AIR QUALITY MONITORING, ASSESSMENT AND MANAGEMENT

Edited by **Nicolás A. Mazzeo**

INTECHWEB.ORG

Air Quality Monitoring, Assessment and Management
Edited by Nicolás A. Mazzeo

Published by InTech
Janeza Trdine 9, 51000 Rijeka, Croatia

Copyright © 2011 InTech
All chapters are Open Access articles distributed under the Creative Commons Non Commercial Share Alike Attribution 3.0 license, which permits to copy, distribute, transmit, and adapt the work in any medium, so long as the original work is properly cited. After this work has been published by InTech, authors have the right to republish it, in whole or part, in any publication of which they are the author, and to make other personal use of the work. Any republication, referencing or personal use of the work must explicitly identify the original source.

Statements and opinions expressed in the chapters are these of the individual contributors and not necessarily those of the editors or publisher. No responsibility is accepted for the accuracy of information contained in the published articles. The publisher assumes no responsibility for any damage or injury to persons or property arising out of the use of any materials, instructions, methods or ideas contained in the book.

Publishing Process Manager Natalia Reinic
Technical Editor Teodora Smiljanic
Cover Designer Jan Hyrat
Image Copyright Jeff Banke, 2010. Used under license from Shutterstock.com

First published June, 2011
Printed in Croatia

A free online edition of this book is available at www.intechopen.com
Additional hard copies can be obtained from orders@intechweb.org

Air Quality Monitoring, Assessment and Management, Edited by Nicolás A. Mazzeo
p. cm.
ISBN 978-953-307-317-0

INTECH OPEN ACCESS PUBLISHER

INTECH open

free online editions of InTech
Books and Journals can be found at
www.intechopen.com

Contents

Preface

Human beings need to breathe oxygen diluted in certain quantity of inert gas for living. In the atmosphere, there is a gas mixture of, mainly, oxygen and nitrogen, in appropriate proportions. However, the air also contains other gases, vapours and aerosols that humans incorporate when breathing and whose composition and concentration vary spatially. Some of these are physiologically inert. An unpolluted atmosphere never existed. From the very beginning of time, the decomposition of vegetable, animal matter and the forest fires have emitted gases and particles. However, as a consequence of technological development, air pollution has become a problem of major concern in the last few decades, since it has caused negative effects on human health, nature and properties.

This book presents the results of research studies carried out by researchers from different countries, presented in seventeen chapters which can be grouped into two main sections. Those sections are: a) air quality monitoring and b) air quality assessment and management. Most chapters are the result of research work done by their authors during several years.

The first three chapters, which form the first section, have been prepared by researchers from Italy, Canada-Saudi Arabia and Thailand. These chapters are focused on the discussion about the difficulties of the air quality network design and on the development and description of the application of an electronic nose to detect odour generated by different air pollutants.

The second section is constituted of fourteen chapters and focuses on air quality assessment and management in different areas. The authors of these chapters are from USA (three chapters), Poland, Italy (two chapters), Brazil (two chapters), India, France, Japan, South Africa, Chile and Mexico. Chapter 4 deals with a monitoring program of total particulate deposition in the vicinity of the coal fired power plant employing passive dry deposition techniques. Chapter 5 investigates the possible occurrence of dusting process by analyzing the atmospheric particulates accumulated on the biological surface and compares them with the particles characteristic of phosphogypsum waste by-product. Chapter 6 presents an application of Principal Component Analysis and Absolute Principal Component Scores to the data set of chemical parameters (ions, organic carbon and elemental carbon) of PM2.5 and PM10 data obtained with sampler.

Chapter 7 is a review article on different techniques of measurement and monitoring of VOCs in emission gases and air quality. Chapter 8 describes the estimation of vehicle emissions of CO, NOx, HC, SO2 and PM in an urban area located in Brazil, from the addition of biodiesel to diesel and evaluates air quality according to PM, CO, NOx, O3, SO2, PAHs, NPAHs and meteorological variables. This chapter illustrates why vertical information is critical in monitoring air quality and how large-scale plume transportation affects surface pollution level. Chapter 9 outlines the importance of remote sensing instruments in multiple applications in monitoring the vertical distribution of air quality and demonstrates how they can unravel difficulties in air quality retrieval from satellite techniques. Chapter 10 presents SO2 concentration measurements undertaken over an island and in the vicinity of a volcano during and off eruption events. Chapter 11 deals with different sampling and analysis techniques for persistent organic pollutants in the atmosphere of remote zones. In chapter 12, the special information on Asian dust–storm particles which is a peculiar natural source of air pollution in East Asia and the Pacific Ocean is reported. Chapter 13 addresses the use of genetic damage biomarkers as early indicators for mainly organic atmospheric pollution, compares the mutagenic responses with particulate matter concentration and discusses the biological effects observed in assays using samples of different particulate matter size. Chapter 14 gives the results of an evaluation of atmospheric aerosols in a gold mining town. The main objective of chapter 15 is to identify the causes of high levels of PM10 concentrations in the Metropolitan Region of the city of Santiago (Chile) in order to contribute to improve the management of air quality in the city. Chapter 16 describes a multi-year assessment of airborne metals, using leaf-surface chemistry. Chapter 17 presents a study of the organic compounds in airborne particles and their impact on climate and air quality, chemical composition and source apportionment, as well as on instrumental determination and atmospheric transformation, besides their toxic effects and to risk human health.

This book provides a source of material for all those involved in the field, whether as a student, scientific researcher, industrialist, consultant, or government agency with responsibility in this area.

It should be emphasized that all chapters have been prepared by professionals who are experts in their research fields. The content of each chapter expresses the point of view of its authors who are responsible for its development. All chapters have been submitted to reviews in order to improve their presentation following several interactions between the Editor-Publisher-Authors. In this sense, the Editor, the Publisher and hard-working air quality professionals have worked together as a team to prepare a book that may become a reference in the field next years. This will have been achieved, mainly, thanks to the group of experts in their research fields joined as authors of this book.

Nicolás A. Mazzeo
National Scientific and Technological Research Council
National Technological University
Argentina

Part 1

Air Quality Monitoring

1

Planning Air Pollution Monitoring Networks in Industrial Areas by Means of Remote Sensed Images and GIS Techniques

Mauro Rotatori, Rosamaria Salvatori and Roberto Salzano
National Research Council of Italy - Institute of Atmospheric Pollution Research
Italy

1. Introduction

Air pollution and its impact have become one of the most important challenge for public authorities. The quantification of emissions as well as their spatial distribution are essential for any air quality program (Aleksandropoulou & Lazaridis, 2004; Sengupta et al., 1996). The selection of the location of monitoring stations is one of the most complex task that occurs in designing air monitoring networks. Several issues, as the harmful effects of pollution on both human health and environment, must be taken into account (Allegrini et al., 2004).
The European directive 2008/50/CE of 21 May 2008 on ambient air quality and cleaner air provides criteria about monitoring network. This directive has been issued in order to improve, clarify, simplify and replace the precedents five acts:

- Council Directive 96/62/EC of 27 September 1996 on ambient air quality assessment and management;
- Council Directive 1999/30/EC of 22 April 1999 relating to limit values for sulphur dioxide, nitrogen dioxide and nitrogen oxides, particulate matter and lead in ambient air;
- Directive 2000/69/EC of the European Parliament and of the Council of 16 November 2000 relating to limit values for benzene and carbon monoxide in ambient air;
- Directive 2002/3/EC of the European Parliament and of the Council of 12 February 2002 relating to ozone in ambient air and;
- Council Decision 97/101/EC of 27 January 1997 establishing a reciprocal exchange of information and data from networks and individual stations measuring ambient air pollution within the Member States.

The Directive 2008/50/CE also introduces new air quality objectives and monitoring requirements for $PM_{2.5}$. In addition to that the EU directive determines criteria for positioning monitoring stations, taking into account a detailed evaluation of environmental features on both local and regional scale.
These objectives can be pursued by territorial analysis, which can be performed using a Geographic Information System (GIS). GIS is a computer-based information system that enables storing, modelling, manipulation, retrieval, analysis and presentation of geographically referenced data (Burrough, 2001). In particular this powerful tool allows a

detailed representation of the investigated territory. Different types of data can be integrated and correlated: chemical, physical, demographic and any kind of environmental information. Numeric records can be stored in a GIS, creating and developing a geo-database. All these information can be analysed and elaborated in order to derive thematic cartography. GIS gives the opportunity to integrate these thematic layers with health data and permit the evaluation of health risk towards pollution (Stedman et al., 1997). The dynamics of these processes can be moreover investigated and monitored over a long period by multitemporal integration. This last procedure consists on join up of data provided by different campaigns carried out in the same study area. The background knowledge of every territorial analysis and successive integration with atmospheric data is made up of satellite imagery retrieving and classification. This final step provides land use maps and can be derived with several classification techniques on satellite images or digital aerial imagery (Foody, 2000; Weirs et al., 2004). The integration of land use maps with concentration maps of pollutants, allows recognition of areas exposed to high pollution levels and the relative exposure during time. The successive step of this territorial analysis allows identification of sites optimal for the installation of monitoring stations following the rules provided by the directives in force. This chapter proposes a combined procedure between data concerning pollutants contents and thematic cartography. This approach can support designing of monitoring networks focused on air quality.

2. Sampling strategies

Campaigns for monitoring pollutants must be planned considering objectives of the survey and features of the investigated process. These two issues are decisive for the selection of the season and the extent of the sampling length and are critical for the choice of the passive samplers location strategy. The passive sampler system, developed by the CNR Institute of Atmospheric Pollution Research, is particularly useful for preliminary evaluations of air quality condition (Bertoni 2000; De Santis et al., 1997). Samplers can in factbe exposed for many months in selected areas of interest, and resulting concentration levels are averaged over a long period. Passive samplers use active carbon as adsorption phase, active carbon is contained in a stainless steel netting inserted in the diffusive cylindrical body. Pollutants adsorbed by active carbon are successively extracted, by solvents or by heating, and analysed with appropriate chemical techniques. Passive samplers are inserted with the open side facing to the holder, which is necessary in order to minimize wind interference. Samplers are then exposed to air for a period long enough to obtain a significant and adequate sample for the analysis. The selection of the exposure length for sampling is regulated mainly by the survey objectives: the impact evaluation of new industrial plants on the environment requires pre-, sin- and post start-up campaigns; the impact evaluation of existing industrial plants requires, instead, to plan campaigns representative of each season in order to estimate all climatic and environmental features of the investigated area. The design of monitoring networks in urban areas requires, as above, the execution of campaigns representative of all the features characterising the examined urban area. On the other hand, the scheduling of campaigns and the exposure time of samplers are obviously influenced dominantly by requirements and funds dedicated by the administrations that dispose the study. For sure, a longer exposition of passive samplers can, in accordance of observed concentrations, be more representative of the study area, as the climatic and environmental conditions are averaged.

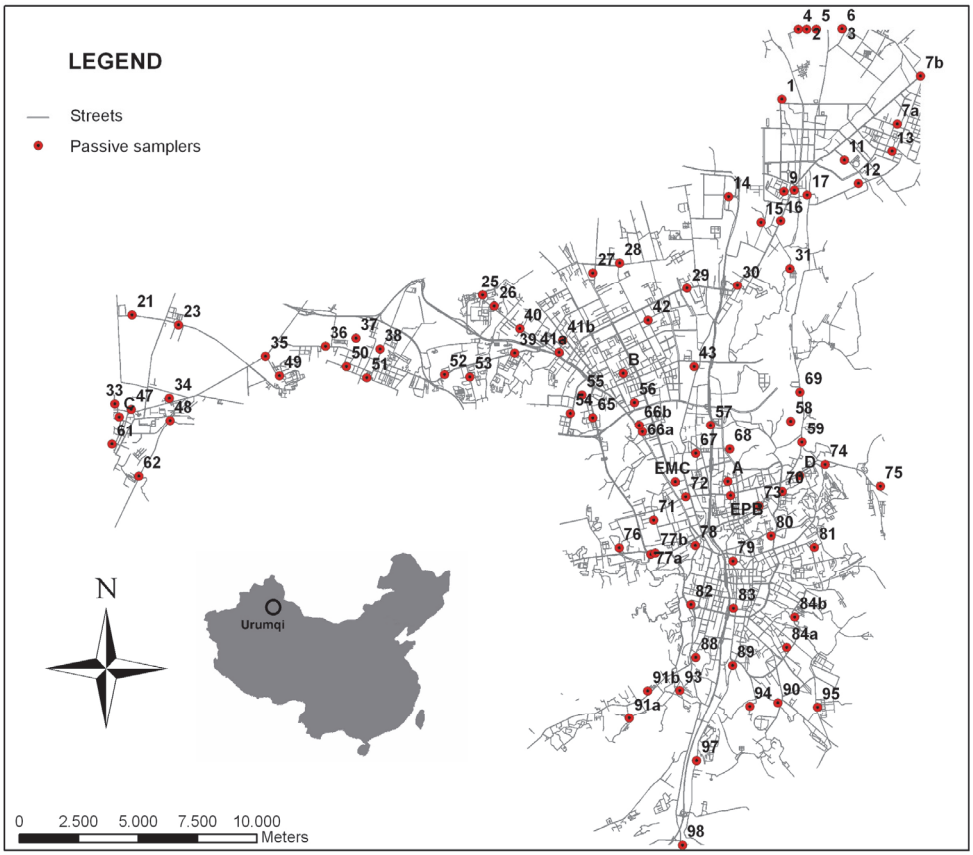

Fig. 1. Example of sampling strategy carried out in Urumqi (China, PRC).

The sampling strategy (Fig. 1) must be selected considering the objectives of the survey (Isaaks & Srivastava, 1989). Strategies can be classified into two major groups: simple and stratified. The first one is characterised by a single sampling grid. The lattice that localizes sampling sites is defined by several features: orientation; order; density. Orientation is the property that defines the alignment of grids with preferential directions of pollutant dispersion. This feature can be selected taking into account the climatic and environmental conditions of the study area and can be regulated in order to consider dominant wind directions, topography and urban characteristics in the case of cities. The order grade of the grid is referred to the distribution of sampling stations in the territory and to the distance that occurs between sites. This distance can be constant and guarantees an homogeneous distribution, or it can be random in order to investigate processes at a more detailed spatial scale. In opposition of that, the random criteria can add clustering problems to the distribution of sampling stations. Both geometric features, previously discussed, influence the final characteristic of the sampling grid. The sampling density is a descriptive parameter that defines the spatial resolution of the lattice and allows evaluation of homogeneity and spatial significance of data. Stratified strategies are instead the result of the combination

between two or more simple grids. This group is more appropriate for monitoring studies with a limited number of stations. It provides a dataset relatively independent from the studied phenomena and at the same time guarantees a good coverage of the study area.

3. Representation of concentration levels of pollutants

The representation of chemical data in a spatial context requires a three step analysis of concentration levels (Fig. 2).

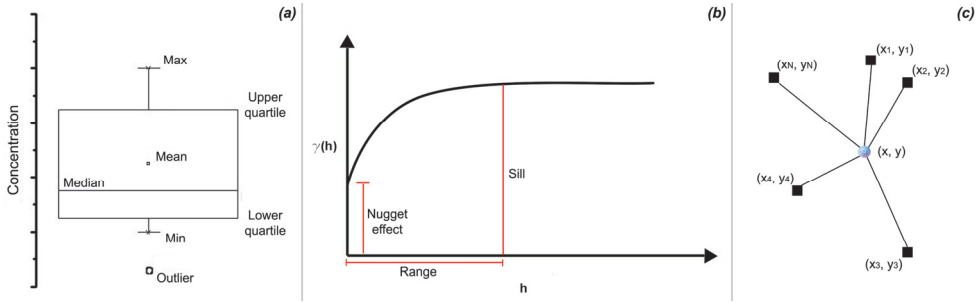

Fig. 2. Examples of statistical tools useful for the representation of concentration levels of pollutants [box diagrams (a), variograms (b) and interpolation algorithm (c)].

3.1 Descriptive analysis

This first step consists on the description, with general statistical parameters, of data obtained during the monitoring campaigns. Different statistic tests are performed (Davis, 1986), in particular to study the statistical distribution of the dataset;variograms are created to define the spatial dependence of pollutants. All these data treatments are propaedeutic to the next steps that are focused on the representation *sensu strictu*.

3.2 Interpolation criteria

The interpolation criteria that can be applied to chemical data provided by diffusive samplers can be classified into two main groups (Armstrong, 1998): deterministic (inverse distance weight, nearest neighbour, linear and polynomial regression), and probabilistic (ordinary and universal kriging). In the first case, the values in the "*unknown*" sites are calculated as linear combination between "*measured*" stations. Probabilistic criteria estimate instead the "*unknown*" value using the spatial dependence model that exists between "*measured*" sites. Kriging, in particular, requires that the investigated process, and consequently the measured dataset respects the "*normality*" and the "*stationariness*" hypothesis (Isaaks & Srivastava, 1989). A complex geostatistical treatment is necessary to support the application of kriging. The core of this probabilistic method consists in the definition of spatial dependence model. The appropriated model is selected fitting experimental variograms with theoric functions. The selection of the interpolation method depends mainly on the sampling strategy and on the number of available samples. Unfortunately there are no objective criteria that support the selection of the most appropriate interpolation method. Each case differs from the others and only the preliminary analysis and the variogram study can help the user to take decisions. It is

possible to evaluate the goodness of resulting maps creating error maps, which can be calculated as the difference between "*measured*" and "*calculated*" values.

Concentration level	SO_2	O_3	NO_x	NO_2	H_2S
			$\mu g/m^3$		
1st	0 – 20.8	0 – 20	0 – 13.3	0 – 13.3	0 – 2.7
2nd	20.8 – 41.7	20 – 40	13.3 – 26.7	13.3 – 26.7	2.7 – 5.3
3rd	41.7 – 62.5	40 – **60**	26.7 – **40.0**	26.7 – **40.0**	5.3 – **8**
4th	62.5 – 83.3	**60** – 80	**40.0** – 53.3	**40.0** – 53.3	**8** – 10.7
5th	83.3 – 104.2	80 – 100	53.3 – 66.7	53.3 – 66.7	10.7 – 13.3
6th	104.2 – **125.0**	100 – 120	66.7 – 80.0	66.7 – 80.0	13.3 – 16.0
7th	> **125.0**	> 120	> 80	> 80	> 16.0

Concentration Level	Benzene	Toluene	Xylenes	VOCs
		$\mu g/m^3$		
1st	0 – 1.6	0 – 8.3	0 – 8.3	0 – 16.7
2nd	1.6 – 3.3	8.3 – 16.7	8.3 – 16.7	16 – 33.3
3rd	3.3 – **5**	1.7 – **25.0**	1.7 – **25.0**	33.3 – **50.0**
4th	**5** – 6.6	**25.0** – 33.3	**25.0** – 33.3	**50.0** – 66.7
5th	6.6 – 8.3	33.3 – 41.7	33.3 – 41.7	66.7 – 83.3
6th	8.3 – 10.0	41.7 – 50.0	41.7 – 50.0	83.3 – 100.0
7th	> 10.0	> 50.0	> 50.0	> 100.0

Table 1. Suitable concentration levels of pollutants for distribution maps. Bold numbers represent the reference values, that are based on annual limits indicated by legislation, when available.

3.3 Classification of pollution levels

The classification of pollution levels for each considered substance can be arbitrary, objective or derived. The first criterion can be applied using statistic parameters as equivalent classes, quartile, standard deviation or whatever the user wants to use for subdividing the range into levels. The classification with an objective criterion is instead based on selecting a reference value that can be indicated, for example, by legislation. In conclusion several derived criteria can be used as calculated indexes. It is possible to calculate ratios respect reference values or coefficients that consider health effects produced by specific pollutants (Table 1).

4. Territorial analysis with remote sensed images

The best locations for air quality monitoring stations can be found analysing the environmental patterns of the region where the network must be located, even if socio-political reasons cannot be neglected. The study of environmental patterns can be conducted

using coverage and land use maps along with census maps. The availability of updated and detailed maps is very limited and to overcome this problem it is only possible to derive these thematic maps by processing remote sensed images. Remote sensors collect and record the electromagnetic energy coming from the Sun and reflected, or emitted, by the Earth surface at different wavelengths. For environmental studies the wavelength range used by sensors (passive optical sensors) is between 450 nm and 2500 nm, although there are passive sensors that can collect images in the thermal infrared wavelengths range (8000 – 10000 nm). Each surface element like soil, different types of vegetation cover, urban areas, reflects the electromagnetic energy as a function of its chemical and physical characteristics, i.e. each surface element shows a different spectral behaviour that can be considered as its fingerprints or its spectral signatures. Images collected at different wavelength intervals (different bands) can be processed in order to assign a surface element to each pixel of images and to analyse the spatial distribution of these elements. At the present time, there are many remote sensors and each of them can collect images characterised by a different spectral range (band). The number of bands, their width and their location in the electromagnetic spectrum define the spectral resolution of the image. Most of the sensors record the reflected energy in the visible range, with three spectral bands centred on blue, green and red light, one or more bands are instead reserved for the spectral range that corresponds to middle and near-infrared and generally only one band is dedicated to measure the radiation in the thermal infrared. Therefore, a remote sensing (RS) image can be composed of different number of bands: a multispectral image is represented by 3 - 7 bands while hyperspectral images can have more the 100 bands, where more than one corresponds to the thermal infrared. In theory, a higher number of bands can allow a more detailed analysis of the spectral characteristics of surface element. The availability of images collected simultaneously at different wavelength ranges, allows selection of the most appropriate set of bands useful for the specific investigation. Visible and near infrared images are, for instance, used mainly for vegetation and land cover studies while images recorded at higher wavelengths are more useful for geological applications. Moreover, images recorded in the thermal infrared can be processed in order to derive radiant temperature of the surfaces. Remote sensors used for environmental investigation can be carried aboard on satellites or aircrafts. In the first case, the geometry of the sun-target-sensor system, is determined by orbital parameters. The resultant image has consequently a fixed and constant pixel size. Aircrafts can, instead, fly at specified altitude that can be selected in order to achieve the requested spatial resolution. These images can also be collected at different day time improving the discrimination of surface elements. Nowadays, the improvement of spatial technologies makes available a wide selection of satellite images with a "*spatial resolution*" ranging between 1km and few metres and a "*pass over*" time ranging between 0.5 and 25 days. Sensors with low spatial resolution pass over the same area daily while sensors with medium or high resolution have pass over time of 3 - 16 days (Table 2).

Such a wide availability of remote sensed images with different spatial and spectral characteristics makes possible the production of thematic maps with a higher level of accuracy and with a scale controlled by the image pixel size. The selection of the most appropriate sensor must be carried out before the information extraction process and must take into account the purposes of the study averaging out between spatial and spectral resolutions. For instance, the most suitable data sets for regional scale studies are the Landsat Thematic Mapper images. Such sensor acquires images with 7 spectral bands, in the

wavelength range between visible and thermal infrared, at ground resolution of 30m per pixel (Table 2). These radiometric and geometrical characteristics allow the investigation of large areas with a spectral resolution suitable for the production of land cover or land use maps with a scale ranging between 1:50.000 and 1:100.000. Image fusion techniques, that combine images with different spatial and spectral resolutions, are a very useful tool to preserve the highest content of information. Moreover, all the other multispectral instruments devoted to Earth observations, as Thematic Mapper, were designed taking into account the spectral properties of natural surfaces. Vegetation cover patterns can be easily discriminated by processing red and near infrared bands (TM3, TM4, TM5) while differences between soils moisture or rock outcrops can be detected using band TM5 and TM7. The complexity of the information embedded in multispectral images is the key that allows, using proper statistical classification algorithms, the elaboration of thematic maps for environmental applications.

	NOAA AVHRR	Landsat 7 ETMP	SPOT5 HRVIR	IRS LISS-I	IKONOS	QuickBird
Image bands (μm)	0.58 – 0.68	0.45 – 0.52[a]			0.45 – 0.52[a]	0.45 – 0.52[a]
	0.725 – 1.1	0.52 – 0.60[a]	0.50 – 0.59[a]	0.52 – 0.59[a]	0.52 – 0.61[a]	0.52 – 0.60[a]
	3.55 – 3.93	0.63 – 0.69[a]	0.61 – 0.68[a]	0.62 – 0.68[a]	0.64 – 0.71[a]	0.63 – 0.69[a]
	10.3 – 11.3	0.76 – 0.90[a]	0.79 – 0.89[a]	0.77 – 0.86[a]	0.77 – 0.88[a]	0.76 – 0.90[a]
	11.5 – 12.5	1.55 – 1.75[a]	1.58 – 1.75[b]	1.55 – 1.70[b]		
		10.4 – 12.5[b]				
		2.08 – 2.35[a]				
		0.52 – 0.90[c]	0.48 – 0.71[c]	0.5 – 0.75[c]	0.45 – 0.90[c]	0.45 – 0.90[c]
Spatial resolution (m)	1100	30[a]/60[b]/15[c]	10[a]/20[b]/5[c]	23[a]/70[b]/5.8[c]	4[a]/1[c]	2.4[a]/0.5[c]
Revisit time (day)	0.5	16	2-3	24	3	3
Swath Width (km)	3000	185	60	70[a,c]/142[b]	11	16.6

Table 2. Characteristics of the most commonly used satellite sensors for Earth Observation.

The definition of land use and land cover classes has been object of several studies but nowadays the scientific community is converged on the CORINE classification system (Bossard et al., 1999), where the detail of classification can be selected according to the study purposes as well as the representation scale. CORINE Land Cover (CLC) is a geographic land cover/land use database encompassing most of the European countries. CLC describes land cover (and partly land use) according to a nomenclature of 44 classes organised hierarchically in three levels. The first level (5 classes) corresponds to the main categories of the land cover/land use (artificial areas, agricultural land, forests and semi-natural areas, wetlands, water surfaces). The second level (15 classes) covers physical and physiognomic entities with a higher level of detail (urban areas, forests, lakes, etc), finally level 3 is composed of 44 classes. Image classification techniques can help to study air quality and its effects on human health. The classification procedures, devoted to the production of the

land use and the land cover maps for air quality studies, support the discrimination between spectral classes related to urban and industrial areas. These classes can be used, by means of integration with data coming from different sources (i.e. census data), to estimate population density or other socio-economic parameters. For example, classes identified in industrial sites could be combined with the number of persons working as well as the type and the amount of pollutants introduced in the atmosphere.

5. Integrated analysis with GIS

As mentioned before, the GIS is a complex database system in which data coming from different sources can be archived. The unique constraint is that data must be georeferred, i.e. stored with their geographical coordinates (Fig. 3). The creation of a GIS, designed to be a decision tool in planning an air quality network, foresees the input of: point data, derived from chemical analysis of atmospheric pollutants or from census archives; linear data, like railways or highways networks as well as traffic fluxes associated to relative feature; surfaces data, derived from remote sensed image processing or other thematic maps. The statistical analysis, the data retrieval and the representation procedures are implemented in a GIS. All these features make GIS as a very powerful tool, which can provide several types of new information. For example, surface information can be derived from point data using interpolation procedures. The geodatabase can be queried in order to extract new calculated values, as areas where pollution levels are higher then a certain value and where the main roads are closer than 50 metres. Data stored in a GIS can be periodically upgraded by the users in order to supply a better overview in monitoring environmental processes. The dynamism of GIS allows processing of multi-temporal data using multivariate statistical analyses. Once pollutant concentrations, collected in different seasonal campaigns, are stored into a GIS, substances can be treated singularly or combined together. The built-in routines can either retrieve seasonal distribution maps or calculate maps of ratios (i.e. benzene/VOCs) or compute multi-temporal maps. Moreover, the areas with concentration values above the average can be highlighted using queries. These results can also be resumed in different summary maps, one for each pollutant (i.e. NO_x, NO_2, O_3 and VOCs respectively). Through the summary maps it is possible to describe the distribution of pollutants all over the monitoring period without loosing information of the single monitoring campaign. Subsequently, from each summary map, areas with values above average for more than two campaigns can be extracted and plotted together in a new map that can be named "*occurrence map*". These areas can be furthermore classified using special tags that allow identification of the recurrence number and of the type of pollutant.
For instance it is possible to attribute the tag "$2rNO_x$" to the areas that registered a NO_x concentration levels above the average values for at least two monitoring campaigns (Fig. 4). This kind of analysis, iterated for each pollutant, can be used to verify the significance of peak values and/or spatial trends. For this purpose a "*multiple-occurrence map*" can be created selecting properly the pollutants to be monitored. All the thematic maps, thus computed, can be overlaid to the land cover and land use maps obtained by remote sensed image classification procedures. This approach permits the correlation between pollution patterns, physical features and processes occurring in the investigated area (Fig. 5). Pollutant distribution can be easily investigated taking into account its possible origins or carriers, such as transportation fluxes, industrial plans, urban wastes, morphology or hydrological networks.

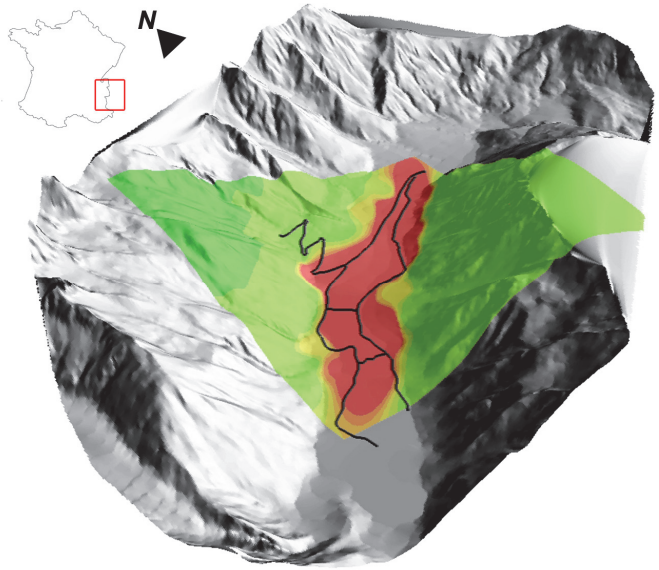

Fig. 3. Example of data integration in a GIS. Concentration levels (colours) of one pollutant are over imposed on a shaded relief (grey tones) obtained from a digital elevation model. Black lines represent the major road network. The study area is Chamonix (France).

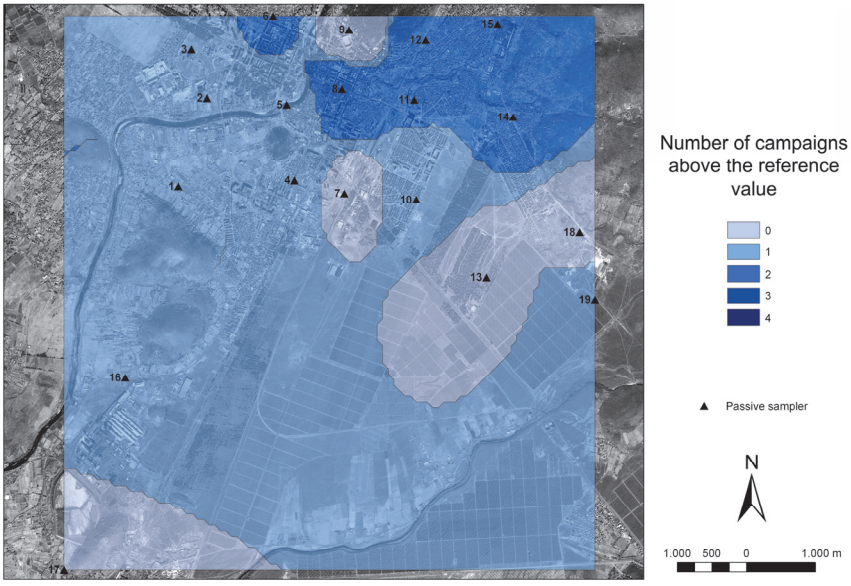

Fig. 4. Example of occurrence map where colours represent the number of campaigns that exceed a reference value defined by legislation or by statistics.

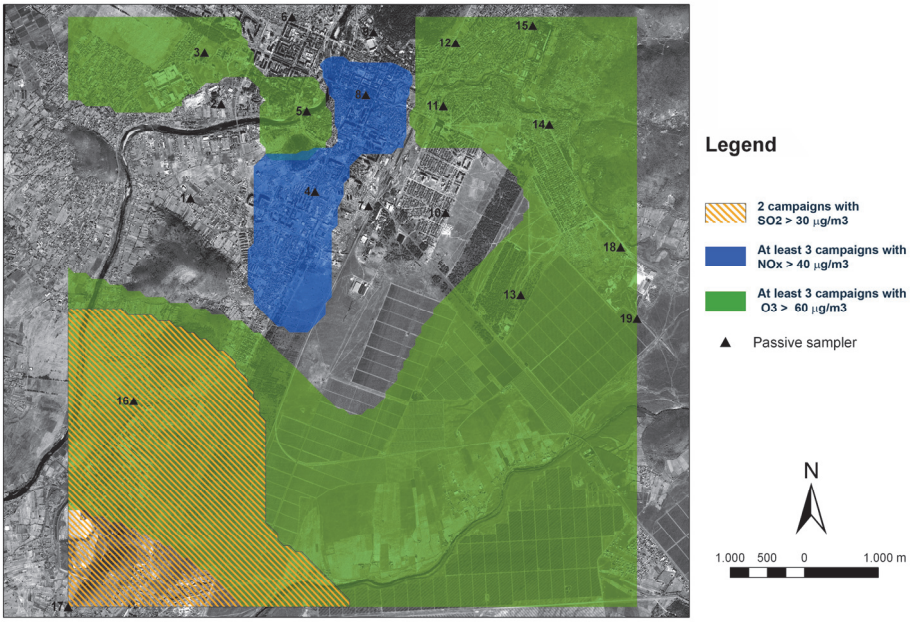

Fig. 5. Example of multiple occurrence map where colours represent areas where pollutants exceeded a reference value for a specified number of campaigns.

In urban areas, the use of very high resolution images can also allow overlaying of supply networks to land cover map as well as to pollutant distribution map. This interactions has been turn out to be a very useful tool to identify the most suitable site for monitoring stations network following the European criteria.

6. Practical applications

6.1 Gela case study

RS – GIS integrated approach was tested in 2005 when an oil enterprise, owner of a refinery plant located in Gela (Southwestern Sicily, Italy), charged CNR – IIA for upgrading its air quality monitoring network. The aim of this study was the identification of the minimum number of monitoring stations, their location, their type and their instrumental equipment in accordance with the Italian and the European legislation. Gela refinery is located in Sicily, 1 km SE of the city of Gela, in an industrial area 500 km^2 wide. Considering the wind direction, the distribution of inhabited areas, it was decided to investigate an area of about 22 x 22 km thus including both the urban areas of Gela and Niscemi (Fig. 6).

A Landsat 5 Thematic Mapper multispectral image (July 20th 2004) was selected to obtain a 1:50.000 land use map; this scale factor was also used to prepare all the cartographic layers of the developed GIS. The identification of different land covers (urban area, bare soils and different kind of vegetation covers) was carried out using the false colours combination of visible and near infrared bands (RGB = TM 4-3-2) provided by Landsat TM. This classification was obtained following the CORINE land cover classification criteria. In details, the performed procedure consisted in a first step where a preliminary classification

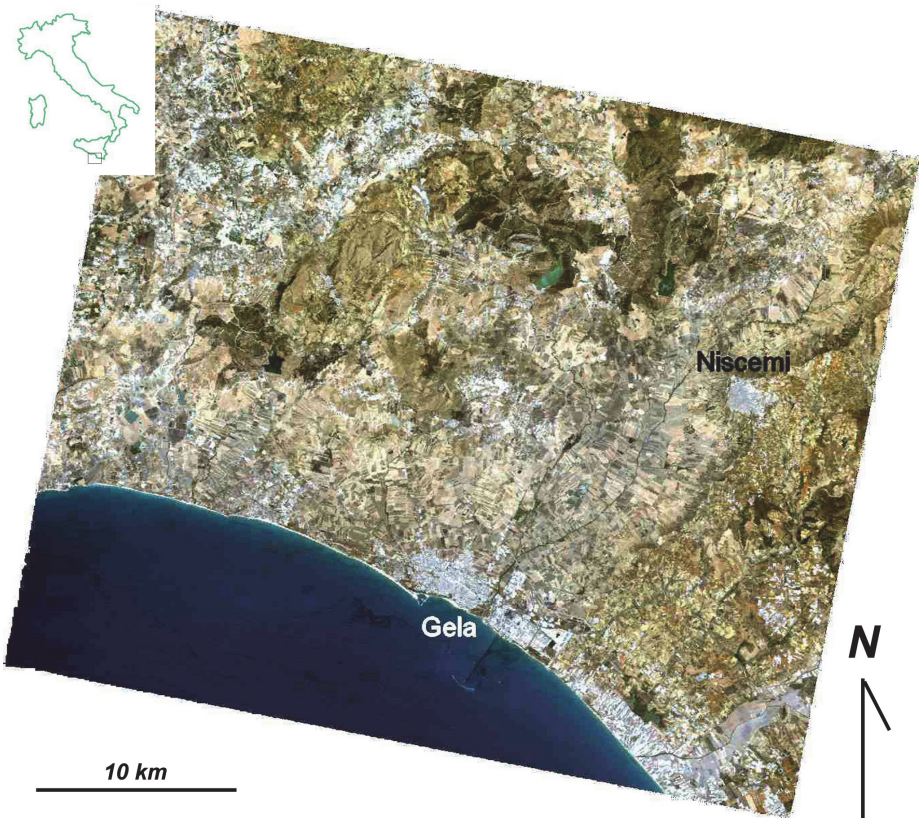

Fig. 6. Location map of Gela and Niscemi (south-western Sicily, Italy).

based on 6 classes (CORINE level 2) was obtained using a maximum likelihood algorithm. The following step was based on the principal component analysis of the original multispectral image combined to the classification of the resulting components. In this new classified image it was possible to discriminate clearly the urban area (in red) from the industrial areas: refinery in blue and dumping ground in magenta (Fig. 7). Both thematic maps were included in the GIS prepared for this case study. Moreover, this discrimination between different land-use classes (agricultural, natural and pasture areas) supported the assignment to each area of a specific weight, successively useful for estimating the value of each parcel and consequently the type of monitoring station that must be located, as stated by the European criteria on air monitoring network.

In addition to the territorial analysis this study included preliminary assessment of air quality using diffusive samplers: 4 seasonal campaigns were performed from January 2005 to November 2005, and the considered substances were NO_x, NO_2, SO_2, O_3, benzene, toluene, xylenes, and VOCs. Diffusive sampler is a device that collects samples of gas or vapour pollutants from air at a rate controlled by physical processes such as diffusion through a static air layer or permeation through a membrane. The main advantage of diffusive sampling is the length of the exposure period (it ranges from weeks to months

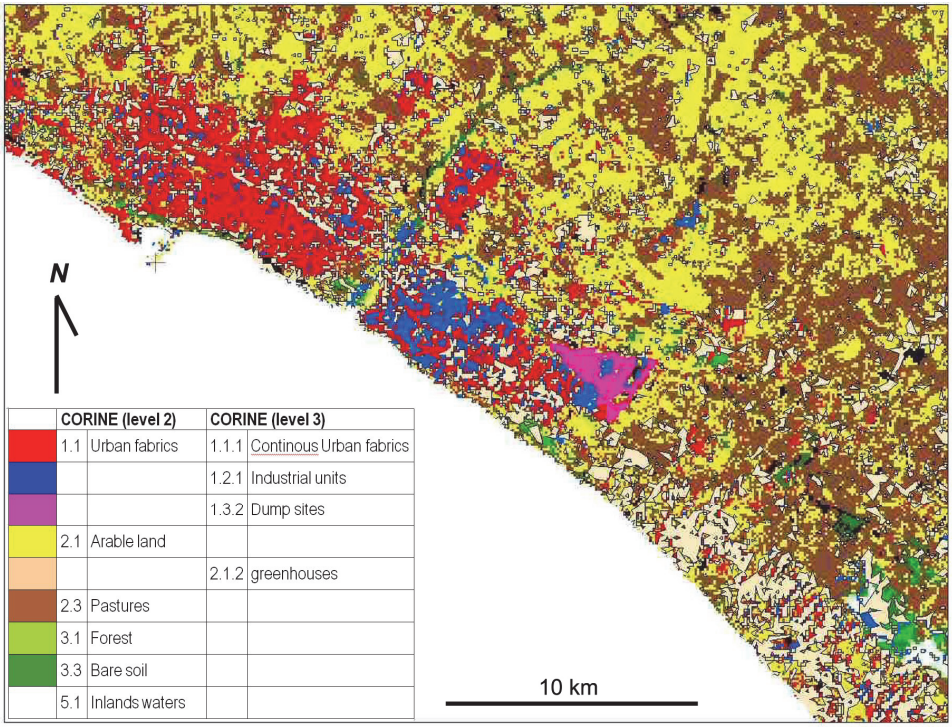

	CORINE (level 2)		CORINE (level 3)	
	1.1	Urban fabrics	1.1.1	Continous Urban fabrics
			1.2.1	Industrial units
			1.3.2	Dump sites
	2.1	Arable land		
			2.1.2	greenhouses
	2.3	Pastures		
	3.1	Forest		
	3.3	Bare soil		
	5.1	Inlands waters		

Fig. 7. Final classified image of the Gela area. Red pixels represent urban areas, blue areas are occupied by refinery facilities and dumping ground in magenta.

depending on observed concentrations) that allows long term sampling campaigns. In this study the selected sampling strategy for positioning diffusive samplers was the "*Stratified Random Sampling*" strategy. This option was adopted because this is an effective and practical method to ensure a uniform coverage of the study area. The study area was divided into a regular square grid with a cell dimension of 2.5 km and samplers were randomly placed within each cell. More than one sampler was placed in the cells located in the inhabited areas (Gela and Niscemi), in order to better assess the effects of pollutants on human health. In conclusion 72 diffusive samplers were distributed in the study area and the exposure time for each seasonal campaign was 30 days. In addition to that the quality of data was supported by samplers used as replicates and blanks. Furthermore, the installation of diffusive samplers was supported by a GPS survey in order to use chemical data in a GIS geodatabase. Pollutants concentration data, obtained by IIA chemical laboratories using chromatographic techniques, were interpolated over the whole study area using the geostatistical tools on the developed GIS. In this case study concentration maps were obtained using an "*Inverse Distance Weight*" algorithm, where the values at the "*unknown*" sites are calculated using relationship based on the distance between "*measured*" stations. The greater the distance, the lower is the effect of measured points on the unknown site. The interpolation process produces a continuum of values placed on the whole study area.

Concentration level	SO_2	O_3	NO_x	NO_2	H_2S
			$\mu g/m^3$		
1st	0 – 20.8	0 – 20	0 – 13.3	0 – 13.3	0 – 2.7
2nd	20.8 – 41.7	20 – 40	13.3 – 26.7	13.3 – 26.7	2.7 – 5.3
3rd	41.7 – 62.5	40 – **60**	26.7 – **40.0**	26.7 – **40.0**	5.3 – **8**
4th	62.5 – 83.3	**60** – 80	**40.0** – 53.3	**40.0** – 53.3	**8** – 10.7
5th	83.3 – 104.2	80 – 100	53.3 – 66.7	53.3 – 66.7	10.7 – 13.3
6th	104.2 – **125.0**	100 – 120	66.7 – 80.0	66.7 – 80.0	13.3 – 16.0
7th	> **125.0**	> 120	> 80	> 80	> 16.0

Concentration level	Benzene	Toluene	Xylenes	VOCs
		$\mu g/m^3$		
1st	0 – 2.7	0 – 8.3	0 – 8.3	0 – 16.7
2nd	2.7 – 5.3	8.3 – 16.7	8.3 – 16.7	16 – 33.3
3rd	5.3 – **8**	1.7 – **25.0**	1.7 – **25.0**	33.3 – **50.0**
4th	**8** – 10.7	**25.0** – 33.3	**25.0** – 33.3	**50.0** – 66.7
5th	10.7 – 13.3	33.3 – 41.7	33.3 – 41.7	66.7 – 83.3
6th	13.3 – 16.0	41.7 – 50.0	41.7 – 50.0	83.3 – 100.0
7th	> 16.0	> 50.0	> 50.0	> 100.0

Table 3. Applied concentration levels of pollutants for the Gela case study. Bold numbers represent the considered reference value, that are based on annual limits indicated by legislation, when available.

For a better result, a pollutant map requires the use of a chromatic scale that can effectively represent the concentration values; therefore the colour scale adopted was calibrated in order to immediately visualize the reference limits imposed by national and European directives (Table 3). This approach turned out to be an objective and flexible criterion, and the maps thus obtained were easily compared and immediately figured out also by non-technical users. Since maps were produced from digital data, any modification of ranges or limit can be easily performed and, for more detail local analysis, it was also possible to represent concentration values following statistical criteria. In conclusion of that, considering all the monitored compounds and each seasonal campaign, 32 concentrations maps were created and integrated in the GIS combined to thematic layers obtained by the previously described territorial analysis. This large amount of maps was unfortunately not easily accessible and information were synthesized in new thematic layers. The first step was to create a "*multitemporal map*" or a summary map overlapping the seasonal campaign maps of each pollutant. Being the product of a series of queries and not the result of numerical calculations on the original concentration values of pollutants, these maps allowed the simultaneous view of the pollutant distribution during the year, maintaining, however, information relating to individual campaigns. From the summary maps for each pollutant, using crossover

functions, areas with concentration values higher than the 4th class for more than 2 campaigns were selected. Since the values of the classes were decided on the basis of current legislation and not on the basis of the statistical distribution of individual pollutant, the 4th class represents the threshold that can be assimilated as reference value for each pollutant.

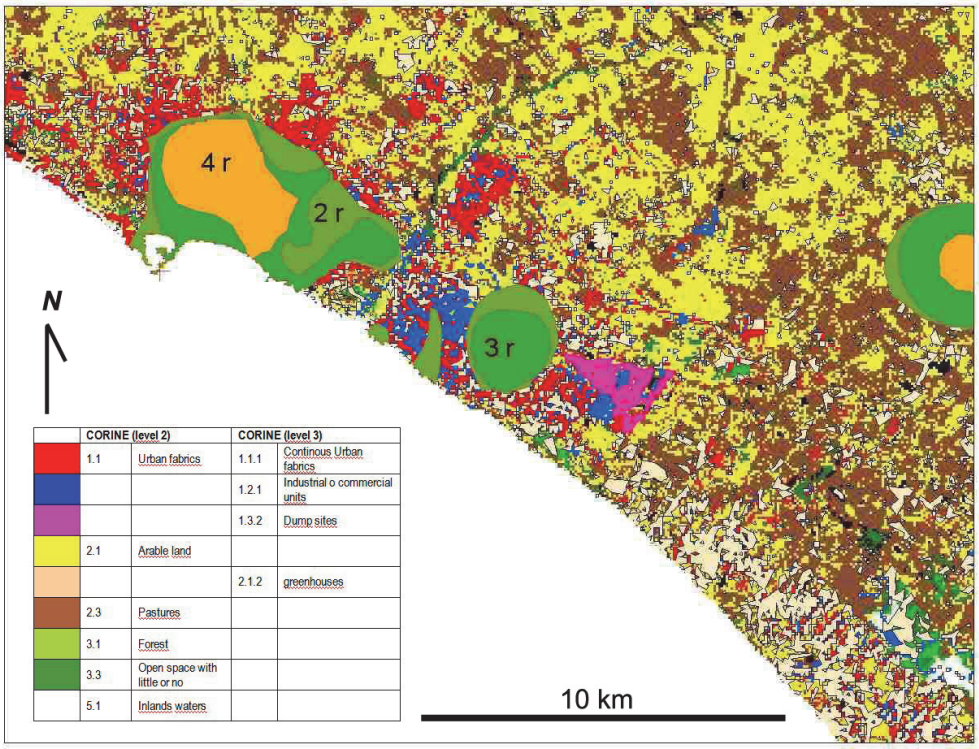

Fig. 8. Occurrence map of NOx in Gela. Orange (4r), dark (3r) and light green (2r) areas show where nitrogen oxides exceed the reference value for 4, 3 or 2 campaigns.

These areas were classified taking into account the number of occurrences, named as "*occurrence map*", highlighting how many times the concentration values were above the reference value and where. Querying the GIS iteratively and performing multi-temporal and multi-pollutants analyses, NO_x, O_3 and VOCs were found to be the most significant compounds that affect air quality in the study area. In conclusion all these maps were collapsed in a single final synthetic map named as "*multiple occurrence map*", where the occurrence maps of these compounds were overlaid. This "*multiple occurrence map*" evidences sites where the effects of pollutants are more relevant. Merging this map with the land cover /use maps, derived by satellite image processing, it was finally possible to evaluate the effect of pollutant on environment and on human activities and health The orange area "*4r*", is the area where the concentration of NO_x was higher than the law limits during the 4 seasonal campaigns. In the land use map this area corresponds to an urban area (Fig. 8).

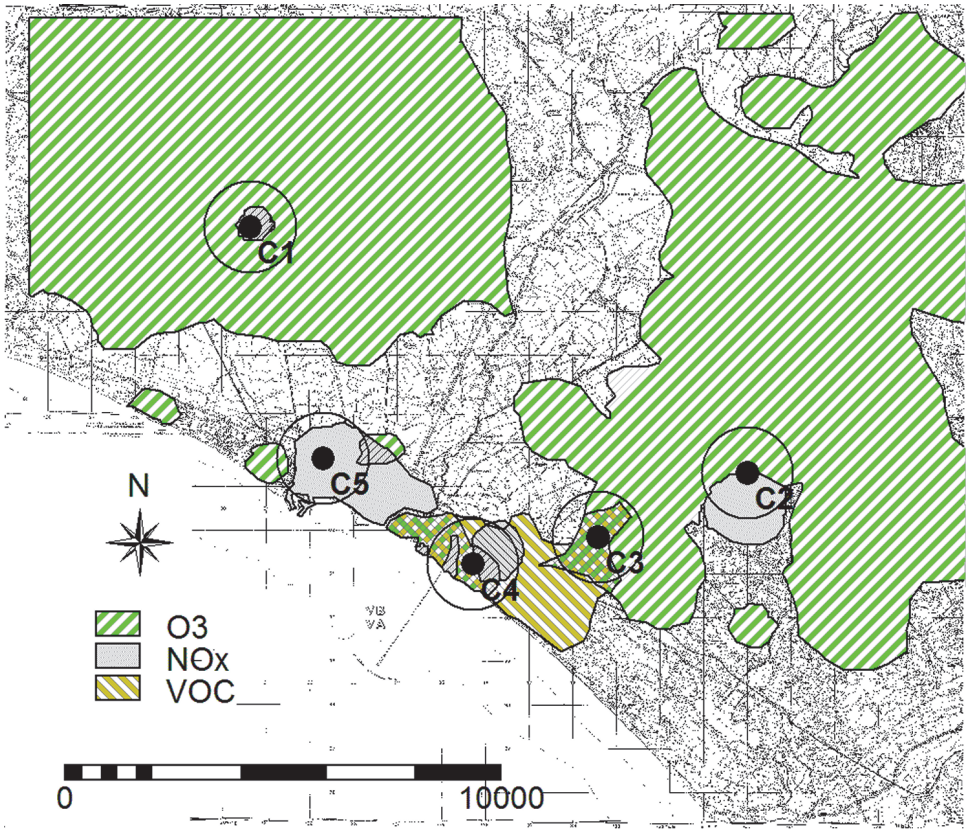

Fig. 9. Localization of monitoring stations in the Gela areas.

The final aim of the study was the selection of the location of new continuous monitoring stations. Giving the environmental asset of the study area: urban areas, industrial plants, agricultural lands, the European Directive suggests at least 3 continuous sampling points. For the sake of a better assessment of the risks for human health, 5 station monitoring network were proposed and this proposal was accepted by the oil company. Based on EUROAIRNET criteria (Larssen et al., 1999), the monitoring stations (Fig. 9) were classified according to the type of pollutant source (urban traffic, industrial, and background) and the characteristics of the area in which they are located (residential, industrial, rural - agricultural).
Furthermore, an additional result obtained overlapping the map of multiple occurrences and the land use map was the identification of the most suitable areas for the location of this 3 different types of monitoring stations taking into account also the logistics and accessibility of sites (power supply, roads network, etc.).

6.2 Scarlino case study

The situation of the industrial area of Scarlino, an industrial area close to coast in Tuscany (Italy), has always been one of the most delicate in Italy from the environmental point of

view, considering the type of industries and the proximity of the industrial area to the city. For this reason the municipality has commissioned to the CNR-IIA a preliminary assessment of air quality aimed to optimize the air quality monitoring network according to the European criteria. In the study area the former monitoring network covered only the industrial area of Scarlino and was focused on monitoring mainly sulphur dioxide (13 stations), that is the most significant pollutant in the emissions of the local industries activities. Few stations were equipped for monitoring nitrogen dioxide (2 stations) and total suspended particulate matter (3 stations). Moreover, this network appeared to meet outdated methodological criteria and not to be consistent with recent EU directives. The study was therefore focused on defining the possible relocation and on retraining the network set up, based on the new criteria established by current legislation. The European criteria require a preliminary evaluation of the air quality in the area of interest; to achieve this result a 4 seasonal monitoring campaigns on NO_x, NO_2, O_3, SO_2, H_2S and VOCs were carried out in the area surrounding the industrial plant (12 x 9 km). Investigated substances were sampled using diffusive samplers that were exposed for 30 days as described above.

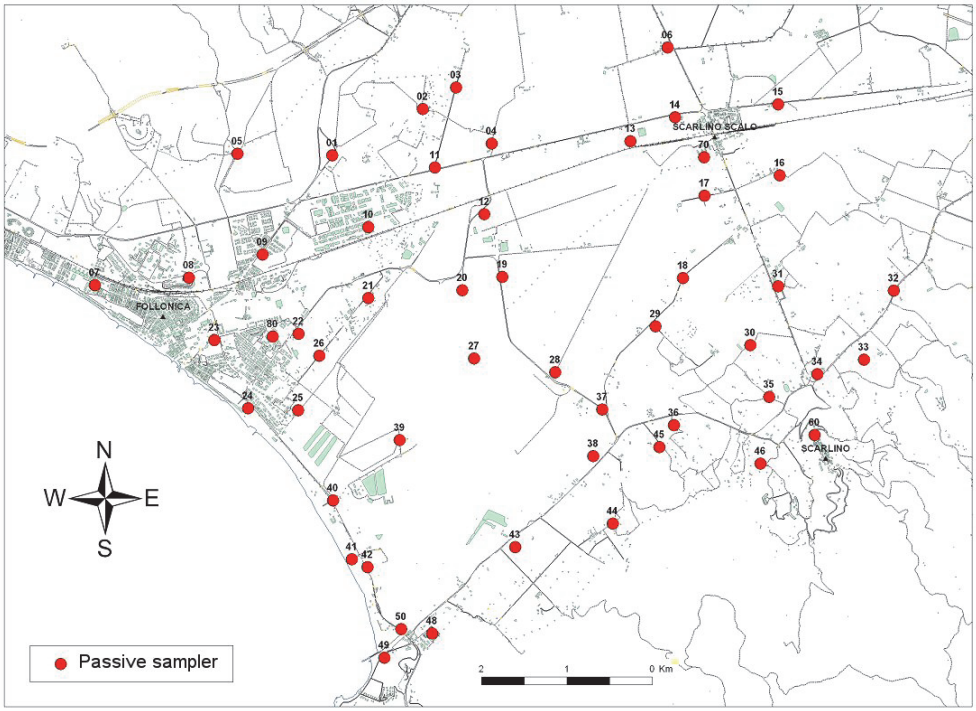

Fig. 10. Location map of passive samplers in the Scarlino area.

Considering the territorial feature of the study area, 52 passive samplers were positioned according to a stratified random strategy: systematic or large-scale and random on local scale. The area was divided with a regular grid (1 x 1 km), and in each cell a sampler was randomly placed. The sampling grid was constructed to take into account the morphology of the study area, the urban fabric and layout of industrial sites. (Fig. 10). Geographic

coordinates of each sampler were collected in order to input the concentration value in the GIS geo-database. The quality of data was ensured placing samplers as replicates and blanks. The values of pollutants concentrations, as stated in the previous case study, were measured at the CNR-IIA chemical labs and included in the developed GIS in order to be statistically processed and spatially interpolated. In this case interpolation was constrained by territorial features as morphology, obtained by the digital elevation model, and by the coastline, defined using satellite imagery (SPOT, September 12th 2006).
The land cover/use map of the study was extracted processing both panchromatic and multispectral bands of a SPOT satellite image acquired on January 7th, 2005. The high spatial resolution, 5 meters for panchromatic band and 10 m for multispectral bands, allowed us to analyse territories with enough detail to realize thematic maps with a scale larger than 1:50.000, and therefore sufficiently accurate for the study purposes. The SPOT image was georeferenced to the 1:25.000 topographic map that represented the base of the GIS. The first stage of image processing was devoted on improving the contrast of each individual spectral band and on increasing the chances of visual interpretation of the image. The integration between bands with different spatial resolution aimed to increase the spatial detail and then to obtain a better detection of the land cover/use classes. In details, the contrast enhancement was performed emphasizing multispectral bands by linear stretching and the band integration was achieved using a pan-sharpening technique which allowed to obtain a synthetic image having the spatial resolution of the panchromatic band (5m/pixel) but preserving the spectral information of the multispectral images (Saroglu et al., 2004; Švab & Oštir, 2006). The final synthetic image has been classified by object-oriented methodology that allows the image interpretation not only based on their spectral characteristics but also on object geometric features and on the mutual relation between these objects. This technique allowed the accurate discrimination between classes of land use characterised by a similar spectral behaviour, in particular between the urban and the industrial zones, but avoiding the possibility of interpretation errors usually associated with pixel-oriented techniques (Yu et al., 2006). Furthermore, the image classification was carried out with an iterative procedure that creates polygons, firstly matched with an higher CORINE land cover class (level 2), and starts to segment the polygon-classes into sub-polygons assigned to a lower level of the CORINE land cover system (level 3). After the segmentation procedures, the classification algorithm k-Nearest Neighbours (k-NN) was used to associate the land cover classes to each polygon. The last step of this phase consists in the integration of this land cover/use maps to the developed GIS.
Similarly to the previous case study, distribution maps of pollutants were obtained using the Inverse Distance Weighting interpolation method. Considering the threshold values specified by regulations, the same 7 classes of the Gela case study were used to represent the distribution maps of the monitored pollutants (Table 3). Using the spatial analysis tool implemented in a GIS, pollutant concentration maps were overlaid to the land cover map and synthesized as already described. It was noted that the concentration values of SO_2, NO_2, benzene, toluene, xylenes were always lower than the 4th class; the occurrence maps emphasized also that in the study area there are no occurrences if the 4th class is considered; even when 3rd class is considered, the occurrences showed a small extent pattern. A Further analysis of the pollutants distribution was then carried out computing the ratio between NO_2 and NO_x, in order to evaluate the areas in which the primary pollutants provide a major contribution i.e. the areas where the ratio tends to lower values. This calculation was performed for each campaign and NO_2/NO_x distribution maps were derived.

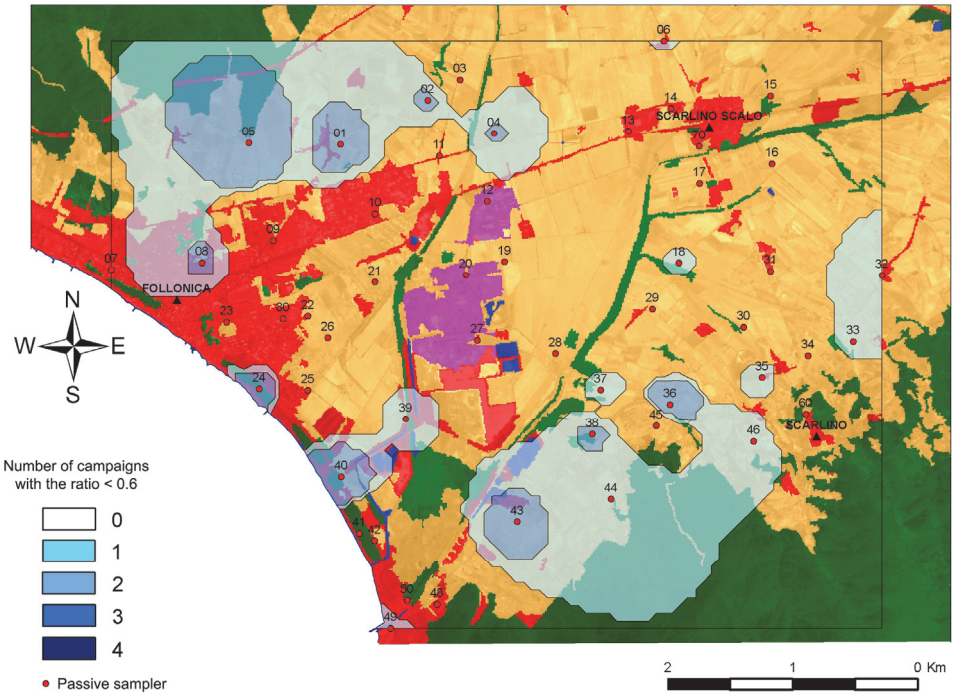

Fig. 11. Occurrence map of the ratio NO_2/NO_x below 0.6 in the Scarlino area overlaid on the land use map. Red areas are urbanized, magenta are industrialized, green are vegetated and brown are rural districts.

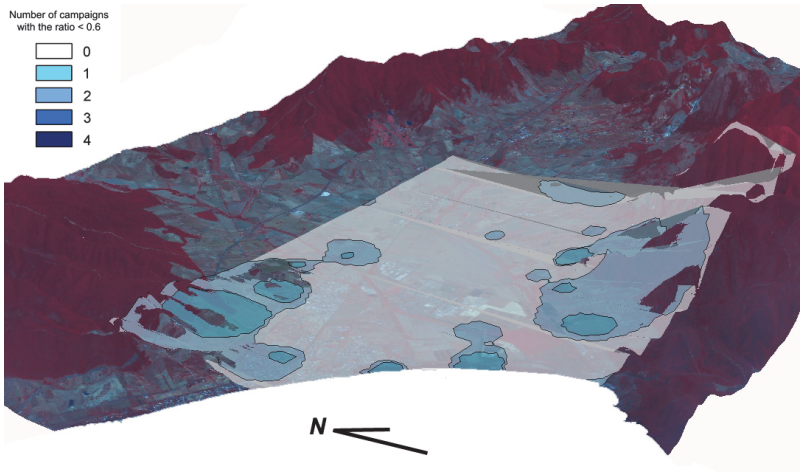

Fig. 12. Integration of $NO_2/NO_x < 0.6$ occurrence map on the digital elevation model associated with a remote sensed image. Red areas represent vegetated hills.

A "*ratio occurrence map*", that indicates how many time the ratio assumed values less than 0.6, was created and overlaid on the land use map (Fig. 11). This map showed the presence of a lower concentration of secondary pollutant in the areas where vegetation is largely present. As a final step, a Digital Elevation Model (DEM), with 10m grid, was derived by the 1:10.000 map provided by technical services of the Municipality. The ratio maps on the DEM clearly shown that these areas correspond with those at higher elevation above sea level (Fig. 12) . The ratio occurrence map, the land use map and the DEM were used as input data for querying the GIS in order to select the most suitable site for the three air quality monitoring stations according to EUROAIRNET criteria (Larssen et al., 1999). The final cartographic product (Fig. 13) shows the localization of monitoring stations that can be defined by a 500m buffer area. The final map presents three possible locations for monitoring stations: one traffic station (A) where two occurrences of NO_2/NO_x ratio less than 0.6 were found (the lower is the ratio, the higher is the amount of primary nitrogen oxide associated to vehicular emissions); one rural station (B) located inland in the valley at the same distance between the industrial and urban area; one industrial station (C) near the industrial hub.

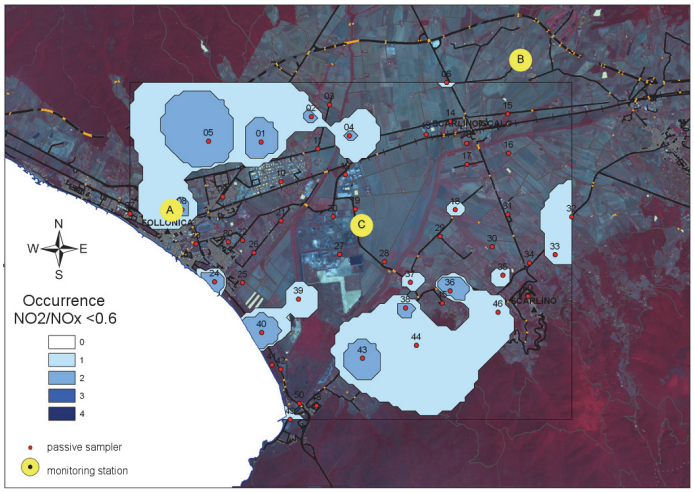

Fig. 13. Location map of monitoring stations in accordance to results obtained during the seasonal campaigns.

7. Conclusions

This chapter presents a combined approach (Fig. 14) for designing monitoring networks of air quality based on integrating Remote Sensing and GIS techniques, following the criteria indicated by European directives. The current EU legislation (Directive 2008/50/EC) on air quality monitoring for the preservation of human health sets still very generic criteria at macro-and micro-scale, but contains an new approach which requires a definition of the spatial and temporal distribution of air pollutants through a preliminary assessment of air quality. The Directive also classifies the monitoring stations according to their purposes (Traffic, Background and Exposure) and the characteristics of the area in which they are located (urban, suburban, industrial, rural).

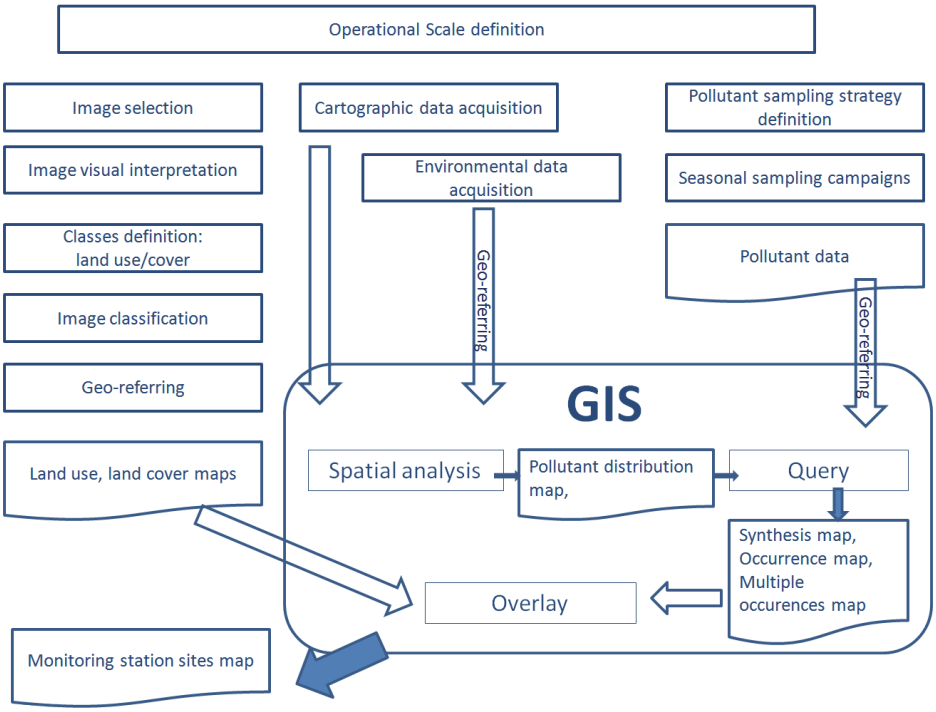

Fig. 14. Flow chart of the proposed approach based on integrating GIS technique and Remote Sensing.

The traffic stations should be placed along main streets, taking into account its type and dimension, the distance from buildings and the mean traffic flow. These stations should be equipped for monitoring nitrogen oxides, nitrogen dioxide, carbon monoxide, benzene, toluene and xylenes. The background stations, which support observations on long-range transport of pollutants, must be placed outside the major urban areas, possibly in rural areas, where only photochemical pollution occurs and where the distance from possible emitting sources is more than tens of km. The stations should be provided with equipment for the measurement of nitrogen oxides and ozone. The exposure stations are aimed to establish the level of exposure of population to pollutants. They should be located at sites with high population density and in adequate number according to the number of inhabitants and their distribution. These monitoring station must be equipped in order to monitor all those pollutants affecting human health protection, such as nitrogen oxides, carbon monoxide, nitrogen dioxide, sulphur dioxide, polycyclic aromatic hydrocarbons (pah) , benzene, toluene, xylenes, PM_{10} and $PM_{2.5}$. Moreover, the EU directive combined to such a preliminary study on air quality, focused on investigating the spatial distribution of pollutant during different seasons, foresees a territorial analysis of the area of interest at local and regional scale. The GIS technique can cater to these requests but it is necessary that all pollutant and environmental data must be georeferenced. Having georeferenced data available it is possible to use interpolation tools and consequently to generate pollutant

distribution maps. GIS supports query and overlapping of such maps and land use/cover maps, derived by remote sensing image processing. The final goal of this approach is to provide smart information that can be integrated with legal and socio-economical features of the study area. The approach here described may represent a flexible, effective and quick methodology to develop management strategies concerning air pollution, such as the definition of control areas or the localization of monitoring stations.

8. References

Aleksandropoulou, V. & Lazaridis, M. (2004). Spatial distribution of gaseous and particulate matter emissions in Greece. *Water, Air and Soil Pollution* Vol.153, (March 2004), pp. 15-34, ISSN 1573-2932.

Allegrini, I.; Novelli, L.; Picchi, S.; Biscotto, M.; Hong, W.; Liu, F.; Yin, Z. & Costabile, F. (2004). In accordance with Framework Directive 96/62/EC, development of an air quality monitoring network in a Chinese city. *Proceedings of the 13th World Clean Air and Environmental Protection*, pp. 22-27, London, United Kingdom, August 22-27 2004.

Armstrong, M. (1998). *Basic linear* geostatistics. Springler, ISBN 978-3540618454, Berlin.

Bertoni G.; Tappa R. & Allegrini I. (2000). Assessment of a new passive device for the monitoring of benzene and other volatile aromatic compounds in the atmosphere. Annali di Chimica, Vol.90, No.3-4, (March-April, 2000), pp. 249-263. , ISSN 1612-8877.

Bossard, M.; Feranec, J. & Otahel, J. (1999). The revised and supplemented CORINE land cover nomenclature. *Technical report* No.38, European Environment Agency, Copenhagen.

Burrough, P.A. (2001). GIS and geostatistics: Essential partners for spatial analysis. *Environmental and Ecological Statistics* Vol.8, No.4, (December 2001), pp. 361-377, ISSN 1573-3009.

Davis, J.C. (1986). *Statistical and data analysis in geology* (2nd Ed.). John Wiley & Sons, ISBN 978-0471080794, New York, USA.

De Santis, F.; Allegrini, I.; Fazio, M.C.; Pasella D. & Piredda, R. (1997). Development of a passive sampling technique for the determination of Nitrogen Dioxide and Sulphur Dioxide in ambient air. Analytica Chimica Acta Vol.346, No.1, (June 1997), pp. 127-134, ISSN 0003-2670.

Foody, G.M. (2000). Estimation of sub-pixel land cove composition in the presence of untrained classes. *Computers & Geosciences* Vol.26, No.4, (May 2000), pp.469-478, ISSN 0098-3004.

Isaaks, E.H. & Srivastava, R.M. (1989). *An* introducytion *to Applied* Geostatistics. Oxford University Press, ISBN 978-0195050134, Oxford, UK.

Larssen, S.; Sluyter, R. & Helmis, C. (1999). Criteria for EUROAIRNET - The EEA Air Quality Monitoring and Information Network. *Technical Report* No.12, European Environment Agency, Copenhagen.

Saroglu, E.; Bektas, F.; Musaoglu, N. & Goksel, C. (2004). Fusion of multisensor remote sensing data: assessing the quality of resulting images. *Proceedings of the XXth ISPRS Congress*, Vol. XXXV, Part B4, pp. 575-579, ISSN 1682-1750, Istanbul, Turkey, July 12-23 2004.

Sengupta, S.; Patil, R.S. & Venkatachalam, P. (1996). Assessment of population exposure and risk zones due to air pollution using the geographical information system. *Computer, Environment and Urban Systems* Vol.20, No.3, (May 1996), pp. 191-199, ISSN 0198-9715.

Stedman, J.R.; Keith J.V.; Campbell, G.W.; Goodwin, J.W.L. & Downing, C.E.H. (1997). New high resolution maps of estimated background ambient NOx and NO_2 concentrations in the U.K. *Atmospheric Environment* Vol.31, No.21, (November 1997), pp. 3591-3602, ISSN 1352-2310.

Švab, A. & Oštir, K. (2006). High-resolution image fusion: methods to preserve spectral and spatial resolution. *Photogrammetric Engineering & Remote Sensing*, Vol.72, No.5, (May 2006), pp. 565-572, ISSN 0099-1112.

Weiers, S.; Bock, M.; Wissen, M. & Rossner, G. (2004). Mapping and indicator approaches fort he assessment of habitats at different scales using remote sensing and GIS methods. *Landscape and Urban Planning* Vol. 67, (March 2004), pp. 43-65, ISSN 0169-2046.

Yu, Q.; Gong, P.; Clinton, N.; Biging, G.; Kelly, M. & Schirokauer, D. (2006). Object-based detailed vegetation classification with airborne high spatial resolution remote sensing imagery. *Photogrammetric Engineering and Remote Sensing*, Vol.72, No.7, (July 2006), pp. 799-811, ISSN 0099-1112.

2

Design of Urban Air Quality Monitoring Network: Fuzzy Based Multi-Criteria Decision Making Approach

Abdullah Mofarrah[1], Tahir Husain[2] and Badr H. Alharbi[3]
[1,2]*Faculty of Engineering and Applied Science, Memorial University, St. John's,*
[3]*National Center for Environmental Technology,*
King Abdulaziz City for Science and Technology, Riyadh,
[1,2]*Canada*
[3]*Saudi Arabia*

1. Introduction

The air quality monitoring network (AQMN) is the essential part for air quality management, strategies planning, and performance assessment (Mofarrah and Husain, 2010). Existing methods of establishing ambient air quality monitoring networks typically evaluate the parameters related to air pollutant concentrations, emission source characteristics, atmospheric transport and dispersion, secondary reactions, deposition characteristics, and local topography (Harrison and Deacon, 1998; Bladauf et al., 2002). In most of the cases, AQMN is designed to measure the pollutants of concern such as particulate matter (PM_{10}), carbon monoxide (CO), sulfur dioxide (SO_2), ozone (O_3), nitrogen oxides (NOx), and total hydrocarbons (Chang and Tseng, 1999). Most of the reported AQMN design methods applied to a specific situation wherein one or two specific objectives are considered (Harrison and Deacon, 1998; Mofarrah and Husain, 2010). However, design of AQMN considering the multiple-criteria including multiple pollutants is complicated because air pollution phenomena are complex and dynamic in nature, depends on the meteorological and topographical conditions and involves not only irregularity of atmospheric movement but also uncertainty of human activities. The objective of this study is to develop a systematic approach for designing urban AQMN considering multi-criteria including multiple air pollutants in the system. The optimization is approached based on the utility scores gained from the fuzzy analytical hierarchy process associated with a candidate station, which is estimated over the representative zone (*RZ*) of the potential station.

2. Fuzzy Analytical Hierarchy Process

Fuzzy Analytical Hierarchy Process (AHP) is the extension of analytical hierarchy process (Saaty, 1980) is used for structuring the problem. AHP is an efficient method in which hierarchical structure is developed by a pair-wise comparison between any two criteria. The levels of the pair-wise comparisons range from 1 to 9, where '1' represents that two criteria

are equally important, while the other extreme '9' represents that one criterion is absolutely more important than the other (Saaty, 1980). The AHP uses objective mathematics to process the subjective and personal preferences of an individual or a group of decision maker (Saaty, 1980). Generally, decision-making processes are subject to insufficiency of data and lack of knowledge (Tesfamariam and Sadiq, 2006). In fact, even if the data are available, criteria often contain linguistic definitions involving human judgment and subjectivity, which introduce uncertainties in the decision making process. In application to actual system traditional AHP is not so effective in capturing uncertainty and subjective judgments of different experts. The fuzzy AHP developed Zadeh (1965) is modified version of AHP, and can be used to handle the fuzziness of the data. It is easier to understand and can effectively handle both qualitative and quantitative data in the multiple-criteria problems. In this paper triangular fuzzy numbers (TFNs) are used to judge the qualitative information related to AQMN design. The TFN is defined by three real numbers, expressed as (*l, m, n*) with a membership function between 0 and 1 (Fig. 1). The parameters *l*, *m*, and *n*, respectively, indicate the smallest possible value, the most promising value, and the largest possible value that describe a fuzzy event (Zadeh, 1965). The mathematical definition of a TFN can be described as (Kaufmann and Gupta, 1988):

$$\mu(x/\tilde{M}) = \begin{cases} 0, & x < l, \\ (x-l)/(m-l), & l \le x \le m, \\ (n-x)/(n-m), & m \le x \le n, \\ 0, & x > n \end{cases} \tag{1}$$

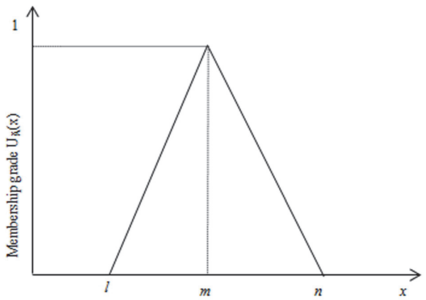

Fig. 1. Construction of triangular membership function

The TFNs for this study are developed in such a way that the most likely value has a membership grade of unity, considering the fact that the lower and upper bonds have a membership value of zero in that fuzzy set. The arithmetic of fuzzy set is little different than regular arithmetic. For example the fuzzy algebraic operations of two TFNs, namely $A(l_1, m_1, n_1)$ and $B(l_2, m_2, n_2)$ are as follows (Kaufmann and Gupta, 1988):

$$A + B = (l_1 + l_2, m_1 + m_2, n_1 + n_2)$$

$$A - B = (l_1 - n_2, m_1 - m_2, n_1 - l_2)$$

$$A.B \approx \min(l_1 l_2, l_1 n_2, n_1 l_2, n_1 n_2), \textit{mostlikely}(m_1 m_2), \max(l_1 l_2, l_1 n_2, n_1 l_2, n_1 n_2) \text{ ; and if } 0 \notin (l_2, n_2)$$

$$A / B = A \,.\, B^{-1} = \min(l_1 / l_2, l_1 / n_2, n_1 / l_2, n_1 / n_2), mostlikely(m_1 / m_2), and$$
$$\max(l_1 / l_2, l_1 / n_2, n_1 / l_2, n_1 / n_2)$$

3. Methodology used in this work

A systematic methodology for designing urban AQMN is developed by using multiple criteria, which covered environmental (e.g., air quality), social (i.e., location sensitivity (*LS*), population density (*PD*), population sensitivity (*PS*), and cost parameter (*CP*). The aim of this AQMN design is to study air pollutants' characteristics, human health, social sensitivity, and cost objective. Thus, the proposed design will protect public health, sensitive locations/receptors from exposures to ambient air pollutants, and it will measure the maximum pollutants' concentration for the study area. The framework of this methodology is shown in Fig. 2. This technique will help the decision maker to optimize the AQMN with limited financial and human resources.

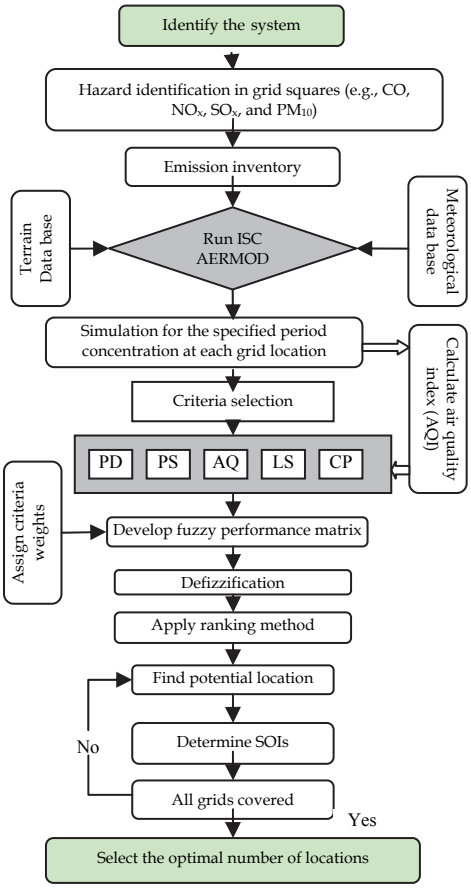

Fig. 2. Framework for designing AQMN

At the beginning, the study area is divided into a continuous grid system in which each grid represents a potential candidate location for monitoring station. Fuzzy synthetic optimization technique is used to identify the potential monitoring sites. The key functions of the methodology are described in the following sections.

3.1 Air quality exceedance index

An air quality index (*AQI*) function is generated comparing the local air quality with the national standards. *AQI* provides overall information about the local air quality. It hints how clean or polluted the local air comparing with the national standards. If the ratio of measured data (C_{ij}) and standard (C_{sj}) grater then one, it means the local air quality is violating the national air quality standards. For this study, concentrations of the major air pollutants such as CO, NO_2, SO_2, and PM_{10} are monitored and subsequently converted into an *AQI* by assigning a probability of occurrence factor to each air pollutants based on their occurrence of exceedance during study periods as eq. 2.

$$AQI_j = \sum_{j=1}^{m} \frac{C_{ij} * p_{ij}}{C_{sj}} \tag{2}$$

C_{ij} = j^{th} pollutant concentration (i.e., CO, NO_2, SO_2, and PM_{10}) in i^{th} grid; C_{sj} = national air quality standard of j^{th} pollutant, p_{ij} is the probability of occurrence of j^{th} pollutant in the i^{th} location over the measurement periods.

Criteria	Assigned scores
Location sensitivity (LS)/ available amenities /grid	LSi
No-basic facility	(1,2,4)
Facilities of low value (e.g., storage facilities)	(1,3,5)
Factories and industry	(2,4,6)
Residential, parks	(3,5,7)
Schools, churches, heritage places	(4,6,8)
Hospitals, sensitive locations	(5,7,9)
Population density (PD)/ number of people /grid	PDi
<50	(1,2,4)
51- 250	(1,3,5)
251-450	(2,4,6)
451-650	(3,5,7)
650-850	(4,6,8)
>850	(5,7,9)
Population sensitivity (PS)/ sensitive population /grid	PSi
<10	(1,2,4)
11-20	(1,3,5)
21-30	(2,4,6)
31-40	(3,5,7)
41-50	(4,6,8)
>50	(5,7,9)
Cost criteria	Ci
Installation cost >$7000	(1,2,4)
$7000-$6000	(1,3,5)
$5900-$5000	(2,4,6)
$4900-$4000	(3,5,7)
$3900-$3000	(4,6,8)
Installation cost <$3000	(5,7,9)

Table 1. Definitions for criteria scores

3.2 Cost objective

An important objective of any AQMN is to minimization of its cost. This objective can also be interpreted as a budgetary constraint. Cost criteria consideration in this evaluation is installation cost. Generally, the installation cost is varied depending on the site location, local labour force and communication facilities. To compare the installation cost within the area of interest a cost index (*CI*) is introduced as:

$$CI_i = Minimize\left[\frac{C_i}{\sqrt{\sum C_i}}\right] \tag{3}$$

where, CI_i = cost index for the grid i, C_i = cost score at the i^{th} location over the study area. Considering the local market and communication facility the installation cost score (C_i) of i^{th} grid was assigned as shown in Table 1.

3.3 Definitions of social criteria

In each grid, the social criteria such as *LS*, *PS*, and PS are consequently converted to a score with the help of pre assigned scale shown in Table 1. Finally, the scores are normalized to get social criteria index (*SCI*) at i^{th} location as shown in eq. 4.

$$SCI_i = Maximized\left[\frac{LS_i}{\sqrt{\sum LS_i}} + \frac{PD_i}{\sqrt{\sum PD_i}} + \frac{PS_i}{\sqrt{PS_i}}\right] \tag{4}$$

3.4 Determining of screening scores

The screening score is the composition components of an environmental parameters (eq. 2), cost objective (eq. 3), and social criteria (eq. 4). It is defined by a dimension less function, called screening score (*SC*). The *SC* combines, under a mathematical approach, and is defined by eq. 5.

$$SC_i = \begin{bmatrix} A_1 \\ A_2 \\ A_3 \\ . \\ A_n \end{bmatrix} \begin{bmatrix} AQI_{ij} & CI_i & LS_i & PD_i & PS_i \end{bmatrix} \times \begin{bmatrix} AQI_{A1} & CI_{A1} & LS_{A1} & PD_{A1} & PS_{A1} \\ AQI_{A2} & CI_{A2} & LS_{A2} & PD_{A2} & PS_{A2} \\ AQI_{A3} & CI_{A3} & LS_{A3} & PD_{A3} & PS_{A3} \\ . & . & . & . & . \\ AQIn & CI_{An} & LS_{An} & PD_{An} & PS_{An} \end{bmatrix} \times \begin{bmatrix} w_j & w_c & w_{LS} & w_{PD} & w_{PS} \end{bmatrix} \tag{5}$$

where, $A_1, A_2, \ldots\ldots, A_n$ are the possible monitoring station location, and w_j , w_c , w_{LS}, w_{Pd}, and w_{PS} are weighting factors for *AQI*, *CI*, *LS*, *PD*, and *PS* respectively.

The *SC* from eq. 5 is also fuzzy value. For decision purpose the comparisons of fuzzy data is not straightforward. To obtained crisp value of *SC*, centroidal method (Yager, 1980) is used. The centroid index of the fuzzy number represents the crisp score of an alternative A_i. If the fuzzy *SC* for a grid A_i is $SC_{Ai}(\alpha_1, \beta_1, \gamma_1)$, then the crisp score of that location can be computed as follows:

$$SC_x(A_i) = \frac{(\beta_1 - \alpha_1)(\alpha_1 + 2/3(\beta_1 - \alpha_1)) + (\lambda_1 - \beta_1)(\beta_1 + 1/3(\lambda_1 - \beta_1))}{(\beta_1 - \alpha_1) + (\lambda_1 - \beta_1)} \quad (6)$$

where, $SC_x(A_i)$ is the crisp score of grid A_i and α_1, β_1, and γ_1 are the lowest, most likely and maximum values of SC_{Ai}. Depending on the SC_x (A_i) values the grids location are screened, and potential locations were ranked for second step analysis.

3.5 Determination of representative zone (RZ)

After the identification and quantification of the objectives of the monitoring network, the second step is to determine the degree of representativeness (*Dr*) and the representative zone (*RZ*) associated with each candidate monitoring location. The *RZ* for a monitoring station is established on the basis of the concept of a sphere of influence area surrounding the potential station, for which the pollutants measurements can either be regarded as representative or can be extrapolated with known confidence. Sphere of influence (SOI) is defined as the zone over which the metrological (MET) data for a given monitoring location can be considered representative (Mofarrah and Husain, 2010). A grid cell *(i*) will belong to the *RZ* of a monitoring station at grid cell (k), if the D_r of cell (*i*) is greater than zero (eq. 7).
The D_r is dictated by a predetermine cutoff value (*Rc*) in the spatial correlation coefficient (*R*) between the pollutant's concentration at the monitoring locations identified and the neighboring locations surrounding it. The spatial correlation coefficient (*R*) gives an indication of the relationship among locations to be selected in the monitoring network (Elkamel et al., 2008). The *R* lies between -1 and +1 (Liu et al., 1986). The computation of *R* is carried out in all radial directions surrounding each potential location until the *R* falls below the predetermined cut-off value (R_c). In this study *RZ* is considered the area surrounding it in which the *R* of this location with the nearby locations is higher than the cut-off value (R_c). This means the pollutants concentration measured at this location are representatively correlated with a certain degree of confidence to any location in the network within the area. Fig. 3 illustrates the general concept of *RZ*. By this concept it is assumed that, when a station is installed in a grid square (i.e A5), the nearby grid squares, as are marked on Fig. 3, are not allowed to be installed with the same class of station if their D_r is higher than zero. When searching for the next station location, the marked grid squares will be skipped for enhancing the solution efficiency.

$$D_r = \begin{cases} \sum_{j=1}^{4} R^2, & if\,(R - R_c) \geq 0 \\ 0, & Otherwise \end{cases} \quad (7)$$

where, *R is* spatial correlation coefficient of the concentrations between two adjacent monitoring locations $x_1 = (x_{11}, x_{12}, \ldots x_{1p})$ and $x_2 = (x_{21}, x_{22}, \ldots x_{2p})$ with a sample size p can be expressed (Elkamel et al., 2008) as:

$$R = \frac{\sum_{i=1}^{p}(x_{1i} - \bar{x}_1)(x_{2i} - \bar{x}_2)}{\sqrt{\sum_{i=1}^{p}(x_{1i} - \bar{x}_1)^2 \sum_{i=1}^{p}(x_{2i} - \bar{x}_2)^2}} \quad (8)$$

where, $\bar{x}_1 = \frac{1}{p}\sum_{i=1}^{p} x_{1i}$ and $\bar{x}_2 = \frac{1}{p}\sum_{i=1}^{p} x_{2i}$ are the average concentrations at location 1 and 2, respectively. Once D_r of the each pathetical location is calculated, the ranking of the potential location can be quantified in terms of grid utility scores. A grid score $U_{(g)}$ for gth candidate location is defined as the sum of SC_x of all grids correlated with gth location as:

$$U_{(g)} = SC_{(xg)} + \sum_{i=1}^{n} D_r \times SC_{xi} \tag{9}$$

where, n is the number of grids correlated with gth location. Highest $U_{(g)}$ means better location for air quality monitoring station. The RZ of the sphere can be defined as the number of square grids place inside it.

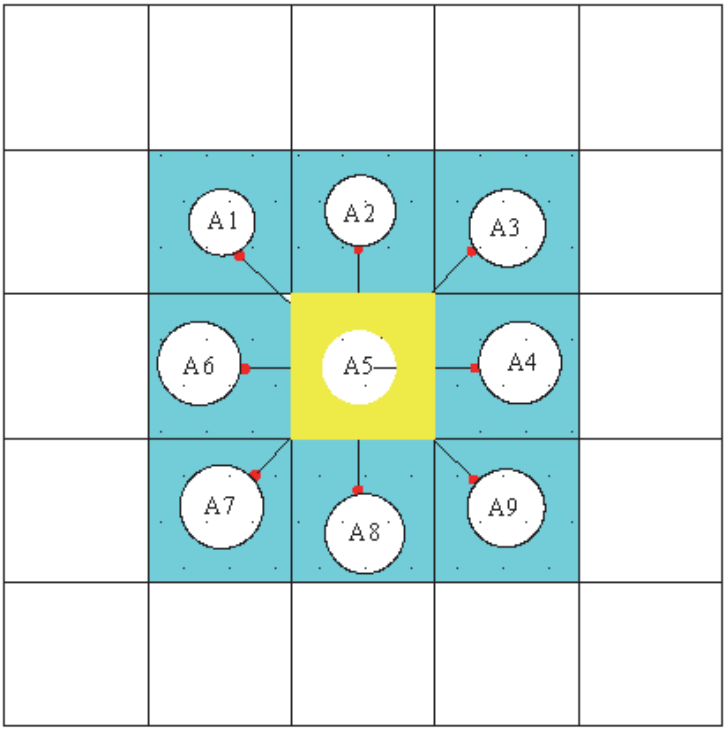

Fig. 3. Representative location zone

4. Application of the methodology

Riyadh, the capital city of Saudi Arabia was considered to demonstrate the proposed methodology. Riyadh is one of the major industrial cities in the Kingdom of Saudi Arabia; it has multiple types of heavy and light industries such as oil refinery, power plant, cement industry etc. The population of the city is above four million with very high growth rates.

Therefore, to maintain the air quality standard the city authorities have planned to re-assess the current air quality monitoring network. There are six existing air quality monitoring stations in Riyadh city owned and operated by different organizations. Most of these existing air AQMNs are not working properly or not serving at satisfactory levels. The main objective of this study is to design the air quality monitoring network for Riyadh city and to identify the optimal station locations to satisfy the future air quality monitoring demands. To design the AQMN three major emission sources such as point sources, area sources and line sources were considered. The detailed emission inventory can be found elsewhere (Mofarrah and Husain, 2010). The major point sources in Riyadh city are power plants, refinery and cement industries. The old and new industrial cities under development are considered as the area source. The automobile sources for the selected major roads based on traffic counts, composition of traffic, and model years were considered as the line sources in this study. The database for emission inventory was developed based on production rate, fuel consumption and the emission factors as suggested by USEPA.

At the beginning, the study area (40km x 60km) was conceptually divided into 441 square grids as subsystems. Each grid component includes environmental parameters (i.e., sulfur dioxide (SO_2), nitrogen dioxides (NO_2), carbon monoxide (CO) and fine particulate matters (PM_{10})), social objectives (i.e., *LS, PD, PS*) and cost criteria (*CI*). The concentration level of each air pollutant was simulated on; hourly, 8-hourly, and 24-hourly basis using Industrial Source Complex (ISC3) air quality software programs. The concentration distribution of selected air pollutants over the study area is shown in Fig. 4. If we compare the pollutants distribution (Fig. 4) with the Saudi Arabian national air quality standard (Table 2), it is clear that some regions within the study are experiencing high level of air pollution threats. For this study, the social and cost objective data of each grid were also modeled as fuzzy variables according to the fuzzy scale mentioned in Table 1.

Pollutant	Measurement period	Limit
SO_2	30 day period, one hour average	730 µg/m^3
	12 month period, 24 hour average	365 µg/m^3
	12month period, annual average	80(µg/m^3)
Inhalable Particulates (fpm)	12-month period, the 24-hour maximum	340(µg/m^3)
	12-month period, the annual average	80(µg/m^3)
Nitrogen Oxides Defined as Nitrogen Dioxide (NO_2)	30 day period, the one-hour average	660(µg/m^3)
	12-month period, the annual average	100(µg/m^3)
Carbon Monoxide (CO)	30-day period, the one-hour average	40 (mg/m^3)
	30-day period, the 8-hour average	10(mg/m^3)

Table 2. Ambient air quality standards for Saudi Arabia (Source Presidency of Meteorology and Environment, Saudi Arabia)

4.1 Criteria weight computation

Based on the importance of each criterion on AQMN design, a fuzzy pair-wise comparisons matrix (PCM) $\tilde{A}_F$ is formed considering C_1, C_2, C_3, C_4 and C_5 are respectively, location sensitive *(LS)*, population sensitive (*PS*), cost, air quality (*AQ)* and population density (*PD)*. The preference scale as shown in Table 3 was used in this case.

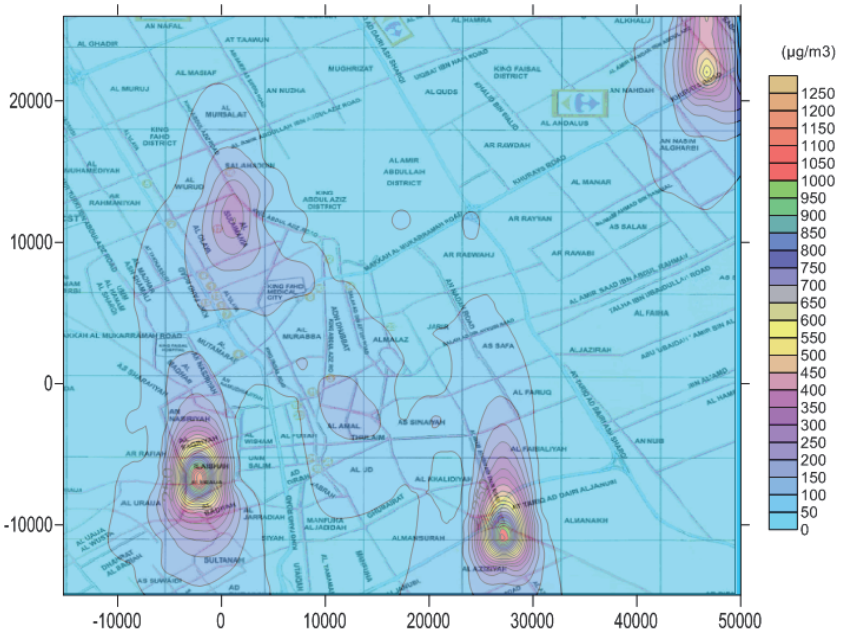

Fig. 4. (a) Distribution of SO_2 for 12month period, annual average

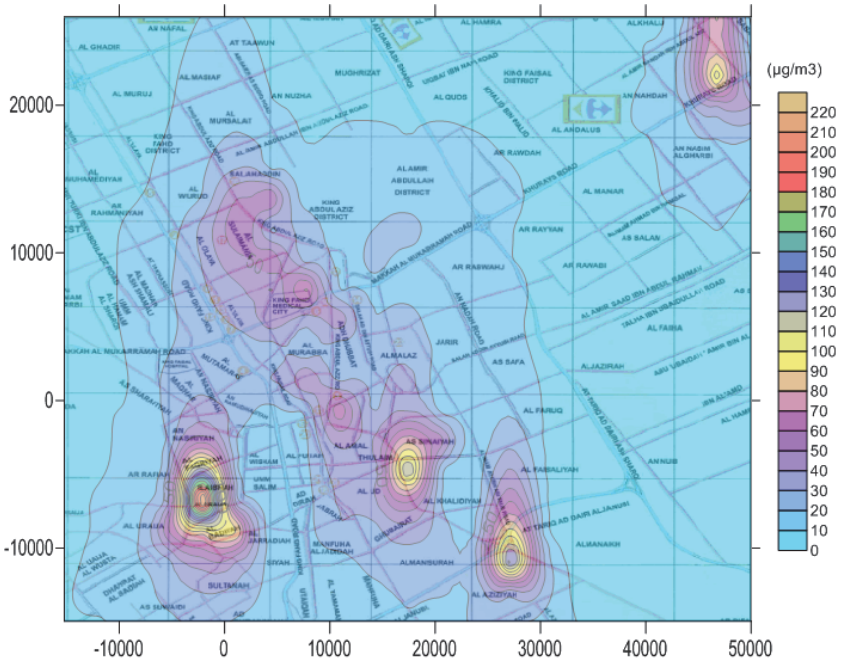

Fig. 4. (b) Distribution of NO_2 for 12month period, annual average

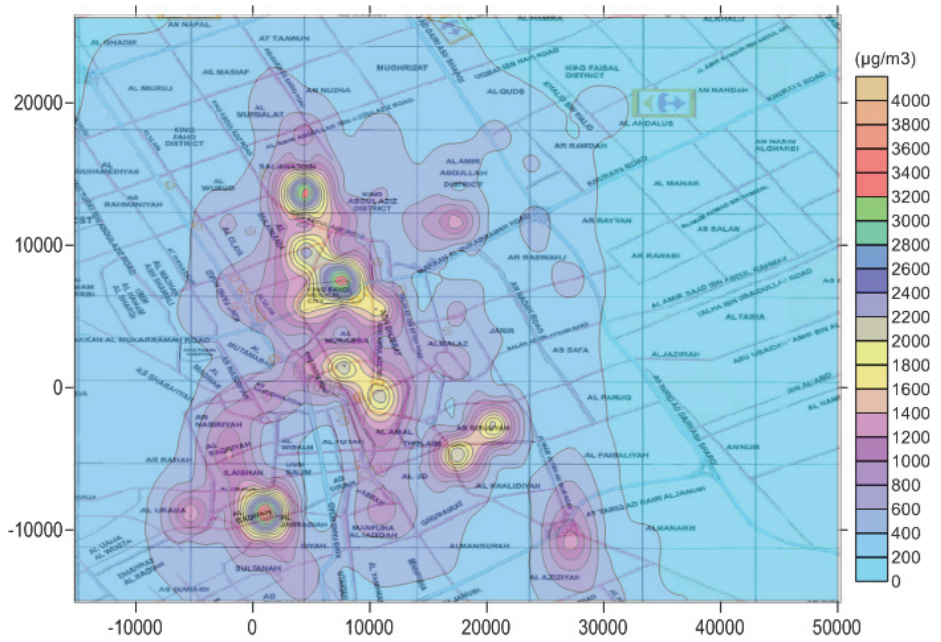

Fig. 4. (c) Distribution of CO for 30-day period, the 8-hour average

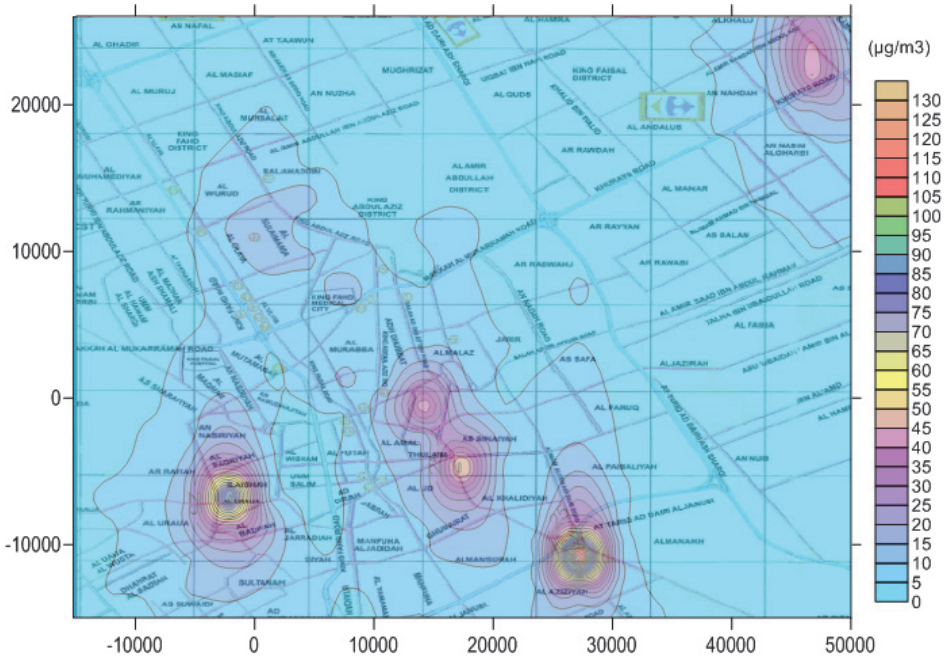

Fig. 4. (d) Distribution of PM_{10} for 12month period, the 24-hour maximum

How important is A relative to B?	Preference index (Saaty 1988)	Fuzzy value (l, m, u; Jie et al. 2006)
Equally important	1	(1, 1, 1)
Moderately more important	3	(1,3,5)
Strongly more important	5	(3,5,7)
Very strongly more important	7	(5,7,9)
Overwhelmingly more important	9	(7,9,11)
	2	(1,2,4)
Intermediate values	4	(2,4,6)
(Need to judge two)	6	(4,6,8)
	8	(6,8,10)

Table 3. Criteria preference scale

$\tilde{A}_F =$

	C_1	C_2	C_3	C_4	$C5$
C_1	1, 1, 1	0.33,0.5,1.0	0.25,0.33,1	0.33,0.5,1	2,3,4
C_2	1, 2,3	1, 1, 1	0.33,0.5,1	0.17,0.2,0.25	0.5,1,1
C_3	1,3,4	1,2,3	1, 1, 1	0.2,0.25,0.33	0.33,0.5,1
C_4	1,2,3	4,5,6	3,4,5	1, 1, 1	0.17,0.2,0.25
$C5$	0.25,0.33,0.50	1,1,2	1,2,3	4,5,6	1, 1, 1

After constructing $\tilde{A}_F$, relative weights of each criterion is calculated by using fuzzy extent analysis (Lee et al., 2006) as follows:

Row	Left	Middle	right
The first row sum	3.92	5.34	8.00
The 2nd row sum	3.00	4.70	6.25
The 3rd row sum	3.53	6.75	9.33
The 4th row sum	9.17	12.20	15.25
The 5th row sum	7.25	9.33	12.50
Total	**26.87**	**38.32**	**51.34**

Criteria	Left	Middle	right
LS (C_1)	3.92/51.34= 0.0763	5.34/38.32 = 0.1393	8.0/26.87 = 0.2978
PS (C_2)	3.00/51.34= 0.0584	7.40/38.32 = 0.1227	6.25/26.87 = 0.2326
Cost (C_3)	3.53/51.34= 0.0688	6.75/38.32 = 0.1762	9.33/26.87 = 0.3474
AQ (C_4)	9.17/51.34= 0.1786	12.20/38.32 = 0.3184	15.25/26.87 = 0.5676
PD (C_5)	7.25/51.34= 0.1412	9.33/38.32 = 0.2436	12.5/26.87 = 0.4653

The weights of *AQ* were re-distributed to the *CO, SO_2, PM_{10}* and NO_2 on the basis of their impotence (i.e., considering the local environment and human health point of view). The complete set of criteria weights are shown in Table 4.

Criteria	*Weights*	***Sub-criteria***			
		CO	*SO_2*	*PM_{10}*	*NO_2*
LS (C_1)	w_1=(0.0763,0.1393,0.2978)	-	-	-	-
PS (C_2)	w_2=(0.0584,0.1227,0.2326)	-	-	-	-
Cost (C_3)	w_3=(0.0688,0.1762,0.3474)	-	-	-	-
AQ (C_4)	w_4=(0.1786,0.3184, .5676)	C_{41} = 20% of C_4	C_{42} = 25% of C_4	C_{43} = 35% of C_4	C_{44} = 20% of C_4
PD (C_5)	w_5=(0.1412,0.2436,0.4653)	-	-	-	

Table 4. Weights of each criteria and sub-criteria

5. Results and discussions

The concentration level of each pollutant was compared with the Saudi National Air quality standards (Table 2) to calculate the air quality index (*AQI*). Social and cost objectives data of each grid were also predicted and converted into fuzzy scores according to Table 1. The step by step calculations of potential location identification is described in the following section by considering few grids. Table 5 shows the *AQIs* and assigned scores of different parameters. The criteria scores (Table 5) are multiplied with the weighting factors (Table 4) to form fuzzy screening scores matrix as shown in the Table 6.

Grid no	*AQI (SO2)*	*AQI (NO2)*	*AQI (CO)*	*AQI (PM10)*	*Assigned scores (LS)*	*Assigned scores (PS)*	*Assigned scores (CI)*	*Assigned scores (PD)*
A1	22.7798	38.8779	58.3944	27.4490	(1,2,4)	(1,2,4)	(3,5,7)	(5,7,9)
A2	22.4193	38.9320	65.7578	24.7020	(1,2,4)	(1,2,4)	(3,5,7)	(5,7,9)
A3	31.5411	51.0081	81.7773	32.3196	(1,3,5)	(1,3,5)	(3,5,7)	(4.6.8)
A4	45.5648	69.3000	97.5538	45.8194	(2,4,6)	(2,4,6)	(3,5,7)	(5,7,9)
A5	66.8583	96.5431	107.2574	58.2306	(2,4,6)	(1,2,4)	(3,5,7)	(4,6,8)
A6	46.5463	78.2129	109.7475	45.0471	(1,2,4)	(1,2,4)	(3,5,7)	(5,7,9)
.	.		.	.	.	.	.	.
.	.		.	.	.	.	.	.
A436	2.486	14.478	19.775	24.351	(1,2,4)	(1,2,4)	(3,5,7)	(5,7,9)
A437	3.204	17.229	21.650	21.579	(1,2,4)	(1,2,4)	(3,5,7)	(5,7,9)
A438	5.808	21.943	25.775	17.283	(1,3,5)	(1,3,5)	(3,5,7)	(4.6.8)
A439	13.402	69.518	73.369	17.328	(2,4,6)	(2,4,6)	(3,5,7)	(5,7,9)
A440	31.328	346.130	343.296	21.558	(1,2,4)	(1,2,4)	(3,5,7)	(5,7,9)
A441	5.118	21.599	23.418	16.571	(1,2,4)	(1,2,4)	(3,5,7)	(5,7,9)

Table 5. *AQI*s and assigned scores for different criteria

Grid no	*AQI (SO2)*	*AQI (NO2)*	*AQI (CO)*	*AQI (PM10)*	*(LS)*	*(PS)*	*(CI)*	*(PD)*
A1	1.017,1.813,3.232	1.389,2.476,4.413	2.086,3.719,6.629	1.716,3.059,5.453	0.076,0.279,1.191	0.058,0.245,0.93	0.206,0.881,2.432	0.706,1.705,4.188
A2	1.001,1.785,3.181	1.391,2.479,4.42	2.349,4.187,7.465	1.544,2.753,4.907	0.076,0.279,1.191	0.058,0.245,0.93	0.206,0.881,2.432	0.706,1.705,4.188
A3	1.408,2.511,4.476	1.822,3.248,5.79	2.921,5.208,9.283	2.02,3.602,6.421	0.076,0.418,1.489	0.058,0.368,1.163	0.206,0.881,2.432	0.565,1.462,3.722
A4	2.034,3.627,6.466	2.475,4.413,7.867	3.485,6.212,11.074	2.864,5.106,9.102	0.153,0.557,1.787	0.117,0.491,1.396	0.206,0.881,2.432	0.706,1.705,4.188
A5	2.985,5.322,9.487	3.449,6.148,10.96	3.831,6.83,12.176	3.64,6.489,11.568	0.153,0.557,1.787	0.117,0.491,1.396	0.206,0.881,2.432	0.565,1.462,3.722
A6	2.078,3.705,6.605	2.794,4.981,8.879	3.92,6.989,12.459	2.816,5.02,8.949	0.076,0.279,1.191	0.058,0.245,0.93	0.206,0.881,2.432	0.706,1.705,4.188
.	.	.	.	.	.	.	.	.
.	.	.	.	.	.	.	.	.
A436	0.646,1.152,2.054	0.706,1.259,2.245	0.87,1.551,2.764	1.056,1.883,3.357	0.076,0.279,1.191	0.058,0.245,0.93	0.206,0.881,2.432	0.706,1.705,4.188
A437	0.769,1.371,2.445	0.773,1.379,2.458	0.771,1.374,2.45	1.362,2.427,4.327	0.076,0.418,1.489	0.058,0.368,1.163	0.206,0.881,2.432	0.565,1.462,3.722
A438	0.98,1.747,3.114	0.921,1.641,2.926	0.617,1.101,1.962	2.468,4.4,7.843	0.153,0.557,1.787	0.117,0.491,1.396	0.206,0.881,2.432	0.706,1.705,4.188
A439	3.104,5.534,9.865	2.621,4.672,8.329	0.619,1.103,1.967	5.695,10.153,18.098	0.153,0.557,1.787	0.117,0.491,1.396	0.206,0.881,2.432	0.565,1.462,3.722
A440	15.455,27.552,49.116	12.263,21.861,38.971	0.77,1.373,2.447	13.312,23.732,42.307	0.076,0.279,1.191	0.058,0.245,0.93	0.206,0.881,2.432	0.706,1.705,4.188
A441	0.964,1.719,3.065	0.836,1.491,2.658	0.592,1.055,1.881	2.175,3.877,6.912	0.382,0.975,2.68	0.117,0.491,1.396	0.138,0.705,2.084	0.706,1.705,4.188

Table 6. Weighted screening scores matrix

The crisp values of weighted fuzzy screening scores (*SC*) of each grid were estimated by applying eq. 6 and reported in Table 7. Based on the top SC_x scores, 50 potential locations were indentified for second step analysis.

Grid no	Grid screening scores (SC)	Crisp values of (SC_x)
A1	0.065,0.133,0.278	0.1586
A2	0.067,0.137,0.285	0.1628
A3	0.076,0.16,0.326	0.1871
A4	0.099,0.198,0.392	0.2298
A5	0.112,0.223,0.436	0.2569
A6	0.099,0.194,0.388	0.2273
.	.	.
.	.	.
A436	0.045,0.098,0.217	0.1202
A437	0.043,0.103,0.223	0.1231
A438	0.055,0.12,0.253	0.1428
A439	0.083,0.171,0.344	0.1990
A440	0.231,0.429,0.806	0.4887
A441	0.06,0.125,0.261	0.1483

Table 7. Grid screening scores

To determine the degree of representativeness (Dr) and the representative zone (RZ) associated with each candidate monitoring location, three different cutoff values (R_c), 0.45, 0.60 and 0.75 were used separately and compared with the coefficient in the spatial correlation (*R*) between the pollutant concentration of the potential monitoring station and the neighboring locations surrounding it. Ten optimal locations and corresponding number of grids coverage were indentified for different cutoff value as shown in Fig. 5. The results show that cutoff value has significant effect on the representative zone (RZ) assessment. However, considering the geometry of the study area and analysis of the different cutoff values it was found that the 0.6 cutoff value is the best suited for the Riyadh city. Hence, the grid scores $U_{(g)}$ and top ten optimal locations distribution with cutoff value 0.6 is evaluated as shown in Fig. 6. Due to heavy industries and high populations' exposure, 1-2 optimal locations were found near a major point source such as power plant at grids A397 to A441 (Fig. 6). However, this part is outside of the present study area, but respecting the study results, we suggested putting at least one air monitoring station at grid A419 or A398.

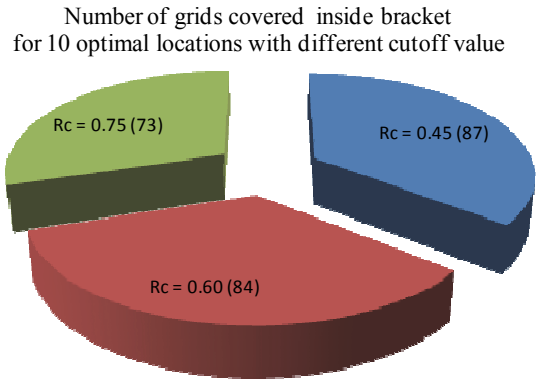

Fig. 5. Ten Optimal stations with number of grids covered for different cutoff values

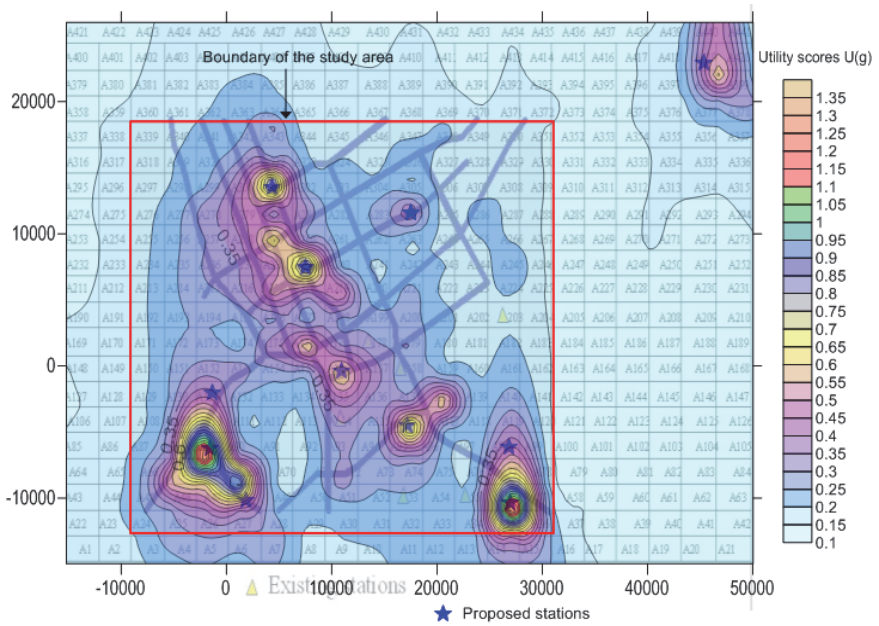

Fig. 6. Location of the ten Optimal stations (for cutoff value 0.6)

For a specific situation the agency can choose either a high or a low value of R_c. A high R_c based network may not necessarily cover more area, but the covered region is well represented. On the other hand a low R_c based network, would offer more coverage of the region, but the covered region may not be satisfactorily represented (Mofarrah and Husain, 2010; Elkamel et al., 2008). The final decision in such a case is of course dependent on the respective agency. It should be noted that the design of an air quality network with higher cutoff values (R_c) is the addition of some more monitoring stations in the network, as compared to that of a network designed with a lower R_c values . The selection of the R_c varies case by case, based on budget, type of air monitoring station, meteorological condition, and the purpose of the monitoring network.

6. Conclusions

The AQMN represents an essential tool to monitor and control atmospheric pollution. The use of some specific criteria in conjunction with the mathematical models provides a general approach to determine the optimal number of monitoring stations. In this study, fuzzy multiple-criteria approach in conjunction with the degree of representativeness technique was used to develop optimal AQMN design. The triangular fuzzy numbers (TFNs) were used to capture the uncertainty associated from human judgement (e.g., assigning weights, scoring). The coverage area of the monitoring station is an essential part of an AQMN which was determined on the basis of representative zone. The effect of the correlation coefficient as well as the cutoff values on coverage of the network was also studied by changing the cutoff values. This methodology provides a systematic approach, which allows multiple-criteria and multiple pollutants in AQMN design. However, the design of an AQMN

depends on many site-specific issues and good upfront planning is therefore crucial in properly assessing the problem and designing an optimal AQMN.

7. Acknowledgement

Financial support provided by the Natural Science and Engineering Research Council of Canada (NSERC) is highly appreciated.

8. References

Baldauf, R.W., Lane, D.D., Marotz, G.A., Barkman, H.W., Pierce, T. (2002). Application of a risk assessment based approach to designing ambient air quality monitoring networks for revaluating non-cancer health impacts, *Environmental Monitoring and Assessment*, vol. 78, pp. 213-227, ISSN 1573-2959

Chang, N. B. and Tseng, C. C. (1999). Optimal Design of Multi-pollutant Air Quality Monitoring Network in a Metropolitan Region using Kaohsiung, Taiwan as an Example, *Environmental Monitoring and Assessment*, vol. 57, no. 2, pp. 121-148, ISSN 1573-2959

Elkamel, A., Fatehifar, E., Taheri, M., Al- Rashidi, M.S. and Lohi, A. (2008). A heuristic optimization approach for Air Quality Monitoring Network design with the simultaneous consideration of multiple pollutants, *Environmental Management*, Vol. 88, pp.507-516 (May 2007), ISSN 1432-1009

Harrison, R.M. and Deacon A.R. (1998). Spatial correlation of automatic air quality monitoring at urban background sites: implications for network design, *Environmental Technology,* vol. 19, pp. 121–132, ISSN 1479-487X

Kaufmann, A. and Gupta, M.M. (1988). *Fuzzy mathematical models in engineering and management science,* Elsevier Science Publishers, ISBN 0-444-70501-5, New York, U.S.A

Lee, H. J., Meng, M.C., and Cheong, C.W. (2006) Web Based Fuzzy Multicriteria Decision Making Tool, *International Journal of the Computer, the Internet and Management* , vol. 14., no.2 (May-August, 2006), pp 1-14, ISSN 0858-7027

Liu, M.K., Avrin, J., Pollack, R.I., Behar, J.V., and McElory J.L. (1986). Methodology for designing air quality monitoring networks, *Environmental Monitoring and Assessment*, Vol. 6, pp. 1-11, ISSN 1573-2959

Mofarrah, A., Tahir Husain, (2010), A Holistic Approach for optimal design of Air Quality Monitoring Network Expansion in an Urban Area, *Atmospheric Environment*, vol. 44, no. 3 (January 2010), pp. 432-440, ISSN: 1352-2310

Saaty, T.L. (1980). *The analytic hierarchy process: planning, priority setting, resource allocation*, McGraw-Hill, ISBN 0070543712: 9780070543713, New York

Tesfamariam, S. and Sadiq, R., 2006. Risk-based environmental decision-making using fuzzy analytic hierarchy process (F-AHP). *Stoch Environ Res Risk Assess*, vol. 21, pp. 35–50 (March 2006), ISSN 1436-3259

Yager, R.R., (1980). On a general class of fuzzy connectives. *Fuzzy Set Syst*, vol. 4, pp. 235–242, ISSN 0165-0114

Zadeh, L. A., 1965, Fuzzy sets, *Information and control*, vol. 8, issue 3 (June 1965), pp. 338–353, ISSN 0890-5401

3

Malodor Detection Based on Electronic Nose

Teerakiat Kerdcharoen[1],
Chatchawal Wongchoosuk[2] and Panida Lorwongtragool[3]
[1]*Department of Physics, Faculty of Science, Mahidol University*
[2]*Department of Physics, Faculty of Science, Kasetsart University*
[3]*Faculty of Science and Technology,*
Rajamangala University of Technology Suvarnabhumi
Thailand

1. Introduction

Recent decades have observed significantly increasing interest in the applications of electronic nose (E-nose) for qualitative analysis of odors. The first E-nose experiments were conducted in the early 1990s. (Shurmer et al., 1990; Shurmer & Gardner, 1992) Since then, E-nose has become a powerful tool to complement or even replace traditional chemical analysis in many applications ranging from quality control of foods (Barié et al., 2006; Panigrahi et al., 2006; Santonico et al., 2008; Tikk et al., 2008) and beverages (Ragazzo-Sanchez et al., 2008; Yu & Wang, 2007; Wongchoosuk et al., 2009b, 2010b), environment protection (Negri & Reich, 2001; Kuske et al., 2005), medical applications (Chan et al.,2009) to public safety (Scorsone et al., 2006; Zhang et al., 2007). Electronic nose employs an array of chemical gas sensors, numbering from 2 up to a few hundred sensors. Research on chemical gas sensors is mainly focused on improving two properties: selectivity (specificity to a molecule or a class of molecules) and sensitivity (strength of signal upon exposure to low concentration of molecules). Both selectivity and sensitivity leads to performance enhancement of an e-nose for specific applications such as bomb detection (Lubczyk et al., 2010), determination of food freshness based on amine detection (Lorwongtragool et al., 2011; Liao et al., 2010), quality control of alcoholic beverages (Wongchoosuk et al., 2009b, 2010b) and hydrogen gas sensing (Wongchoosuk et al., 2010a).

Chemical sensors can be classified into 4 types (James et al., 2005) based on their transduction, a mechanism that converts chemical interaction into a sensor signal: (1) Optical, (2) Thermal, (3) Electrochemical and (4) Gravimetric. Electrochemical transduction has so far dominated research activities on gas sensors, because its interface setup is more straightforward than other transduction methods. (Choopun et al., 2007; Lorwongtragool et al., 2011) Nevertheless, many research groups including us have been working on many transduction principles, i.e., optical (Uttiya et al, 2008) and gravimetric (Tuantranont et al, 2008), in parallel in order to take advantage of hybrid methodology that could dramatically enhance the performance of electronic nose. Due to the simplicity of the electronics involved, most commercial chemical gas sensors adopt electrical transduction technology in which the metal oxide semiconductors assume the most used sensor architecture according to their low-cost, high sensitivity and simplicity in function. (Korotcenkov, 2007) Thus, one

could easily integrate several functional elements such as sensitive layer, signal converter and control electronics within the same device of a size as required for most applications. Notwithstanding the simple working principles of metal oxide gas sensors, the gas-sensing mechanism at the microscopic level is quite complex and so far still insufficiently understood. (Korotcenkov, 2005; Surnev et al., 2003) As widely known, the gas sensors having the same metal oxide materials can have completely different gas-sensing properties depending on the preparation conditions. It is commonly believed that the chemo-resistive change of the metal oxides is caused by catalytic redox reactions at the sensing surface. Such reactions are controlled by electronic structure, chemical composition, crystal structure and relative orientation of the oxide surface to the analyte molecules, thereby allowing tuning their gas-sensing properties by modifying such parameters. Structural engineering by reducing grain size and modifying crystallite microstructure has been widely accepted as the best method to optimize the metal oxide gas sensors. It can be said that metal oxide gas sensors have nowadays been the most robust technology for gas detection in most applications. As will be seen in this chapter, most E-noses employ this type of gas sensors, except for section 2.1 where carbon nanotube/polymer gas sensors were developed for amine detection.

In this chapter, we have explored the applications of E-nose for malodor detection in three areas: (1) animal malodor, (2) human body odor and (3) indoor air quality.

2. Animal malodor

Among the numerous applications of an E-nose, detection of malodor involving with animal often refers to odor assessments of animal products and animal waste. The changes in the sensory properties of the both animal products and waste are mainly caused by the decomposition of organic matters. The major cause of these unpleasant and unacceptable odors is the growth and metabolism of microorganisms such as bacteria, yeasts and moulds leading to formation of the various toxic volatile organic compounds (VOCs) (Gram & Dalgaard, 2002; Huis in't Veld, 1996). In this section, a review of E-nose applications for 54malodor detection as caused by animal products and animal waste is given.

2.1 Animal products

Quality of animal products is very important because they are protein sources for human and some animals. Mechanisms of food spoilage can be classified into four types, as follows (Berk, 2009; Ghaly et al., 2010) :

i. Microbial spoilage: degradation of food components due to the activity and/or presence of microorganisms
ii. Enzymatic spoilage: undesirable changes due to the activity of enzyme in enzyme catalyzed reactions
iii. Chemical spoilage: irreversible changes such as discoloration due to non-enzymatic chemical reactions between intrinsic food components or the action of environment to the food components (e.g. Maillard browning and lipid oxidation)
iv. Physical spoilage: undesirable changes in the physical structure of the food (e.g. sugar crystallization in preserves, separation of emulsions and collapse of gels).

Early studies acknowledged that microorganism activity is a crucial cause of food spoilage because it can affect to both quality and safety. During propagation process of food spoilage, some physical properties may be observed such as changes in color, taste and smell, etc

(Wilkes et al., 2000). Analytical techniques commonly used to determine quality of food are gas chromatography-mass spectrometry (GC-MS) technique, bacterial and sensory analysis (Zhang et al, 2010). Up to the present, many researchers have tried to push E-nose forward as one of the standard techniques in food industry to evaluate food quality (Berna, 2010). Because the results of an E-nose are normally reported in terms of aroma pattern yielded from the response of chemical sensor array, therefore several scientists tried to correlate E-nose data with the standard techniques. (Blixt & Borch, 1999; O'Sullivan et al., 2003). The E-nose has been applied in a wide range of animal products, including: animal flesh product (e.g. meat (Blixt & Borch, 1999; Panigrahi et al., 2006; Vernat-Rossi et al., 1996; Winquist et al., 1993;), fish and seafood (Alimelli et al., 2007; Huang et al., 2011; Kent et al., 2004; Lorwongtragool et al., 2011; **Ólafsdóttir**, et al., 1997, 2004; Rajamäki et al., 2006; Zhang et al., 2009), dairy product (e.g. cheese and milk) (Ampuero & Bosset, 2003; Drake et al., 2003; Seregély et al., 2006) and egg product (Suman et al., 2007; Yongwei et al., 2009)). Most applications are associated with using E-nose to determine the degree of microbial spoilage. In the literature, development of E-nose system for food monitoring has been conducted in the same direction. E-nose is expected to be usable for on-line analysis in quality control (Blixt & Borch, 1999; Vernat-Rossi et al., 1996). In 1996, E-nose with a limited number of semiconductor gas sensors (six sensors: TGS822, TGS812, TGS824, TGS825, TGS880 and TGS800) was demonstrated to discriminate cured meat products such as dry sausages of various origins or cured hams of different qualities. It was also used for analysis of the volatile compounds of bacterial strains (Vernat-Rossi et al., 1996). The experiment was done by pumping (10 ml min^{-1}) headspace generated by bacteria after 48 h to a gas sensor array. Fig. 1 shows analysis diagram of the volatile compounds of bacterial strains.

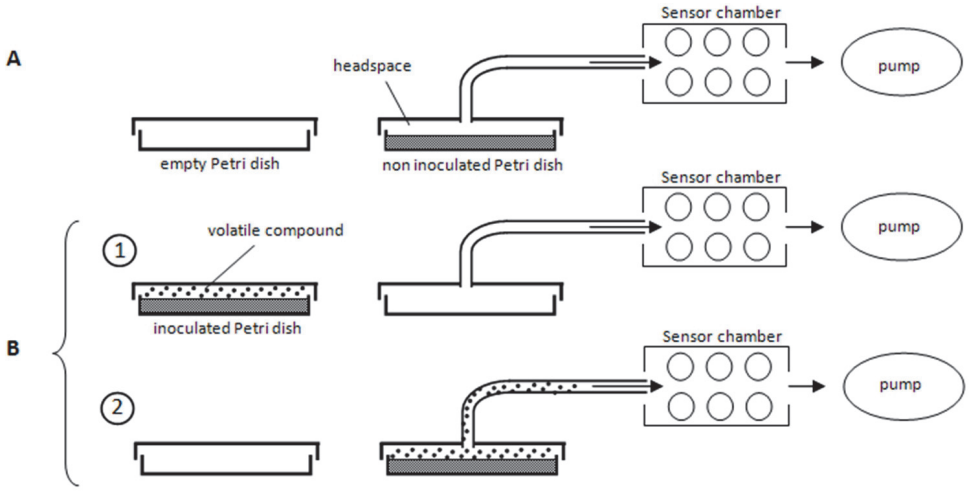

Fig. 1. Analysis of the volatile compounds of bacterial strains. (A) Preliminary analysis to train the gas sensor. Volatile compounds of a non-inoculated Petri dish are introduced for 40 s through the measurement chamber. (B) The two stages of the volatile-colapound analysis: (1) return to baseline for the gas-sensor signal; extraction of the headspace of an empty Petri dish for 10 min; (2) extraction of volatile compounds from an inoculated Petri dish and analysis for 40 s. (Vernat-Rossi et al., 1996)

The performance of E-nose has been demonstrated for quality estimation of ground beef and pork (Winquist et al., 1993). The studies were performed by using a sensory array composed of 10 metal oxide semiconductor field-effect transistors, four Tagushi type sensors and one CO_2 -sensitive sensor. With the same sensor array, Blixt and Borch (Blixt & Borch, 1999) showed that the degree of spoilage of vacuum-packed beef could be determined quantitatively. They also developed mathematical model, describing the relationships between the degree of spoilage, as determined by a sensory panel, and the sensor signal magnitudes of the electronic nose. This relationship is given in equation (2.1)

$$Y = b_0 + b_1 \times S_1 + b_2 \times S_2 + ... + b_n \times S_n \tag{2.1}$$

where Y is the degree of spoilage, b_x is the unweighted regression coefficient obtained from partial least-squares regression (PLS), and S_x is the standardized sensor signal magnitude of the electronic nose. The factor 1/(weight of meat (g))$^{1/2}$ was used as the standardized sensor signal.

It is noticed that most applications for evaluating food quality prefer metal oxide gas sensors as a sensor array (Berna, 2010). Metal oxide semiconductor gas sensors can respond highly and rapidly to volatile compounds. However, this type of gas sensors work at high temperature, thereby consuming higher electrical power than others (Fleischer& Meixner, 1997; Tomchenko et al., 2003) Gas sensors with lower power consumption are therefore in higher demand nowadays. Many research groups have developed alterative sensing materials that can be sensitive to volatile compounds at lower temperature. Hybrid metal oxide and multi-walled carbon nanotube (SnO_2/MWCNTs, WO_3/MWNTs films) was found to present excellent sensitivity towards NO2 at room temperature (Espinosa et al., 2007; Su & Pan, 2011). Conducting polymer as well as polymer/conductive filler composite are new sensing materials that can be applied to indicate quality of food products. Conductive filler such as carbon black, carbon nanotube and graphite can be loaded into the polymer matrix at the level near the conduction percolation threshold to obtain high gain sensors. For example, four nanocomposite sensor materials based on conductive polymer loaded with carbon black were demonstrated for potential applications in real time analysis and quantification of the odor given off from a selection of food borne pathogens including *Salmonella spp.*, *Bacillus cereus* and *Vibrio parahaemolyticus*. (Arshak et al., 2007)

Applications of E-nose involving fish and seafood freshness monitoring were also widely interested. Freshness monitoring of such protein-based products is usually based on chemical contents decomposed by microbial and chemical spoiling process, generally known as total volatile basic nitrogen (TVB-N) such as trimethylamine (TMA), ammonia (NH3) and dimethylamine (DMA). (Dapkevicius et al., 2000; Gram & Huss, 1996; Önal, 2006; Pacquit et al., 2006; Seo et al., 2011;) Because many fish species contain high content of free amino acid and trimethylamine oxide (TMAO), TMA is formed from the reduction of TMAO by bacterial activity (Howgate, 2010a, 2010b).

In order to apply the E-nose efficiently for a specific application, the gas sensor array containing in the E-system should be highly sensitive and selective to the volatile compounds presented in the samples. Lorwongtragool and co-workers have designed a new type of polymer/SWNT-COOH gas sensors that are highly sensitive to the presence of amine based volatile compounds (Lorwongtragool et al., 2011). Fig. 2 shows the sensor responses of polymer/SWNT-COOH nanocomposites to dimethylamine, dipropylamine,

pyridine, and ammonium hydroxide at the concentrations of 50-1000 ppm. This E-nose was shown to be an efficient device for fish freshness monitoring.

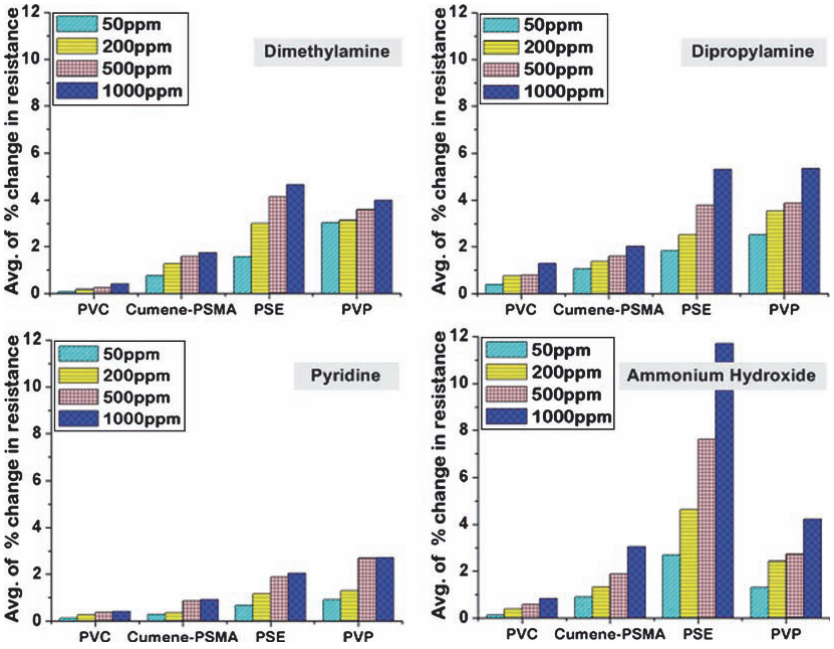

Fig. 2. The average of percent change in resistance of each sensor in static condition when exposed to (a) dimethylamine (b) dipropylamine, (c) pyridine, and (d) ammonium hydroxide at the concentrations of 50-1000 ppm (Lorwongtragool et al., 2011)

2.2 Animal waste

This section illustrates the literature and our recent works on malodor measurement in farms. Problems of most livestock industries often concern with unpleasant odor generated by animal waste resulting in conflict between producers and the local public. In fact, many factors that cause air pollution are associated with farm management (Hamelin et al., 2010;Ivanova-Peneva et al., 2008; Melse & Timmerman, 2009; Sheridan et al., 2002; Van der Werf et al., 2005; Pan et al., 2006, 2007). Numerous animal farms has employed E-nose for odor monitoring such as pig (Brose et al., 2001; Lorwongtragool et al., 2010), poultry (Sohn et al., 2008), sheep (Cramp et al., 2009) and cattle farms (Lane & Wathes, 1998). With complexity of odor in the livestock farm, odor monitoring, reducing and controlling are required due to the impacts of health risks of human and quality of livestock production (Pan & Yang, 2007).

Over 400 compounds identified by GC-MS technique are normally generated from anaerobic process in pig farm area. The compounds identified include many acids, alcohols, aldehydes, amides, amines, aromatics, esters, ethers, fixed gases, halogenated hydrocarbons, hydrocarbons, ketones, nitriles, other nitrogen-containing compounds, phenols, sulfur-containing compounds, steroids, and other compounds (Schiffman et al., 2001). Although analytical instruments such as gas chromatography and mass spectrometry can identify

individual components in a complex odor, the data obtained are lacking the qualitative characteristics as perceived by the human nose (Hyung et al., 1997). Moreover, GC-MS technique as well as other traditional technique (e.g. human assessment) does not support the monitoring on site and at real time due to the method of sampling. Schiffman, et al. (Schiffman et al., 2001) collected the odor onto Tenax® cartridges and Tedlar® *bags* to be analyzed by GC-MS. Odor threshold and sensory assessments were carried out by human assessors. The flexibility of E-nose has shown its ability beyond the human panels with its long operating hours and good reproducibility. Since E-nose containing air flow unit in the system can suck the air directly into the sensing unit, it can be a better choice than taking air into a gas sample bag that posses many difficulties (Trabue et al., 2006). Fig. 3 shows schematic diagram of the portable E-nose system using for detection of unpleasant odor in pig farm (Lorwongtragool et al., 2010).

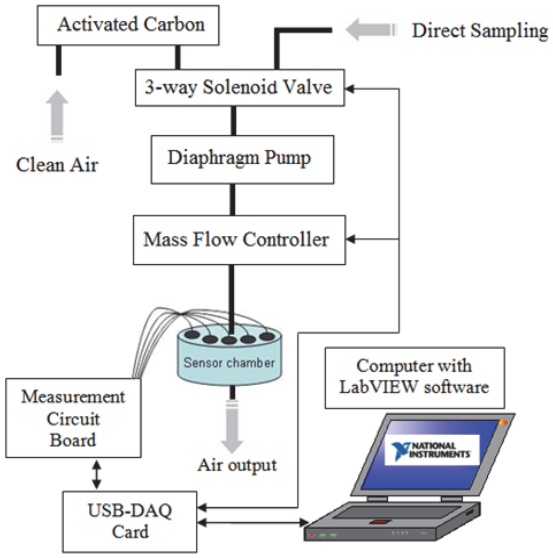

Fig. 3. Schematic diagram of the portable e-nose system (Lorwongtragool et al., 2010).

The odor measurement by using E-nose works under switching between the reference gas (purified air) and odorous gases (non-purified air) pumped into the sensor chamber from the point of sampling. The reference gas was obtained from purification of air with activated carbon. Direction and rate of flow are controlled by 3-way solenoid valve and a mass flow controller, respectively. The USB-DAQ card used as interface device sends analog signal for flow rate adjustment and receives a set of digital signal back for reading the real-time flow rate value. Odor can be directly sampled from interested point by pumping. Because it is well-known that the air inside a pig farm concerning usually consists of ammonia and hydrogen sulfide (Kim et al., 2008; Timmer et al., 2005), so the gas sensor array should be chosen appropriately to detect these gases.

Polyethylene odor sampling duct may be constructed to provide well-mixed (homogenous) air samples. Sohn et al. (Sohn et al., 2008) used a temporary duct with a design of Australian Standard AS 4323.1 as shown in Fig. 4. The complex odour-generating mechanisms within

poultry housing were continuously monitored by E-nose based on 12 metal oxide semiconductor sensors.

Fig. 4. Tunnel ventilated broiler shed showing polyethylene sampling duct attached to an exhaust fan. (Sohn et al., 2008)

Actually, the E-nose used to monitor the odor in the farm area is useful for supporting farm management. Numerous published papers have used the E-nose to study the parameters relating to changes of malodorous odors and used as one of the equipment to find out the final solution for odor reduction. According to Lorwongtragool et al. (Lorwongtragool et al., 2010), the E-nose based on eight commercial metal oxide gas sensors used as assessment technique finally led to an optimized feed menu and cleaning schedule to control and reduce the odor in pig farm. Environmental conditions such as season, temperature, wind, and humidity, etc. that are difficult to control and manage bring the emitted odor to spread to neighbor areas have been evaluated by E-nose (Pan et al., 2006, 2007). In addition, E-nose with applying analysis software can highly improve the accuracy and precision of livestock farm odor evaluation.

Recently, the non-specific conducting polymer was used as chemical gas sensing materials in E-nose system for monitoring odor emissions from a biofiltration system in a piggery building (Sohn et al., 2009). Based on PCA analysis the odor samples collected at the outlet of the biofilter and those from the inlet and post-humidifier were discriminated. Data pre-processing techniques including normalising and outlier handling could also enhance the odor discrimination performance.

E-nose can also be used to detect illness of animals (Cramp et al., 2009; Lane & Wathes, 1998). There are only a few published papers reported about using E-nose to diagnose or detect unusualness of animal; for examples, detection of perineal odors associated with oestrus in the cow (Lane & Wathes, 1998) and detection of cutaneous myiasis in sheep (Cramp et al., 2009). In early stage, the flystrike (Cutaneous myiasis) is difficult to detect,

therefore cutaneous myiasis causes the death of millions of sheep each year due to the larvae of flies burrowing into and feeding on body tissues (Krajewski et al., 2009; Lane & Wathes, 1998; McGraw & Turiansky, 2008). Since a characteristic unpleasant odor is generated from flystrike, this leads to a potential application of E-nose technology to detect the flystrike in advance.

The E-nose combined with non-linear signal measurement techniques and linear discriminant analysis (LDA) extracts signal features and process those features for classification of odor groups. Schematic diagram of the experimental system is given in Fig. 5 (Lane & Wathes, 1998). The E-nose system composed of six metal oxide gas sensors chosen on the basis of GC-MS profile of flystrike odor. Each of the odor sample and clean air is drawn through the E-nose chamber by using diaphragm vacuum pump. The direction of air flow is controlled by two solenoid valves to switch between sample odor and clean air. This experiment can accurately distinguish flystrike odor on days 1, 2 and 3 of development from that of dry wool in all experiments ($P < 0.05$).

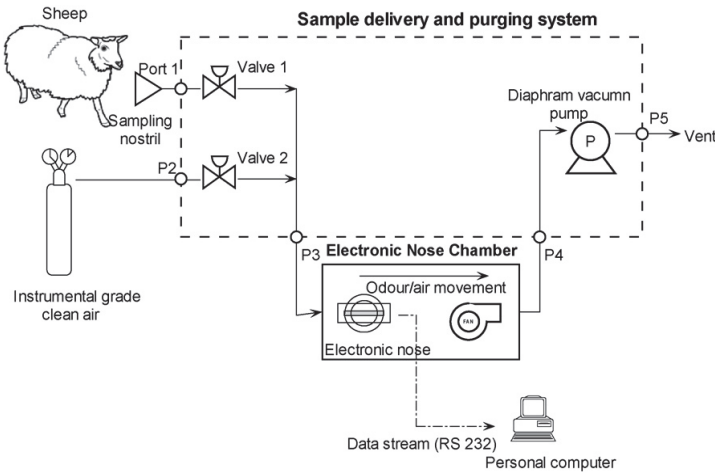

Fig. 5. Schematic diagram of the experimental system, which included the odor or clean air source, the sensor array enclosed in an airtight chamber, an odor delivery system, moisture trap and computer for data logging and recording (Cramp et al., 2009)

3. Human body odor

3.1 Historicatl background

Human body odor refers to unpleasant and pleasant scents that can be emitted from many parts of the body such as skin, armpit, mouth, feet, etc. In fact, most of body odors were considered socially unpleasant while there are only a few of them that are believed to serve as attractants. The human body odor was first investigated systematically in 1936 (Yaglou et al., 1936). They studied the perceived air quality on different numbers of persons who were seated in an experiment-controlled room. They found the relationship of ventilation rates per person required to provide a certain acceptable odor intensity as emitted from the human body in a definite space. Their work has then become the basis of European guidelines for ventilation rates in buildings for more than 50 years.

However, during that time, no scientific instrument existed to measure perceived air quality or human body odor directly. Thus, human panel test, assisted by statistical analysis, had been the only mean to evaluate perceived air quality. The perceived air quality (AQ) in decipols can be written down as (Fanger, 2001):

$$AQ = 112\left[\ln\left(\frac{\exp(-0.18-5.28\overline{AA})}{1+\exp(-0.18-5.28\overline{AA})}\times 100\right)-5.98\right]^{-4} \tag{3.1}$$

Where $\overline{AA}$ is the mean vote of air acceptability (from -1 to +1) measured from untrained panel of impartial subjects who enter the space and judge the acceptability of the air quality.

Nowadays, analytical instruments such as gas chromatograph–mass spectrometry (GC-MS) and electronic nose (E-nose) have become available for detection and analysis of human body odor with both qualitative and quantitative capabilities. Human body odor consists of various volatile organic compounds (VOC). By using stir bar sorptive extraction in connection with thermal desorption, Penn and co-workers (Penn et al., 2007) found on average 241 peaks in the GC–MS of armpit sweat, 179 in saliva and 163 in urine per individual. The list of 152 identified VOCs in the GC–MS profiles from armpit sweat is displayed in Table 1.

RT (min)	**Identification**
	alcohols and phenols
9.98	2-phenylethanol
12.3	a-terpineol
12.47	γ-terpineol
12.9	2-phenoxyethanol
13.34	citronellol
13.82	geraniol
16.48	eugenol
18.93	isoeugenol
21.93	1-tridecanol
26.83	pentadecanol
27.75	a hexadecadienol
29.51	hexadecanol
	Aldehydes
12.74	decanal
13.93	p-anisaldehyde
14.38	geranial
15.46	undecanal
18.1	dodecanal
20.61	tridecanal
20.83	lilial
23	tetradecanal
23.58	pentylcinnamaldehyde
26.04	E-2-hexylcinnamaldehyde
28.09	hexadecanal

RT (min)	Identification
	Ketones
8.98	acetophenone
9.49	2-nonanone
14.99	2-undecanone
15.42	an isopropylacetophenone
17.47	jasmone
17.69	2-dodecanone
19.45	γ-irone
19.66	β-ionone
20.22	2-tridecanone
20.54	Z-α-irone
22.52	2-tetradecanone
18.27	a-ionone
23.09	benzophenone
24.08	1-ethyl-3-methyl-β-ionone
24.92	2-pentadecanone
27.54	2-hexadecanone
28.7	2-acetyl-3,5,5,6,8,8-hexa-methyl-5,6,7,8- tetrahydronaphthalene
29.22	7-acetyl-6-ethyl-1,1,4,4-tetramethyl tetralin (Musk 36A)
	Esters
11.4	benzyl acetate
12.07	2-phenylethyl acetate
12.73	dihydromyrcenol acetate
14.82	cis-2-tert-butylcyclohexyl acetate
16.37	a-terpinyl acetate
16.43	citronellol acetate
16.62	neryl acetate
17.16	geranyl acetate
17.86	methyl-N-methylanthranilate
18.28	2-hexyl-2-pentenoate
18.79	E-cinnamyl acetate
21.24	a-trichloromethylbenzyl acetate
21.95	pentyl salicylate
22.21	isooctanedioldibutyrate
22.69	isoeugenol acetate
23.3	isopropyl dodecanoate
23.73	methyl-cis-dihydrojasmonate
24.15	3Z-1-hexenyl salicylate
24.46	1-hexyl salicylate
25.01	methyl trans-jasmonate
25.73	a hexenyl salicylate
26.65	benzyl benzoate
27.38	ethyl tetradecanoate
27.53	2-ethylhexyl salicylate
28.23	a branched isopropyl hexadecanoate

RT (min)	Identification
30.06	ethyl pentadecanoate
30.32	2-phenylethyl phenylacetate
30.93	methyl palmitate
32.29	decyl octanoate
32.36	dodecyl hexanoate
32.4	hexyl dodecanoate
32.99	ethyl hexadecanoate
33.7	isopropyl hexadecanoate
35.64	ethyl heptadecanoate
36.47	a branched dodecyl benzoate
37.35	2-ethyl-hexyl 4-methoxycinnamate
38	dodecyl octanoate
38.72	dodecyl benzoate
43.19	tridecyl benzoate
47.56	tetradecyl octanoate
49.15	tetradecyl benzoate
	Hydrocarbons
7.67	p-cymene
12.26	1-dodecene
12.5	dodecane
15.15	tridecane
17.55	1-tetradecene
17.77	tetradecane
18.22	β-caryophyllene
19.72	trans-muurola-4(14),5-diene
19.96	a methyl biphenyl
20.36	α-farnesene
20.38	pentadecane
21.77	4-methylpentadecane
22.56	hexadecane
23.28	5-phenylundecane
23.53	4-phenylundecane
23.99	3-phenylundecane
24.94	2-phenylundecane
25.04	heptadecane
25.49	6-phenyldodecane
25.66	a sesquiterpene
25.77	5-phenyldodecane
26.96	a propyl-substituted dodecane
27.48	octadecane
27.57	2-phenyldodecane
28.09	6-phenyltridecane
28.64	4-phenyltridecane
29.4	3-phenyltridecane
29.54	3-methyloctadecane

RT (min)	Identification
30.13	1-nonadecene
30.22	nonadecane
30.38	2-phenyltridecane
32.19	3-methylnonadecane
32.93	eicosane (C-20 linear hydrocarbon)
35.79	heneicosane (C-21 linear hydrocarbon)
38.79	docosane (C-22 linear hydrocarbon)
41.49	tricosane (C-23 linear hydrocarbon)
43.44	tetracosane (C-24 linear hydrocarbon)
	Amines
12.65	2-pentylpyrrole
13.28	2-phenoxyethylmethylamine
15.19	an aliphatic amine
16.34	nicotine
16.81	4-sec-butylaniline
20.37	N,N-dimethyl-1-dodecylamine
30.24	N,N-dimethyl-1-hexadecylamine
35.88	N,N-dimethyl-1-octadecylamine
	Amides
17.18	methyl N,N-diethylthiocarbamate
18.04	a hydroxy acetanilide
21.98	n-propylbenzamide
	Carboxylic acids
12.24	octanoic acid
14.76	nonanoic acid
21.03	8-methylundecanoic acid
21.9	dodecanoic acid
22.8	a methyl dodecanoic acid
23.18	9-methyldodecanoic acid
25.74	10-methyltridecanoic acid
26.8	myristic acid (tetradecanoic acid)
28.36	a methyltetradecanoic acid
28.65	a methyltetradecanoic acid
28.84	9-pentadecenoic acid
29.31	pentadecanoic acid
30.76	a methylpentadecanoic acid
31.7	9-hexadecenoic acid
32.49-33.00	palmitic acid (hexadecanoic acid)
34.37	9-heptadecenoic acid
37.31	oleic acid
38.03	stearic acid (octadecanoic acid)
	Lactones
12.27	γ-heptanolactone
16.7	γ-nonanolactone
18.6	coumarin

Table 1. Compounds identified from armpit samples (Penn et al., 2007).

The changes in body odor associated with aging were investigated by Haze and co-workers (Haze et al., 2001). They found that 2-Nonenal compound only presents in the odor of individuals over the age of 40 years. The 2-Nonenal compound and other aldehydes were produced from oxidative degradation of monosaturated fatty acids such as palmitoleic acid and vaccenic acid. Some VOCs associated with aging that were detected by GC/MS are displayed in Table 2.

Compounds	**Detection rate (%)**	
	<40 y (n=9)	>40 y (n=13)
Hydrocarbons		
1-Octene	11	8
Decane	11	23
Undecane	22	23
Dodecane	67	69
Alcohols		
1-Butanol	11	8
1-Hexanol	11	15
2-Ethylhexanol	89	85
Octanol	11	8
1-Decanol	11	15
Amyl alcohol	11	8
Hexadecanol	11	8
Octadecanol	11	8
Acids		
Acetic acid	22	23
Butyric acid	22	15
Ketones		
4-Methyl-2-pentanone	11	8
6-Methyl-5-heptenone	89	77
Aldehydes		
Hexanal	33	23
Heptanal	11	15
Octanal	89	85
Nonanal	89	85
Decanal	89	69
2-Nonenal	0	69

Table 2. Some compounds detected from body odor by GC/MS (Haze et al., 2001).

Comparison of compounds extracted from the samplings of male and female was also studied by Curran and co-workers (Curran et al. 2005a). Some compounds such as dodecanoic acid, propanedioic acid-methyl ester, octanal, and tetradecanoic acid could be extracted from the male subjects only and they were not present in any of the female profiles. Overall, the individual human body odors can be determined by several factors, which are either stable over time (genetic factors) or vary with environmental or internal conditions. The human body odor can thus be classified into three types (Curran et al. 2005b).):

i. "Primary odor" of a person contains constituents that are stable over time regardless of diet or environmental factors.

ii. "Secondary odor" contains constituents that are present due to diet and environmental factors.
iii. "Tertiary odor" contains constituents that are present because of the influence of outside sources (i.e., lotions, soaps, perfumes).

For identification of an individual using the human body odor, detection of the primary odor class should be used because they are stable over time and diverse across people.

3.2 Evaluation of body odor strength

There are more refined and less subjective ways to measure odor strength in direct way. For instance, the concept of dilution-to-threshold principle can be used quite accurately to reduce uncertainties associated with subjective impressions (Nicell, 2003; Henshaw et al., 2006; Kim & Park, 2008). In the cosmetic industry, human olfaction has been commonly employed to evaluate the odor strength of armpit for the development of deodorants. The armpit odor comprises a complex set of chemicals as shown in section 3.1. However, to simplify the odor strength of armpit, only a single component such as isovaleric acid can be used for training the sensory panel (Hooper et al., 1982). Isovaleric acid (3-Methylbutanoic acid) is a natural fatty acid that can represent the sweaty primary odor (Amoore, 1967, Leyden et al., 1981) which contributes mainly to the armpit malodor. Molecular structure of isovaleric acid is shown in Fig. 6.

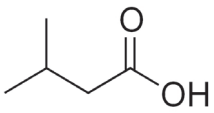

Fig. 6. Isovaleric acid ($(CH_3)_2CHCH_2COOH$)

Hooper and co-workers (Hooper et al., 1981, 1982) assigned the concentrations of isovaleric acid levels on a scale 0 to 5 corresponding to subjective impression by human nose, as shown in Table 3.3. Their test was carried out by a team of three female assessors of ages ranging from 20 to 40 years. They were selected for olfactory evaluation on the basis that each person is able to rank correctly the odor levels of the series of aqueous isovaleric acid solution listed in Table 3.

Level	Concentration of aqueous isovaleric acid solution (mM)	Subjective impression
0	0	No odor
1	0.12	Slight
2	0.48	Definite
3	1.99	Moderate
4	7.88	Strong
5	32.33	Very strong

Table 3. The concentration of the isovaleric acid levels that correspond to subjective impression using human nose.

Recently, evaluation of body odor strength based on isovaleric acid solutions as prepared according to the intensity scale can also be performed using gas sensor array in stead of the

human nose (Wongchoosuk et al., 2009a). The response of a gas sensor array to the isovaleric acid is displayed in Fig. 7.

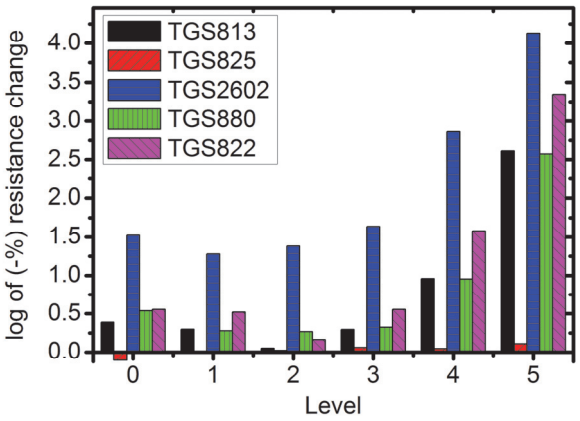

Fig. 7. Logarithmic plot of the sensor response to isovaleric acid at different intensity level (Wongchoosuk et al., 2009a).

3.3 Instrument and method for real-time human odor detection

Even though GC-MS method can be used to detect VOCs emitted from human body odor, they are quite time-consuming, complicated and so costly. Therefore, it is impractical to use it in real-time or at point of use, especially where quick screening for detecting human body odor is the case. One of the most state-of-the-art technologies that can be used for real-time human odor detection is electronic nose (E-nose). Recently, there have been increasing interests in the application of E-nose for measurement of human body odors. If successful, many new applications await in such area as healthcare monitoring, biometrics, homeland security and cosmetics. The first success in distinguishing between two different people by detecting human odor from the armpit region using E-nose was reported by Wongchoosuk and co-workers (Wongchoosuk et al., 2009a). Schematic diagram of the E-nose system for real-time human odor detection is exhibited in Fig. 8.

To allow an identification of human odors, principal component analysis (PCA) was employed to perform pattern recognition and discrimination. PCA is a popular statistical technique usually used to visualize in two or three uncorrelated dimensions transformed from all correlated information. In principles, PCA process contains five following steps (Wongchoosuk et al., 2009a):

i. Get data from matrix, $X_{M\times N}$. The row M represents different repetition of the experiment and the column N represents the number of independent sensors.
ii. Normalize the data matrix, $Norm(X_{M\times N})$, by the mean subtraction. The mean of each N column is calculated and subtracted from the data set. Hence, the new data set produces the mean equal to zero.
iii. Calculate the covariance matrix, $Cov(X_{M\times N})$, and calculate eigenvectors and eigenvalues of the covariance matrix. The calculated eigenvectors must be unit eigenvectors.

iv. Rearrange the eigenvectors and eigenvalues. The eigenvectors are ordered by eigenvalues from highest to lowest, $(\overline{Cov(\mathrm{X}_{M\times N})})_{\max\to\min}$.

v. Obtain the PCA result by matrix multiplication and transpose, $\left((\overline{Cov(\mathrm{X}_{M\times N})})_{\max\to\min} \otimes Norm(X_{M\times N})\right)^T$. The obtained new dataset with orthogonal linear transformation have been plotted in two or three dimensions containing the most relevant of the data set.

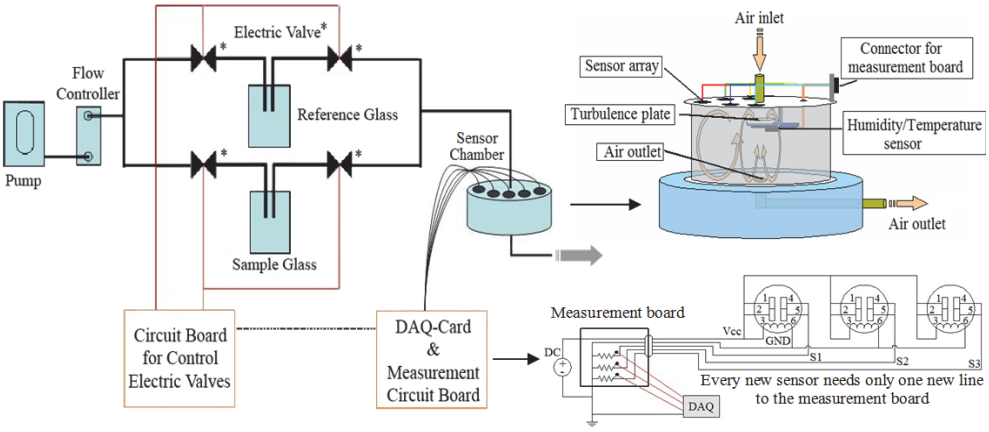

Fig. 8. Schematic diagram of the E-nose system (Wongchoosuk et al., 2009a).

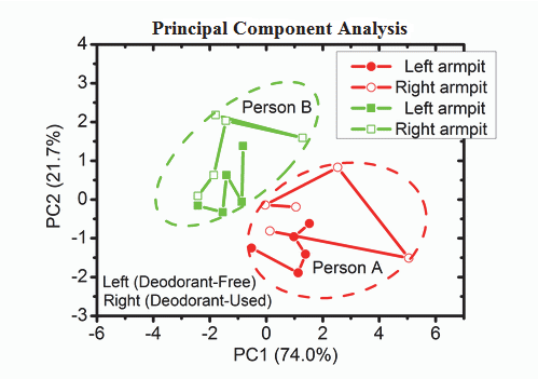

Fig. 9. Discrimination of two persons (Wongchoosuk et al., 2009a).

By using typical E-nose with PCA, Wongchoosuk and co-workers showed obviously discrimination between person A and person B and the use of deodorant may not change the odor fingerprint (Fig. 9). To recognize and discriminate more persons, the method for sensor signal correction should be developed. It is well-known that sensor drift effect is a serious impairment of chemical sensors. The sensor signals alter over time. Therefore, they will produce different responses for the same odor. To correct the sensor drift effect, a mathematical model has been applied to the raw sensor signal via the following formulation:

$$S'(t) = S(t) - F(t) + \overline{F(t)} \tag{3.2}$$

Where $S'(t)$ represents the corrected sensor signal. $S(t)$ is the smoothed raw sensor signal. $F(t)$ is defined as spline interpolation calculated from relationship between the averaged values of their 10 neighboring data points that switch from reference to sample of each loop. $\overline{F(t)}$ is a mean valve of $F(t)$. The Eq. 2 can be demonstrated in Fig. 10.

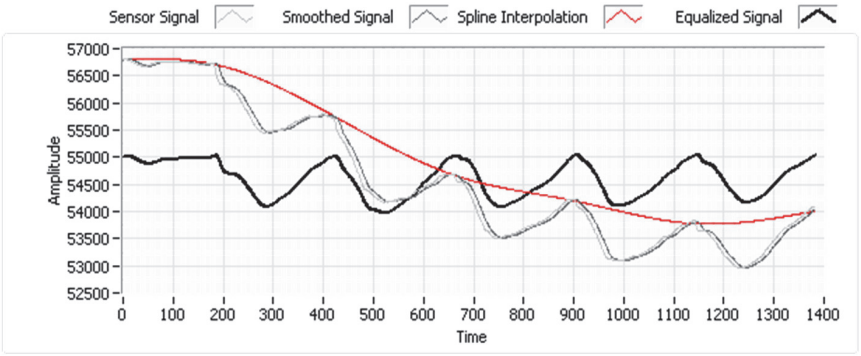

Fig. 10. Correction of sensor drift.

The real armpit measurement by E-nose is shown in Fig. 11. It clearly shows the sensor drift effect that makes the difference of the baseline shift, especially the signal from sensor 1 and

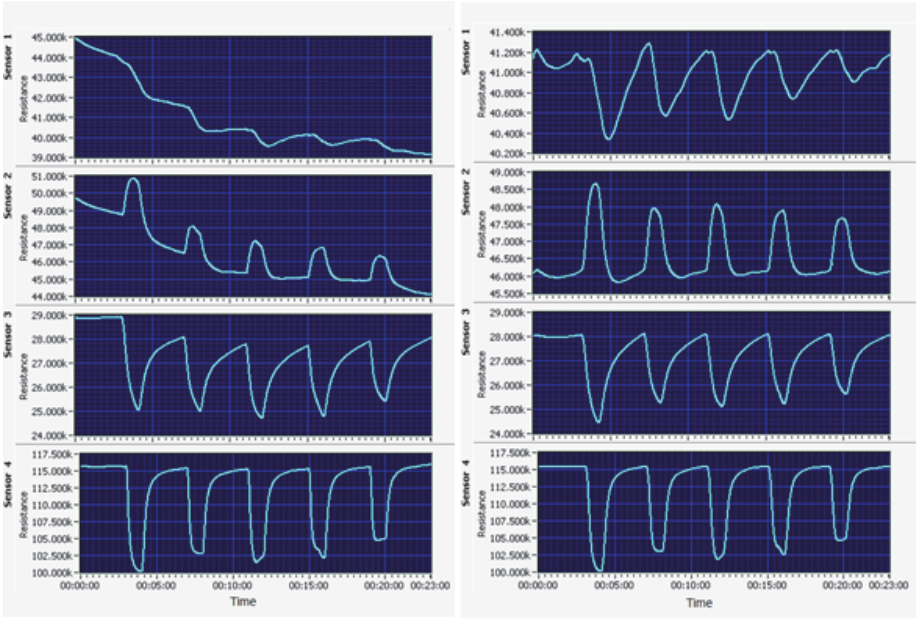

Fig. 11. Raw sensor signals (L-hand side) and corrected sensor signals by using mathematical model (R-hand side).

sensor 2. The drift effect of sensor signal may arise from the temperature variation under long time measurement and humidity generated from armpits (sweat) during the measurement. After correction by using the mathematical model, the sensor signal becomes more homogeneity. It will be useful for reorganization and discrimination of many persons because it helps to reduce the humidity and temperature effects.

To add 95% confidence ellipse for an XY scatter plot in PCA results, the equation of an ellipse is given by the following equation:

$$\frac{(X - X_0)^2}{a^2} + \frac{(Y - Y_0)^2}{b^2} = 1 \tag{3.3}$$

$$\text{Where } a = \sqrt{\frac{\sum_i^N x_i^2}{N}} \text{ and } b = \sqrt{\frac{\sum_i^N y_i^2}{N}} \tag{3.4}$$

The X_0 and Y_0 can be calculated from the center of mass of XY scatter plot. The ellipse is rotated from the horizontal by the following angle:

$$\theta = 0.5 \tan^{-1}\left(\frac{2\sum_i^N (x_i - \bar{x})(y_i - \bar{y})}{\sum_i^N (y_i - \bar{y})^2 - \sum_i^N (x_i - \bar{x})^2} \right) \tag{3.5}$$

The PCA result shows clear classification of four persons within 95% confidence ellipses as shown in Fig .12. The results confirm that each human body has a unique odor pattern. Even though odor of each person can be changed under diverse living conditions such as eating, drinking, sexual activities, health or hormonal status, the E-Nose is still able to identify the people from armpit odor region.

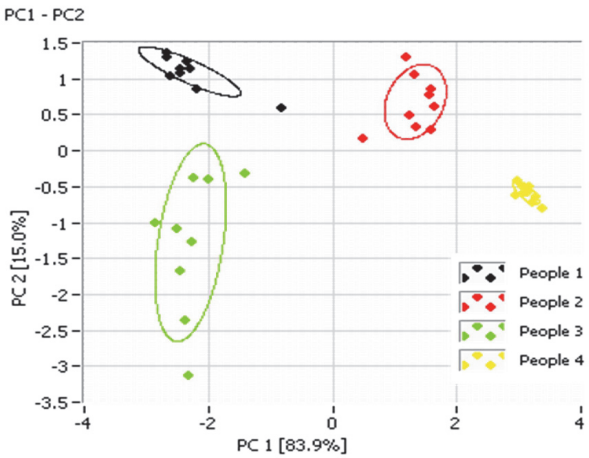

Fig. 12. Discrimination of four persons.

Based on the results as shown above, it is expected that E-nose has potential for helping identify terrorists from a distance in the near future.

4. Indoor air monitoring

Most people spend more than 80% (90% in industrial countries) of their time indoors (Austin et al., 1992), i.e., in offices, houses, stores, restaurants, public or private transportation vehicles, movie theatre, etc. Typically, several hundreds of indoor chemical contaminants including by-products of the combustion (CO_2 , CO), cigarette smoke, particulate matter, mineral fibers etc. can be found. A list of typical indoor air pollutants is displayed in Table 4. In spite of the very low concentrations, some of these compounds are extremely toxic such as CO, NO_2 or formaldehyde. Only as low as 667 ppm of CO may cause up to 50% of the body's hemoglobin to convert to carboxyhemoglobin (Tikuisis et al.,1992) that is ineffective for delivering oxygen to bodily tissues. Exposure to 100 ppm of NO_2 can produce pulmonary edema that may be fatal or may lead to bronchiolitis obliterans while formaldehyde was proved to be carcinogenic. Concisely, indoor air quality can greatly affect morale, emotion, productivity, and health status of people. Therefore, development of technical devices for indoor air monitoring has become an important issue of public interest. In 1988, Fanger (Fanger, 1988) proposed a method for assessing the air quality and introduced that discomfort as caused by indoor air quality based on human sensory panels. However, his method is too time consuming and cannot be used for continuous measurements in long time monitoring and control.

Inorganic Pollutants	Organic Pollutants	Physical Pollutants	Biological Pollutants
Carbon dioxide	Volatile Organic Compounds	Particulate matter	House dust mites
Carbon monoxide	Formaldehyde	Asbestos	Dander from furred animals
Nitrogen dioxide	Pesticides	Radon	Fungi
Sulphur dioxide	Polynuclear Aromatic hydrocarbons		Bacteria
Ozone	Polychlorinated biphenyls		

Table 4. Typical indoor air quality contaminants

In the last decades, gas sensor systems (E-nose) have been developed for monitoring air quality instead of human sensory panels. In an E-nose system, the gas sensors may be considered the most important component. For developing individual gas sensor, there is a great deal of effort on improving the sensitivity and selectivity using nanotechnology. A list of nanostructure gas sensors for indoor chemical contaminant monitoring is given in Table 5.
In many cases, individual gas sensor, that provides only one output signal, is not sufficient for monitoring a wide range of gases. The combination of several gas sensors yielding an E-nose is therefore necessary to measure, maintain and control indoor air quality in real-world applications. Unfortunately, typical commercial E-nose architectures are not suitable for such usage. Most of them are usually designed for fixed location that relies on wired connectivity. Moreover, they are power consuming and very limited in local data processing

capabilities (Vito et al., 2008). Therefore, design of new E-nose architectures such as networked or wireless E-nose is a current interesting topic of E-nose development for indoor air monitoring.

Pollutants	Detection range	Sensing material	Ref.
CO	5–1200 ppm	CuO Nanowires	(Liao et al., 2009)
CO_2	500-2500 ppm	La-SnO_2	(Marsal et al., 2003)
NO_2	5-500 ppb	In_2O_3 Nanowires	(Zhang et al.,2004)
SO_2	2-32 ppm	SnO_2−NiO	(Hidalgo et al.,2005)
O_3	0.2-0.4 ppm	WO_3	(Vallejos et al., 2007)
VOCs	100-1000 ppm	Au-ZnO	(Wongchoosuk et al., 2009b)
CH_2O	0.8-12 ppm	NiO	(Lee et al., 2007)
Pesticide	0.1-1.0 ppm	SnO_2	(Huang et al., 2003)

Table 5. List of nanostructure gas sensor responding to some indoor air quality contaminants.

4.1 Typical E-nose

In principles, an E-nose consists of three main parts: (i) air flow system, (ii) detection system, and (iii) control and data analysis system. The air flow system refers to the way to deliver aroma molecules into the detection system. There are two main types of flow systems, including static and dynamic flow systems. The static system has no vapor flow around the gas sensors and the gas sensors are exposed to vapor at a constant concentration. In the dynamic system, E-nose is subjected to continuous flow of vapor with controllable flow rate during measurement. The simple gas sensor chambers for static and dynamic systems are displayed in Fig. 13.

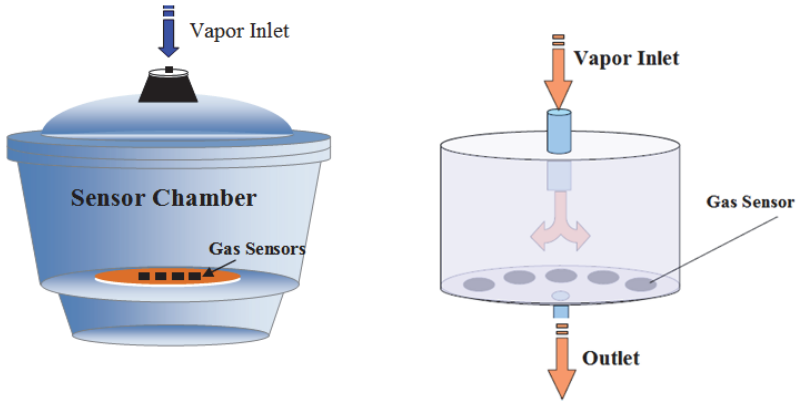

Fig. 13. Static (L-side) and dynamic (R-side) sensor chambers for static and dynamic systems, respectively.

The air flow rate in a dynamic E-nose system is usually controlled by a mass flow controller. Mass flow rate ($\dot{m}$) can be calculated from the density of the gas or liquid (ρ), its velocity (v), and the cross sectional area (A) of the flow by the following equation;

$$\dot{m} = \rho v A \tag{4.1}$$

For an ideal compressible gas, the equation of mass flow rate (Benson, 2008) can be written down as;

$$\dot{m} = \frac{pA}{\sqrt{T}} \sqrt{\frac{\gamma}{R}} M \left(1 + \frac{\gamma - 1}{2} M^2\right)^{-\frac{\gamma+1}{2(\gamma-1)}} \tag{4.2}$$

Where p is total pressure, T is total temperature, R is gas constant, γ is specific heat ration and M is mach number.

A detection system consists of a gas sensor array embedded in a sensor chamber. There are many types of gas sensors used in E-nose such as metal oxide semiconductors (MOS), conducting polymers (CP), quartz crystal microbalance (QCM), surface acoustic wave (SAW), etc. Each type has specific gas detection principle. The MOS and CP rely on the change in electrical conductivity of the sensing materials for detecting aroma molecules. MOS is usually operated under high temperature. When it is heated, oxygen will be adsorbed onto the sensing surface with a negative charge. Then, donor electrons in the crystal surface are transferred to the adsorbed oxygen, resulting in leaving positive charges in a space charge layer. Thus, the surface potential is formed to serve as a potential barrier against electron flow. Electrical conductivity of MOS is low when it presents in pure air. In the presence of a deoxidizing gas or malodor, the surface density of the negatively charged oxygen decreases, so the barrier height in the grain boundary is reduced. The reduced barrier height results in increasing conductivity of MOS. In a CP gas sensor, swelling of vapor molecules into the polymer film is the basis of sensing mechanism. The swelling decreases the number of connected pathways of the conducting component of the composite material leading to an increase in the electrical resistance of the film. For a pure CP, insertion of analyte molecule into polymer matrix generically increases interchain distance that affects the electron hopping between different polymer chains (Bai & Shi, 2007). The interchain electron transfer can be described by the following relationship (Vercelli et al., 2002):

$$\left(\ln \frac{\sigma}{\sigma_0}\right)^{-1} = \left(\frac{\varepsilon_p}{\left(\varepsilon_s - \varepsilon_p\right) B}\right) X^{-1} + B^{-1} \tag{4.3}$$

Where σ and σ_0 are the conductivity before and after exposure to solvent vapor, respectively. ε_p and ε_s are the relative permittivity of the solvent and the polymer, respectively. B is a constant and X is the molar fraction of absorbed vapor for sensing polymer. A simple linear circuit, called as voltage divider (see Fig. 14), can be used for basic measuring of the resistance of MOS or CP gas sensor array.

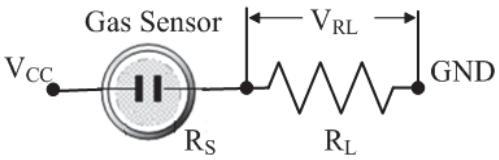

Fig. 14. Basic measuring circuit for MOS or CP gas sensor.

Sensor resistance (R_s) can be calculated by the following equation:

$$R_s = \left(\frac{V_{cc}}{V_{RL}} - 1 \right) \times R_L \tag{4.4}$$

For QCM and SAW gas sensors, a change in the mass of the piezoelectric sensor coating due to gas absorption results in a change in the resonant frequency on exposure to a vapor (Arshak et al., 2004). The QCM utilizes bulk acoustic wave traveling through the entire bulk of the crystal while the SAW uses surface acoustic wave that propagates along the surface of the crystal at a depth of one wavelength at operating frequencies between 100 and 400MHz (Pearce et al., 2003). The resonant frequency of the QCM sensor is related to the change of the mass of QCM loading by the following equation (Sauerbrey, 1959):

$$\Delta f = \frac{-2 f_0^2 \Delta m}{A \sqrt{\rho_q \mu_q}} \tag{4.5}$$

Where Δf is the change in resonant frequency, f_0 is resonant frequency, Δm is mass change due to adsorption of vapor, A is the piezoelectrical active crystal area, ρ_q is density of quartz and μ_q shear modulus of quartz.
In case of the SAW sensor, the change in frequency with sorption of a vapor is given by (Pearce et al., 2003):

$$\Delta f_{SAW} = \frac{\Delta f_p c_v K_p}{\rho_p} \tag{4.6}$$

Where Δf_p is the change in frequency caused by the membrane, c_v is the vapor concentration, K_p is the partition coefficient and ρ_p is the density of polymer membrane.
Both air flow system and detection system are normally controlled by computer via USB, RS-232 or parallel port. Pattern recognition and machine learning such as artificial neural networks (ANN), linear discriminant analysis (LDA), support vector machine (SVM), and principal components analysis (PCA) are typically used in data analysis on a computer.

4.2 Networked E-nose

Networked E-nose can be developed based on a typical E-nose by modifying only one main part (control and data analysis system). If an E-nose can work and analyze the results over a network system such as LAN, WiFi or ZigBee, the E-nose can be defined as networked E-nose. Development of a networked E-nose for indoor air monitoring is demonstrated below:

4.2.1 Air flow system

Schematic diagram of an air flow system for networked E-nose is displayed in Fig. 15.
The measurement works under switching between the reference gas (clean air) and indoor air (malodor) pumped into the network E-nose from the point of sampling. The reference gas was generated by purifying the sucked-in air with activated carbon. The flow was controlled by a mass flow controller and 3-way solenoid valve. Switching between the clean air and the indoor air was used to obtain the baseline and signal, respectively.

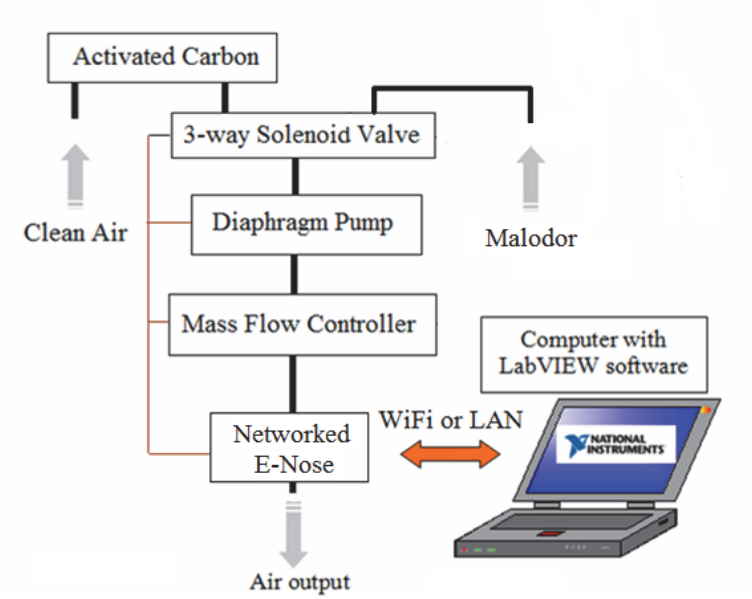

Fig. 15. Schematic diagram of air flow system

4.2.2 Detection system

The commercial MOS gas sensors widely known as TGS (Tagushi) gas sensors can be used for the sensing part. The resistance measurement is performed as shown in Fig. 16 by applying a constant excitation current of I_C=10μA to each sensor element and measure the voltage drop U_1 via V_1.

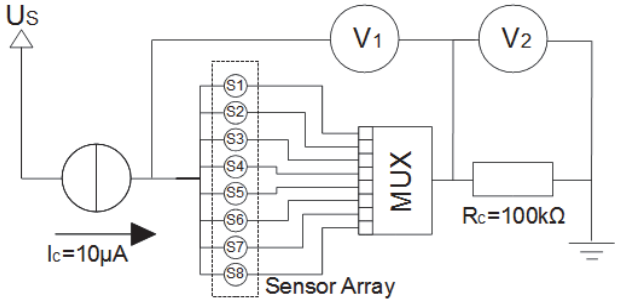

Fig. 16. Resistance measurement principle

The resistance can be calculated by the formula

$$R=U_1/I_C \tag{4.7}$$

An 8-Channel multiplexer was used to address each gas sensor. The voltage U_1 was measured between the input to all sensors and the output of the multiplexer (MUX). The

differential voltage U_1 was measured using the first channel of a 24-Bit Delta-Sigma ADC defined as V_1. The second channel measures the voltage drop U_2 defined as V_2 over a fixed resistor R_C=100kΩ that is in series with the multiplexers and the sensor matrix. Therefore, it is possible to measure the constant current and calculate corrections if the current changes due to temperature effects or external noise.

4.2.3 Control and data analysis system

From section 4.2.2, the ADC, MUX and excitation current source are part of a measurement system controlled by a Microchip PIC24HJ microcontroller. Additionally, a digital-analog converter (DAC) was used to set the flow rate of a mass flow controller and one ADC input of the microcontroller was used to measure the flow rate feedback. Also the 3-way solenoid valves were controlled by the microcontroller. The microcontroller is interfaced to an Ethernet controller, so the measurement system can make an Ethernet connection to a personal computer (PC) on board the measurement software written in LabView. By connecting the measurement system to a small WiFi-Router, this E-nose could become a flexible solution for use in a wireless sensor network. It is possible to use encrypted communications to the PC that can make the system to be secure. The PCB board that contains the metal oxide gas sensors and a temperature/humidity sensor was plugged onto the measurement system PCB board. This creates a flexible setup with interchangeable sensors. A photograph of a networked E-nose is displayed in Fig. 17.

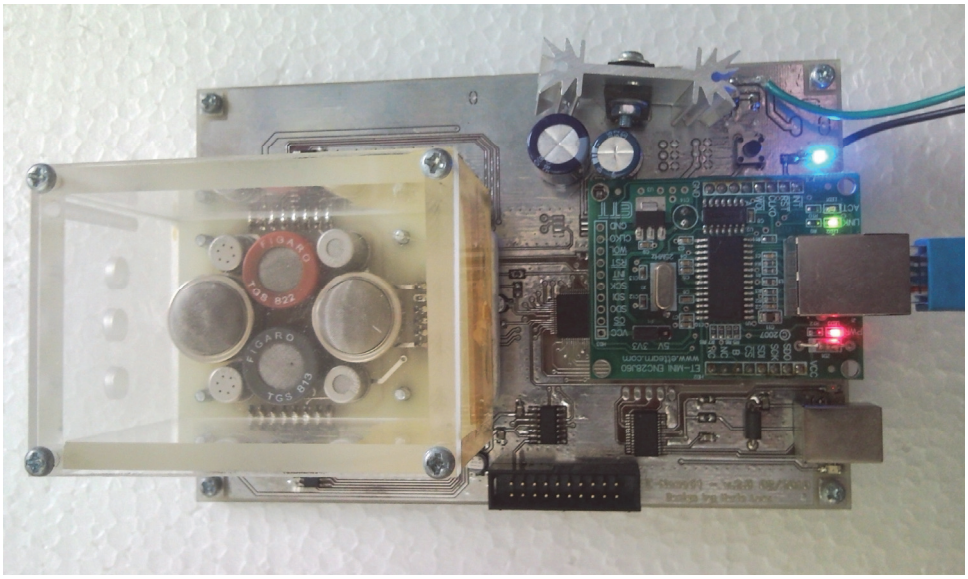

Fig. 17. Photograph of a networked E-nose (15 cm x 10 cm) developed by Center of Nanoscience and Nanotechnolohy, Faculty of Science, Mahidol University.

4.2.4 Other networked E-nose

A wireless E-nose based on IEEE 802.15.4 (ZigBee wireless network) has been developed for environment quality classification as shown in Fig. 18 (Pogfay et al., 2010).

Fig. 18. Photographs of a wireless E-nose based on ZigBee wireless network (Pogfay et al., 2010).

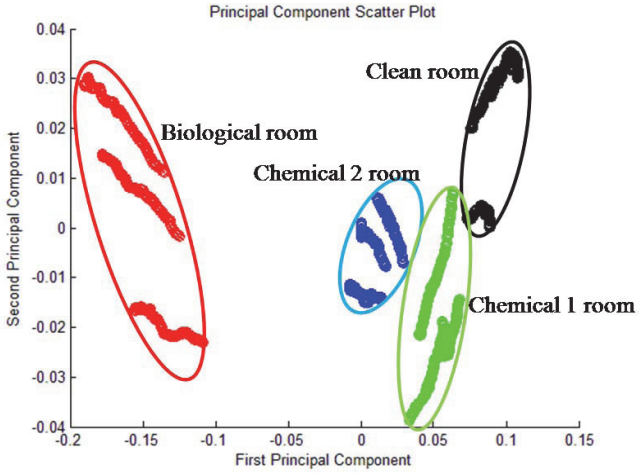

Fig. 19. 2-D PCA plot for environment quality classification (Pogfay et al., 2010).

The advantage of this ZigBee wireless network lies in its ability to offer low power consumption (50 mW) and extend the line of sight distance up to 1 mile. By combined with PCA analysis, the wireless E-nose can clearly classify the air environment from different rooms as shown in Fig. 19.

A smart wireless E-nose (Pan & Yang, 2009) has been designed to be compact in size, energy efficient, and low cost as shown in Fig. 20. This E-nose has been applied for online monitoring of livestock farm odors. Based on field applications like livestock farm monitoring, the circuit and environmental factor noises can strongly affect the output signals. To overcome the problems, a modified Kalman filtering technique has been developed for improving the sensor sensitivity and precision of odor strength measurement for livestock farm odors (Qu et al., 2009). The new odor strength measurement equation based on the noise analysis of MOS gas sensors can be modeled by (Qu et al., 2009):

$$y_k = Cx_k + d_k + s_k \tag{4.8}$$

where C is a measurement matrix, x_k is the system state vector, d_k is the direct current noise component with the same frequency as the signal and s_k is the white noise.

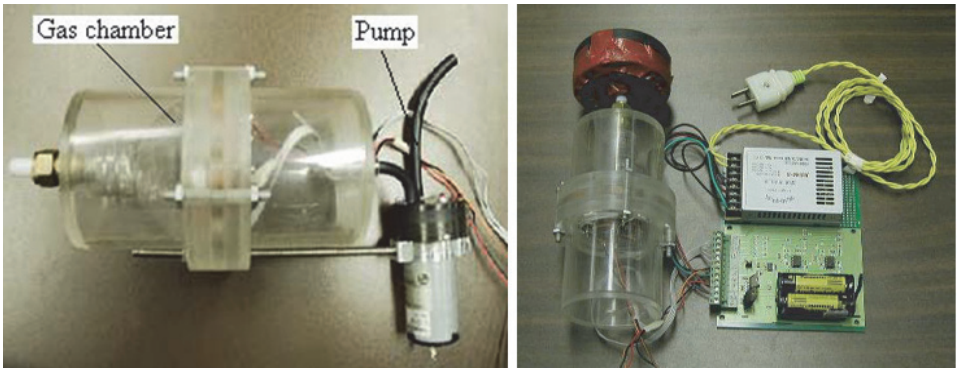

Fig. 20. The smart wireless E-nose (Qu et al., Pan & Yang, 2009).

5. Acknowledgements

Mahidol University and National Research Council of Thailand are acknowledged for supports.

6. References

Alimelli, A.; Pennazza, G.; Santonico, M.; Paolesse, R.; Filippini, D.; D'Amico, A.; Lundström, I. & C. Di Natale. (2007). Fish freshness detection by a computer screen photoassisted based gas sensor array. *Analytica Chimica Acta*, Vol. 582, No. 2, pp. 320-328

Amoore, J.E. (1967). Specific Anosmia: A Clue to the Olfactory Code. *Nature*, Vol. 214, pp. 1095–1098

Ampuero, S. & Bosset J.O. (2003). The electronic nose applied to dairy products: a review. *Sensors and Actuators B*, Vol. 94, pp. 1–12

Arshak, K.; Adley, C.; Moore, E.; Cunniffe, C.; Campion, M. & Harris, J. (2007). Characterisation of polymer nanocomposite sensors for quantification of bacterial cultures. *Sensors and Actuators B*, Vol. 126, pp. 226–231

Arshak, K.; Moore, E.; Lyons, G.M.; Harris, J. & Clifford, S. (2004). A review of gas sensors employed in electronic nose applications, *Sensor Review*, Vol. 24, pp. 181–198

Austin, B.S.; Greenfield, S.M.; Weir, B.R.; Anderson, G.E. & Behar, J.V. (1992). Modeling the indoor environment. *Environmental Science & Technology*, Vol.26, pp. 851–858

Bai, H. & Shi, G. (2007). Gas sensors based on conducting polymers. *Sensors,* Vol. 7, pp. 267-307

Barié, N.; Bücking, M. & Rapp, M. (2006). A Novel Electronic Nose Based on Miniaturized SAW Sensor Arrays Coupled with SPME Enhanced Headspace-analysis and Its Use

for Rapid Determination of Volatile Organic Compounds in Food Quality Monitoring. *Sensors and Actuators B*, Vol. 114, pp. 482–488

Benson, T. (2008). Mass Flow Rate Equations. http://www.grc.nasa.gov/WWW/k-12/airplane/mchkdrv.html

Berk, Z. (2009). Spoilage and Preservation of Foods. *Process Engineering and Technology*, pp. 351-354, ISBN: 978-0-12-373660-4

Berna, A. (2010). Metal Oxide Sensors for Electronic Noses and Their Application to Food Analysis. *Sensors,* Vol. 10, pp. 3882-3910, ISSN 1424-8220

Blixt, Y. & Borch, E. (1999). Using an electronic nose for determining the spoilage of vacuumpackaged beef. *International Journal of Food Microbiology*, Vol. 46, pp. 123–134

Brose, G.; Gallmann, E.; Hartung, E. & Jungbluth, T. (2001). Detection of the dynamics of odour emissions from pig farms using dynamic olfactometry and an electronic odour sensor. *Water Science and Technology*, Vol. 44, No. 9, pp. 59–64

Chan, H.P.; Lewis, C. & Thomas, P.S. (2009). Exhaled Breath Analysis: Novel Approach for Early Detection of Lung Cancer. *Lung Cancer*, Vol. 63, pp. 164–168

Choopun, S.; Hongsith, N.; Mangkorntong, P. & Mangkorntong, N. (2007). Zinc oxide nanobelts by RF sputtering for ethanol sensor. *Physica E*, Vol. 39, No. 1, pp. 53-56

Cramp, A.P.; Sohn, J.H. & James, P.J. (2009). Detection of cutaneous myiasis in sheep using an 'electronic nose'. *Veterinary Parasitology*, Vol. 166, pp. 293–298

Curran, A.M.; Rabin, S.I., Prada, P.A. & Furton, K.G. (2005a). Comparison of the Volatile Oranic Compounds Present in Human Odor using SPME-GC/MS. *Journal of Chemical Ecology*, Vol.31, pp. 1607- 1619

Curran, A.M.; Rabin, S.I., Prada, P.A. & Furton, K.G. (2005b). Analysis of the Uniqueness and Persistence of Human Scent. *Forensic Science Communications*, Vol. 7, No. 2

Dapkevicius, M. L.N. E.; Nout, M. J. R; Rombouts, F. M.; Houben, J. H. & Wymenga, W. (2000). Biogenic amine formation and degradation by potential fish silage starter microorganisms. *International Journal of Food Microbiology*, Vol. 57, pp. 107–114

Drake, M.A.; Gerard, P.D.; Kleinhenz, J.P. & Harper, W.J. (2003). Application of an electronic nose to correlate with descriptive sensory analysis of aged Cheddar cheese. *Lebensm.-Wiss. U.-Technol.,* Vol. 36, pp. 13–20

Espinosa, E.H.; Ionescu, R.; Chambon, B.; Bedis, G.; Sotter, E.; Bittencourt, C.; Felten, A.; Pireaux, J.-J.; Correig, X. & Llobet, E. (2007). Hybrid metal oxide and multiwall carbon nanotube films for low temperature gas sensing. *Sensors and Actuators B*, Vol. 127, pp.137–142

Fanger, P.O. (1988). Introduction of the olf and the dezipol units to quantify air pollution perceived by humans indoors and outdoors, *Energy and Buildings,* Vol.12, pp. 1–6

Fanger, P.O. (2001). Perceived Air Quality and Ventilation Requirements, *Indoor air quality handbook*, pp. 22.1-22.11. McGraw-Hill

Fleischer, M. & Meixner, H. (1997). Fast gas sensors based on metal oxides which are stable at high temperatures. *Sensors and Actuators B*, Vol. 43, pp. 1–10

Ghaly, A.E.; Dave, D.; Budge, S. & Brooks M.S. (2010). Fish Spoilage Mechanisms and Preservation Techniques: Review. *American Journal of Applied Sciences*, Vol. 7, No. 7, pp. 859-877

Gram, L. & Dalgaard, P. (2002). Fish spoilage bacteria – problems and solutions. *Current Opinion in Biotechnology*, Vol. 13, No. 3, pp. 262-266

Gram, L. & Huss, H.H. (1996). Microbiological spoilage of fish and fish products. *International Journal of Food Microbiology*, Vol. 33, pp.121-137

Hamelin, L.; Godbout, S.; Thériault, R. & Lemay, S.P. (2010). Evaluating ammonia emission potential from concrete slat designs for pig housing. *Biosystems Engineering*, Vol. 105, No. 4, pp. 455-465

Haze, S.; Gozu, Y.; Nakamura, S.; Sawano, K.; Ohta, H.; & Yamazaki, K. (2001). 2-Nonenal Newly Found in Human Body Odor Tends to Increase with Aging. *Journal of Investigative Dermatology*, Vol.116, pp. 520-524

Henshaw, P.; Nicell, J. & Sikdar, A. (2006). Parameters for the Assessment of Odour Impacts on Communities. *Atmospheric Environment*, Vol. 40, pp. 1016–1029

Hidalgo, P.; Castro, R.H.R.; Coelho, A.C.V. & Gouvêa, D. (2005). Surface Segregation and Consequent SO_2 Sensor Response in SnO_2−NiO, *Chemistry of Materials*, Vol.17, pp. 4149–4153

Hooper, D.C.; Johnson, G.A. & Peter, D. (1981). Deodorant Compositions. *US Patent 4278658*

Hooper, D.C.; Johnson, G.A. & Peter, D. (1982). Detergent Product Containing Deodorant Compositions. *US Patent 4322308*

Howgate, P (2010a). A critical review of total volatile based and trimethylamine as indices for freshness of fish. Part.1. Electric *Journal of Environmental, Agricultural and Food Chemistry*, Vol. 9, No. 1, pp. 29-57, ISSN: 1579-4377

Howgate, P (2010b). A critical review of total volatile based and trimethylamine as indices for freshness of fish. Part.2. *Electric Journal of Environmental, Agricultural and Food Chemistry*, Vol. 9, No. 1, pp. 58-88, ISSN: 1579-4377

Huang, X.; Liu, J.; Pi, Z. & Yu, Z. (2003) Detecting Pesticide Residue by Using Modulating Temperature Over a Single SnO_2-Based Gas Sensor, *Sensors*, Vol. 3, pp. 361-370

Huang, X.;Xin, J. & Zhao, J. (2011). A novel technique for rapid evaluation of fish freshness using colorimetric sensor array, *Journal of Food Engineering*, doi: 10.1016/j.jfoodeng.2011.03.034

Huis in't Veld, J. H. J. (1996). Microbial and biochemical spoilage of foods: an overview. *International Journal of Food Microbiology*, Vol. 33, No. 1, pp. 1-18

Hyung G. B.; Krishna C. P.; Soad M.K.; Philip J. H. & Tom H. M. (1997). Application of unsupervised clustering methods to the assessment of malodour in agriculture using an array of conducting polymer odour sensors. *Computers and Electronics in Agriculture*, Vol. 17, No. 2, pp. 233-147

Ivanova-Peneva, S.G.; Aarnink, A.J.A. & Verstegen, M.W.A. (2008). Ammonia emissions from organic housing systems with fattening pigs. *Biosystems Engineering*, Vol. 99, No.3, pp. 412 – 422

James, D.; Scott, S. M.; Ali, Z. & O'Hare,W. T. (2005). Chemical Sensors for Electronic Nose Systems. *Microchimica Acta,* Vol. 149, No.1-2, pp. 1-17

Kent, M.; Oehlenschlager, J.; Mierke-Klemeyer, S.; Manthey-Karl, M.; Knöchel, R.; Daschner, F. & Schimmer, O. (2004). A new multivariate approach to the problem of fish quality estimation. *Food Chemistry*, Vol. 87, No. 4, pp.531-535

Kim, K. H. & Park, S.Y. (2008). A Comparative Analysis of Malodor Samples between Direct (Olfactometry) and Indirect (Instrumental) Methods. *Atmospheric Environment*, Vol. 42, pp. 5061–5070

Kim, K. Y.; Ko, H. J.; Kim, H. T.; Kim, Y. S.; Roh, Y. M.; Lee, C. M. & Kim, C. N. (2008). Quantification of ammonia and hydrogen sulfide emitted from pig buildings in Korea. *Journal of Environmental Management*, Vol. 88, pp. 195–202

Krajewski, A.; Allen, B.; Hoss, D.; Patel, C. & Chandawarkar, R. Y. (2009). Cutaneous myiasis. *Journal of Plastic, Reconstructive & Aesthetic Surgery*, Vol.62, pp. e383 - e386

Korotcenkov, G. (2005). Gas response control through structural and chemical modification of metal oxide films: state of the art and approaches. *Sensors and Actuators*, Vol. 107, No. 1, pp. 209-232

Korotcenkov, G. (2007). Metal oxides for solid-state gas sensors: What determines our choice?. *Materials Science and Engineering B*, Vol. 139, No. 1, pp. 1-23

Kuske, M.; Romain, A.C. & Nicolas, J. (2005). Microbial volatile organic compounds as indicators of fungi. Can an electronic nose detect fungi in indoor environments?. *Building and Environment*, Vol. 40, No. 6, pp. 824-831

Lane, A.J.P. & Wathes D.C. (1998).An Electronic Nose to Detect Changes in Perineal Odors Associated with Estrus in the Cow. *Journal of Dairy Science,* Vol. 81, No. 8, pp. 2145-2150

Lee, C.Y.; Chiang, C.M.; Wang Y.H. & Ma, R.H. (2007). A self-heating gas sensor with integrated NiO thin-film for formaldehyde detection, *Sensors and Actuators B: Chemical,* Vol.122, pp. 503-510

Leyden, J.J.; McGinley, K.J.; Hölzle, E.; Labows, J.N. & Kligman, A.M. (1981). The Microbiology of the Human Axilla and Its Relationship to Axillary Odor. *Journal of Investigative Dermatology*, Vol. 77, pp. 413–416

Liao, F.; Yin, S.; Toney, M. F. & Subramanian, V. (2010). Physical discrimination of amine vapor mixtures using polythiophene gas sensor arrays. *Sensors and Actuators B*, Vol. 150, No. 1, pp. 254-263

Liao, L.; Zhang, Z.; Yan, B.; Zheng, Z.; Bao, Q.L.; Wu, T.; Li, C.M.; Shen, Z.X.; Zhang, J.X.; Gong, H.; Li, J.C. & Yu, T. (2009). Multifunctional CuO nanowire devices: p-type field effect transistors and CO gas sensors, *Nanotechnology,* Vol.20, pp. 085203(1-6)

Lorwongtragool, Panida; Wisitsoraat, A. & Kerdcharoen, T. (2011). An Electronic Nose for Amine Detection Based on Polymer/SWNT-COOH Nanocomposite. *Journal of Nanoscience and Nanotechnology*, in press

Lorwongtragool, P.; Wongchoosuk, C. & Kerdcharoen, T., Portable artificial nose system for assessing air quality in swine buildings, *Proceedings of ECTI-CON2010 7th International Conference of Electrical Engineering/Electronics, Computer, Telecommunications and Information Technology Association*, pp. 532 - 535, ISBN 978-1-4244-5606-2, Chaing Mai, THAILAND, May 19-21, 2010

Lubczyk, D.; Siering, C.; Lörgen, J.; Shifrina, Z. B.; Müllen, K. & Waldvogel, S. R. (2010). Simple and sensitive online detection of triacetone triperoxide explosive. *Sensors and Actuators B*, Vol. 143, No. 2, pp. 561-566

Marsal, A.; Cornet, A. & Morante, J.R. (2003). Study of the CO and humidity interference in La doped tin oxide CO_2 gas sensor, *Sensors and Actuators B: Chemical,* Vol.94, pp. 324-329

McGraw, T.A. & Turiansky, G. W. (2008).Cutaneous myiasis. *Journal of the American Academy of Dermatology*, Vol. 58, No. 6, pp. 907-926

Melse, R. W. & Timmerman, M. (2009). Sustainable intensive livestock production demands manure and exhaust air treatment technologies. *Bioresource Technology*, Vol. 100, No. 22, pp. 5506–5511

Negri, R.M. & Reich, S. (2001). Identification of Pollutant Gases and its Concentrations with a Multisensor Array. *Sensors and Actuators B*, Vol. 75, pp. 172–178.

Nicell, J.A. (2003). Expressions to Relate Population Responses to Odor Concentration. *Atmospheric Environment*, Vol.37, pp. 4955–4964

Ólafsdóttir, G.; Martinsdóttir, E.; Oehlenschläger, J. ;Dalgaard, P.; Jensen, B.; Undeland, I.; Mackie, I.M. ; Henehan, G.; Nielsen, J. & Nilsen H. (1997). *Trends in Food Science & Technology*, Vol. 81, pp.258-265

Ólafsdóttir, G.; Nesvadba, P.; Natale, C. D. Careched, M.; Oehlenschläger, J.; Tryggvadóttir, S. V.; Schubring, R.; Kroeger, M.; Heia, K. Esaiassen, M.; Macagnano, A. & Jørgensen, B. M. (2004). Multisensor for fish quality determination. *Trends in Food Science & Technology*, Vol. 15, pp. 86–93

Önal, A. (2006). A review: Current analytical methods for the determination of biogenic amines in foods. *Food Chemistry*, Vol. 103, pp. 1475–1486

O'Sullivan, M.G; Byrnea, D.V.; Jensen, M.T.; Andersen, H.J. & Vestergaard, J. (2003). A comparison of warmed-over flavour in pork by sensory analysis, GC/MS and the electronic nose. Meat Science, Vol. 65, pp. 1125–1138

Pacquit, A.; Lau, K. T.; McLaughlin, H.; Frisby, J.; Quilty, B. & Diamond, D. (2006). Development of a volatile amine sensor for the monitoring of fish spoilage. *Talanta*, Vol. 69, pp. 515–520

Panigrahi, S.; Balasubramanian, S.; Gu, H.; Logue, C.M. & Marchello, M. (2006). Design and Development of a Metal Oxide Based Electronic Nose for Spoilage Classification of Beef. *Sensors and Actuators B,* Vol. 119, pp. 2–14

Pan, L.; Yang, S.X. & DeBruyn, J. (2007). Factor Analysis of Downwind Odours from Livestock Farms. *Biosystems Engineering*, Vol. 96, No. 3, pp. 387–397

Pan, L.; Yang, S.X.; Otten, L. & Hacker, R.R. (2006). Component and Factor Analysis of Pork Farm Odour using Structural Learning with the Forgetting Method. *Biosystems Engineering*, Vol. 94, No. 1, pp. 87–95

Pan, L. & Yang, S. X. (2007). Analysing livestock farm odour using an adaptive neuro-fuzzy approach. *Biosystems Engineering*, Vol. 97, pp. 387 – 393

Pan, L. & Yang, S. X. (2009). An Electronic Nose Network System for Online Monitoring of Livestock Farm Odors. *IEEE/ASME Transactions on Mechatronics*, Vol. 14, pp. 371-376

Pearce, T.C.; Schiffman, S.S.; Nagle, H.T. & Gardner, J.W. (2003) Handbook of Machine Olfaction, WILEY-VCH

Penn, D.J.; Oberzaucher, E.; Grammer, K.; Fischer, G.; Soini, H.A.; Wiesler, D.; Novotny, M.V.; Dixon, S.J.; Xu Y.; & Brereton, R.G. (2007). Individual and Gender Fingerprints in Human Body Odour, *Journal of the Royal society interface*, Vol.4, pp. 331-340

Pogfay, T.; Watthanawisuth, N.; Pimpao, W.; Wisitsoraat, A.; Mongpraneet, S.; Lomas, T.; Sangworasil, M. & Tuantranont, A. (2010). Development of Wireless Electronic Nose for Environment Quality Classification, Proceedings of ECTI-CON 2010, pp. 540 – 543

Qu, J.; Chai, Y. & Yang, S. X. (2009). A Real-Time De-Noising Algorithm for E-Noses in a Wireless Sensor Network. *Sensors*, Vol. 9, pp. 895-908

Ragazzo-Sanchez, J.A.; Chalier, P.; Chevalier, D.; Calderon-Santoyo, M. & Ghommidh, C. (2008). Identification of different alcoholic beverages by electronic nose coupled to GC. *Sensors and Actuators B*, Vol. 134, No.1, pp. 43-48

Rajamäki, T.; Alakomi, H.-L.; Ritvanen, T.; Skyttä, E.; Smolander, M. & Ahvenainen, R. (2006). Application of an electronic nose for quality assessment of modified atmosphere packaged poultry meat. *Food Control*, Vol. 17, No. 1, pp. 5-13

Santonico, M.; Pittia, P.; Pennazza, G.; Martinelli, E.; Bernabei, M.; Paolesse, R.; D'Amico, A.; Compagnone, D. & Di Natale, C. (2008). Study of the aroma of artificially flavoured custards by chemical sensor array fingerprinting. *Sensors and Actuators B*, Vol. 133, No. 1, pp. 345-351

Sauerbrey, G. (1959). Verwendung von Schwingquarzen zur Wägung dünner Schichten und zur Mikrowägung, *Zeitschrift für Physik*, Vol. 155, pp. 206–222.

Schiffman, S.S.; Bennett, J.L. & Raymer, J.H. (2001). Quantification of odors and odorants from swine operations in North Carolina. *Agricultural and Forest Meteorology*, Vol. 108, No. 3, pp. 213–240

Scorsone, E.; Pisanelli, A.M. & Persaud, K.C. (2006). Development of an Electronic Nose for Fire Detection. *Sensors and Actuators B*, Vol. 116, pp. 55–61

Seo, S.-G.; Ma, Z.-K.; Jeon, J.-M.; Jung, S.-C. & Lee, W.-B. (2011). Measurements of key offensive odorants in a fishery industrial complex in Korea. *Atmospheric Environment*, in press

Seregély, Z.; Farkas, J.;. Tuboly, E &Dalmadi, I. (2006). Investigating the properties of egg white pasteurised by ultra-high hydrostatic pressure and gamma irradiation by evaluating their NIR spectra and chemosensor array sensor signal responses using different methods of qualitative analysis. *Chemometrics and Intelligent Laboratory Systems*, Vol. 82, pp. 115 – 121

Sheridan, B.; Curran, T.; Dodd, V. & Colligan, J. (2002). Biofiltration of Odour and Ammonia from a Pig Unit-a pilot-scale Study. *Biosystems Engineering*, Vol. 82, No. 4, pp. 441–453

Shurmer, H.V.; Gardnera, J.W. & Corcoran, P. (1990). Intelligent vapour discrimination using a composite 12-element sensor array. *Sensors and Actuators B: Chemical*, Vol. 1, No. 1-6, pp. 256-260

Shurmer H. V. & Gardner, J. W. (1992). Odour discrimination with an electronic nose. *Sensors and Actuators B: Chemical*, Vol. 8, No.1, pp. 1-11

Sohn, J. H.; Dunlop, M.; Hudson, N.; Kim, T. & Yoo, Y. H. (2009). Non-specific conducting polymer-based array capable of monitoring odour emissions from a biofiltration system in a piggery building. *Sensors and Actuators B: Chemical*, Vol. 135, No. 2, pp. 455-464

Sohn, J. H.; Hudsonb, N.; Gallagher, E. & Dunlop, M. (2008). Implementation of an electronic nose for continuous odour monitoring in a poultry shed. *Sensors and Actuators B*, Vol. 133, pp. 60–69

Suman, M.; Riani, G. & Dalcanale, E. (2007). MOS-based artificial olfactory system for the assessment of egg products freshness. *Sensors and Actuators B*, Vol. 125, pp. 40–47

Su, P.-G. & Pan, T.-T. (2011). Fabrication of a room-temperature NO2 gas sensor based on WO3 films and WO3/MWCNT nanocomposite films by combining polyol process with metal organic decomposition method. *Materials Chemistry and Physics*, Vol. 125 pp.351–357

Surnev, S.; Ramsey, M.G. & Netzer, F.P. (2003). Vanadium oxide surface studies. *Progress in Surface Science*, Vol. 73, No. 4-8, pp. 117-165

Tikk, K.; Haugen, J.-E.; Andersen, H. J. & Aaslyng, M. D. (2008). Monitoring of warmed-over flavour in pork using the electronic nose – correlation to sensory attributes and secondary lipid oxidation products. *Meat Science*, Vol. 80, No. 4, pp. 1254-1263

Tikuisis, P.; Kane, D.M.; McLellan, T.M.; Buick, F.; Fairburn, S.M. (1992). Rate of formation of carboxyhemoglobin in exercising humans exposed to carbon monoxide. *Journal of Applied Physiology,*Vol.72, pp. 1311–1319

Timmer, B.; Olthuis, W.; Berg, A. v. d. (2005). Ammonia sensors and their applications—a review. *Sensors and Actuators B*, Vol. 107, pp. 666–677

Trabue, S.L.; Anhalt, J.C. & Zahn, J.A. (2006). Bias of Tedlar Bags in the Measurement of Agricultural Odorants. *Journal of Environmental Quality*, Vol. 35, No. 5, pp.1668–1677

Tomchenko, A. A.; Harmer, G. P.; Marquis, B. T. & Allen, J. W. (2003). Semiconducting metal oxide sensor array for the selective detection of combustion gases. *Sensors and Actuators B*, Vol. 93, pp. 126–134

Tuantranont, A.; Lomas, T.; Jaruwongrungsee, K.; Jomphoak, A. & Wisitsoraat, A. (2008). Symmetrical PolyMUMPs-Based Piezoresistive Microcantilever Sensors With On-Chip Temperature Compensation for Microfluidics Applications. *IEEE Sensors Journal*, Vol. 8, No. 5, pp. 543-547

Uttiya, S.; Kerdcharoen, T.; Vatanayon, S. & Pratontep, S. (2008). Effect of structural transformation to the gas sensing properties of phthalocyanine thin films. *Journal of the Korean Physical Society*, Vol. 52, No. 5, pp. 1575-1579

Vallejos, S.; Khatko, V.; Aguir, K.; Ngo, K.A.; Calderer, J.; Gràcia, I.; Cané, C.; Llobet E. & Correig, X. (2007). Ozone monitoring by micro-machined sensors with WO_3 sensing films, *Sensors and Actuators B: Chemical,* Vol.126, pp. 573-578

Van der Werf, H.M.G.; Petit, J. & Sanders, J. (2005). The environmental impacts of the production of concentrated feed: the case of pig feed in Bretagne. *Agricultural Systems*, Vol. 83, No. 2, pp.153–177

Vercelli, B.; Zecchin, S.; Comisso, N.; Zotti, G.; Berlin, A.; Dalcanale, E. & Groenendaal, L.B. (2002). Solvoconductivity of polyconjugated polymers: The roles of polymer oxidation degree and solvent electrical permittivity. *Chem. Mater.*, Vol. 14, pp. 4768-4774

Vernat-Rossi, V.; Garcia, C.; Talon, R.; Denoyer, C. &. Berdagué, J.-L. (1996). *Sensors and Actuators B: Chemical*, Vol. 37, No. 1-2, pp. 43-48

Vito, S.D.; Massera, E.; Burrasca, G.; Girolamo, A.D.; Miglietta, M.; Francia, G.D. & Sala, D.D. (2008). TinyNose: Developing a wireless e-nose platform for distributed air quality monitoring applications, *Proceedings of 2008 IEEE Sensors Conference*, pp. 701-704

Wilkes, J. G.; Conte, E. D.; Kim, Y.; Holcomb, M.; Sutherland, J. B. & Miller, D. W. (2000). Sample preparation for the analysis of flavors and off-flavors in foods. *Journal of Chromatography A*, Vol. 880, No. 1-2, pp. 3-33

Winquist, F.; Hornsten, E G; Sundgren, H & Lundstrom, I. (1993). Performance of an electronic nose for quality estimation of ground meat. *Meas. Sci. Technol*, Vol. 4, pp.1493-1500

Wongchoosuk, C.; Lutz, M. & Kerdcharoen, T. (2009a). Detection and Classification of Human Body Odor using an Electronic Nose. *Sensors,* Vol. 9, pp. 7234-7249

Wongchoosuk, C.; Choopun, S.; Tuantranont, A. & Kerdcharoen, T. (2009b) Au-doped Zinc Oxide Nanostructure Sensors for Detection and Discrimination of Volatile Organic Compounds. *Materials Research Innovation*, Vol. 13, pp. 185-188

Wongchoosuk, C.; Wisitsoraat, A.; Phokharatkul, D.; Tuantranont, A. & Kerdcharoen, T. (2010a). Multi-walled Carbon Nanotubes Doped Tungsten Oxide Thin Film for Hydrogen Gas Sensing. *Sensors,* Vol.10, pp. 7705-7715, ISSN 1424-8220

Wongchoosuk, C.; Wisitsoraat, A.; Tuantranont, A. & Kerdcharoen, T. (2010b). Portable Electronic Nose Based on Carbon Nanotube-SnO_2 Gas Sensors: Feature Extraction Techniques and Its Application for Detection of Methanol Contamination in Whiskeys. *Sensors and Actuators B*, Vol. 147, pp. 392-399

Yaglou, C.P.; Riley, E.C. & Coggins D.I. (1936). Ventilation Requirements. *ASHVE Transactions*, Vol.42, pp. 133-162

Yongwei, W.; Wang, J.; Zhou, B. & Lu, Q. (2009). Monitoring storage time and quality attribute of egg based on electronic nose. *Analytica Chimica Acta*, Vol. 650, pp. 183–188

Yu, H. & Wang, J. (2007). Discrimination of LongJing green-tea grade by electronic nose. *Sensors and Actuators B*, Vol. 122, No. 1, pp. 134-140

Zhang, D.; Liu, Z.; Li, C.; Tang, T.; Liu, X.; Han, S.; Lei, B. & Zhou, C. (2004). Detection of NO2 down to ppb Levels Using Individual and Multiple In_2O_3 Nanowire Devices, *Nano Letters*, Vol.4, pp. 1919–1924

Zhang, Z; Li, G.; Luoc, L. & Chen, G. (2010). Study on seafood volatile profile characteristics during storage and its potential use for freshness evaluation by headspace solid

phase microextraction coupled with gas chromatography–mass spectrometry. *Analytica Chimica Acta*, Vol. 659, No. 1-2, pp. 151-158

Zhang, S.; Xie, C.; Bai, Z.; Hu, M.; Li, H. & Zeng, D. (2009). Spoiling and formaldehyde-containing detections in octopus with an E-nose. *Food Chemistry*, Vol. 113, No. 4, pp. 1346-1350

Zhang, S.; Xie, C.; Zeng, D.; Zhang, Q.; Li, H.; & Bi, Z. (2007). A feature extraction method and a sampling system for fast recognition of flammable liquids with a portable E-nose. *Sensors and Actuators B*, Vol. 124, No. 2, pp. 437-443

Part 2

Air Quality Assessment and Management

4

"Nuisance Dusts" – Validation and Application of a Novel Dry Deposition Method for Total Dust Fall

Gary T. Hunt
TRC Corporation, Wannalancit Mills, Lowell, MA
USA

1. Introduction

Nuisance dust complaints received from residents living in the vicinity of a coal fired power plant in the eastern United States prompted development of a monitoring program to quantify the frequency of incidents as well as the magnitude of the problem (if any). Nuisance dusts (in this context defined as visible dust deposits on solid surfaces) while regulated by some state and local agencies, have no quantitative standards or guidelines associated with them that define acceptable levels (concentrations) in ambient air or deposited on surfaces. Methods historically used to measure and/or characterize airborne dusts have included manual (Wheeler, J.P. and J.P. Stancliffe, 1998., ASTM D6966-08.) and automatic wipe sampling techniques (Wheeler, J.P. and J.P. Stancliffe, 1998.) use of adhesive tapes (Wheeler, J.P. and J.P. Stancliffe, 1998.) passive sampling using open faced containers (Estokova, A, N. Stevulova and L. Kubincova, 2010, ASTM D-1739-98, Reapproved 2004., James P. Lodge, Jr, Editor Lewis Publishers, 1989.) and vacuum or suction sampling apparatus (Byrne, M.A., 2000., ASTM D-5438-05, 2005.) While all of these techniques have been employed for collection of surface dusts they were not suitable for the current application for one or more of the following reasons: 1) not suitable for gravimetric measurements (wipe sampling for example) , 2) designed for the collection of wet and dry dusts combined and not dry surface dusts only (passive collection in open faced containers for example), 3) qualitative characterization only of dry dusts present on surfaces (adhesive tape sampling for example 4) ease in deployment and recovery at multiple stations simultaneously.

In order to meet the needs of the monitoring program the preferred method was characterized as follows: 1) ease in deployment and recovery of dust collection devices at multiple stations simultaneously, 2) samples represent passive dry dust fall on surfaces (these types of dusts were the basis for the nuisance complaints), 3) inexpensive, 4) citizens/homeowners could participate with minimal training 5) ability to collect gravimetric data (weight of particulate per unit time and unit surface area), 6) field samples after gravimetry were suitable for further chemical analyses employing non destructive techniques without the need for pretreatment (filter based device). As a result, a pre-existing filter sampling technique (Dzubay, T. and R. Barbour, 1983**.)** was selected for use in dust fall monitoring. The filter sampling technique was modified and a monitoring program designed to meet the above characteristics.

The total dust fall monitoring program included measures for validation of the customized monitoring method as well as collection of data defining what constitutes background particulate levels in the study area. These background levels were needed as a "benchmark" in assigning significance to the program's collected data in the absence of published regulatory values. The monitoring program was designed to measure total dust fall (non-respirable) as surface dust deposits and relied on passive particulate collection devices. Preconditioned and pre-weighed filter media were deployed at ten (10) sites in the metropolitan area. Residential hosts who agreed to participate in the program on a voluntary basis operated the majority of the sites used. Criteria for site selection included coverage of all wind vectors in the vicinity of coal handling processes at the power plant as well as residential properties where nuisance dust complaints had been recorded previously. Filter collection media were employed for sampling events expected to last one calendar week or seven (7) days. This provided an exposure period that maximized collection of particulate matter, and yet limited non-detected values. All residential hosts received training in filter deployment, recovery, handling and shipping procedures.

2. Program purpose and objectives

The primary purpose of the program was to conduct a total particulate or "total dust fall" monitoring program in the vicinity of the coal fired power plant employing passive dry deposition techniques. It was anticipated that the results of this program would assist the facility in determining the fate of dusts potentially released during coal handling events at the facility, as well as, in the identification of likely sources of dust deposits observed in off-site residential properties.

3. Experimental methods

3.1 Approach and methodology

The method employed in the collection of passive dry dust-fall was not a standard reference method. EPA Federal Register or sanctioned methods were not available for use in collection of the type of measurements needed for this program. This is attributable to the fact that nuisance dusts are not currently regulated at the EPA or federal level. While there are National Ambient Air Quality Standards (NAAQS) for $PM_{10,}$ $PM_{2.5}$ previously for TSP or Total Suspended Particulate there are no promulgated standards for total particulate or visible dusts. While nuisance dusts are regulated by some state and local agencies no quantitative standards or guidelines exist for defining acceptable levels of these types of dusts in ambient air. The method employed in the conduct of the validation and subsequent field program represents a novel or unique approach for the monitoring of total dust fall or particulate.

Preconditioned and pre-weighed filter media were deployed at ten (10) sites in the metropolitan area where the coal fired power plant was located. The majority of the sites used were operated by residential hosts who agreed to participate in the program on a voluntary basis. Criteria for site selection included coverage of all wind vectors in the vicinity of the power plant as well as properties where nuisance dust complaints had been made previously.

Filter collection media were deployed for sampling events expected to last one calendar week or seven (7) days. This sampling period was selected so as to provide an exposure period to maximize collection of particulate matter and limit non-detected values. All site

hosts received training in filter deployment, recovery, handling and shipping procedures. It was particularly important that filters be recovered in the event that precipitation took place during a sampling event. Filters were then re-deployed after the precipitation had passed. Samples were subsequently recovered and packaged for shipment to TRC. After inspection all valid samples were shipped to the laboratory for gravimetry.

3.2 Method validation - program design

The primary purpose of the method validation study was to collect performance data representative of the sample collection and analyses method used during the term of the dust fall monitoring program. Accordingly it was necessary that the method validation exercise be performed under actual field conditions. Specific objectives of the method validation program were as follows:

- Examine what influences if any are associated with the sample collection process itself. For example, what influences are associated with exposure of the filter media and cassette to sunlight and other environmental factors such as temperature?
- What influences if any are associated with the sample shipping and handling process? This includes all of the following factors: initial filter preparation and weighing process, packaging and shipping to field, field deployment and sample collection, recovery, repackaging and return shipment to lab, lab handling and final weighing process.
- Fate of particulate matter collected on filters as a result of the passive collection field sampling process. This includes the % recovery of known quantities of particulate matter deposited on filters prior to field deployment.

A series of filter samples were placed on a rectangular wood board surface (16 ¼" by 17 ½") and deployed in a residential suburban location for an approximate one-week period; the term of an actual sampling event during the field program performed in the vicinity of the coal fired power plant. Twenty filter samples were arranged on the board surface as shown in the schematic provided as Figure 1. As shown in the filter placement schematic (Figure 1) four types of filters were used in the field validation program. Field or trip blanks were also part of the program but these were not deployed in the actual sample collection process. As shown in the schematic a total of twenty (20) samples were collocated representing four (4) distinct types or categories of samples.

Each category or filter type was comprised of five (5) identical filters. The four (4) filter types and the significance of each were as follows:

Regular Exposed Filters – These filters were identical to those used in the dustfall monitoring program itself. Data from these filters represented actual dustfall deposited on the filters by passive deposition from the atmosphere. The results from this five (5) sample set represented the precision or repeatability of the sample collection and analyses process. As such these data complemented the collocated filter sample data collected on a station specific basis during the actual field program. These data were used to define method performance in terms of precision.

Coal Spiked Exposed Filters – These filters were identical to the regular exposed filters with the exception that the filter surface on each has been spiked with a known amount of coal dust. Actual coal dust used at the host power plant was placed manually on the surface of a pre-weighed filter by the laboratory and the net weight of dust deposited was calculated. These filters were deployed as shown in Figure 1. This filter set represented a classic matrix spike employing the technique of standard additions. The results of these filters provide some measure on the accuracy of the method in actual field use.

Regular Unexposed – These filters were deployed while in the shipping package and were not exposed to the atmosphere. The covered filters were exposed, however, to direct sunlight and other environmental factors in place during the sample collection period such as temperature variability. While unexposed this filter set was not subject to any environmental effects such as wind and rain or filter tampering attributable to birds or small animals.

Coal Spike Unexposed – These filters were identical to the regular unexposed filters with the exception that the filter surface on each has been spiked with a known amount of coal dust. Actual coal dust used at the host power plant was placed manually on the surface of a pre-weighed filter and the net weight of dust deposited was calculated. These filters were deployed as shown in Figure 1. The results from this set provided recovery data for known quantities of particulate deposited on filters and subjected to the filter handling, shipping and weighing processes.

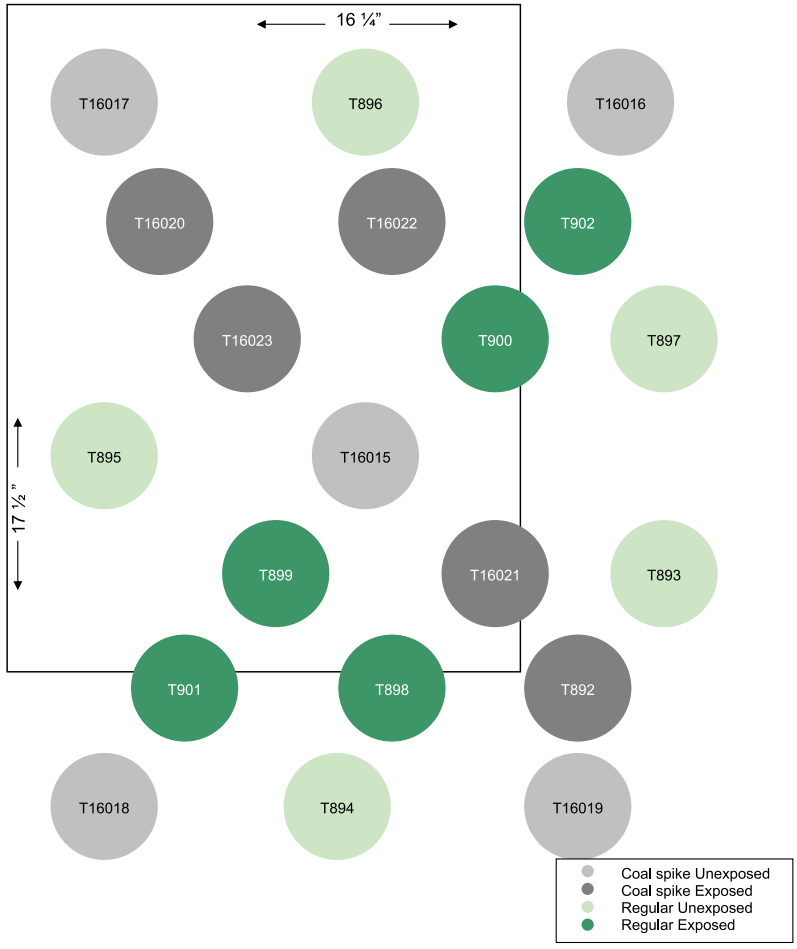

Fig. 1. Total Dust Fall Method Validation – Field Performance Study/Filter Placement Schematic

3.3 Gravimetry

Gravimetry for all filters was performed at Chester Lab Net Tigard, Oregon). Before sampling, the filters were equilibrated at constant temperature and relative humidity conditions and weighed. After sampling, the filters were again equilibrated at constant temperature and humidity conditions and weighed to obtain a net total dust fall mass. The filter weighing procedure employed by Chester Lab Net was based upon the Federal Register method in place for PM2.5 (40CFR50 Appendix L).

3.4 Filter preparation

Teflon filters (47 mm diameter) were received from the manufacturer and stored in a climate controlled weigh room. Temperature of the filters and room were kept at 70 ± 2°F, and at 35 ± 5% relative humidity. All filters were subsequently coated with a light layer of mineral oil to enhance adhesion of coarse particulate matter to the filter matrix. Teflon filters were placed in a chamber designed to nebulize a mineral oil solution under nitrogen purge. The filter was attached to a vacuum, and the nebulized oil was driven onto the filter by both the vacuum source behind the filter and the positive pressure of the nitrogen purge in front of the filter. The oil coating solution consisted of a commercial grade mineral oil dissolved in reagent grade hexane. The concentration of mineral oil in hexane solution was approximately 0.025 % (w/w). The mineral oil reagent was procured commercially as Kaydol. (Synonyms: Drakeol, Parol, Peneteck, Slab Oil or White Mineral Oil). The oil coating procedure employed by Chester was based upon a prior procedure published by Dzubay.

Fig. 2. Teflon Filter (47mm) Oil Coated in Sampling Cassette with Shipping Container (Ready for Field Use)

All filters after coating were reweighed to determine the weight of the oil coating. For 47 mm filters, the weight of oil should be 300 ± 50 mg. A higher concentration of mineral oil may be used. The greater the concentration of oil, the less time is required during the actual coating and therefore the greater the chance for error during the coating process. This concentration (0.025%) was recommended for beginning the process. If greater concentrations are needed, they can be made later. An actual photograph of an oil coated Teflon filter used during the field monitoring program is shown in Figure 2.

4. Results and discussions

4.1 Collocated filters (unexposed)

Results for the five (5) sample set are summarized in Table 1. This includes tare and gross weights for each of the filters as well as % recovery values. As shown the mean recovery value was 100%. These data represent a quantitative recovery of the filter tare weight. As a result of the sample preparation, shipping and weighing processes there were no noticeable gains or losses in filter weight. These data suggest that losses and gains in filter tare weights while unexposed to the atmosphere were not a factor during the course of the field program. Further, any observed losses or gains in filter weights were directly attributable to passive dry deposition of atmospheric particulate matter.

LabNet ID	Tare Wt.(mg)	Gross Wt.(mg)	Percent Wt. Recovered (%)
04-T893	164.439	164.435	100.00
04-T894	159.15	159.142	99.99
04-T895	152.172	152.165	100.00
04-T896	155.106	155.096	99.99
04-T897	149.193	149.181	99.99
		Average:	100.00

Table 1. Method Validation - Field Performance Data Unexposed Filters – No Coal Spike Percent Recovery Data

4.2 Coal spiked filters (unexposed)

Results for the five (5) sample set are summarized in Table 2. This includes filter tare weights as well net weights of coal applied and recovered on a filter specific basis. As shown the mean recovery value was >99%. These data represent a quantitative recovery of the amounts of coal dust deposited on each of the filters. The quantities of coal dust applied to the filter surface (see Table 2) expressed as dust fall rates were variable ranging from 127.6 μg/24hrs to 216 μg/24hrs (based upon 7 days or 168 hours per sampling event). The mean dust fall rate of 177.8 μg/24hrs applied to the filters is approximately 40% higher than the mean dust fall rate of 126.1 μg/24hrs observed at the Fire Station Site (Station 10) downtown in the metropolitan area around the power plant. As a result of the sample preparation, shipping and weighing processes there were no noticeable gains or losses in filter gross weight. These data suggest that losses and gains in filter weights attributable to

coal or other types of particulate deposited on the filter surface while unexposed to the atmosphere were not a factor during the course of the field program. Further, any observed losses or gains in filter weights were directly attributable to passive dry deposition of atmospheric particulate matter. These data also provide evidence on the overall integrity of the handling, shipping and weighing processes applied to all filter samples after completion of the field sampling or filter exposure period.

LabNet ID	Tare Wt.(mg)	Gross Wt (mg) After Coal Spike	Net Wt (ug) of Coal	Gross Wt.(mg) After Exposure	Net Wt (ug) After Exposure	Percent Recovery (%)
03-T16015	144.507	145.400	893	145.415	908	101.68
03-T16016	152.854	154.051	1197	154.056	1202	100.42
03-T16017	145.923	147.435	1512	147.383	1460	96.56
03-T16018	145.954	147.336	1382	147.304	1350	97.68
03-T16019	148.827	150.066	1239	150.075	1248	100.73
					Average % Recovery:	**99.41**

Table 2. Method Validation - Field Performance Data Coal Spiked Filters – Unexposed – Percent Recovery Data

4.3 Filters un-spiked (exposed)

Five (5) identical unexposed filter samples were deployed as shown in Figure 1. These samples essentially represented a set of five (5) collocated filter samples. The results of these analyses are summarized in Table 3. As shown the mean concentration of the set expressed as a net weight of particulate was 272.2 µg with a standard deviation of 57.08 µg; the mean expressed as a dust fall rate was 39.34 µg/24hrs with a standard deviation of 8.25 µg/24hrs. These standard deviation values expressed as a % of the mean is approximately 21%. This value is in good agreement with much of the method precision data to follow for collocated filter samples. Average % difference data derived from analyses of collocated filter pairs for the majority of the sites ranged from 20-25 %.

LabNet ID	Tare Wt.(mg)	Gross Wt.(mg)	Net Wt.(ug)	Rate of Deposition ug/24 Hours
04-T898	148.632	148.938	306	44.22
04-T899	140.626	140.803	177	25.58
04-T900	143.334	143.645	311	44.94
04-T901	143.687	144.017	330	47.69
04-T902	145.85	146.087	237	34.25
	Average:		**272.20**	**39.34**
	Standard Deviation:		**57.08**	**8.25**

Table 3. Method Validation - Field Performance Data - Exposed Filters (166 Hours of Exposure)

4.4 Coal spiked filters (exposed)

This filter set represents a "classic matrix spike" employing the technique of standard additions. The results of these filters provided some measure on the accuracy of the method in actual field use. These filters were deployed as shown in Figure 1. The results of these analyses are summarized in Table 4. The net weight values shown for this set of filter samples represents both the amount of coal applied to each filter initially with the addition of atmospheric particulate deposited while the filters were exposed on location during the week-long sampling event. Recovery data were therefore calculated on the basis of background corrected weights. The latter value was derived on a filter specific basis employing the average or mean particulate weight shown in Table 3 as a correction factor. The background corrected weight in combination with the net weight of coal dust applied initially was the basis for calculation of the % recovery data shown in Table 4. Recovery data for the five (5) sample set ranged from 71.7 % to 85.2 % with a calculated mean of 78.8 %. These data suggest an approximate loss of 20% of the particulate deposited on the filter surface during the filter exposure period.

These losses were likely attributable to environmental factors such as periodic rainfall during the week-long exposure period. The field logs for the method validation exercise document a limited amount of rainfall exposure that was experienced during the sampling event when the filter array was unattended and not accessible to the field operator. These data suggest a negative bias of approximately 20% associated with the sample collection process. Accordingly, dust fall rates measured during the actual field program may be understated when rainfall takes place during a sampling event and the filter is not covered and/or secured indoors by the site operator as required.

LabNet ID	Tare Wt. (mg)	Gross Wt (mg) After Coal Spike	Net Wt (ug) of Coal	Gross Wt. (mg)	Net Wt. (ug)	Rate of Deposition ug/24Hrs	Background* Corrected Net Wt.(ug)	Percent Recovery (%)
03-T16020	145.702	147.243	1541	147.179	1477	213.44	1204.8	78.18
03-T16021	156.139	157.522	1383	157.403	1264	182.66	991.8	71.71
03-T16022	155.404	156.856	1452	156.866	1462	211.27	1189.8	81.94
03-T16023	149.854	150.800	946	150.932	1078	155.78	805.8	85.18
04-T892	150.486	151.735	1249	151.72	1234	178.32	961.8	77.01
							Average % Recovery:	**78.80**

*Refer to Table 3

Table 4. Method Validation - Field Performance Data Coal Spiked Filters – Exposed Matrix Spikes (166 Hours of Exposure)

4.5 Filters un-spiked (exposed) - July 26-30 2004

Results of the initial method validation indicated that dust fall rates may be influenced by rainfall that takes place during a sampling event. Dust fall rates, as a result of rain fall events

may be understated. More specifically, rainfall may cause dust already deposited on the filter surface to migrate to the perimeter of the sampling cassette and/or be lost from the filter surface. In order to examine this finding further the field method validation program was repeated during the calendar period July 26-30 2004. The method validation repeat was limited to an array of exposed filters only, including both spiked and un-spiked sets.

Five (5) identical unexposed filter samples were deployed as shown previously in Figure 1. These samples essentially represented a second set of five (5) collocated filter samples. The results of these analyses are summarized in Table 5. As shown the mean concentration of the set expressed as a net weight of particulate was 53.5 µg with a standard deviation of 6.26 µg; the mean expressed as a dust fall rate was 22.48 µg/24hrs with a standard deviation of 2.63 µg/24hrs. These standard deviation values expressed as a % of the mean is approximately 11.7 %. This value is better than the 21% value reported for the collocated filter set in the initial method validation event and the method precision data reported for collocated filter samples. Average % difference data derived from analyses of collocated filter pairs for the majority of the sites ranged from 20-25 %.

It should be noted that the dust fall data from the second set of filter samples represents an exposure period of fifty-seven (57) hours during the during the calendar period July 26-30 2004. Based upon field sampling records filters were not exposed to rainfall during this sampling event. These data were subjected to statistical analyses for the purpose of identifying outliers in the five (5) collocated filter sample set. As a result of these analyses, results from one of the five samples (Lab ID 04-T952) was identified as an outlier and eliminated from the mean and standard deviation reported in Table 5. The mean net weight for the remaining four (4) samples of 53.5 µg was used for background correction of the filter set spiked with coal dust and reported in Table 6 to follow.

July 26-30, 2004 (57 Hours of Exposure)					
LabNet		**Tare**	**Gross**	**Net**	**Rate of Deposition**
ID		**Wt.(mg)**	**Wt.(mg)**	**Wt.(µg)**	**µg/24 Hours**
04-T951		173.828	173.873	45	18.91
04-T952 *		168.638	168.747	109 *	45.8 *
04-T953		157.497	157.557	60	25.21
04-T954		166.394	166.444	50	21.01
04-T955		158.848	158.907	59	24.79
		Average:		**53.5**	**22.48**
		Standard Deviation:		**6.26**	**2.63**

*This sample was determined to be an outlier, and was not included in the average and standard deviation calculations.

Table 5. Method Validation - Field Performance Data Exposed Filters

4.6 Coal dust spiked filters (exposed) - July 26-30 2004

This second set of five (5) filters was deployed as shown in Figure 1. The results of these analyses are summarized in Table 6. The net weight values shown for this set of filter samples represents both the amount of coal applied to each filter initially with the addition of atmospheric particulate deposited while the filters were deployed on location. Recovery data were therefore calculated on the basis of background corrected weights. The latter value was derived on a filter specific basis employing the average or mean particulate

weight of 53.5 µg shown in Table 5 as a correction factor. The background corrected weight in combination with the net weight of coal dust applied initially was the basis for calculation of the % recovery data shown in Table 6. Recovery data for the five (5) sample set ranged from 97.1 % to 99.6% with a calculated mean of 98.5 %. These data represent a complete quantitative recovery of the coal dust applied in the laboratory to the set of five (5) filter samples. These data indicate that a quantitative recovery of dust can be expected when measures are taken to protect filters from rainfall during sampling events. Furthermore, these recovery data serve to further validate the combined sample collection and analyses procedures employed during the actual dust fall monitoring program. This includes filter preparation, gravimetry, shipping, handling, field deployment and exposure.

July 26-30, 2004 (57 Hours of Exposure)								
LabNet ID	**Tare Wt. (mg)**	**Gross Wt (mg) After Coal Spike**	**Net Wt (µg) of Coal**	**Gross Wt.(mg)**	**Net Wt. (µg)**	**Rate of Deposition µg/24Hrs**	**Background* Corrected Net Wt. (µg)**	**Percent Recovery (%)**
04-T946	168.621	169.535	914	169.562	941	395.38	887.5	97.10
04-T947	166.525	167.527	1002	167.566	1041	437.39	987.5	98.55
04-T948	175.078	176.462	1384	176.51	1432	601.68	1378.5	99.60
04-T949	183.463	184.579	1116	184.614	1151	483.61	1097.5	98.34
04-T950	166.61	167.737	1127	167.778	1168	490.76	1114.5	98.89
Average % Recovery 98.50								

*Refer to Table 5

Table 6. Method Validation - Field Performance Data Coal Spiked Filters – Exposed Matrix Spikes

4.7 Field blanks

A pair of filters were identified as field blanks. These filters were identical to the unexposed category with the exception that they were not deployed as part of the field validation study. The field blank results are indicative of the sample preparation, handling shipping and gravimetry processes. The results of the field blank analyses indicated identical weights for both filters prior to field deployment and upon completion of the sample collection process.

4.8 Total dust fall data

Total dust fall measurements were collected during the entire term of the program spanning from February 18 2003 through February 4 2004. All samples were collected as weekly sampling events and results reported in units of µg/24 hours of sample collection. The numbers of sampling events collected at each of the eleven (11) stations employed in the network at full expansion however varied due to the fact that all stations were not employed for the entire duration of the program. This coupled with the fact that not all samples

collected met sample validation and acceptance criteria resulted in different numbers of valid data sets at each of the locations. Table 7 summarizes total dust fall rates on a site-specific basis. The data provided includes mean deposition rates for each of the sites, the maximum deposition rate observed at each site and the number of data points per site. These same data are shown graphically in Figure 3 in bar graph format. This includes average or mean deposition rates on a station specific basis. The numbers of data points included in each of the mean rates is also shown.

Station #	Site Description/Location	(N=)*	Dates of Operation**	X	Max
Station 1	Residential/ ½ Mile NW of Facility	8	2/18/03 - 4/15/03	82.5	247.8
Station 2	Residential/1000 Feet W of Facility	30	2/18/03-11/4/03	123.2	658.1
Station 3	Residential/ ⅓ Mile W of Facility	21	2/18/03-8/19/03	84.5	392.6
Station 5	Background Residential/1 Mile SW of facility (Over Water)	25	2/18/03-10/7/03	72.0	203.0
Station 6	Residential/ 8/10 Mile E of Facility (Over Water)/ Remote Setting/Regional Background.	28	2/18/03-1/27/04	27.1	109.0
Station 7	On Facility Property /1000 Feet N Coal Storage and Handling Processes	32	2/18/03-1/27/04	40.4	166.4
Station 8	Residential/2000 Feet N of Facility	22	6/10/03-2/3/04	40.0	176.8
Station 9	Residential/2000 Feet NW Facility	10	6/10/03-2/3/04	28.1	67.0
Station 10	Urban Background Downtown/Fire Station/8/10 Mile SW Facility (Upwind)	24	6/10/03-1/27/04	126.1	249.9
Station 11	Residential/ 2000 Feet SW Facility	7	9/9/2003-12/23/03	19.0	34.4
		206	**2/18/03-2/3/04**	**69.1**	

*Includes only valid sampling sessions

**Ending date indicates completion of last valid sampling session

Table 7. Total Dust Fall Data Summary – Site Specific Basis - µg/24 Hours – February 2003 – February 2004

4.9 Total dust fall levels- background assignments and contributions

Three (3) stations well beyond the immediate vicinity of the power plant were designated as representative of different background environments for analyses of dust fall data. These stations and associated dust fall rates were as follows: Station 6- Remote (mean = 27 µg/24hrs), Station 10 Fire Station Urban (mean = 126 µg/24hrs) and Station 5 Shoreline (72 µg/24 hrs).

Wind trajectory data were examined for all sampling events. Based upon these analyses criteria were developed for assignment of specific samples as predominantly upwind or downwind of the coal handling processes during each weekly sampling event. These criteria (upwind greater than 20% and downwind less than 5%) were used to identify samples representing upwind only or background dust fall levels in the vicinity of the power plant. Background data for the immediate vicinity of the power plant were identified from examination of all data collected at stations 1,2,3,5,7,8,9 and 11. There were 30 samples that

met the pre established predominantly upwind criteria. The mean concentration for this data set is 65.9 µg/24 hrs. Three different dust fall rates corroborate this as a representative number for background in the Metropolitan area as follows: Station 6/10 average all events = 78.9 µg/24 hrs (pool of all data from stations with highest and one of the lowest dust fall rates), average all samples 69.1 µg/24hrs (N=206) and Shore Drive Station 5 = 72 µg/24 hrs. The latter site was situated approximately one mile due south/southwest of the facility over open water and removed from the Metropolitan Area.

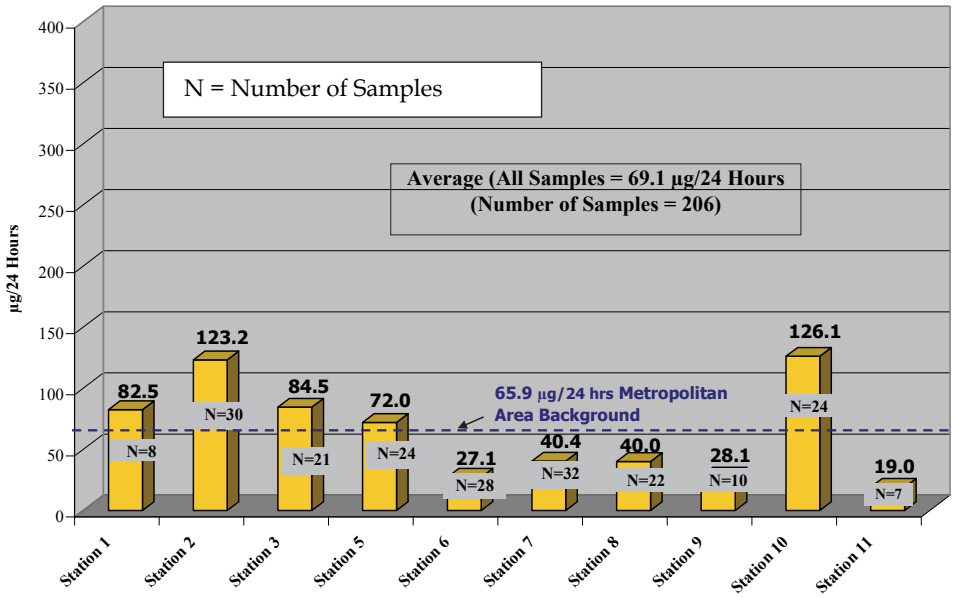

Fig. 3. Total Dust Fall Program – Average Rate of Deposition – Site Specific Basis – February 18, 2003-February 4, 2004

4.10 Collocated total dust fall filter samples

Collocated filter sample media were deployed at eight (8) of the sites in the network. Initially filter pairs were collected only at the Berm Site (Station 7) but as the program evolved over a longer time period this feature was expanded to include all active sites in the network. The use of collocated filter samples was expanded to all sites still active in the August-September time period. Two (2) of the ten (10) sites included in the network were not in active use at this time as the site host had withdrawn from the program. This included Sites 1 and 3. The data set available for Site 7 includes a total of twenty-seven (27) valid sampler pairs representing the calendar period February 25 2003-January 27, 2004. The results of these analyses are displayed in bar graph format in Figure 4. As shown the average % difference (% RPD) for Station 7 was 20.3 %. Collocated sampler results for Station 10 are displayed graphically in Figure 5. The average % difference (%RPD) for the sixteen (16) samples collected at Station 10 was 20.0 %. This value is equivalent to performance data collected at the Berm Site discussed previously.

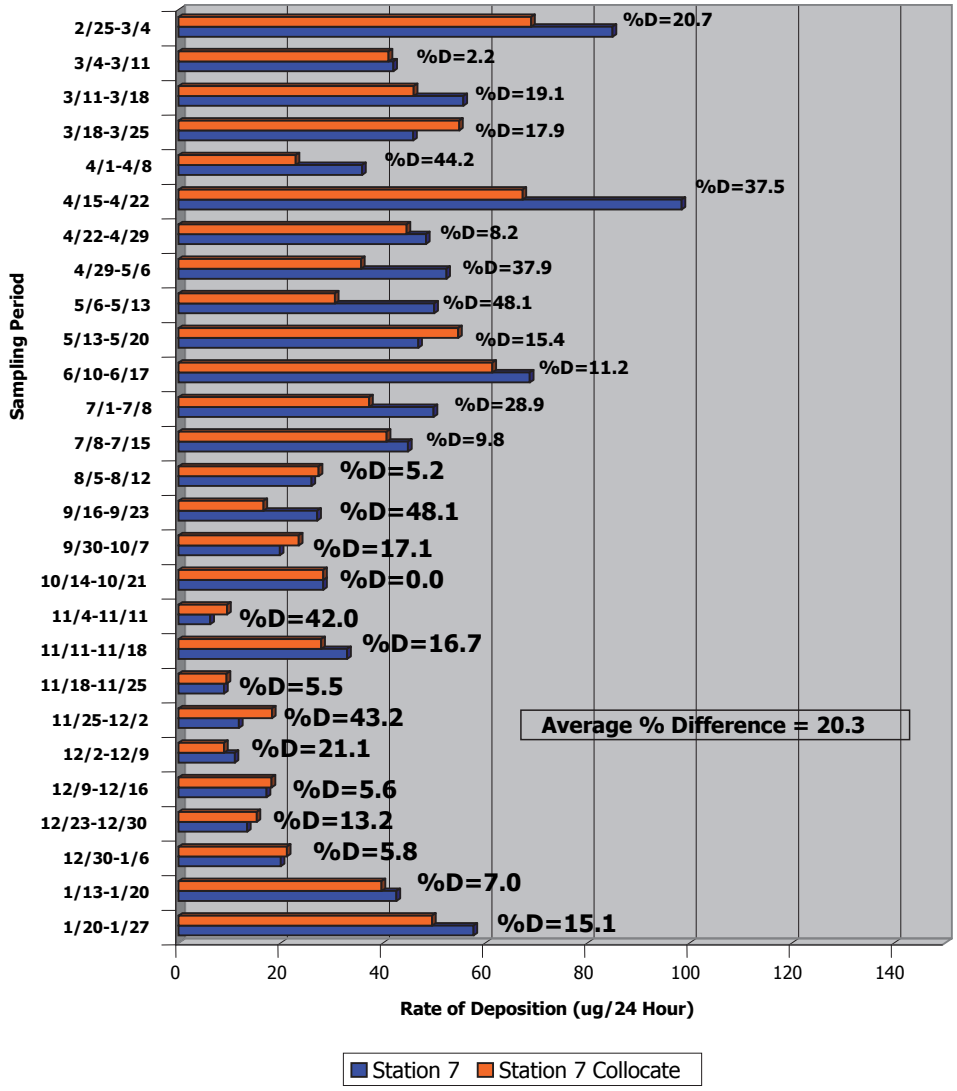

Fig. 4. Total Dust Fall Program Station 7 – Collocated Sample Precision Data – February 25, 2003 – January 27, 2004

The average % difference for the majority of the sites ranged from 20-25 %. The observed variability in the precision of collocated filter pairs is likely attributable to one or more of the following:

- Indicative of actual variability in particulate loadings collected by passive deposition on each of the samples in the pair. The filters although they are side by side are not truly collocated in the same air space and do not obviously occupy identical places on the horizontal collection surface.

- Indicative of host attentiveness to filter placement and perhaps filter deployment and recovery process. Two of the stations with the lowest average % difference data were the Berm (Station 7) and the Fire Station (Station 10). Filters at these stations were deployed and recovered by TRC personnel on a regular basis.
- Particulate loadings on the filters themselves were a factor. As with any sampling and analyses method as concentrations/gravimetric loadings decrease and approach the method sensitivity the variability in the measurement is higher. This is particularly true in comparison of data from Station 10 (Fire Station) to data collected at Station 6. The highest particulate loadings were observed at the Fire Station concurrent with one of the lowest average % difference values. Conversely, the lowest particulate loadings were observed at the Station 6 concurrent with the highest average % difference. This value approached 56 % for the complete data set.

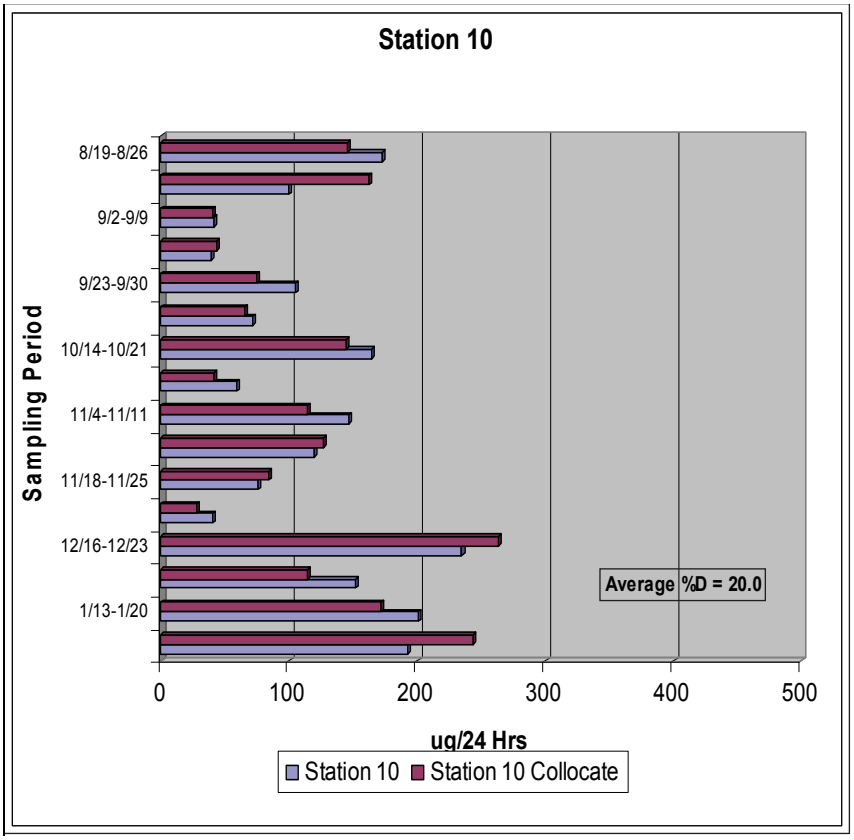

Fig. 5. Collocated Sampler Precision Data

The collocated sampler precision data were employed during this program to evaluate the validity of a particular sampling session. More specifically, if there was significant variability in the precision of collocated sampler data in a particular session (> 20-25 %) for

all sample pairs this would suggest that the samples and data from the affected session not be used in the program data set. As a result samples from a number of sampling sessions were deemed invalid and not incorporated into the final program data population and hence not used in subsequent data analyses. In instances where there was significant disparity in the gravimetric results from a single collocated pair the higher loading or concentration would be used for comparison to background. This represents a more conservative approach. In all cases where collocated filter data were deemed valid the two samples were averaged in representing the dust fall loading at a given site during all sampling events.

5. Conclusions

The use of Teflon filters coated with mineral oil represents a cost effective and reliable approach for passive collection and measurement of total particulate or dust fall. Field validation of this novel approach indicates that dusts can be collected quantitatively with little or no losses of dusts deposited on the filter surfaces attributable to field deployment and recovery as well as shipping and handling procedures. The overall precision of the sample collection and analysis procedure (as defined by collocated sampling devices) has been determined to be +/- 20-25% (RPD).

The filter sampling devices can be readily deployed and recovered at numerous locations simultaneously and require little operator training. As a result citizen participants represent candidate field sampling personnel for programs conducted in response to "nuisance dust" complaints. Since the method has been designed and optimized for the collection of passive particulate deposition particular attention must be paid to recovery of all filters prior to precipitation events or periods of inclement weather conditions.

The method was applied for monitoring of "nuisance dusts" in an Eastern United States urban setting in which a coal fired power plant was located. The results of this field program conducted during the calendar period February 2003 - February 2004 indicated that background concentrations for total dust fall in the subject metropolitan area were in the range of 65-70 ug/24 hr (based upon surface area of 47mm Teflon filter).

Field samples are readily suited for gravimetric analyses as well as other non destructive analytical procedures for use in forensics analyses of particulate deposited on the filter surface. These applications include qualitative and semi-quantitative elemental analyses (XRF) as well as microscopic examination (PLM, TEM and SEM). Further analyses such as these can prove valuable in a determination of the sources or origins of the particulate matter deposited on filter surfaces.

6. References

Wheeler, J.P. and J.P. Stancliffe, 1998. Annals of Occupational Hygiene: 42(7), pp 477-488

Byrne, M.A., 2000. Annals of Occupational Hygiene: 44(7), pp 523-528

Estokova, A, N. Stevulova and L. Kubincova, 2010. Global NEST: 12(1), pp 20-26

ASTM D-5438-05, 2005. Standard Practice for Collection of Floor Dust for Chemical Analysis. American Society of Testing and Materials, Philadelphia, USA

ASTM D-1739-98, Reapproved 2004. Standard Test Method for Collection and Measurement of Dust Fall (Settleable Particulate Matter). American Society of Testing and Materials, Philadelphia, USA.

ASTM D6966-08. Standard Practice for Collection of Settled Dust Samples using Wipe Sampling Methods for Subsequent Determination of Metals. American Society of Testing and Materials, Philadelphia, USA.

James P. Lodge, Jr, Editor Lewis Publishers, 1989. Particle Fallout Container Measurement of Dust Fall from the Atmosphere in Methods of Air Sampling and Analysis, Third Edition.

Dzubay, T. and R. Barbour, 1983. Journal of The Air Pollution Control Association: 33(7), 692

5

Characterization of Particles Transmitted by Wind from Waste Dump of Phosphatic Fertilizers Plant Deposited on Biological Sample Surfaces

M.I. Szynkowska, A. Pawlaczyk and J. Rogowski
Institute of General and Ecological Chemistry, Technical University of Lodz, Łódź, Poland

1. Introduction

There are many methods available aiming at studying atmospheric contamination but often their application is limited by problems connected with sample preparation difficulties or an insufficient amount of material for analysis. Therefore, there is an increasing necessity of applying methods which enable a direct solid sample characterization and provide information concerning the state of environmental pollution (Szczepaniak&Biziuk, 2003). Surface analysis techniques have become more and more widely used in recent years and their rapid development since 1970s has resulted in many applications including probing physical and chemical properties of surface. The thickness of the studied surface layer depends upon the method employed and varies from a few uppermost layers to several microns deep (Robinson, 1995; Szczepaniak&Biziuk, 2003; Szynkowska, 2005). Scanning electron microscopy with energy-dispersive X-ray analysis (SEM-EDS) and time-of-flight secondary ion mass spectrometry are powerful methods allowing a direct observation, comparison and characterization of different spectrum of materials. What is more, a large depth of field gives an opportunity to investigate even three-dimensional objects, which is especially significant in observation of usually very heterogeneous biological samples (Goldstein et al., 1992; Seyama &Soma, 2003; Seyama, 2003; Szynkowska, 2005). The techniques mentioned above are considered a relatively fast and basically non-destructive approach, which can be successfully used as a complementary method to the wet chemical analysis requiring sample homogenization and dissolution (Kempson&Skinner, 2005; Szynkowska et al., 2008a; Szynkowska et al., 2008b; Williamson et al., 2004). Additionally, XRD technique can be applied in environmental monitoring research to identify crystalline phases of studied samples.

Phosphogypsum deposited in the phosphatic fertilizer waste disposal place in Wiślinka near Gdańsk (Northern Poland) is a main by-product of a wet process of phosphoric acid production. During the wet process phosphoric acid is produced by the reaction of phosphate rock with sulfuric acid, and then used for the production of phosphatic fertilizers. Phosphoric acid and phosphogypsum obtained in the wet process contain a number of impurities like calcium sulfate dehydrate and HF. For every ton of phosphoric acid obtained even up to 5 tons of this waste by-product are produced. The chemical

composition of by-products and the quantity of impurities depend on the origin of the phosphate rock used in the phosphoric acid industry as well as the dissimilarities in the parameters of the process plant operation or the age of phosphogypsum.
Dumping of phosphogypsum into open air can create environmental and health concerns as the piled material, dominated mainly by calcium sulphate dehydrate (94-98% wt.), contains approximately up to 5-6% of many impurities including heavy metals, fluoride and radionuclides, which have been identified as a potential environmental hazard. These toxic substances can be transported by wind over long distances or percolate through the dump and, in consequence, contaminate soil or groundwater. This continuous process may lead to the increase in the content of spread substances in various components of our environment and can be built into the food chain. Therefore, more detailed studies are necessary in order to fully understand the transfer process of toxic substances into the adjacent environment and to assess their impact (Al-Masri et al., 2004; Arocena et al., 1995; Rutherford et al., 1995).
The increasing awareness about possible negative effects caused by elevated levels of toxic substances not only in air, water or soil, but especially in biological material has caused a huge development of plant studies as a complementary tool to instrumental methods. The amount, size or composition of trapped surface material depend on many factors, e.g. distance from the source of pollution or wind strength. The surface characterization of biological samples using SEM-EDS and ToF-SIMS methods could be especially helpful in understanding where and how airborne particulate matter becomes incorporated into or is lost from the plant matrix as well as to assign a specific type of particles to their potential origin (Kempson&Skinner, 2005; Szynkowska et al., 2008b). SEM-EDS and ToF-SIMS are versatile tools particularly used for morphological and chemical characterization of various materials, which cover a number of areas of application. Nowadays they are employed, for example in environmental and forensic researches, due to their unique properties such as almost a non-destructive analysis and a relatively small amount of sample required. XRD analysis can be used to identify crystalline phases in various phosphate rock and phosphogypsum samples.
The main objective of this chapter was to investigate the possible occurrence of dusting process by analyzing the atmospheric particulates accumulated on the biological surface and to compare them with the particles characteristic of phosphogypsum waste by-product. The other objective of this study was to compare the usefulness of applied methods (SEM-EDS, ToF-SIMS, XRD) as a complementary tool for the assessment of air pollution.

2. Material studied

Biological samples were collected from the area near Gdańsk (Northern Poland), where a huge phosphogypsum waste disposal site is located. In general, the state of pollution of this rural area is affected mainly by the presence of phosphate stack, where approximately over 16 mln tons of phosphogypsum are deposited. In order to correlate the composition of the material deposited on various biological indicators, different phosphogypsum samples as well as phosphate rocks were investigated. The studied rock material comes from Tunisia, Morocco and Syria.
The studied material consists of samples of moss and lichen taken from the neighborhood of a phosphate waste disposal place as well as various phosphogypsum samples (fresh, old, recultivated) stored in the dump and phosphate rock material used in the process of phosphoric acid production. For comparison purposes moss and lichen material was also

collected from a clean area, not affected by any industrial or environmental activity (Lodz city, Lagiewniki Forest).

3. Methods

Scanning electron microscopy with energy dispersive X-ray spectrometer, SEM-EDS (Hitachi, Japan; Thermo Noran, USA) and time- of- flight secondary ion mass spectrometer ToF-SIMS IV (ION-TOF GmbH, Germany) were applied for particle distribution studies and an identification of type and composition of airborne particulate deposited on samples and present in the stored by-product.
Before the SEM-EDS measurements, the samples were placed on carbon plasters and coated with carbon target by Cressington 208 HR system. SEM micrographs, EDS spectra from the single points and chosen microareas and maps showing elemental composition and surface distribution were obtained using the SEM-EDS method. The accelerating voltage was 25 kV. The ToF-SIMS positive and negative spectra and images were carried out using ToF-SIMS IV spectrometer equipped with 25 keV bismuth primary ion gun. Primary ion beam current was set to 0.5 pA during analysis. Flood gun was used to compensate for the surface charging during analysis. In the case of phosphogypsum and phosphate rock, the samples were pressed into tablets in order to gain better mass and lateral resolution.
The phase composition of biological, phosphate rock and phosphogypsum samples was examined using polycrystalline difractometer X`PERT PRO MPD (PANanalytical) equipped with a copper tube. HighScore Plus software and PDF-2 database were used for the phase identification.

4. Results and discussion

The study was dedicated to verify a possible existence of the emission of dumped material spread by wind into the adjacent environment based on the examination of particulate matter deposited on lichen and mosses samples.
At present SEM-EDS and ToF-SIMS techniques are more and more commonly applied to study particles present on the surface of various biological material as complementary methods to the wet quantitative chemical analysis for an identification of the source of pollution making it possible to distinguish exogenous elements from internal ones. In our studies they were used to provide information about phosphogypsum chemistry, composition and a possible impact on living organisms.
SEM-EDS maps of elemental distribution on phosphogypsum surface revealed many impurities besides main gypsum ingredients. The elements such as S, O, Ca, Na, K were quite regularly distributed over the surface of waste. Gypsum formed characteristic geometric sticks resembling posts with the grain size of 20-200 μm. Additionally, some amount of much smaller size particles, rather spherical and attached to much bigger gypsum grains and rich in Al, Si (over 2.5 μm), mainly enriched in F (below 2.5 μm), and containing Ba (around 2.5 μm) and Sr (even below 1 μm) were observed on EDS maps (Fig. 1). Moreover, SEM-EDS spectra collected from single points of phosphogypsum surface showed other impurities of this waste e.g. the presence of Fe, Mn or P, which were not detected on EDS maps performed for whole microareas. It should be pointed out that a potential detection limit of SEM-EDS analysis is about 0.1-0.5 wt. % for most elements. The results obtained from the microscope also indicated some differences among samples taken

from various parts of the dump, probably caused by a various phosphate rock source and a general decrease in metal intensity during the waste storage. This finding stays in agreement with literature data. There is a general consensus that the content and composition of waste by-product impurities depend mainly on the origin of phosphate rock (besides the type of the wet process applied or efficiency of factory operation) (Arocena et al., 1995; Rutherford et al., 1995; Williamson et al., 2004).

Stockpiled phosphogypsum in Wislinka is derived from various types of phosphoric rock originating mainly from Tunis, Buckra and Togo or Morocco. However, some elements like Sr, Ce or W were observed in higher amounts in fresh samples. Furthermore, EDS spectra demonstrated that a recultiveted sample presents a higher content of e.g. Ba, Pb, Cd and they were in contrast to other phosphogypsum material. Since 2001 the recultivation process with sewage sludge from the mechanical-biological treatment plant (consisting domestic and industrial sewage) has been applied in the considerable part of the disposal place in order to expand luxuriant vegetation, which possibly changed the sanitary conditions and loads of metals.

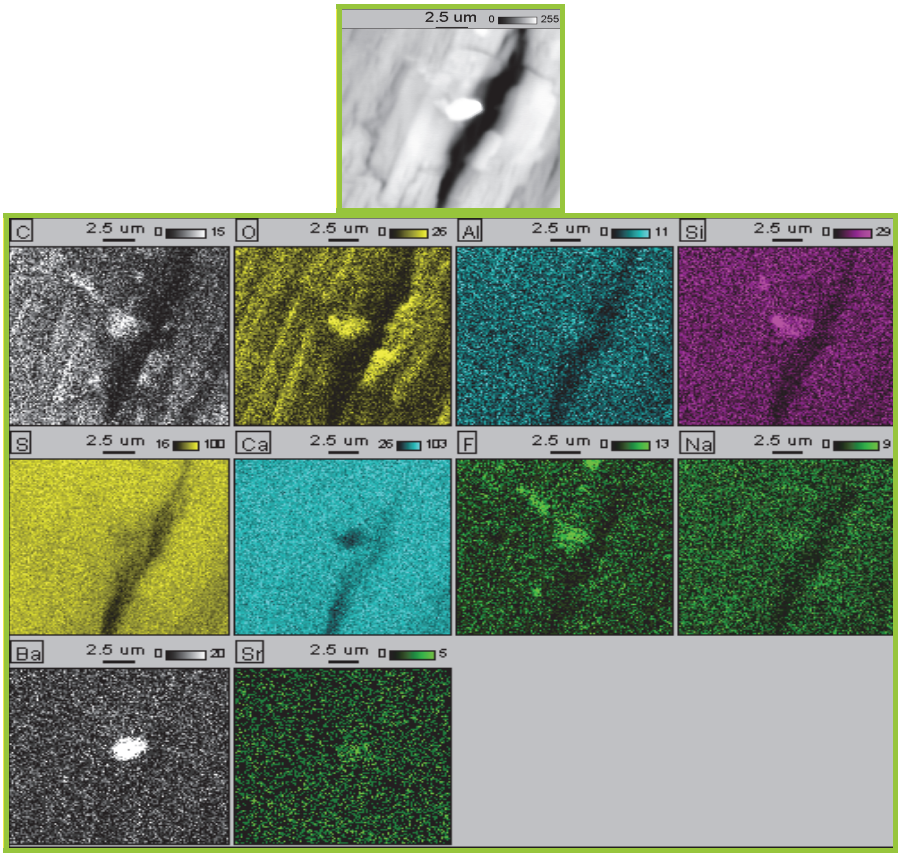

Fig. 1. SEM-EDS micrograph and maps of distribution of elements on the surface of phosphogypsum (x8000)

The ToF-SIMS analysis showed that phosphogypsum can be characterized by the following characteristic secondary ions: $CaOH^+$, Ca_2O^+, $CaPO_2^+$, $Ca_2O_2^+$, $CaPO_3^+$, CaH^+, CN^-, CNO^-, Cl^-, SO^-, PO_2^-, SO_2^-, PO_3^-, SO_3^-, SO_3H^-, SO_4^-, SO_4H^- and SiO^- (Fig. 2). Generally, among phosphogypsum contaminants enhanced levels of fluorine were identified as potential environmental hazards, which restricts its utilization as building materials or agricultural fertilizers. The wastes stockpiled in Wislinka contain about 0.2-0.3% of soluble fluorine compounds. Moreover, this part of Poland is located in the area with significantly high fluoride concentrations in water of natural origin. A potential leaching process of these impurities may cause their further transfer into the adjacent environment and, in consequence, to the food chain. Summarizing, the obtained information concerning the composition and chemical properties of phosphogypsum is incredibly important from the point of view of the waste management decisions and environmental or health risk assessments.

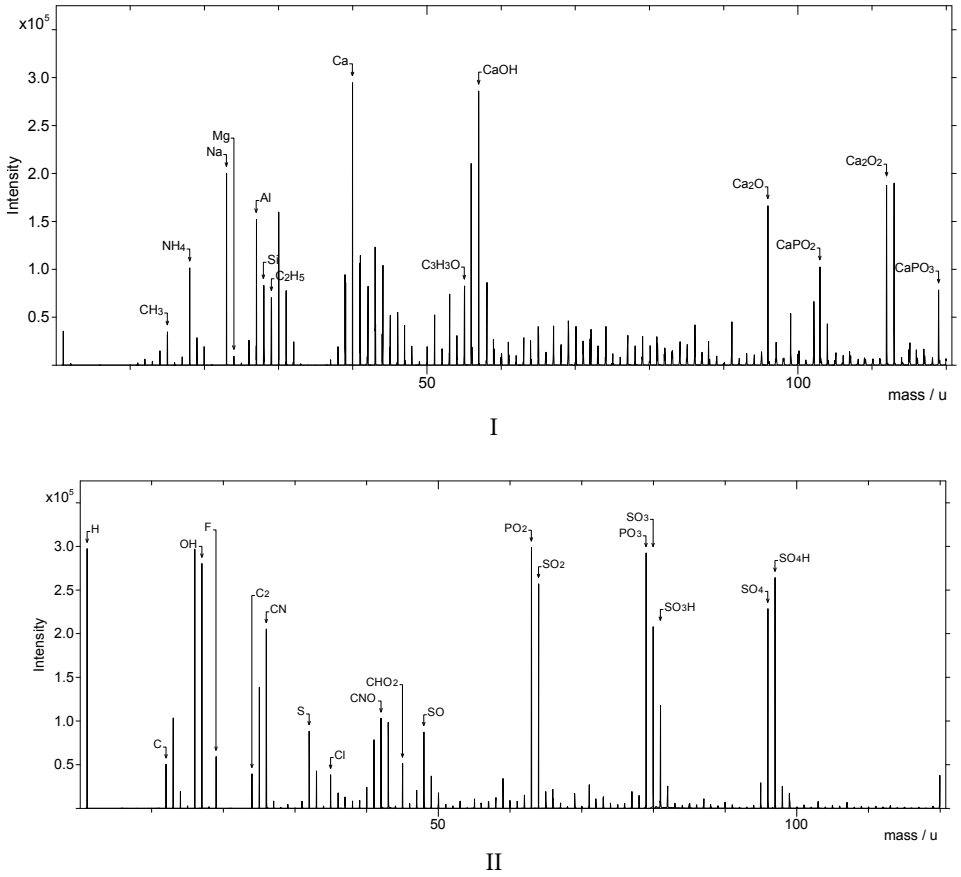

Fig. 2. ToF-SIMS positive (I) and negative (II) ion spectra of phosphogypsum from Wiślinka

The results of analysis of phosphogypsum particles on moss and lichen surfaces revealed that the composition of analysed phosphogypsum material corresponds to the chemical composition and morphology of particles deposited on biological samples collected from the vicinity of a phosphatic fertilizer dump. There is a well-known fact that elevated concentrations of heavy metals in bioindicators such as lichens in the surroundings of industrial areas are caused mainly by trapping the relatively large particles. This caught particulate matter may remain within the surface over a long time or may be solubilised by e.g. acid precipitation (Kempson&Skinner, 2005). SEM-EDS analysis of the particulate matter deposited on the surface of chosen biological samples (moss, lichen) showed apart from the posts typical of gypsum containing mainly Ca, O and S also considerable amounts of particles with the size and composition corresponding to waste impurities identified earlier on the phosphogypsum surface. The grain size can be classified mostly to a very fine fraction below 5 μm (Figs. 3-5). The presence of small Fe-rich spherical shaped particles may originate from both the dusting process and high-temperature combustion process. What is more, some irregular particles exceeding 50 μm were also found on the biological surfaces (Fig. 4). These enriched in P, O and Si contaminants may be a trace of a wet process of phosphoric acid production.

This work shows that the inhomogenous dispersion of the studied particulate matter on the surface of bioindicators strongly depends on the distance from the waste disposal site. The presence of many windblown air contaminants on the studied surface of biological samples collected in the vicinity of a dump area reflects the level of pollution of this relatively rural area. It was clear that the amount of anthropogenic dust on the biological surface is increasing towards the dump. Therefore, its presence at considerable distances from the dump can prove that there exists a dusting process form the waste disposal place, which can pose a health hazard to the inhabitants by potential inhalation of fine fraction material, which is transported by wind over great distances and contains toxic substances including fluorine and heavy metals.

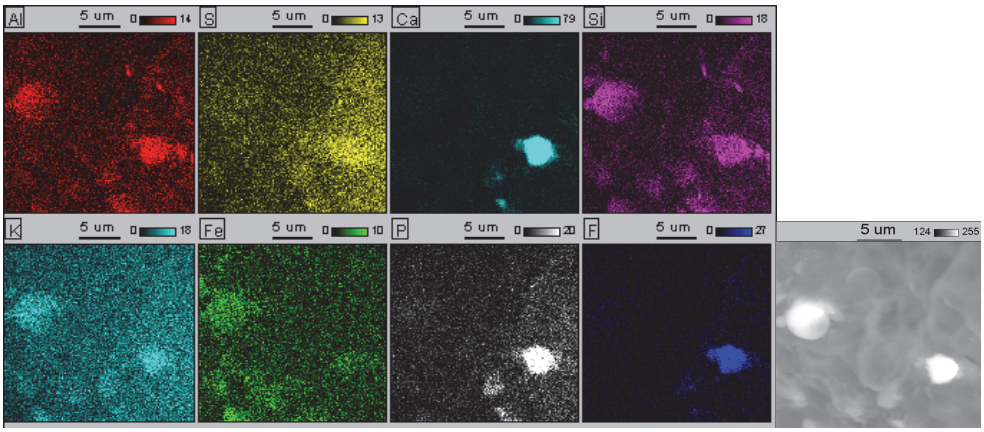

Fig. 3. SEM-EDS micrograph and maps of distribution of particles deposited on lichen surface (x6000). Particles rich in Al, S, Ca, Si, K, Fe, P, F are present.

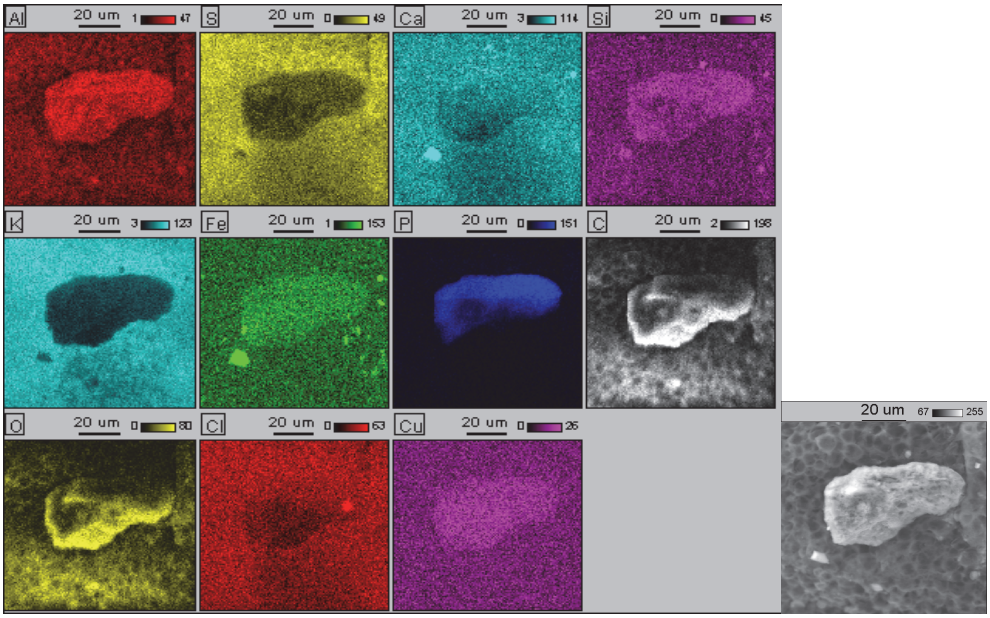

Fig. 4. SEM-EDS micrograph and maps of distribution of particles deposited on lichen surface (x1500). Particles rich in Al, Ca, Si, Fe, P, O, Cl , Cu are present.

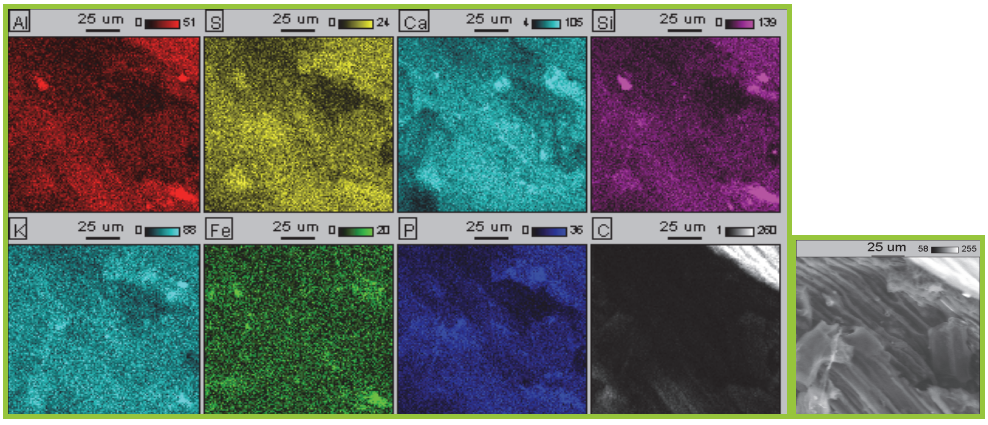

Fig. 5. SEM-EDS micrograph and maps of distribution of particles deposited on moss surface (x1000). Particles rich in Al, S, Ca, K, Fe, P are present.

ToF-SIMS analysis showed that the particles on the studied surfaces of moss and lichen samples are characterized by an emission of the following secondary ions: Na^+, Mg^+, Al^+, Si^+, K^+, Ca^+, $CaOH^+$, Fe^+, $CaPO_3^+$, F^-, CN^-, S^-, Cl^-, PO_2^-, SO_2^-, PO_3^-, SO_3^-, SO_4^-, SO_4H^- (Figs. 6, 7). The material of probable airborne source consisting mainly of P or S was characterized by their substantial sizes and amorphous shapes in contrast to other contaminants.

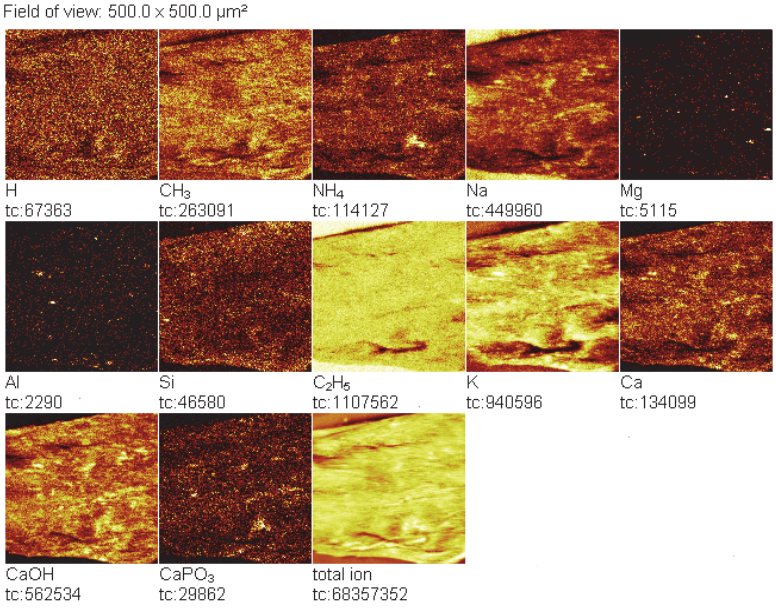

I

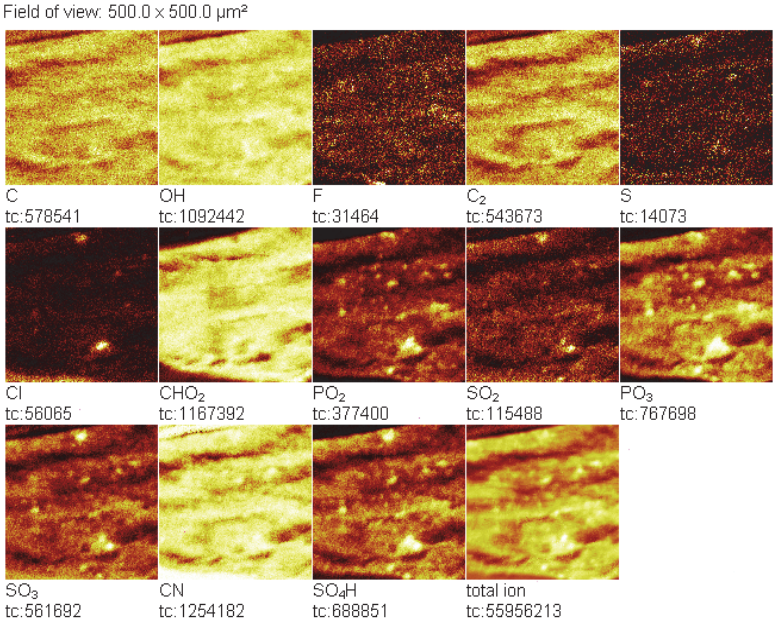

II

Fig. 6. ToF-SIMS positive (I) and negative (II) ion images of moss from Wislinka

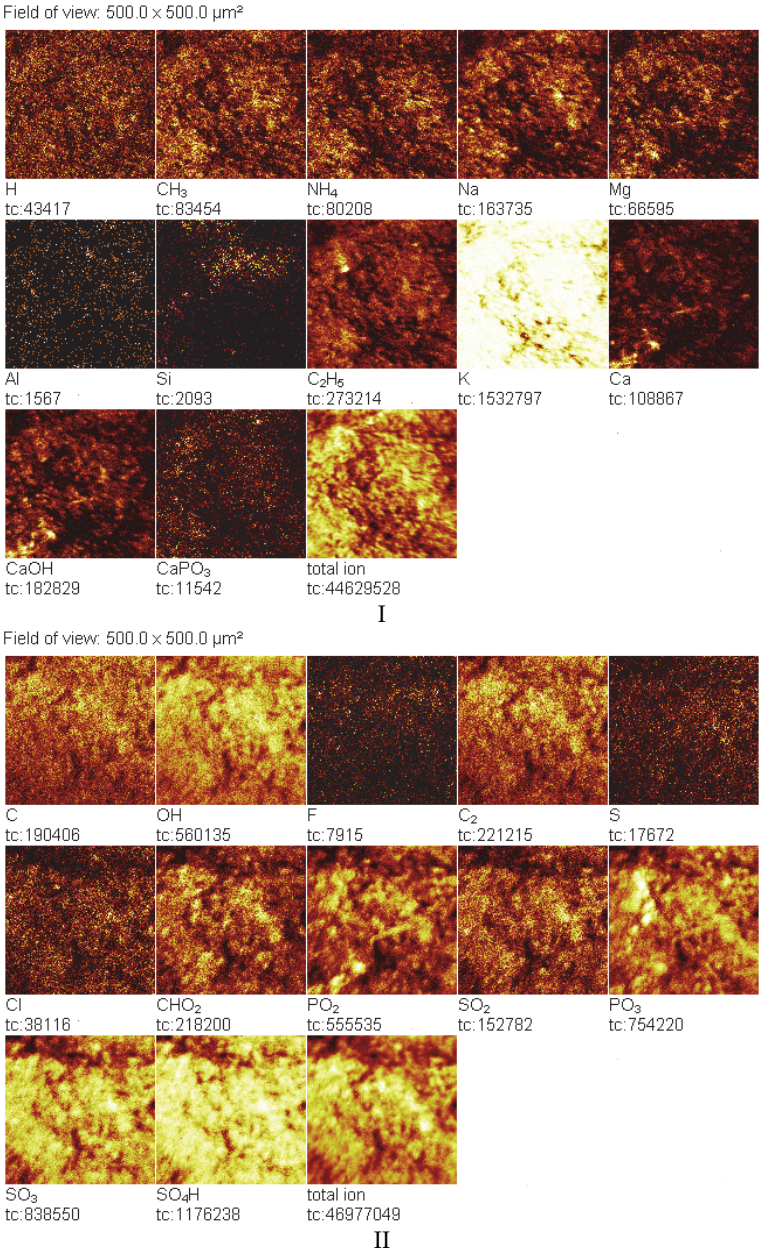

Fig. 7. ToF-SIMS positive (I) and negative (II) ion images of lichen from Wiślinka

In order to get a better insight into the process of air industrial contamination, also samples coming from unpolluted places were examined. In general, their surfaces were not covered

with any deposited particles of anthropogenic origin. Figures 8 and 9 present for comparison ToF-SIMS positive and negative ion images of moss and lichen, respectively from the control site and ecologically clean area.

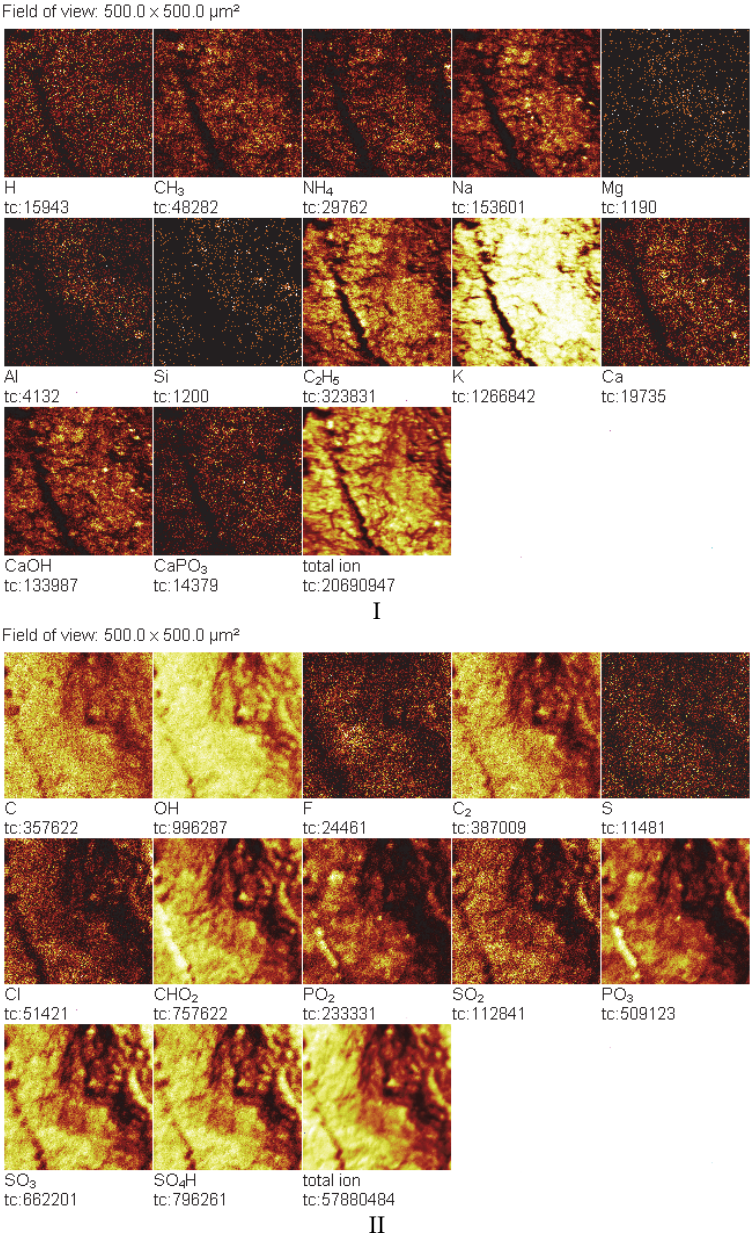

Fig. 8. ToF-SIMS positive (I) and negative (II) ion images of moss from the control site

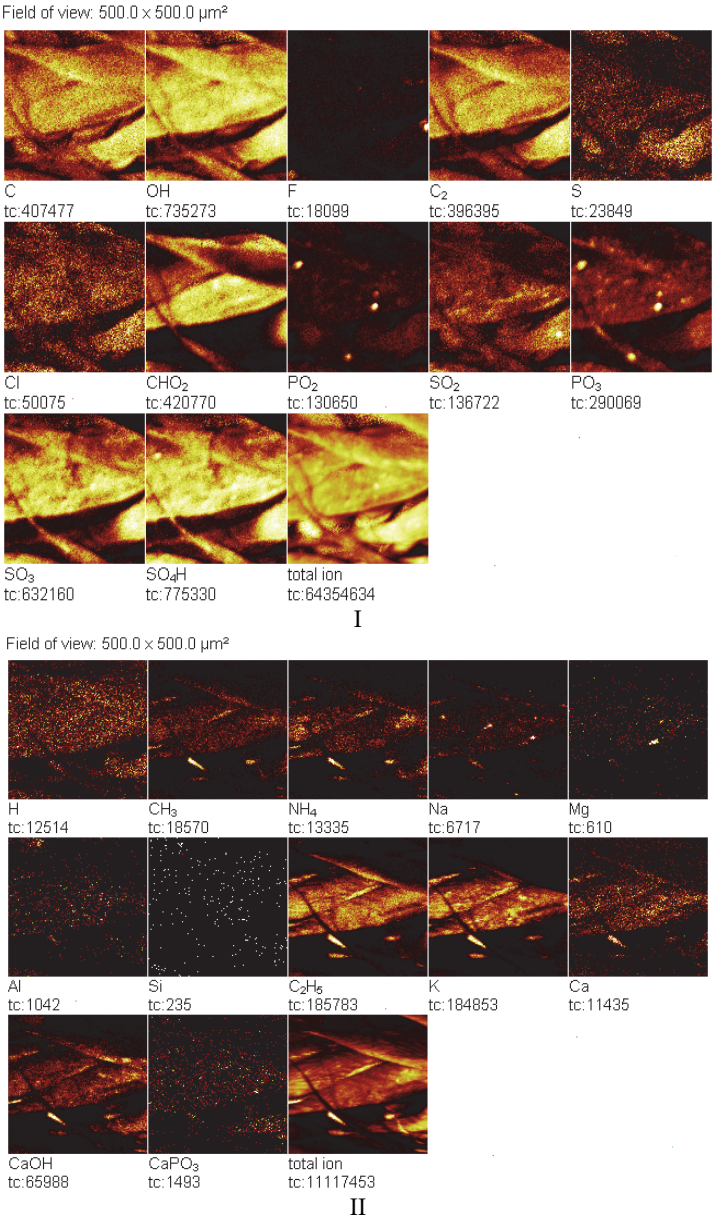

Fig. 9. ToF-SIMS positive (I) and negative I (II) on images of moss from the control site

The obtained ToF-SIMS spectra showed that the peak intensities of Ca^{+}, and PO_2^{-} ions characteristic of gypsum are significantly different for moss and lichen samples collected from the polluted and control sites (Fig. 10). These results confirmed that the phosphate waste disposal place has an impact on the surrounding environment.

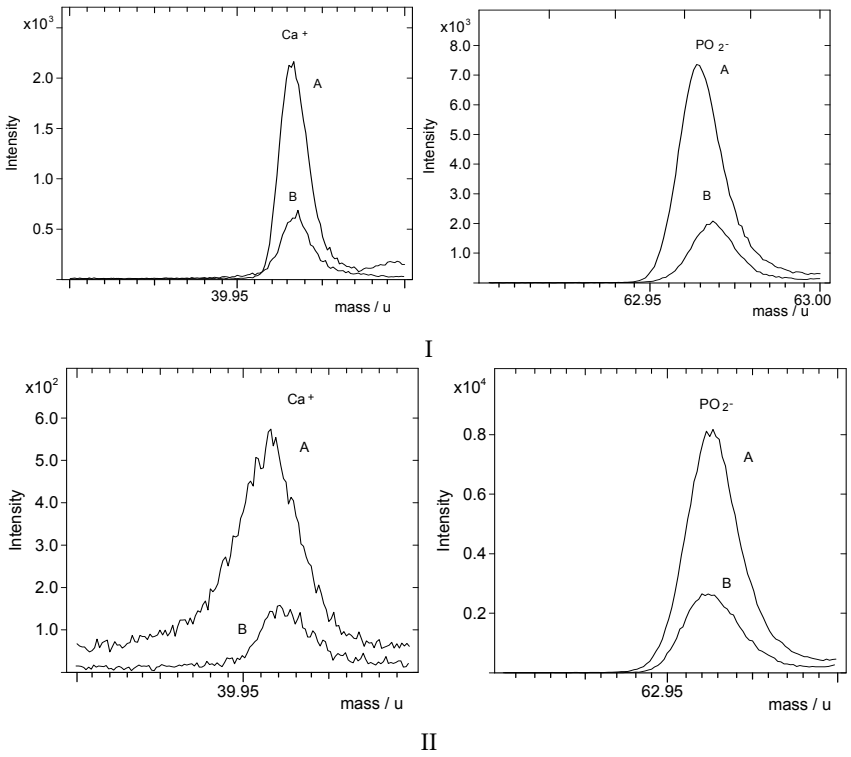

Fig. 10. Ca^{+}, and PO^{2-} ion peaks from the ToF-SIMS spectra of the moss (I) and lichen (II) from Wiślinka (A) and from the control site (B), respectively

The analysis of crystalline phases of different phosphogypsum samples confirmed that this waste by-product is mainly composed of calcium sulfate dihydrate. Additionally, for comparison purposes four phosphogypsum samples obtained directly from the production line and originating from Morocco, Syria, Tunisia and Kola phosphate rocks were investigated. Three of them were formed as a result of the dihydrate method of production of phosphoric acid (Morocco, Syria, Tunisia), while only one sample was created by the hemihydrate process. In general, all gypsum samples show almost the same crystalline composition with minor exceptions. Anhydrite ($CaSO_4$), bassanite ($CaSO_4 \cdot H_2O$), CaO, $CaPO_3(OH) \cdot 2H_2O$ (brushite), SiO_2, Fe_3O_4, H_3PO_4, $SrSO_4$, Na_2SiF_6, $Na_5Fe_3F_{14}$ were present on diffraction patterns (Fig. 11). The results show as well that magnetite was detected only in samples from Tunisia and Syria, whereas Na_2SiF_6 was detected in samples from Kola and Tunisia. $Na_5Fe_3F_{14}$ was detected in apatite-based phosphogypsum. No fluorine compounds were detected in the analysed samples because the XRD spectrum was dominated by the peaks of bassanite and gypsum.

Similarities observed in XRD spectra of older phosphogypsum collected directly from the stack and phosphogypsum obtained from Morocco phosphate rock suggest the same source of rock of both materials. Some amount of P_2O_5 or SiO_2 in phosphogypsum material identified with the XRD technique can be attributed to the residues of unreacted particles of

phosphate rock. Burshite is an apatite precursor, hence its presence in the phopshogypsum waste is not surprising.

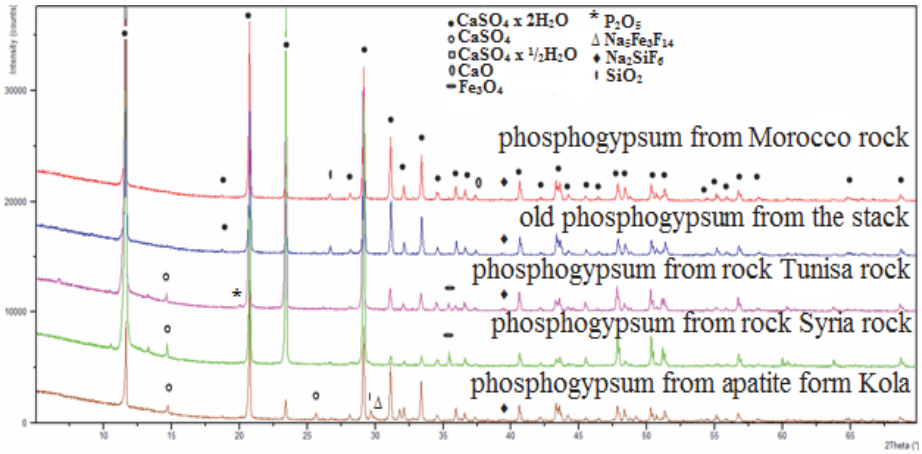

Fig. 11. Diffraction patterns of various phosphogypsum samples collected directly from the stack (old) with an unknown source of phosphate rock and obtained from the production line (originating from Morocco, Syria, Tunisia and Kola rocks).

In order to obtain information about the possible migration of phosphogypsum impurities into the environment, waste material was collected from different places of stack. The comparison of XRD patterns (Fig. 12) of two phosphogypsum samples proved that the composition is almost the same with hydroxyapatite, calcium sulfate dihydrate, bassanite (hemihydrate form) and anhydrite as main components. The only difference is the presence of celestine ($SrSO_4$) in the sample collected near the trench. The lack of celestine in the composition of fresh phosphogypsum can support the suggestion that the process of leaching of phosphogypsum contaminants and their subsequent transportation into the adjacent environment take place. In general, strontium, which is present in sedimentary formations, usually accompanies calcium and as a result of transformation of deposits enriched with Ca, strontianite is created ($SrCO_3$). Strontianite after the reaction with sulphur may form celestine. It is thought that this compound may pose a threat to the local environment by an excessive concentration of a highly soluble amount of strontium. Probably rain water, which flows down the stack surface, causes the accumulation of Sr in the trench surrounding the dump in the acid environment. Moreover, the distribution of this element is facilitated by the tendency of Sr to migrate to the surface formations. Some previous studies concerning the analysis of the level of selected elements in surface waters (Vistula River) confirmed that the samples collected in the vicinity of the waste dump contained an elevated concentration of Sr (Dembska et al, 2006). On the contrary, fresh phosphogypsum seems to be more enriched with H_3PO_4. According to literature, the increase in deposition time causes the decrease in acidity by washing out the residue of acids from the production of phosphoric acid (Nowak, 2006).

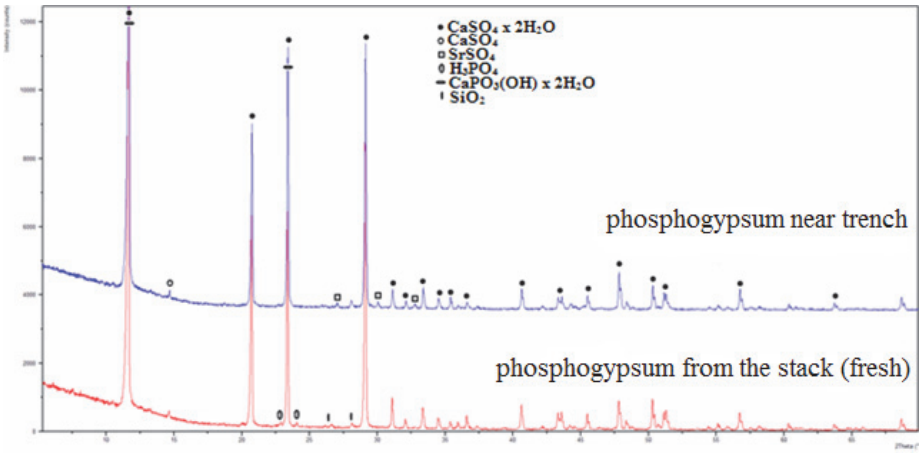

Fig. 12. Diffraction patterns of two phosphogypsum samples taken from the same area

XRD analysis showed that biological samples contain a limited amount of crystalline phases (Fig. 13). On the other hand, the XRD diffraction patterns did not confirm the existence of any compounds characteristic of deposited waste material on the surface of biological material taken from the area situated near the dump, probably due to a small amount of contaminants accumulated on the surface in relation to the whole sample. Generally, in the case of the biological material, obtained diffraction patterns revealed that quartz (SiO_2) was the main component.

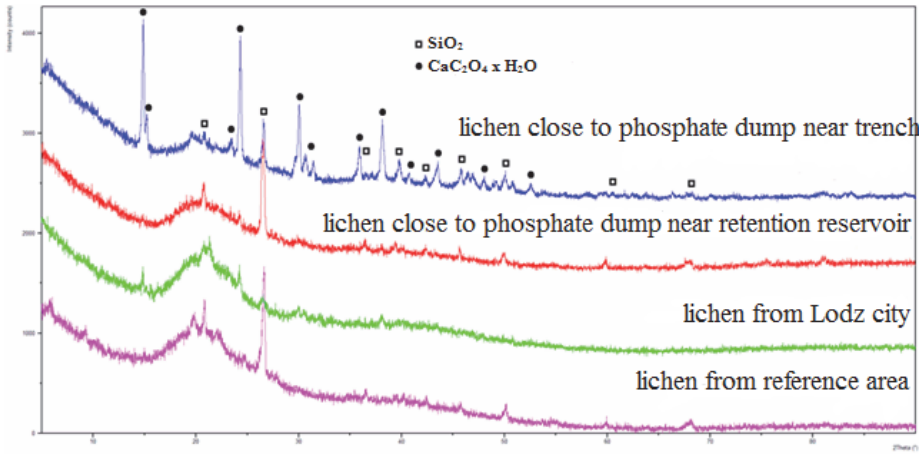

Fig. 13. Diffraction patters of lichen samples collected from the area situated in the neighborhood of the phosphate waste disposal place (near trench and retention reservoir), from urbanized Lodz area and from the reference clean site (Lagiewniki Forest).

The potential source of SiO_2 could be contamination from soil or fly ashes. Small differences observed on the diffraction patterns of various biological samples can be attributed to different forms of SiO_2 – crystalline and amorphous. Additionally, some biological samples

contained $CaC_2O_4 \cdot H_2O$ (whewelite). This organic mineral is created as a result of precipitation of calcium oxalates, leached from organic material and it does not seem to be specific for a sample collection place.
It should be emphasized that a detailed interpretation of XRD results was limited by a considerable amount of amorphous compounds present in the studied materials and other organic phases characteristic of plant material, whose identification was not possible due to the lack of adequate diffractive standards in the data powder base. Moreover, the detection limit of the technique used is above 0.5%, which limits the verification of the presence of trace components. Although, all analysed samples showed similar profiles of diffraction patterns, some essential differences among samples collected from ecologically clean areas, metropolitan area or the surroundings of waste disposal site were observed. The samples were collected after the recultivation process (the surface of stack was covered with a mixture of soil, grass seeds and sewage sediments), which could significantly reduce the effect of dusting on the local area.

5. Conclusions

The obtained SEM-EDS and ToF-SIMS results showed that the surface of biological material collected in the vicinity of the phosphatic fertilizer waste dump was covered with particles whose chemical composition corresponds to the chemistry and morphology of stockpiled waste by-product. The performed surface studies of biological material revealed that the observed particles showed various morphology (size and shape) but are characterized by similar chemical composition. It was found that gypsum is a main component of the analyzed particles with the admixture of Al, Si, K, Fe, Na, P, F, and S. The presence of elements and molecules typical of phosphogypsum and its impurities on the surface of biological indicators suggests that there exists a dusting process form the waste disposal place, which can pose a health hazard to the inhabitants by potential inhalation of the material carried by wind and containing toxic substances including fluorine and heavy metals due to the fact that many of the deposited particles consisted of the fraction less than 10 μm. Moreover, the degree of covering of the biological surface by anthropogenic dust decreased with the distance from the waste disposal site. This observation can suggest that the dusting process from the waste disposal place is responsible for the phosphogypsum contamination of phosphatic fertilizer dump neighborhood.
The XRD technique revealed significant differences between phosphogypsum material: fresh and older. Moreover, various phase composition in both phosphate rock and phosphogypsum was identified. X-ray diffraction patterns of phosphogypsum in general show mainly calcium sulfate dehydrate with impurities such as silicon oxide. In the case of phosphogypsum sample taken from the trench around the stack, in addition to the diffraction peak of gypsum, also calcium and strontium sulfate as well as phosphoric acid peaks were observed in comparison with the fresh material.
Phosphate rock was composed of fluorapatite, silicon oxide, calcite, magnetite or perovskite. It was also stated that during the time of storage, the acidity of waste by-product decreases to the deeper parts of dump due to the washing process. Moreover, the presence of strontium sulphate in fresh prosphogypsum may suggest that Sr can be introduced into the surrounding environment by the dusting process, while the content of this element in waste reaches even 1%. Unfortunately, it was not possible to detect compounds characteristic of stockpiled phosphogypsum on the surface of biological samples due to the low surface

concentration. It should also be emphasized that the samples were taken after the recultivation process with sewage sludge, which could considerably reduce the dusting process from the dump.
This study also showed a versatile application of ToF-SIMS and SEM-EDS methods as powerful tools for the identification of particulate matter on the surface of chosen biological samples as well as for the assignment of individual particles to their potential origin. Surface-analysis techniques make it possible to combine information about both changes of the surface of bioindicators and the state and source of environmental pollution. Our results also confirmed the usefulness of adapting moss and lichen samples (apart from their well known accumulation ability) as notable trapping organisms of mostly windblown airborne particles.

6. Acknowledgment

Authors thank to dr Joanna Bojarska from the Institute General and Ecological Chemistry at Technical University of Lodz for XRD measurements.

7. References

Al-Masri M.S., Amin Y., Ibrahim S., Al-Bich F., Applied Geochemistry 2004; 19, 747.
Arocena J.M., Rutherford P.M., Dudas M.J., The Science of the Total Environment 1995; 162, 149.
Dembska G., Grynkiewicz M., Wiśniewski S., Aftanas B., Wiadomości Chemiczne, vol. 2006, 60, 302.
Goldstein J.I., Newbury D.E., Joy D.C., Roming A.D., Lyman C.E., Fiori C., Lifshin E., Scanning Electron Microscopy and X-Ray Microanalysis, Plenum Press, New York, 1992.
Kempson I.M., Skinner W.M., The Science of the Total Environment 2005; 338, 213.
Nowak W., Rekultywacja biologiczna hałdy fosfogipsu w Zakładach Chemicznych Wizów S.A., Zeszyty Naukowe Uniwersytetu Przyrodniczego we Wrocławiu, vol. 545, 195-203, Rolnictwo LXXXVIII, Wrocław 2006.
Robinson J.W., Undergraduate instrumental analysis, Marcle Dekker, Inc., New York, 1995.
Rutherford PM., Dudas M.J., Arocena J.M., Waste Management and Research 1995; 13, 407.
Seyama H., Applied Surface Science 2003; 203-204, 745.
Seyama H., Soma M., Analytical Sciences 2003; 19, 487.
Szczepaniak K., Biziuk M., Environmental Research 2003; 93, 221.
Szynkowska M.I., Scanning Electron Microscopy. Encyclopedia of Analytical Science (Eds. P.J. Worsfold, A. Townshend and C.F. Poole), Elsevier, Oxford, 2005, pp. 134-142.
Szynkowska M. I., Pawlaczyk A., Paryjczak T., Polish Journal of Chemistry, 2008a, 82, 32.
Szynkowska M.I., Pawlaczyk A., Rogowski J., Applied Surface Science, 2008b, 255/4, 1165.
Williamson B.J., Mikhailova I., Purvis O.W., Udachin V., The Science of the Total Environment 2004; 322, 139.

6

Role of the Ionic Component and Carbon Fractions in the Fine and Coarse Fractions of Particulate Matter for the Identification of Pollution Sources: Application of Receptor Models

Pierina Ielpo[1], Claudia Marcella Placentino[2], Isabella Cafagna[2], Gianluigi de Gennaro[2], Martino Amodio[2], Barbara Elisabetta Daresta[2] and Alessia Di Gilio[2]
[1]*Water Research Institute – National Research Council*
[2]*Chemistry Department - University of Bari*
Italy

1. Introduction

Particulate matter (PM) is a very complex mixture of many inorganic and organic compounds of primary and secondary origin and this is the main reason why the desired reduction of its concentration and the identification of its many sources constitute a very difficult task. It is widely recognised that atmospheric particles are responsible for adverse effects on the ecosystem, the climate and the health of human beings (Pope & Dockery, 2006). Epidemiological studies have shown a consistent association of the mass concentration of urban air thoracic particles (PM10 particles with an aerodynamic diameter smaller than 10 μm), and its sub-fraction fine particles (PM2.5 particles with an aerodynamic diameter smaller than 2.5 μm), with mortality and morbidity among cardio-respiratory patients (WHO, 2005). Recent studies indicate that PM10 is associated to respiratory responses while PM2.5 may contribute to cardiovascular diseases (Wyzga, 2002). The chemical characteristics of the particulate fractions and biological mechanisms responsible for these adverse health effects are still unknown as well as the aerosol parameters (mass, particle size, surface area, etc) involved in the health impacts (Hauck et al., 2004). In addition, there is an indication that the increase in the atmospheric aerosol burden delays the global warming attributed to the increase in greenhouse gasses (GHG: CO_2, CH_4, N_2O, halocarbons). Whether the increase in GHGs since preindustrial times is producing a warming of 2.3 Wm^{-2},anthropogenic contributions to aerosols (primarily sulphate, organic carbon, black carbon, nitrate and dust) together produce a cooling effect, with a total direct radiative forcing of -0.5 Wm^{-2} and an indirect cloud albedo forcing of -0.7 Wm^{-2} (IPCC, 2007).

In recent years many studies have been carried out to determine the chemical composition of atmospheric particulate matter (Vecchi et al., 2007). Most of these studies were devoted to the identification of the main particle sources, with the purpose to identify viable strategies for their reduction. In this chapter we focus the attention mostly on the ionic component of

particulate matter. The ionic component of particulate consists in ionic species, soluble in water. Although this fraction has not a particular toxicological interest, it provides information about sources of PM. Also, the analysis of temporal trends of these chemical species considered as typical indicators of specific sources in given atmospheric conditions allows us to understand the emissions and the meteo-climatic conditions governing the particulate concentrations in atmosphere (Seinfeld & Pandis, 2006; Vardoulakis & Kassomenos, 2008). The ionic component of PM consists of sulfate, ammonium and potassium, which are found almost exclusively in the fine fraction (below 2.5 μm particulate size) while chloride, calcium, sodium and magnesium dominate in the coarse fraction (above 2.5 μm particulate size), and nitrate is present in both fractions (Wall et al., 1988).

The calcium, potassium and magnesium cations are associated mainly with oxides, hydroxides and carbonates. Their natural sources are the erosion and fragmentation of the rocks and the resuspension of dust by wind (Nicholson, 1988). The Sahara desert, for example, is a major source of natural dust in Europe, due to its proximity to Africa. In fact the coasts of countries bordering the Mediterranean basin may be affected by intrusions of Saharan air masses (Almeida et al., 2005; Querol et al., 2004). The dusts can be released into the atmosphere by resuspension and they can be carried at different altitudes (from sea to 4-6 km above sea level) across thousands of kilometers. Moreover, dusts can be generated by mining or construction activities. These sources are produced by human activities, therefore they are anthropogenic sources.

Sodium and chloride ions (and also magnesium), main constituents of sea salt, are in significant concentrations in particulate matter of marine origin (Seinfeld & Pandis, 2006). Potassium is used as a simple indicator of biomass burning (Andreae, 1983; Hays et al. 2005; Saarikoski et al., 2007). This last term includes natural fires, caused for example by lightning, but also fires due to human activities such as combustion of vegetation in agricultural practices to clean the soil; the combustion in domestic boilers, stoves or open fires for heating and cooking are other examples of biomass burning.

At present, the secondary inorganic particulate (SIA) is receiving a special scientific interest given that it can have a significant fraction of the total mass in PM, particularly in rural and natural background sites. The SIA consists mainly of ammonium sulfate and nitrate, obtained as a result of atmospheric reactions between the sulfuric and nitric acid with ammonia (Seinfeld & Pandis, 2006). Therefore, its precursors are sulfur dioxide, nitrogen oxides and ammonia. The SIA is not directly attributable to local sources, unlike the primary particulate. In fact, the contribution to PM from the single source of gaseous precursors is not clearly identified from the investigations on PM collected. This is because PM is distributed on a large spatial scale (regional). This is determined by the high formation and life time in the atmosphere of the SIA**,** and that leads to a temporal shift and spatial dispersion of the contribution locally released, resulting in an averaging of a number of contributions, mixed in a wider area. This typical feature of SIA, in particular of ammonium sulphate, makes very difficult to identify the origin of secondary particles.

Anthropogenic secondary ammonium sulphate is produced in large quantities by the oxidation of sulfur dioxide deriving from combustion of fossil fuels (especially coal). However, there is a natural contribution considering that the sulphate is directly released by marine aerosols and by erosion of rocks. Therefore, sulphate can have or primary origin either it can be the result of oxidation of sulfur dioxide derived from local or non-local production activities. Indeed, this species could be released in atmosphere from plants placed in remote regions, and reach the site investigated after transport over hundreds of

kilometers. Other potential sources are the oxidation of sulfur compounds with low number of oxidation (hydrogen sulfide, sulfides, sulfoxides, etc.) resulting from volcanic eruptions and landfills, or even derived from dimethylsulphate produced by some marine organisms. In particular, recent studies have shown that the sulphate in the PM present in many coastal regions of Europe and the Mediterranean area, could be due to atmospheric oxidation of dimethyl sulphide emitted by marine microorganisms (Ganor et al., 2000; Kouvarakis & Mihalopoulos, 2002; Luria et al., 1996; Meinrat & Crutzen, 1997; Mihalopoulos et al., 1997; Putaud et al., 1999;).

Experiments show that during summer there is an increase of sulphate compared to nitrate. Among the several reasons for this there are the reduction of emissions of nitrogen oxides, generally produced by domestic heating, the increase of photochemical activity, which would favor the conversion of sulfur dioxide to sulphate, or the possible contribution of marine biogenic source of sulphate, higher in peak productivity periods. Also the demonstrated losses of nitrate during the collection of PM (Schaap et al, 2004; Turpin et al, 2000), lower in the winter, can contribute to such result.

As already mentioned, in the countries of southern Europe the influence of Saharan desert (Saharan dust) is important, while other contributions such as natural re-suspension of dust, sea salt, biogenic sulfate may be relevant in high concentrations of PM, under specific meteo-climatic conditions. However, it should be considered that long-range transport (LRT) processes of anthropogenic particulate from the Center and Eastern Europe may have a significant influence on levels of PM observed in countries such as Italy (Abdalmogith & Harrison, 2005; Amodio et al., 2008; Güllü et al., 2005).

As already said, the ionic component of the PM constitutes a rich source of information necessary for the control of atmospheric concentrations of this pollutant.

Generally after the collection of particles on a suitable support, the ionic species are solubilized in deionized water (water subjected to processes reducing the ionic content) and analyzed by ion chromatography. This analytical technique allows to separate chemical species according to their different affinities for the ion exchange resin. The order of separation of ions allows the identification, while the concentration can be obtained by measuring of their electrical conductivity.

In addition to the traditional determination of ions in the PM, there are systems that allows to automatically collect the particles in the field, extract the ions and analyze them. These systems have the advantage to not accumulate the PM suspended in atmosphere directly on a filter. This prevents that chemical reactions between collected species take place and it avoids the difficulty of measuring a PM composition on the filter different from the actual one present in the atmosphere. When this occurs sampling artifacts take place. In sampling artifacts the ionic species involved are mainly nitrate, chloride and ammonium, because they form volatile salts. Another advantage of continuous measurement is the possibility to obtain the concentration data in continuous mode averaged in very small time ranges (eg. one hour, half hour or less). In this way information about the temporal evolution of these species is obtained, resulting in a better understanding and interpretation of the pollution phenomena.

The ionic component together with the organic one represents most part of particulate mass. Thus, to complete the general picture, it is necessary to introduce the carbonaceous species. They constitute a major fraction of atmospheric particulate matter. They are formed by organic matter (OM), elemental carbon (EC), and carbonate carbon (CC) (Birch & Cary, 1996; Chow et al., 1993, 2001).

The organic matter (OM) includes thousands of organic compounds (such as aliphatic, aromatic compounds, carboxylic acids and carboxylic compounds with polar substituents, etc) with widely varying chemical and physical properties. OM has both primary and secondary origin: the primary organic carbon is emitted directly by combustion, industrial, geological and natural sources. In particular, urban and industrial primary particulates OC are formed during fossil fuels' combustion and are emitted mainly as sub-micrometer particles. Primary biogenic OC aerosol sources consist of plant debris (cuticular waxes, leaf fragments), lipids, soot and humic and fulvic acids, different pollens and microbial particles, and their size distribution seems to be made up of both a fine and a coarse fraction (Artaxo & Hansson, 1995). Secondary organic carbon can be formed in the atmosphere from gas to particle conversion of semi- and low-volatility organic compounds either as result of the condensation of low vapour pressure volatile organics, when concentrations exceed saturation levels, or from physical or chemical adsorption of gaseous species on aerosol particle surfaces: this process that can happen in subsaturation conditions (Pankow, 1987). Elemental carbon(EC) has a graphitic-like structure and it is essentially a primary pollutant emitted directly in the particle phase during the incomplete combustion of fossil fuels and biomass carbonaceous fuels. In fact, the main sources of elemental carbon in the atmosphere are diesel vehicles (Rogge et al., 1991; Schauer et al., 1996, 2003) and it is emitted mainly as submicron fraction. Carbonate carbon in particulate matter consists mainly of the resuspended crustal material, such as desert dust, street abrasion and construction sites (Chow et al., 1993, 2001). While CC represents an important fraction of atmospheric PM10, it isn't a significant portion of PM2.5.

Carbonaceous species cause serious health effects and have significant impacts on the global radiation balance and on the global climate change through direct and indirect radiation forcing. About health effects all particles with a diameter of 10 μm or smaller are harmful because they can readily penetrate and deposit in the tracheo-bronchial tree reaching the lungs. When lodged in the lungs particles can act as adsorption sites for inhaled vapors and mists. Elemental carbon is an example of such a particulate. Carbon readily adsorbs hydrocarbons, including PAHs (Polycyclic Aromatic Hydrocarbons), on its surface and retains these toxicants in the lungs for periods of time far exceeding their usual residence time. Particles with diameters of less than 2.5 μm are particularly dangerous because they are small enough to reach the small airways and alveoli into the lung tissue, this finding was supported by various observations (Churg & Brauer, 2000).

Moreover, EC is the principal light-absorbing species in the atmosphere and it is one of the dominant species that result in the global warming (Dan et al., 2004; O'Brien & Mitchel, 2003) and visibility reducing (Martins et al., 1996; Na et al., 2004) by absorbing and scattering solar radiation.

Instead OC, play an important role in the formation of cloud condensation nuclei that lead to a higher albedo of cloud and finally to the global climate change (Dan et al., 2004; Hitzenberger et al., 1999). It is an effective light scattering and may contribute significantly to both visibility degradation and the direct aerosol climatic forcing (Malm & Day, 2000; Tegen et al., 1996;).

Developing effective control strategies to reduce the atmospheric concentrations of PM requires identifying sources and quantifying their contributions. One approach is to use receptor-based source apportionment models to distinguish sources. Much literature about different source apportionment techniques for airborne particulate matter is available (Currie et al., 1984; Dzubay et al., 1984; Gordon et al., 1984; Henry et al., 1984; Massart et al., 1997; Stevens & Pace, 1984).

The two main approaches of receptor models are Chemical Mass Balance (CMB) and multivariate factor analysis (FA). CMB gives the most objective source apportionment and it needs only one sample; however, it assumes knowledge of the number of sources and their emission pattern. On the other hand, FA attempts to apportion the sources and to determine their composition on the basis of a series of observations at the receptor site only (Henry, 1984). Among multivariate techniques, Principal Component Analysis (PCA) is often used as an exploratory tool to identify the major sources of air pollutant emissions (Bruno et al., 2001; Guo et al., 2004; Marcazzan et al., 2003; Thurston & Spengler, 1985). The great advantage of using PCA as a receptor model is that there is no need for a priori knowledge of emission inventories (Chio et al., 2004). The application of receptor models allowed to identify the number of the pollutant sources, their profiles and contributions.
In this chapter the application of PCA and APCS (Absolute Principal Component Scores) to the data set of chemical parameters (ions, organic carbon and elemental carbon) of PM2.5 and PM10 samples will be shown (Bruno et al., 2008; Caselli et al., 2006).

2. Chemical composition of fine and coarse PM fractions: results and discussion

The fine fraction is defined as the part of particulate matter sampled by the sampling head with cutting of 2.5 μm (PM2.5), while the coarse fraction of particulate matter is the weight given by the difference between PM10 and PM2.5.
In this chapter the chemical composition of fine and coarse fractions simultaneously collected in three sites of the Bari territory (South-East Italy) during winter and summer sampling campaigns will be discussed.

2.1 Sampling campaigns

Three sampling sites at different distances from the sea in the Bari province were chosen:
- Pane e pomodoro beach (P&P), a coastal site in Bari town;
- San Nicola sport stadium (SN), an urban background site of the Bari city;
- Casamassima (CS), an urban site of Bari province.

Pane e pomodoro beach sampling site is situated in the South of Bari and the particulate sampling system unit was placed at 10m from the sea.
San Nicola sport stadium site is placed at 5.2 km from the city center and 5.7 km from the sea, in south-west direction (see figure 1).
Casamassima site is located at 15 Km from Bari, 15.5 km from P&P beach site; the angular distances of the sites are shown in figure 1.
All the considered sampling sites are affected by urban and semi-industrial human activities, although in different way.
Two sampling campaigns were performed during the winter (from 10th to 27th March 2007) and the summer (from 14th June to 5th July 2007) in the three sampling sites.
Low-volume particle samplers (FAI Instruments model Hydra Dual sampler, Roma, Italy) were used to collect PM2.5 and PM10 samples. PM2.5 samples were collected on quartz fiber filters, while PM10 samples were collected on polycarbonate membranes. Both the filters were weighed, before and after the particulate sampling, by a microbalance with the smallest scale division of 0.0001 mg (Sartorius series Genius). The relative humidity (RH) and temperature in the weighing room were 44 ± 7 % and 22 ± 3 °C.

Fig. 1. Satellite map of the three sampling sites

A quarter of each sample (PM2.5 and PM10) was extracted, in two step, with 10 ml of deionized water for 20 minutes using ultrasonic agitation. These solutions were analyzed by ion chromatography to obtain the following ions Cl^-, NO_3^-, SO_4^{2-}, $C_2O_4^{2-}$, Na^+, NH_4^+, K^+, Mg^{2+} and Ca^{2+}. Organic carbon (OC), elemental carbon (EC) and carbonates (CO_3^{2-}) analysis were performed on rectangular punches of filter deposit of PM2.5 by a thermal optical method (Sunset Laboratory Inc, Tigard, OR, USA) (Amodio et al. 2008).
On PM2.5 and PM10 samples collected during the summer campaigns ions and OC, EC and CO_3^{2-} analyses were performed. On PM10 samples collected during the winter only ions were determined.

2.2 Fine fraction of samples collected in Pane e Pomodoro sampling site

For the samples collected in P&P beach site the comparison between the daily concentration trends of each species and PM2.5, showed a different behaviour during the winter campaign than the summer one.

In wintertime PM2.5 concentration showed high correlation with EC, OC, oxalate, and ammonium sulphate (r values ranging from 0.98 to 0.93). The correlation is quite high with nitrate and potassium (r values among 0.85 and 0.82), while it is much lower with magnesium, calcium and sodium chloride. It is well known that sulphate, ammonium and nitrate are typical components of secondary particulate matter; EC is considered as a tracer of primary emissions, mostly of vehicular traffic; OC originates as a part from primary sources and part from secondary aerosols formation processes. Thus in the samples collected during the winter the PM2.5 is mostly composed of secondary aerosol and primary aerosol resulting from combustion processes. During the winter the correlation between sodium and chloride concentrations is 0.30, while their average concentrations ratio is 0.44, a value very far from that characteristic one of sea water. Only the PM2.5 sample collected on 17th March shows a ratio getting up to the theoretical value (1,8) (Almeida et. al,. 2005). It 's interesting to note that during this day the wind blew with average speed of 3m/s from east-northeast for 53.33.% of the day (LIBD airport site). During the summer campaign the correlation between PM2.5 and the other species concentrations showed values lower than those of the winter campaign, except for calcium, magnesium and sodium, although the correlation of all elements didn't exceed the value of 0, 54.

Considering the correlation between single cation and anion, the ammonium and sulphate concentrations correlation does not change from winter to summer, keeping high values in both seasons (0.97 and 0.98, respectively).

The correlation between ammonium and nitrate concentrations decreases noticeably from winter to summer from 0.94 to -0.14 respectively. By expressing the analyte concentrations in nano equivalent, their different value between summer and winter samplings becomes more evident. During the winter, the daily data of individual samples and their average, have showed that the sum of the cations averages (104neq/m^3) is less than the sum of the anions averages (127neq/m^3).

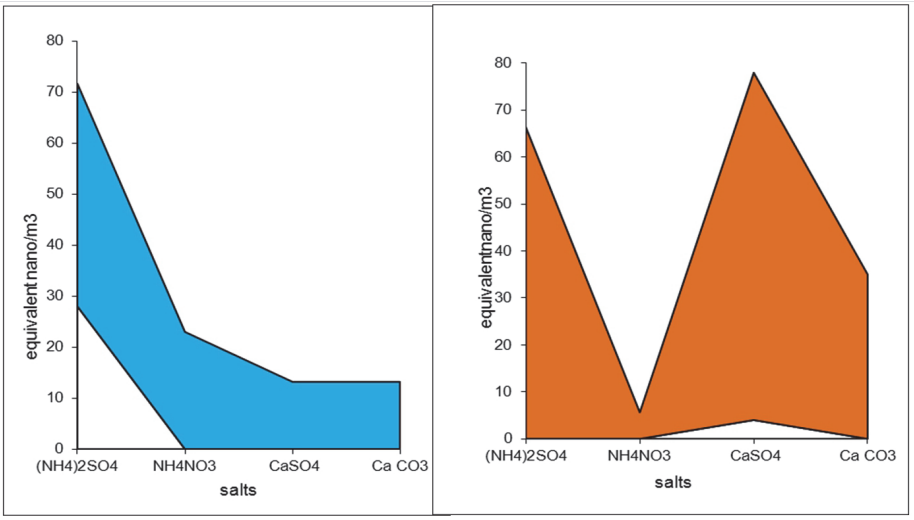

Fig. 2. Patterns of ammonium sulphate, ammonium nitrate, calcium sulphate, calcium carbonate concentrations during the winter (in blue) and summer (in orange) season

During the summer the sum of the cations averages (170neq/m^3) exceeds the anions one (143neq/m^3). Moreover during the summer the calcium average (among samples) concentration increases from 13.2 ng to 78.0 ng. Figure 2 shows the minimum and maximum concentrations of ammonium sulphate, ammonium nitrate, calcium suphate, calcium and carbonate calculated on the basis of simple stoechiometric considerations.
During the summer the correlation between chloride and sodium concentrations increased up to 0.87, while the winter value was 0.30.
However, during summer, the sodium and chloride concentrations didin't show a clear marine component because their ratio was slightly bigger than winter one but very different compared to the typical value (1.8) in seawater. One explanation for this observation may be searched in the action of nitrogen oxides on sodium chloride that leads to the solute concentration depletion (Kerminen et al., 1998).

2.3 Fine fraction of samples collected in St. Nicola sport stadium sampling site

The samples collected in St. Nicola sport stadium showed a correlation between PM2.5 and the other analytes, during both sampling periods, lower than the Pane e Pomodoro site one. As observed for the samples collected in P&P site, during the wintertime, the values of the correlation coefficients between PM2.5 and species deriving from combustion and secondary particulate matter were high: 0.93 for OC and 0.57 for K^+. Moreover chloride, calcium, magnesium and sodium concentrations were weakly correlated with PM2.5 ones (r values ranging between 0.26 and -0.35).
During the winter, the correlation between chloride and sodium concentrations was 0.08; it was considerably lower than Pane e Pomodoro one and the ratio between the chloride and sodium average concentrations was 0.215.
The correlation between ammonium and sulphate concentrations shows high values, quite similar (r = 0.87 and r = 0.88 respectively) during the winter and summer seasons. These values were slightly lower than Pane e Pomodoro ones.

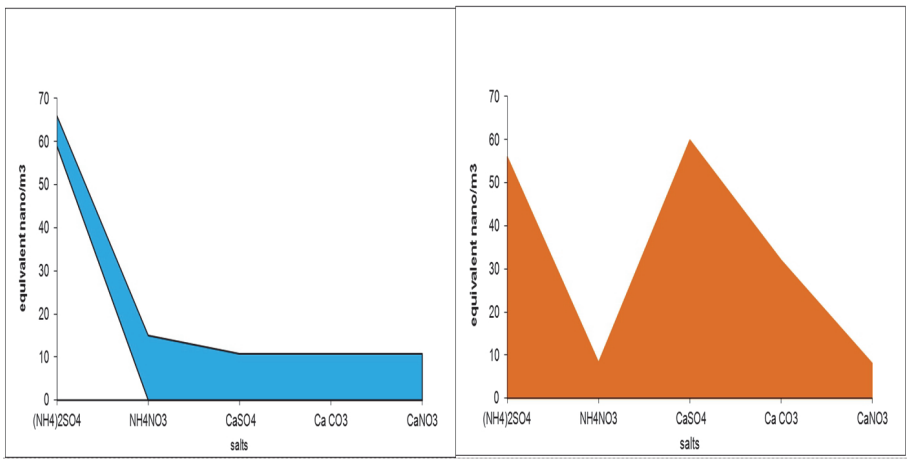

Fig. 3. Patterns of ammonium sulphate, ammonium nitrate, calcium sulphate and calcium carbonate and calcium nitrate concentrations during the winter (in blue) and summer (in orange) season

The correlation between nitrate and ammonium concentrations decreased from winter to summer as seen for the samples collected in Pane e Pomodoro site, but in St. Nicola site nitrate concentration was poorly correlated with ammonium one (r = 0.34) also during the winter.
Considering the ionic balance between anions and cations expressed in nano equivalent, also for this site there was an excess (20%) of anions during the winter, while there was an excess (13%) of cations in summer. It should be noted that the non-analyzed part of the particulate mass consists of silicates. Moreover a percentage of anions is contained in the organic matter (OC).
Also for this site, the correlation between sodium and chloride concentrations increased from winter (r = 0.07) to summer (r = 0.51), having in both seasons lower values than Pane e Pomodoro site ones.
Figure 3 shows the minimum and maximum concentrations, calculated on a stoechiometric basis, of ammonium sulphate, ammonium nitrate, calcium sulphate, calcium carbonate and calcium nitrate.

2.4 Fine fraction of samples collected in Casamassima sampling site and comparison among different sites in the two sampling campaigns

During the winter in Casamassima sampling site, the most far from the sea, the correlation between the PM2.5 and the analytes investigated followed, even if with some differences, the general trend shown in the other two sites. In fact observing figure 4 the correlation coefficient trends are similar in the three sampling sites, except for the last four analytes in samples collected in St Nicola sport stadium site.

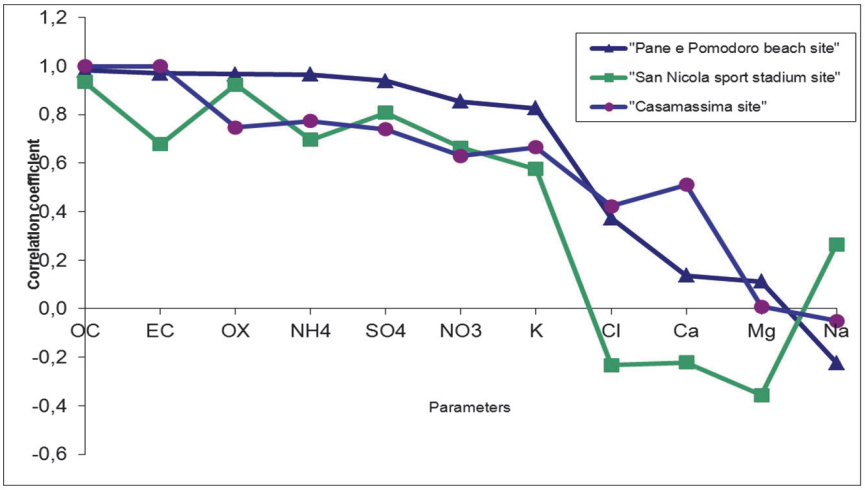

Fig. 4. Correlation between PM2.5 and each ion concentrations for the three sites during the winter campaign

OC, EC, oxalate, chloride, magnesium and sodium concentration values were found similar to the Pane e Pomodoro site ones, while ammonium sulphate, nitrate and potassium have similar trends to the St. Nicholas site ones; the calcium and PM2.5 concentrations show for this site higher correlation than the other site ones.

About correlation among investigated analytes figure 5 shows the chloride and sodium concentrations for all three sites during both sampling campaigns.

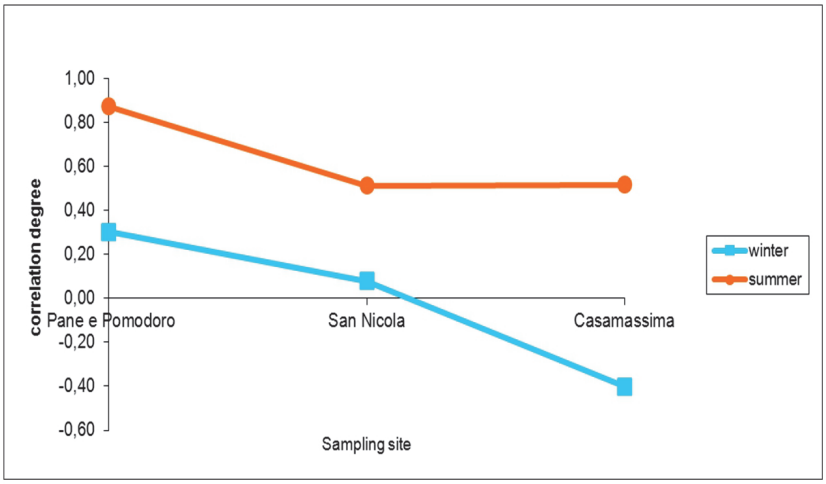

Fig. 5. Correlation between chloride and sodium concentrations in the three sampling sites during both sampling campaigns

Increasing distance from the sea, the correlation between chloride and sodium decreases, keeping higher values in the summer than the winter. The correlation between the two elements terrigenous, calcium and carbonate, is similar in all three sampling sites, keeping higher values in summer than the winter for all sites.
Figures 6 and 7 show the trends of the correlation coefficient between ammonium and nitrate and ammonium and sulphate respectively.

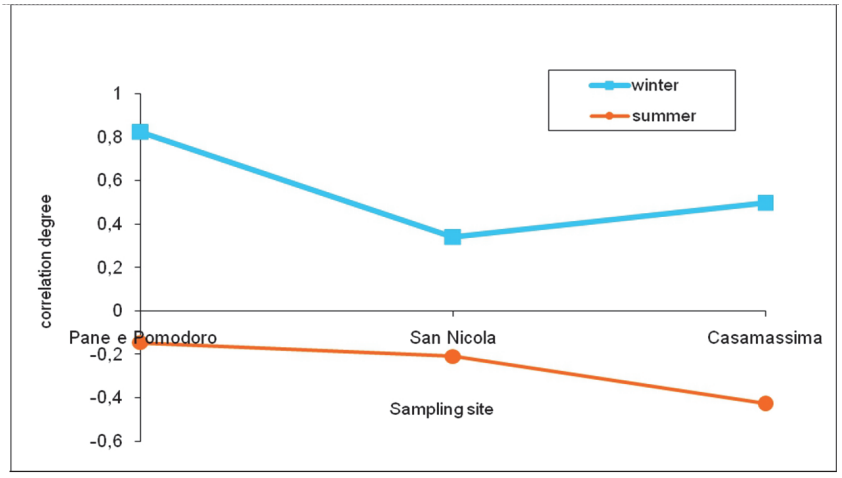

Fig. 6. Correlation between nitrate and ammonium concentrations in the three sampling sites during both sampling campaigns

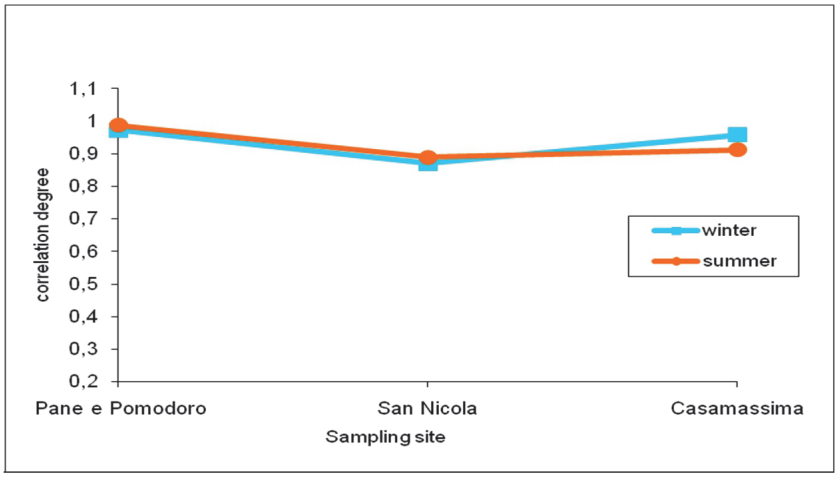

Fig. 7. Correlation between ammonium and sulphate concentrations in the three sampling sites during both sampling campaigns

The figure 7 shows that the ammonium and sulphate have a high correlation in all sites during the both sampling campaigns. Observing figure 6 we can see that during the winter campaign ammonium and nitrate are less correlated; during summer campaign they are anti correlated.

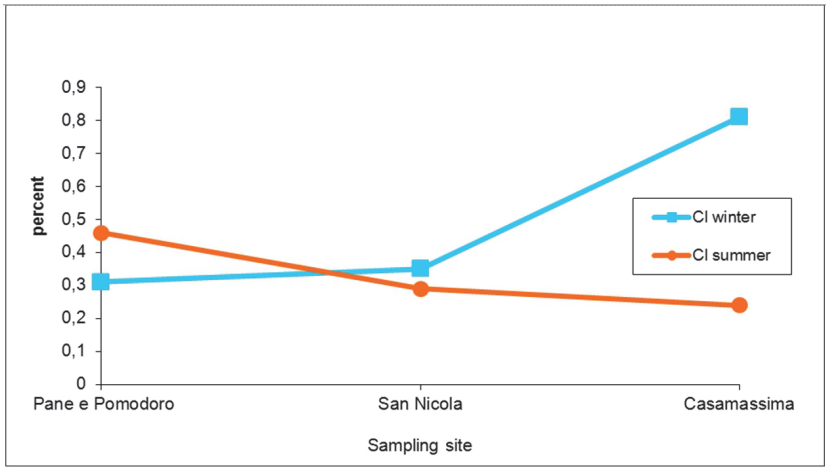

Fig. 8. Percentage of chloride in the three sampling sites during both sampling campaigns

Figure 8 shows as the percentage of chloride[1] during the summer decreases with distance from the sea, while during the winter it has the opposite trend: this suggests that part of the

[1]The percentage of chloride is obtained as ratio between the chloride mass and total PM mass; the ratio is multiplied for 100.

chloride monitored during the winter has a different origin than the sea spray. To understand the chloride trends it should be considered the depletion of chloride by nitric acid and nitrogen oxides cited earlier (Kerminen et al., 1998).
The percentage of EC for all sites presents high values and shows a downward trend moving from the Pane e Pomodoro site to Casamassima one, more marked during the winter than the summer.
The percentages of all other analytes didn't show site specificity, but it depended only on the season, so that moving from winter to summer the average value of OM decreased from 31.6% to 20.0% for the three sites; the nitrate value varied from 4.7% to 1.6%, while the percentage of sulphate and calcium and carbonate increased from 15.6% to 17%, from 1.7% to 4.9% and from 4.1% to 7.5% respectively.

2.5 Results of comparison between coarse and fine fractions

The sampler used was enable to collect simultaneously the PM2.5 and PM10 fractions of particulate matter, so that it was possible to measure contemporary the amount of fine and coarse particles until 10μm using the two sampling heads: PM2.5 and PM10. In this way it is possible to calculate the PM2.5 and PM10 ratio for each sampling. For our samples this ratio has varied in a range from 0.2 to 0.91.
It was observed that the PM2.5 and PM10 ratio was higher in winter (mean value = 0.77) and lower in summer (mean value = 0.56). The difference was more evident in coastal site. These results may be attributed to several factors:

- resuspension of coarse fraction in PM10;
- lower frequency of precipitations which remove mainly coarse fraction of PM by washout;
- higher frequency of African dusts episodes, so coarse PM, in summer months.

Analyzing data it's been pointed out that during the winter fine particles percentage is greater than the coarse one for all sites. Moreover for the samples collected in Pane e Pomodoro site, during the both sampling campaigns, fine particles percentage was less than the other two sites ones.
Considering the portioning of the analytes between the coarse and fine fractions, it is noted that each analyte has showed a different portioning percentage between the fine and coarse fractions depending more on the season than on the sampling site.
About the portioning percentage of majority elements between the fine and coarse fractions we have observed that EC is almost completely contained in the fine fraction with a percentage of 6% about; moreover the EC portioning percentage didn't depend on the sampling site. This confirms that the EC is mainly due to combustion sources (vehicular traffic).
About the OC portioning percentage we have observed that it was much more site-specific than EC, especially for the coarse fraction. In fact in the coastal site the OC percentage contained in the fine particles is five times than one contained in the coarse particles, while the innermost site (CS site), where the sampling station is located near the agricultural area, showed similar percentages of organic matter in the two PM fractions.
During the summer the sulphate average percentage in the fine fraction is three times that contained in the coarse fraction.
During the winter the sulphate average percentage in the fine fraction is one time and half that contained in the coarse fraction.
Nitrate, during the summer, has showed a behaviour opposite to the sulphates one, in fact, the nitrate average percentage is bigger than the coarse fraction one. In the winter the nitrate percentage was increased in both fractions, but it was bigger in coarse particulates.

As mentioned above the carbonate concentration values are available only for the summer campaign. As shown in figure 9, carbonate has showed an anomalous behaviour, because for the two sites, the average percentage is bigger in the fine fraction than coarse one, while for the samples collected in Casamassima site it has a bigger percentage in the coarse fraction than in the fine one.

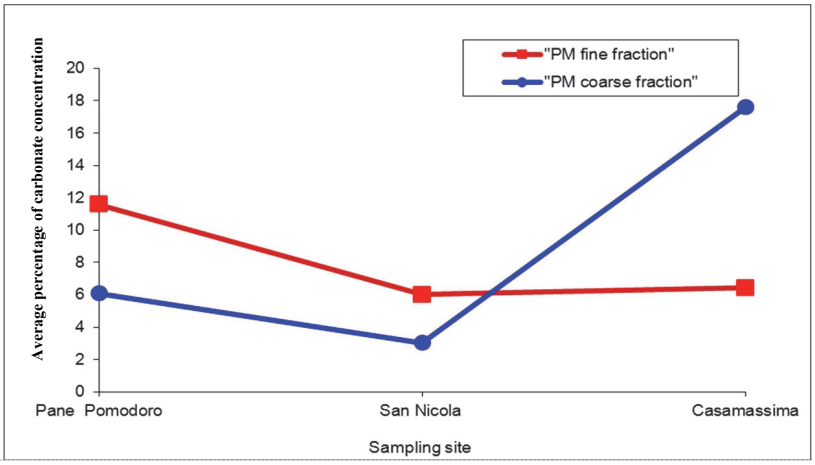

Fig. 9. Portioning of carbonate in the fine and coarse PM fractions during the winter campaign.

Among majority elements contained in soluble particulate the ammonium contained in PM10 showed, in many samples, concentration values slightly lower than PM2.5 ones. Because of the PM10 contains the PM2.5 and the sampling was performed simultaneously with the same bi-channel pump, this is clearly the result of an experimental artefact.

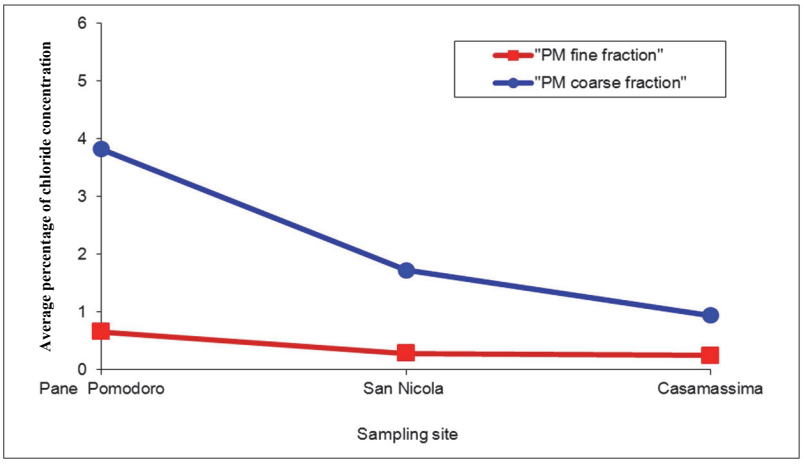

Fig. 10. Portioning of chloride in fine and coarse PM fractions during the summer campaign.

From literature it is known that, during the sampling, ammonia may suffer a depletion, especially if it is present as chloride and nitrate salt: these salts are highly volatile.
Minority elements such as chloride, sodium and magnesium showed similar patterns each others with a bigger percentage in the coarse particles than in the fine ones in all sampling site and in both campaigns. Moreover during the summer, there is a decrease of chloride and sodium percentage from coastal site in the innermost (see figure 10).
Also calcium percentage in the coarse particles was bigger than the fine one, especially during the winter.
During the summer, where it is possible to compare calcium and carbonate concentrations, the behaviour of the two ions was similar, so that it 's possible to conclude that a large percentage of calcium is present as carbonate, mostly in Casamassima sampling site.

3. Application of receptor models

The results of multivariate statistical methods, such as Principal Component Analysis and Absolute Principal Component Scores, applied to dataset will be shown to identify similar PM sources in the two PM fractions.

3.1 Principal Component Analysis (PCA) and Absolute Principal Component Scores (APCS)

PCA is a statistical method that identifies patterns in data, revealing their similarities and differences (Massart et al., 1997; Todeschini, 1998; Zhuang & Dai, 2007). PCA creates new variables, the principal components scores (PCS), that are orthogonal and uncorrelated to each other, being linear combinations of the original variables. They are obtained in such a way that the first PC explains the largest fraction of the original data variability, the second PC explains a smaller fraction of the data variance than the first one and so forth (Abdul-Wahab et al., 2005; Sousa et al., 2007; Wang & Xiao, 2004). Thus the first step is the search of the Eigenvalues and Eigenvectors of the data correlation matrix. Only the most significant p Eigenvectors (or factors) are taken into account.
Generally two methods are used in order to chose p Eigenvectors: Kaiser method (PCs with eigenvalues greater than 1) and ODVx ones (PCs representing at least X% of the original data variance). In our method we have chosen the second one and we have taken into account p Eigenvectors until the sum of their Eigenvalues reaches at least 90% of the total variance. Varimax rotation is the most widely employed orthogonal rotation in PCA, because it tends to produce simplification of the unrotated loadings to easier interpretation of the results. It simplifies the loadings by rigidly rotating the PC axes such that the variable projections (loadings) on each PC tend to be high or low. The results of PCA application are generally shown in the graphics: the loading and score plot.
Moreover the reconstruction of the source profile and contribution matrices can be successfully obtained by APCS (Absolute Principal Component Scores) method (Caselli et al., 2006), in which the first steps correspond to PCA method. In the following the total steps of APCS method are summarized. The normal approach to obtain a data set for receptor modeling is to determine an adequate number of not correlated chemical concentrations in an enough high number of samples. The mass balance equation can thus be extended to account for all m elements in the n samples as the sum of the contributions by p independent unknown sources, equation 1

$$C_{ij} = \sum_{k=1}^{p} M_{ik} A_{kj} \quad (1)$$

$$X = FxA + E \quad (2)$$

$$Z = PCSxV^T \quad (3)$$

$$E_X\% = \sqrt{\frac{1}{nm}\sum_{i=1}^{n}\sum_{j=1}^{m}\left[\frac{\left(Xr_{ij} - X_{ij}\right)}{X_{ij}}\right]^2}\ x100 \quad (4)$$

where C_{ij} in the equation 1 is the i^{th} concentration measured in the j^{th} sample, M_{ik} is the concentration of the i^{th} parameter in the k^{th} source, and A_{kj} is the fraction of the k^{th} source contributing to the j^{th} sample. In matrix form equation 1, taking into account the data error, becomes the equation shows in 2, where X (nxm) is the measured concentration matrix.
F (nxp) is the source contribution matrix. A (pxm) is the source profile matrix. E is the error matrix. The solution of equation 2 is not unique but, in any case, the solutions must be found according to a set of physical constraints. For example, all the terms of the matrices F and A must be non-negative numbers.
In APCS the first step is the search of the Eigenvalues and Eigenvectors of the data correlation matrix G. Only the most significant p Eigenvectors (or factors) are taken into account.
Generally p Eigenvectors are taken into account until the sum of their Eigenvalues reaches at least 80% of the total variance. The p Eigenvectors are then rotated by an orthogonal or oblique rotation. The aim of the rotation is to transform the Eigenvectors, that are an abstract representation of the source (factors) profiles into values, which have a physical meaning. After the rotation all the components should assume positive values; small negative values are set zero. An abstract image of the source contributions to the samples can be obtained by multivariate linear regression, see equation 3, where Z is the scaled data matrix, PCS is the principal component scores matrix, and V^T is the transposed rotated loading (Eigenvectors) matrix. In order to pass from the abstract contributions to real ones, a fictitious sample Z_0, where all concentrations are zero, is built (Thurston & Spengler, 1985).
Using the matrix V^T and the equation 3 the vector PCS_0, corresponding to Z_0, is calculated and subtracted from all the vectors that form PCS. The matrix obtained in this way is referred to as Absolute Principal Component Scores (APCS) matrix. The APCS matrix can be identified with the estimated contribution matrix F_r. Also in this case small negative values are usually set zero. Then, a regression on the data matrix X allows to obtain the estimated source profiles matrix Ar. If the APCS matrix is bordered with a unit column vector, the regression gives for each parameter also a possible contribution of the not explained variance. At last the product of the matrices F_r and A_r allows to recalculate the data matrix X_r. If F and A are unknown, the agreement between X and X_r is the only assessment for the effectiveness of their reconstruction.
In order to evaluate the goodness of reconstruction of the data matrix, the percent relative root mean square errors (RRMSE) for X (E_X%) is defined as shown equation 4.

3.2 Application of PCA and APCS methods to PM2.5 and PM10 samples data set

In figure 11 it's possible to observe the plot (loading plot) obtained by application of Principal Component Analysis to data set of chemical parameters of PM2.5 samples. The

data matrix was formed by 86 samples x 12 parameters. Six factors (PCs) were calculated explaining up to 90% of the total variance. Factor loadings of the variables were used to identify source profiles.
The first Principal Component (PC1) explains 50% of the total data variance, while the second Principal Component (PC2) explains 15%.

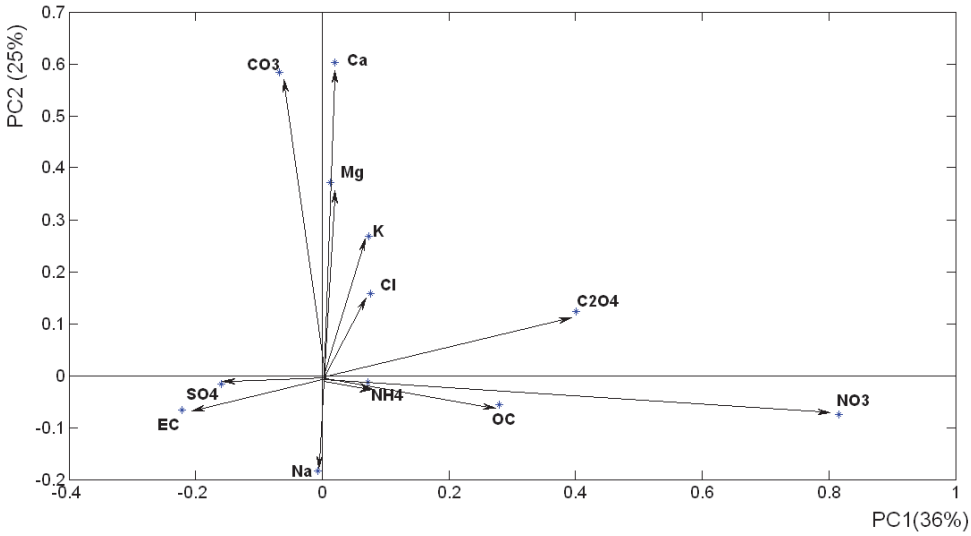

Fig. 11. Loading plot for PM2.5 samples data set

It' possible to observe the contribution of CO_3^{2-}, Ca^{2+} e Mg^{2+} on the second component and NO_3^-, OM e OC on the first one. The first and second PCs allowed to discriminate between samples collected in the cold and the warm season (observing figure 12). The winter samples were collocated along the PC1, with high loadings for NH_4^+, SO_4^{2-}, NO_3^-, OC, EC, and $C_2O_4^{2-}$, while the summer samples along the PC2, showing high loadings for Cl^-, Na^+, Mg^{2+}, Ca^{2+} and CO_3^{2-}.
In figure 12 the score plot obtained by application of Principal Component Analysis to data set of chemical parameters of PM2.5 samples is shown. Observing figure 12 two clusters, identified by two semiprobability ellipses, for winter and summer samples are evident. The semi axes of ellipse is two times the scores standard deviation. One ellipse shows major samples dispersion along the first PC, while the other shows major samples dispersion along the second PC.
On the contrary, it 's not possible to individuate clusters for the different sampling sites.
The application of APCS method allowed to identify the number of the pollutant sources, their profiles and contributions. Applying the APCS method to data matrix of PM2.5 samples and considering a total variance of 90% six pollutant sources were obtained. In figure 13 the grouping of parameters in six factors (named sources) is highlighted. In the figure the weight percentage of each source is also shown.
In the first factor OC, CO_3^{2-}, NO_3^-, SO_4^{2-}, Cl^- and EC are grouped though ether. The presence of OC with NO_3^- and SO_4^{2-} suggests a source of secondary organic matter. The weight percentage of this source is 38%.

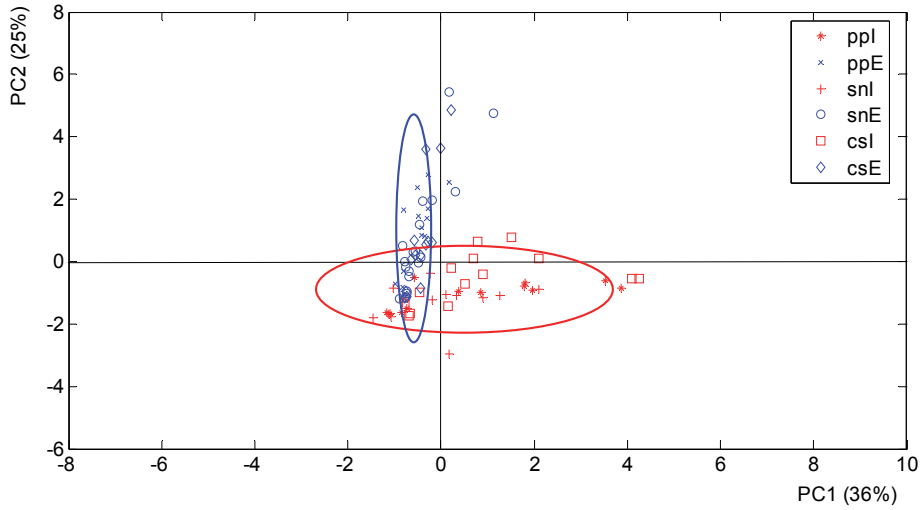

Fig. 12. Scores plot for PM2.5 samples data set. ppI represents samples collected in Pane e Pomodoro sampling site during the winter; ppE represents samples collected in Pane e Pomodoro sampling ste during the summer; snI represents samples collected in San Nicola sport stadium sampling site during the winter; snE represents samples collected in San Nicola sport stadium sampling ste during the summer; csI represents samples collected in Casamassima sampling site during the winter; snE represents samples collected in San Nicola sport stadium sampling site during the summer. Winter samples are highlighted in red colour, while summer samples in blue.

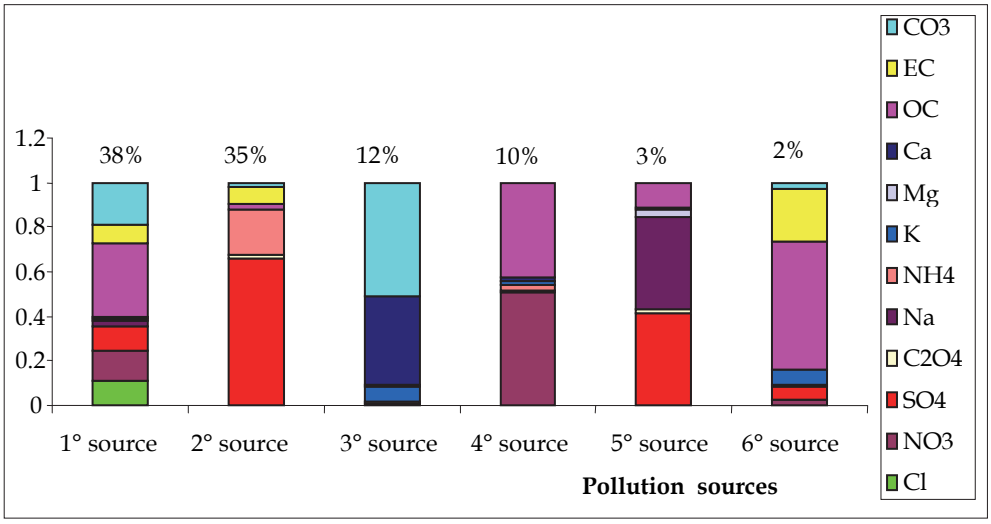

Fig. 13. Source's profiles obtained for PM2.5 samples data set

In the second factor, among grouped parameters, $NH_4^+$and SO_4^{2-} are those relevant: this source can be identified with secondary particulate produced from oxidation of SO_2 and from the action of NH_3 on oxidation products.
The third factor presents mostly Ca^{2+} and CO_3^{2-}. The calcium carbonate identifies this source.
OC and NO_3^- are the dominant parameters in the fourth factor. Considering that the contribution of this source is more relevant during the winter (see figure 4d) it can be identified with point combustions (domestic heating plants).
About fifth factor it 's characterized by Na^+, SO_4^{2-}, Mg^{2+}. It'd suggest a sea source but the Cl^- contribution is absent. So it's not easy to identify this source.
The sixth factor presents mostly OC and EC: this source can be identified with mobile combustion sources (vehicular traffic).
In figure 14(a,b,c) and figure 14(d,e) the source's contribution percentage values for each source in the different sampling sites and seasons are shown on the left, while the source's profile percentage for the considered source (figure 14a shows the 1° source) is shown on the right of the figure. The first and second sources that together represent the 73% (38%+35%) of total PM mass, mainly constituted by OC and SO_4^{2-}, respectively, were identified with organic and inorganic secondary particulate matter. As one can see observing figure 14a and 14b they were almost constant in different seasons and sites.

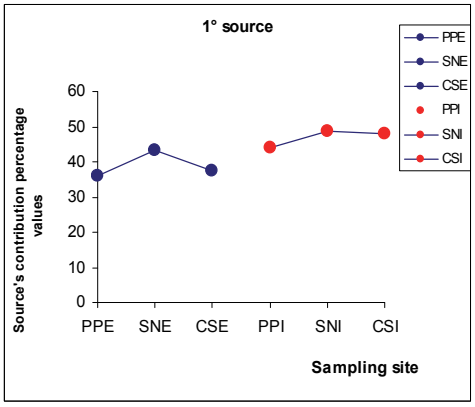

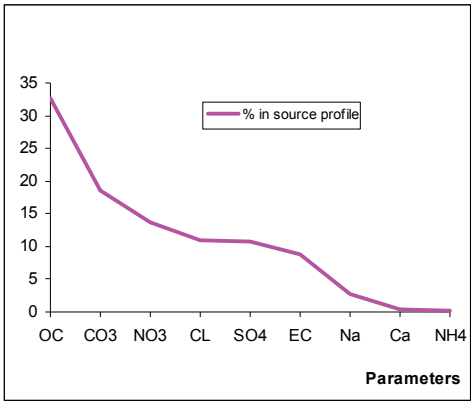

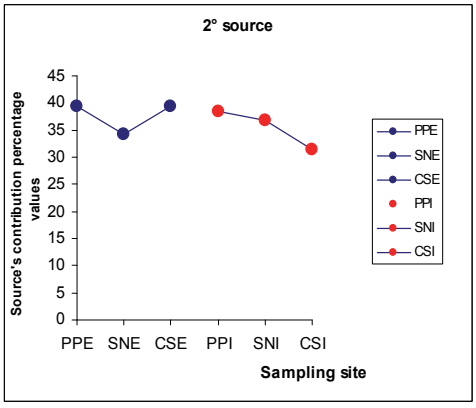

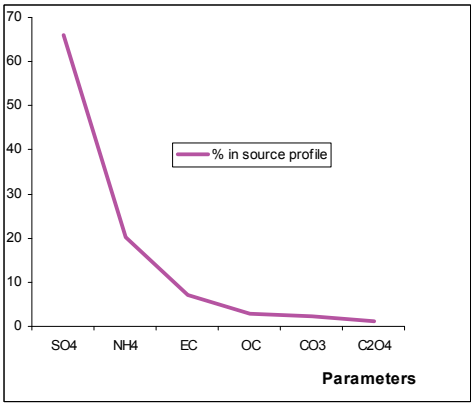

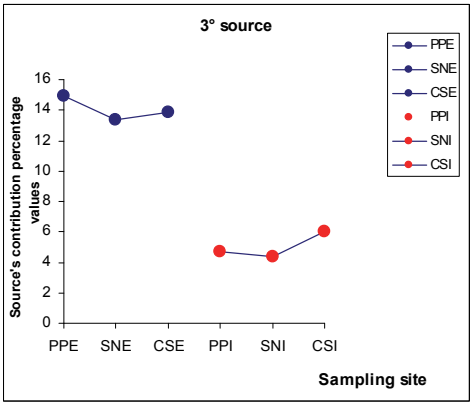

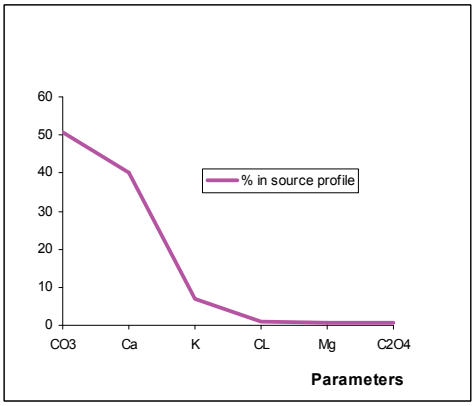

Fig. 14. (a,b,c). Percentage of source's contributions and percentage source's profiles for PM2.5 samples data set

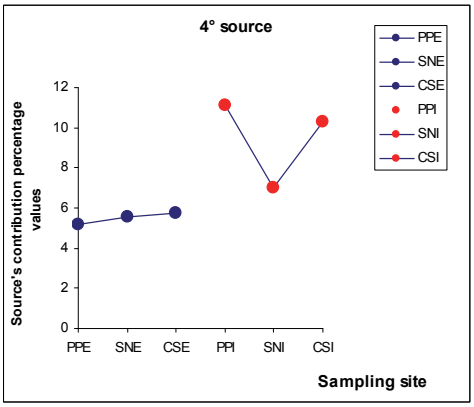

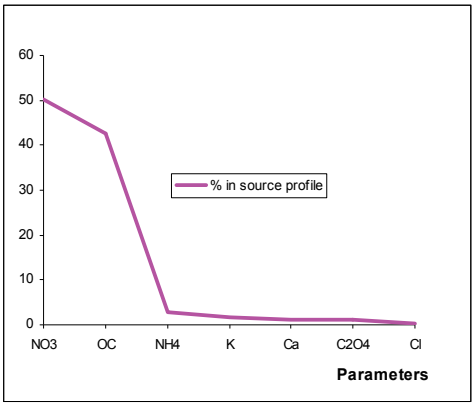

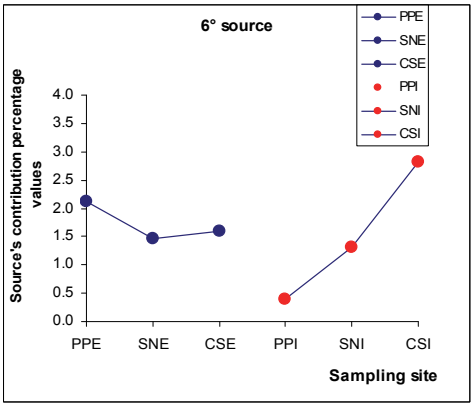

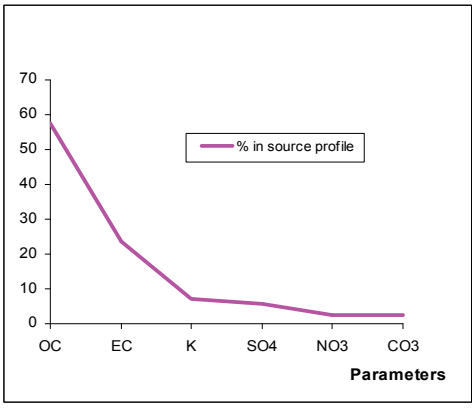

Fig. 14. (d,e). Percentage of source's contributions and percentage source's profiles for PM2.5 samples data set

The third source showed summer levels nearly three times winter ones. It was constituted by calcium carbonate.
The fourth source, more high in winter, may be due to point combustion sources.
The sixth one shows similar values among sites during the summer, while it shows more site variability during the winter: as we said above, considering the source's profile, it can be attributed to diffuse and or mobile combustion sources.
The PCA and APCS methods have been applied also to PM10 samples collected in the three sampling site during the summer. Observing the loading plot for PM10 samples data set shown in figure 6 we can see that NO_3^-, SO_4^{2-} and OM show a high contribution on the first component explaining the 50% of the total variance, while Cl^-, Mg^{2+} and Na^+ show high values on the second one that explains the 15% of the total data variance. PCA method with a total variance of 90% identifies five factors.

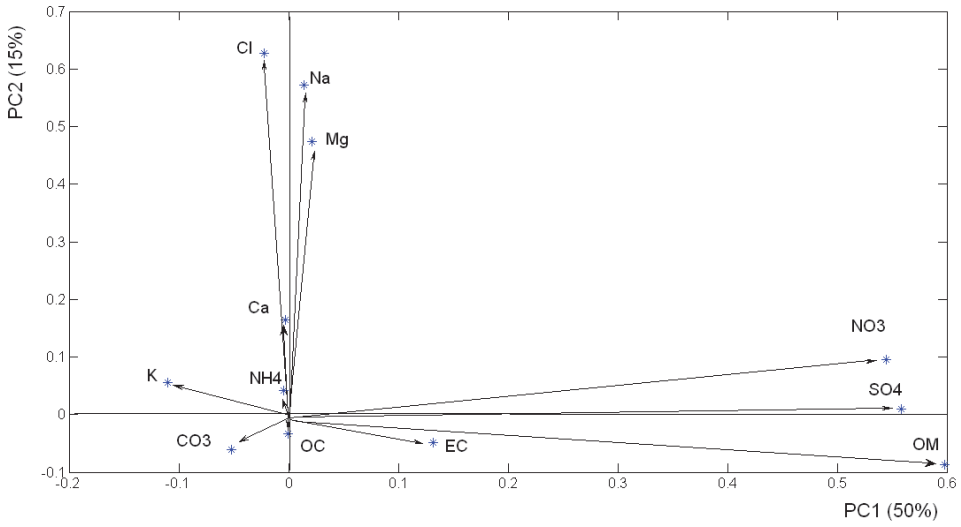

Fig. 15. Loading plot for PM10 samples data set

In the score plot of the first two PCs of PM10 samples data set, shown in figure 16, a cluster due to samples collected in Casamassima site can be easily observed.
Applying the APCS method to the data set of PM10 samples it's been possible to obtain source's profiles and contributions. In figure 17 profiles of the five factors (sources) are shown.
The composition of the first factor is mostly due to Ca^{2+} and CO_3^{2-}: this source can be identified with calcium carbonate.
The second factor shows SO_4^{2+} e NO_3^-: this suggests a secondary inorganic source.
The third factor shows a relevant presence of OC: this source is similar (for composition) to the first and fourth source of PM2.5.
Fourth factor shows a composition due to Na^+, Cl^-, Ca^{2+} and Mg^{2+}: this source can be identified as the sea source.
Fifth factor shows Na^+, Mg^{2+} e SO_4^{2+}.

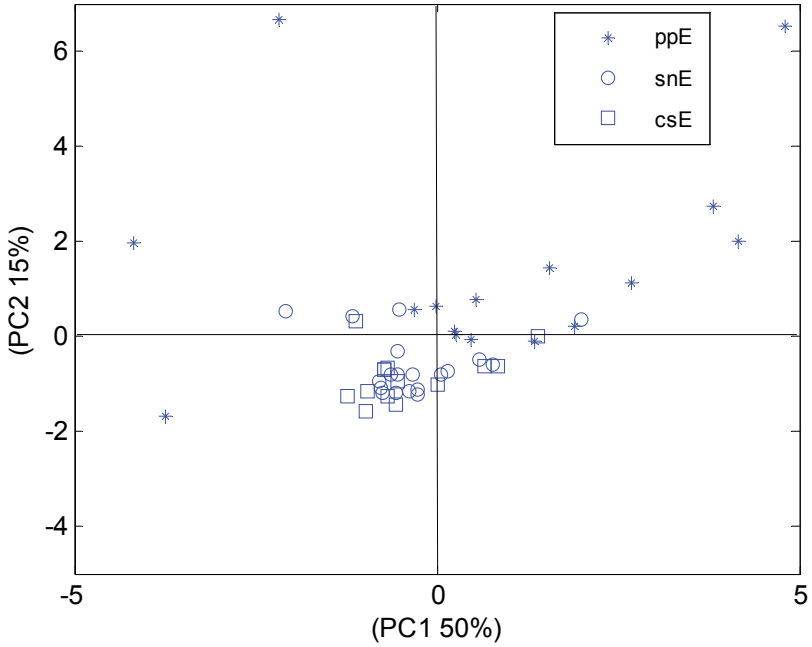

Fig. 16. Scores plot for PM10 samples data set

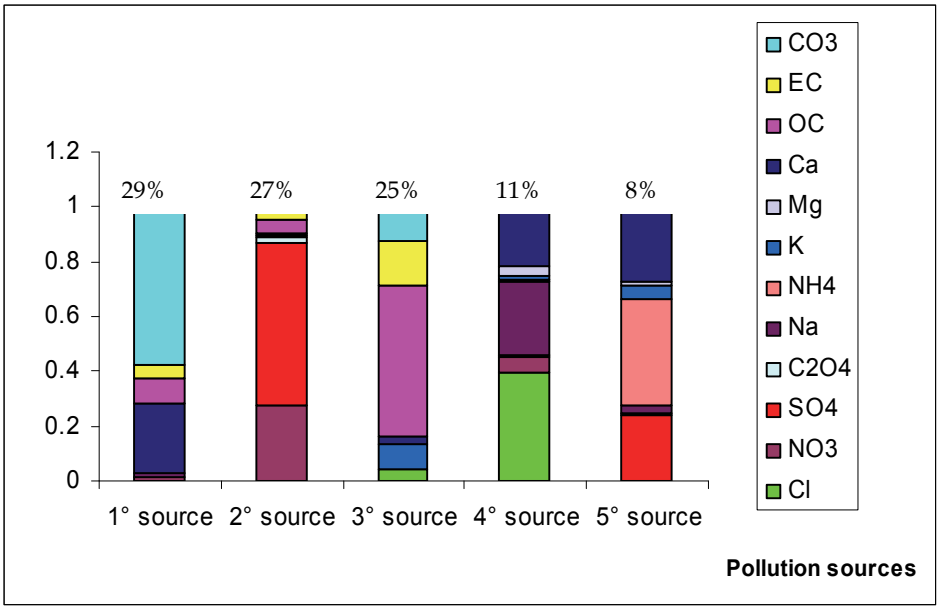

Fig. 17. Source's profiles obtained for PM10 samples data set

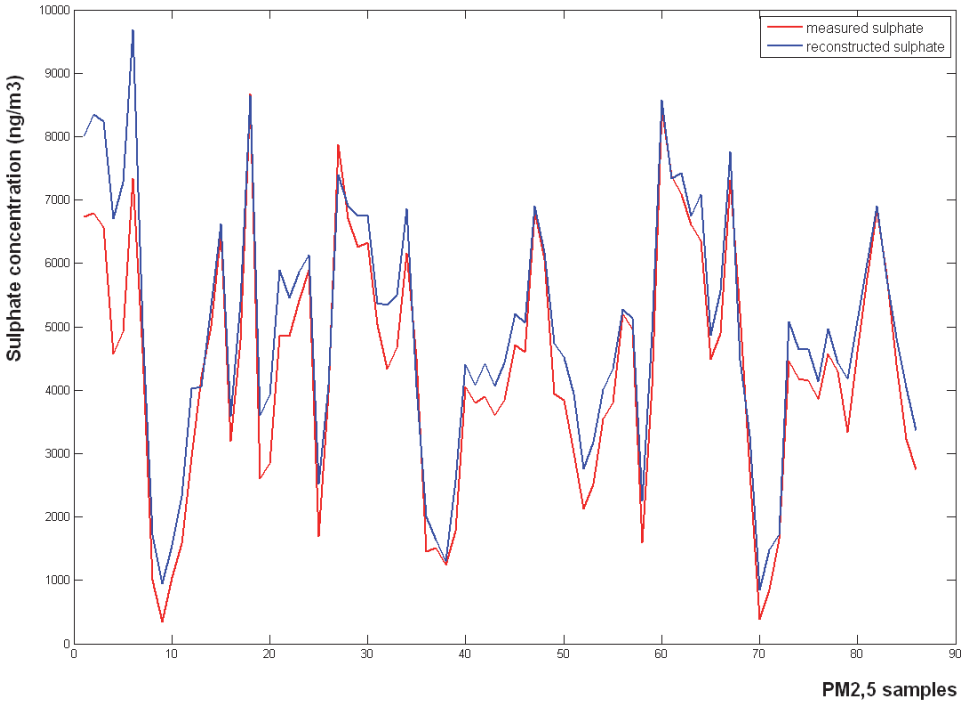

Fig. 18. Comparison between measured and reconstructed matrix of SO_4^{2-} concentration in PM2.5 samples

Observing the measured and reconstructed trends of SO_4^{2-} concentration (figure 18) it's possible to observe a good overlap between the red and blue curves. This confirms the goodness of the method used.
Moreover when factor analysis is applied on real samples the only way to check the goodness of the apportion procedure is the root mean square (RRMSE) error of the reconstructed data matrix (equation 4). In our case the RRMSE is 4,6%.

4. Conclusion

The chemical composition of PM2.5 and PM10 simultaneously collected during winter and summer seasons in three sites of South-East Italy territory and having different distances from the sea, was examined.
It was observed that the PM2.5 and PM10 ratio was higher in winter (mean value = 0.77) and lower in summer (mean value = 0.56). The difference was more evident in coastal site.
The PM2.5 analysis evidences a good correlation between chloride and sodium in each season and in all sites, but higher in the site of Pane e Pomodoro during summer. These findings confirm the presence of marine spray also in fine fraction of PM.
Nitrate and ammonium were correlated in cold season, mainly in urban sites, due to the NOx production from vehicular traffic.

Sulphate and ammonium are always very correlated in all sites. Moreover, it was noted that sulphate and ammonium were in almost stoechiometric ratio for ammonium sulphate. These outcomes support the hypothesis of a common PM contribution, in the whole Bari territory, consisting in ammonium sulphate.
The application of PCA and APCS on the main chemical constituents of PM2.5 and PM10 identified similar PM sources. Differences were observed in their distribution.
The source characterized by Ca^{2+} and CO_3^{2-} was found in both PM fractions: the percentage weight contribution of this source to the total mass is 29% for PM10 and 12% for PM2.5 respectively. While in the PM2.5 first and fourth source are identified with organic matter and vehicular traffic (explaining toghether 40% of the total mass), in the PM10 they became a single source explaining 25% of the total mass. Moreover in PM10 was identifiable a marine source (with high amount of Cl^-, Na^+ and Mg^{2+}), while in PM2.5 this source is not well identified, in fact Na^+ and Mg^{2+} were found in the same source with SO_4^{2-}, but without Cl^-.
The similar PM sources found in this study were organic and inorganic secondary compounds, point and diffuse combustion processes, calcium carbonate and sea salt.
Differences were observed in distribution of the source: secondary and combustion compounds were mainly in PM2.5, while primary and natural species were prevalent in coarse PM.

5. Acknowledgment

The authors wish to thank Professor Maurizio Caselli (Bari University, Italy) for his teaching and scientific advice during the many years of collaboration activities. This research activity was funded by PCOST project 'Studio del Particolato COSTiero' (2005-2007) evaluated eligible for funding by MIUR (Italian Research and University Ministry) and funded by Bari University.

6. References

Abdalmogith, S.S. & Harrison, R.M. (2005). The use of trajectory cluster analysis to examine the long-range transport of secondary inorganic aerosol in the UK. *Atmospheric Environment*, Vol.39, pp. 6686–6695

Abdul-Wahab, S.A.; Bakheit, C.S. & Al-Alawi, S.M. (2005). Principal component and multiple regression analysis in modelling of ground-level ozone and factors affecting its concentrations. *Environ. Modell. Softw*, Vol.20, No.10, pp. 1263-1271

Almeida, S.M.; Pio, C.A.; Freitas, M.C.; Reis, M.A. & Trancoso, M.A. (2005). Source apportionment of fine and coarse particulate matter in a sub-urban area at the Western European Coast. *Atmospheric Environment*, Vol.39, pp. 3127–3138

Amodio, M.; Bruno, P.; Caselli, M.; de Gennaro, G.; Dambruoso, P.R.; Daresta, B.E.; Ielpo, P.; Gungolo, F.; Placentino, C.M.; Paolillo, V. & Tutino, M. (2008) Chemical characterization of fine particulate matter during peak PM10 episodes in Apulia (South Italy). *Atmospheric Research*, Vol.90, pp. 313–325

Andreae, M.O. (1983). Soot carbon and excess fine potassium: long-range transport of combustion-derived aerosols. *Science*, Vol.220, No.4602, pp. 1148–1151

Artaxo, P. & Hansson, H.-C. (1995). Size distribution of biogenic aerosol particles from the Amazon Basin. *Atmospheric Environment*, Vol.29, pp. 393– 402

Birch, M.E. & Cary, R.A. (1996). Elemental carbon-based method for monitoring occupational exposure to particulate diesel exhaust. *Aerosol Science and Technology*, Vol.25, pp. 221–241

Bruno, P.; Caselli, M.; de Gennaro, G. & Traini, A. (2001). Source apportionment of gaseous atmospheric pollutants by means of an absolute principal component scores (APCS) receptor model. *Fresen. J Anal. Chem.*, Vol.371, No.8, pp. 1119-1123

Bruno, P.; Caselli, M.; de Gennaro, G.; Ielpo, P.; Daresta, B.E.; Dambruoso, P.R.; Paolillo, V.; Placentino, C.M. & Trizio, L. (2008). Application of Receptor Models to Airborne Particulate Matter. *Microchemical Journal*, Vol.88, pp. 121-129

Caselli, M.; de Gennaro, G. & Ielpo, P. (2006). A comparison between two receptor models to determine the source apportionment of atmospheric pollutants. *Environmetrics*, Vol.17, No.5, pp. 507-516

Chio, C.P.; Cheng, M.T. & Wang, C.F. (2004). Source apportionment to PM in different air quality conditions for Taichung urban and coastal areas, Taiwan. *Atmos. Environ.*, Vol.38, No.39, pp. 6893-6905

Chow, J.C.; Watson, J.G.; Pritchett, L.C.; Pierson, W.R.; Frazier, C.A. & Purcell, R.G. (1993). The DRI thermal/optical reflectance carbon analysis system: description, evaluation and applications in US air quality studies. *Atmospheric Environment*, Vol.27A, pp. 1185–1201

Chow, J.C.; Watson, J.G.; Crow, D.; Lowenthal, D.H. & Merrifield, T.M. (2001). Comparison of IMPROVE and NIOSH carbon measurements, *Aerosol Sci. Technol.*, Vol.34, No.1,pp. 23–34

Churg, A & Brauer, M. (2000). Ambient atmospheric particles in the airways of human lungs. *Ultrastructure Pathology*, Vol.24, pp. 353–361

Currie, L.A.; Gerlach, R.W.; Lewis, C.W.; Balfour, W.D.; Cooper, J.A.; Dattner, S.L.; De Cesar, R.T.; Gordon, G.E.; Heisler, S.L.; Hopke, P.K.; Shah, J.J.; Thurston, G.D. & Williamson, H.J. (1984). Interlaboratory comparison of source apportionment procedures: results for simulated data sets. *Atmospheric Environment*, Vol.18, No.8, pp. 1517–1537

Dan, M.; Zhuang, G.; Li, X.; Tao, H. & Zhuang, Y. (2004). The characteristics of carbonaceous species and their sources in PM2.5 in Beijing. *Atmospheric Environment*, Vol.38, pp. 3443–3452

Dzubay, T.G.; Stevens, R.K.; Balfour, W.D.; Williamson, H.J.; Cooper, J.A.; Core, J.E.; De Cesar, R.T.; Crutcher, E.R.; Dattner, S.L.; Davis, B.L.; Heisler, S.L.; Shah, J.J.; Hopke, P.K. & Johnson, D.L. (1984). Interlaboratory comparison of receptor model results for Houston Aerosol. *Atmospheric Environment*, Vol.18, No.8, pp. 1555–1566

Ganor, E.; Foner, H.A.; Bingemer, H.G.; Udisti, R. & Setter, I. (2000). Biogenic sulphate generation in the Mediterranean Sea and its contribution to the sulphate anomaly in the aerosol over Israel and the Eastern Mediterranean. *Atmospheric Environment*, Vol.34, pp. 3453-3462

Gordon, G.E.; Pierson, W.R.; Daisey, J.M.; Lioy, P.J.; Cooper, J.A.; Watson, J.G. & Cass, G.R. (1984). Considerations for design of source apportionment studies. *Atmospheric Environment*, Vol.18, No.8, pp. 1567–1582

Güllü, G.; Dogan, G. & Tuncel, G. (2005). Atmospheric trace element and major ion concentration over the eastern Mediterranean Sea: identification of anthropogenic source regions. *Atmospheric Environment*, Vol.39, pp. 6376–6387

Guo, H.; Wang, T. & Louie, P.K.K. (2004). Source apportionment of ambient non-methane hydrocarbons in Hong Kong: Application of a principal component analysis/absolute principal component scores (PCA/APCS) receptor model. *Environ. Pollut.*, Vol.129, No.3, pp. 489-498

Hauck, H.; Berner, A.; Frischer, T.; Gomiscek, B.; Kundi, M.; Neuberger, M.; Puxbaum, H. & Preining, O. (2004) AUPHEP-Team, AUPHEP-austrian project on health effects of particulates-general overview. *Atmospheric Environment*, Vol.38, No.24, pp. 3905–3981

Hays, M.D.; Fine, P.M.; Geron, C.D.; Kleeman, M.J. & Gullett, B.K. (2005). Open burning of agricultural biomass: Physical and chemical properties of particle-phase emissions. *Atmospheric Environment*, Vol.39, No.36, pp. 6747-6764

Henry, R.C.; Lewis, C.W.; Hopke, P.K. & Williamson, H.J. (1984). Review of receptor model fundamentals. *Atmospheric Environment*, Vol.18, No.8, pp. 1507–1515

Hitzenberger, R.; Berner, A.; Giebl, H.; Kromp, R.; Larson, S.M.; Rouc, A.; Koch, A.; Marischka S. & Puxbaum, H. (1999). Contribution of carbonaceous material to cloud condensation nuclei concentrations in European background (Mt. Sonnblick) and urban (Vienna) aerosols. *Atmospheric Environment*, Vol.33, pp. 2647–2659

IPPC. (2007). IPCC Fourth Assessment Report: Climate Change 2007, Cambridge University press, Cambridge, In: *Internet,* 9th march 2011, Available from: <http://www.ipcc.ch/publications_and_data/publications_and_data_reports.shtml>

Kerminen, V.-M.; Teinilä, K.; Hillamo, R. & Pakkanen, T. (1998). Substitution of chloride in sea-salt particles by inorganic and organic anions. *J. Aerosol Sci.*, Vol.29, No.8, pp. 929-942

Kouvarakis, G. & Mihalopoulos, N. (2002). Seasonal variation of dimethylsulfide in the gas phase and of methanesulfonate and non-sea-salt sulfate in the aerosols phase in the Eastern Mediterranean atmosphere. *Atmospheric Environment*, Vol.36, pp. 929–938

Luria, M.; Peleg, M.; Sharf, G.; Siman Tov-Alper, D.; Spitz, N.; Ben Ami, Y.; Gawii, Z.; Lifschitz, B.; Yitzchaki, A. & Seter, I. (1996). Atmospheric sulfur over the eastern Mediterranean region. *Journal of Geophysical Research*, Vol.101, pp. 25917-25930

Malm, W.C. & Day, D.E. (2000). Optical properties of aerosol at Grand Canyon National Park. *Atmospheric Environment*, Vol.34, pp. 3373–3391

Marcazzan, G.M.; Ceriani, M.; Valli, G. & Vecchi, R. (2003). Source apportionment of PM10 and PM2.5 in Milan (Italy) using receptor modelling. *Sci. Total Environ.*, Vol.317, No.1-2, pp. 137-147

Martins, J.V.; Artaxo, P.; Hobbs, P.V.; Liousse, C.; Cachier, H.; Kaufman, Y. & Plana-Fattori, A. (1996). Particle-size distributions, elemental compositions, carbon

measurements, and optical properties of smoke from biomass burning in the Pacific Northwest of the United States, In: Biomass Burning and Global Change, Vol. 2., Levine, J.S., pp. 716–732, MIT Press, Cambridge, MA

Massart, D.L.; Vandeginste, B.G.M.; Buydens, L.M.C.; de Jong, S.; Lewi, P.J. & Smeyers-Verbeke, J. (1997). *Data Handling in Science and Technology. Handbook of Chemometrics and Qualimetrics*, vols. 20A and 20B, Elsevier, Amsterdam

Meinrat, O.A. & Crutzen, P.J. (1997). Atmospheric Aerosols: Biogeochemical Sources and Role in Atmospheric Chemistry. *Science*, Vol.276, pp. 1052-1058

Mihalopoulos, N.; Stephanou, E.; Kanakidou, M.; Pilitsidis, S. & Bousquet, P. (1997). Tropospheric aerosol ionic composition above the Eastern Mediterranean Area. *Tellus B*, Vol.49, No.3, pp. 314–326

Na, K.; Sawant, A.A.; Song, D. & Cocker, D.R., III (2004). Primary and secondary carbonaceous species in the atmosphere of Western Riverside County, California. *Atmospheric Environment*, Vol.38, pp. 1345–1355

Nicholson, K.W. (1988). A review of particle resuspension. *Atmospheric Environment*, Vol.22, pp. 2639-2651

O'Brien, D.M. & Mitchel, R.M. (2003). Atmospheric heating due to carbonaceous aerosol in Northern Australia-confidence limits based on TOMS aerosol index and sun-photometer data. *Atmospheric Research*, Vol.66, pp. 21–41

Pankow, J.F. (1987). Review and comparative analysis of the theory of partitioning between the gas and aerosol particulate phases in the atmosphere. *Atmospheric Environment*, Vol.21, pp. 2275–2283

Pope, A.C., III & Dockery, D.W. (2006). Critical Review: Health Effects of Fine Particulate Air Pollution: Lines that connect. *J Air Waste Manag Assoc*, Vol.56, pp. 709–742

Putaud, J.P.; Davison, B.M.; Watts, S.F.; Mihalopoulos, N.; Nguyen, B.C. & Hewitt, C.N. (1999). Dimethylsulfide and its oxidation products at two sites in Brittany. *Atmospheric Environment*, Vol.33, pp. 647–659

Querol, X.; Alastuey, A.; Rodrìguez, S.; Viana, M.M.; Artìñano, B.; Salvador, P.; Mantilla, E.; Garcìa do Santos, S.; Fernández Patier, R.; de la Rosa, J.; Sánchez de la Campa, A. & Menéndez, M. (2004). Levels of PM in rural, urban and industrial sites in Spain. *Sci Total Environ*, Vol.334–335, pp. 359–376

Rogge, W.F.; Hildemann, L.M.; Mazurek, M.A.; Cass, G.R. & Simoneit, B.R.T. (1991). Sources of fine organic aerosol: 1. Charbroilers and meat cooking operations. *Environ. Sci. Technol.*, Vol.25, pp. 1112–1125

Saarikoski, S.; Sillanpää, M.; Sofiev, M.; Timonen, H.; Saarnio, K.; Teinilä, K.; Karppinen, A.; Kukkonen, J. & Hillamo, R. (2007). Chemical composition of aerosols during a major biomass burning episode over northern Europe in spring 2006: Experimental and modelling assessments. *Atmospheric Environment*, Vol.41, No.17, pp. 3577-3589

Schaap, M.; Spindler, G.; Schulz, M.; Acker, K.; et al. (2004). Artefacts in the sampling of nitrate studied in the "INTERCOMP" campaigns of EUROTRAC-AEROSOL. *Atmospheric Environment*, Vol.38, pp. 6487-6496

Schauer, J.J.; Rogge, W.F.; Hildemann, L.M.; Mazurek, M.A.; Cass, G.R. & Simoneit, B.R.T. (1996). Source apportionment of airborne particulate matter using organic compounds as tracers. *Atmospheric Environment*, Vol.30, pp. 3837–3855

Schauer, J.J.; Mader, B.T.; Deminter, J.T.; Heidemann, G.; Bae, M.S.; Seinfeld, J.H.; Flagan, R.C.; Cary, R.A.; Smith, D.; Huebert, B.J.; Bertram, T.; Howell, S.; Kline, J.T.; Quinn, P.; Bates, T.; Turpin, B.; Lim, H.J.; Yu, J.Z.; Yang, H. & Keywood, M.D. (2003). ACE-Asia intercomparison of a thermal-optical method for the determination of particle-phase organic and elemental carbon. *Environmental Science & Technology*, Vol.37, No.5, pp. 993–1001

Seinfeld, J.H. & Pandis, S.N. (2006). *Atmospheric Chemistry and Physics, from Air Pollution to Climate Change* (2nd edition), Wiley and Sons, New York, N.Y.

Sousa, S.I.V.; Martins, F.G.; Alvim-Ferraz, M.C.M. & Pereira, M.C. (2007). Multiple linear regression and artificial neural networks based on principal components to predict ozone concentrations. *Environ. Modell. Softw*, Vol.22, pp. 97-103

Stevens, R.K. & Pace, T.G. (1984). Overview of the mathematical and empirical receptor models workshop (Quail Roost II). *Atmospheric Environment*, Vol.18, No.8, pp. 1499–1506

Tegen, I.; Lacis, A.A. & Fung, I. (1996). The influence on climate forcing of mineral aerosols from disturbed soils. *Nature*, Vol.380, pp. 419–422

Thurston, G.D. & Spengler, J.D. (1985). A quantitative assessment of source contributions to inhalable particulate matter pollution in metropolitan Boston. *Atmospheric Environment*, Vol.19, No.1, pp. 9-26

Todeschini, R. (1998). *Introduction to chemometrics,* pp. 37-60, EdiSES s.r.l, ISBN 8879591460, Napoli

Turpin, B.J.; Saxena, P.; Andrews, E. (2000). Measuring and simulating particulate organics in the atmosphere: problems and prospects. *Atmospheric Environment*, Vol.34, No.18, pp. 2983-3013

Vardoulakis, S. & Kassomenos, P. (2008). Sources and factors affecting PM10 levels in two European cities: Implications for local air quality management. *Atmospheric Environment*, Vol.42, No.17, pp. 3949-3963

Vecchi, R.; Marcazzan, G. & Valli, G. (2007). A study on nighttime–daytime PM10 concentration and elemental composition in relation to atmospheric dispersion in the urban area of Milan (Italy). *Atmospheric Environment*, Vol.41, pp. 2136–2144

Wall, S.M.; John, W. & Ondo, J.L. (1988). Measurement of aerosol size distributions for nitrate and major ionic species. *Atmospheric Environment*, Vol.22, No.8, pp. 1649-1656

Wang, S. & Xiao, F. (2004). AHU sensor fault diagnosis using principal component analysis method. *Energ Buildings*, Vol.36, No.2, pp. 147-160

World Health Organization. (2005). Fact Sheet EURO/04/05, In: *Internet,* 9th march 2011, Available from: <http://www.euro.who.int/document/mediacentre/fs0405e.pdf>

Wyzga, R.E. (2002). Air Pollution and Health: Are Particulates the Answer?, *Proceedings of NETL Conference, PM2.5 and Electric Power Generation: Recent Findings and Implications*, Pittsburgh, PA, April 9-10, 2002

Zhuang, X.S. & Dai, D.Q. (2007). Improved discriminate analysis for high-dimensional data and its application to face recognition. *Pattern Recogn.*, Vol.40, No.5, pp. 1570-1578

7

Monitoring and Reporting VOCs in Ambient Air

Anjali Srivastava and Dipanjali Majumdar
National Environmental Engineering Research Institute, Council of Scientific and Industrial Research, India

1. Introduction

Volatile organic compounds (VOCs) are part of the large hydrocarbon family, a vast array of aliphatic, aromatic hydrocarbons, their halogenated derivatives, alcohols, ketones and aldehydes. VOCs have a property of conversion into vapour or gas without any chemical change. They are highly reactive hydrocarbons and participate in atmospheric photochemical reactions. Some of them have negligible photochemical activity; however they play an important role as heat trapping gases in atmosphere. VOC of both primary and secondary origin in ambient air have immense importance as they have direct as well as indirect effects on climate change, ecology and human health.

Many VOCs are of natural origin while many owe their existence to anthropogenic activities. Natural sources of VOCs include forests, termites, oceans, wetlands, Tundras and volcanoes. Estimated global emission rate of biogenic VOCs is 1150 Tg yr^{-1} (Guenther et. al., 1995).

The anthropogenic sources of VOCs consist of vehicular emissions, petroleum products, chemicals, manufacturing industries, painting operations, varnishes, coating operations, consumer products, petroleum handling, auto refinishing, cold clean degreasing, printing inks, dry-cleaning etc.

In presence of oxides of nitrogen and sunlight, VOCs form ozone and other products. Oxidation of VOCs by reaction with hydroxyl radicals is the main removal process. The oxidation of complex organic molecules leads to the fragmentation, production of a range of reactive free radicals and more stable smaller molecules such as aldehydes. VOCs are cause of concern firstly due to its role in formation of ground level ozone and smog and secondly due to some of them being carcinogenic, mutagenic and teratogenic in nature. Adverse effects of ozone on human health, crop viability and yields are well documented. Wide range of VOCs, imply wide range of reaction rates, which means large range of transport distances. Many VOCs have low reactivity and thus long atmospheric life times and can be classified as Persistent Organic Pollutants (POPs). Some VOCs are Hazardous Air Pollutants (HAPs) by virtue of their toxicity.

International concerns regarding VOCs arise due to their ability of long range transport, distribution and accumulation in various components of environment, their toxic nature and significant contribution from natural sources. Ambient air monitoring of VOC is aimed to control or avoid adverse impacts on humans and ecology. This should also result in knowledge of types and category of VOCs in terms of photochemical ozone creating potential of VOCs, concentrations of VOC species, their dispersion routes and fate in

environment. However there are many issues embedded in measurement of ambient VOCs, starting from the definitions of VOCs to monitoring and reporting protocols.
In this chapter we will discuss the various methods in practice for defining, sampling, analysing and reporting of VOCs. The chapter also stresses the need for a uniform method to deal with VOCs for the purpose of comparison and better understanding.

2. Definitions of VOCs

Definition of VOCs vary according to context. A very general definition is "VOCs are organic substances which are volatile and are photo chemically reactive". Below are the definitions of VOCs used by various organisation.
UNECE (United Nations Economic Commission for Europe):
All organic compounds of anthropogenic nature, other than methane, those are capable of producing photochemical oxidants by reacting with nitrogen oxides in the presence of sunlight are VOCs
WHO (World Health Organisation):
World Health Organisation has defined VOC Based on 'Boiling Point' range,
"Any organic compound" will be denoted as very volatile organic compound (VVOC) if the boiling point is in the range of < 0°C to up to 50 °C; and the will be denoted as volatile organic compound (VOC) if the boiling point falls within the range from 50°C - 100°C up to 240 - 260 °C.
ASTM (international standards developing organization):
Any compound of carbon evaporating under specific test conditions; water and exempt volatile solvents (methylene chloride, p-chlorobenzotrifluoride, acetone, volatile methyl siloxanes) are not included as VOC.
ISO 16000-6 (International Organization for Standardization):
Any organic compound in the indoor air of homes, offices and public buildings as well as organic compounds, which emit from construction materials and are detected in the test chamber"
- This definition relates to Indoor Air Quality
European Union (Directive 2001/81/EC):
"volatile organic compounds" and "VOC" mean all organic compounds arising from human activities, other than methane, which are capable of producing photochemical oxidants by reactions with nitrogen oxides in the presence of sunlight".
US EPA Definition of VOC - Volatile Organic Compounds
"Volatile organic compounds (VOC)" means any compound of carbon, excluding carbon monoxide, carbon dioxide, carbonic acid, metallic carbides or carbonates, and ammonium carbonate, which participates in atmospheric photochemical reactions

3. Estimation of VOCs

Any technique of measuring VOCs must consist of three major components namely,
- the means of sampling of air sample
- the means of extraction, and
- the means of detection of the target analytes;

3.1 Methods of sampling

The first step of monitoring of VOCs is the collection of air sample. Different methods of VOC sampling in air are practiced worldwide for this purpose (Demeestere et. al., 2007).

- *Active sampling* is done by drawing a specified volume of the air using a pump through an adsorbent tube with a constant, usually low air flow rate. In some cases sampling can be done for long term where the collection of air sample is done as average samples intermittently over a long period, or sampling at a very low air flow rate.
- *Grab sampling* is done for a very short periods of time (10-30 seconds) generally using evacuated polished stainless steel or aluminium canisters. However, evacuated canisters can also be used for time integrated sampling over minutes to days using a suitable flow restrictive inlet. The VOCs are enriched afterwards in the laboratory. The lesser sensitivity of this technique limits its use for microenvironments such as indoor air or occupational environment studies since fairly high concentrations are required.
- *Passive sampling* consists of adsorbents normally contained in a thin tube. The cross section of the tube and the distance between the opening of the tube and the adsorbent surface determines the sampling rate of the passive sampler.

Instruments with photoionization detector (PID) are often used for measuring total VOCs (TVOCs) in air directly. These are also known as combustible gas meter or explosivity meter. These instruments are not chemical-specific, they measure the total organic or flammable vapor concentrations in the air mass under consideration. The detection limits of these instruments are typically higher in the parts per million range.

There are more sophisticated methods in practice which measure chemical specific VOCs in the air sample. The primary step of the methods requires pre-concentration of the target VOCs. There are two pre-concentration methods widely used which are cryogenic trapping and adsorptive sampling either in passive or active mode.

3.1.1 VOC pre-concentrations on solid sorbents

Both Active and passive sample pre-concentration is done on solid adsorption badges and packed tubes. Enrichment of VOC onto solid sorbents, either by active or passive sampling is a well established sample preparation technique for VOC in air.

Passive sampling: In passive (diffusive) sampling, sorbent material is exposed to air for a period in the order of days. Tube type or badge type samplers are used for sorbent holding in passive sampling.

Active sampling: Active sampling occurs by pumping air through a bed of sorbent(s) in a tube, at a rate typically in the range of 10–100 $mLmin^{-1}$ range for a period in the order of minutes or hours. VOC enriched sorbents are typically desorbed by thermal desorption or chemical desorption. A recent work reported in Kolkata in a microenvironment namely in passenger cars used active sampling followed by chemical desorption for sample pre-concentration (Som et al., 2007).

Cryogenic sample pre-concentration: In this process an air flow is passed through a cooled tube usually filled with glass beads. Sample preparation in this method is typically done with the aid of cryogenic fluids where trapping temperatures kept between −150 to −170°C. Recent applications where this technique is combined with canister sampling are reported for analysis of indoor environments (Hsieh et al., 2006).

3.2 Method of extraction

After pre-concentration of VOCs they need to be desorbed for further analysis. There are many extraction techniques presently in practice such as chemical and thermal desorption, Solvent extraction, Solid phase micro-extraction etc.

3.2.1 Chemical desorption

Subsequent to pre-concentration of VOCs in solid sorbent, especially activated charcoal, desorption is done using some organic solvent. Carbon disulfide (CS_2) is widely used for this purpose; Methanol and acetonitrile are also used by some researchers. Typically 1-2ml of solvent is used for desorbing target VOCs from the exposed solid sorbent. It is kept for 45 - 60 min with occasional stirring for desorption.

3.2.2 Thermal desorption

A very effective method of extraction from solid sorbent is thermal desorption. In this non-destructive method the sampling tube with exposed solid sorbent is subjected to high temperature typically in the range of 200°C to 380°C depending upon the characteristics of the solid sorbent. The target VOCs are desorbed and collected for further analysis. Cryogenic focus trap is often used followed by thermal desorption of target compounds for their collection. Alternatively they can be used directly for subsequent analysis.

3.2.3 Solvent extraction

In this method dissolving airborne VOC in an appropriate liquid solvent for pre-concentration can be achieved using impingers and denuders. Derivatization reagents can also be added converting the analytes in reaction products more suitable for subsequent separation and/or detection. This method is of particular use for the analysis of carbonyl compounds in air, with 2,4-dinitrophenylhydrazine (DNPH) the most widely used derivatization agent, forming hydrazones which can be analysed via HPLC and UV–vis or fluorescence detection (Dutta et al., 2009). Alternatively, DNPH impregnated cartridges of silica gel, florisil or octadecyl silane are widely used for collecting carbonyl compounds from air (Fujita et al., 2003, Hell´en et al., 2006). After elution with acetonitrile a very low detection limits (LODs) can be achieved by HPLC–MS analysis (Hell´en et al., 2006). Although the sensitivity of these methods are mostly sufficient, they are time consuming and not easily applicable for continuous measurements. However, Motyka et al. (2006) described a novel combined wet denudation–chemiluminescence method, based on the Trautz–Schorigin reaction, allowing continuous determination of formaldehyde in air with a LOD of 0.6 $\mu g\ m^{-3}$.

3.2.4 Solid phase micro-extraction based techniques

SPME is based on the equilibrium partitioning of target analytes between the sampled matrix and a stationary phase, coated on a fused silica fiber. Among the liquid-like and solid polymeric stationary phases available in a wide variety of polarity. As an alternative to thermal desorption, Barro et al. (2004) introduced the combined use of adsorbent cartridges and SPME for analysis of trace levels of chlorobenzenes in air. If automated, the adsorbent/HS-SPME method allows high-throughput analysis of VOC at the sub ngm^{-3} level.

3.2.5 Membrane extraction

In this method analytes are transferred from a donor to an acceptor phase through a single or multi-membrane device, where distinction can be made between non-porous and (solvent impregnated) porous membranes. Membrane extraction techniques are suitable for passive sampling over extended periods, e.g. for monitoring indoor air quality. An obstacle, however, is the necessity to calibrate each compound individually. (Zabiegala et al., 2003; 2006)

3.3 Method of analysis

A number of advanced analytical techniques are engaged for analysis of chemical specific VOCs subsequent to sampling and extraction. Gas Chromatography (GC) among them is most widely used separation technique where the target compounds are separated inside a column containing liquid stationary phase adsorbed on to the surface of a inert solid packing material by a inert gaseous mobile phase. Temperature of the column is controlled for obtaining a good separation and resolution of the analytes. The analytes are separated depending upon their various physical properties like polarity, molecular weight, structure etc. There are plenty of detectors that are used as a common practice such as Flame ionization (FID), Thermal conductivity (TCD), Electron capture (ECD), Nitrogen-phosphorus, Flame photometric (FPD), Photo-ionization (PID), Hall electrolytic conductivity. All the detectors have specific target pollutant group but the most accurate and versatile detector is the Mass detector. This detector has one specific advantage over the others that it can identify the unknown compounds as well. Other chromatographic methods are also used for some specific group of VOCs like for analysis of carbonyls High performance liquid chromatography (HPLC) is employed followed by solvent extraction.

4. Challenges in monitoring VOCs

Measurement of VOCs in ambient air is often difficult, because of the variety of VOCs of potential concern, the variety of potential techniques for sampling and analysis, and the lack of standardized and documented methods.

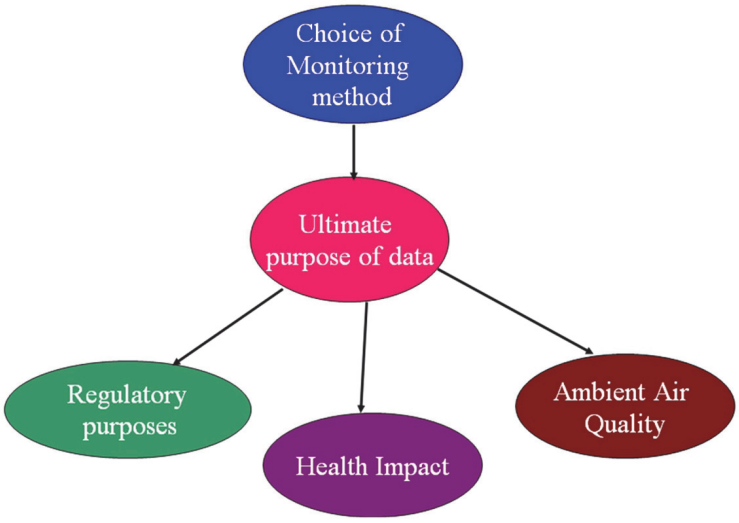

Fig. 1. Selection of monitoring method depending upon the use of data.

Volatile Organic Compounds (VOCs) present a particularly unique testing dilemma since there are a large number of different compounds defined as VOCs. The process of accurately and consistently measuring the quantity of total VOCs emitted is a concern to industry, researchers and regulatory agencies. Measurement of VOCs can be divided into two categories

- Source Emissions
- Ambient Air

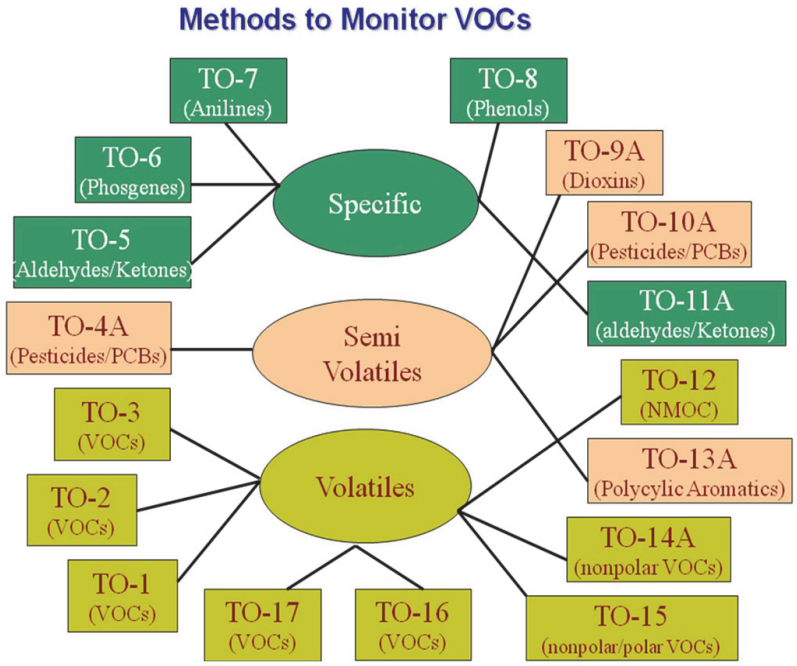

Fig. 2. Selection of monitoring method depending upon the pollutant type.

4.1 Source emission monitoring

There are three primary mechanisms for evaluating VOC emissions.

- Material Balance
- Emission Factors
- Emission Testing

All of above can be used for source emissions and reporting format depends on the compliance requirement.

USEPA has promulgated number of methods for VOC measurement which is applicable to source emission monitoring. Below is tabulated (table 1) the list of such methods along with respective application.

The correct determination of VOC emission rates is dependent on multiple factors. One factor is the ultimate purpose of the data. If testing is performed for regulatory purposes, then the regulating agency must define the pollutant and the reporting units. Usually regulating agencies require knowledge of total VOC emission, control efficiency of control equipments and concentration limits. Commonly used methods are M18, M25 and M25A. These methods suffer from limitations of detection technology and in all the methods accept M18 TVOC is reported as "Carbon" or "Methane". M18 uses FID & MS as a detector. M18 is excellent for speciating individual compounds, testing for Toxic Air Pollutants (TAPs) and Hazardous Air Pollutants (HAPs), for mass emission tests when there are only a few VOCs in the gas

Method number	Title/application
USEPA M18	VOCs by GC analysis, sampling and on-line systems
USEPA M21	VOC leaks (fugitive emissions).
USEPA M25a	Gaseous VOC concentration by Flame Ionisation Detector
USEPA M25b	Gaseous VOC concentration by infrared analyser
USEPA M25c	Non-methane organic carbon in landfill gases
USEPA M25d	VOC of waste samples
USEPA M25e	Vapour Phase organic concentration in waste samples
OSW M0010	Semi VOCs by GC after sampling with a modified Method 5 (MM5) train
OSW M0011	Aldehydes by sampling with a MM5 train and 2,4-DNPH. Analysis by GC-M5 or HPLCUV
OSW M0030.	Sampling with a 2-tube VOST and analysis by GC. For medium volatility VOCs
OSW M0031	Sampling with a 3-tube VOST, and analysis by GC. For medium to very high volatility organic compounds.
OSW M0040	Bag sampling for high volatility, high concentration compounds.
USEPA M106	Determination of VCM (Vinyl Chloride Monomer)
USEPA M107	VCM of in-process waste water samples
USEPA M107a	VCM of solvents
USEPA M204A	VOCs in liquid input stream
USEPA M204B	VOCs in captured stream
USEPA M204C	VOCs in captured stream (dilution technique)
USEPA M204D	Fugitive VOCs from temporary total enclosure
USEPA M204E	Fugitive VOCs from building enclosure
USEPA M204F	VOCs in liquid input stream (distillation)
USEPA M305	Potential VOC in waste
USEPA M307	Emissions from solvent vapour emissions
USEPA M308	Sampling for methanol with a heated system. Analysis by GC-FID
USEPA M318	Extractive FTIR for measuring emissions from the mineral wool and wood Fibreglass industry.
USEPA M310A	Residual hexane
USEPA M310B	Residual solvent
USEPA M3201C	Residual n-hexane in EDPM rubber
USEPA M312A	Styrene in SBR latex (GC)
USEPA M312B	Styrene in SBR latex by capillary GC
USEPA M312C	Styrene in SBR latex produced by emulsion polymerisation
USEPA M320	Vapour-phase, organic and inorganic emissions by extractive FTIR

Table 1. Key promulgated USEPA methods for VOC monitoring

stream and for characterising a gas stream. Method 18 utilizes gas chromatography to separate the VOC compounds from each other and from other interferences in the gaseous stream. The detector used in this method is specifically calibrated for each VOC compound present using known standards to develop response factors and linear operating ranges for the method. This method is capable of providing true results in terms of individual VOC components which when totalled provide a total VOC concentration. The main advantage of this method is that results are reported "as VOC".

Method 25 measures TGNMO (total gaseous non-methane organic) by first separating the VOC components from methane, carbon monoxide and carbon dioxide. The remaining VOC compounds are chemically converted to methane molecules, which are quantitatively measured by a FID (flame ionization detector). This method provides a measurement of the VOC composition in terms of its carbon content. This method normalizes the response factor for individual VOC components since the carbon in each component is converted to methane before performing the quantification. This method has detection limit of about 50 ppm carbon cannot be used on many outlets where the concentration is often considerably less than that. This method reports VOC "as Carbon".

Method 25A is an instrumental method in which the VOC is introduced into a FID chamber without first separating the VOC components. The FID is calibrated with a standard gas such as methane or propane and the method results are often reported in terms of the calibration gas used (e.g., "as propane"). The main problem with this method is the variation of the FID response to VOC components other than hydrocarbon compounds. VOC compounds containing oxygen or halogen atoms may differ as much as two-fold in FID response from similar hydrocarbon compounds. This method is sensitive to low concentrations, relatively easy to use, low cost and may be converted to "as VOC" results for simple gas streams where the composition is known.

4.2 Ambient air monitoring

Measurement of VOCs in ambient air is often difficult, because of the variety of VOCs of potential concern, the variety of potential techniques for sampling and analysis, and the lack of standardized and documented methods. Measuring TVOC concentrations does not provide reliable indication of potential health impacts of air pollution. In case of ambient air monitoring of VOC is aimed to control /avoid adverse impacts on humans and ecology must result in knowledge of

- Types of VOCs
- Concentrations of VOCs
- Their dispersion routes
- Their fate in environment
- Category of VOCs in terms of photochemical ozone creating potential
- VOCs in terms of their health end point

VOCs that are of importance due to their toxicity are listed in Table 2.

Very little guidance is available for the determination of toxic organic compounds in ambient air. As a result, while monitoring VOCs as air pollutant one is required to develop his own monitoring strategies, including selection of monitoring methods, sampling plan design, and specific procedures for sampling, analysis, logistics, calibration and quality control and averaging time. The choice of monitoring method for ambient measurement of VOCs depends on the ultimate purpose of the data such as:

- regulatory purpose
- Health impact
- Impact on Climate change
- Impact on ecology

Compound	Category
acrylamide	cat.2 carcinogen and mutagen
acrylonitrile	cat.2 carcinogen
azinphos-methyl	very toxic
benzene	cat.1 carcinogen
benzo(a)anthracene	cat.2 carcinogen
benzo(b)fluoranthene	cat.2 carcinogen
benzo(k)fluoranthene	cat.2 carcinogen
benzo(j)fluoranthene	cat.2 carcinogen
benzo(a)pyrene	cat.2 carcinogen, mutagen and teratogen
butadiene	cat.2 carcinogen
carbon disulphide	cat.2 teratogen
1-chloro-2,3-epoxypropane	cat.2 carcinogen
chloroethene (vinyl chloride)	cat.1 carcinogen
dibenzo(a,h)anthracene	cat.2 carcinogen
1,2-dichlorethane	cat.2 carcinogen
dichlorvos	very toxic
dieldrin	very toxic
diethyl sulphate	cat.2 carcinogen and mutagen
dimethyl sulphate	cat.2 carcinogen
dnoseb	cat.2 teratogen
endosulfan	very toxic
endrin	very toxic
1,2-epoxypropane	cat.2 carcinogen
2-ethoxyethanol	cat.2 teratogen
2-ethoxyethyl acetate	cat.2 teratogen
4,4′-methylenebis(2-chloroanaline)	cat.2 carcinogen
4,4′-methylenediphenyl diisocyanate	very toxic (inhalation)
nitrobenzene	very toxic
2-nitropropane	cat.2 carcinogen
phenol	very toxic (inhalation)
phorate	very toxic
phosgene	very toxic
polychlorinated biphenyls	IARC group 2A
2-propen-1-ol	very toxic (inhalation)
pyrene	very toxic
1,1,2,2-tetrachloroethane	very toxic

Table 2. List of VOCs Identified to be of Importance due to their Toxicity

USEPA has compiled compendium of methods to monitor VOCs and toxics in ambient air (Table 3). It gives description of technical aspects of the available methods. However none of these methods recommend any averaging period. Literature shows that concentration of VOCs have been reported as ppmv/ ppbv and also microgram per meter cube for samples collected as grab sample or for time periods varying from few seconds to hours.

Compendium Method No	Type of Compounds	Determined Sample Collection Device	Analytical Methodology
TO-12	Volatile organic compounds	Tenax® solid sorbent	GC/MS
TO-22	Volatile organic compounds	Molecular sieve sorbent	GC/MS
TO-32	Volatile organic compounds	Cryotrap	GC/FID
TO-4A	Pesticides/PCBs	Polyurethane foam	GC/MD
TO-52	Aldehydes/Ketones	Impinger	HPLC
TO-62	Phosgene	Impinger	HPLC
TO-72	Anilines	Adsorbent	GC/MS
TO-82	Phenols	Impinger	HPLC
TO-9A	Dioxins	Polyurethane foam	HRGC/HRMS
TO-10A	Pesticides/PCBs	Polyurethane foam	GC/MD
TO-11A	Aldehydes/ketones	Adsorbent	HPLC
TO-122	NMOC	Canister or on-line	FID
TO-13A	Polycyclic aromatic	Polyurethane foam	GC/MS
TO-14A	Volatile organic compounds (nonpolar)	Specially-treated canister	GC/MS and GC/MD
TO-15	Volatile organic compounds (polar/nonpolar)	Specially-treated canister	GC/MS
TO-16	Volatile organic compounds	Open path monitoring	FTIR
TO-17	Volatile organic compounds	Single/multi-bed adsorbent	GC/MS, FID, etc.

Table 3. List of USEPA Compendium of Methods for VOC / Toxic Air Pollutant Monitoring

5. Issues in reporting of VOCs

Regulations in the World as a common practice are based on limits for mass emissions of total VOC (TVOC) during a year. Most of the inconsistencies are there in reporting the TVOCs. TVOCs concentrations are reported

- as Total Organic Carbon (TOC), which is the concentration of carbon in the gas stream, and usually expressed in milligrams per cubic metre (mg m^{-3});
- as TOC expressed in terms of the equivalent concentration of a specified VOC, such as propane/Toulene, and;
- as the sum of the concentrations of specific, individual VOCs in a sample.

The Total VOC is often referred as total hydrocarbon (THC)or total organic carbon (TOC). But when THC is measured as carbon or as propane then THC cannot be used to represent Total VOC. In real situation gas stream is complex and consist of unknown compounds of variable properties; THCs are reported either as carbon or as propane. When an average MW is not available, the data is often reported on a mass basis 'as carbon' or in terms of

another surrogate. To convert 'as propane' to 'as carbon' the results must be multiplied by 3 as there are 3 carbon atoms in propane

This procedure involves two errors: response factors and total VOC molecular weight.

gms/hr (as Carbon) = K *ppm *12.01*Flow rate; where K is ….. emission factor

gms/hr (as VOC) = K *ppm *Flow rate*(MW VOC/ no. C)

e.g., Benzene is 92% carbon by weight

Ethanol is 52% carbon by weight

VOC (g/hr) = THC(g/hr) / (MW of C in VOC) / (MW of VOC)

For Benzene = THC (g/hr) / (72 / 78) = THC/ 0.92

For a mixture of gas stream benzene 25%, ethanol 50% and toluene 25%, VOC (g/hr) = THC (g/hr) / [(0.25) (72/78) + 0.5 (24/46) + 0.25 (84/91)]

= THC/ 0.72

Similarly this issue is present in measurement of ambient concentrations as well.

Thus there is need for development of uniformity in ambient VOC measurement including specific standards, at least for HAPs. Uniform reporting format e.g. TVOC as ppmv & individual VOC as $\mu g/m^3$ is also required. Averaging period and uniform detection methodology is to be standardized. Moreover VOC is not to be reported as THC and NMHC.

6. References

Barro, R.;Ares, S.; Garcia-Jares, C.; Llompart, M.; Cela, R.(2004) Development of a sensitive methodology for the analysis of chlorobenzenes in air by combination of solid-phase extraction and headspace solid-phase microextraction, *Journal of Chromatography A*, Vol.1045, No. 1-2, pp.189-196.

Demeestere, K.; Dewulf, J.; Witte, B. D.; Langenhove, H. V. (2007) Sample preparation for the analysis of volatile organic compounds in air and water matrices. *Journal of Chromatography A,* Vol. 1153, pp. 130–144.

Dutta, C.; Som, D.; Chatterjee, A.; Mukherjee, A. K.; Jana, T. K.; Sen S. (2009) Mixing ratios of carbonyls and BTEX in ambient airof Kolkata, India and their associated health risk. Environ Monit Assess Vol. 148, pp. 97–107

Fujita, E.M.; Harshfield, G.; Sheetz, L.(2003). Performance audits and laboratory comparisons for SCOS97-NARSTO measurements of speciated volatile organic compounds, *Atmospheric Environment*, Volume 37, pp. 135-147

Guenther, A.; Hewitt, C. N.; Erickson, D.; Fall, R.; Geron, C.; Graedel, T.; Harley, P.; Klinger, L.; Lerdau, M.; Mckay, W. A.; Pierce, T.; Scholes, B.; Steinbrecher, R.; Tallamraju, R.; Taylor, J.; and Zimmerman. (1995). Global-Model of Natural Volatile Organic-Compound Emissions, J. Geophys. Res.- Atmos.,Vol. 100, No. (D5), pp. 8873–8892,.

Hell´en, H.; Hakola, H.; Pirjola, L.; Laurila, T.; Pystynen, K.H. (2006). Ambient air concentrations, source profiles, and source apportionment of 71 different C2-C10 volatile organic compounds in urban and residential areas of Finland, Environ. Sci. Technol.,Vol. 40, No. 1, pp. 103-8.

Hsieh, L.-L.; Chang, C.-C.; Sree, U.; Lo, J.-G. (2006). Determination of volatile organic compounds in indoor air of buildings in nuclear power plants, Taiwan. *Water Air and Soil Pollution,*Vol. 170,pp.107-121,

K, Motyka; P, Mikuska; Z, Vecera. (2006). Continuous chemiluminescence determination of formaldehyde in air based on Trautz–Schorigin reaction, *Analytica Chimica Acta*, Vol. 562, No. 2, pp. 236-244

Som, D.; Dutta, C.; Chatterjee, A.; Mallick D.; Jana T.K.; S. Sen (2007). Studies on commuters' exposure to BTEX in passenger cars in Kolkata, India, *Science of the Total Environment*, Vol. 372, pp. 426–432

Zabiegala, B.; G´orecki, T.; Namiesnik, J.. (2003). Calibration of permeation passive samplers with siliconemembranes based on physico-chemical properties of the analytes, *Anal. Chem.*, Vol. 75 pp. 3182-3192.

Zabiegala, B.; Partyka, M.; G´orecki, T.; Namiesnik, J.(2006) Application of the chromatographic retention index system for the estimation of the calibration constants of permeation passive samplers with polydimethylsiloxane membranes, *Journal of Chromatography A*, Vol. 1117, No. 1, pp 19-30

8

Estimated Atmospheric Emissions from Mobile Sources and Assessment of Air Quality in an Urban Area

Elba Calesso Teixeira[1,2,3], Camila D. P. Mattiuzi[4],
Flavio Wiegand[1], Sabrina Feltes[1] and Felipe Norte[1]
[1]*Fundação Estadual de Proteção Ambiental Henrique Luis Roessler, Porto Alegre, RS,*
[2]*Programa de Pós-Graduação em Sensoriamento Remoto e Meteorologia, UFRGS, Porto Alegre, RS,*
[3]*Universidade Feevale, Programa de Pós-Graduação em Qualidade Ambiental, Novo Hamburgo, RS,*
[4]*Engenharia Ambiental, UFRGS/FEPAM, Porto Alegre, RS, Brazil*

1. Introduction

During the last decades, the world has gone through a period of economic and technological development that brought many benefits to modern life. Due to these developments, there was a worldwide expansion of the number of automotive vehicles on the roads increasing pollutant emissions into the atmosphere, thus frequently contributing to a worse air quality, particularly in large urban areas (Colvile et al., 2001). Although a set of improvements implemented in the vehicles, such as electronic injection systems, post-combustion catalytic converter, and changes in fuel, which have contributed to a decrease in pollutant emissions into the atmosphere, the increase in the vehicle numbers has brought about a severe deterioration in the quality of the air.

Vehicular emissions are one of the major primary sources of fine particles (Sheesley et al., 2007). Emissions from diesel engines are chemically complex and contain hundreds of chemical substances divided into gaseous and particulate phases (Kagawa, 2002; Kerminen et al., 1997). The particulate phase, significantly high when considering the one produced by gasoline-powered vehicles, has a significant amount of fine and ultrafine particles, making this one of the severest problems referring to quality of air in large urban areas, as seen in Asian countries and developing countries (Kim Oanh, 2006; Gupta & Kumar, 2006).

Diesel vehicles are the major emissions sources of several compounds in the atmosphere, amongst which the polycyclic aromatic hydrocarbons (PAHs) and the nitro-polycyclic aromatic hydrocarbons (NPAHs) (Desantes et al., 2005; Maricq, 2007; Phuleria et al., 2007; Ravindra et al., 2008). PAHs are complex organic molecules, whose structure, in addition to the carbon and hydrogen atoms, contains at least two benzene rings (Karavalakis et al.,

2010). Nitro-polycyclic aromatic hydrocarbons are also present in diesel-vehicle emissions, and they differ from PAHs due to the presence of at least one group –NO_2 in an aromatic ring (Andrade-Eiroa et al., 2010). These compounds are widely distributed in the atmosphere and are well know as mutagenic and carcinogenic agents (Karavalakis et al., 2010; Andrade-Eiroa et al., 2010).

Type and concentration of PAHs and NPAHs emitted depend on the type of fuel used and on the operating conditions of the combustion process (Ravindra et al., 2008; Karavalakis et al., 2010). These compounds are distributed in the atmosphere in the gaseous phase, and they are mainly adsorbed onto the particulate matter (Chetwittachan et al., 2002).

Emissions from gasoline vehicles contain a great deal of fine particles, which nevertheless show small adsorption when compared to particles from diesel emissions. In addition, diesel engines have a higher rate of ultrafine particle emissions (<1.0 μm). Since these particles show a large specific area, PAHs show a trend to adsorb onto the surface of gaseous particles from diesel emissions. PAHs with five or more rings are usually associated with fine atmospheric particles from diesel exhaust.

Like in other parts of the world, in Brazil, we can consider that the prevailing urban pollution comes from vehicles, i.e., it is a direct consequence of a greater number of vehicles on the roads. In view of this, the search for a non-fossil fuel which would decrease atmospheric emissions pointed out biodiesel as the most adequate and beneficial alternative, not only in terms of the environment but of the economy as well.

Biodiesel is a fuel with a high rate of oxygenation, obtained from vegetable oils or animal fat through a reaction of transesterification, with similar properties as diesel oil (Knothe, 2007). The use of this fuel has been discussed in several countries due to an increase in environmental awareness and the high price of diesel oil. Currently, many countries such as the USA, Japan, Brazil, India, amongst others, use biodiesel and petrodiesel blends in their cars, since this blend can be used without any prejudice to the existing motors.

Agarwal (2007) reviewed the combustion characteristics with regard to fuel economy and biodiesel feasibility. There is clearly a decrease in regulated emissions –HC, CO, PM–, except for NO_x, which tends to increase when the diesel engine is fueled with biodiesel. Biodiesel impact on the environment and its effects on health are also being studied by the characterization of the emissions. Lin et al. (2006) reported that PAHs emissions decreased with the increase of biodiesel amounts in the diesel-biodiesel blend. Jung et al. (2006) reported that the addition of biodiesel decreased the amount and size of particles emitted by the vehicle exhaust and increased the oxidation rate of the particles.

Biodiesel differs from diesel produced from oil in several factors, many of which directly influence the emissions. Biodiesel has two oxygen atoms per molecule more, and this represents 10-12% of its molecular weight; since it is a plant-derived fuel, it does not contain sulfur (Coronado et al., 2009); it has a greater number of cetanes (which indicates a better quality of ignition of a diesel fuel) (Knothe, 2006); and it has a higher lubricity and viscosity (Fontaras et al., 2010).

Therefore, this fuel arises as an alternative to the dependence on oil and its derivatives. Biodiesel production provides a new market for oilseeds, thereby generating a new branch of agribusiness, with a multiplier effect on various segments of the economy dealing with vegetable oils, alcohol, diesel oil, as well as inputs and byproducts from the production of the vegetable ester. In addition to all these benefits, biodiesel use also offers an excellent potential of reducing atmospheric pollutants.

The present chapter of the book aims to describe the estimation of vehicle emissions of CO, NO_X, HC, SO_2 and PM in an urban area located in the state of Rio Grande do Sul, from the addition of biodiesel to diesel, in accordance with Brazilian regulations as of 2008. In addition, air quality will be described according to various atmospheric parameters (PM, CO, NOx, O_3, SO_2, PAHs, NPAHs) and meteorological variables.

2. Area of study

The area chosen for this study was the metropolitan area of Porto Alegre (MAPA) located at 29°30'S – 30°30'S / 50°25'W – 51°55'W in the east of the state of Rio Grande do Sul, Brazil (Figure 1). According to the Brazilian Institute of Geography and Statistics (IBGE, 2010), this region comprises an area of 9,800 km², representing 3.76% of the total area of the state, and it has a population of 3,979,561 inhabitants, i.e., 37.21% of the total population of Rio Grande do Sul.

The metropolitan area of Porto Alegre is the most urbanized area of the state and includes 31 counties. The counties comprising the MAPA are: Alvorada, Araricá, Arroio dos Ratos, Cachoeirinha, Campo Bom, Canoas, Capela de Santana, Charqueadas, Dois Irmãos, Eldorado do Sul, Estância Velha, Esteio, Glorinha, Gravataí, Guaíba, Ivoti, Montenegro, Nova Hartz, Nova Santa Rita, Novo Hamburgo, Parobé, Portão, Porto Alegre, Santo Antônio da Patrulha, São Jerônimo, São Leopoldo, Sapiranga, Sapucaia do Sul, Taquara, Triunfo and Viamão.

The capital Porto Alegre has approximately 40% of the fleet of diesel vehicles, and its population represents 35.6% of the total population of the MAPA. Therefore, Porto Alegre is indisputably one of the most relevant cities for this estimation, since the county certainly has an intense traffic of vehicles.

The metropolitan area of Porto Alegre is characterized by different industrial typologies, including several stationary sources such as the Alberto Pasqualini oil refinery, two steel mills (Siderúrgica Riograndense and Aços Finos Piratini, which do not use coke) and two coal-fired power plants (Termochar and São Jerônimo). Despite the different industrial sources around Porto Alegre contributing to the total emissions, the major contributions come from an estimated 620,000 vehicles on local roads, representing 20% of the total 3.1 million vehicles of the state (Teixeira et al., 2008).

Due to the geographical location of the MAPA, the seasons are well defined and the rain is evenly distributed all over the year. Winter in this region is strongly influenced by cold air masses migrating from polar regions, and in summer there is a greater influence of tropical, maritime and continental air masses.

According to Köppen's international climate classification system, the area of study has a climate described as Cfa subtropical climate with an average temperature above 22°C during the warmest month of the year (Livi, 1999).

The prevailing wind directions are east (E), east southeast (ESE), and southeast (SE) (Livi, 1999). During the day, wind reaches its lowest speed at dawn and early morning, and highest speed in the late afternoon, between 5-7 p.m. This pattern is related to energy availability at the surface (sensible heat) during the day, intensifying local and mesoscale atmospheric circulations. The prevailing wind results from interactions of mesoscale phenomena, especially sea/land breezes (from the Atlantic Ocean and the Patos Lagoon) and valley/mountain breezes (from the nearby Serra Geral mountains to the north of the MAPA).

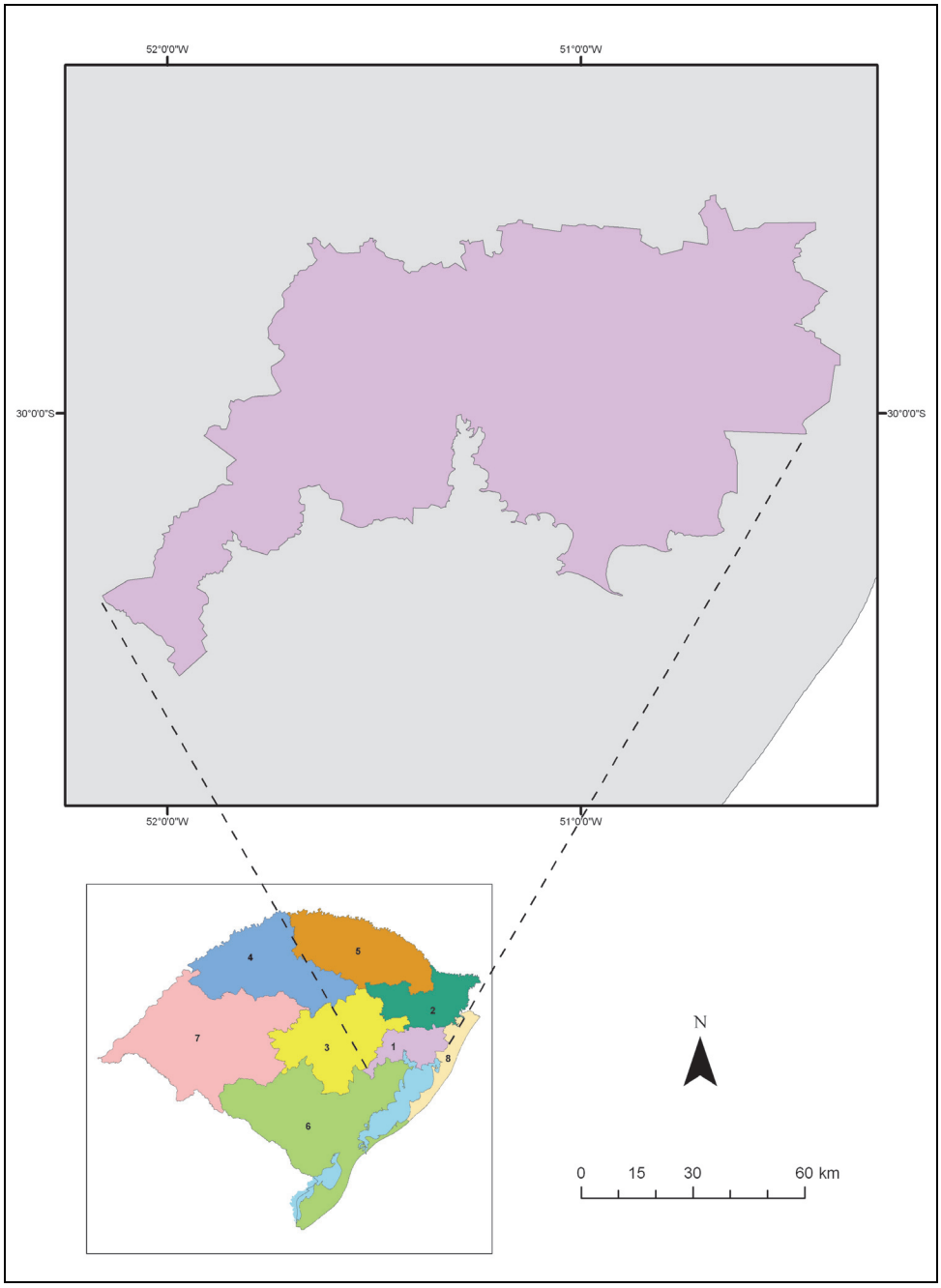

Fig. 1. Location of the Metropolitan Area of Porto Alegre

3. Methodology

3.1 Emission estimation

The method for collecting emission data in the MAPA was based on the methods for preparing vehicular emission inventories of the US Environmental Protection Agency (US EPA, 2002). Emission factors provided by the Sao Paulo State Environmental Company (CETESB, 2008) with adjustments for the area of study, amongst which the numbers of diesel vehicles on the roads in 2008 and 2009. Thus, the emissions of the following pollutants were measured: carbon monoxide (CO), hydrocarbons (HC), nitrogen oxides (NO_x), and particulate matter (PM), for the scenarios of use of diesel blended with biodiesel at 2, 5, 10, and 20%.

The working method of the present study consisted of two steps:

1. Data collecting and organization;
2. Intermediate calculations to generate the variables for the general equation (1).

$$E_{\text{pollutant,year}} = \sum_{\text{year}-\text{model}} \left(Fe \times N \times C \times A \times 10^{-6} \right) \quad (1)$$

E = pollutant emission rate (ton/year)
Fe = pollutant emission factor (g/km)
A = vehicle autonomy (km/L)
C = fuel consumption (L/year)
N= number of vehicles

All steps of calculations were developed by using Microsoft Office Excel software. Initially, the diesel fleet was subdivided into two classes: trucks, vans and pickups, and buses and minibuses, with their corresponding values for kilometers driven and autonomy.

Fleet and fuel consumption for the 31 counties located within the MAPA in 2008 and 2009 were provided by the Traffic Department of Rio Grande do Sul (DETRAN/RS) and the Brazilian Oil Agency (ANP), respectively.

There is a significant discrepancy between the volume referred to as actual consumption and the theoretical volumes, as it is not possible to affirm that a vehicle refueling in a given county will circulate only within that area. With this in mind and based on statistical data from IBGE, a weighting was done with respect to the urban and rural population of each county in order to obtain a more realistic consumption profile of that area.

Emission factors are obtained in g/KWh in national and international approaches, and they were also applied to calculating the estimated atmospheric emissions. These values were obtained in function of average speed, air temperature, vehicle technology, amongst other variables. According to Brazilian regulations, the Sao Paulo State Environmental Company (CETESB) performs annual calculations of emission factors, which are then used as reference for all studies conducted in Brazil in this field (CETESB, 2008).

In the present study, the exponential correlation referring to the emission factors was taken into account when preparing the inventory (Figure 2). Calculation adjustment to biodiesel was done by applying Equation 2 (US EPA, 2002) added of the values of coefficient "a" (Table 1) and, by considering variables "b" to be close to null, transforming the second term in a unit value.

Results obtained by using the general equation (1) and the adjustment through equation (2) give us a forecast of the decrease in pollutant emissions in the MAPA, as will be seen later.

$$E_{\text{pollutant,year}} = \exp\left[a \times (vol\%biodiesel)\right] \times \exp b \tag{2}$$

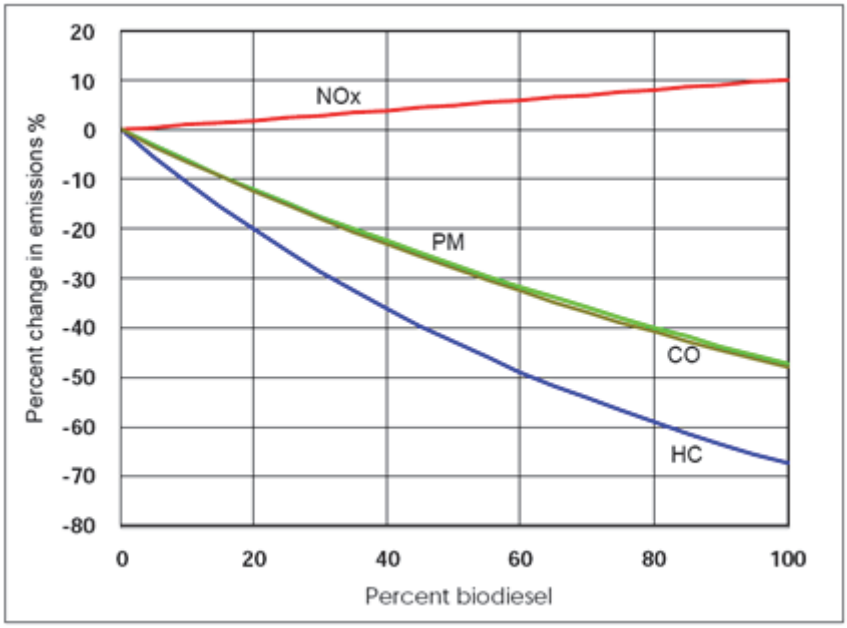

Fig. 2. Mean pollutant emissions by using different biodiesel percents in diesel engines, US EPA (2002)

	Coefficient "a"
NO_X	0.0009794
PM	-0.006384
HC	-0.011195
CO	-0.006561

Table 1. Values of coefficient "a"

Figure 3 shows the block diagram in which are presented all the stages of the calculation methodology, since the data collecting and organization, through the corrections, until obtaining the final results of the emissions.

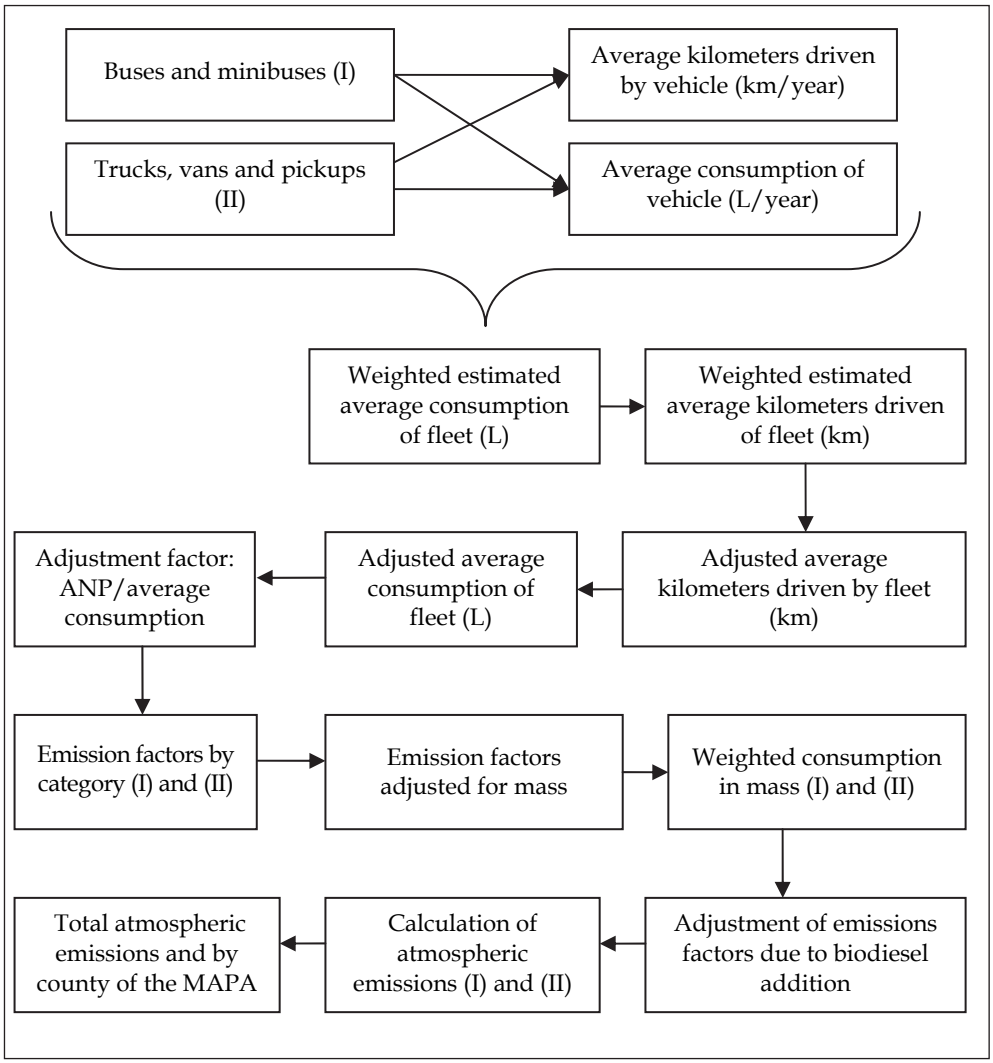

Fig. 3. Block chart of the calculation system

3.2 Air quality

3.2.1 Sampler automatics

The equipment used for the sampling included a sulfur oxide analyzer (using UV fluorescence method), a PM_{10} analyzer (using beta radiation method), a nitrogen oxide analyzer (AC31M using chemiluminescence method), a carbon monoxide analyzer (CO11M using infrared absorption), an ozone analyzer (O341M, absorption of UV light with wavelength of 254 nm, LCD/UV photometry ozone analyzer), Total hydrocarbon (HC 51 M FID Total hydrocarbon analyzer model). All equipment is manufactured by Environnement S.A.

The analysis of the 16 major PAHs (US EPA, 1999) was performed by chromatography coupled with a Shimadzu GCMS-QP5050A mass spectrophotometer detector. (For further details about the analyses, see American Society for Testing and Materials [ASTM], 2004; modified by Dallarosa et al., 2005a, b; 2008). After isolation, derivatization of the extracts was performed by cleanup, according to the method proposed by Jinhui & Lee (2001). After that, NPAHs analysis was performed by gaseous chromatography by electron capture detection (GC/ECD – Varian CP-3800) and silica gel column (CP - Sil 19 CB, 30 m x 0.25 µm x 0.25 mm).

4. Results and discussion

4.1 Emissions

Figure 4 shows the estimated emissions by diesel vehicles on the roads in 2008 and 2009 in the MAPA. In this area, there were 80,316 and 83,548 diesel vehicles in 2008 and 2009, respectively. An increase of 3.8% in the total diesel fleet can be seen. This increase was already expected due to the increase in vehicle sales in the state of Rio Grande do Sul during the last year.

Figure 5 shows a comparison between the diesel fleets of the MAPA and of Porto Alegre. Among the counties of the MAPA, Porto Alegre is probably the major contributor of atmospheric emissions, since as already mentioned before, it represents approximately 40% of the total diesel fleet in the area.

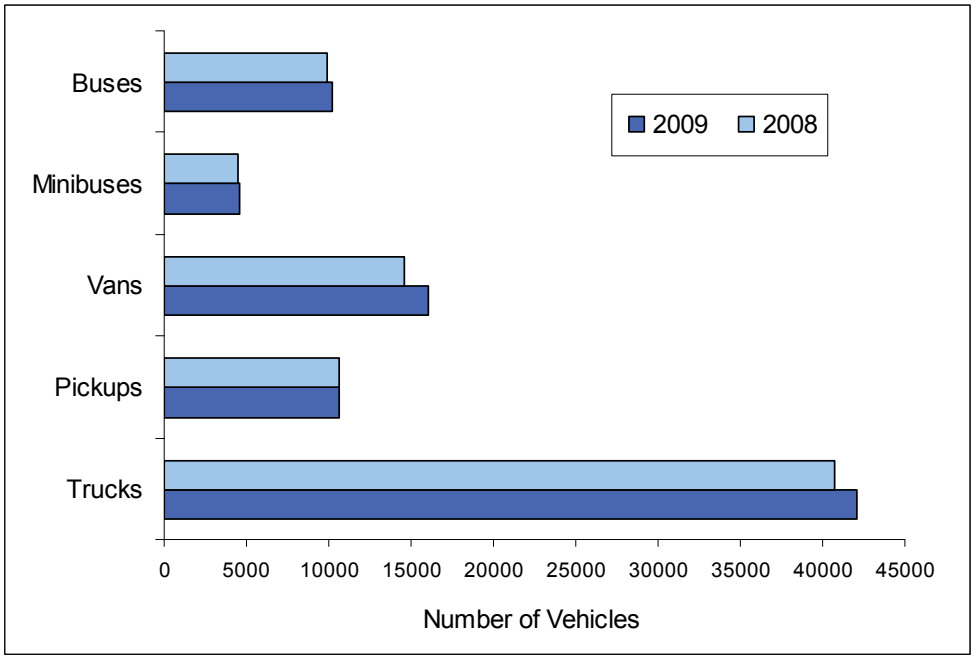

Fig. 4. Diesel fleet by vehicle type in the Metropolitan Area of Porto Alegre in 2008 and 2009

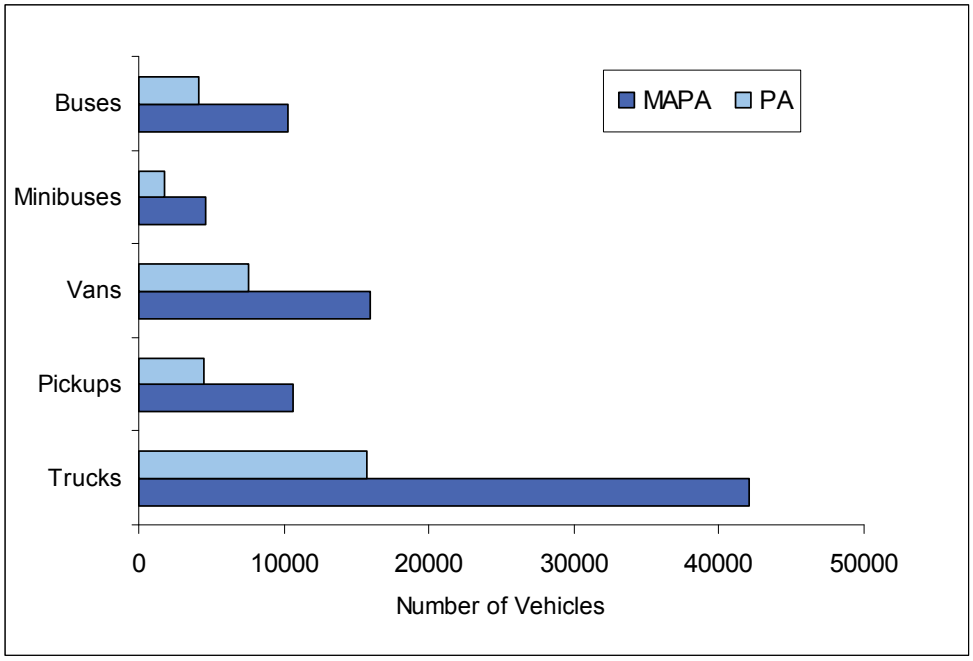

Fig. 5. Distribution of type of diesel vehicles in the Metropolitan Area of Porto Alegre and the city of Porto Alegre in 2009

Below we present the variations in atmospheric emissions of NO_X, CO, HC, and PM for 2008 and 2009 for different biodiesel amounts added to the diesel: 2, 5, 10, and 20%. A decrease in PM, CO, and HC emissions, as well as slight increase in NO_X emissions has been observed.
Figure 6 shows an increase in NO_X emissions when biodiesel was added. This might be explained due to the high oxygen levels in biodiesel molecules and to improved combustion conditions: temperature and pressure in the combustion chamber are higher, boosting the formation of larger amounts of nitrogen oxides in engines running on biodiesel, by combining oxygen with the nitrogen present in the air (Coronado et al., 2009).
Figure 7 shows the decrease in carbon monoxide emissions with the increase in biodiesel percent in the blend. This decrease might be attributed to the oxygen present in biodiesel molecules, producing a more efficient combustion reaction by moving the direction of the combustion reaction toward the production of CO_2 (Maziero et al., 2006).
Figure 8 shows a decrease in unburned hydrocarbon emissions by the addition of biodiesel to the diesel. This decrease is due to the complete combustion, during which CO_2 and water are mainly formed, as opposed to what occurs during diesel combustion (Coronado et al., 2009).
The decrease in particulate matter emissions, as shown in Figure 9, is due to higher oxygen levels in the biodiesel molecule, which allows the complete burning of the fuel. Consequently, there is a decrease in particulate matter emissions. The absence of sulfur in biodiesel contributes to less sulfate particles forming during combustion, thus contributing even more to a decrease in particulate matter emissions (Dwivedi et al., 2006).

Although the variation of SO_X emissions with the addition of biodiesel is not provided in the present study, these emissions decreased proportionally to the percent of diesel added to the blend. This occurs because biodiesel is a vegetable-derived fuel and it is free of sulfur.

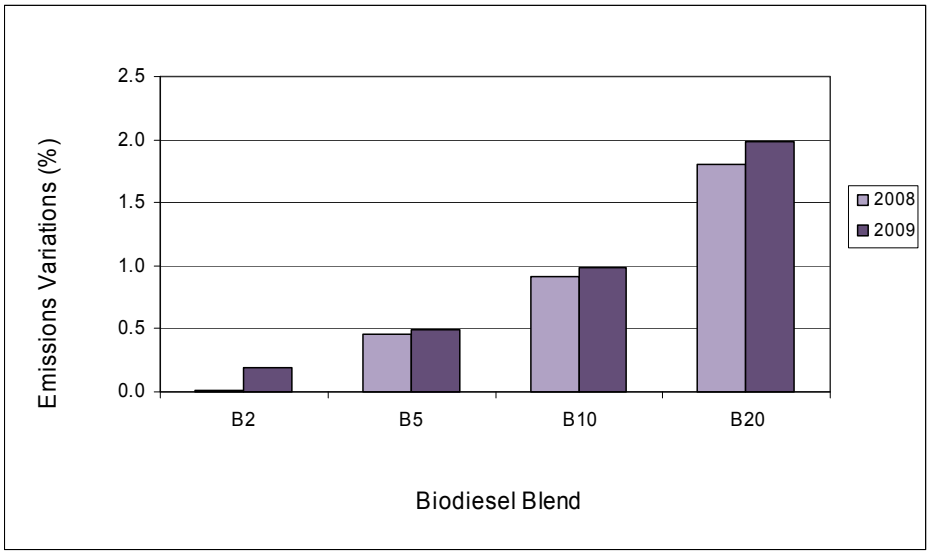

Fig. 6. Variation of atmospheric emissions of NO_X at different biodiesel blends added to diesel oil.

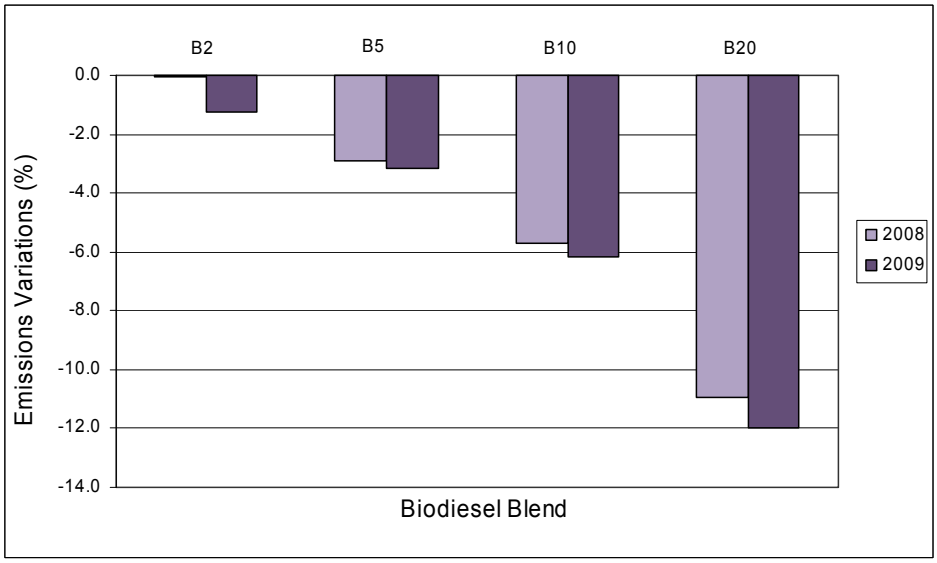

Fig. 7. Variation of atmospheric emissions of CO at different biodiesel blends added to diesel oil

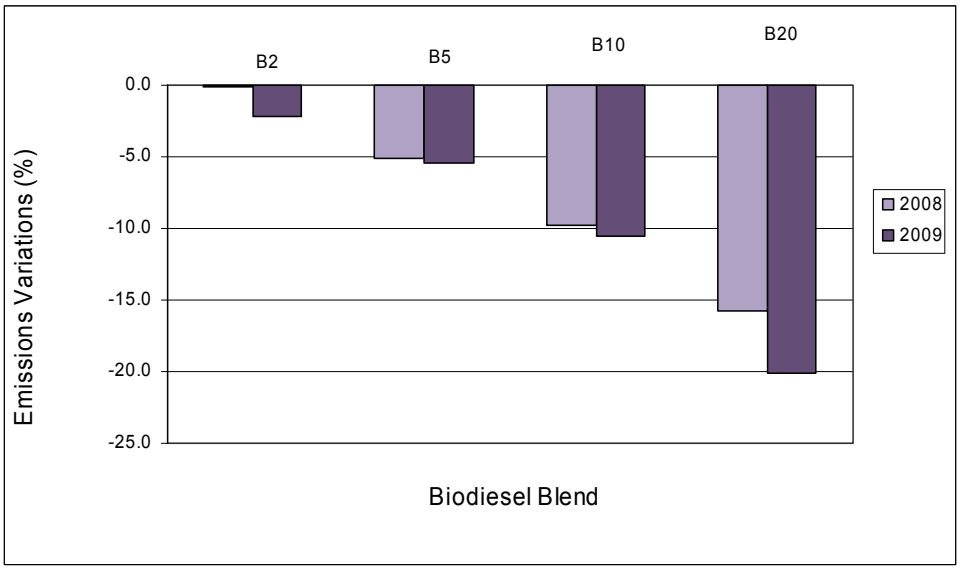

Fig. 8. Variation of atmospheric emissions of HC at different biodiesel blends added to diesel oil

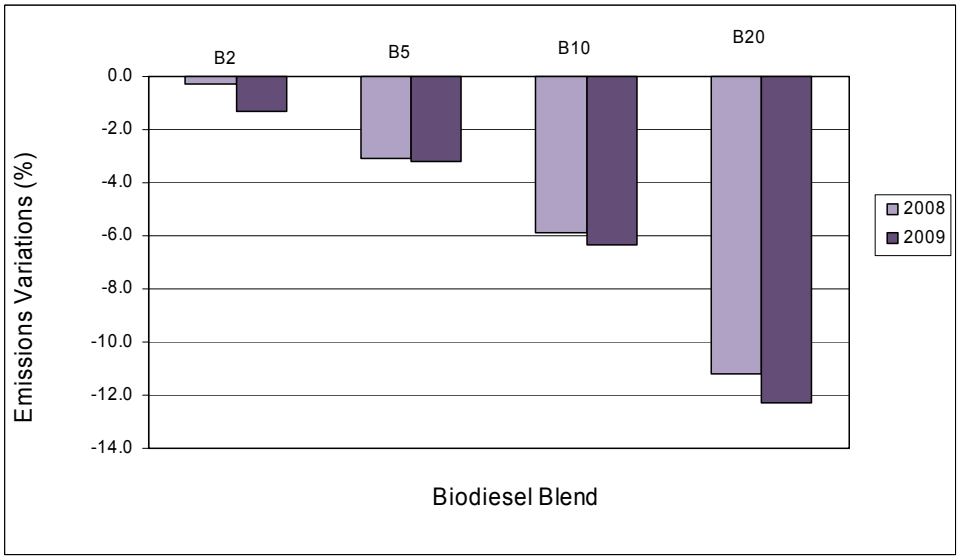

Fig. 9. Variation of atmospheric emissions of PM at different biodiesel blends added to diesel oil

Table 2 shows the compared results on pollutant emissions from diesel oil added of different biodiesel blends. Results reported by Morris et al. (2003) and by the National Biodiesel

Board (NBB, 2010) showed higher agreement with the estimated emission values for B20 in the present study. Data on CO, HC, NO_X and PM reported by Oliveira & Costa (2002) and NBB for B20 showed the highest agreement with results of the present study. At lower percents of biodiesel in diesel, results did not show significant variations, with only slight variations in the values found. This might indicate a change of trend. The error margin of the estimated and measured values is sometimes greater than the absolute values found.

B2					
Pollutant	CO	HC	NO_X	MP	SO_X
MAPA (2009)	-1.3	-2.2	0.2	-1.3	-
Corrêa (2005)	-0.1	-0.4	-1.3	-	-
B5					
Pollutant	CO	HC	NO_X	MP	SO_X
MAPA (2009)	-3.1	-5.4	0.5	-3.2	-
Corrêa (2005)	-0.2	-0.6	-1.3	-	-
Oliveira & Costa (2002)	-	-	0.7	-2.5	-5
B10					
Pollutant	CO	HC	NO_X	MP	SO_X
MAPA (2009)	-6.2	-10	1	-6.4	-
Corrêa (2005)	-0.3	-1.1	-3.7	-	-
Oliveira & Costa (2002)	-	-	1.3	-5	-9.5
B20					
Pollutant	CO	HC	NO_X	MP	SO_X
MAPA (2009)	-12	-20	2	-12	-
NBB (2010)	-12	-20	2	-12	-
Park et al. (2009)	-20	-35	3.7	-20	-
Oliveira & Costa (2002)	-	-	2.5	-10	-19
Morris et al. (2003)	-13	-	2.4	-8.9	-20

Table 2. Compared results (%) of various studies on pollutant emissions from diesel oil added of different biodiesel rates

4.2 Air quality

Table 3 shows the total average concentrations of PM_{10}, $PM_{2.5}$, CO, NO_X, NO_2, O_3, SO_2 measured in the MAPA for 2006, 2007, 2008 and 2009; and PAHs, NPAHs and $PM_{2.5}$ for 2006 and 2007. An increase in the pollutant studied is seen in 2007, except for PM_{10} and CO, whose data are from 2006. PAHs and NPAHs were higher in 2007.

Between 2006 and 2009, CO shows a decrease in the atmosphere (Table 3). This compound originates mostly from mobile sources. Despite the greater number of vehicles on the roads in recent years, the addition of catalytic converters to automobiles has substantially reduced CO emissions from the combustion of common gasoline. However, CO emissions during the ''cold start'' of engines, when the catalyst is cold and has not reached operating temperature, can still be substantial, even for those vehicles that are equipped with catalytic converters (Gaffney & Marley, 2009).

Studies about macro-regions of Rio Grande do Sul (Teixeira et al., 2010) showed that the MAPA had higher CO concentration in the air due to gasoline-fueled vehicles. Even if the

annual mean concentration of CO is decreasing, there are concerns about an increase in the number of vehicles on the roads and, consequently, in fuel consumption. Canoas, Sapucaia do Sul and Porto Alegre are the areas within the MAPA that have the greatest number of gasoline-fueled vehicles. During 2008 and 2009, gasoline consumption in these areas was 468,870 m^3 and 507,331m^3, respectively. These counties are probably the major contributors of atmospheric emissions (approx. 40.0%) in the MAPA, due to their great number of gasoline-fueled vehicles, with CO emissions of approximately 110,241 tons annually.

The annual SO_2 mean concentration was higher in 2007, with a slight decrease up to 2009 (Table 3). Despite vehicles having shown to be major contributors of SO_2 emissions, some stationary sources located in the MAPA, e.g. an oil refinery and coal-fired power plants, are probably also related to SO_2 emissions and have contributed to the higher emission levels measured in 2007. Some authors (Geng et al., 2009) have reported SO_2 in urban areas from vehicles and coal-fired power plants. These activities might speed up SO_2 concentration in the atmosphere (Nguyen & Kim, 2006).

High SO_2 and/or NO_2 emissions might result in the formation of secondary particulate matter of several orders of magnitude higher than the emissions of the primary fly ash PM originating for example from a coal fire power station (Gaffney & Marley, 2009). Moreover, since these secondary particles are very small (<1 μm) they have long atmospheric residence times and can travel long distances (Finlayson-Pitts & Pitts, 2000). Highly scattering aerosols, such as sulfates and nitrates, have been shown to have an overall effect of cooling in the lower atmosphere by scattering the incoming solar radiation (Charlson & Wigley, 1994). In presence of SO_2 and NO_X they can also form acid rain. In the atmosphere, SO_2 and NO_2 react with hydroxyl radicals and, in the presence of water vapor, form H_2SO_4 and HNO_3, respectively (Erduran & Tuncel, 2001).

Frequently, exhaust gases from motor vehicles contribute significantly to atmospheric particles emissions, mainly fine and ultrafine. The particulates associated with diesel exhaust are very small (<1 μm). Along with their small size, these particles have a very large surface area onto which other organic contaminants present in the diesel exhaust can adsorb. Polycyclic organic matter compounds with five or more membered rings are usually associated with diesel PM. Table 3 shows PM_{10} average concentrations in the MAPA from 2006 to 2009. The Brazilian legislation on PM_{10} establishes an annual average of 60 μm/m^3. It can be seen that the values were above the level established in the Brazilian legislation (National Council of the Environment [CONAMA], 2002), indicating that there is a contribution from vehicles, especially from heavy traffic that is usually associated with diesel particulates. Heavy traffic of diesel-fueled vehicles is characteristic of the area of sampling.

Table 3 shows the average annual concentrations in fine particles (<2.5 μm). Although there is no legislation in Brazil concerning fine particles, an increase in theses particles was reported in 2007, confirming the influence of heavy vehicles.

As already mentioned, the area studied herein (MAPA) has a lot of traffic of heavy diesel trucks, and only in Porto Alegre diesel consumption was 171,133 m^3 and 224,280 m^3 in 2008 and 2009, respectively.

The heavy traffic of diesel engines significantly contributes to produce ultrafine particles (Vallius et al., 2000). These ultrafine particles have a very large surface area onto which the organic contaminants present in the diesel exhaust can adsorb. The emission depends on a number of factors such as vehicle age, engine design and operating conditions, lubricant oil

and fuel quality, as well as environmental conditions (Maricq, 2007; Yanowitz et al., 2000). It is believed that with the higher percent of biodiesel added to diesel there will be a significant decrease in ultrafine particles emissions and, consequently, the quality of air will improve.

The average annual concentrations of NO_X, NO_2, and O_3 were higher in 2007 and 2009. In recent years, despite the higher number of vehicles on the roads, there was an improvement in fuel and lubricant oil quality, vehicle maintenance and operating conditions. Not all diesel vehicles had electronic injection until 2008; therefore, they were probably contributing to a higher concentration of NO_X in the atmosphere. Diesel vehicles on the roads are a major source of NO_X. Studies have estimated that diesel engines produce five times the amount of NO_X per mass of fuel burned when compared to gasoline vehicles (Gaffney & Marley, 2009). NO_X emissions react in the presence of sunlight through a series of photochemical reactions involving hydroxyl-, peroxy- and alkoxy radicals, to form the secondary pollutant ozone (Finlayson-Pitts & Pitts, 2000). NO reacts with peroxy radicals (RO_2) or O_3 producing NO_2, which can suffer a photolysis. The atomic oxygen thus released combines with molecular oxygen to form O_3 again.

Studies by Teixeira et al. (2009) about photochemical variables in the MAPA showed that the rise of NO_X and NO_2 concentrations in the area of study during the first hours of the day (7:00h –10:00h) is mainly due to the increase in traffic flow (rush hours). This is also associated with weak winds and atmospheric stability (characteristic of the "nocturnal stable boundary layer", that still persists in the first hours of the morning. These authors also report that the area of study suffers strong influence of mobile sources and NO is mainly emitted by vehicle exhausts; considering the reactivity of O_3 with NO, it reacts with O_3 to form NO_2, which acts as an O_3 sink.

$$NO + O_3 \rightarrow NO_2 + O_2 \quad (3)$$

Ozone is not the only oxidant formed from the reactions of NO_2 in the atmosphere. Other atmospheric oxidants are also formed such as hydrogen peroxide (H_2O_2), which can also react with SO_2 to form sulfuric acid aerosol, and others. Therefore, NO_X emissions are currently regulated in vehicle exhaust in order to control the formation of ozone in the atmosphere.

Year	PM_{10} $\mu g.m^{-3}$	$PM_{2.5}$ $\mu g.m^{-3}$	CO $\mu g\ .m^{-3}$	NO_X $\mu g.m^{-3}$	NO_2 $\mu g.m^{-3}$	O_3 $\mu g.m^{-3}$	SO_2 $\mu g.m^{-3}$	PAHs $ng.m^{-3}$ $PM_{2.5}$	NPAHs $ng.m^{-3}$ $PM_{2.5}$
2006	64.31	29.9	1.61	248	132	125	19.8	7.81	3.07
2007	56.25	39.2	1.42	313	178	155	41.1	8.54	7.52
2008	60.11	--	0.74	205	90.0	110	22.6	--	--
2009	58.1	--	0.77	257	110	118	8.25	--	--

Table 3. Average concentration of PM_{10}, CO, NO_X, NO_2, O_3, SO_2, measured in the MAPA for 2006, 2007, 2008 and 2009; PAHs, NPAHs and $PM_{2.5}$ for 2006 and 2007.

Besides the regulated pollutants, other pollutants are also emitted by vehicles, especially diesel engines, e.g. polycyclic aromatic hydrocarbons. Some compounds have shown carcinogenic and mutagenic properties (Chang et al., 2006; Kawanaka et al., 2004; Villalobos-Pietrini et al., 2007). Studies conducted by several authors (Dallarosa et al., 2008; Sheu et al.,

1997) on PAHs in fine particles have shown that the highest concentration of these compounds is found in particles <2.5 μm. Along with their small size, these particles have a very large surface area onto which other organic contaminants present in the diesel exhaust can adsorb. Polycyclic organic matter compounds with five or more membered rings are usually associated with diesel particulates.

Combustion related PAHs tend to be associated with fine mode vehicle emissions. The concentration of PAHs may vary due to meteorological conditions but high concentrations with high temperature and high solar intensity are considered favorable to photochemical and/or chemical reaction in the atmosphere (Harrison et al., 1996). Photochemical transformations are also considered significant processes for the removal of atmospheric PAHs. Ravindra et al. (2008) reported that PAHs in the vapor phase are more susceptible to such reactions than in the particulate phase. These same authors reported that at moderate temperatures the rate of PAH photo-decomposition may decrease with increased PAH particle loading.

Table 3 shows the average annual concentrations of PAHs and NPAHs in fine particles (<2.5 μm) in 2006 and 2007. Although the time span is of only two years, it is possible to see that these compounds increased in 2007 together with nitrogen oxides. These data confirm the influence of diesel vehicles, since the sampling sites are located near the BR-116 highway, which is under the strong influence of heavy traffic.

Table 4 shows a comparison of PAHs and NPAHs concentrations in the MAPA and other regions of the world. Concentrations in the MAPA were directly influenced by vehicle traffic. The area of Santiago (Chile) shows a higher PAHs concentration, because in addition to being an urban area, it is surrounded by hills and mountains ranging from 500 to 2500 m above sea level, producing limited air circulation and weak dispersion mechanisms, especially during winter, with low thermal inversion heights (Sienra & Rosazza, 2000).

NPAHs concentrations found in the MAPA (Table 4) were higher than those found by Albinet et al. (2007), even if taking into account differences in the equipment used for atmospheric particles and different meteorological conditions. Perhaps the area studied herein had a stronger influence of heavy vehicles; in addition, there might be formation of NPAHs during the sampling process (Albinet et al., 2007), since PAHs deposited on the filter are converted to NPAHs by the passage of NO_2.

Various authors have demonstrated that higher PAHs concentration are seen in winter (Fang et al., 2005) and that this can be attributed to various factors, amongst which increased consumption of combustible fossil fuels, increased condensation of PAHs in the gaseous phase at low temperatures (Garban et al., 2002) and some PAHs undergoing only little photochemical degradation under solar radiation in winter (Lee et al., 2002). Moreover, PAHs concentration in winter is higher than in spring/summer, mainly because stationary and mobile source emissions are higher. Lower PAHs concentrations during the summer sampling period have also been attributed to the washing out effect of particulates during rainy days, and photochemical degradation during high solar radiation (Fang et al., 2006). Most PAHs are attached to particulates and they are washed out in rainy summer days.

Other authors (Dallarosa et al., 2005a; 2008) reported that the higher PAHs concentration in atmospheric particles (PM_{10}) in the MAPA were related to events of thermal inversion, weak winds and low atmospheric pressure prevailing over the state. This, together with periods of heavier traffic, especially in winter, has directly influenced the accumulation of PAHs associated with particulates in the atmosphere.

Studies conducted by several authors (Dallarosa et al., 2008; Fang et al., 2006, Chang et al., 2006, Bourotte et al., 2005, and others) in different regions of world on PAHs in fine particles have shown that the highest concentration of these compounds are found in particles <2.5 μm.

NPAHs studies are based on the measuring of certain compounds in specific regions, and they try to assess the influence of emission sources and seasonality (samples collected at different seasons of the year: summer and winter) on them, as well as to propose the mechanisms by which NPAHs are formed in the atmosphere. Most studies use analytical methods already publish in the literature, only with adjustments to the particular conditions of the study.

The various papers on NPAHs published since 2000 are concentrated in the Northern Hemisphere, especially in countries as Japan (Tang et al., 2002; 2005; Kakimoto et al., 2001) and Italy (Di Filippo et al., 2007; 2009; 2010), each with three studies. In the Southern Hemisphere, we have Chile (Sienra et al., 2000; 2006) and Brazil, the latter with a study conducted in Sao Paulo by Vasconcellos et al. (2008). The latter study was based on the occurrence and the measuring of NPAHs in the air of three cities of the state of Sao Paulo (Araraquara, Piracicaba and Paulínia). Figure 10 shows a global overview on the location of the studies on NPAHs published since 2000.

Forty-seven NPAHs have been analyzed in the studies published since 2000. Despite this large number, studies have focused on a limited number of compounds: nitrofluoranthene, nitropyrene, nitroanthracene, nitronaphthalene, nitrophenanthrene, and their isomers. The most abundant NPAHs studied were: 1-nitropyrene (monitored in 90.5% of the studies: 19 out of 21 studies); 9-nitroanthracene (61.9%; 13/21); 2-nitrofluoranthene (61.9%; 13/21); 2-nitropyrene (57.1% ; 12/21); 3-nitrofluoranthene (52.4%; 11/21); 1-nitronaphthalene (47.6%; 10/21); 2-nitrofluorene (47.6%; 10/21).

The compound 1-nitropyrene (1-NP) has been detected in many types of combustion processes, including particles emitted by diesel and gasoline vehicles and by coal burning. The compounds 2-nitrofluoranthene (2-NFl) and 2-nitropyrene (2-NP) have not been detected in processes of direct emissions, although they are amongst the most abundant NPAHs present in the atmospheric particulate matter. Their presence might be due to the atmospheric transformations of fluoranthene and pyrene.

When analyzing emissions from diesel vehicles with regard to the presence of 1-nitronaphthalene and 2-nitronaphthalene, only 1-nitronaphthalene was found (Bamford et al., 2003). Atkinson et al. (1987) observed that in the gaseous phase reactions with naphthalene initiated by OH^- radicals produced 1 and 2-nitronaphthalene at almost identical amounts. Therefore, the fact that 2-nitronaphthalene having appeared in 57.1% of the studies reinforces the hypothesis of investigation on the mechanisms by which NPAHs are formed in the atmosphere, with the purpose of monitoring certain NPAHs.

PAHs are emitted directly from combustion whereas NPAHs, as already mentioned before, are primarily emitted and formed in the atmosphere, by gas and heterogeneous phase reactions of PAHs induced by atmospheric oxidants (OH, NO_3, O_3). PAH derivatives have a particular interest because they seem more toxic than their related parent PAHs. For instance, NPAHs could contribute with 10% to the total mutagenicity of inhalable suspended particles in polluted areas (Atkinson & Arey, 1994; Albinet et al., 2007). A correct quantification of these compounds in ambient air is very important.

	Sampler type	Source	PAHs ng.m^{-3}	NPAHs ng.m^{-3}
MAPA-Brazil 2006/2007	$PM_{2.5}$	urban, traffic	7.8-8.5	3.07-7.52
Ravindra et al. 2006	PM	different anthropogenic activities	0.9-8.7	--
Bourotte et al. 2005	$PM_{2.5}$	urban	10.8	--
Sienra et al. 2005	PM_{10}	traffic	5.45–61.93	--
Sienra et al. 2005	PM_{10}	traffic	1.79–10.91	--
Albinet et al. 2007	PM_{10}	traffic	7.6	--
Albinet et al. 2007	high volume cascade impactor	traffic	4.9	--
Albinet et al. 2007	PM_{10}	traffic	--	0.247
Albinet et al. 2007	high volume cascade impactor	traffic	--	0.954
Albinet et al. 2007	PM_{10}	urban	0.5	--
Albinet et al. 2007	high volume cascade impactor	urban	0.5	--
Albinet et al. 2007	PM_{10}	urban	--	0.152
Albinet et al. 2007	high volume cascade impactor	urban	--	0.034

Table 4. Compared concentrations of PAHs and NPAHs in the Metropolitan Area of Porto Alegre, Brazil, and other regions of the world.

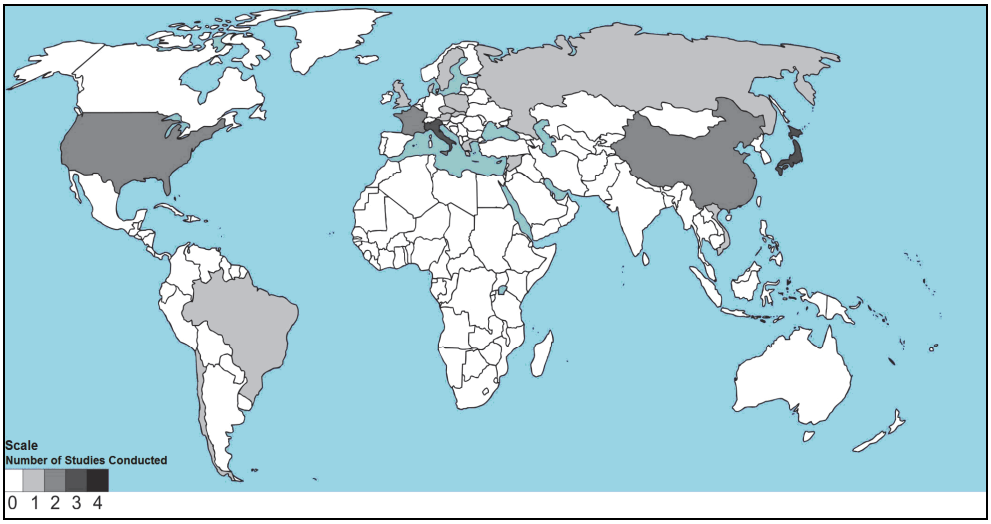

Fig. 10. Studies conducted in the world about NPAHs monitoring, identified in the literature and published as of 2000.

5. Conclusion

The major benefit of biodiesel to the environment is the significant decrease in atmospheric pollutant emissions compared to petroleum diesel oil. Estimated data on biodiesel addition to diesel oil indicate a decrease in pollutant levels, particularly for B20. Pollutant emissions showed a decrease in PM, CO, and HC, while NO_X experienced a slight increase.

Vehicle emissions were usually the most significant source of air pollution in general in the Metropolitan Area of Porto Alegre (MAPA). This was intensified by emissions from diesel engines.

The characterization of atmospheric pollutants in the Metropolitan Area of Porto Alegre showed that it is influenced by mobile sources and, particularly, by diesel engines.

The increase in average annual concentrations of PAHs and NPAHs in the fine particles (<2.5 μm) in 2007, together with nitrogen oxides, confirms the influence of heavy traffic in the MAPA.

Studies conducted by several authors as of 2000 about NPAHs show that most of these compounds were related to direct emissions (vehicular emissions, particularly emissions from diesel engines), except for 2-nitrofluoranthene, 2-nitropyrene and 2-nitronaphthalene, which are formed by reactions of PAHs with hydroxyl radicals (OH^-).

The subject of future studies will be organic compounds associated with ultrafine atmospheric particles and ways to optimize the sampling methods to achieve a more accurate assessment of the influence of mobile sources.

6. Acknowledgements

We are grateful to FINEP, FAPERGS and CNPq for their financial support.

7. References

Agarwal, A.K. 2007. Biofuels (alcohols and biodiesel) applications as fuels for internal combustion engines. *Progress in Energy and Combustion Science*, Vol. 33, No. 3, pp. 233-271.

Albinet, A.; Leoz-Garzilandia, E.; Budzinski, H. & Villenave, E. (2007). Sampling precaution, for the measurement of nitrated polycyclic aromatic hydrocarbons in ambient air. *Atmospheric Environment*, Vol. 41, No. 23, pp. 4988–4994.

American Society for Testing and Materials [ASTM]. 2004. Standard Test Method for Determination of Gaseous and Particulate Polycyclic Aromatic Hydrocarbons in Ambient Air (Collection on Sorbent-Backed Filters with Gas Chromatographic/Mass Spectrometric Analysis). Designation: D6209 – 98.

Andrade-Eiroa, A.; Leroy, V. & Dagaut, P. (2010). Advances in PAHs/nitro-PAHs fractioning. *Analytical Methods*, Vol. 2, No. 12, pp. 2017-2024.

Atkinson R.; Arey J.; Zielinska B. & Aschmann, S.M. (1987). Kinetics and products of the gas-phase reactions of OH radicals and N205 with naphthalene and biphenyl. *Environmental, Science and Technology*, Vol. 21, No. 4, pp. 1014-1022.

Atkinson, R. & Arey, J. (1994). Atmospheric chemistry of gas phase polycyclic aromatic hydrocarbons: formation of atmospheric mutagens. *Environmental Health Perspectives*, Vol. 102, pp. 117–126.

Bamford, H.A.; Bezabeh, D.Z.; Schantz, M.M.; Wise, S.A. & Baker, J.E. (2003). Determination and comparison of nitrated-polycyclic aromatic hydrocarbons measured in air and diesel particulate reference materials. *Chemosphere*, Vol. 50, pp. 575–587.

Brazilian Institute of Geography and Statistics [IBGE]. (2010). Rio Grande do Sul, In: *Banco de Dados*, 01.2010, Available from: <http://www.ibge.gov.br>

Bourotte, C.; Forti, M.C.; Taniguchi, S.; Bícego, M.C. & Lotufo, P.A. (2005). A wintertime study of PAHs in fine and coarse atmospheric particles in São Paulo city, Brazil. *Atmospheric Environment*, Vol. 39, pp. 3799–3811.

Chang, K.F.; Fang, G.C.; Chen, J.C. & Wu, Y.S. (2006). Atmospheric polycyclic aromatic hydrocarbons (PAHs) in Asia: A review from 1999 to 2004. *Environmental Pollution*, Vol. 142, pp. 388-396.

Charlson, R.J. & Wigley, T.M.L. (1994). Sulfate Aerosol and Climate Change. *Scientific American*, Vol. 270, No. 2, pp. 48-57.

Chetwittachan, T.; Shimazaki, D. & Yamamoto, K. (2002). A comparison of temporal variation of particle-bound polycyclic aromatic hydrocarbons concentration in different urban environments: Tokyo, Japan and Bangkok, Thailand. *Atmospheric Environment*, Vol. 36, pp. 2027-2037.

Colvile, R.N.; Hutchinson, E. J.; Mindell, J. S. & Warren, R. F. (2001). The transport sector as a source of air pollution. *Atmospheric Environment*, Vol. 35, pp. 1537-1565.

Coronado, C.R.; Carvalho Jr., J.A. & Silveira, J.L. (2009). Biodiesel CO_2 emissions: A comparison with the main fuels in the Brazilian market. *Fuel Processing Technology*, Vol. 90, pp. 204-211.

Corrêa, S.M. (2005). Impacto do biodiesel na qualidade do ar da cidade do Rio de Janeiro. *Proceedings of XXV Encontro Nacional de Engenharia de Produção*, Porto Alegre-RS/Brazil, Oct/Nov 2005.

Dallarosa, J.; Monego, J.G.; Teixeira, E.C.; Stefens, J.L. & Wiegand, F. (2005a). Polycyclic aromatic hydrocarbons in atmospheric particles in the metropolitan area of Porto Alegre, Brazil. *Atmospheric Environment*, Vol. 39, pp. 1609–1625.

Dallarosa, J.B.; Teixeira, E.C.; Pires, M. & Fachel, J. (2005b). Study of the profile of polycyclic aromatic hydrocarbons in atmospheric particles (PM_{10}) using multivariate methods. *Atmospheric Environment*, Vol. 39, pp. 6587–6596.

Dallarosa J.; Teixeira E.C.; Meira L. & Wiegand F. (2008). Study of the chemical elements and polycyclic aromatic hydrocarbons in atmospheric particles of PM_{10} and $PM_{2.5}$ in the urban and rural areas of South Brazil. *Atmospheric Research*, Vol. 89, pp. 76-92.

Desantes, J.M.; Berrmúdez, V.; Garcia, J.M. & Fuentes, E. (2005). Effects of current engine strategies on the exhaust aerosol particle size distribution from a Heavy-Duty Diesel Engine. *Journal of Aerosol Science*, Vol. 36, pp. 1251-1276.

Di Filippo, P.; Riccardi, C.; Gariazzo, C.; Incoronato, F.; Pomata, D.; Spicaglia, S. & Cecinato, A. (2007). Air pollutants and the characterization of the organic content of aerosol particles in a mixed industrial/semi-rural area in central Italy. *Journal of Environmental Monitoring*, Vol. 9, pp. 275-282.

Di Filippo, P.; Riccardi, C.; Pomata, D.; Gariazzo, C. & Buiarelli, F. (2009). Seasonal abundance of particle-phase organic pollutants in an urban/industrial atmosphere. *Water, Air, and Soil Pollution*, Vol. 211, No. 1-4, pp. 231-250.

Di Filippo, P.; Riccardi, C.; Pomata, D. & Buiarelli, F. (2010). Concentrations of PAHs, and nitro- and methyl- derivatives associated with a size segregated urban aerosol. *Atmospheric Environment*, Vol. 44, pp. 2742-2749.

Dwivedi, D.; Agarwal, A.K. & Sharma, M. (2006). Particulate emission characterization of a biodiesel vs. diesel-fuelled compression ignition transport engine: A comparative study. *Atmospheric Environment*, Vol. 40, pp. 5586-5595.

Erduran, M.S. & Tuncel, S.G. (2001). Gaseous and particulate air pollutants in the northeastern Mediterranean Coast. *Science of the Total Environment*, Vol. 281, pp. 205-215.

Fang, G.C.; Wu, Y.S.; Chen, J.C.; Fu, P.P.; Chang, C.N.; Ho, T.T. & Chen, M.H. (2005). Characteristic study of polycyclic aromatic hydrocarbons for fine and coarse particulates at Pastureland near Industrial Park sampling site of central Taiwan. *Chemosphere*, Vol. 60, No. 3, pp. 427-433.

Fang, G.C.; Wu, Y.S.; Chen, J.C.; Chang, C.N. & Ho, T.T. (2006). Characteristic of polycyclic aromatic hydrocarbon concentrations and source identification for fine and coarse particulates at Taichung Harbor near Taiwan Strait during 2004–2005. *Science of the Total Environment*, Vol. 366, pp. 729–738.

Finlayson-Pitts, B.J. & Pitts Jr., J.N. (2000). *Chemistry of the Upper and Lower Atmosphere: Theory, Experiments, and Applications*, (1st Ed), Academic Press, ISBN-13: 978-0122570605.

Fontaras, G.; Kousoulidou, M.; Karavalakis, G.; Tzamkiozis, T.; Pistikopoulos, P.; Ntziachristos, L.; Bakeas, E.; Stournas, S. & Samaras, Z. (2010). Effects of low concentration biodiesel blend application on modern passenger cars. Part 1: Feedstock impact on regulated pollutants, fuel consumption and particle emissions. *Environmental Pollution*, Vol. 158, No. 5, pp. 1451-1460

Gaffney, J.S. & Marley, N.A. (2009). The impacts of combustion emissions on air quality and climate – From coal to biofuels and beyond. *Atmospheric Environment*, Vol. 43, pp. 23–36.

Garban, B.; Blanchoud, H.; Motelay-Massei, A.; Chevreuil, M. & Ollivon, D. (2002). Atmospheric bulk deposition of PAHs onto France: trends from urban to remote sites. *Atmospheric Environment*, Vol. 36, pp. 5395-5403.

Geng, F.; Zhang, Q.; Tie, X.; Huang, M.; Ma, X.; Deng, Z.; Yu, Q.; Quan, J. & Zhao, C. (2009). Aircraft measurements of O3, NO_X, CO, VOCs, and SO_2 in the Yangtze River Delta region. *Atmospheric Environment*, Vol. 43,pp. 584–593.

Gupta, I. & Kumar, R. (2006). Trends of particulate matter in four cities in India. *Atmospheric Environment,* Vol. 40, pp. 2552-2566.

Harrison, R.M.; Smith, D.J.T. & Luhana, L. (1996). Source apportionment of atmospheric polycyclic aromatic hydrocarbons collected from an urban location in Birmingham, U.K. *Environmental, Science and Technology*, Vol. 30, pp. 825-832.

Jinhui, X. & Lee, F.S.C. (2001). Analysis of nitrated polynuclear aromatic hydrocarbons. *Chemosphere*, Vol. 42, pp. 245–250.

Jung, H.J.; Kittelson, D.B. & Zachariah, M.R. (2006). Characteristics of SME biodiesel-fueled diesel particle emissions and the kinetics of oxidation. *Environmental Science and Technology*, Vol. 40, pp. 4949–4955.

Kagawa, J. (2002). Health effects of diesel exhaust emissions - a mixture of air pollutants of worldwide concern. *Toxicology*, Vol. 181-182, pp. 349–353.

Kakimoto, H.; Yokoe, H.; Matsumoto, Y.; Sakai, S.; Kanoh, F.; Murahashi, T.; Akutsu, K.; Toriba, A.; Kizu, R. & Hayakawa, K. (2001). Considerations of atmospheric behaviors of polycyclic aromatic hydrocarbons, nitropolycyclic aromatic hydrocarbons and inorganic pollutants based on their interrelationships. *Journal of Health Science*, Vol. 47, pp. 385–393.

Karavalakis, G.; Fontaras, G.; Ampatzoglou, D.; Kousoulidou, M.; Stournas, S.; Sâmaras, Z. & Bakeas, E. (2010). Effects of low concentration biodiesel blends application on modern passenger cars. Part 3: Impact on PAH, nitro-PAH, and oxy-PAH emissions. *Environmental Pollution*, Vol. 158, pp. 1584-1594.

Kawanaka, Y.; Matsumoto, E.; Sakamoto, K.; Wang, N. & Yun, S. (2004). Size distributions of mutagenic compounds and mutagenicity in atmospheric particulate matter collected with a low-pressure cascade impactor. *Atmospheric Environment*, Vol. 38, pp. 2125-2132.

Kerminen, V.M.; Mäkelä, T.E.; Ojanen, C.H.; Hillamo, R.E.; Vilhunen, J.K.; Rantanen, L.; Havers, N.; Bohlen, A. & Klockow, D. (1997) . Characterization of the particulate phase in the exhaust from a diesel car. *Environmental Science and Technology*, Vol. 31, No. 7, pp. 1883–1889.

Kim Oanh, N.T. (2006). Particulate air pollution in six Asian cities: Spatial and temporal distributions, and associated sources. Atmospheric Environment, Vol. 40, pp. 3367-3380.

Knothe, G. (2006). Propriedades do Combustível. In: *Manual de Biodiesel*, Knothe, G.; Gerpen, J.V.; Krahl, J. & Ramos, L.P., pp. 83-88, Editora Blucher, ISBN: 978-85-212-0405-3, São Paulo, Brazil.

Knothe, G. (2007). Some aspects of biodiesel oxidative stability. *Fuel Process Technology*, Vol. 88, pp. 669–77.

Lee, S.C.; Ho, K.F. & Chiu, G.M.Y. (2002). Characterization of selected volatile organic compounds, polycyclic aromatic hydrocarbons and carbonyl compounds at a roadside monitoring station. *Atmospheric Environment*, Vol. 36, pp. 57–65.

Lin, Y.C.; Lee, W.J. & Hou, H.C. (2006). PAH emissions and energy efficiency of palm-biodiesel blends fueled on diesel generator. *Atmospheric Environment*, Vol. 40, pp. 3930-3940.

Livi, F.P. (1999). Elementos do Clima: o contraste de tempos frios e quentes. In: *Atlas Ambiental de Porto Alegre,* MENEGAT, R., pp. 73-74, Editora da Universidade Federal do Rio Grande do Sul, ISBN: 8570259123, Rio Grande do Sul, Brazil.

Maricq, M.M. (2007). Chemical characterization of particulate emissions from diesel engines: A review. *Journal of Aerosol Science*, Vol. 38, pp. 1079-1118.

Maziero, J.V.G.; Corrêa, I.M.; Trielli, M.A.; Bernardi, J.A. & D'Agostini, M.F. (2006). Avaliação de emissões poluentes de um motor diesel utilizando biodiesel de girassol como combustível. *Engenharia na Agricultura*, Vol. 14, No. 4, pp. 287-292.

Morris, R.E.; Pollack, A.K.; Mansell, G.E.; Lindhjem, C.; Jia, Y. & Wilson, G. (2003). Impact of biodiesel fuels on air quality and human health. Summary Report. National Renewable Energy Laboratory, NREL/SR-540-33793.

National Biodiesel Board [NBB]. (2010). Biodiesel emissions. In: *Biodiesel*, 03.2010, Available from: <http://www.biodiesel.org/pdf_files/fuelfactsheets/emissions.pdf>

National Council of the Environment [CONAMA]. (2002). Resolução nº 315, de 29 de outubro de 2002. Controle da Poluição do Ar – PROCONVE/PROMOT, 06.2010, Available from: <http://www.mma.gov.br/port/conama/legiabre.cfm?codlegi=337>

Nguyen, H.T. & Kim, K.H. (2006). Evaluation of SO_2 pollution levels between four different types of air quality monitoring stations. *Atmospheric Environment*, Vol. 40, pp. 7066-7081.

Oliveira, L.B. & Costa, A.O. (2002). Biodiesel: uma experiência de desenvolvimento sustentável, *Proceedings of Congresso Brasileiro de Energia*, Rio de Janeiro, Brazil.

Park, S.; Kim, H. & Choi, B. (2009). Emission characteristics of exhaust gases and nanoparticles from a diesel engine with biodiesel-diesel blended fuel (BD20). *Journal of Mechanical Science and Technology*, Vol. 23, pp. 2555-2564.

Phuleria, H.C.; Sheesley, R.J.; Schauer, J.J.; Fine, P.M. & Sioutas, C. (2007). Roadside measurements of size-segregated particulate organic compounds near gasoline and diesel dominated freeways in Los Angeles, CA. *Atmospheric Environment*, Vol. 41, No. 22, pp. 4653-4671.

Ravindra, K.; Sokhi, R. & Grieken, R.V. (2008). Atmospheric polycyclic aromatic hydrocarbons: Source attribution, emission factors and regulation. *Atmospheric Environment*, Vol. 42, pp. 2895-2921.

São Paulo State Environmental Company [CETESB]. (2008). Relatório de qualidade do ar no Estado de São Paulo em 2007, In: *Qualidade do Ar: Publicações e Relatórios*, 01.2010, Available from: <http://www.cetesb.sp.gov.br/ar/qualidade-do-ar/31-publicacoes-e-relatorios>

Sheesley, R.J.; Schauer, J.J.; Zheng, M. & Wang,B. (2007). Sensitivity of molecular marker-based CMB models to biomass burning source profiles. *Atmospheric Environment*, Vol. 41, pp. 9050-9063.

Sheu, H.L.; Lee, W.J.; Lin, S.J.; Fang, G.C.; Chang, H.C. & You, W.C. (1997). Particle-bound PAH content in ambient air. *Environmental Pollution*, Vol. 96, No. 3, pp. 369–382.

Sienra, M.D.R. & Rosazza, N.G. (2000). Occurrence of nitropolycyclic aromatic hydrocarbons in urban particulate matter PM_{10}. *Atmospheric Research*, Vol. 81, pp. 265–276.

Sienra, M.R.; Rosazza, N.G. & Préndez, M. (2005). Polycyclic aromatic hydrocarbons and their molecular diagnostic ratios in urban atmospheric respirable particulate matter. *Atmospheric Environment*, Vol. 75, pp. 267–281.

Tang, N.; Tabata, M.; Mishukov, V.F.; Sergineko, V.; Toriba, A.; Kizu, R. & Hayakawa, K. (2002). Comparison of Atmospheric Nitropolycyclic Aromatic Hydrocarbons in Vladivostok, Kanazawa and Toyama. *Journal of Health Science*, Vol. 48, no. 1, pp. 30-36.

Tang, N.; Hattori, T.; Taga, R.; Igarashi, K.; Yang, X.; Tamura, K.; Kakimoto, H.; Mishukov, V.F.; Toriba, A.; Kizy, R. & Hayakawa, K. (2005). Polycyclic aromatic hydrocarbons and nitropolycyclic aromatic hydrocarbons in urban air particulates and their relationship to emission sources in the Pan–Japan Sea countries. *Atmospheric Environment*, Vol. 39, No. 32, pp. 5817-5826.

Teixeira, E.C.; Feltes, S. & Santana, E. (2008). Estudo das emissões de fontes móveis na região metropolitana de Porto Alegre, Rio Grande do Sul. *Química Nova*, Vol. 31, pp. 244-248.

Teixeira, E.C.; Santana, E.; Wiegand, F. & Fachel, F. (2009). Measurement of surface ozone and its precursors in an urban area in South Brazil. *Atmospheric Environment*, Vol. 43, pp. 2213–2220.

Teixeira, E.C.; Santana, E.; Wiegand, F.; Feltes, S.; Mattiuzi, C. & Palagi, A. (2010). 1º Inventário das emissões atmosféricas de fontes móveis do Estado do Rio Grande do Sul. Fundação Estadual de Proteção Ambiental Henrique Luís Roessler – FEPAM/RS, ISBN 978-85-98053-09-7.

United States Environmental Protection Agency [US EPA]. (1999). Compendium of methods for the determination of toxic organic compounds in ambient air: determination of polycyclic aromatic hydrocarbons (PAHs) in ambient air using gas chromatograph/mass spectrometer (GC/MS). Method TO-13A. US Government Printing Office, Washington DC.

United States Environmental Protection Agency [US EPA]. (2002). A comprehensive analysis of biodiesel impacts on exhaust emissions. 02. 2010, Available from: <http://www.epa.gov/otaq/models/analysis/biodsl/p02001.pdf >

Vallius, M.J.; Ruuskanen, J.; Mirme, A. & Pekkanen, J. (2000). Concentrations and estimated soot content of PM_1, $PM_{2.5}$, and PM_{10} in a subarctic urban atmosphere. *Environmental, Science and Technology*, Vol. 34, pp. 1919–1925.

Vasconcellos, P. C.; Sanchez-Ccoyllo, O.; Balducci, C.; Mabilia, R. & Cecinato, A. (2008). Occurrence and concentrations levels of nitro-PAH in the air of three Brazilian cities experiencing different emissions impacts. *Water, Air and Soil Pollution*, Vol. 190, pp. 87-94.

Villalobos-Pietrini, R.; Hernández-Mena, L.; Amador-Muñoz, O.; Munive-Colín, Z.; Bravo-Cabrera, J.J.; Gómez-Arroyo, S.; Frías-Villegas A. & Ortiz-Muñiz R. (2007). Biodirected mutagenic chemical assay of PM_{10} extractable organic matter in Southwest México City. *Mutation Research*, Vol. 634, pp. 192-204.

Yanowitz, J.; McCormick, R. L. & Graboski, M.S. (2000). In-use emissions from heavy-duty diesel vehicles. *Environmental, Science and Technology*, Vol. 34, pp. 729–740.

9

Applications of Remote Sensing Instruments in Air Quality Monitoring

Chuen Meei Gan, Barry Gross,
Yong Hua Wu and Fred Moshary
City University of New York
United States

1. Introduction

Aerosols have become an area of intensive study both for the complex climate forcing questions that arise due to direct aerosol and indirect (aerosol–cloud) mechanisms and for air quality concerns that have arisen due to exposure to fine particulate matter. While the climate questions regarding aerosols are certainly of great importance, our focus in this chapter is to explore using remote sensing techniques the unique concerns of aerosol dynamics in an urban environment and how such understanding can ultimately be used to improve air quality modelling and forecast.

The difficulties of urban air quality forecast modelling can be grouped into two major factors. First, urban areas have extremely variable multiple pollutant emission sources and inventories of these emissions are difficult to be quantified in a common way without limitations and uncertainties (Koji & Lovei, 2001; Zhao & Frey, 2004). Second, meteorological and radiation processes which drive the aerosol generation and transport are significantly affected by complexities in the urban atmosphere coupling. In particular, urban structures can significantly affect diurnal heating processes through surface roughness mechanisms which modify wind and turbulent mechanisms as well as radiation trapping due to surfaces which absorb radiation (e.g. asphalt) and are a root cause of Urban Heat Island (UHI) mechanisms (Liu et al., 2006; Taha, 1999; Atkinson, 2003; Piringer et al., 2007; Mestayer et al. 2005). These mechanisms have a direct effect on the mixing layer which is the region that is directly affected by processes or events that occur at the earth's surface (e.g. heat transfer and turbulence). Most important for air quality applications, the planetary boundary layer (PBL) height effectively defines a total available volume for pollutant transport and dispersion (Stull, 1988) and errors in prediction of PBL dynamics will affect how the pollution forecasts are distributed. Therefore, methods that can directly explore PBL height dynamics should provide some insights into underlying difficulties observed in current air quality models are needed.

The most direct and attractive approach is so called active remote sensing techniques which can be used to range different components of the atmosphere. Once these atmospheric parameters are profiled, further analysis can then be used to estimate the PBL height. For instance, sodar and radar wind profilers monitor wind speed and by looking at statistical

fluctuations of wind speed, we can estimate the turbulent structure of the atmosphere. Since the PBL is a region where turbulent behavior dominates over the shear dynamics seen in the upper atmosphere, enhanced fluctuations in wind speed are a good indicator of PBL height. On the other hand, direct observations of the aerosol pollutants themselves are particularly valuable both as a means to monitor PBL heights and as a means of tracking the vertical structure of the aerosols directly (Kovalev & Eichinger, 2004). Ceilometers have the advantage of being eye safe and can run continuously (e.g. 24 hours / 7 days) and unattended but the signal to noise ratio (SNR) is low and vertical range is limited even if extensive temporal and spatial averaging is used. Therefore, for high mixing layers such as those in summer where convective heating causes the layer to grow, ceilometers are not suitable. In this case, the elastic lidar system (Nd:YAG laser) which has much better SNR are the only realistic choice. Unfortunately, this system is not eye safe and therefore cannot run without external observers. This makes continuous operation impractical. In addition, due to the limitations of large telescope optics, lidar signals cannot see near to surface and transmitter/receiver overlap occurs only sufficiently far from the ground (> 500 meters). This makes certain applications such as tracking surface pollutants inaccessible although merging ceilometer and lidar together may address this overlap issue. However, despite these difficulties, the optical techniques which track the aerosols directly in general outperform the turbulence based approaches as well as allow us to explore other processes so that the major focus of this chapter will be on lidar and ceilometer based techniques and their potential to address air quality questions and assess current and future air quality models.

To assess the potential of lidar based methods, we rely heavily on data and instrumentation directly available in research conducted in New York City (NYC) which is an excellent representative of the complexities of the urban environment. In particular, long term ground based multi-wavelength lidar observations have been performed at City College of New York (CCNY). A noise sensitive wavelet transform method together with additional constraints has been developed to better determine the convective boundary layer from lidar measurements (Emeis et al., 2008; Davis et al., 2000). This method is then applied over multiyear observations to assess the Weather Research and Forecast (WRF) Model (Flagg & Taylor, 2008; Gan et al., 2011). In doing these comparisons, seasonal performance issues are a particular focus (Zhang et al., 2009).

The above discussion focused on local emission and dynamics and therefore long range transport events are not considered. However, one of the strongest benefits for lidar is the direct observation of aloft layers which can affect local pollutants as well as making it difficult for satellite observations. Because of the increased extend of urban mixing layers in general; it is possible for aloft layers to mix with local emission layers. Therefore we also add a section to illustrate how this mechanism can affect PBL pollution by a case study of Aug 2007 Idaho and Montana Fires. We evaluate this smoke plume transport event using in-situ and satellite measurements combined with back-trajectory analysis (Gan et al., 2008). This section clearly illustrate why vertical information is critical in monitoring air quality and how large-scale plume transportation effect surface pollution level.

The structure of this chapter is as follows. In section 2, a brief introduction of meteorology of the PBL and the urban heat island (UHI) is given. A brief survey of current methods in

measuring air quality is discussed in section 3. Next, we give an introduction to air quality models with particular attention to those used within Weather Research and Forecast (WRF) model coupled with the Community Multiscale Air Quality (CMAQ) model environment in section 4. In section 5, descriptions of the vertical remote sensing instruments are given along with PBL height retrieval method and their advantages/disadvantages are enumerated. In section 6, discussion of the performance of air quality models in urban areas is given with special focus on the high pollution summer events. The comparisons between measurements and WRF model are presented and anomalies which may explain difficulties with CMAQ model forecasts are given. We explore the potential of remote sensing instruments to identify and quantify smoke events and their effect on local surface pollution in section 7. A summary of the chapter and overall conclusions are given in section 8.

2. Meteorology

The planetary boundary layer (PBL), also known as the mixing layer, is defined as the lowest layer of the troposphere (ranging from 100 to 3000 meters) which is directly modified by the transport processes and responds to surface forcing. Detail descriptions of PBL structure such as residual, stable and entrainment layer can be found in Stull, 1988. The diurnal variation of temperature near the earth surface is the most important driver of the PBL diurnal variability. The layer above the PBL is called the free atmosphere which shows little diurnal variation in temperature. Solar radiation and the heat capacity of the relevant surfaces provide a strong atmosphere land coupling dynamics which must be modeled properly for accurate PBL dynamics.

While modeling the PBL height dynamics is important for climate and meteorology, the important issue for air quality is that the PBL thickness also defines the total volume available for the pollutants to inhabit and be transported. For example, a high emission of local pollutants with low PBL height will result a high level pollution near the surface. This is critical since many studies have linked high surface pollution of particulate matter (PM2.5) to both respiratory and pulmonary health problems (Dockery et al., 1989; Girardot, 2006). For this reason, EPA has enforced strict pollution standards as shown in Fig. 1 and the Clean Air Act (CAA).

In addition to the modifying of the temperature and wind distribution, the urban surface also affects the PBL dynamics by the heat storage of urban materials. This is commonly called the urban heat island (UHI) which describes the lack of radiative cooling of both the atmosphere and surfaces in urban areas compared to their non-urbanized surrounding during nighttime. With increasing urban development, UHI may increase in frequency and magnitude especially in summer. (Voogt, 2004; Arrau & Peňa 2010)

Based on comprehensive multi-national (European) analysis (Piringer et al., 2007), the need to parameterize the affects of the UHI is crucial. For example, Mestayer et al. (2005) presents extensive measurements within city centers show that turbulent sensible heat flux is the dominant mode of heat transfer during the middle of the day but before sunrise, the largest heat transfer is limited by storage of energy within urban materials. In fact, unlike natural vegetation surfaces, the convective sensible heat flux remains positive over the diurnal cycle through release of heat stored the urban canopy. This mechanism is particularly important for air quality predictions since collapse of the urban boundary layer (UBL) due to

underestimates in the turbulent flux can result in dramatic increases in surface pollution forecasts (Doraiswamy et al., 2010). For these reasons, direct evaluation of the UBL height is important in diagnosing the performance of operational air quality models driven by high resolution meteorological forecasts.

Air Quality Index Levels of Health Concern	Numerical Value	Meaning
Good	0 to 50	Air quality is considered satisfactory, and air pollution poses little or no risk
Moderate	51 to 100	Air quality is acceptable; however, for some pollutants there may be a moderate health concern for a very small number of people who are unusually sensitive to air pollution.
Unhealthy for Sensitive Groups	101 to 150	Members of sensitive groups may experience health effects. The general public is not likely to be affected.
Unhealthy	151 to 200	Everyone may begin to experience health effects; members of sensitive groups may experience more serious health effects.
Very Unhealthy	201 to 300	Health alert: everyone may experience more serious health effects
Hazardous	301 to 500	Health warnings of emergency conditions. The entire population is more likely to be affected.

Fig. 1. EPA has assigned a specific color to each AQI category to make it easier for people to understand quickly whether air pollution is reaching unhealthy levels in their communities.

3. Current air quality monitoring efforts

3.1 AIRNow network

Current efforts to monitor fine particulate mass are based on the deployment of surface sensors which filters the particulates and can access the mass concentration directly. For example, AIRNow is an online network which is developed by EPA, NOAA, NPS and local agencies to provide real-time national air quality information daily for the public over 300 cities across the US. The air quality information is presented in a color map associated with the Air Quality Index (AQI) as shown in Fig. 1 and can be used to generate spatial maps and forecasts which are collected using either federal reference or equivalent monitoring techniques or techniques approved by the state or local agencies. The data are displayed on the website (http://airnow.gov) after the end of each hour so that it can be "real-time". Therefore the data as such are not fully verified and validated through the quality assurance procedures monitoring organizations use to be officially submit and certify data on the EPA AQS (Air Quality System) even though some preliminary data quality assessments are performed. Thus, these data are not used to formulate or support regulation, guidance or

any other Agency decisions or positions as it is for the purpose of reporting the AQI. The AQI represents how clean or unhealthy of the air and what associated health effects might result.

3.2 Satellite efforts

Fire hotspots and smoke plume signatures are readily seen in satellite imagery, and many satellite sensors like GOES, MODIS (Kaufman, 1993) and TOMS (Torres et al., 2002 and Herman et al., 1997) are widely used to map the geographical distribution and aerosol transport on large scales. MODIS and TOMS (sun synchronous polar orbiting satellites) provide global coverage approximately once a day and can only provide snap-shots of large-scale aerosol spatial distribution during the time of satellite overpass, which is not very suitable for tracking and monitoring large scale aerosol events. On the other hand, although GOES (Geostationary satellite) has a single channel, unlike MODIS and TOMS, it provides coverage of the entire globe at 30 minutes intervals providing a summary of the extent of aerosol coverage, which gives a strong indication of the aerosol intensity. This gives GOES the advantage of being useful in tracking the time-history and spatial distribution of aerosol transport. Important features may sometimes go unnoticed by sun synchronous satellites, making it challenging and sometimes difficult to complete a picture. GOES can then further be used to validate features common to MODIS and OMI imagery. The goal here is to use the GOES AOD (aerosol optical depth) product to identify transport by utilizing its multi-time passes in a single day to verify features which are common in geographical area to MODIS and OMI.

While satellite measurements are critical for understanding transport and air quality prediction schemes, the lack of any vertical information of the aerosol column limits the use of these satellite measurements for air quality applications. In particular, due to the presence of possible aerosol plumes as well as poorly mixed aerosols in the PBL, connecting satellite derived AOD to surface level air quality measurements such as PM2.5 or PM10 is very difficult. Efforts such as the IDEA product, attempt to connect satellite AOD measurements directly to PM2.5 using a static relationship between AOD and surface PM2.5 measurements.

$$PM2.5 = 60\tau \tag{1}$$

The coefficient in Equation 1 is statistically determined from coincident measurements from a sky radiometer and surface sampler measurements (Zhang et al., 2009). However, the cloud clearing of the sky radiometer insures that plumes are unlikely to be accounted for and all viable sky radiometer measurements occur when the PBL is the only aerosol source. Therefore, the presence of plumes will bias the surface PM2.5 measurements to higher values and any assessments of plume interaction with the PBL must first isolate the AOD contributions.

In particular, as we will explore fully in section 6, we unambiguously show that long term advected smoke plumes can either be transported aloft without any interaction with the PBL, or can mix with the PBL and change the air quality parameters at the surface. In both cases, lidar measurements are critical to properly apportion the PBL AOD contributions from the total column and to connect it to surface particulate matter. In particularly, we show that a combination of passive and active ground instruments and satellite

measurements respectively, can provide a unique and clear picture on how PBL air quality can be affected by plumes mixing down into the PBL.

4. Air quality models and data analysis

4.1 Model description (WRF-CMAQ)

In performing comparisons to assess model performance, it is important to distinguish two different methods in running the WRF-CMAQ model. One approach is the use of retrospective analysis to better diagnose (Otte, 2008a, 2008b) the potential underlying physical parameterizations of a given model or comparisons between different models. These schemes in fact benefit from auxiliary near surface measurements which can be used to "nudge" the model during the processing. This form of data assimilation is useful as a means of identifying limitations in the model directly. This is in contrast to the natural forecast mode where the meteorological models do not benefit from additional surface data. This nudging mechanism had been applied to the MM5 model environment and had not been available within the WRF environment. However, recent implementations within WRF ARW 3.1-1 (Skamarock et al., 2008) have incorporated these observational assimilation capabilities. In particular, the nudging process ingested 3 hours surface observed data and every 6 hours upper data to adjust the annual model results.

Furthermore, it is possible to use WRF model for better observations of the differences in the PBL scheme itself since the modular structure of WRF allows different PBL parameterizations to use the same underlying surface layer schemes which in our case are the Pleim-Xiu (PX) Surface Layer Scheme (Pleim & Gilliam, 2009). In particular, two hind cast runs which are compared to our lidar and ceilometer measurements are considered whose detailed characteristics are given in Table 1. In particular, we note that our main focus is on the comparison of the Modified Blackadar (BLK) and the Asymmetric Convective Model - version 2 (ACM2) schemes are among the schemes most accurately modeling the PBL height in comparison to radiosonde and wind profiler measurements (Baker et al., 2009; Hong et al., 2006). This is also consistent with comprehensive tests made by the Environmental Protection Agency (EPA) where it was shown that the nonlocal schemes, BLK and ACM2 (PX) were better in general compared to the local schemes YSU and the Mellor-Yamada-Janjic (MYJ) PBL scheme.

On the other hand, while the nudging may improve the model error for surface temperature, humidity, and wind (although this is not an independent comparison), it may not help estimate vertical features since the upper air observation network very sparse. In addition, it must be emphasized that comparison studies in urban centers have not been made and is therefore, a major focus. During these retrospective analyses, when using the PX Land Surface Model, the pixel nearest the urban CCNY validation site is classified as 88% "Urban and Build-Up land" as defined by the USGS 24 land use category (Anderson et al., 1976). Finally, we also want to restate that our study is limited to summer where the biggest air quality issues regarding particulates in an urban environment occur and the most severe difficulties in the diurnal structure of the CMAQ air quality forecasts seem to occur (Doraiswamy et al., 2010). While summer 2007 measurements used retrospective analysis, summer 2010 forecast data were made using the MYJ PBL scheme which uses the 1.5-order (level 2.5) turbulence closure model of Mellor and Yamada (1982) to represent turbulence above the surface layer (Janjic 1990, 1994, 2001) and has become a popular model for PBL representation. (see Table 1)

Schemes	2007 WRF Run 1	2007 WRF Run 2	2010 WRF Run
PBL	Modified Blackadar	ACM2	MYJ 2.5
Surface Layer	Pleim-Xiu	Pleim-Xiu	NOAH Unified 5-layer Land-surface
Microphysics	WSM6	Morrison II	Ferrier Gridscale
Cumulus	Kain-Fritsch	Kain-Fritsch	Cumulus-Betts-Miller-Janjic
Shortwave Radiation	Dudhia	Dudhia	Lacis-Hansen
Longwave Radiation	RRTM	RRTM G	Fels-Schwartzkopf

Table 1. WRF-CMAQ Model Parametric Schemes

4.2 Data analysis for PBL heights

The first point to be made is for operational mesoscale air quality applications, the New York State Department of Environmental Conservation (NYSDEC) WRF-CMAQ runs provided to us were a final spatial resolution of 12- by 12-km grid and temporal resolution of hourly dataset. Therefore, we can expect that connecting point measurements with our lidar and ceilometers sensors may result in extensive variability. However, we note that since the PBL measurements from WRF are per hour, we are able to reduce much of the variability in our point measurements by similar one hour averaging of the lidar PBL retrievals. Due to natural wind flow, the one hour averages should be reasonably representative of the 12 km spatial footprint. To improve the data matchup quality, we also introduce the following filters into the lidar matchups.

Filter 1: Only cloud free cases are considered. This is in fact a limitation of the lidar measurements since operation under cloudy conditions can result in strong backscatter signals that would often saturate the detector. Since we are ultimately concerned with cases where pollution exceedence is of major concern and to avoid local coastal contamination issues, we remove from our comparisons all sea-breeze cases identified through wind data from Hybrid Single Particle Lagrangian Integrated Trajectory (HYSPLIT) Model.

Filter 2: We restrict comparisons to cases where at least five PBL measurements are made within the hour and the standard deviation is less than 20% of the mean. This limits comparisons to cases where temporal homogeneity is reasonably met.

4.3 Data analysis for PM2.5

While our first concern is the PBL heights, we also look to assess the performance of the WRF driven CMAQ forecast predictions. As mentioned earlier, the CMAQ model performance for summer conditions in urban conditions results in strong overestimating pollution spikes which are not in agreement with the AIRNow TEOM measurements.

Particulate size distributions in CMAQ are represented as the superposition of three lognormal subdistributions, called modes, including the aitken mode (i-mode), accumulation mode (j-mode), and coarse mode (c-mode). In general, a large number of species with different optical and density properties are represented but all particles are assumed to share the same size distribution. In this study, we estimate the PM2.5 from the CMAQ output by simply summing the aitken and accumulation mode or (i+j) method (EPA, 1999a, 1999b; Jiang et al., 2006). In comparing with the TEOM measurements, we use three sites within the 12km area (see Table 2) and filter the cases to those in which the standard deviation of the three sites is < 20 % of the mean.

Site Name	Latitude	Longitude
CCNY	40.81976 N	-73.94825 W
Manhattanville PO	40.81133 N	-73.95321 W
IS 52	40.81618 N	-73.90200 W

Table 2. TEOM Stations Locations

5. Instrumentations and methodology

5.1 Lidar

An elastic lidar with three wavelengths (355 nm, 532 nm and 1064 nm) is operated year round in CCNY (40.8N, 73.9W). Measurement at wavelength 1064nm is mainly used in this study as this channel has minimum contribution from molecular scattering and is better for aerosol observation by increasing the backscatter contrast between the PBL and free troposphere layers. More details about lidar specifications and system configuration can be found in Wu et al., 2009.

The lidar return signal is based on the scattering of the laser transmitted energy by atmospheric particles including aerosol, dust and molecules. The instantaneous magnitude of the return signal provides information on the backscatter properties of the atmosphere at a certain height determined by the time delay of the pulse echo. While processing the raw lidar data, we must include the fact that the atmosphere attenuates the signal both before and after hitting the backscattering target. To account for this, the instantaneous return signal strength is given by the basic LIDAR equation:

$$P_r(z) = E_o . \frac{c\Delta t}{2} . \frac{A}{z^2} . \beta(z) . e^{-2\int_{z1}^{z2} \sigma(z')dz'} \quad (2)$$

where $P_r(z)$ is the instantaneous power received from distance z [Watt], E_o is the effective pulse energy (include all optics attenuation) [Joule=Watt-second], c is the speed of light [meter per second], Δt is the laser pulse width [second], A is the receiver aperture area [meter^2], z is the distance between system and target [meter], $\beta(z)$ is the volume backscatter coefficient at distance z [per meter-steradian] and the exponential term is the two-way atmospheric transmittance, which accounts for the attenuation of transmitted and backscattered power by extinction at various distances (z′) between the transceiver and target.

The PBL contains greater aerosol concentration because the aerosols are trapped in the PBL by a potential temperature inversion. Therefore, the backscatter signal strength is dramatically reduced when it transits from the PBL into the free troposphere. This sharp change of signal is used to estimate the PBL height. These changes in backscatter signal caused by varying aerosol concentration provide a very powerful tool for remotely observing the two-dimensional structure of the PBL. In general, the PBL is characterizes by intense mixing in a statically unstable situation where thermals of warm are rise from the ground. The PBL reaches its maximum depth in late afternoon. It grows by entraining, or mixing down into it, the less turbulent air from above. The resulting turbulence tends to mix heat, moisture, pollutants and momentum uniformly in the vertical. (Stull, 1988; Kovalev & Eichinger, 2004; Brooks, 2003; Davis et al., 2000)

5.2 Ceilometer

Another remote sensing instrument that is used in this study is a ceilometer (model CL31) which is manufactured by Vaisala. This instrument is a device that is originally designed to determine the height of a cloud base. Due to the higher backscatter signal of a cloud, the pulse powers are dramatically less and therefore can be made eye-safe but works on the same principle as lidar system. Furthermore, unlike the lidar transmitter which is not eye-safe, the ceilometer utilizes a single NIR (Near Infra Red) channel at 910 nm. While designed for cloud detection, ceilometers can also be used to measure the aerosol concentration within the atmosphere (Eresmaa et al., 2006; Haji et al., 2009). However, it is also clear that the low signal pulse power will result in higher noise and significant temporal and spatial averaging would need to be applied to bring the noise contamination down to acceptable levels. Besides, the limitation of this instrument is unable to observe PBL height that is higher than 1.2 km where the noise is dominant.

5.3 Wavelet covariance transform method

From extended studies of the performance of the available lidar methods applied to a large set of lidar observations, the wavelet covariance transform (WCT) method has been shown to be the most robust technique for an automated PBL height detection (Davis et al, 2000; Brooks, 2003; Baar et al. 2008). This method is intuitive and is based on scanning the backscatter profile with a localized impulse function and maximizing the covariance between the backscatter profile and the impulse function. While many possible wavelet shapes are possible, we find that a step function Haar wavelet defined as below can be used.

$$h\left(\frac{z-b}{a}\right)=\begin{cases}1: & b-\frac{a}{2}\le z\le b\\ -1: & b\le z\le b+\frac{a}{2}\\ 0: & elsewhere\end{cases} \tag{3}$$

where z is the profile height and a and b describe the width and translation of the function, respectively. The covariance (Gamage & Hagelberg, 1993) is simply the convolution or localized transform, $W_f(a,b)$, of the Haar function with the lidar backscatter profile.

$$W_f(a,b)=a^{-1}\int_{z_b}^{z_t}B(z)h\left(\frac{z-b}{a}\right)dz \tag{4}$$

where z_b and z_t are the bottom and top altitudes in the lidar backscatter profile, and $B(z)$ is the lidar backscatter as a function of altitude, z. The locations of these maxima and minima, b_i^{max} and b_i^{min} , and the associated values of the covariance transform, $W_f(a_{max}, b_i^{max})$ and $W_f(a_{max}, b_i^{min})$, are the locations and relative strength of step like boundaries in the lidar backscatter profile, $B(z)$. The index i refers to the case of multiple local minima or maxima. For clear conditions, $W_f(a,b)$ takes a clear local maximum at the PBL height because of the high backscatter values in the mixing layer and significantly lower backscatter values in the free atmosphere (Fig. 2).

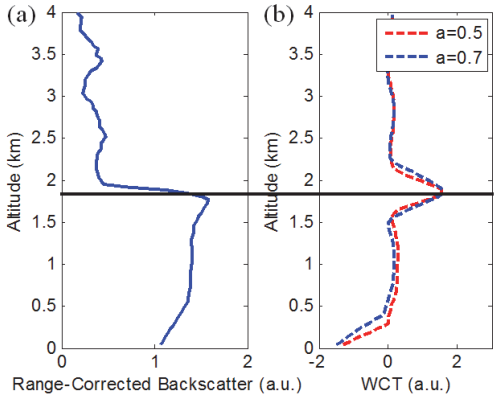

Fig. 2. (a) Single Lidar signal (log scale) profile (b) Resulting wavelet convariance transform.

However, when strong residual or plume layers occur, $W_f(a,b)$ will have multiple local minima and maxima as shown in Fig. 3 (a). These multiples maxima confuse the algorithm making it difficult to extract a unique PBL height. For example, Fig. 3 (b) illustrates 4 hours lidar measurements where an aloft plume occurs in the morning. The backscatter from the plume is higher than the backscatter from the PBL which gives the wrong estimation of PBL height. This renders the selection of the correct PBL height ambiguous and it is this ambiguity that needs to be addressed for better model validation.

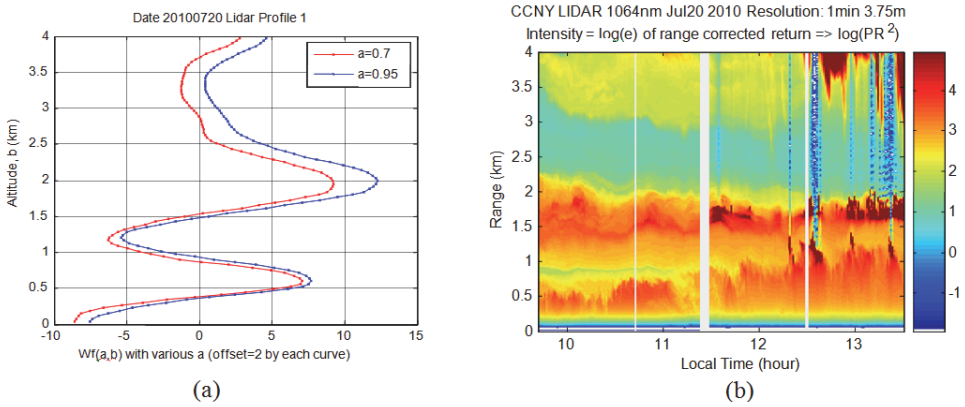

Fig. 3. (a) Single lidar WCT profile (b) Lidar measurements on Jul 10, 2010.

To account for the different structures expected in the PBL height, we separate the lidar profiles into classes. The "transition" class occurs between 8:00-12:00 EST and 18:00-22:00 EST when the PBL is growing / collapsing and residual layers are present growing, while the mature PBL class extends from 12:00-18:00 EST. In order to decrease the noise level and smooth the atmosphere transition, a sliding spatial and temporal averaging is applied to the lidar backscatter dataset. In this study, the averaging temporal interval Δt is 20 minutes with a sliding window of 10 minutes while the averaging spatial interval Δz is 80 meters with a

sliding window of 40 meters. The temporal resolution is 10 minutes and spatial resolution is 40 meters. Since the PBL height predicted by the WRF model is hourly, 10 minutes temporal resolution is sufficient for comparison. When making final comparisons however with the WRF outputs, the 10 minutes retrievals are further averaged to 1 hour. To better separate the convective layer from the residual or plume layer, we apply a few modifications that will be briefly discussed below.

Our first modification is applying cloud screening to the dataset before WCT. Clouds are characterized by a steep increase of the range-corrected lidar signal at the cloud base followed by a strong decrease of the signal with increasing cloud penetration depth. From these properties, the use of the WCT and together with a minimum backscatter threshold is sufficient to easily identify cloud pixels in the lidar profile. For such marked cases, no PBL height is provided.

Furthermore, the selection of an appropriate spatial resolution a is the main challenge for a successful retrieval of the PBL height. For rather small values of a, signal noise dominates the vertical profile of W_f masking the maxima that defines the PBL top. On the other hand, large value of a may fail to resolve the PBL height when further aerosol layers are present in the lower free troposphere. In general, we found that a smaller a (0.5 km) is needed during the transition regime whiles a larger a (0.7 km) is optimum for the afternoon time dataset. The larger value allows us to balance the effects of lower SNR due to the higher altitude where the signal strength is degraded with the reduction of vertical structure of the PBL due to turbulent mixing during this period

In addition, to isolate the convective growth layer from the residual layer, we make use of general trends (e.g. climatology) in the PBL searching range to limit the PBL height retrieval. For example, we restrict the PBL searching range to 1 km in the morning and night period while a range from 1 to 3.5 km is used for the afternoon period. The restriction in morning is necessary since the residual layer is often very deep from the previous day.

Finally, the PBL height determined by the algorithm is checked for continuity. On a running scale, a given interior point is compared to its adjacent points and if it is outside a range (e.g. ± 250 meters with spatial resolution of 40 meters and temporal resolution of 10 minutes) on both sides, it is discarded. If only one side is outside the range, a mean value of both points will be calculated. This scheme is iterated until no further changes occur. This reduces the number of false hits caused by noise or other layers such as residual layer, plume layer and internal turbulence.

6. Discussions

6.1 PBL statistic variations in NYC

In order to have a general idea of the PBL temporal dynamics in an urban area such as NYC, we overlay the PBL trend grouped by seasons. Due to the weather and human factors, the lidar observations are normally limited from 10:00 to 18:00. Therefore, the results as shown in Fig. 4 (a-b) only illustrate the daytime trend. Table 3 summarizes the number of observation days and averaged maximum PBL height that occur during daytime for each month. The most important observations is the high PBL height (2-2.5 km in summer) as compared to winter seasonal trends (1-1.5 km in winter) (e.g. January, Febraury and December). In addition to the general increase of the maximum PBL height, the diurnal increase from morning through late afternoon is much more dramatic and indicative of the surface heating process in general during the summer and spring.

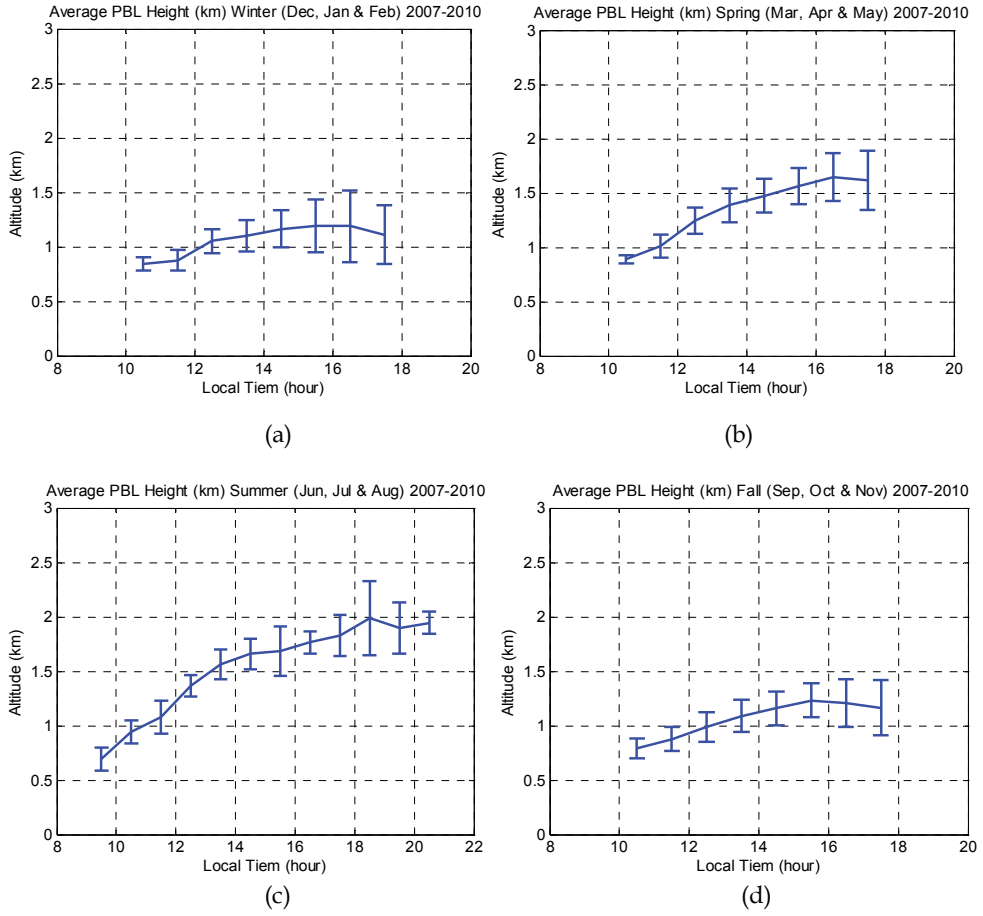

Fig. 4. Monthly PBL trend average over 4 years (2007-2010).

Month	1	2	3	4	5	6	7	8	9	10	11	12
No. Days	12	16	29	28	30	16	32	24	26	25	22	11
Max Height (km)	0.99	1.30	1.88	1.78	1.80	2.05	2.23	2.02	2.21	1.11	1.18	1.48

Table 3. Summary of number of observation days and maximum PBL height.

6.2 Assessment of model PBL height retrieval

The main results when comparing both the BLK and ACM2 data are given in Fig. 5 (a-b). First, we note the BLK has somewhat slightly better correlation (R=0.87) than the ACM2 scheme (R=0.84) although both schemes seem to result in statistically significant

overestimations of the PBL height. However, as seen in the histogram analysis of Fig. 6, the bias of the BLK scheme is somewhat smaller than that observed in the ACM2 scheme with a mean bias of m=180 meters for BLK and m=340 meters for the ACM2 scheme On the other hand, the fluctuation of the deviation is quite high with the std for the BLK scheme about σ_{BLK}=300 meters while the ACM2 schemes standard deviation is σ_{ACM2}=280 meters. Keeping in mind that the lidar based methods matched against meteorologically based methods such as the parcel method show no appreciable bias and average deviations between on the order ±200 meter (Hennemuth & Lammert, 2006), we believe the model biases are significant and there is room for more model development. Still, the results illustrate that at least for ACM2, the over bias is significant and all things considered, the BLK scheme performs best under the study period.

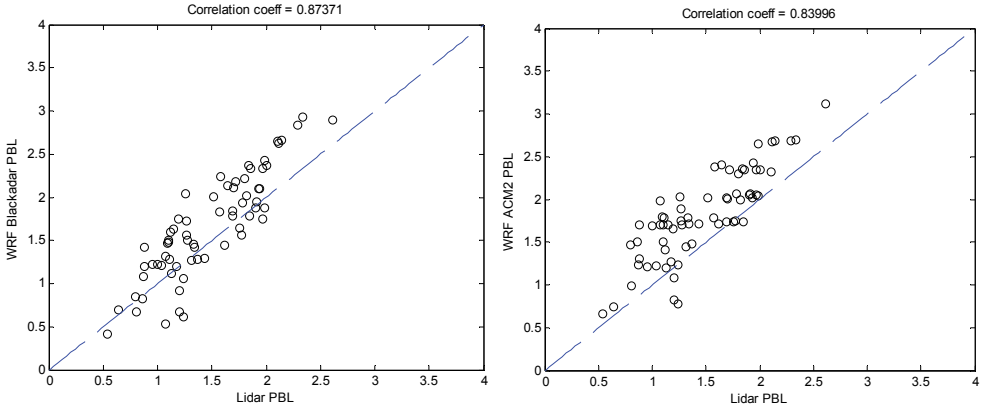

(a) (b)

Fig. 5. WRF versus Lidar PBL heights in unit km (a) Blackadar (b) ACM2.

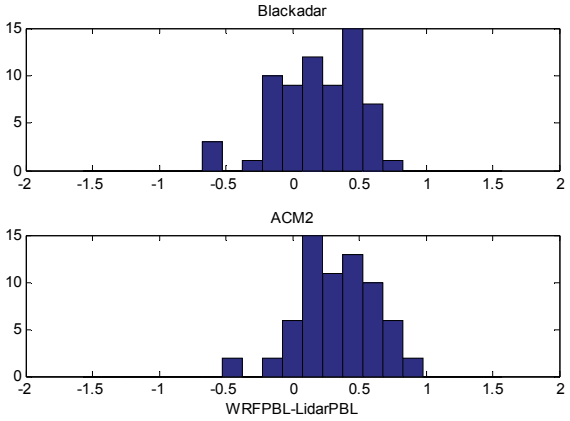

Fig. 6. Statistics of PBL height model versus measurement errors (WRF PBL – Lidar PBL in unit km) summer 2007 (a) Blackadar (b) ACM2.

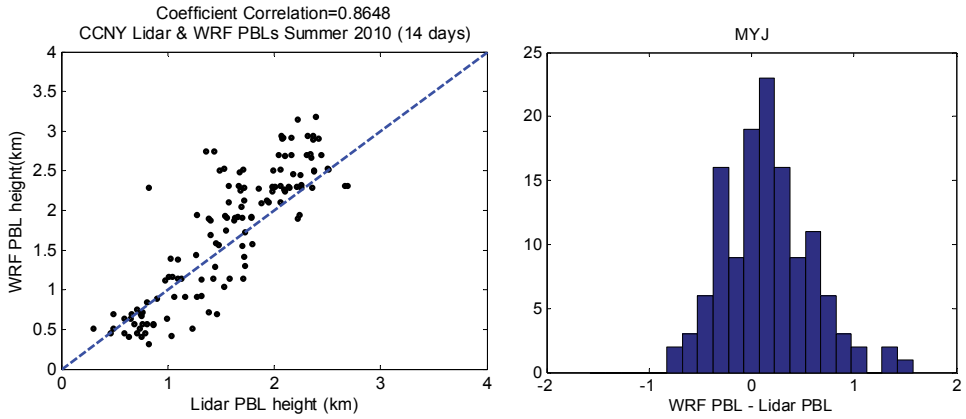

(a) (b)

Fig. 7. (a) Linear regression of WRF PBL height with lidar derived PBL height for selected 14 days on June, July and August, 2010 (b) Statistics of PBL height model versus measurement errors (WRF PBL – Lidar PBL in unit km) summer 2010.

The results for the 2010 PBL height comparisons using the MYJ scheme in forecast mode are given in Fig. 7 (a). We note however that even though the correlation is comparably high (R~0.86) to the 2007 hind cast data, the fluctuations for the 2010 forecast data is much larger as seen in the histogram data as shown in Fig. 7 (b) with a standard deviation σ_{MYJ}~550 meters in comparison to σ_{BLK}~320 meters and σ_{ACM2}~280 meters. This is consistent with the fact that forecast uncertainties are expected to significantly increase the fluctuations of all dynamical parameters.

6.3 Assessment of CMAQ PM2.5

In looking at the performance of CMAQ as illustrated in Fig. 8, a strong diurnal spike behavior is observed in the CMAQ surface layer PM2.5 which is not seen in the TEOM measurements. The direct source of this over bias is not clear with possible contributing factors being unrealistic gradients in the PM2.5 vertical profiles or overestimation in the primary emission associated with urban rush hour traffic (Doraiswamy et al., 2010). However, the use of ceilometer backscatter profile data can be used to explore how realistically, the primary emissions are distributed vertically. Before doing this, it is useful to illustrate indirectly that vertical distribution of PM2.5 is at least partially a factor that must be taken into account seriously. In Fig. 9, we plot for the summer 2007 case, the linear correlation coefficient binned by hour between the TEOM PM2.5 measurements and the path averaged PM2.5 mass from the CMAQ model for different vertical height levels. Most dramatic is the enhancement of the correlation for the pre-sunrise particulate matter emission case when the altitude is large. This illustrates that to some extent, the primary emission is not the dominant problem and that these emissions are in practice being more evenly distributed in the UBL. On the other hand, we see a complete change once sufficient heating has taken place during the day. In this case, the particulate matter mass in the CMAQ model is better mixed in agreement to observations and the best correlation should occur when the CMAQ particulates is closest to the surface.

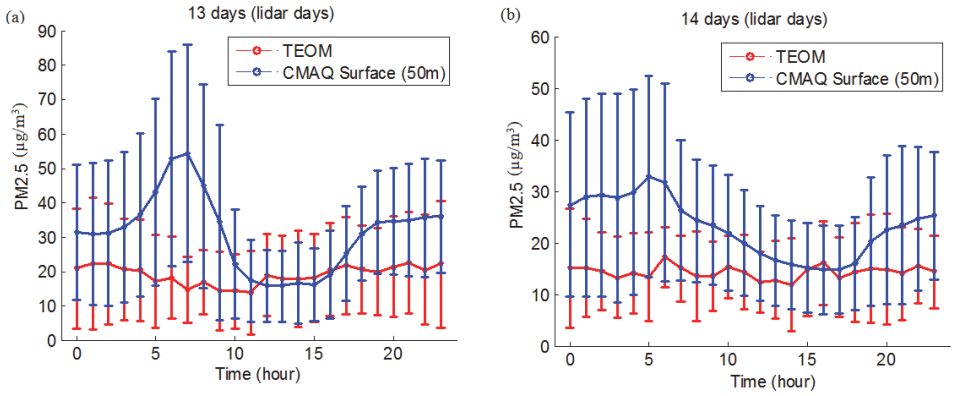

Fig. 8. Summer averaged PM2.5 mass concentration (μg/m³) diurnal cycle comparison of CMAQ and TEOM. (a) Summer 2007, (b) Summer 2010.

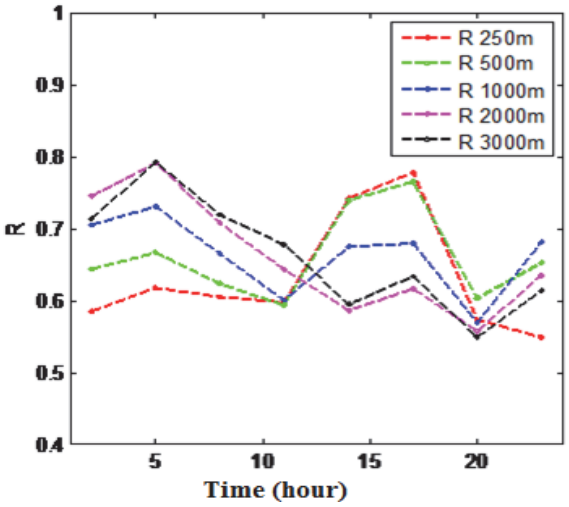

Fig. 9. Linear correlation coefficient binned by hour between the TEOM PM2.5 Summer 2007 measurements and the path averaged PM2.5 mass from the CMAQ model for different vertical height levels. (R: correlation coefficient; 250 meters: path average from the surface to 250 meters altitude)

For a more direct comparison, we plot in Fig. 10 path averaged CMAQ PM2.5 and the ceilometer backscatter over the diurnal cycle for different altitude ranges. In panel (a), the results reemphasize how the CMAQ PM2.5 distribution is compressed near the surface during the morning spike anomaly. In fact, as the altitude increases, the PM2.5 diurnal distribution becomes peaked during mid-day and evidence of the spike behavior is removed. On the other hand, the ceilometers path averaged backscatter in panel (b) does

not observe these pollutant spikes even at the lowest vertical bins. While a small increase is seen in the ceilometer backscatter relative to mid day, the contrast between morning and mid-day is much smaller with a contrast coefficient $C(X)=X_{max}-X_{min})/(X_{max}+X_{min})$ of approximately 12% compared to ~50% for the CMAQ near surface measurements. In addition, the ceilometer contrast is clearly much more in line with the TEOM measurements. It is also interesting to see that as the height of the ceilometer path increases, we recover the general diurnal trend seen in the CMAQ data retrievals.

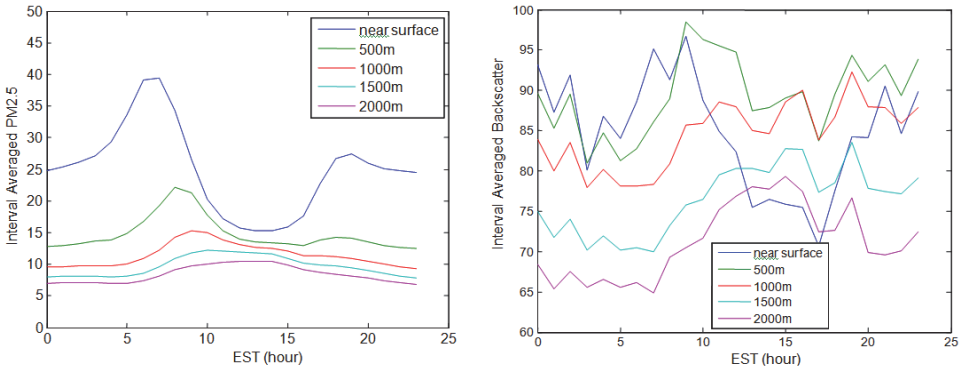

(a) (b)

Fig. 10. Cumulative path averaged parameters for different altitude ranges over the diurnal cycle (a) CMAQ $PM_{2.5}$ ($\mu g/m^3$) (b) Un-calibrated ceilometer backscatter (10^{-9} m^{-1} sr^{-1}).

Further evidence that boundary layer mechanisms giving rise to problems with the near surface PM2.5 estimates can be seen by inter-comparing the summer 2007 and 2010 CMAQ predictions. In Fig. 11, the 3-dimensional structure of the CMAQ PM2.5 outputs are compared. For convenience, the different PBL height retrievals are superimposed. The most important observation is that the summer 2010 mixing layer heights are significantly larger on average for summer 2010 during the sunrise/sunset periods. For the 2007 data, the extremely compressed PBL clearly tends on average to trap the primary emissions not letting them vent upwards. Since the emission inventories are not expected to be significantly different when averaged over seasonal scales, the different PBL height behavior is clearly the dominant mechanism. The difference in PBL height is directly observed in Fig. 12 where the different PBL height retrievals are plotted. Besides the significant growth of the nocturnal PBL, we note a significant increase in the magnitude and persistence of the PBL profile.

Finally, it is important to remember that when we compared the vertical structure of the CMAQ against the ceilometers in Fig. 9-10, we found that the strong surface emission behavior in the diurnal pattern predicted by CMAQ within the first 500 meters of the surface are not seen in the ceilometer data. However, it may be argued that since we are matching PM2.5 to optical backscatter, there may be significant problems in the comparison. Although we argued that this should not be a significant issue since the TEOM-Ceilometer regression has high correlations in the first 500 meters, it is useful to consider a more direct matchup where we use the CMAQ extinction variable based on semi-empirical parameterization connecting the CMAQ component masses to optical extinction (Malm et

al., 1994). In Fig. 13 (a), the averaged optical extinction data is displayed and in Fig. 13 (b), the accompanying seasonally averaged relative humidity (RH). The first point is that the CMAQ extinction parameter has the same near surface behavior with the PM2.5 mass so that it is not unreasonable to diagnose the CMAQ PM2.5 with the lidar and ceilometer backscatter. In this direction, it is clear that CMAQ primary emissions are not properly being distributed vertically. On the other hand, enhanced extinction is seen in the CMAQ retrievals in the upper atmosphere but when compared to the WRF RH profile is a direct consequence of the enhanced scattering due to hygroscopic humidification. This enhanced backscatter does in fact exist in our lidar images where increased humidity at the top of the PBL is often accompanied by enhanced RH due to temperature inversion and an increase of hazy layers capping the PBL in the afternoon but occurs too high to be of interest in our ceilometer retrievals.

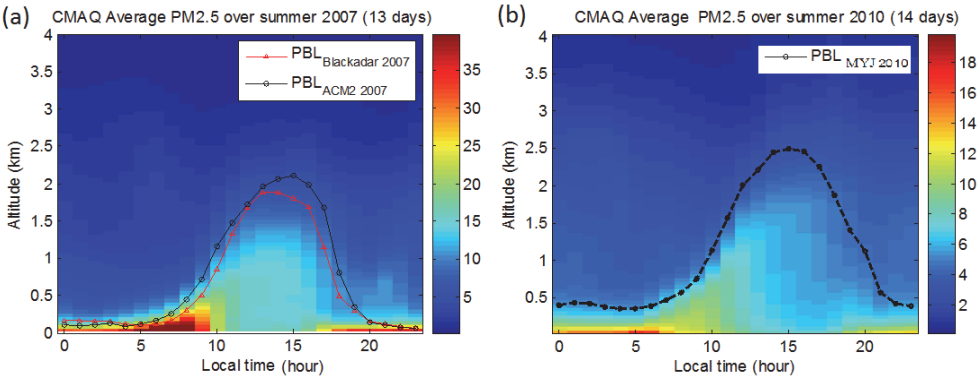

Fig. 11. The 3-Dimensional structure of the CMAQ predicted PM2.5 mass concentration ($\mu g/m^3$) (a) Summer 2007 (b) Summer 2010.

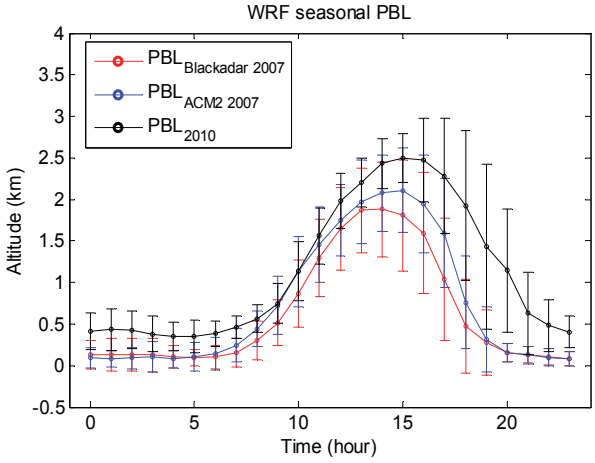

Fig. 12. Dirnal Average of PBL height retrievals for different schemes.

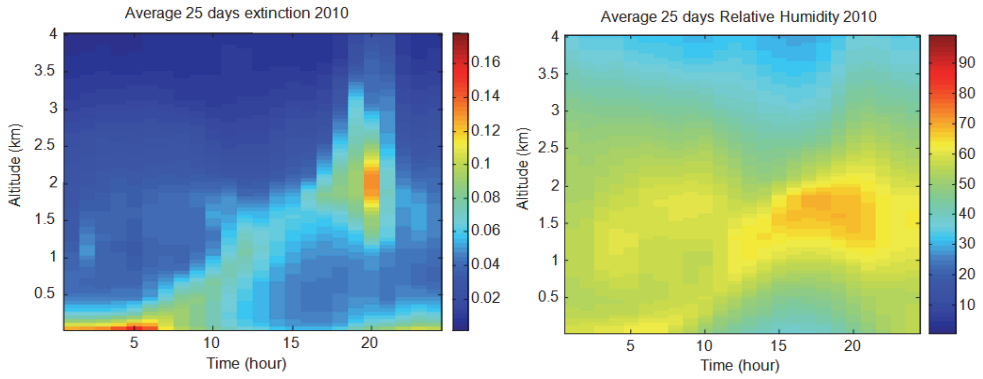

(a) (b)

Fig. 13. (a) Optical extinction (km^{-1}) at wavelength 550 nm based on the MALM paramterization within the CMAQ product (b) Simultaneous WRF RH (percent) retrievals.

7. Case study – august 2007 Idaho and Montana fires

In section 3, we briefly mentioned satellite based approaches to measure pollutants focusing on MODIS AOD as a proxy for PM2.5. However, this approach does not work if aloft plumes are present since they modify the column AOD. These plumes not only affect the PM2.5 retrieval but also can physically interact with the PBL and change the surface PM2.5 concentrations.

7.1 Plume identification using polar satellites

To determine the nature of the aerosol plumes, a number of more advanced multi-spectral satellites including OMI, POLDER, and MODIS to name a few have the added capability of limited aerosol classification. In order to illustrate the phenomenon, we choose the mid August (Aug) 2007 fires, which were continuously burning across Idaho and Montana with columns of thick smoke transported eastwards across North America, affecting much of the United States. Although it was assumed that this event significantly affected air quality in the north east, observations from satellites are not conclusive and in fact during the plume transport, surface samplers often showed low pollutant levels. The advanced warning provided by the satellites was crucial to ensuring that this transport event was captured by the CCNY lidar as well as other lidars from the Micro-pulse Lidar Network (MPLNET). However, the column AOD does not directly determine the surface pollution when plumes are present since the aloft plumes cannot be differentiated from the satellite measurements. Therefore, lidar (ground based or space based) must be employed to quantify the AOD in the plume and thereby correct for the plume contribution to the satellite AOD.

As an example of how we could do this, we look at a special case of heavy smoke plumes from Idaho-Montana. The plumes were initially transported as high altitude lofted layers which was observed by the CCNY lidar system (40.8N, 73.9W) over two days and was subsequently observed to mix with the late afternoon PBL. The source of the plume is shown in Fig. 14 (a) as fire hot spots and smoke signatures captured by MODIS onboard the Aqua satellite on Aug 13. By Aug 14 and 15, the smoke plumes began to canvas the North Eastern United States as seen

in Fig. 14 (b) and were visually identifiable from the quick view imagery, as well as through the large AOD measurements seen from the GOES and MODIS satellites.

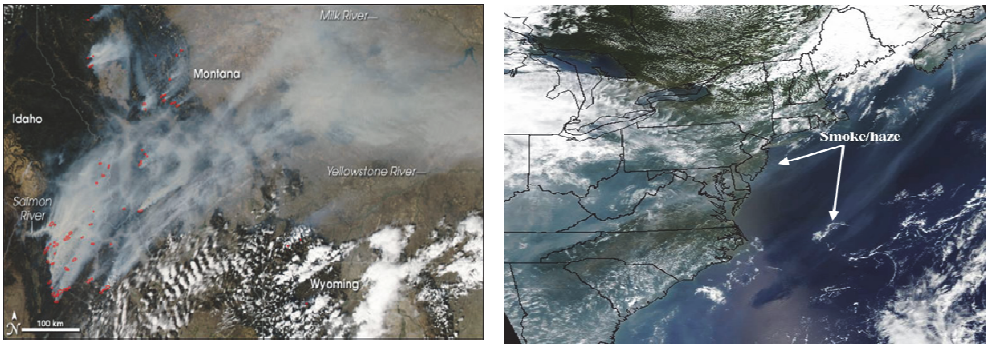

Fig. 14. (a) Images showing smoke and fires area (Montana and Idaho) captures by MODIS aboard Aqua satellite on Aug 13, 2007. This image of the area was captured by MODIS on NASA's Aqua satellite at 2:00 p.m. local time (U.S. Mountain Daylight Time). Locations where that sensor detected active fires are highlighted in red. (b) MODIS Terra close-up view of the smoke and haze over the Great Lakes and the northeastern United States on Aug 15, 2007 at 1625 UTC.

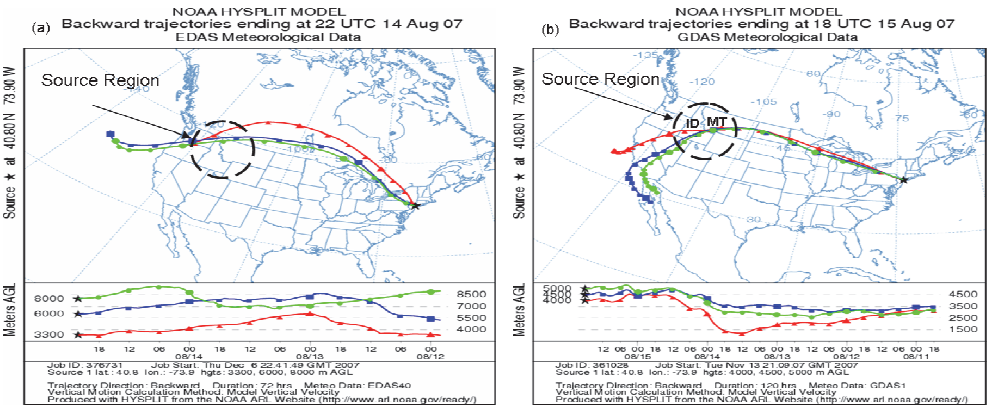

Fig. 15. HYSPLIT 5-day backward trajectory analysis ending at (a) 22:00 UTC on Aug 14 at three altitudes between 3 and 8 km and (b) 18:00 UTC on Aug 15, 2007 between 4 and 5 km.

Modeled backward trajectories from HYSPLIT (DeMott et al., 2003; Jorba et al., 2004; Hondula et al., 2009) provide a means to identification of the source region and the transport patterns of the air parcels at varying altitudes as specified by lidar observations. In Fig. 15, we show the back-trajectory of the air parcels over 120 hours from CCNY for Aug 14 and 15, illustrating the horizontal and vertical motion of the air mass. The trajectory results clearly show the air mass interacting with the aloft layers from the Idaho and Montana forest fire regions. This backward mode then allowed us to run HYSPLIT in prediction mode, which can then be compared to observations. Running the smoke forecast tool produced by NOAA Air Resource Laboratory (ARL) using the HYSPLIT dispersion model with the MODIS aerosol loadings shows how well

the model performs. In particular, MODIS aerosol retrieval continuously shows high aerosol optical depth over the source region over all three days in Fig. 16 (b, d, f). However, we can see that on Aug 13 as shown in Fig. 16 (b), very low aerosol loadings over the NYC region occur, implying that the smoke plumes had not made its way to this area as yet, as predicted

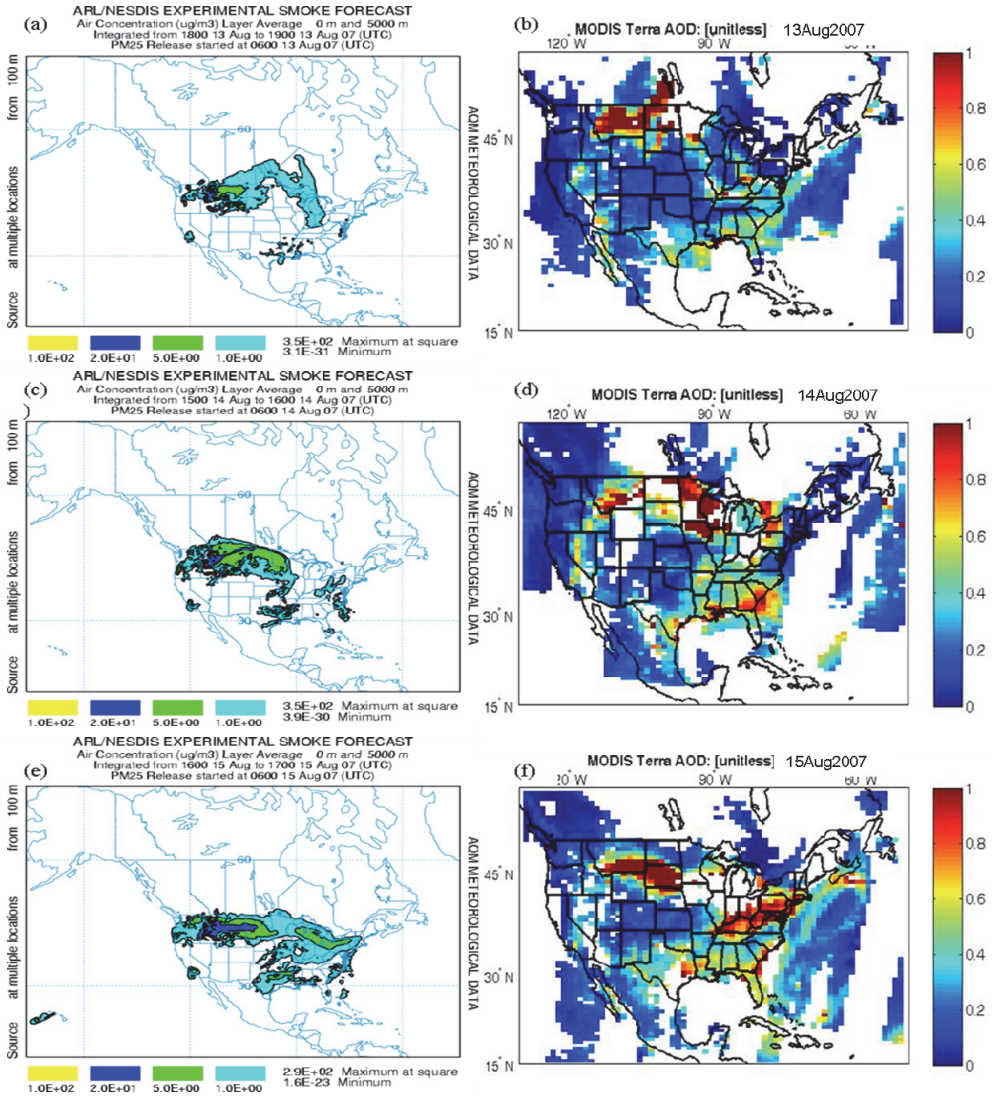

Fig. 16. MODIS Terra AOD at 550 nm on (b) Aug 13, (d) Aug 14, and (f) Aug 15, 2007. NOAA ARL smoke forecast for (a) Aug 13, (c) Aug 14, and (e) Aug 15, 2007. The smoke forecasts are 1-hour average output maps of primary PM2.5 air concentrations between the ground and 3 km. Smoke Forecast Model courtesy of NOAA's Air Resource Laboratory using the HYSPLIT Dispersion Model.

by the model. On the other hand, we can see much higher aerosol loading on Aug 14 and 15 as shown in Fig. 16 (d and f), which is consistent with the CCNY lidar observations and model predictions. The quality of the predictions is also seen in the timing of the plume front. A more careful examination of the observations and model predictions show that by 1600 UTC, the plumes were first making their way into central New York and did not make it into the NYC Area. This is consistent with the timing of the plumes observed from the CCNY lidar system where the first plumes were seen at 2000 UTC.

To further identify the nature of the plume coefficient as well as the underlying aerosol environment, we plot in Fig. 17 the angstrom coefficient derived from MODIS AOD. The Angstrom exponent α quantifies the slope of the wavelength dependence of the optical depth and is an indicator of the size of the atmospheric particles. In particular, when the Angstrom exponent is larger than one, fine mode aerosols dominate the column, while for Angstrom exponents less than one; coarse mode aerosols dominate the column [Kaufman, 1993]. In particular, we note that the plume as well as the background aerosol angstrom coefficient is quite high, which is indicative of highly concentrated fine mode aerosols. However, to identify the aerosols as biomass burning, we need to obtain information on the absorbing nature of the aerosols, which is beyond the capabilities of MODIS. Therefore, we utilize the UV (ultraviolet) aerosol measurements from AURA's OMI sensor, which allows for the determination of the absorbing index (AI) parameter known for its strong indications of biomass burning. These results are reported in the next section.

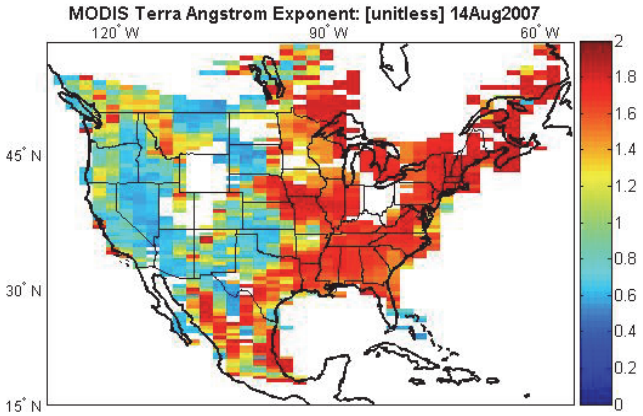

Fig. 17. Mosaic of Angstrom Exponents over North America derived from MODIS on Aug 14, 2007.

The Aura OMI instrument can differentiate UV-absorbing aerosols such as dust and biomass burning from the weakly absorbing aerosols and clouds (Braak et al. 2007) Absorbing and non-absorbing aerosols are separated based on the UV aerosol index, which is positive for absorbing (e.g. dust) and negative for non-absorbing aerosols (Torres et al. 2002). Since we have already eliminated dust due to the MODIS observed high angstrom coefficient, a high AI coefficient is a good indicator of biomass burning. In Fig. 18 (a), we see the strong biomass signature of the fire source. By Aug 14, the biomass plume had been transported to the northeast US. Although the AI is slightly smaller, the biomass signature is still quite clear. By Aug 15, the plumes are observed to be heading out to sea and mixing

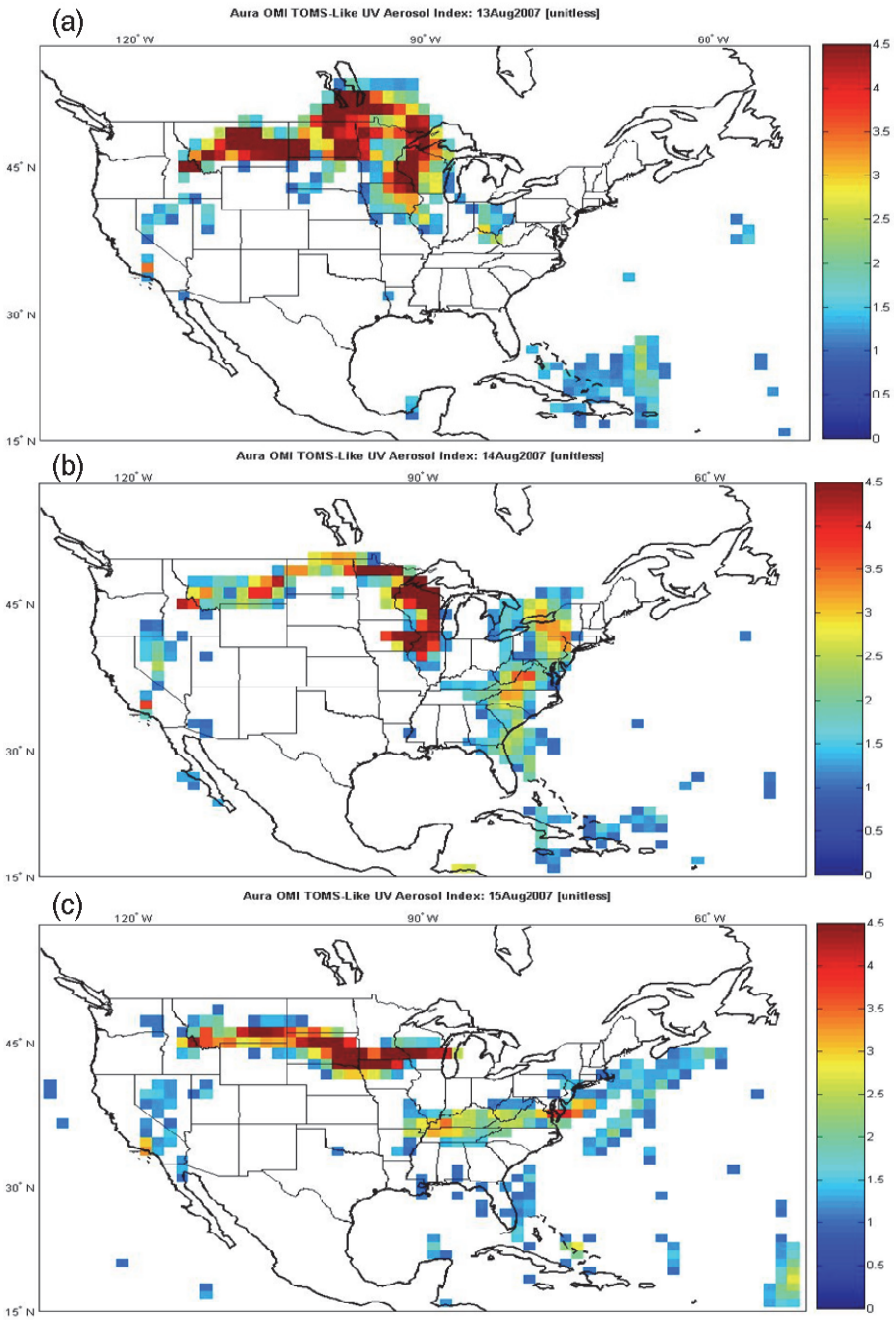

Fig. 18. TOMS OMI UV Aerosol Index for (a) Aug 13, 2007, (b) Aug 14, 2007, (c) Aug 15, 2007 at 354nm.

strongly with native maritime type aerosols, reducing the overall absorbing index. The smoke areas in the OMI imagery of UVAI, was found to coincide well with areas where MODIS (Fig. 17) reported increased aerosol loading compared to its surrounding background. We observe UV Absorbing Index as high as 4, which is indicative of highly absorbing aerosols.

We have also examined the biomass nature of the plume directly using the MOPITT Carbon Monoxide (CO) product, which is a good indicator of biomass aerosols and smoke. The results in Fig. 19 show the CO concentrations over the NYC area for the plume event as a function of pressure level. Clear increases in biomass burning are seen on Aug 14 and 15, marked by the increase in CO concentrations. Note however, that little difference in CO concentration is seen between the 14th and 15th due to the inability of the satellite sensor to see to the PBL layer.

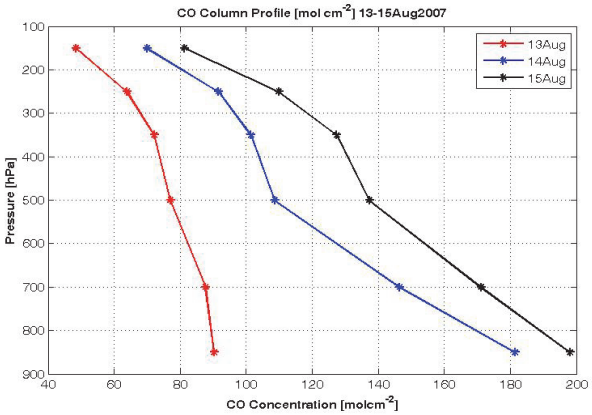

Fig. 19. MOPITT column profile of carbon monoxide concentration of Aug 13-15, 2007 at six pressure levels: 850, 700,500, 350, 250, and 150 hpa.

7.2 Plume transport using seostationary satellites

In all the previous observations, the satellites were polar orbiting so very few observations can be made daily. However, geostationary observations can be used to explore transport of pollution with high temporal resolution. In fact, the GOES Aerosol and Smoke product (GASP) provides aerosol optical depth retrievals over the United States at 4 km spatial resolution and 30 minutes intervals (Prados et al., 2007; Knapp et al., 2002a, 2002b, 2005). Retrievals are performed over land and ocean providing a full view of the earth daily. The GOES AOD retrieval method uses the visible channel of the GOES-12 Imager data to retrieve aerosol information. The GOES retrieval method is a three-step process. First, a background image composite is created of the visible imagery for each satellite observation time, using the visible image from the past 28 days including the current image. The second minimum reflectance (second darkest pixel) is selected and used in the background composite. Secondly, an atmospheric correction is applied and the Radiative Transfer (RT) model, which assumes a continental aerosol model from the Look Up Table (LUT) generated with the 6S RT model, is used to connect the top of the atmosphere (TOA) reflectance to a surface reflectance. In the final step, the calculated surface reflectance, the LUT, and the

GOES visible image are used to retrieve the aerosol optical depth at 550 nm (Prados et al., 2007; Knapp et al., 2002a, 2002b, 2005). Since the GASP product must assume an aerosol type (background continental), it may be thought that the AOD might be quite inaccurate when applied to smoke. However, the GOES visible channel is fairly insensitive to absorbing effects and since the particle size distributions are quite compatible, we might expect fairly good quantitative measures of AOD.

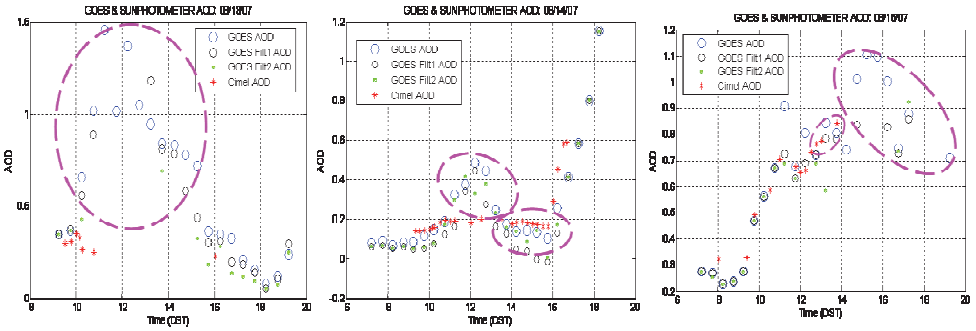

Fig. 20. Comparison of the AERONET sun-photometer (Cimel) derived AOD and GASP AOD products at CCNY on Aug 13-15, 2007

In Fig. 20 we show a comparison of the AERONET sun-photometer derived AOD and GASP AOD products at CCNY for Aug 13-15, 2007. The GASP pixel was centered over CCNY and the AOD was averaged over a 0.1° x 0.1° grid for every 30 minutes of data. Although the GASP product uses a single channel, we still see excellent temporal agreement between the GASP AOD and the sun-photometer AOD product when both data sets exist. However, the GASP measurements are often given when the sky radiometer measurements are not available. These gaps in the sun-photometer data exist due to the presence of clouds in the instruments field of view, where an automated cloud-screening algorithm has been applied. In the original formulation, the GASP AOD has not been properly cloud screened, and therefore, a high optical depth value due to broken clouds is observed, as indicated by the circled regions in Fig. 20. However, when applying a more conservative cloud screening technique to the GOES data (courtesy of NOAA/STAR team), most of the cloud pixels were removed while still leaving the plume AOD measurements unaffected.

7.3 Evaluation of the plume vertical structure using active lidar and passive radiometry

The CCNY lidar co-located with a CIMEL sun-photometer is available for extensive ground measurements. Lidar measurements of the smoke event from Aug 13 to 15 are illustrated in Fig. 21. (a) shows that on Aug 13, we observe prior to the smoke plume arrival over NYC, a clear atmosphere above CCNY with no visible evidence of plumes aloft. On Aug 14, the vertical profile retrieved by the lidar shows a distinct aerosol layer, identified by its strong aerosol backscatter in the late afternoon at about 7 km altitude in Fig. 21 (b). However, by the following day (Aug 15), as the boundary layer developed and the smoke plumes continued to pollute the free troposphere over CCNY, the most noticeable impact of the smoke was its downward advection and mixing with the boundary layer by 14:00 EST.

In examining the spatial extent of the vertical plume structure, we also looked at the NASA Micro-Pulse Lidar NETwork (MPLNET) for simultaneous measurement with the CCNY lidar. The MPLNET operates a lidar at GSFC (39º N, 76º W), downwind from the CCNY lidar, which also has a collocated sun-photometer instrument. Fig. 22 displays the MPLNET/NASA Goddard Space Flight Center Micro Pulse Lidar normalized relative backscatter ratios measured on 14-15 August, the same days as CCNY lidar observations. In Fig. 22, we can see smoke plumes between 3 and 10 km on Aug 14 and between 2 and 6km on Aug 15, similar to that observed over the CCNY site, with the exception that the Aug 14 plumes over GSFC had already began descent, although no boundary layer mixing was evident. Backward trajectories ending at GSFC also showed similar air parcel patterns from the source as that ending at CCNY. It is also important to highlight the fact that the boundary layer mixing on Aug 15 occurred about the same time (14:00 EST) at both locations, which is consistent with the HYSPLIT trajectory analysis.

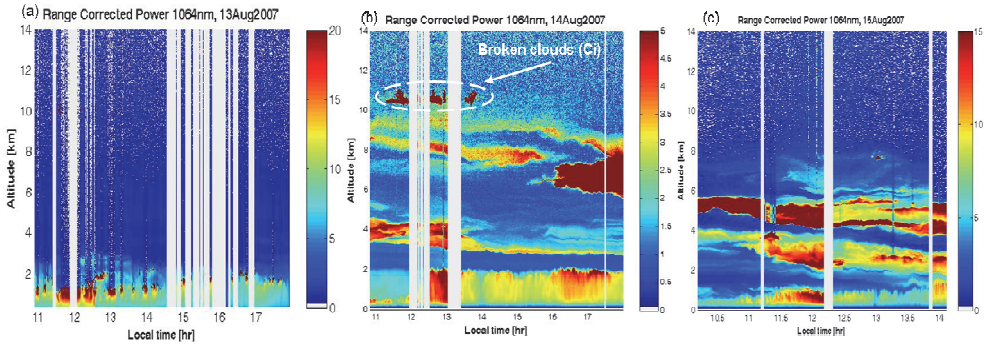

Fig. 21. CCNY range corrected lidar returns at 1064nm showing high altitude plume formation from Idaho, Montana, and Wyoming fires. a) Aug 13: before evidence of smoke plume arrival to NYC b) Aug 14: onset of plumes with lofted layer and no evidence of PBL interactions c) Aug 15: plumes advect downwards interacting with PBL.

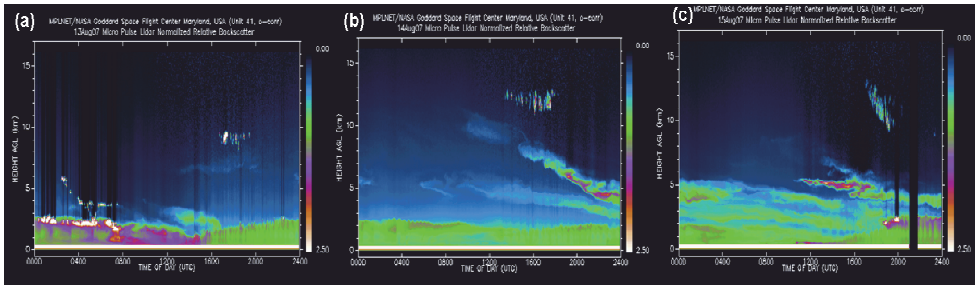

Fig. 22. MPLNET/NASA Goddard Space Flight Center Micro Pulse Lidar normalized relative backscatter ratios measured on (a) Aug 13 before the onset of the smoke plumes, (b) Aug 14, the onset of the smoke plumes descending towards the boundary layer but no visible mixing, and (c) Aug 15, plume advected downwards and mixed with the surface air.

7.4 Plume properties and identification

Unlike the MPLNET, the CCNY lidar has multi-wavelength capabilities allowing us to look for spectral characteristics of the aerosol useful for identification. For example, the plume angstrom coefficient derived from the lidar backscatter measurements as a function of altitude, which we define as:

$$\beta_{aer}(\lambda_1, \lambda_2) = C\lambda^{-\alpha(\lambda_1, \lambda_2)} \tag{5}$$

where C is an arbitrary constant, β is the aerosol backscatter coefficient, and α is the angstrom exponent can help distinguish between small smoke particles and large dust particles in an aloft plume. In doing this calculation, care must be made that channels are calibrated. The 532 nm channel is calibrated based on clear molecular reference signals but the 1064 nm channel requires more care since the molecular reference at 1064 nm channel is too weak. To do this, we employed (Gan et al., 2008; Wu et al., 2010) a cloud base calibration method which results in accuracies ~15%. In Fig. 24 (c) we note that the plume has a large (~2) and stable angstrom exponent as a function of altitude, which is a

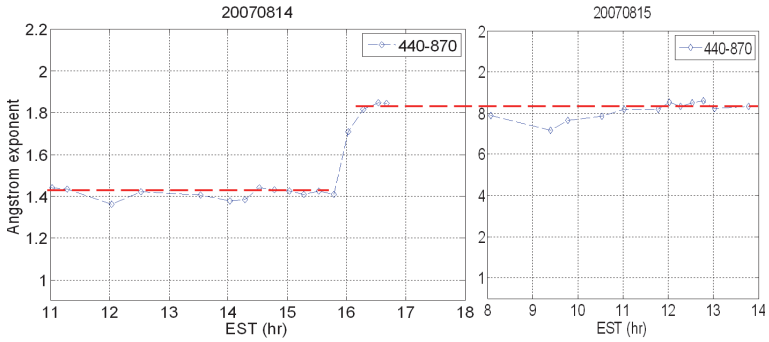

Fig. 23. Column integrated angstrom coefficient derived from sun photometer AOD measurements using 440 – 870 nm channels.

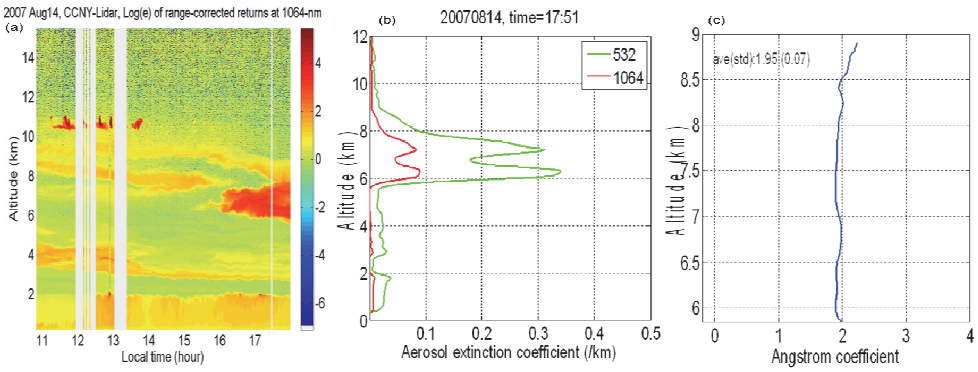

Fig. 24. (a) Lidar range corrected power at 1064 nm, (b) Extinction coefficient obtained from lidar at 17:51 EST, (c) Angstrom coefficient (unitless) using two wavelengths obtained using Equation 5.

clear indication of small particles. These results are reinforced when the sky radiometer angstrom coefficient is calculated, as illustrated in Fig. 23. In particular, we note changes in the angstrom signature (increasing from 1.4 to 1.8 by late afternoon on Aug 14) indicating an increase of fine mode particulates entering the air column. Furthermore, the angstrom coefficients remained fairly constant and stable over the entire 2-days episode, indicating that we are dealing with the same type of particulates, not necessarily coming from a single source. These results are also in good quantitative agreement with the CCNY lidar derived angstrom coefficients.

7.5 Smoke influence on local air quality

We have already noted the advection of the plume into the PBL, so it is natural to explore any ground signatures that indicates an increase in air pollution in the PBL. Fig. 25 shows the near surface particulate loadings on August 13-14 obtained from the NYSDEC. On Aug 14, as expected, the PM2.5 loadings were low. These observations showed no evidence of boundary layer interaction with upper troposphere plumes, and at the surface scattering coefficients and particulate loadings remained low, which is a characteristic of clear and relatively unpolluted air within the boundary layer. On the other hand, by the afternoon of Aug 15, there was a large-scale descent of smoke plumes, resulting in a significant increase in the surface PM2.5 loadings, compared to the state prior to plume interaction. What is interesting is that the semi-empirical relation between PM2.5 and column AOD assuming a well mixed PBL layer (Zhang et al., 2009) Equation 1 would lead to dramatically large overestimates of the surface pollution. However, by using the lidar extinction, we can quantify the AOD of the plume and subtract that contribution from the GOES satellite. The resulting matchup is much improved (Fig. 25) even when the plume interacts with the PBL resulting in tangible increases in the PM2.5 concentration.

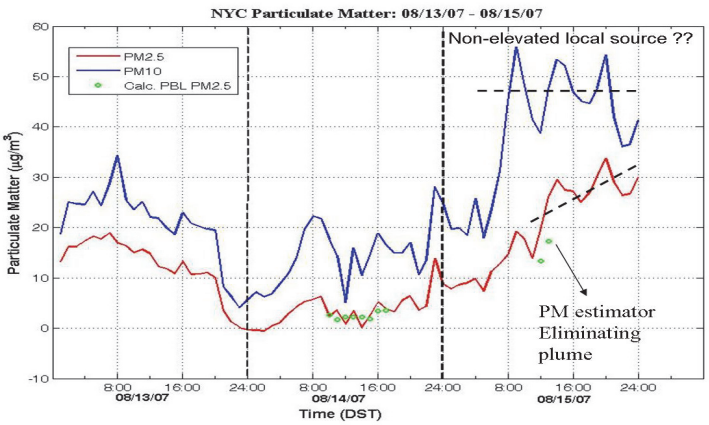

Fig. 25. Ground level PM2.5 and PM10 surface loadings for NYC on Aug 13-15, 2007.

8. Summary

To summarize, the use of vertical profiling sensors has found multiple applications in improving our understanding of pollution and transport processes. In this chapter, we show

not only the importance of remote sensing instruments in monitoring the vertical distribution of air quality but also demonstrate how they can unravel difficulties in air quality retrieval from satellite techniques.

We first illustrate that current meteorological forecast models can reliably determine the PBL height even in urban environments in cases where convective heating is the dominant mechanism. We find in such cases correlations ($R > 0.85$) occur although some over biases are observed in the non-local (BLK and ACM2) schemes. In making these comparisons, the use of the Wavelet Covariance Transform (WCT) method to analyze the lidar profiles together with additional constraints was important in isolating the convective layer from residual and plume layers. In addition, eyesafe 24 hour / 7 days ceilometer measurements were used to understand the most critical anomalies in the CMAQ PM2.5 forecasts. Using the vertical information, the over biases are shown to be most attributable to CMAQ forcing the pollution too near the surface and less to errors in the emission inventories.

Finally, satellite and active sensors were used to demonstrate how long distance plume transport events can affect local pollution including clear observation of how plumes can advert into the PBL and enhance local PM2.5 surface concentrations. Although forest fires are basically local phenomena, they can also contribute to changes of the atmosphere on a regional or even global scale by generating large amounts of aerosol particles, which can be transported over large distances. Therefore, our analysis of the transport of the Idaho and Montana forest fire plumes over the eastern United States during Aug 2007, demonstrates the importance of pollution monitoring and prediction. In particular, we find direct evidence that even long term transport of lofted plume layers can mix with PBL modifying the surface level air-quality

9. Acknowledgment

This chapter is partially supported by NOAA-CREST #NA17AE1625 and NOAA-ISET #NA06OAR4810187. The views, opinions and findings contained in this report are those of the author(s) and should not be construed as an official NOAA or U.S. Government position, policy, or decision. The authors greatly appreciate datasets and helpful advice that were supplied by Jia-Yeong Ku from NYSDEC.

10. References

Anderson, J. R., Hardy, E. E., Roach, J. T., & Witmer, R. E. (1976). A Land Use And Land Cover Classification System For Use With Remote Sensor Data, USGS Geological Survey Professional Paper 964.

Atkinson, B. W. (2003) Numerical modeling of urban heat-island intensity, Bound.-Layer Meteor., 113, 285–310.

Baar, H., Ansmann, A., Engelmann, R. and Althausen, D. (2008). Continuous monitoring of the boundary-layer top with lidar. Atmos. Chem. Phys. Discuss., 8, 10749-10790.

Baker, D., Downs, T., Ku, M., Hao, W., Sistla, G., Kiss, M., Johnson, M. and Brown, D. (2009). Sensitivity Testing of WRF Physics Parameterizations for Meteorological Modeling and Protocol in Support of Regional SIP Air Quality Modeling in the OTR Ozone Transport Commission Modeling Committee.

Braak, R., Torres, O., Veihelmann, B., Veefkin, J. P., Kroon, M. and Levelt, P. (2007). OMI UV absorbing index as a tracer for transport of Australian biomas burning aerosols', Geophys. Res. Abstracts, 9.

Brooks, I. M. (2003). Finding Boundary Layer Top: Application of a Wavelet Covariance Transform to Lidar Backscatter Profiles, J. Atmospheric & Oceanic Technology, Vol. 20, 1092-1105.

Davis, K. J., Gamage, N., Hagelberg, C. R., Kiemle, C., Lenschow, D. H. & Sullivan, P. P., (2000). An Objective Method for Deriving Atmospheric Structure from Airborne Lidar Observations, J. Atmospheric & Oceanic Technology, Vol. 17, 1455-1468.

DeMott, P. J., Sassen, K., Poellot, M. R., Baumgardner, D., Rogers, D. C., Brooks, S. D., Prenni, A. J. and Kreidenweis, S. M. (2003). African dust aerosols as atmospheric ice nuclei, Geophysical Research Letters, Vol. 30, No. 14, 1732, doi:10.1029/2003GL017410

Doraiswamy, P., Hogrefe, C., Hao, W., Civerolo, K., Ku, J.Y. & Sistla, G. (2010). A Retrospective Comparison of Model-Based Forecasted PM2.5 Concentrations with Measurements, J. Air & Waste Manage. Assoc. 60(11):1293-308.

Dockery, D.W., Speizer, F.E., Stram, D.O., Ware, J.H., Spengler, J.D. and Ferris, B.G. Jr. (1989). Effects of inhalable particles on respiratory health of children Am. Rev. Respir. Dis.; (United States); Journal Volume: 139:3 Pages: 587-594

Emeis, S., Schafer, K. & Munkel, C. (2008). Surface-based Remote Sensing of the Mixing-Layer Height – a review, Meteorological Zeitschrift, Vol. 17, No. 5, 621-630.

EPA (1999a). User Manual for the EPA Third-Generation Air Quality Modeling System (Models-3Version 3.0), EPA-600/R-99/055, pp.1-1–1-18, United States Environmental Protection Agency.

EPA (1999b). Science Algorithms of the EPA Models-3Community Multiscale Air Quality (CMAQ) Modeling System, PART II: Chapters 9-18, EPA-600/R-99/030, pp. 10-1 – 10-23, United States Environmental Protection Agency.

Eresmaa, N., Karppinen, A., Joffre, S. M., Rasanen, J. and Talvitie, H. (2006). Mixing height determination by ceilometer, Atmos. Chem. Phys., 6, 1485-1493.

Flagg, D., & Taylor, P. A. (2008). Sensitivity Morphology in Urban Boundary Layer Modeling at the Mesoscale, AMS 18th Symposium on Boundary Layers and Turbulence, 7A.3.

Gamage, N. & Hagelberg, C. (1993). Detection and analysis of microfronts and associated coherent events using localized transform, J. Atmos. Sci, 50, 750-756.

Gan, C. M., Charles, L., Gross, B., Moshary, F. and Ahmed, S. (2008). Analysis of the interaction of aerosol transport layers on local air quality, IGARSS IEEE International Vol.4.

Gan, C. M., Wu, Y., Gross, B., and Moshary, F. (2011). Application of Active Optical Sensors to Probe the Vertical Structure of the Urban Boundary Layer and Assess Anomalies in Air Quality Model $PM_{2.5}$ Forecasts, To appear Atmos. Environ.

Girardot, S. P.(2006). Characterization of ambient ozone and fine particulate matter (PM(2.5)) concentrations, human exposure, and pulmonary health effects in the Great Smoky Mountains National Park, EMORY UNIVERSITY, Thesis ID 3212358

Haij, de, M.J., Wauben, W.M.F., Klein Baltink, H. and Apituley, A. (2009). Determination of the mixing layer height by a ceilometer *Proceedings of the 8th International Symposium on Tropospheric Profiling, ISBN 978-90-6960-233-2 Delft, The Netherlands.*

Hennemuth, B., & Lammert, A. (2006). Determination of the atmospheric boundary layer height from radiosonde and lidar backscatter, Boundary-Layer Meteorology 120: 181–200

Herman, J. R., Bhartia, P. K., Torres, O., Hsu, C., Seftor, C. and Celarier, E. (1997). Global distribution of UV absorbing aerosols from Nimbus 7/TOMS data. J. Geophys. Res. 102, 16,911-16,922.

Hondula, D. M., Sitka, L., Davis, R. E., Knight, D. B., Gawtry, S. D., Deaton, M. L., Lee, T. R., Normile, C. P. and Stengera, P. J. (2009). A back-trajectory and air mass climatology for the Northern Shenandoah Valley, USA, *Int. J. Climatol.* DOI: 10.1002/joc.1896

Hong, S.Y., Noh, Y. & Dudhia, J. (2006). A New Vertical Diffusion Package with an Explicit Treatment of Entrainment Processes, Mon. Wea. Rev., 134, 2318–234.

Janjić, Z.I. (1990). The step-mountain coordinate: physical package. *Mon. Wea. Rev.*, 118, 1429-1443.

Janjić, Z.I. (1994). The step-mountain eta coordinate model: further developments of the convection, viscous sublayer and turbulence closure schemes. *Mon. Wea. Rev*., 122, 927-945.

Janjić, Z.I. (2001) Nonsingular Implementation of the Mellor-Yamada Level 2.5 Scheme in the NCEP Meso model, National Centers for Environmental Prediction, Office Note #437

Jiang, W., Smyth, S., Giroux, E., Rothand, H. & Yin, D. (2006). Differences between CMAQ fine mode particle and PM2.5 concentrations and their impact on model performance evaluation in the lower Fraser valley, Atmospheric Environment, 40, 4973-4985.

Jorba, O., Pe' Rez, C., Rocadenbosch, F. and Baldasano, J. M. (2004). Cluster Analysis of 4-Day Back Trajectories Arriving in the Barcelona Area, Spain,from 1997 to 2002, Journal of Applied Meteorology Vol. 43 pp. 887-901

Kaufman, Y. J. (1993). Aerosol optical thickness and atmospheric path radiance, J. Geophys. Res., 98(D2), 2677–2692.

Knapp, K. R. (2002a). Quantification of aerosol signal in GOES 8 visible imagery over the United States, J. Geophys. Res., VOL. 107, NO. D20.

Knapp, K. R., Vonder Haar, T. H. and Kaufman, Y. J. (2002b). Aerosol Optical Depth Retrieval from GOES-8: Uncertainty study and Retrieval validation over South America, J. Geophys. Res., VOL. 107, NO. D7.

Knapp, K. R., Frouin, R., Kondragunta, S. and Prados, A. (2005). Towards Aerosol Optical Depth Retrievals over land from GOES visible radiances: determine surface reflectance, International Journal of Remote Sensing, VOL. 26, NO. 18.

Koji, M. and Lovei, M. (2001). Urban Air Quality Manegement Coordinating Transport, Enviroment and Energy Policies in Develoing Countries, World Bank Technical paper No. 508.

Kovalev, V.A. & Eichinger, W.E. (2004). Elastic Lidar: Theory, Practice, and Analysis Methods, Wiley-Interscience, USA.

Liu, Y., Chen, F., Warner, T., & Basara, J. (2006). Verification of a Mesoscale Data-Assimilation and Forecasting System for the Oklahoma City Area During the Joint Urban 2003 Field Project, J. Appl. Meteor., 45, 912–929.

Malm, W.C., Sisler, J.F., Huffman, D., Eldred, R.A. & Cahill, T.A. (1994). Spatial and seasonal trends in particle concentration and optical extinction in the United States, *Journal of Geophysical Research-Atmospheres* 99 (D1) (1994), pp. 1347–1370.

Mellor, G.L. and T. Yamada (1982). Development of a turbulence closure model for geophysical fluid problems. *Rev. Geophys. Space Phys.,* 20, 851-875.

Mestayer, PG., Durand, P., Augustin, P., Bastin, S., Bonnefond, J. M., Benech, B., Campistron, B., Coppalle, A., Delbarre, H. and Dousset, B. et al. (2005) The urban boundary layer field campaign in Marseille (UBL/CLU-ESCOMPTE): Set-up and first results, Boundary-Layer Meteor., 114: 315–365.

Otte, T. L. (2008a). The impact of nudging in the meteorological model for retrospective air quality simulations. Part I: Evaluation against national observation networks, J. Appl. Meteor. Climatol., 47, 1853-1867.

Otte, T. L. (2008b) The impact of nudging in the meteorological model for retrospective air quality simulations. Part II: Evaluating collocated meteorological and air quality observations", J. Appl. Meteor. Climatol., 47, 1868-1887.

Piringer, M. et al. (2007). The surface energy balance and the mixing height in urban areas - activities and recommendations of COST-Action 715, Boundary-Layer Meteor. 124:3–24.

Pleim, J. E. & Gilliam, R. (2009). An indirect data assimilation scheme for deep soil temperature in the Pleim-Xiu land surface model, J. Appl. Meteor. Climatol., 48, 1362-1376.

Prados, A.I., Kondragunta, S., Ciren, P. and Knapp, K. R. (2007). GOES Aerosol/Smoke Product (GASP) over North America: Comparisons to AERONET and MODIS observations, J. Geophys. Res. 112.

Skamarock, W. C. et al. (2008). A Description of the Advanced Research WRF Version 3, NCAR TECHNICAL NOTE NCAR/TN–475+STR.

Stull, R.B. (1988). An Introduction to Boundary Layer Meteorology, Kluwer Academic Publishers, Dordrecht/Boston/London.

Taha, H. (1999) Modifying a mesoscale meteorological model to better incorporate urban heat storage: A bulk-parameterization approach, J. Appl. Meteor., 38, 466–473.

Torres, O., Decae, R., Veefkind, P. and G. de Leeuw (2002). OMI Aerosol Retrieval Algorithm, OMI Algorithm Theoretical Basis Document, Volume III, Version 2.

Wu, Y., Chaw, S., Gross, B., Moshary, F. & Ahmed, S. (2009). Low and optically thin cloud measurements using a Raman-Mie lidar, Appl. Opt. 48, 1218-1227.

Wu, Y, Gan, C. M., Gross, B., Moshary, F. and Ahmed, S. (2010). Calibration of lidar at 1064-nm channel using the water-phase and cirrus clouds, To Appear Applied Optics.

Zhang, H., Hoff, R.M. and Engel-Cox, J.A. (2009). The relation between Moderate Resolution Imaging Spectroradiometer (MODIS) aerosol optical depth and PM2.5 over the United States: a geographical comparison by EPA regions, J.Air & Waste Manage. Assoc., 59, 1358-1369.

Zhao, Y. and Frey, H. C. (2004). Development of Probabilistic Emission Inventory of Selected Air Toxics for an Urban Area, Air & Waste Management Association, Pittsburgh, PA.

Arrau, C. P. & Peňa, M. A. (2010). Urban Heat Island Causes, In: *Home Urban Heat Island Effect*, 03.10.2011, Available from: http://www.urbanheatislands.com/home

Voogt, J. A. (2004). Urban Heat Islands: Hotter Cities, In: *ActionBioscience.org*, 03.10.2011, Available from: http://www.actionbioscience.org/environment/voogt.html#primer

10

The Surveillance of the Air Quality in the Vicinity of an Active Volcano: Case of the Piton de la Fournaise

Chatrapatty Bhugwant[1], Miloud Bessafi[2] and Bruno Siéja[1]
[1]*Observatoire Réunionnais de l'Air, Technopole de La Réunion, Sainte-Clotilde, La Réunion island,*
[2]*Université de La Réunion, Saint-Denis Messag Cedex 9, La Réunion island*
France

1. Introduction

Atmospheric pollution may be of both anthropogenic and natural origin (Levine, 1996; Finlayson and Pitts, 1999; IPCC, 2000; Delmas et al., 2005). Concerning natural pollution, most active volcanoes emit, among others, gases (eg. sulphur dioxide) and particles into the atmosphere during eruption events (Hobbs et al., 1991; Bhugwant et al., 2009). It is thus important to conduct the monitoring of these pollutants for active volcanoes all over the world, in order to take the adequate measures of air pollution (eg. to establish evacuation plans for the surrounding population) and also to study the long-term trends and effects caused by volcanic activity. In this sense, since a decade the World Health Organization (WHO), the European Community and the French Ministry of Environment (MEDDTL: Ministère de l'Ecologie, du Développement Durable, du Transport et du Logement) have established SO_2 guideline levels, following the severity of the impact of this pollutant on human health and on the environment (WHO, 2005).
Previous experimental (ground-based and air-borne) studies indicate that major volcanic eruptions such as Mount St Helens (May 1980), El Chicon (March-April 1982) and Pinatubo (June 1991) injected large amounts of solid particles and volatile gases in the troposphere and the stratosphere, up to an altitude of 25 km high (Turco et al., 1993; Trepte et al., 1993; Krueger et al., 1995; Schneider et al., 1999). Another study showed, in a statistical approach, the global distribution of volcanic SO_2 degassing during the last century (1900-2000) and further indicated that each eruption (even for non monitored ones) could affect the stratosphere, based on empirical observations (Hamler et al., 2002). More recently, the eruption of the Eyjafjallajökull volcano in Iceland, which began on April 14th 2010 and ended in October 2010, caused enormous disruption to air travel across western and northern Europe, due to huge amounts of ash and particles emitted in the atmosphere.
Volcanic eruptions may cause irreversible environmental and ecological impacts (burial by ash, mud, etc.), via lava or pyroclastic flows, dusts and ash falls and/or gaseous emissions, while they may also increase the economic burden in socio-economic sectors, by causing infrastructure and habitation damages (e.g. houses, buildings, roads, fields and forests covered with ash and/or lava) (Munich Re, 1998; Brosnan, 2000). It is now clearly

established that the volcanic pollutants have damaging effects on both human health and ecology. The human health effects from air pollution vary in the degree of severity, covering a range of minor effects to serious illness such as impaired pulmonary function as well as premature death in certain cases (Brantley and Myers, 2000).

Volcanic eruptions mostly emit water vapour, sulfur dioxide (SO_2), hydrochloric acid (HCl), hydrofluoric acid (HF) and carbon dioxide (CO_2) (Tabazdeh et al., 1993; Evans and Staudacher, 2001; Kinoshita, 2003; Dubosclard et al., 2004). Once emitted in the atmosphere, they contribute to acid rain and may also affect the stratosphere (Galindo et al., 1998).

The atmospheric SO_2 emitted during volcanic eruptions is chemically transformed into sulphate aerosols (H_2SO_3 and H_2SO_4) during transport (McKeen et al., 1984). These sulphate aerosols may remain in suspension in the atmosphere for several years mainly in the stratosphere, while in the troposphere they are washed out in between weeks (Graf et al., 1993). A recent epidemiological study showed that the SO_2 emitted during the eruption of the Piton de la Fournaise volcano might have a potential sanitary impact on the surrounding population (Viane et al., 2009).

The mean residence time of ambient SO_2 concentration is about 1 day, in absence of sink processes such as rainfall (Delmas et al., 2005). However, the public may be exposed to sulfur dioxide concentrations that are higher than typical outdoor air levels. The effects of exposure to any hazardous substance depend on the dose, the duration, the way one may be exposed, the personal traits and habits. Short-term exposures to high levels of sulfur dioxide can be life-threatening (ATSDR, 1999; WHO, 2005).

The study of gaseous and particulate emissions in the atmosphere induced by natural events such as volcanic eruptions may therefore help for a better comprehension of their impact, especially on the atmospheric chemistry and on human health.

However, up to now, very few studies based on atmospheric measurements have been undertaken with links to sources such as volcanic eruptions in the southern hemisphere, especially at Reunion island, where atmospheric measurements such as SO_2 and particles are still scarce (Bhugwant and Brémaud, 2001; Bhugwant et al., 2002; Halmer, 2005; Bhugwant et al., 2009).

This chapter presents the SO_2 concentration measurements, undertaken over Réunion island and in the vicinity of the Piton de La Fournaise volcano during and off eruption events from 2005 to 2010. This volcano is located in the south-eastern part of the Réunion island, a tiny island found in the south-western Indian Ocean (21° S; 55,5° E). It is surrounded by quite densely inhabited regions from the north-eastern to the southern part of it. This active volcano erupts regularly, at least once a year, with notable amount of degassing. However, due to the geographic configuration, coupled with the meteorological conditions which prevail regionally (easterlies) and locally (land/sea breezes) over the island, the volcanic plumes are regularly transported towards the inhabited regions located downwind and may cause sanitary and environmental impacts.

The SO_2 concentration was measured continuously with an analyser in different parts of the island and with passive diffusion samplers in the vicinity of the Piton de La Fournaise volcano since 2005. The tremor activity of the Piton de La Fournaise volcano and the meteorological data (winds and rainfall) were measured at several locations over the island for each eruption. The analysis of these datasets have contributed towards explaining the spatial distribution and the temporal evolution of the volcanic SO_2 emissions, mainly due to dynamical (transport) and deposition (wet/dry) processes.

2. Guideline values for the SO_2 concentration levels

It has been shown that high SO_2 concentration levels present in ambient air may cause considerable environmental and sanitary impacts (EPA, 1997). It is thus important to conduct the monitoring of this pollutant, in order to take the adequate measures of air pollution and also to study its long-term trends and effects. In this sense, since a decade the World Health Organization (WHO), the European Community and the French Ministry of Environment (MEDDTL : Ministère de l'Ecologie, du Développement Durable, du Transport et du Logement) have established guidelines for the SO_2 concentration levels, following the severity of the impact of this pollutant on human health and the environment.
The French National air quality criteria is mainly based on the Decree n°2002-213 of 15th February 2002 and recently on the Decree n°2010-1250 of the 21st October 2010, concerning the air quality survey, in particular for SO_2, and its effects on the human health and the environment, in the air quality objectives, in the alert thresholds and in the limit values (ADMINET, 2002, 2010).
The European Council Directive (1999) also defines the limit values for sulfur dioxide in the ambient air (see Table I). The objectives of this directive are, to establish limit values and alert thresholds for sulfur dioxide concentrations in ambient air intended to avoid, prevent and/or reduce harmful effects on human health as well as on the environment.
The Table I summarizes briefly the main SO_2 guideline values (critical levels) for the human health and for the vegetation, in order to establish the regulation context of this study (Council Directive, 1999 ; ADMINET, 2002; WHO, 2005).

LIMIT VALUES AND THE ALERT THRESHOLD FOR SULFUR DIOXIDE - EC 1999

Limit values must be expressed in µg/m^3. The volume must be standardised at a temperature of 293 °K and a pressure of 101,3 kPa.

	Averaging period	Limit Value	Margin of Tolerance	Date by which limit value is to be met
1- Hourly limit value for the protection of human health	1 hour	350 µg/m^3, not to be exceeded more than 24 times a calendar year	500 µg/m^3 (43%) on the entry into force of this Directive, reducing on 1 January 2001 and every equal months thereafter by equal annual percentages to reach 0 % by January 2005	1 January 2005
2- Daily limit value for the protection of human health	24 hours	125 µg/m^3, not to be exceeded more than 3 times a calendar year	None	1 January 2005
3- Limit value for the protection of ecosystems	Calendar year and winter (1 October to 31 March)	20 µg/m^3	None	1 July 2001

Table I. (a) Council directive 1999/30/EC of 22 April 1999 relating to limit values for sulfur dioxide, in ambient air.

II. Alert threshold for sulfur dioxide

500 µg/m^3 measured over three consecutive hours at locations representative of air quality over at least 100 km^2 or an entire zone or agglomeration, whichever is the smaller.

LIMIT VALUES AND THE ALERT THRESHOLD FOR SULFUR DIOXIDE - ADMINET 2002

The volume must be standardised at a temperature of 293 °K and a pressure of 101,3 kPa. The annual reference period is the calendar year.

Quality Objective : 50 µg/m^3, on annual average.

Recommendation and information threshold (**SRI**) : 300 µg/m^3 on hourly average.

Alert threshold (**SA**) : 500 µg/m^3 on hourly average, exceeded during consecutive three hours.

Limit values for the protection of the human health :

- Centile 99,7 (that is authorized 24 hours of overtaking a calendar year of 365 days) hourly concentrations: 350 µg/m^3. This value is applicable as from the 1st January 2005. Before this date, the applicable limit value is the value of 2005 increased by the following margins not to be exceeded :

Calendar year considered :	**2001**	**2002**	**2003**	**2004**
Sets the margins not to be exceeded (µg/m^3) :	120	90	60	30

- Centile 99,2 (i.e. 3 authorized days for values exceeding a calendar year of 365 days) daily average concentrations : 125 µg/m^3.
- Limit values for the protection of the ecosystems : 20 µg/m^3 on average annual average and 20 µg/m^3 on average over the period going from the 1st October till the 31st March.

Table I. (b) Decree n° 2002-213 of the 15th February 2002 of the French Ministry of Environment relating to limit values for sulfur dioxide, in ambient air.

TARGET VALUES FOR SULFUR DIOXIDE - WHO 2005

WHO air quality guidelines and interim targets for SO_2 : 24-hour and 10-minute concentrations

	24-hour average (µg/m^3)	**10-minutes average (µg/m^3)**	**Basis for selected level**
Interim target-1 (IT-1)[a]	125	-	
Interim target-2 (IT-2)	50	-	Intermediate goal based on controlling either motor vehicle emissions, industrial emissions and/or emissions from power production. This would be a reasonable and feasible goal for some developing countries (it could be achieved within a few years) which would lead to significant health improvements that, in turn, would justify further improvements (such as aiming for the AQG value).
Air quality guideline (AQG)	20	500	

[a]Formerly the WHO Air Quality Guideline (WHO, 2005).

Table I. (c) WHO Air quality guidelines, Global update 2005.

3. Experimental set-ups and measurements

The ORA measured SO_2 concentrations using passive diffusion samplers on 10 inhabited sites (1 to 10) located in the vicinity of the Piton de La Fournsaise volcano from mid 2005 to late 2007. During the April-2007 eruption however, SO_2 concentrations were measured using passive diffusion samplers on 12 (11 to 22) additional inhabited sites located close to the Piton de La Fournaise volcano. Since 2009, 4 more sites (23 to 26) have been added to reinforce the SO_2 survey in the vicinity of the volcano (Figure 1). All the selected sampling sites are located in inhabited areas, with almost no traffic circulation and at more than 1 to 2 km away from busy highways, in order to avoid local anthropogenic contamination.

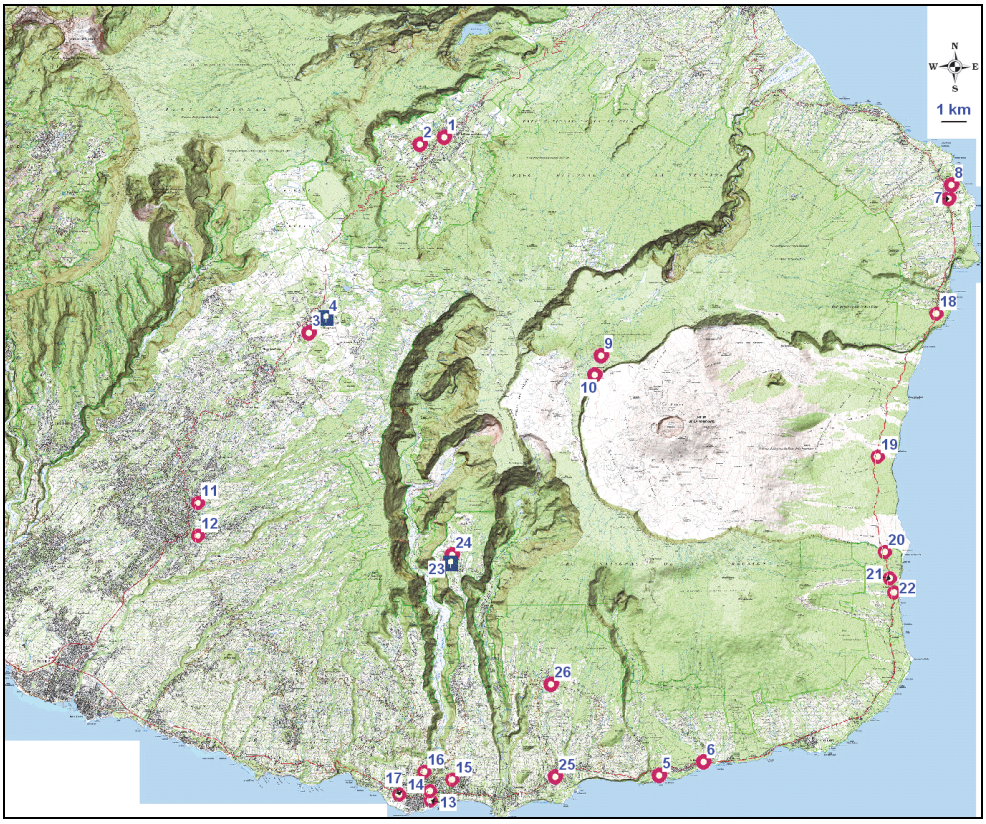

©IGN - ® autorisation N°9876

Fig. 1. Map with indication of the sampling sites (red circles) dedicated for the SO_2 measurements with passive diffusion tubes from 2005 to 2010

3.1 Atmospheric measurements

3.1.1 SO_2 measurement using passive diffusion samplers

Passive diffusion samplers (Ferm, 1991) were used at 10 sites located around the Piton de La Fournaise volcano for the measurement of the ambient SO_2 concentration since September

2005. The measurements by passive diffusion samplers are based on the property of molecular diffusion of gases and species-specific collection on an impregnated filter specific to the SO_2 pollutant measured. The passive diffusion samplers, which were exposed over a period of one week to 10 days, provided quantitative SO_2 concentration measurements and the spatial distribution of this pollutant during and off volcanic eruptions of the Piton de La Fournaise volcano.

The uncertainty on the SO_2 concentrations measured by passive samplers was evaluated during two inter-comparison phases in late 2005, with two series of SO_2 tubes sampled on the sites. One of the series was analysed by the Joint Research Center (JRC) and the other one by the Gradko International Limited (Bhugwant et Siéja, 2005, 2006). This sampling technique has also been tested in different tropical and subtropical regions (Carmichaël et al., 2003; Ferm and Rodhe, 1997).

On the monitoring sites, the samplers are installed mesh side down in the underside of a plastic disc screwed at the top of a wooden pole and left in position for one week to 10 days (see Figure 2).

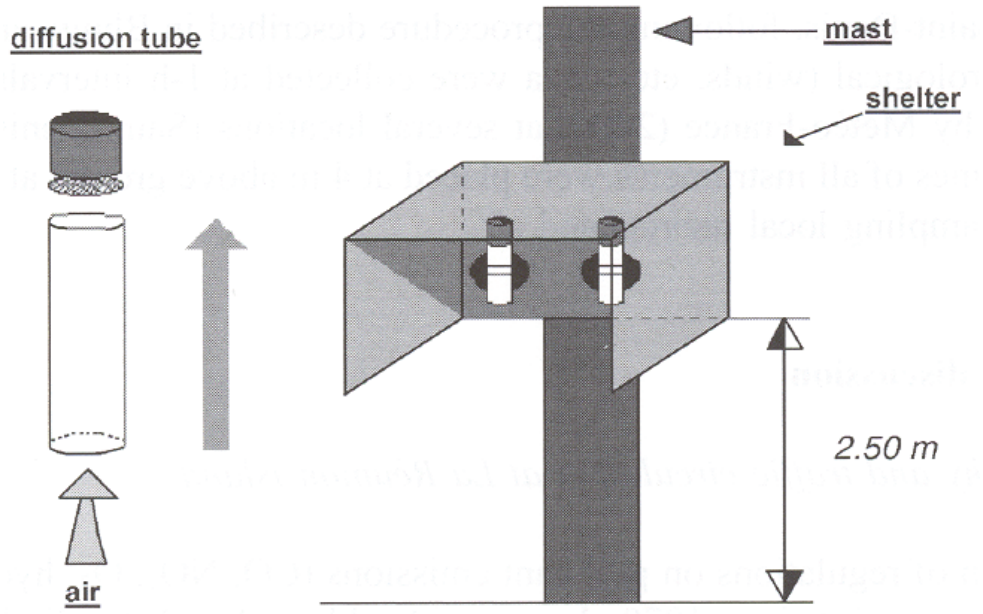

Fig. 2. Schematic representation of a SO_2 passive diffusion tube (left) and the sampling system (right : shelter and mast) for protecting against meteorological conditions (UV radiation, rains …).

After they are taken off, the exposed samples are stored in a refrigerator, in order to stabilize the trapped air samples. Then, they are sent to Gradko International Limited for subsequent laboratory analysis, via Ion Chromatography, in order to calculate the SO_2 concentration. The precision of the samplers, expressed as mean percentage difference between duplicates was found to be in the 10-25% range for SO_2 (Ayers et al., 1998).

3.1.2 SO_2 monitoring using SF-2000 analyser

The ORA also measured SO_2 concentration continuously with automatic analysers in an atmospheric network composed of fixed stations at different parts over Réunion island (Figure 3). During the April-May 2007 eruption, an SO_2 analyser SF-2000 (SERES) model was installed temporarily at two additional sites located in the south-western and southern parts of the island (see points 20: TR_1 and 22: TR_2 respectively, in Figure 3).

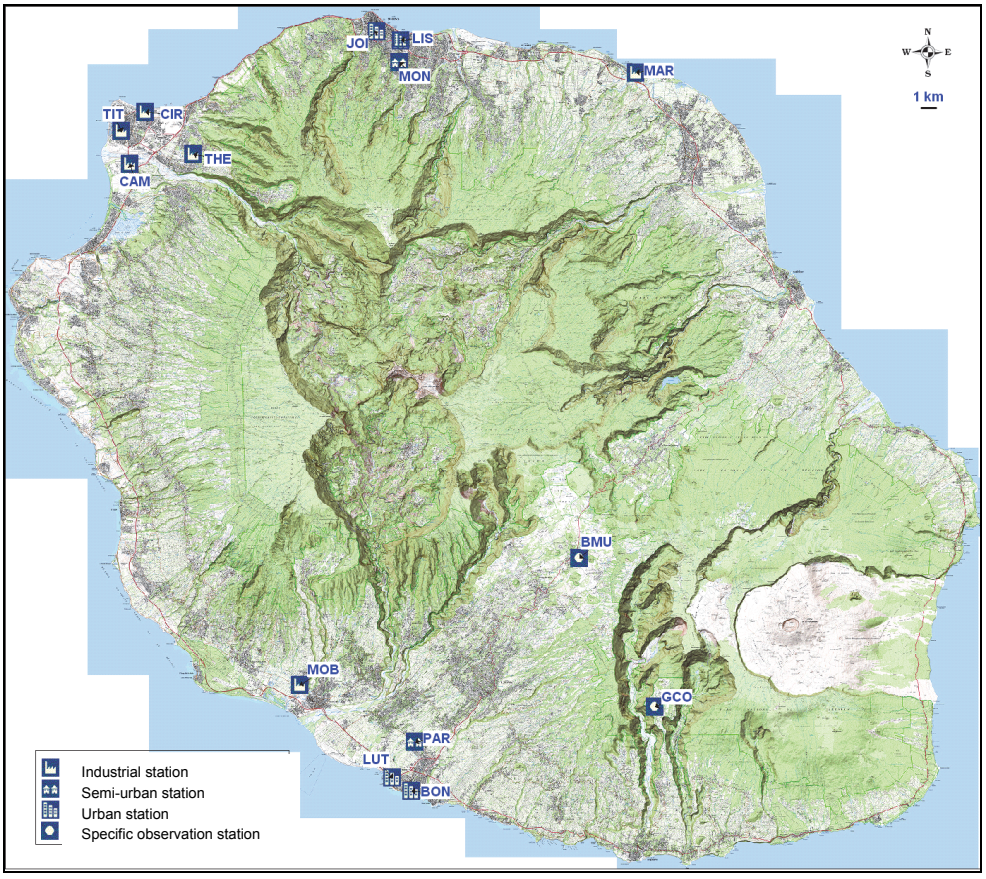

©IGN - ® autorisation N°9876

Fig. 3. Map of Réunion island, with indication of the atmospheric network composed of fixed atmospheric stations over different parts of the island

The instrument analyses ambient air by the ultraviolet (UV) fluorescence technique, at a time-base of 15 minutes, subsequently averaged to 1 hour, for analysis with other datasets such as tremor intensity, winds and rainfall.
Sulfur dioxide molecules are brought to fluorescence once irradiated by ultraviolet radiation in the 190-390 nm wavelength range.
This UV fluorescence is the maximum for a wavelength found in the 210-230 nm range produced by a UV radiation generator which uses a zinc vapour lamp. In the case of the SF-

2000 analyser, the UV radiation of 215 nm wavelength produced by the zinc vapour lamp excites SO_2 molecules contained in the sampling vat, as shown by the equation (1) :

$$SO_2 + h\nu \rightarrow SO_2^* \qquad \text{adsorption - excited state} \qquad (1)$$

The excited SO_2^* molecule regains its initial energetic state E by emitting a radiation of wavelength λ', as indicated in the equation (2):

$$SO_2^* \rightarrow SO_2 + h\nu' \qquad \text{unexcited state} \qquad (2)$$

The re-emitted energy is lower than hν, the excitation energy, and hence the wavelength of the UV fluorescence radiation λ' (240-240 nm) is greater than that of the stimulation source wavelength λ (=215 nm). The fluorescence phenomenon stops when the excitation source is suppressed. The intensity of radiation of the sample is proportional to the SO_2 concentration: $[SO_2] = k \times I_F$, where k is the proportionality factor and I_F is the measured intensity (Ruidavets et al., 2005).
The SO_2 concentration measured by the SF-2000 analysers at the four locations situated in the north-western part of the island is carried out continuously since January 2001. However, only atmospheric data collected during summer 2005 and spring 2007 will be discussed in this work, as notable volcanic pollutants emitted during these eruption episodes were dispersed over different inhabited parts of the island.

3.2 Seismic network

The Observatoire Volcanologique du Piton de la Fournaise (OVPF) is in charge of the seismic and deformation network which has been implemented over the Piton de la Fournaise volcano since 1980. This network is composed, among others, of 25 seismic stations, with 1Hz and large band instruments (Aki and Ferrazzini, 2000; Staudacher at al., 2009). It records the seismic activity and deformation of Piton de la Fournaise 24 hours throughout a day and transfers data by radio in real time to the observatory. The seismic stations closer to the volcano enclosure (Staudacher at al., 2009) and to the eruption site are best representative of the eruptive tremor, and have been studied in particular for the April-May 2007 eruption (Bhugwant et al., 2005, 2009).

3.3 Meteorological data

The local meteorological parameters such as wind speed, wind direction, and rainfall are measured from the instruments onboard a tower at 10 m above the ground level, close to most of the sampling locations. These meteorological stations are managed by the French Meteorological Service (Météo-France, 2000). The wind fields calculated from the ECMWF (European Center for the Medium-Range Weather Forecast) data archives are also analysed (not shown) in order to study the dynamical processes prevailing on regional scale over Réunion Island (Bhugwant et al., 2009).

3.4 Tropospheric SO_2 concentration variability measured from satellite data

The Ozone Monitoring Instrument (OMI) is dedicated to detect and measure volcanic eruptions degassing and anthropogenic pollution from space. The OMI is a hyperspectral UV-Visible spectrometer with a resolution of 13x24 km at nadir. In order to gain more information about the spatial distribution of the SO_2 and the characteristics (composition, etc.) of the volcanic plumes, satellite data retrieved each day from the Aura OMI satellite

following the eruptions were analysed (Carn et al., 2003, 2007; Yang et al., 2007; Bhugwant et al., 2009).

3.5 Field observations of the Piton de la Fournaise activity

It is now well established that the Piton de la Fournaise volcano is one of the most active volcanoes in the world, with one eruption every 8 months, over the last century. Since 1998, a particular intense volcanic activity is observed, with 2 to 4 eruptions per year. These eruptions are mainly basaltic, producing generally lava fountains of 50 to 100 m high and fluid lava flows of aa or pahoehoe type and of aphyric to olivine-rich composition. Most eruptions of Piton de la Fournaise last between 2 weeks and 1 month. However, the March 1998 eruption lasted 196 days. As the driving force of every eruption is the trapped gas, they always accompany each eruption. However, significant gas emissions are observed at Piton de la Fournaise during intense eruptions only (Bhugwant et al., 2001, 2009).

3.6 Sanitary and environmental survey

Following the recent population control, Réunion island holds a population of 730 000 inhabitants (INSEE, 2010). About 24% of the population of the island lives in the vicinity of the Piton de La Fournaise volcano and may thus be exposed to sanitary hazards during eruption episodes. Moreover, a large part region localised close to the Piton de La Fournaise is composed of agricultural lands and also forests with endemic species, which may be subject to environmental impacts (eg. acid rains) during eruptions.

4. Results & discussions

4.1 Spatial SO_2 concentration distribution during late December 2005 eruption

The methodology applied to calculate the spatial distribution of the SO_2 concentrations measured at different locations over Réunion island is the kriging interpolation method (Carletti et al., 2000).

The Figure 4 presents the GIS (geographic information system) plot of the spatial distribution of the mean SO_2 concentration measured during an eruption event which occurred on late December 2005-early January 2006, i.e., from 27th December 2005 to 3rd January 2006. The mean SO_2 concentration shown in this figure consists of the data obtained from both passive diffusion samplers and the automatic analysers on the atmospheric stations. It may first be observed that the highest SO_2 concentration (~ 70 $\mu g/m^3$) is mostly confined on the southern and the south-eastern parts of the island. Then, it decreases rapidly after a few kilometres from the eruption vent. Importantly, it may be seen that the eastern to north-eastern part of the island is weakly concerned by the SO_2 concentration emitted during this eruption event. The main causes are, among others, the ranges of mountains Cilaos, Mafate and Salazie (see Figure 2), which constitute a natural barrier for the transfer of atmospheric pollutants downwind, over the eastern to northern parts of the island. Moreover, due to the conjunction of the important relief of the island and the easterlies prevailing over the south-western Indian Ocean, the air masses originating from the south-eastern part of the island tend to by-pass it (Météo-France, 2000). Also, the geographic configuration of the island tends to generate microclimates over the island. Consequently, the windward side of the island is more windy with high rainfall levels throughout the year while the leeward side of it is drier with less winds. This parameter may also in part explain the low SO_2 concentration observed on the eastern to northern sectors.

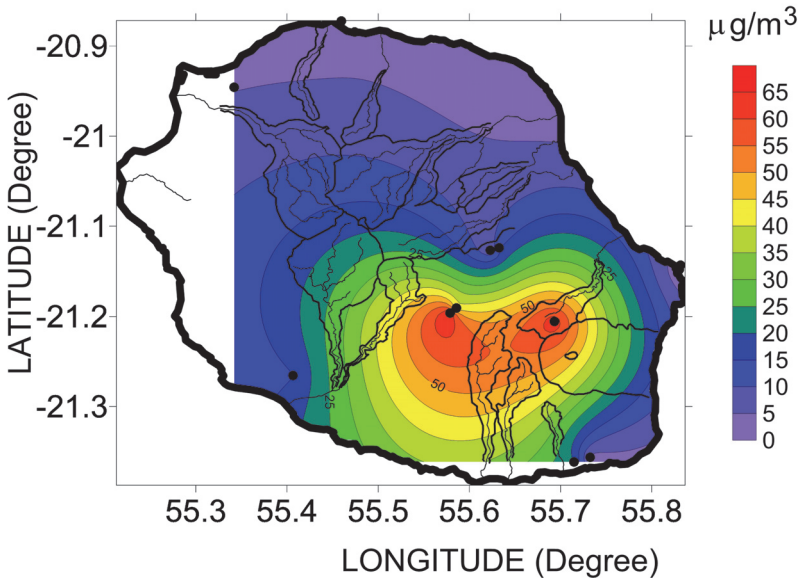

Fig. 4. Contour plot of the mean SO_2 concentration calculated by kriging interpolation method from thirteen measurement locations during 27th December 2005-3rd January 2006 period over Réunion Island (black circles : SO_2 sampling locations).

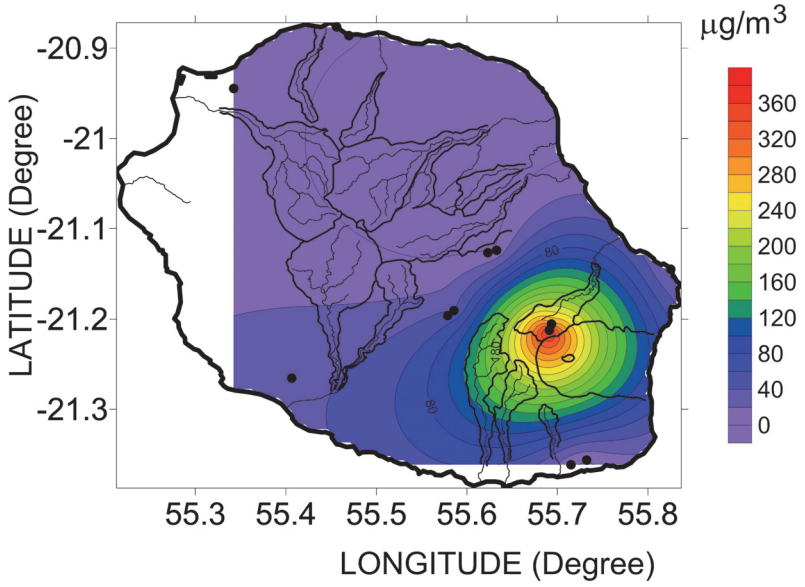

Fig. 5. Contour plot of the mean SO_2 concentration calculated by kriging interpolation method from thirteen measurement locations during 3rd January 2006-12th January 2006 period over Réunion island (black circles : SO_2 sampling locations).

4.2 Spatial SO_2 concentration distribution during early January 2006 eruption

The Figure 5 presents the plot of the spatial distribution of the mean SO_2 concentration obtained by passive diffusion samplers and automatic analysers during an eruption event which occurred from late December 2005 to mid-January 2006, i.e., from 3rd January 2006 to 12th January 2006. The highest SO_2 concentration (~ 370 µg/m^3) is observed on the northern to south-western parts of the Piton de la Fournaise volcano. Interestingly, it may be seen that the high SO_2 levels are constrained in a mountainous sector with a very low density of population. The contaminated air masses follow gullies and rivers lane found in the vicinity of the volcano (on the north-western to southern part of it) to attain the littoral regions of the island. The comparison of the two figures (4 and 5) shows that, in spite of the relief and the meteorology, the source intensity is also a dominating factor which can explain the sulfur dioxide variability observed for these two eruptive episodes.

4.3 Spatial SO_2 concentration distribution during mid-April 2007 eruption

The Figure 6 presents the plot of the spatial distribution of the mean SO_2 concentration obtained by passive diffusion samplers and automatic analysers during an eruption event which occurred from early April 2007 to early May 2007, i.e., from 18th April 2007 to 26th April 2007. The highest SO_2 concentration (~ 190 µg/m^3) is mainly concentrated on the northern to south-western parts of the Piton de la Fournaise volcano while moderate levels are also measured up to the southern to south-western part of the island.
Since the SO_2 surveillance in the vicinity of this volcano, it may be seen that during the previous eruptions, regularly the volcanic plumes are preferentially transported to the southern to north-western parts of Réunion island.

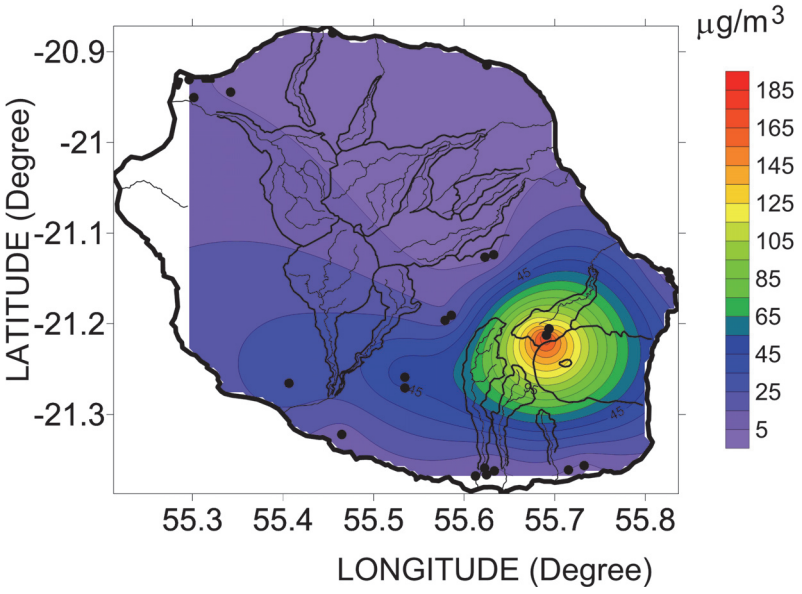

Fig. 6. Contour plot of the mean SO_2 concentration obtained by kriging interpolation method from twenty-three measurement locations during 18th April-26th April 2007 period over Réunion island (black circles : SO_2 sampling locations).

4.4 Temporal evolution of SO_2 concentration in 2006 and 2007

The Figure 7 presents the monthly mean SO_2 concentration measured by automatic analysers in atmospheric stations at different parts of Réunion island in 2006 and 2007. In absence of any eruption, the monthly mean SO_2 concentration exhibits low levels, varying in the 3-12 µg/m³ range at all the monitoring sites.

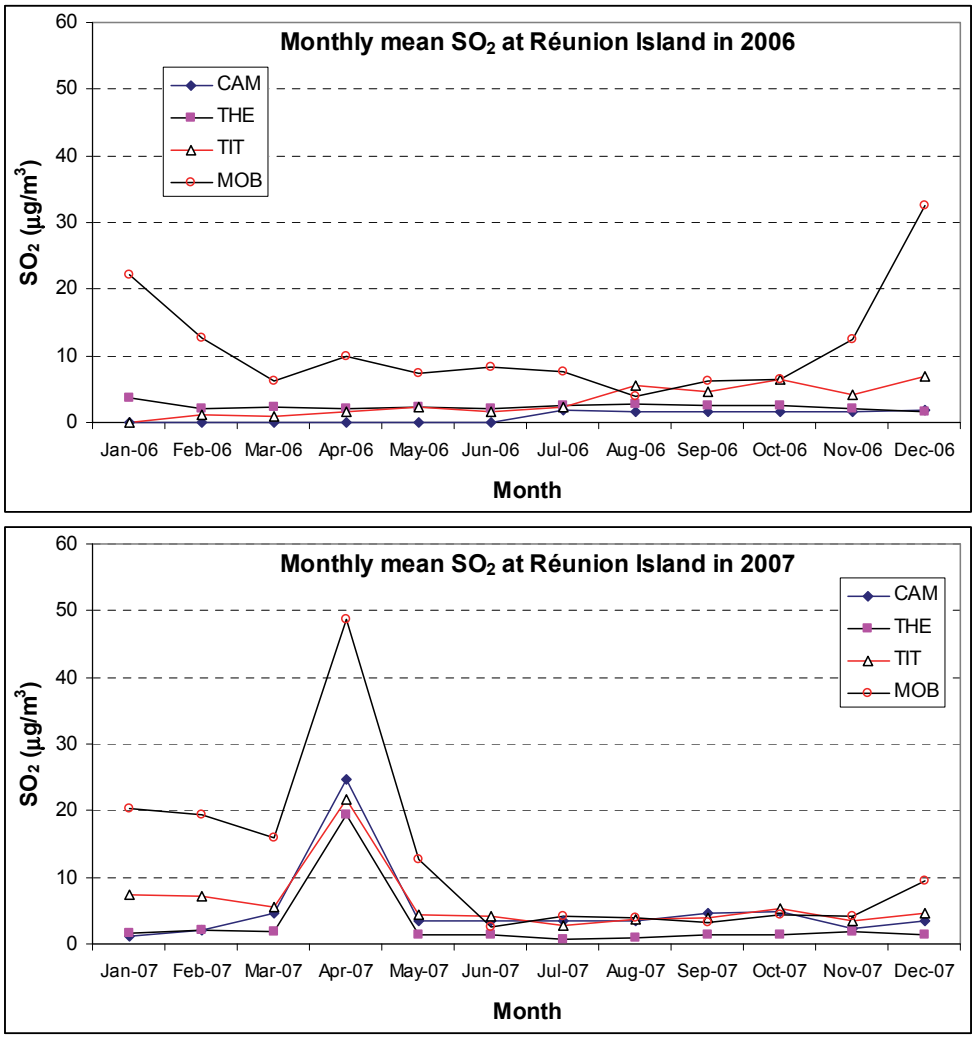

Fig. 7. Monthly mean SO_2 concentration measured continuously with automatic analysers at different atmospheric stations over Réunion island in 2006 and 2007.

The highest SO_2 concentration (~ 50 µg/m³) is observed at the MOB station (which is closest to the Piton de la Fournaise volcano) while the other stations are also but less impacted by the SO_2 emitted in April 2007. This assessment is coherent with the results presented in Figure 6.

Importantly, it may be seen that the atmospheric stations located in the north-western parts of the island show low values while the MOB station exhibit high values during each eruption event registered in 2006 and 2007. The results also suggest a regional impact of the contaminants emitted during the Piton de la Fournaise volcano eruption and the implications on human health for the population exposed to atmospheric pollution.

4.5 Winds spatial distribution over Réunion island

Dynamical processes such as winds (direction and speed) have notable influence on atmospheric constituent variability. It is thus important to study the winds regime prevailing over the island in order to assess their influence on the SO_2 concentration variability. The Figure 8 presents the wind roses annual mean distribution over Réunion island, calculated from winds data collected over meteorological stations located in different parts of the island from 1976 to 1995 (Météo-France, 2000). It may be seen that the hilly landscape of the island plays an essential role in the winds distribution. On one hand, it contributes to strengthen the winds in certain sectors, and, on the other hand, to place certain regions under cover. The land/sea breezes as well as the slope breezes, the constituent of which is perpendicular in the coasts, are clearly evidenced on most of the meteorological stations. The local winds distribution induced by the important relief of the island, coupled with the easterlies prevailing regionally over the south-western Indian Ocean, notably contribute to the dispersion of the SO_2 over the island during and off eruption events.

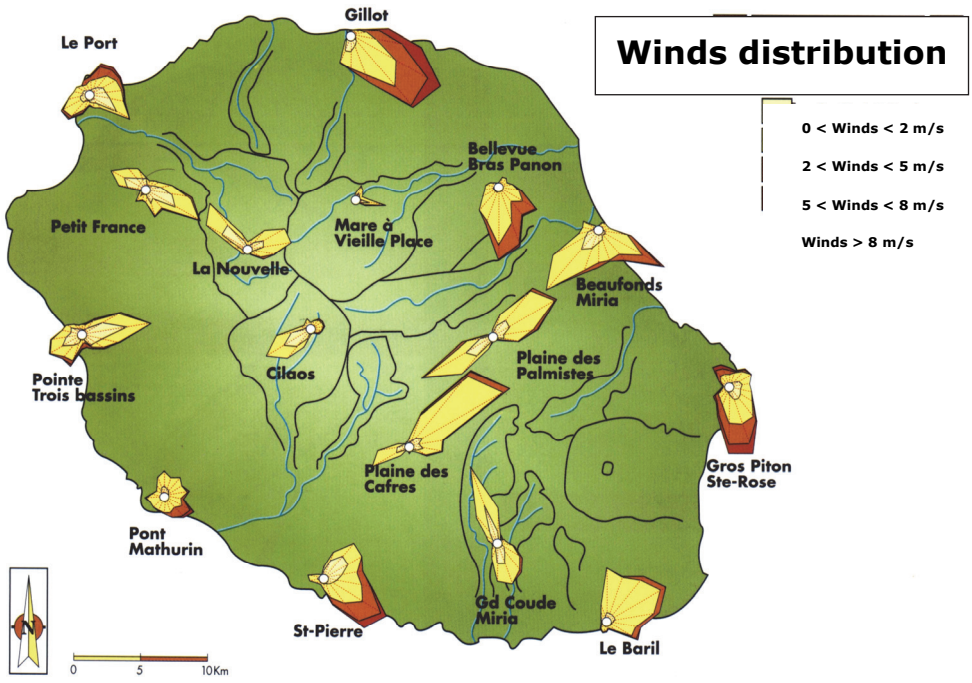

Fig. 8. Wind roses annual mean distribution illustrating the winds spatial distribution over Réunion island obtained from winds data collected from 1976 to 1995 (Source : Météo-France, 2000).

4.6 Spatial distribution of rainfall in early winter (April)

In order to gain more information about the spatial distribution and the temporal evolution of the SO_2 concentration; additional meteorological data collected over the island was also analysed. Figure 9 presents the spatial distribution of the monthly mean rainfall measured in April (from 1998 to 2008) over Réunion island. It may be seen that the maximum rainfall occurs in the southern to north-eastern regions, with a maximum rainfall of ~ 1 200 mm in the East of the island. A comparison with the 4 to 6 suggest that this parameter is the main factor which may explain the lower SO_2 levels observed in the south-eastern to the northern regions, especially during eruption events.

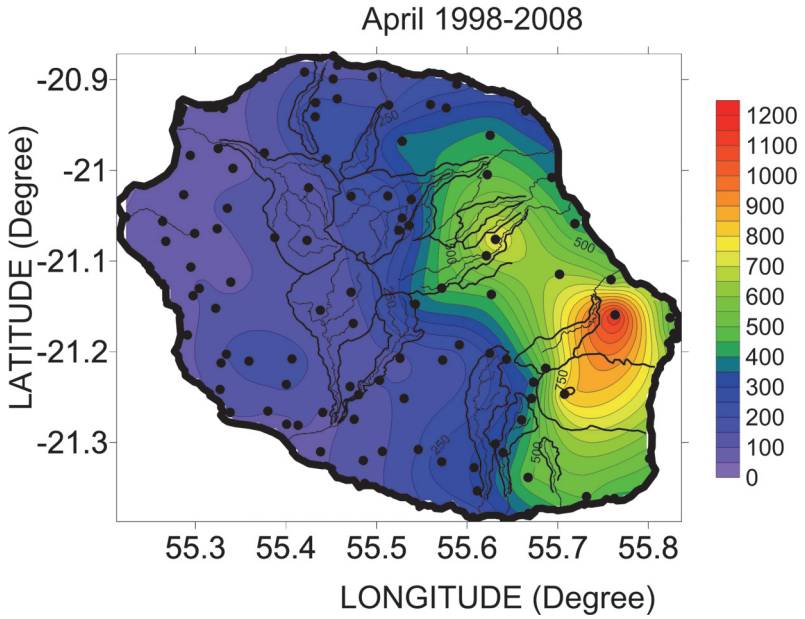

Fig. 9. Monthly mean rainfall measured in April from 1998 to 2008 at different parts of Réunion island (black circles : meteorological stations).

5. Conclusions

In this chapter the spatial distribution of SO_2 concentration and its temporal evolution during several eruptions of the Piton de La Fournaise volcano has been analysed, in conjunction with other parameters, such as seismic and meteorological data.

A good correlation has been established between the seismic variability and the SO_2 concentration variation in the vicinity of the volcano (Bhugwant et al., 2009).

The analysis of SO_2 data collected in parallel with meteorological parameters show that the rainfall influences notably the SO_2 spatial variability in particular over the eastern to northern regions of Réunion island, via scavenging processes.

The conjunction of the important relief of the island coupled with the winds (easterlies and land/sea breezes) also contribute to the spatial distribution and the temporal evolution of the SO_2 concentration measured at different parts of it.

Importantly, the results of several years of SO_2 measurements also show that the QO (Quality Objective) as well as the LV (Limit values for the protection of the ecosystems), based on an annual average, were not exceeded over the island during the 2005-2010 period. However, the SRI (Recommendation and information threshold) as well as the SA (alert threshold) was exceeded in some inhabited regions close to the volcano during previous eruptions, in particular during the April-May 2007 eruption (Bhugwant et al., 2009).
Recently, a preliminary epidemiological study showed that the SO_2 emitted during the eruption of the Piton de la Fournaise volcano might have a potential sanitary impact on the surrounding population. Consequently, this investigation should be carried out in order to establish quantitatively the links between atmospheric pollution induced by eruption events and sanitary impacts.
This preliminary work may be of interest in particular to epidemiologists (eg. to establish the sanitary impact on the surrounding population) and to decision-makers (eg. for crisis managements during eruption episodes).
A close collaboration between the various supervisory boards (ORA, OVPF and Météo-France) may help to establish a decision-making tool to the decision-makers, in particular, to draw up evacuation plans in case of pollution alerts. The recent tools deployed, i.e., the atmospheric data collected from the satellite since a few decades is also a supplement to the ground-based measurements, for the monitoring of atmospheric plumes during future eruptions of this active volcano.

6. Acknowledgements

The present work is supported in part by the French 'Ministère de l'Outre-Mer' (MOM) Program. We acknowledge the French 'Minsitry of Environment' for the financial support of the ORA atmospheric network.
We also gratefully acknowledge the ORA staff for the technical support and for the atmospheric data sampling. We also thank the OVPF staff for preparing the tremor data. Météo-France is also gratefully acknowledged for providing the meteorological data.

7. References

ADMINET, http://admi.net/jo/20020219/ATEP0190081D.html, (in French), 2002.
ADMINET, http://www.legifrance.gouv.fr/affichTexte.do?cidTexte=JORFTEXT000022941254&dateTexte=&categorieLien=id, (in French), 2010.
Aki, K., Ferrazzini, V., 2000. Seismic monitoring and modeling of an active volcano for prediction, J. Geophys. Res., 105, B7, 16617-16640.
ATSDR, 1999. Agency for Toxic Substances and Disease Registry, Public Health Statement, Toxicological Profile for Sulfur Dioxide, CAS # 7446-09-5.
Ayers, G.P., Keywood, M.D., Gillett, R., Manins, P.C., Malfroy H., Bardsley, T., 1998. Validation of passive diffusion samplers for SO_2 and NO_2, Atmos. Environ., vol. 32, 20, Pages 3587-3592.
Benkovitz, C.M., Scholtz, M.T., Pacyna, J., Tarrason, L., Dignon, J., Voldner, E.C., Spiro, P.A., Logan, J.A. Graedel, T.E., 1996. Global gridded inventories of anthropogenic emissions of sulfur and nitrogen, *J. Geophys. Res.*, 27, 101, 29,239-29,253.

Bhugwant, C., Brémaud, P., 2001. Simultaneous Measurements of Black Carbon, PM10, Ozone and NOx Variability at a locally polluted island in the Southern Tropics, J. Atmos. Chem., Vol. 39, N° 3, 261-280(20).

Bhugwant, C., Siéja, B., Perron, L., E. Rivière, E., Staudacher, T., 2002. Impact régional du dioxyde de soufre d'origine volcanique induit par l'éruption du Piton de la Fournaise (Ile de la Réunion) en juin-juillet 2001, Pollution Atmosphérique, (in French), vol. 44, nº176.

Bhugwant, C., Siéja, B., 2005. Campagnes de mesures de la qualité de l'air réalisées sur Saint Pierre en 2004 et 2005 (in French), Bilan d'Etude, N° 5, ORA.

Bhugwant, C., Siéja, B., 2006. Surveillance des concentrations de SO_2 autour du volcan en 2005 (in French), Rapport d'étude, ORA.

Bhugwant, C., Siéja, B., Bessafi, M., Staudacher, T. & Ecormier, J. 2009. Atmospheric sulfur dioxide measurements during the 2005 and 2007 eruptions of the Piton de La Fournaise volcano: Implications for human health and environmental changes. Journal of Volcanology and Geothermal Research, 184, 208-224.

Brantley, S.R., Myers, B., 2000. Mount St. Helens - From the 1980 Eruption to 2000, USGS Fact Sheet, 036-00, http://vulcan.wr.usgs.gov/Volcanoes/MSH/Publications/FS036-00/.

Brosnan, D.M., 2000. Coral Reefs: Volcanic Impacts, Ecological impacts of the Montserrat volcano: A pictorial account of its effects on land and sea life, Sustainable Ecosystems Institute, http://www.sei.org/impacts.html.

Carletti, R., Picci, M., Romano, D., 2000. Kriging and Bilinear Methods for Estimating Spatial Pattern of Atmospheric Pollutants, Environ. Monitor. Assess., 63, 2, 341-359, DOI: 10.1023/A:1006293110652.

Carmichaël, G.R., Ferm, M., Thongboonchoo, N., Woo, J.H., Chan, L.Y., Murano, K., Viet, P.H., Mossberg, C., Bala, R., Boonjawat, J., Upatum, P., Mohan, M., Adhikary, S.P., Shrestha, A.B., Pienaar, J.J., Brunke, E.B., Chen, T., Jie, T., Guoan, D., Peng, L.C., Dhiharto, S., Harjanto, H., Jose, A.M., Kimani W, Kirouane, A., Lacaux, J.P., Richard, S., Barturen, O., Cerda, J.C., Athayde, A., Tavares T., Cotrina, J.S., Bilici, E., 2003. Measurements of sulfur dioxide, ozone and ammonia concentrations in Asia, Africa and South America using passive samplers. Atmos Environ., 37:1293–1308., doi:10.1016/S1352-2310(02)01009-9.

Carn, S.A., Krueger, A.J., Bluth, G.J.S., Schaefer, S.J., Krotkov, N.A., Watson, I.M. and Datta, S., 2003. Volcanic eruption detection by the Total Ozone Mapping Spectrometer (TOMS) instruments: a 22-year record of sulfur dioxide and ash emissions. In: Volcanic Degassing (eds. C. Oppenheimer, D.M. Pyle and J. Barclay), Geological Society, London, Special Publications, 213, pp.177-202.

Carn, S.A., Krotkov, N.A., Yang, K., Hoff, R.M., Prata, A.J., Krueger, A.J., Loughlin, S.C., Levelt, P.F., 2007. Extended observations of volcanic SO_2 and sulfate aerosol in the stratosphere, Atmos. Chem. Phys. Discuss., 7, 2857-2871.

Council Directive, 1999. 1999/30/EC of 22nd April 1999 relating to limit values for sulfur dioxide, nitrogen dioxide and oxides of nitrogen, particulate matter and lead in ambient air, *Official Journal,* L 163, 29/06/1999, P. 0041-0060.

Delmas, R., Mégie G., Peuch, V.-H., 2005. Physique et chimie de l'atmosphère, in French, 640 pages, Ed. Belin.

Dubosclard, G., Allard, P., Cordesses, R., Donnadieu, F., Hervier, C., Coltelli, M., Privitera, E., Kornprobst, J., 2004. Doppler radar sounding of volcanic eruption dynamics at Mount Etna. Bull. Volcanol., 66, 5, 443-456.

Evans, B.M., Staudacher, T., 2001. In situ measurements of gas discharges across fissures associated with lava flows at Reunion island, *J. Volcanol. Geotherm. Res.*, 106, 255-263.

EPA, 1997. Summary Report, http://www.epa.gov/air/airtrends/aqtrnd97/brochure/so2.html

Ferm, M, 1991. A Sensitive Diffusional Sampler. IVL publication B-1020, Swedish Environmental Research Institute, Box 47086, 402 58 Goteborg, Sweden.

Ferm, M., Rodhe, H., 1997. Measurements of Air Concentrations of SO2, NO2 and NH3 at Rural and Remote Sites in Asia, *Journal of Atmospheric Chemistry,* 27, 17–29, 1997.

Finlayson-Pitts, B.J., Pitts Jr., J.N., 1999. Chemistry of the Upper and Lower Atmosphere, Theory, Experiments and Applications. Ed. B.J. Finlayson-Pitts & J.N. Pitts Jr., Academic Press.

Galindo, I., Ivlev, L.S., Gonzalez, A., Ayala, R., 1998. Airborne measurements of particle and gas emissions from the December 1994–January 1995 eruption of Popocatepetl volcano (Mexico), *J. Volcanol. Geotherm. Res.*, 83, 197-217.

Graf, H.-F., Kirchner, I., Robock, A., Schult, I., 1993. Pinatubo eruption winter climate effects: Model versus observation, *Climate Dynamics*, 9, 81-93.

Halmer, M.M., Schmincke, H.-U., Graf, H., 2002. The annual volcanic gas input into the atmosphere, in particular into the stratosphere: a global data set for the past 100 years. *J Volcanol. Geotherm. Res.*, 115: 511-528.

Halmer, M.M., 2005. Have volcanoes already passed their zenith influencing the ozone layer? *Terra Nova*, 17, 500-502, doi: 10.1111/j.1365-3121.2005.00641.x.

Hobbs, P., Radke, L., Lyons, J., Ferek, R., Coffman, D., Casadevall, T., 1991. Airborne measurements of particle and gas emissions from the 1990 volcanic eruptions of Mount Redoubt, J. Geophys. Res., 96(D10), 18735-18752.

IPCC, 2000. Guidelines for National Greenhouse Gas Inventories.

Kinoshita, K., Kanagaki, C., Tupper, A., Iino, N., 2003. Observation and analysis of plumes and gas from volcanic islands in Japan, Proceedings of PHYSMOD2003, Int. Workshop on Physical Modelling of Flow and Dispersion Phenomena, Prato, Italy, 3-5 September.

Krueger, A.J., Walter, L.S., Bhartia, P.K., Schnetzler, C.C., Krotkov, N.A., Sorid, I., Bluth, G.J.S, 1995. Volcanic sulfur dioxide measurements from the total ozone mapping spectrometer, *J. Geophys. Res.*, 100, 14057-14076.

Levine, J.S., 1996. Biomass Burning and Golbal Change. Remote sensing, modeling and Inventory development, and Biomass burning in Africa. Ed. J. S. Levine, 1.

McKeen, S.A., Liu, S.C., Kiang, C.S., 1984. On the chemistry of stratospheric SO_2 following volcanic eruptions, *J. Geophys. Res.*, 89, 4, 873-881.

Météo-France, 2000. Atlas climatique de La Réunion (in French). Bureau d'étude climatologique, Direction Interrégionale de La Réunion. Annual report, No. 1657.

Munich Re, 1998. World Map of Natural Hazards, Munich Reinsurance Company.

Ruidavets, J. B., Cournot, M.; Cassadou, S., Giroux, M., Meybeck, M.; Ferrières, J. 2005. Ozone air pollution is associated with acute myocardial infarction, *Circulation.* 2005, American Heart Association, Inc., 111: 563-569.

Schneider, D.J., Rose, W.I., Coke, L.R., Bluth, G.J.S., Sprod, I.E., Krueger, A.J., 1999. Early evolution of a stratospheric volcanic eruption cloud as observed with TOMS and AVHRR, *J. Geophys. Res.*, 104, D4, 4037-4050.

Staudacher, Th., Ferrazzini V., Peltier A., Kowalski Ph., Boissier P., Catherine Ph., Lauret F., Massin F., 2009. The April 2007 eruption and the Dolomieu collapse, two major events on Piton de la Fournaise (La Réunion island, Indian Ocean), J. Volcanol. Geotherm. Res., 184, 126-137.

Tabazadeh, A., Turco, R.P., 1993. Stratospheric chlorine injection by volcanic eruptions: HCl scavenging and implications for ozone, *Science*, 260, 1082-1086.

INSEE, TER (Tableau Economique de La Réunion), n° 1084, 3014, (in French), 2010.

Trepte, C.R., Veiga, R.E., McCormick, M.P., 1993. The poleward dispersion of Mount Pinatubo Volcanic Aerosol, J. Geophys. Res., 98, D10, 18,563-18,570.

Turco, R.P., Drdla, K., Tabazadeh, A., Hamill, P., 1993. Heterogeneous chemistry of polar stratospheric clouds and volcanic aerosols, NATO ASI Series, 8, 65-134.

Viane, C., Bhugwant, C., Siéja, B., Staudacher, T. & Demoly, P. 2009. Comparative study of the volcanic gas emissions and the hospitalizations for asthma of the Reunion island population between 2005 and 2007. Revue Francaise D Allergologie, 49, 346-351.

WHO, 2005. Air quality guidelines for particulate matter, ozone, nitrogen dioxide and sulphur dioxide, global update 2005.

Yang, K., Krotkov, N.A., Krueger, A.J., Carn, S.A., Bhartia, P.K., Levelt, P.F., 2007. Retrieval of large volcanic SO_2 columns from the Aura Ozone Monitoring Instrument (OMI): comparison and limitations. *J. Geophys. Res.*, 112, D24S43, doi:10.1029/2007JD008825.

11

Remote Zones Air Quality - Persistent Organic Pollutants: Sources, Sampling and Analysis

Alessandro Bacaloni, Susanna Insogna and Lelio Zoccolillo
Department of Chemistry, University of Rome "La Sapienza"
Italy

1. Introduction

Concern about air quality has been rising since the Industrial Revolution and the so-called "Second Industrial Revolution" characterized by internal combustion engine, electrical technology and above all synthesis of new chemicals. Since then humankind has been facing the consequences of its thoughtless release of pollutants in atmosphere, consequences as reducing smog, acid rains and photochemical smog. Notwithstanding the seriousness of single episodes, these were local, or at most regional, phenomena. Nowadays, the variety of pollutants and the extent of pollution are greater than even in history, and air pollution problems are reaching up to global scale. In the last decades, it was established that manmade chemicals, such as polychlorinated biphenyls, chlorofluorocarbons and volatile chlorinated hydrocarbons, were present even in the remotest zones of the Earth, according to their volatility and half-life. This evidence stimulated the scientific community to monitor air quality of remote zones, areas considered a short time ago as uncontaminated.
This chapter deals with different sampling and analysis techniques for persistent organic pollutants (POPs) in the atmosphere of remote zones. Features, sources and environmental fate of POPs are presented in the first section. The second section focuses on logistic and experimental difficulties connected to surveys in remote zones. The third section focuses on recent developments and improvements concerning sampling and analytical methods for POPs in air. The most significant findings on the presence of POPs in remote zones are shown in the last section.

2. Persistent organic pollutants

Persistent organic pollutants (POPs) are carbon-based chemical compounds and mixtures that, to a varying degree, resist photolytic, biological and chemical degradation. POPs are characterised by low water solubility and high lipid solubility, leading to their bioaccumulation in fatty tissues. They are also semi-volatile, enabling them to be transported long distances in the atmosphere before deposition occurs.
The Agency for Toxic Substances and Disease Registry defined persistent organic pollutants as "organic substances that possess toxic properties, resist degradation, bio-accumulate and are transported, through air, water and migratory species, across international boundaries and deposited far from their place of release, where they accumulate in terrestrial and aquatic

ecosystems" (ATSDR, 1995; Syracuse Research Corporation, 2000). Where the term "substance" stands for "a single chemical species, or a number of chemical species which form a specific group by virtue of (a) having similar properties and being emitted together into the environment; or (b) forming a mixture normally marketed as a single article" (SCAR, 2009).

POPs are chemicals that can be produced both intentionally and unintentionally. POPs can be chemicals currently or once used in agriculture, disease control, manufacturing, or industrial processes. To give an example as intentionally produced POPs, they can be cited PolyChlorinated Biphenyls (PCBs) and DichloroDiphenylTrichloroethane (DDT). PCBs have been used in several industrial applications (e.g., as dielectric fluids in transformers, capacitors, coolants, and as additives to paints and lubricants). DDT is a pesticide still used in malaria vector control in some countries. On the other hand, POPs can be chemicals unintentionally produced, generally as by-products. Polycyclic Aromatic Hydrocarbons (PAHs) and dioxins are POPs which result from industrial processes and incomplete combustion of organic matter (e.g., municipal and medical waste incineration and trash burning).

POPs can cause cancer, allergies and hypersensitivity, reproductive disorders, and disruption of the immune system; they can damage the central and peripheral nervous systems. Some POPs are endocrine disrupters: by altering the hormonal system, they can damage the reproductive and immune systems and have teratogenic effects (Stockholm Convention Secretariat, 2011). Some of these compounds can persist in the environment for periods of years. POPs are noted for their semi-volatility; such a physico-chemical characteristic that permits these compounds to occur both in the vapour phase and adsorbed on atmospheric particles. These properties of unusual persistence and semi-volatility, coupled with other characteristics, pre-dispose POPs to long environmental persistence and to long-range transport through the atmosphere, have resulted in POP ubiquity all over the world. The significant half-life and lipophilicity in human and animal fats of POPs allow them to biomagnify and bioconcentrate in organic tissue up to 70,000 fold and thereby potentially achieving toxicological relevant concentrations.

In virtue of their peculiar characteristics, POPs have been causing a growing concern to scientists and policy makers. Indeed, from 1990, several international initiatives were started aimed at reducing and/or possibly eliminating POP emissions and discharge, recognizing the need for global actions (such as international protocols and conventions) to protect and safeguard human health and the environment.

"The Stockholm Convention on Persistent Organic Pollutants" can illustrate the importance and the consideration of scientific community, concerning sources, behaviour, fate and effects of POP**s**. The Stockholm Convention is a global treaty realized and signed to date by 151 Nations and administered by the United Nations Environment Programme. The treaty was realized with the aim to protect human health and the environment from chemicals that remain intact in the environment for long periods, become widely distributed geographically, accumulate in the fatty tissue of humans and wildlife, and have adverse effects to human health or to the environment (Stockholm Convention Secretariat, 2011).

The Stockholm Convention, which was adopted in 2001 and entered into force in 2004, and its subsequent ratifications and amendments, requires Parties to take measures to eliminate or reduce the release of POPs into the environment. To date twenty-one chemicals have been recognized as POPs causing adverse effects on humans and the ecosystem. These 21 are listed in Table 1 and can be placed in three categories: pesticides, industrial chemicals and by-products.

Initial POPs	Additional POPs (2009 amendment)
Aldrin	Chlordecone
Chlordane	Hexabromobiphenyl
DDT	Hexabromodiphenyl ether and
Dieldrin	Heptabromodiphenyl ether
Endrin	α-Hexachlorocyclohexane
Heptachlor	β-Hexachlorocyclohexane
Hexachlorobenzene	Lindane
Mirex	Pentachlorobenzene
Polychlorinated biphenyls	Perfluorooctane sulfonic acid, its salts and
Polychlorinated dibenzofuran	perfluorooctane sulfonyl fluoride
Polychlorinated dibenzo-p-dioxins	Tetrabromodiphenyl ether and
Toxaphene	pentabromodiphenyl ether

Table 1. Chemicals currently listed as POPs in the Stockholm Convention (Stockholm Convention Secretariat, 2011).

It must be recognized that relatively few substances possess the necessary properties to make them POPs. However, the number of substances that can have adverse effect on environment is higher.

Concerning this, in view of their knowledge contribution regarding the presence volatile chlorinated hydrocarbons (VCHCs) in the Antarctic environment, the authors believe that even substances as VCHCs should be considered as POPs and thus they should be regulated by international protocols and conventions. This even in consideration of massive industrial and commercial usage and release of VCHCs into the atmosphere, their ecotoxicity and above all in consideration of VCHC concentration levels retrieved in Antarctic waters and atmosphere, sometimes 1,000 folds higher than listed POPs (Zoccolillo et al., 2007; Zoccolillo et al., 2009).

Actually, the Stockholm Convention includes provisions for adding to the list further substances that exhibit the characteristics of POPs. At present, actions are promoted to identify further POP candidates and initiate international action on their control.

It is understood that such an international agreement has an effect limited to the substances listed and identified as POPs. In addition, the effect is limited even in consideration that, as long as materials and goods produced before the ban remain in use or are not definitively destroyed, they will represent an emission source of POPs.

Notwithstanding, in virtue of cited international conventions and protocols, many POPs are no longer produced and used in industrialized areas, a great number of developing nations have only fairly recently begun to restrict their production, use and release. Therefore, even in consideration of POP persistence, the evaluation of the occurrence of POPs in the environment is still an open question. Indeed, as a result of massive releases into the environment over the past decades, POPs are now widely distributed, including regions where POPs have never been used.

2.1 Sources

The use of many POPs has declined or ceased in North America and Europe since the 1990s. On the other hand, in Asia, Africa and South America, where adequate environmental sensitivity and abatement measures for atmospheric pollutants are missing, the population

increase and the subsequent growing energy demand, the burning of fossil fuels, the metal extraction, the intensive agriculture and the massive pesticide usage (for ensuring public health) lead to the introduction into the atmosphere of significant masses of persistent contaminants.
Thus, most of POPs are still in use or existing in many countries, but the actual quantity that specific countries may be currently using is unknown. There are not central registers of individual country use, although some organizations, like the FAO, United Nations Economic Commission for Europe, and the World Bank have begun to assemble aggregate use data (Ritteren et al., 1995).
POPs may enter the environment by several routes, e.g. by manufacture, use and disposal of specific chemical products and by-products and by the emissions from combustion and incineration processes. (It should be pointed out that while POPs as pesticides usually originate, according to specific applications, from agricultural or industrial use, POPs as PCBs are typically emitted from industrialised areas). In addition, it should be considered that materials and goods produced before the ban and containing POPs that are still in use or not definitively destroyed, represent an emission source of POPs even in countries where POPs are banned.

2.2 Environmental distribution

By definition, POPs are chemicals more persistent, mobile, and bio-available than other substances. These properties are conferred by POP molecular structure and, for halogenated POPs, they can be associated with the halogenation degree (e.g., DDT and PCBs). The physico-chemical properties of these compounds favour sufficiently high atmospheric concentrations.
According to the environmental partitioning of POPs, the physical properties of greatest importance are water solubility, vapour pressure, Henry's law constant, octanol-water partition coefficient, and the organic carbon-water partition coefficient; these properties are strongly dependent on environmental conditions such as temperature. Persistence in the environment is the other important property of a substance in terms of global transport. Persistence can be reduced by biotransformation, abiotic oxidation and hydrolysis, and photolysis. The relative importance of these processes depends on the rates at which they occur under natural environmental conditions (Rittern et al., 1995).

2.3 Global diffusion

At ambient temperatures semi-volatile POPs can evaporate from water, soil and vegetation into the atmosphere; in addition if their use/application is dispersive, POPs as DDT and VCHCs can be directly emitted into the atmosphere. Once in atmosphere these substances are unaffected by breakdown reactions and are transported over long distances by winds before re-deposition that can occur via wet precipitation (rain or snow) and dry deposition. The chemicals travel through the atmosphere and the planet in several stages, with many volatilization/deposition cycles, according to the theory of global distillation and fractionation and cold condensation (Wania & Mackay, 1993; Wania et al., 1998). In such a way the most volatile compounds can redistribute globally. The process is quite complex, involving temporary deposition and re-volatilization and is influenced by weather conditions and chemical-physical properties of the compounds, such as Henry’s constant, vapour pressure, octanol-water distribution coefficient and atmospheric half-life.

Long-range atmospheric transport can move POPs away from source regions to remote and pristine locations such as Polar Regions. In Polar Regions POPs condense and the low temperatures reduce or block evaporation, producing relatively high environmental levels. The Polar Regions thus act as "cold traps" leading to an accumulation of chemicals in environmental matrices. That the dominant pathway for the transport of POPs to the Antarctic is the atmosphere, is indicated by comparable levels of POP contamination in seawater from north and south of the Antarctic Convergence, which separates sharply defined and distinct water masses (Montone et al., 2003).
The presence of POPs in remote zones as Antarctic and Arctic regions should not be underestimated. Remote zones are areas very vulnerable to contamination; ecosystems and food chains are simple, short, and consequently particularly fragile and take a long time to recover from damage. Even little chemical alteration in these pristine areas has the capability to cause global change phenomena. Therefore, a continuous atmospheric monitoring of POPs in remote zones should be made: to hold in check the level of chemical contamination, but even in order to help to explain the diffusion and distribution processes of environmentally important chemical compounds, and at the same time in order to evaluate any eventual concentration trends (e.g., resulting from a stricter application of environmental protection protocols).

3. Remote zones

Remote zones represent the preferential observatory for understanding the evolution of our Planet and global change processes. Unfortunately, there is no disguising the fact that researches in these areas can represent a challenge in scientific terms. In addition, geographic distance and wildness of sites implies heavy capital expenditure by research units and involvement of highly trained staff able to realize surveys even in case of unexpected difficulties.
The remotest zone of the Earth is probably the Antarctic continent. Atlantic Pacific and Indian Oceans surround this continent; Antarctica is about 1000, 3800 and 2500 km from South America, Africa and Australia, respectively. Antarctica, on average, is the coldest, driest, and windiest continent, and has the highest average elevation of all the continents. Antarctica can be considered as a "frozen desert" with little precipitation; the South Pole itself receives less than 10 cm per year, on average. Temperatures reach a minimum of −80/−90 °C in the interior during winter and reach a maximum of 5/15 °C near the coast during summer. For a long time its climate, remoteness and physical geography discouraged exploration of the continent.

3.1 Remote zones contamination

In virtue of Antarctic climatic and geographic features, remote zones contamination studies are referred above all to Antarctica; insomuch as, Antarctica was designated by United Nations Environment Programme (UNEP) as a region for the global assessment of persistent toxic substances.
As about 98% of the continent is permanently covered by ice, Antarctica, the remotest continent in the Southern Hemisphere, is usually perceived as a symbol of the last great wilderness untouched by human disturbance. Unfortunately, the Antarctic environment is no longer pristine, even Antarctica is affected by global anthropogenic activities notwithstanding the peculiar characteristics of this continent. Indeed, in Antarctica there is

no industrial activity or agriculture. Antarctica has a negligible non-native population, human presence is concerned largely with scientific investigations and related logistics operations (about 1,000 in winter to about 5,000 in the summer) (SCAR, 2009). Natural "barriers" such as oceanic and atmospheric circulation protect Antarctica from lower latitude water and air masses characterize Antarctica. Notwithstanding persistent organic pollutants were found in air, snow, mosses, lichens and marine organisms, showing that these contaminants are transported from other continents in the Southern Hemisphere (Bargagli, 2008). To give an example, pesticides have been neither produced or applied in Antarctica, but since 1960s several pesticides have been reported in biotic and abiotic matrices from Antarctica and the Southern Ocean (UNEP, 2002)

3.2 POP sources in remote zones

The Antarctic region in characterised by the almost total absence of local pollution sources. Pollutants reach Antarctica almost exclusively by long-range transport processes. Source identification of POPs and input sources in the Antarctic area is a very important and complex task.

As POPs released to the environment have been shown to travel vast distances from their original source, they can reach remote zones. For instance, since in Antarctica there are no agriculture or insects, chemicals as organochlorine pesticides are not used, their presence in Antarctic ecosystem can be due almost exclusively to long-range atmospheric transport from areas where these substances are still used and produced.

The main sources of POPs in the Southern Hemisphere are urbanized areas characterized by intensive agriculture, and tropical and subtropical regions, in particular South America, where pesticides are largely used. Another source of POPs is e.g. PCBs used in older electrical devices that were deposited as landfill in some developing countries (Iwata et al., 1993). In addition, population growth and industrial development in several countries of the Southern Hemisphere are changing the global pattern of persistent anthropogenic contaminants and new classes of chemicals have already been detected in the Antarctic environment (Bargagli, 2008; Zoccolillo et al., 2009).

Locally, the greatest impact can be expected where research is carried out at long-term stations with a slight emission of some POPs. In addition, pelagic fisheries are an important operation in some parts of the region, and tourism is an increasingly important activity (SCAR, 2009). Unlike pesticides, some industrial POPs such as PCBs were used in Antarctica leading to contamination in neighbouring areas, e.g. at McMurdo Station (Ross Island) (Risebrough et al., 1990). The impact of scientific bases and related activities on the environment are more efficiently recorded by sediment analysis.

4. Air analysis of POPs

The sampling and the analysis of persistent organic pollutants in atmosphere remain a challenge, especially when the atmosphere of remote zone is considered, taking into account low POP atmospheric concentrations.

Undoubtedly, the most crucial step is the sampling step. The gathered sample has to be representative of the monitored atmosphere; the sample has to represent an aliquot of the monitored atmosphere with the same composition and characteristics. Furthermore, from sampling to analysis time no sample contamination (analyte addition), degradation (analyte transformation) or loss (analyte loss), have to occur. Thus, sampling devices have to be appropriate even according to storage and transport conditions.

When a gas-phase component of the atmosphere has to be measured, two main approaches are operable during the sampling step: air sampling and analyte sampling. Air sampling consists in collecting an aliquot of atmosphere in special containers, the whole-air samplers, as plastic bags, glass vessels and stainless-steel containers. Analyte sampling consists in (passive or active) collecting only the gaseous analyte in a suitable "trap" avoiding air gathering. The approach's choice depends on several factors as chemical and physical characteristics of the air contaminant, its expected concentration, presence of interfering substances and ambient temperature and humidity. The selection of the sampling method depends also on analytical method detection limit: prior to sampling the minimum sample volume allowed by the analytical method has to be determined. Collection of the minimum volume is necessary to collect enough contaminant to meet the method's detection limit and thus measuring the expected concentration level. Therefore when the minimum volume exceeds e.g. 10 L, whole air sampling approach is unfeasible (the volume of whole air samplers is limited, in addition such an approach would be uneconomical) and thus analyte sampling approach has to be followed. This last is the case with semi-volatile compounds characterized by very low atmospheric levels, as PCBs.
Due to the low concentrations of POPs in atmosphere, an enrichment step is always required, i.e. a direct analysis of the air sample is unworkable. This step takes place just prior to analysis when a whole-air sample is collected, or at the same time of analyte sampling when the analyte is collected and then concentrated into the "trap".
The enrichment or trapping techniques can be based on three principles that "entrap" chemicals: absorption, adsorption and condensation. The analytes can be: a) collected into a solvent or on impregnated surfaces; b) collected onto adsorbents via passive or active sampling or onto fibres; c) condensed in cryotraps. The choice of the enrichment techniques strongly depends on the sample and on the contaminants to be collected.
Once decided the sampling method in accordance to needed sample type (instantaneous or time-integrated sample), sample number and above all expected chemical concentration and detection limit, the analytical question has to be faced. Compared to other chemicals and matrices, the analysis of POPs in atmosphere is time-consuming, complex, difficult, and expensive. Extremely sensitive, specific and efficient analytical procedures are required because the analysis must be performed for very low concentrations in the pg m^{-3} and sub pg m^{-3} range. Depending on the case, the pre-treatment step will consist in enrichment and desorption of the chemicals (in case of air sampling) or in extraction of the chemicals from the "traps" (in case of analyte sampling).
In consideration of chemical nature of chosen substances, analytical separation is generally carried out by high-resolution gas chromatography (GC). The detection can be realized by flame ionization detector (FID) or sometimes by electron capture detector (ECD), for electron-absorbing components such as halogenated compounds. However usually, detection and thus a certain identification of chemicals, is performed by high resolution mass spectrometer (MS) operated in electron impact ionization mode and in selected ion monitoring (SIM) mode

4.1 POP sampling and analysis in the atmosphere of remote zones

Air quality studies in remote zones require above all specific sampling and analytical methods that consider extreme environmental conditions. Sampling and analytical methods and equipment have to be specifically planned and modified in order to overcome several hurdles. Sampling devices have to own specific features able to realize representative gatherings even at very low temperatures, made up in material resistant to transport under

adverse conditions and with relatively long-time storage capacity taking into account that several weeks might elapse between collection time and analysis. In addition, when sample collection has to be carried out at remote sites, the sampling equipment should be portable. On the other hand, analytical methods have to be at the cutting edge, as the low concentration levels of chemicals in the considered matrix; at times, a significant improvement concerning the current analytical methodology, in terms of precision and limits of detection can be required.

Whole-air samplings can be performed with a battery operated diaphragm pump and stainless steel canisters (Figure 1). As the pump is battery operated and oil-free, in situ samplings can be performed even in absence of electric current and no contamination of the air sample during the collection can occur. As the canisters are made in stainless steel with interior surface fully deactivated with SUMMA® electro polish technique, any adsorption, deposition and release phenomena are avoided. In addition, air can be collected in them under pressure, consequently a greater volume of sample is available for performing several analyses and, at the same time, any contamination from external environment is thus avoided and on-line analyses can be carried out without a lift pump. The sampling apparatus described is durable, quite light, easy to transport and allows long-term storage. The commercially available apparatus is inappropriate for the severe Antarctic temperatures. Therefore, it has to be suitably modified: a) covering the pump with insulating materials (expanded polyurethane foam and a woollen cap) and then connecting its air way-in to a stainless steel probe; b) realizing a self-warmed and insulated warming system to warm up the pump and compensate the battery charge loss during the sampling operations and to store the pump inside it during transport to the sampling site, to minimize temperature effects; c) replacing canister's original connections and valves with 316 stainless steel connections with metal-to-metal seals and 316 stainless steel diaphragm valves in order to guarantee canister's hermetic seals even at extremely low temperatures and during sudden changes of temperature. The sampling system can be easily cleaned with evacuation/helium filling operations prior to air collection. (Zoccolillo et al., 2009).

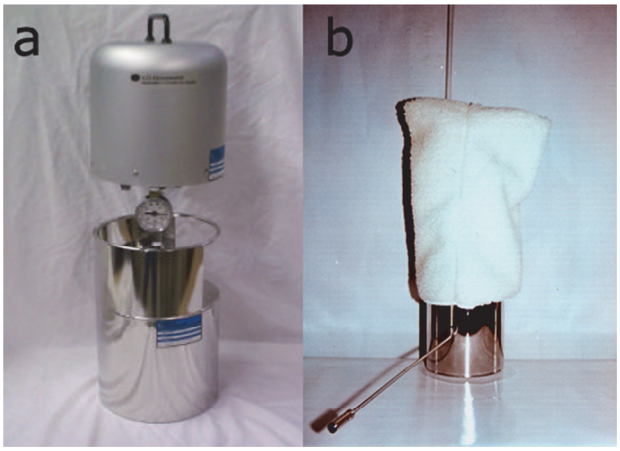

Fig. 1. Air sampling equipment: diaphragm pump and canister. Original apparatus (a) and modified apparatus in usage conditions for polar climate with woollen blanket and stainless steel probe (b) (Zoccolillo et al., 2010).

After whole-air sampling, a specific analytical methodology, characterized by high precision and accuracy and low limits of detection, has to be employed to quantify volatile organic compounds as VCHCs in air samples where the investigated substances can occur at pptv and sub-pptv levels. Volatile organic compounds can be analysed even in only slightly contaminated air samples, such as those from remote zones, with a specifically developed analytical technique based on a cryofocusing trap injector coupled to a gas chromatograph with mass spectrometric detection (CTI-GC-MS). The cryofocusing-trap-injector is the result of appropriate low cost modifications to an original purge-and-trap device to make it suitable for direct air analysis. Air samples, collected in stainless steel canisters, are introduced on-line directly into the CTI-GC-MS system; the volatiles contained in the air are cryo-concentrated into a cold trap at -120 °C and the entrapped volatiles are subsequently directly injected into the capillary column by means of rapid thermal desorption at 200 °C for the subsequent analysis of volatiles by GC-MS. Qualitative and quantitative analysis is performed by external standardization by means of certified gaseous standard mixture of the investigated VCHCs in synthetic air (Zoccolillo et al., 2010).
Active sampling of POPs from the atmosphere can be made with polyurethane foam plugs (PUF). Ambient air samples (from 1000 to 2500 m^3), collected over a period of 4-5 days using a high-volume sampling system, pass through the PUF and the compounds in the gas phase are adsorbed on the PUF. To be more precise, air is pulled through a glass-fibre filter to remove particles and subsequently passes through the PUF sorbent plugs to extract vapour phase organic compounds from the filtered air. The complete system is housed in a clear-anodized aluminium outdoor shelter (Figure 2).

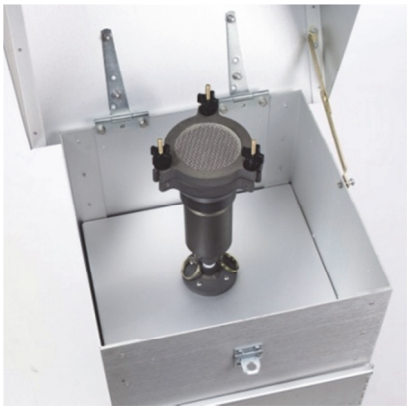

Fig. 2. Head of a PUF (polyurethane foam) sampler.

For POP determination, the PUF is Soxhelt-extracted with organic solvents for several hours. After concentration and clean-up, the extracts are analysed by gas chromatography-mass spectrometry (GC-MS) (Gambaro et al., 2005; Kallenborn et al., 1998) or by gas chromatography-electron capture detection (GC-ECD) (Montone et al., 2003). In order to minimize the interfering substances contamination and to provide acceptable blanks, prior the sampling the PUF plugs have to be cleaned by a long Soxhlet extraction, then the cleaned PUF plugs are dried in a dessicator, packed in glass flasks and sealed in plastic bags until sampling (Montone et al., 2003). PUF plugs are convenient to handle and economical, but can exhibit breakthrough of semivolatile and volatile compounds (Camel & Caude, 1995).

Passive sampling of POPs from the atmosphere can be made with semipermeable membrane devices (SPMDs). These samplers are constituted by a thin film of triolein lipid enclosed in lay-flat, low-density polyethylene membrane (Figure 3). The polymer consists of transport corridors of less than 10 Å in diameter; these pores allow for the selective diffusion of hydrophobic organic chemicals, which are then sequestered in the lipid phase. SPMDs have to be deployed in appropriate screen to protect them from direct wet-deposition and sunlight (Figure 3).

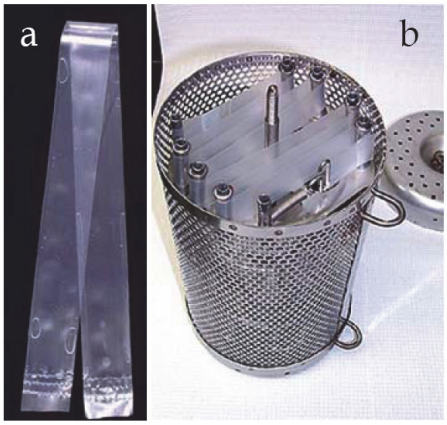

Fig. 3. a) Semipermeable membrane device (SPMD); b) SPMDs deployed inside a stainless steel container.

For POP determination, SPMDs are dialysed with the appropriate solvent and the extract, after clean up, is analysed by GC-MS (Ockenden et al., 2001a). SPMDs are deployed over weeks/months/years in the chosen site. Deployment time of the SPMD is analyte-dependent; in addition, it depends on instrument limit of detection, SPMD blank level, uptake rates and typical atmospheric concentration of the POP. The capacity of the SPMD depends on the quantity of lipid in the sampler and uptake rates by SPMDs depend on permeability of the membrane. Uptake rates are influenced by ambient temperature and wind speed; performance reference compounds can be used to "correct" for site-specific differences in uptake rates. SPMDs are easily contaminated, thus SPMD field blanks have to be taken to the field in sealed containers but not exposed, in order to evaluate the degree of contamination. Despite cited drawbacks, SPMDs are ideal samplers for studies into spatial differences in concentrations and profiles of POPs in the atmosphere, to identify sites where further investigations are required and for producing time-integrated data (Ockenden et al., 2001a).

4.2 Quality control

Quality control of the analytical procedure for POP determination in samples from remote zones is a very critical step in consideration of low atmospheric POP levels and the time lag between sampling and analysis. The risk of contamination is higher in particular for Antarctic air samples due to the much longer transport and storage time.
Suitable analytical quality control and quality assurance programs have to be run in the sampling site and in the laboratory, during sample gathering and analysis in order to guarantee data reliability.

With the purpose of assuring the overall quality and validity of experimental data, a systematic and detailed sampling strategy and blank choice have to be carried out. In order to prevent any contamination during sampling operations, clean room protocols should be attended. All the samplings should be performed downwind and away from local contamination sources, e.g. scientific stations. The operators should wear special clean room clothing and polyethylene gloves even during sampling, over their warm clothing. Immediately after the gathering, an opportune storage procedure (different according to the sampling method and sampling device) is applied in order to maintain unaltered the sample characteristics. The laboratories where the analysis will be performed, should be "Class 100 clean room", as classified by ISO Standard 14644-1. The chemicals used for sample treatment have to be ultra-clean reagents. The labware has to be extensively cleaned and conditioned with tested procedures to prevent any contamination.
Improvement of the storage containers to suppress the risk of contamination during storage should be realized prior to actual sampling. For instance, in order to evaluate the storage capability of a canister at very low temperatures and in case of sudden temperature changes, the canisters can be maintained at -20 °C (or at lower temperature if feasible) for a lapse of time comparable to Antarctic expedition duration and brought back to room temperature during the storage. Canister content, e.g. air with the lowest levels of organic contaminants, can be analysed immediately after the collection and after a variable storage time. No significant deviations of the composition during the storage should be noticed, at the investigated concentration level (Zoccolillo et al., 2009).
The risk of sample contamination has always to be investigated by taking field blanks. At least one field blank should be processed with each sampling episode. As an example, a field blank for POP sampling with PUF consists of a sample cartridge containing PUF and filter (spiked with a standard solution) shipped to the field, installed on the sampler and passively exposed at the sampling area. It is then sealed and returned to the laboratory for extraction, cleanup, and analysis, such as an actual sample.
A part from field blanks, procedural blanks have to be evaluated by analysing different types of blank samples, according to sampling and analytical procedures, e.g. laboratory method blanks and solvent blanks.
Finally, the samples processed have to give highly reproducible results by using traceable standards. Unfortunately, gas standard reference materials, with similar composition of remote zone atmosphere, are lacking.

5. Levels of POPs in remote zones air

While measurements of POPs in the Northern Hemisphere are quite well documented, Southern Hemisphere measurements, and particularly POP measurements are still sparse and relatively limited. There is a limited atmospheric database on POPs in remote areas. Data about air levels of POPs are very sparse and originate mainly from cruises close to the Antarctic continent and from a few sampling campaigns on the continent itself.
The studies concerning the atmospheric content of POPs in Antarctica mostly focused PCBs, organo-chlorine pesticides as hexachlorocyclohexanes and dioxins and emerging pollutants such as VCHCs and PAHs, that were determined in atmospheric samples collected at different Antarctic sites. The studies carried out by several research groups all over the world, focused on long-range transport processes, latitudinal distribution of POPs, concentration temporal tends, scientific expedition impact and on future emerging pollutants.

5.1 Long-range transport studies

Measurements of POPs in the atmosphere of remote zones can be useful to estimate the contribution of long-range atmospheric transport to the input of different classes of POPs in the southern hemisphere. The results obtained by several research groups are consistent with the hypothesis of global fractionation and long-range transport.

The possibility of atmospheric long-range transport episodes from South America to Signy Island was pointed out by Kallenborn in 1998 which measured POPs such as polychlorinated biphenyls and pesticides in ambient air at Signy Island (Antarctica), a sub-Antarctic sampling station, over a period of 17 weeks in the austral summer of 1994. Mean concentrations for single polychlorinated biphenyls (0.02-17 pg m^{-3}), for chlordanes (0.04-0.8 pg m^{-3}), DDT compounds (0.07-0.40 pg m^{-3}) and γ-hexachlorocyclohexane (22 pg m^{-3}), were comparable to those in Arctic air (Kallenborn et al., 1998). Previous studies realized in by Tanabe et al. (1983), Weber & Montone (1990) and Larsson et al. (1992) provided further evidence of atmospheric transport of PCBs and organo-chlorine pesticides in the Antarctic environment. Tanabe et al. (1983) measured PCBs and chlorinated hydrocarbon pesticides such as DDTs and hexachlorocyclohexanes (HCHs) in air sampled in proximity of the Japanese research stations in Antarctica and adjacent oceans during December 1980 to March 1982. The atmospheric concentrations of chlorinated hydrocarbons seemed to decrease in the transport process from northern lands to Antarctica, but the compositions of PCBs, DDT compounds and HCH isomers were relatively uniform throughout this process. Regional and seasonal variations were found in aerial concentrations of these pollutants at Syowa Station and adjacent seas in Antarctica. Larsson et al. (1992), monitored PCBs, p,p'-DDT, p,p'-DDE and γ-HCH in the lower atmosphere of Ross Island, in Antarctica for 2 yr. Geometrical means were 15.2 pg m^{-3} for PCBs, 2.0 pg m^{-3} for p,p'-DDT, 1.0 pg m^{-3} for p,p'-DDE and 25.8 pg m^{-3} for γ-HCH. Atmospheric levels of γ-HCH were positively correlated with temperature, and a significant difference was found between spring-summer and summer-winter concentrations. No season related differences were found for the other chlorinated hydrocarbons, possibly owing to their lower vapour pressure and the cold climate. Periods with increased atmospheric levels of PCBs and DDT compounds were recorded. Chlorinated pesticides in air were measured from the Greenpeace ship Gondwana between New Zealand and Ross Island, January-March, 1990. Geometric mean concentrations: α and γ-HCHs 4.0 and 3.8 pg m^{-3}, hexachlorobenzene 60 pg m^{-3}, heptachlor epoxide 0.52 pg m^{-3}, chlordanes and nonachlors 1.8 pg m^{-3}, p,p'-DDE and p,p'-DDT 0.81 pg m^{-3} (Bidleman et al., 1993). Concentrations of DDTs in Antarctic air were similar to those in the Arctic. A trend of decreasing pesticide concentration at higher latitudes was noted. Further evidence of atmospheric transport of PCBs in the Antarctic environment was provided by Fuoco et al. (1996) whose studies of Antarctic lake sediment found high contributions of atmospheric particulate matter and concluded that it is the primary vehicle of transport and diffusion of PCB in the environment. Montone et al. (2005) determined the atmosphere content of a large number of organo-chlorine compounds (HCB, HCHs, pp'-DDE, pp'-DDD, pp'-DDT and 11 PCB) in a survey performer in November of 1995 in the open ocean between 23°S and 62°S. Air mass back trajectories were used to assess the origin of the air masses that arrived at the sampling point at low altitude. Organo-chlorine levels in the atmosphere ranged from not detected (<0.6) to 25.3 pg m^{-3} for HCB (with a mean concentration of 15 pg m^{-3}), 3.9–32.5 pg m^{-3} for ΣHCHs (α-HCH + γ-HCH) (with a mean concentration of 8.8 pg m^{-3} for Lindane), 3.7– 102.6 pg m^{-3} for PDDTs (pp'-DDT + pp'-DDD + pp'- DDE) and 46.2 up to 985.0 pg m^{-3} for PCBs (Montone et al., 2005). Choi et al. (2008)

deployed passive air samplers for one year at the Korean polar research stations at Ny-Alesund, Norway (2005-2006) and King George Island, Antarctica (2004- 2005) to assess levels and patterns of polychlorinated biphenyls (PCBs) and organo-chlorine pesticides in polar regions. The observed backward trajectories suggested that long-range transport from source regions in Northern Europe and Russia and the southern tip of South America, respectively affect the Arctic and Antarctic areas. The results were consistent with the hypothesis of global fractionation and long-range transport. The authors also observed relatively high levels of PCB-11, averaging 60 pg m^{-3}, suggesting an unusual source of PCB-11 to the Southern Hemisphere. The average level of Σ_{205}PCB (excluding three mono-CBs and PCB-11) was five times higher in the Arctic (95 pg m^{-3} range) than in the Antarctic (19 pg m^{-3}). The difference of concentration in terms of Σ_{205}PCBs reflects the hemispheric distribution of global PCB emissions. Levels of Σ_9PCB at Ny-Ålesund were similar to those reported for other Arctic sites, while levels at King George Island were lower than at other sites on the Antarctic Peninsula but 1 order of magnitude higher than background levels measured at a more remote Antarctic site. Light homologues were predominant in all samples, consistent with the hypothesis of global fractionation and predictions of long-range transport potential (Choi et al., 2008).

5.2 Latitudinal distribution studies

To establish POP background air concentrations in oceanic regions and to assess their latitudinal distribution, POP data concentration can be collected during cruises such as the Atlantic cruise from the United Kingdom to Halley, Antarctica (Lohmann et al., 2004).

With the purpose of give evidence of POP transport from the northern hemisphere to the southern and to reconstruct their trends in concentrations, Lakaschus and co-workers collected POP data during two cruises across the Atlantic Ocean between the Arctic Ocean (Ny-Alesund/Svalbard, 79°N; 12°E) and the Antarctic Continent (Neumayer Station/Ekstroem Ice Shelf, 70d°S; 8.2°W) in 1999/2000 (Lakaschus et al., 2002). Hexachlorocyclohexanes (HCHs) were determined simultaneously in air and seawater. The concentrations of α-HCH and γ-HCH in air and surface waters of the Arctic exceeded those in Antarctica by 1-2 orders of magnitude. Between Cape Town and Neumayer Station the average gaseous concentrations of α-HCH and γ-HCH were 1.1 pg m^{-3} and 1.4 pg m^{-3} and decreased further to 0.36 ± 0.03 pg m^{-3} and 0.15 ± 0.04 pg m^{-3} on the Ekstroem Ice Shelf at Neumayer Station. By comparison of results obtained from archived samples taken (by the same research group) in 1987/1997 and those from 1999, a systematic decrease of α-HCH was observed at all sampling locations (Lakaschus et al., 2002). Booij and co-workers collected POP data during a cruise from the island of Texel (The Netherlands) to Walvis Bay (Namibia) and Cape Town (South Africa). Aerosol and surface water samples were collected and different classes of organic pollutants were determined (Booij et al., 2007). The content of PCBs, hexachlorobenzene (HCB), 1,1-dichloro-2,2-bis(4-chlorophenyl)ethene (4,4'-DDE), and polyaromatic hydrocarbons (PAHs) were determined. The air concentrations of HCB ranged from 56 to 145 pg m^{-3}, a value typical for background levels for air (4–140 pg m^{-3}) (Barber et al., 2005). Atmospheric 4,4'-DDE concentrations ranged from 0.1 to 0.9 pg m^{-3} and were smaller than the values of observed by Iwata et al. (1993) in the same area during one cruise carried out in April 1990 (1.3–6.3 pg m^{-3}). During the same cruise, the atmospheric content of polycyclic aromatic hydrocarbons (PAHs) and of one emerging class of pollutants (polychlorinated naphthalenes, PCNs) were determined. The highest PAH concentrations occurred in the European samples, and in samples close to West Africa and South Africa.

Consistently low PAH concentrations were measured in the southern hemisphere open ocean samples (190-680 pg m^{-3}). Concentrations showed a diurnal cycle, the day/night ratios of phenanthrene, 1-methylphenanthrene and fluoranthene were typically ~1.5-2.5:1. The highest PCN concentrations occurred in the European samples, but high values were also detected off the West African coast, and in the sample taken closest to South Africa (Jaward et al., 2004).

5.3 Temporal trend studies

Studies regarding atmospheric temporal trends of POPs as organo-chlorine pesticides can be carried out by measuring the atmospheric content of HCB, heptachlor, α- and γ-HCH, heptachlor epoxide.

Dickhut et al. (2005) determined hexachlorobenzene (HCB), heptachlor, α- and γ- HCH and heptachlor epoxide in air, seawater, sea ice, and snow. Samples were collected during the austral winter (September-October 2001) and summer (January-February 2002) along a transect in the Western Antarctic Peninsula. By comparison with previous studies they concluded HCB and HCH levels decreased over the last twenty years, ΣHCH showed a half-life of 3 years in Antarctic air. On the other hand, heptachlor epoxide levels did not show such a reduction, possibly due to its continued use in the southern hemisphere. They detected peak heptachlor atmospheric concentrations in coincidence with air masses moving into the region from lower latitudes. Levels of γ-HCH were 1.2-200 times higher in annual sea ice and snow compared to α-HCH, likely due to greater atmospheric input of γ-HCH. Based on the ratio of α/γ-HCH <1 in Antarctic air, sea ice and snow they concluded that there is a predominance of influx of γ-HCH versus technical HCH to the regional environment. In addition, they also observed that the α/γ-HCH in seawater was >1, likely due to more rapid microbial degradation of γ- versus α-HCH. Also this study concluded that the water/air fugacity ratios for HCHs demonstrate continued atmospheric influx of HCHs to coastal Antarctic seas, particularly during late summer (Dickhut et al., 2005). The spatial distribution of α-HCH and the net direction of air/water gas exchange were determined between November 1997 and February 1998 by Jantunen et al. (2004). Air and water samples were collected during a cruise between South Atlantic Ocean (South Africa) and Antarctica SANAE Base (70°S, 3°E). The α-HCH concentrations in air and surface water resulted much lower than in Arctic regions, consistent with the historically lower usage of technical HCH in the Southern Hemisphere. The water/air fugacity ratios of α-HCH were lower than or equal to 1.0, indicating steady state or net deposition conditions. The results of one analysis of the enantiomeric fractionation showed that the α-HCH in water was enantioselectively metabolized and that the two isomers [(-)α-HCH and (+)α-HCH] in the air boundary layer reflected those in surface water, showing the bidirectional nature of gas exchange (Jantunen et al., 2004).

5.4 Scientific expedition and station impact studies

Unlike pesticides, only some industrial POPs such as PCBs were used in Antarctica (Risebrough et al., 1990). Therefore, scientific expedition and bases can be a source of POPs.

In order to study the impact of scientific expeditions and bases, areas neighbouring stations and zones where occurred scientific operations, can be monitored. A concentration gradient was observed with distance from the main buildings of scientific bases in the Antarctic, which strongly indicated the influence of local sources (Choi et al., 2008).

5.5 Recent studies

Recent studies carried out in Antarctica, increased the limited atmospheric database on POPs in remote areas by reporting POP concentrations during the austral summer and hypothesizing their possible sources.

Montone et al. (2003) reported atmospheric levels of PCBs near the Brazilian Antarctic Research Station, at King George Island, during a sampling survey undertaken in the austral summer of 1995-1996. Single PCB congeners ranged from below detection limit to 33.2 pg m^{-3}. The lower chlorinated congeners (PCB-101 and below) predominated in the air samples and represented 66.7% of the total PCB concentrations. Atmospheric levels of PCBs were correlated with meteorological conditions (as well as to the general synoptic atmospheric circulation of the region) and the higher levels were associated with the passage of the frontal system coming from South America over the Drake Passage causing a local increase in air temperature and surface winds from northwest, north and northeast (Montone et al., 2003). Gambaro et al. (2005) monitored the air near Italian Antarctic Research Station. Gas-phase concentration of individual PCB congeners in the air of Terra Nova Bay ranged from below detection limit 0.25 pg m^{-3}. The gas-phase ΣPCB concentrations ranged from 0.61 to 1.78 pg m^{-3} with a mean concentration of 1.06 pg m^{-3}. Over 90% of the total PCB content was due to congener with one to four chlorine atoms and only about 10% with five to seven chlorines, whereas higher chlorinated PCBs were below detection limits. In agreement with other studies, the results emphasized that the PCB profile was dominated by tri-CB and tetra-CB with relatively high contributions from mono-CB and di-CB (Gambaro et al., 2005). In addition, investigations on POP distribution in Antarctica were made by Ockenden at al. (2001b) which monitored the air for PCBs at two sites in the southern hemisphere, one over land and the other over water. They found that the highest concentrations were observed when temperatures were greater and the air concentrations were higher over water than over land. POP concentrations were found to be higher in air samples from the Antarctic Peninsula and sub-Antarctic islands than in those from continental sites (Bargagli, 2005).

5.6 Future emerging pollutants

According to substances not yet listed in the Stockholm Convention (see § 2), concern is growing on manmade chemicals that for their physical-chemical properties can reach remote zones, potentially explicating their ecotoxic effect on fragile ecosystems.

Zoccolillo et al. (2009) measured some volatile chlorinated hydrocarbons in the proximity of the Italian Antarctic Research Station (Mario Zucchelli Station), at Edmonson Point, Thethys Bay and Talos Dome. The VCHCs investigated were present in all samples in concentrations varying from tens to hundreds of ng m^{-3}. Surprisingly, it emerged that the Italian air gathered in rural areas had a comparable level of chemicals, whereas POPs as PCBs show a substantial difference in concentration between temperate and remote zones; in addition, VCHC concentration levels were 1,000 fold higher that other POPs. These results can be considered evidence that other organic compounds may represent future emerging pollutants in Polar Regions and suggest that future monitoring and regulating actions should be undertaken. Other contaminants like polybrominated dyphenil ethers (PBDEs), perfluorooctanesulfonic acid (PFOS) and endosulfan, not yet included in the POPs list but being considered for inclusion in the Stockholm Convention, have already been taken into consideration in a few studies carried out in Antarctica. On the other hand, some organo-

chlorine compounds (mirex, dieldrin, and chlordane) included in the Stockholm Convention have been recently investigated, but data are still very limited.
Although the presence of useful research studies and data in recent literature, a coordinated action is still lacking. An international coordinated project should be promoted on key targets in order to cover actual gaps such as temporal trends of contaminants, processes controlling distribution and transport of POPs in polar environments, including mass transfer at the environmental interfaces (air-water, air-snow, air-biota), and monitoring of future emerging pollutants in polar regions (SCAR, 2009).

6. Conclusion

The Stockholm Convention in 2001 banned manufacture and new use of 21 POPs. Unfortunately, such action has a limited effect, because the number of substances that can have adverse effect on environment is higher, insomuch as many new chemicals are under consideration for listing under the Stockholm Convention. In addition, as long as materials and goods produced before the Stockholm Convention ban remain in use or are not definitively destroyed, they will represent an emission source of POPs.
In this scenario, the scientific community has to keep on studying the environmental sources, behaviour and impact of POPs, especially in remote zones due to vulnerability of Polar Regions to organic contaminants that originate from lower latitudes. At present, not many research groups reported on POP atmospheric levels in remote zones, probably due to the difficulty connected with such a determination in terms of sampling and analytical techniques. Despite reported POP atmospheric concentrations seem to be below those documented to have biological effects, it is impossible to directly transfer toxicological data and models developed in temperate climate on polar biological systems. Polar living beings are endemic species with a long evolutionary story in bio-geographical isolation, more vulnerable to the adverse effects of persistent contaminants. The length of the food chains enhances the biomagnifications of POPs, potentially threatening the health of wildlife. Therefore, it is to be hoped a continuous monitoring of POPs, and other manmade chemicals that behave similar to POPs, in the atmosphere remote zones with the suitable sampling and analytical techniques, in order to better understand their transport pathways and environmental fate, and to monitor their presence and their concentration trends in fragile ecosystems.

7. Acknowledgement

This work was financed by the Italian National Program for Antarctic Research (PNRA).

8. References

ATSDR Toxicological profiles: Polycyclic Aromatic Hydrocarbon (PAHs) (1995) US Department of Health and Human Services, Public Health Services, Agency for Toxic Substances and Disease Registry. CRC Press

Barber, J.L., Sweetman, A.J., van Wijk, D. & Jones K.C. (2005) Hexachlorobenzene in the global environment: Emissions, levels, distribution, trends and processes. *Sci Total Environ*. Vol. 349, pp. 1-44

Bargagli, R. (2008). Environmental contamination in Antarctic ecosystems. *Sci. total environ.*, Vol.400, pp. 212-216

Bargagli, R. (2005). Antarctic ecosystems: environmental contamination, climate change and human impact. Berlin; Springer-Verlag; 2005. 394 pp.

Bidleman, T.F., Walla, M.D., Roura, R., Carr, E. & Schmidt, S. (1993). Organochlorine pesticides in the atmosphere of the Southern Ocean and Antarctica, January-March 1990. *Mar. Pollut. Bull.* Vol. 26, pp. 258-262

Booij, K., van Bommel, R., Jones, K.C. & Barber, J.L. (2007). Air-water distribution of hexachlorobenzene and 4,4'-DDE along a North-South Atlantic transect. *Marine Pollution Bulletin*. Vol. 54, pp. 814-819

Camel, V. & Caude, M. (1995). Trace enrichment methods for the determination of organic pollutants in ambient air. *J. Chromatogr. A,* Vol. 710, pp. 3-19

Choi, S.D., Baek, S.Y., Chang, Y.S., Wania, F., Ikonomou, M.G., Yoon, Y.J,. Park ,B.K. & Hong, S. (2008). Passive air sampling of polychlorinated biphenyls and organochlorine pesticides at the Korean Arctic and Antarctic research stations: Implications for long-range transport and local pollution. *Environ Sci Technol*. Vol. 42, pp. 7125-7131

Dickhut, R.M., Cincinelli, A., Cochran, M. & Ducklow, H.W. (2005). Atmospheric concentrations and air-water flux of organochlorine pesticides along the western Antarctic Peninsula. *Environ Sci Technol*. Vol. 39, pp. 465-470

Fuoco, R., Colombini, M.P., Ceccarini & A., Abete, C. (1996). Polychlorobiphenyls in Antarctica. *Microchemical Journal* Vol. 54, pp. 384-390

Gambaro, A., Manodori, L., Zangrando, R., Cincinelli, A., Capodaglio, G. & Cescon, P. (2005). Atmospheric PCB concentrations at Terra Nova Bay, Antarctica. *Environ. Sci. Technol.* Vol. 39, pp. 9406-9411.

Iwata, H., Tanabe, S., Sakai, N. & Tatsukawa, R. (1993). Distribution of Persistent Organochlorines in the Oceanic Air and Surface Seawater and the Role of Ocean on Their Global Transport and Fate. *Environ Sci Technol*. Vol. 27, pp. 1080-1098

Jantunen, L.M., Kylin, H. & Bidleman, T.F. (2004). Air-water gas exchange of [alpha]-hexachlorocyclohexane enantiomers in the South Atlantic Ocean and Antarctica. *Deep Sea Research II*. Vol. 51, pp. 2661-2672

Jaward, F.M., Barber, J.L., Booij, K. & Jones, K.C. (2004). Spatial distribution of atmospheric PAHs and PCNs along a north-south Atlantic transect. *Environmental Poll*. Vol. 132, pp. 173-181

Kallenborn, R., Oehme, M., Wynn-Williams, D.D., Schalabach, M. & Harris, J. (1998). Ambient air levels and atmospheric long-range transport of persistent organochlorines to Signy Island, Antarctica, *Sci. total environ.*, Vol. 220, pp. 167-180

Lakaschus, S., Weber, K., Wania, F., Bruhn, R. & Schrems, O., (2002). The air-sea equilibrium and time trend of hexachlorocyclohexanes in the Atlantic Ocean between the Arctic and Antarctica. *Environ Sci Technol*. Vol. 36, pp. 138-145

Larsson, P., Järnmark, C. & Södergren, A. (1992). PCBs and chlorinated pesticides in the atmosphere and aquatic organisms of Ross Island, Antarctica. *Marine Pollution Bulletin*. Vol. 25, pp. 281-287

Lohmann, R., Jaward, F.M., Durham, L., Barber, J.L., Ockenden, W., Jones, K.C., Bruhn, R., Lakaschus, S., Dachs, J. & Booij, K. (2004). Potential contamination of shipboard air samples by diffusive emissions of PCBs and other organic pollutants: implications and solutions. *Environ Sci Technol*. Vol. 38, pp. 3965-3970

Montone, R.C., Taniguchi, S., Boian, C. & Weber, R.R. (2005). PCBs and chlorinated pesticides (DDTs, HCHs and HCB) in the atmosphere of the southwest Atlantic and Antarctic oceans. *Marine Pollution Bulletin*. Vol. 50, pp. 778-782

Montone, R.C., Taniguchi, S. & Weber, R.R. (2003). PCBs in the atmosphere of King George Island, Antarctica. *Sci. total environ.*, Vol.308, pp. 167-173

Ockenden, W.A., Lohmann, R., Shears, J.R. & Jones, K.C. (2001a). The significance of PCBs in the atmosphere of the Southern Hemisphere. *Environ Sci Pollut Res.* Vol. 8, pp 189-194

Ockenden, W.A., Corrigan, B.P., Howsam, M. & Jones, K.C. (2001b). Further developments in the use of semipermeable membrane devices as passive air samplers: application to PCBs. *Environ. Sci. Technol.* Vol. 35, pp. 4536-4553

Risebrough, R.W., De Lappe, B.W. & Ypunghans-Haug, C. (1990). PCB and PCT contamination in Winter Quarters Bay, Antarctica. *Mar. Pollut. Bull.*, Vol. 21, pp. 523-529

Ritteren, L, Solomon, K.R. & Forget, J. (1995). *Persistent organic pollutants*, Retrieved from <http://www.chem.unep.ch/pops/ritter/en/ritteren.pdf>

SCAR (2009) *Persistent Organic Pollutants (POPs) in the Antarctic environment,* Retrieved from: <http://www.scar.org/publications/occasionals/POPs_in_Antarctica.pdf>

Stockholm Convention Secretariat. (n.d.). The POPs, In: Stockholm Convention on Persistent Organic Pollutants (POPs), Access in 03/08/2011, Available from: <http://chm.pops.int/Convention/The%20POPs/tabid/673/language/en-US/Default.aspx>

Syracuse Research Corporation. Toxicological profile for polychlorinated biphenils (PCBs) (2000) Under Contract No. 205-1999-00024 Prepared for: U.S. Department of Health and Human Services, Public Health Service Agency for Toxic Substances and Disease Registry, November.

Tanabe, S., Hidaka, H. & Tatsukawa, R. (1983). PCB and chlorinated hydrocarbon pesticides in the Antarctic atmosphere and hydrosphere. *Chemosphere.* Vol. 12, pp 277-288

UNEP. (2002). Regionally based assessment of persistent toxic substances – Antarctica regional report. Geneva: United Nations Environmental Programme; 2002. Chemicals.

Wania, F., Haugen, J.E., Lei, Y.D. & MacKay, D. (1998). Temperature dependence of atmospheric concentrations of semivolatile organic compounds. *Environ Sci Technol*. Vol. 32, pp. 1013-1021

Wania, F. & Mackay, D. (1993). Global fractionation and cold condensation of volatile organochlorine compounds in polar regions. *Ambio*, Vol. 22, pp. 10-18

Weber, R.R. & Montone, R.C. (1990). *Distribution of organochlorines in the atmosphere of the South Atlantic and Antarctic Oceans*, D.A. Kurtz, Lewis Publishers Inc., Chelsea

Zoccolillo, L., Amendola, L. & Insogna, S. (2010). On-line analysis of volatile chlorinated hydrocarbons in air by gas-mass. Improvements in preconcentration and injection steps. *J. Chromatogr. A*. Vol. 1217, pp. 3890-3895

Zoccolillo, L., Amendola, L. & Insogna S. (2009). Comparison of atmosphere/aquatic environment concentration ratio of volatile chlorinated hydrocarbons between temperate regions and Antarctica. *Chemosphere.* Vol. 76, pp. 1525-1532

Zoccolillo, L., Amendola, L., Cafaro, C. & Insogna S. (2007). Volatile chlorinated hydrocarbons in Antarctic superficial snow sampled during Italian ITASE expeditions. *Chemosphere*. Vol. 67, pp. 1897-1903

12

Asian Dust Storm as a Natural Source of Air Pollution in East Asia; its Nature, Aging, and Extinction

Chang-Jin Ma
Fukuoka Women's University
Japan

1. Introduction

Asian dust–storm (hereafter called "ADS") often occurred at desert and loess areas in northwest of China traverse China continent and can be extended to Pacific Ocean passing through Korea and Japan in every spring time. This dust is blown up by strong wind behind the cyclone and delivered in free troposphere by westerly jet. Even though ADS is a peculiar phenomenon occurred in China continent, this ADS have led to the significant environmental change in East Asia and North Pacific ocean for a long time. A new theory states that dust storms might deflect sunlight, thus slowing down climate change. However, there is growing proof that dust storms are a health hazard. Dust clouds harbour viruses, fungi and bacteria as well as heavy metals and other pollutants.
Although ADS can cause many disasters, it is said that ADS make a contribution to the neutralization of acid rain caused by consumption of a large amount of fossil fuels. This ADS finally dissipates when the particles are removed from the atmosphere by dry and wet removal processes. Gravitational settling of large particles (>10 μm) occurs near the source within the first day of transport. Wet removal occurs sporadically throughout the 5-10 day lifetime of the remaining smaller size dust particles.
Here, the special information on ADS particles which is a peculiar natural source of air pollution in East Asia and the Pacific Ocean is reported.

2. Physicochemical properties of ADS sources

Numerous studies on the ADS particles have been performed and reported (Braaten et al., 1986; Darzi et al., 1982; Duce et al., 1980; Iwasaka et al., 1988; Lafon et al., 2004; Ma et al., 2004c; Song et al., 2006; Song & Carmichael, 1999; Zhang et al., 2003). It is presumed that the chemistry of ADS particles can be influenced by absorption of atmospheric gases and subsequent oxidation of the absorbed gases on the surface during long-range transport. It is however desirable to explain how man-made pollutants and sea-salt aerosol react with natural ADS particles. In order to understand these denaturations of ADS particles, information of the nature of original sands at the local source areas is prerequisite.

However, unfortunately, relatively little is known about the individual dust sands in various source regions (Nishikawa et al., 2000).
The primary goal of this section is to report the comparative characteristics of the original sands collected at four different desert regions in China.

2.1 Experimental methods

2.1.1 Description of sampling sites and sampling method of desert sands

The sedimentation of the whole gigantic particles (e.g., larger than 10 μm) happens near the source region of dust storm (Husar et al., 2001). It is a generally acknowledged fact that Taklimakan desert, which is a long way off from receptor areas, does not exert much impacts on receptor areas. In light of this, four desert areas (Yinchuan, Wuwei, Dulan, and Yanchi) located nearby Gobi desert were chosen in the present study (see Fig. 1).

Fig. 1. Map showing the desert areas of sand collection

Yinchuan lies in the middle of the Yinchuan or Ningxia Plain. It is sheltered from the deserts of Mongolia by the high ranges of the Helan Mountain on its west. Yinchuan has a temperate continental climate with an annual average temperature of 8.5 °C, with 158 frost-free days. Its annual rainfall averages 200 mm. Wuwei is situated in the central part of

Gansu province, on the east end of Hexi Corridor. Wuwei has a temperate semiarid climate with an annual average temperature of 8.7 °C, with frost free period of 165 days and annual precipitation of 158 mm. Dulan County belongs to West Lake Mongolia & Tibetan Autonomous prefecture, Qinghai Province. The mean annual temperature is 3 °C with a January average of -10 °C and a July average of 15 °C, and the mean annual precipitation is 188 mm, 78% of which falls from May through September. Yanchi lies in the semi-deserts of the arid north west. There is less rain but more wind all the year round, and weather is extremely dry. The mean annual temperature is 9.2 °C (-7 °C (January) to 20.4 °C (July)) with mean annual precipitation of 225 mm (Li et al., 2007).
To obtain a representative sand sample, three different points (within a 500 m radius) were selected separately and randomly for each desert. A spade which is one of common tools used to sample soil was applied to collection of surface sands.

2.1.2 Chemical identification

The same amounts (2 g of dried sands) of desert sands collected among three different points were evenly mixed. The mixed desert sands were dissolved in 20 ml of pure deionized water and mixed in an ultra-sonicator for 20 min. After ultrasonic extraction, the sample was allowed to be filtered through the **Nuclepore®** filter with a 0.2 μm pore size.
To determine the elemental concentration, both soluble and insoluble fractions of sands were submitted for Particle Induced X-ray Emission (PIXE) installed in Quantum Science and Engineering Center, Kyoto University. Since the self-absorption of emitted characteristic X-ray can occur when specimens are thick, the insoluble solid sands were pulverized and homogenously deposited onto a polycarbonate substrate film. Then they were irradiated by the proton beam of PIXE system. Due to analytical difficulties with the liquid samples by PIXE, a 20 μl water soluble fraction was mounted on a polycarbonate substrate film and dried under infrared lamp. PIXE analysis was performed with a proton beam of 6 mm diameter and 2.0 MeV energy from a Tandem Cockcroft. Beam intensities of 10 to 60 nA were employed with the total dose of about 20 μC. X-ray with the energy of 14.8 keV emitted from the target was detected by a Si (Li) detector which had a resolution of 152 eV at 5.9 keV. The more detailed analytical procedures and experimental set-up used for PIXE analysis have been described elsewhere (Ma et al., 2001).
To analyze the chemical structure and mixing state of surface and inner individual sands, X-ray fluorescence (XRF) microprobe system equipped at Super Photon ring 8 GeV (SPring-8) BL37XU was applied. Hayakawa (2000) established this BL-37XU at SPring-8 that allows chemical analysis for a wide variety of specimens. This method has been successfully used to carry out the reconstruction of elemental map with the quantification of multiple elements at femto gram level sensitivity (Hayakawa et al., 2001). More details about the analytical procedures and experimental set-up for XRF microprobe analysis can be found in Hayakawa et al. (2001).

2.2 Results and discussion

2.2.1 Morphology, color, and size distribution

The morphology of original desert sands collected from four different desert areas was displayed in Fig. 2. Nearly all of sands have irregular shape with yellowish coloration, whereas some sands show peculiar colors such as bluish, blackish, and reddish. Minerals are colored because certain wavelengths of light are absorbed. It is suggested that this color dissimilarity is influenced largely by chemical composition and atomic structure of the mineral.

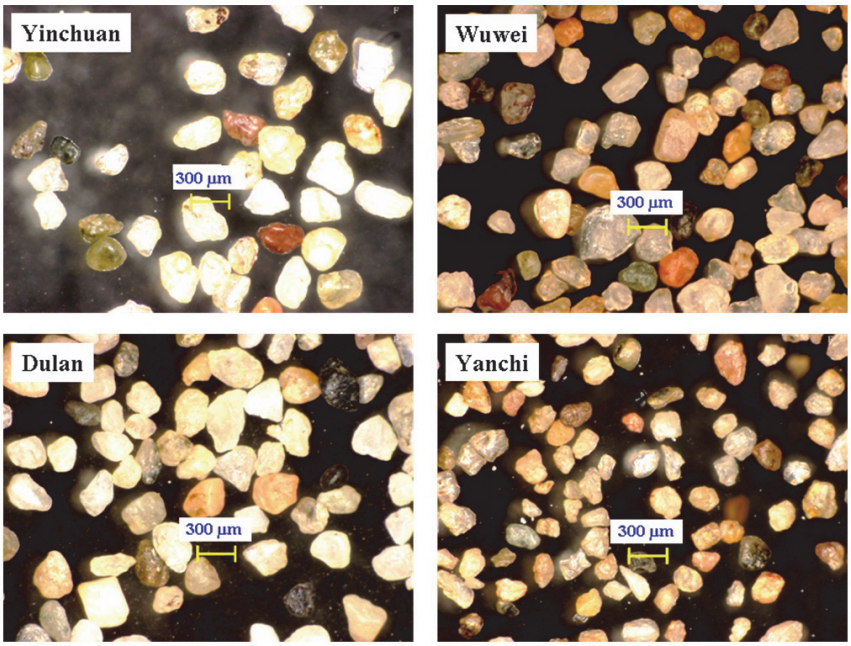

Fig. 2. Microscopic image of sands collected at four desert areas in China (x100)

The shape of size distribution for sands collected at Yinchuan, Wuwei, and Dulan sites is monomodal to show the maximum level between 200 and 300 μm. On the other hand, the maximum level for Yanchi desert sands is displayed between 100 μm and 200 μm. The size of sands at Wuwei desert area is relatively wide spread in the range up to 600 μm.

2.2.2 Chemical properties of bulk and individual sands

In order to conduct quantitative elemental analysis, the masses of deposited sand powders onto polycarbonate substrate film have to be precisely measured. However, due to the small amount of pulverized sands homogenously mounted onto polycarbonate substrate film, it is not possible to conduct mass measurement. Hence, the concentration ratios of Z/Si are listed for soluble and insoluble fractions of the four kinds of desert sand in Table 1. Here, the concentration ratios of Z/Si were calculated by the initial result (μg cm^{-2}) of PIXE analysis. As might be expected, there is a tendency towards higher Z/Si ratios for soil derived elements such as : Si>Fe>K>Ca at Yinchuan, Si>K>Fe>Ca at Wuwei, Si>Ca>Fe>K at Dulan, and Si>Ca>K>Fe at Yanchi. Unfortunately, Al concentration cannot be reliably determined by our PIXE system. Although it has negligible ratio, S was detected in insoluble fraction of Wuwei sample with 0.0003 S/Si ratio and soluble fraction of Dulan sample with 0.0282 S/Si ratio. In addition, Cl was contained in every desert sand with the exception of the insoluble portion of Yanchi area. As reported by Mason (1966), some crustal rocks (such as shale and limestone) contain S and Cl. Therefore one should give attention to data interpretation about the aging processes of dust particles with sea-salts and man-made S. The relative elemental ratios summarized in Table 1 can be a means to assess the transformation of dust particles during long-range transport and other aging processes.

	Insoluble fraction				Soluble fraction			
	Yinchuan	Wuwei	Dulan	Yanchi	Yinchuan	Wuwei	Dulan	Yanchi
Si	1.0000	1.0000	1.0000	1.0000	1.0000	1.0000	1.0000	1.0000
S	N.D.[a]	0.0003	N.D.	N.D.	N.D.	N.D.	0.0282	N.D.
Cl	0.0008	0.0017	0.0036	0.0027	0.0386	0.0281	0.0404	N.D.
K	0.0530	0.0878	0.0761	0.1009	0.2231	0.1569	0.1818	0.1693
Ca	0.0473	0.0239	0.7011	0.2116	0.5063	0.3132	0.9620	0.3488
Ti	0.0035	N.D.	N.D.	N.D.	N.D.	N.D.	N.D.	N.D.
V	0.0042	0.0032	0.0076	0.0044	0.0000	0.0060	0.0107	0.0105
Cr	0.0015	0.0010	0.0056	0.0024	0.0077	0.0037	0.0098	0.0064
Mn	0.0046	0.0019	0.0072	0.0050	0.0100	0.0085	0.0176	0.0174
Fe	0.1666	0.0506	0.2077	0.0988	0.3682	0.3208	0.4007	0.4345
Cu	0.0018	0.0008	0.0022	0.0008	N.D.	N.D.	0.0063	0.0066
Zn	0.0011	0.0004	0.0017	0.0008	N.D.	N.D.	0.0036	0.0021
Sr	0.0014	0.0012	0.0027	0.0012	N.D.	N.D.	0.0081	0.0030
Pb	0.0003	0.0002	0.0008	0.0004	0.0059	0.0023	0.0025	0.0008

[a] Non-Detected.

Table 1. The concentration ratios of Z/Si for four kinds of desert sands as a function of water solubility

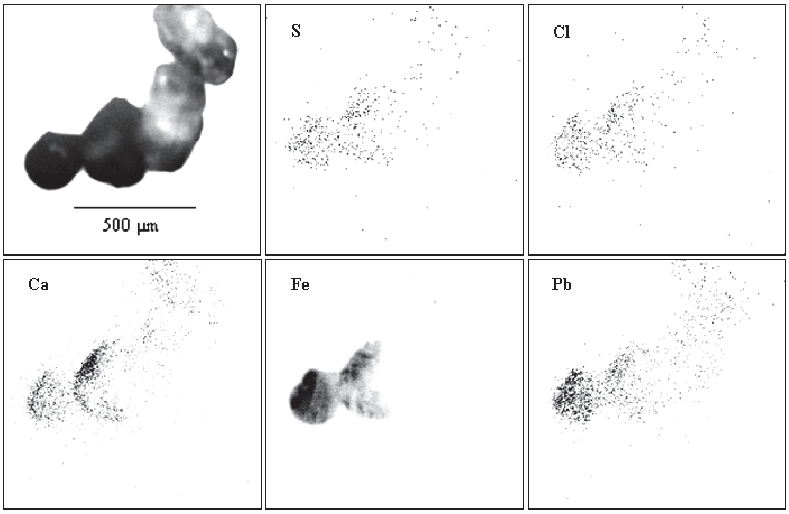

Fig. 3. The reconstructed XRF elemental maps corresponding to individual sands collected in at Yinchuan desert area

An example of XRF elemental maps and microscopically imaged desert sands (top left) collected at Yinchuan desert area in China are presented in Fig. 3. It was possible to draw the distribution of components in and/or on desert sands. From XRF elemental maps, it can be visually confirmed that S, Cl, and Pb were present overall sand surface as the minor components. In contrast, Fe distribution is partially concentrated on sand surface. However, the elemental distribution on sand surface can be influenced by the degrees of an angle between Si (Li) detector recording the fluorescence X-rays and sample holder.

3. Chemical transformation of individual ADS particles

During long-range transport of air masses containing ADS particles over oceans, ADS particles can capture gases or coagulate solid particles and react with each other, leading to a change in chemical compositions (Duce et al., 1980; Hwang et al., 2008; Iwasaka et al., 1988; Ma et al., 2004c; Nishikawa and Kanamori, 1991). Zhang et al. (2003) made an investigation for the elemental composition and size of individual ADS particles and their mixture state with sea salt, sulfate, and nitrate. They reported that about 60-85% of dust particles collected at southwestern Japan was internally mixed with sea salt. Chemical transformation of ADS particles can alter the marine ecosystem and radiative properties of dust clouds (Zhang and Iwasaka, 1998). Hwang et al. (2008) reported that ADS particles were mixed with sea-salts entrained over the Yellow Sea, as well as air pollutants from the eastern China coastal areas.

Microbeam Particle Induced X-ray Emission (PIXE), often called micro-PIXE, is a variation of PIXE that has become very important in recent years. It is a combination of the microbeam technique with PIXE analysis (Johansson and Campbell, 1988). By using micro-PIXE analytical system, Ma et al. (2000) carried out the single particle analysis for the coarse particles collected in an ADS event. In doing so, they pointed out that the significant Cl was detected in individual dust particles. However, they did not fully discuss the internal mixing state in view of reaction between dust particles and sea-salts. Because other Cl sources such as gaseous Cl and non sea-salt particulate Cl can also influence on the aging processes of ADS particles (Ma et al., 2008). Hence, in order to clearly discuss the mixing processes of ADS particles with sea-salts from micro-PIXE data, one should simultaneously analyze Na in individual ADS particles that were captured at receptor area. However unfortunately, as mentioned above, until now light elements including Na have not been determined by micro-PIXE. Broadening the range (including $Z<14$) of analyzed elements by micro-PIXE is urgently needed to assess the aging processes of ADS particles.

In the present work, an attempt was made to broaden the range of analyzed elements by employing the double detector system at micro-PIXE. This section shows the preliminary results of the double detector system and its application to the interpretation of the mixing state of individual ADS particles with sea-salt.

3.1 Experimental methods

3.1.1 Sampling of ambient ADS particles

An intensive measurement of ambient ADS particles was performed at a ground-based site in Fukuoka, Japan (33.40°N; 130.26°E) on April 20, 2005. Because of its closeness to the Asian mainland, this area can be directly exposed to the outflow of air masses from the Asian continent during springtime.

For the sampling of ambient ADS particles, a low pressure Andersen impactor (LPAI) samplers (Tokyo Dylec Co., LP-20) was operated on April 20 (12:00-15:00), 2005. As one of multi-stage particle sampling instruments, this LPAI with multi-orifice was designed to measure the size distribution and mass concentration of particulate matter. Particles are sampled directly on substrate material (80 mm diameter Nuclepore® filter) arranged behind the jet-nozzles of an impactor. The detailed cut-off particle diameter of each stage for the LPAI was already mentioned in other papers by Ma et al. (2004a) and Ma and Kim (2008). During the sampling period, the ranges of temperature and relative humidity (RH) were 18.8-21.7 °C and 41-56%, respectively.

3.1.2 The novel double detector system of micro-PIXE

Table 2 indicates the properties of double X-ray detectors. The HP-Ge X-ray detector has moderate energy resolution and poor detection efficiency below 2 keV because of its Ge L-shell absorption edge and backscattering proton absorber (60 μm thick polypropylene). The Si(Li) X-ray detector was set at a symmetrical position with the HP-Ge X-ray detector with respect to the beam axis. The energy resolution of the Si(Li) detector is excellent, and this higher energy resolution results in a better signal-to-background ratio and smaller peak overlapping, especially in the low-energy regions. The detector window is 8 μm-thick Be and attached with an annular type absorber (100 μm-thick Mylar) with a center hole (3 mm in diameter). This Si(Li) detector can finally provide a fairly good detection efficiency for X-rays below 2 keV. Details of this double X-ray detectors system for PIXE Analysis have been described elsewhere (Sakai et al., 2005).

X-ray detector	Model	Window ( )[b]	Absorber	Distance[c]	Prioty element	Detectable elements
HP[a]-Ge	IGLET-X-11145	Be (25 μm)	Polypropylene 60 μm	22 mm	Middle-Heavy	≥ Si
Si(Li)	LS30135	Be (8 μm)	Mylar 100 μm	18 mm	Light	≥ Na

[a]High-purity

[b]Thickness

[c]Detector - window distance

Table 2. Specification of two different X-ray detectors

3.2 Results and discussion

Fig. 4 shows the micro-PIXE elemental spectra for the seven arrow-marked individual ADS particles that were collected on the 2nd stage (5.07 μm aerodynamic diameter) of LPAI.

Outer blackly filled and inner greyly filled spectra were formed by scanning the whole area retaining seven particles (a blackly filled square at right side of Fig. 4) and each indicated particle, respectively. The scanning of microbeam on each individual particle enabled us to draw more clearly separated peaks of each element including light elements (e.g., Na, Mg, and Al). First of all, the micro-PIXE spectra displayed in Fig. 4 shows a severe particle-to-particle variation of the elemental composition among individual coarse particles collected during our intensive field measurement campaign. From the inner greyly filled spectra, individual particles can be classified into two distinct groups (i.e., above four particles (group 1) and below three particles (group 2) groups). In the particles belonged to group 1, Na and Cl coexist with soil-derived components such as Al, Si, K, Ca, and Fe. The particles of group 1 are the typical example of internally mixed particles which contain a uniform mixture of components from each of the sources. The coexistence of sea salt and mineral components also indicates that ADS particles were experienced aging processes namely, chemical transformation, in the course of their long-range transport. Whereas, only marine components (e.g., Na, Cl, S, and Mg) were detected in the particles of group 2.

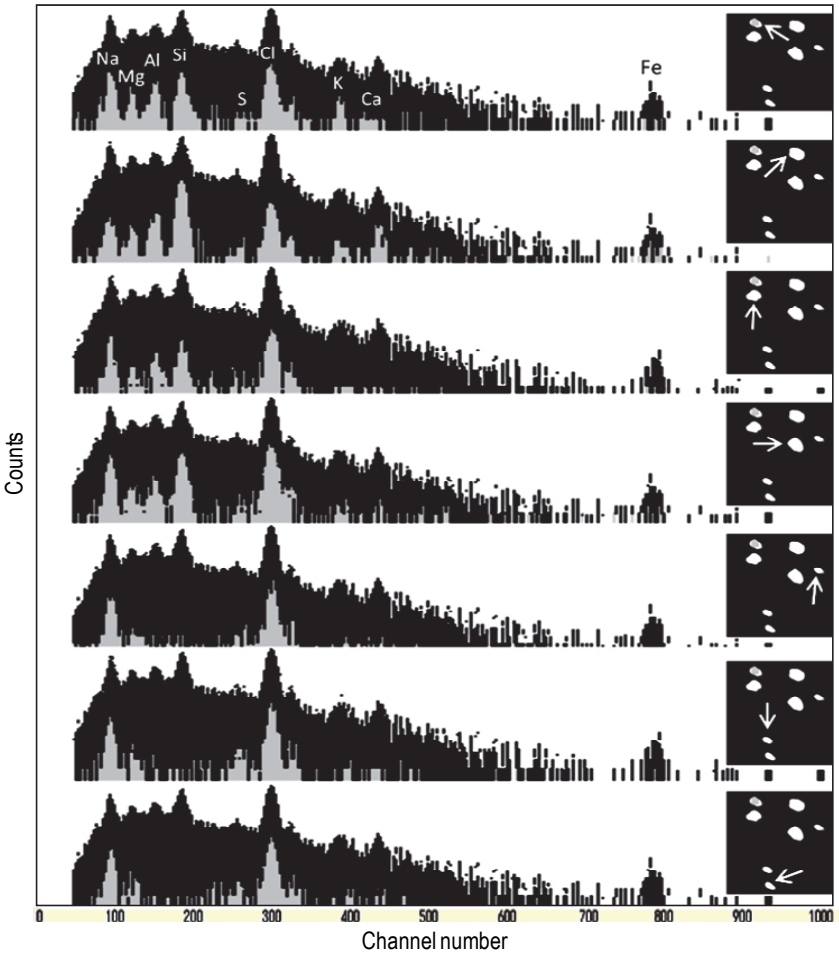

Fig. 4. Micro-PIXE elemental spectra for individual ADS particles collected on the 2nd stage (5.07 μm aerodynamic diameter) of LPAI

Fig. 5 displays an example of micro-PIXE elemental maps taken on two particles (5.07 μm aerodynamic diameter) collected during ADS event. Two combined masks of total elements are schematically shown on the last insert.

The particle displayed at top portion of scanning area is containing marine components (e.g., Cl, Na, and S). Whereas, several crustal elements (e.g., Si, Al, and Ca) are principally distributed in and/or on a particle located at bottom of scanning area. On the other hand, Mg and Ca, which are minor (or relatively minor) composition in both sea-salt (Mg: 0.128 wt.% and Ca: 0.0418 wt.%) and dust sand (Mg: 1.57 wt.% and Ca: 5.83 wt.%) (The standards of China loess and Simulated Asian mineral dust, 1998) are weakly coexisting in and/or on two particles. From this elemental map and mask replayed corresponding to individual two particles we can reasonably suggest that two particles are externally mixed particles (i.e., each particle arises from only one source).

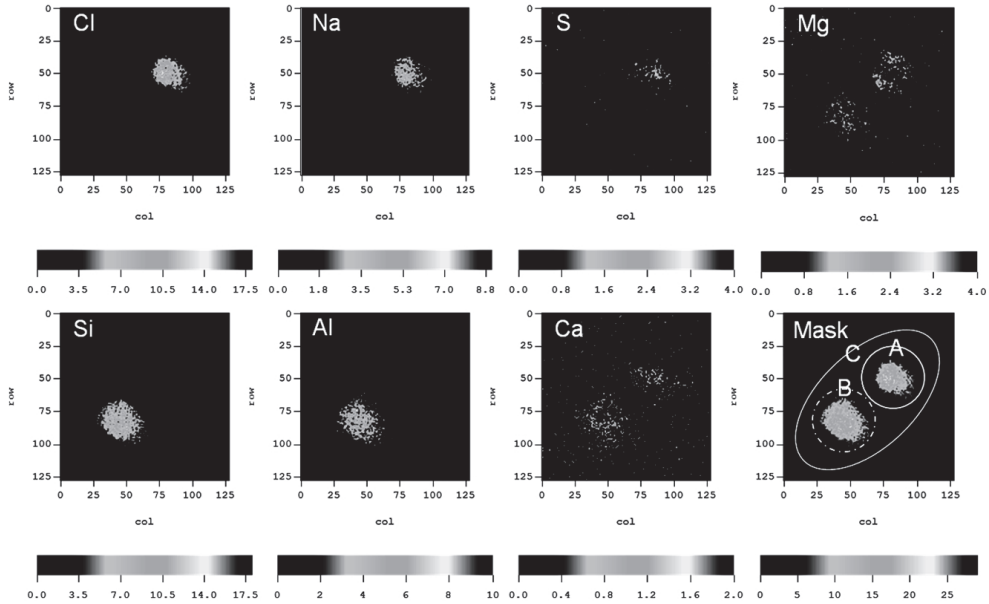

Fig. 5. An example of micro-PIXE elemental maps taken on two particles collected during ADS event. Scanning area of microbeam is 25×25 μm²

Micro-PIXE analysis has the scanning ability of microbeam with a 1-2 μm beam spot size. By scanning this microbeam, we can obtain spatial distribution of trace elements in individual particles. As a result, it is possible to know the portion-to-portion variation of elemental compositions in a particle. Fig. 6 shows an example of the micro-PIXE elemental spectra for two different portions of an ADS particle with 5.07 μm aerodynamic diameter. Outer white and inner black spectra were formed by scanning the whole and each square portion on a particle, respectively. According to this analytical result, the top portion of particle contains both sea-salt and silicon. However, only sea-salt components were detected in the bottom portion of particle. It can therefore be said that the chemically transformed ADS particle shows heterogeneous elemental distribution. This heterogeneous elemental distribution in an ADS particle might be caused by two dissimilar aging processes (i.e., (a): collision (or coagulation) of dust particles and sea-salts and (b): in-cloud scavenging of both particles). The modification of ADS particles occurred most probably due to the collisions and coagulations of dust particles and sea-salts (Zhang and Iwasaka, 2004). Zhang and Iwasaka (2004) suggested that the interaction of ADS particles and sea-salt is an important process in size and compositional changes of ADS particles during their long range transport, consequently affecting mass transformation and optical properties in the atmosphere. Moreover, a cloud formation process contributes significantly to the chemical modification of ADS particles (Ma et al., 2004b). From the study on individual cloud droplets by an X-ray fluorescence microprobe analysis, Ma et al. (2004b) reported that a large number of crustal particles were incorporated into cloud droplets during their long-range transport.

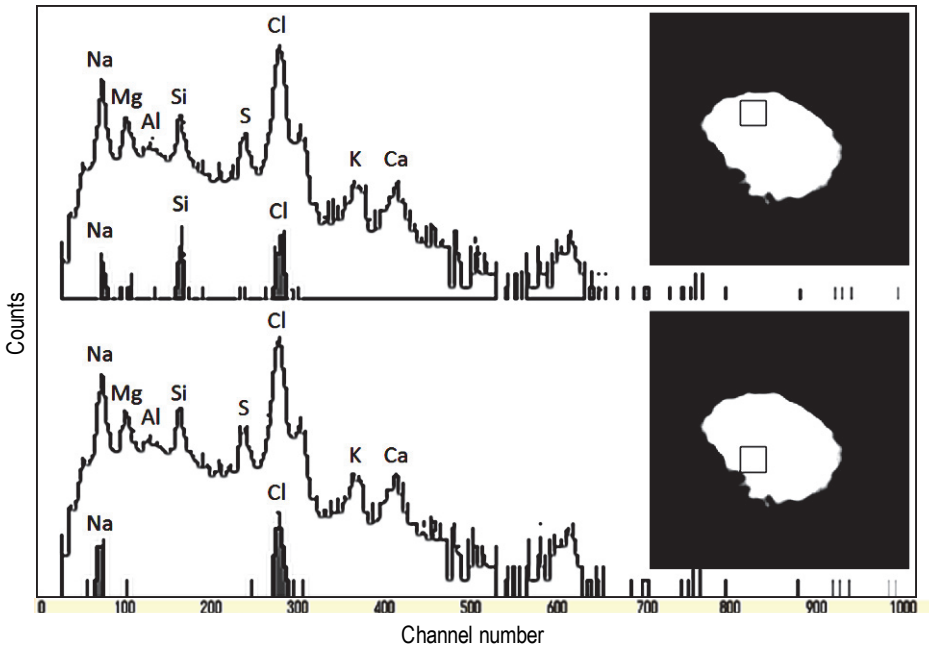

Fig. 6. Micro-PIXE elemental spectra for two different portions of an ADS particle

Fig. 7 illustrates a presumable explanation for the transformation processes of the ADS particles with sea-salt by heterogeneous nucleation. Two types of transformation processes of the ADS particles can be identified, i.e., the coalescence of two different droplets formed by heterogeneous nucleation on a separated ADS particle and a sea-salt and ((a) of Fig. 7) and the collision of an ADS particle to the droplet formed by a sea-salt nucleation ((b) of Fig. 7). Although ADS particles are insoluble in water, they begin to serve as centers with the condensation of water vapor. ADS particles are less soluble than marine of anthropogenic aerosols, their solubility weathered by condensation-evaporation cycles can be increased (Desboeufs et al., 2001). In addition, these homo/heterogeneous nucleation processes can be homomolecular (involving a single species) or heteromolecular (involving two or more species) (Desboeufs et al., 2001). According to the transformation processes of the ADS particles with sea-salt (as illustrated in Fig. 7), the possible reasons of portion-to-portion dissimilarity shown in Fig. 6 (i.e., (a) upper scanned portion: Na, Si, and Cl and (b) below scanned portion: Na and Cl) of elemental distribution on and/or in an ADS particle can be potentially evaluated by below three aging processes of the ADS particles.

As the first aging process ((a) of Fig. 7), both ADS and sea-salt particles were transferred into different cloud droplets via nucleation scavenging. This in-cloud scavenging of particles is called rainout. During this rainout processes, sea-salt particles were perfectly melted; however, hydrophobic ADS particle were keeping a horizontal water film on its surface (Desboeufs et al., 2001). Both cloud droplets were then consolidated, when they grew and diffuse in cloud layer. Finally, descending air parcel by high pressure and evaporation of water from cloud droplet made a new particle which contained partially sea-salt crystal on its surface.

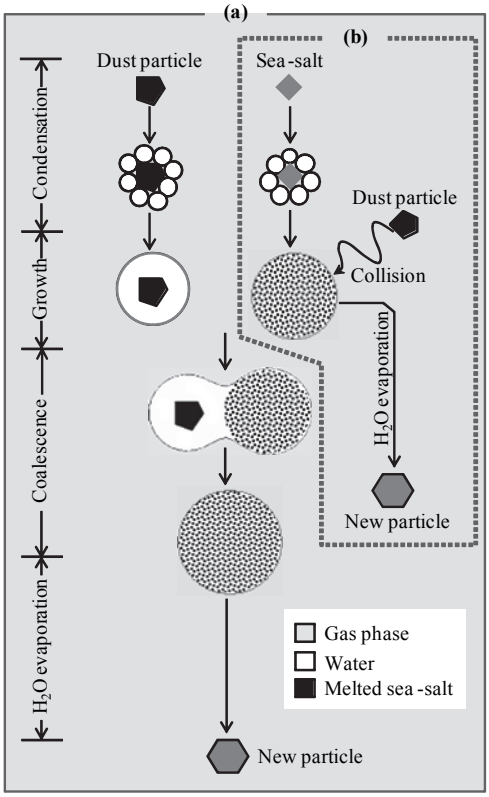

Fig. 7. An illustrative explanation of the transformation processes of the ADS particles with sea-salt via nucleation scavenging

As the second aging process ((b) of Fig. 7), an ADS particle that did not take up any water (i.e., it cannot be dissolved in cloud droplet by itself) was scavenged by a cloud droplet (i.e., through collision) formed by rainout of sea-salt. Then a chemically different particle was born. As distinct from nucleation scavenging, the collisions and coagulations of an ADS particle and a sea-salt can be thought as the third aging process. This homogeneous particle-to-particle reaction is probably due to the modification of ADS particle.

4. Removal of ADS particles by rainout and washout

If the relative humidity of the air parcel reaches a critical humidity, the value of which depends on the size and chemical composition of the aerosol present, the droplets become activated, grow freely by water vapor diffusion, and cloud droplets are formed. This in-cloud scavenging of particles is called rainout. Cloud and precipitation contribute significantly to the removal of Asian dust storm particles from the atmosphere (Ma et al., 2004). Numerous studies including laboratory, field, and model simulation have been carried out to determine the chemical composition of rain and the scavenging efficiency of aerosol particles by raindrops (Baez et al., 1995; Chate & Kamra, 1997; Hallberg et al., 1997).

Since the chemical content of raindrops is variable according to the mechanisms such as condensation nuclei inside clouds, pollutant scavenging, collision, coalescence and break-up of falling raindrops, and evaporation, chemical processes in the atmosphere as the washout of particles and gases are not sufficiently described by the usual determination of elemental concentration in rain water (Ma et al., 2001; Tenberken & Bächmann, 1996). Since the analysis of rain as bulk phase will lead to a loss of detailed information, the sampling and analysis of individual and size-classified raindrops must be performed (Tenberken & Bächmann, 1996; Ma, 2001). In recent years, Ma's "Collodion-film replication technique" (Ma, 2001) has provided a new method by which chemical analysis of individual raindrops can be carried out. Tenberken and Bächmann 4) applied the capillary zone electrophoresis method to the analysis of a single droplet.

Avila and Rodà (1991) introduced the red rain. The red rain, rain event carrying dust from Sahara desert, North African sources, are frequently falling with average frequency of around 3 events per year at Barcelona and surroundings in NE Spain 8). Red rains show a high load of dissolved ions (Rodà et al., 1993) and particulate matter (Berganetti et al., 1989).

In Japan, a yellow rain, which is rain colored yellow by particulate matter with high pH value (6.35) due to the alkaline dust storm particles, was reported in the end of Mar. 2000 (Ma et al., 2002).

The purpose of this section is to introduce the physiochemical properties of the individual cloud base droplets collected in the western Japan during ADS event. Also the elemental masses in size-classified raindrops collected on the yellow rainfall event were theoretically and experimentally compared.

4.1 Scavenging of ADS particles by cloud droplet

4.1.1 Sampling and analysis of individual cloud droplets

The sampling of individual cloud droplets was carried out at the Kyoto Prefectural acid rain monitoring site (200 m elevation) in the range of Mt. Taiko and the summit of Mt. Taiko (683 m elevation) on the west coast of Japan, respectively during dense Asian dust storm event on 22 Mar. 2002. These mountainous sampling sites (35.37^{o} N, 135.81^{o} E) are located at Yasaka in the north part of Kyoto Prefecture, Japan. This mountainous sampling site is not only a clean region without local pollution sources, but also a geographically advantageous position where can be directly exposed to ADS in some cases. The summit of Mt. Taiko was exposed by cloud during dense Asian dust storm event. For the collection of individual cloud droplets, the replication technique introduced for sampling of individual drizzle droplet by Ma et al. (2001) was applied. About 200 µl of collodion solution (3%) is mounted onto a 47 mm diameter non-hole Nuclepore® filter just before exposure to cloud. When cloud droplets adhere freely onto the thin layer of collodion film (130±10 µm) they gently settled without bounce-off. This procedure not only allows us to get information about the physical properties of droplets but also enable us to analyze the retained components in and/or on cloud droplet. During sampling periods the temperature was ranged from 9.5 ^{o}C and 11.4 ^{o}C and the average relative humidity was around 100%. About 500 separated individual cloud droplets were collected on 20 sheets of collodion film at cloud base level.

In order to characterize the chemical nature of solid residual particles retained in individual cloud droplets, the X-ray microprobe system equipped at SPring-8 BL-37XU was applied.

The analytical procedures and experimental set-up used for XRF microprobe analysis were already mentioned.

4.1.2 Replication of individual cloud droplets

Droplets, unlike dust particles, are unstable. Any contact with a solid surface or another droplet makes the droplet disappear as an entity. Therefore, unlike dust particles for example, droplets cannot be collected on a filter paper for subsequent physicochemical analysis in the laboratory. Also it is difficult to collect cloud as individual droplets because a single cloud droplet has a tiny volume. From this point of view, collodion film method can be one of profitable methods for the study on the physical characteristics as well as for subsequent chemical analysis of individual droplets. The replicas of individual cloud droplets were formed separately on the thin collodion film as shown in Fig. 8.

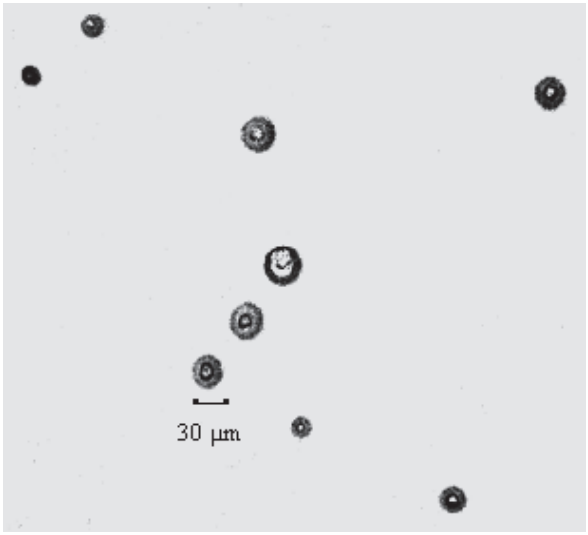

Fig. 8. Replicas of individual cloud droplets formed on collodion film

4.1.3 Chemical properties of residuals in individual cloud droplets

The droplet residues consisted of crustal components were reconstructed as elemental maps. Fig. 9 shows the four kinds of XRF elemental maps of dry residuals in individual cloud droplets. Each elemental map size is 750 μm × 750 μm. Large amount of cloud droplets containing Ca are present on this mapping area (lower left panel). In addition, as a one of substantial fractions of the droplet residues, map of Zn was drown at right upper of Fig. 9. We cloud find the significant distribution of crustal components on the maps of residual particles in individual cloud droplet. This cleanly indicates that a large number of crustal particles were incorporated into cloud droplets during their long-range transport. In other words, soil particles with high amounts of insoluble fractions had high scavenging efficiencies by rain out mechanisms. These XRF elemental maps of residual particles indicate that the internal and external mixture of particles containing different chemical nature was still preserved in the droplet phase.

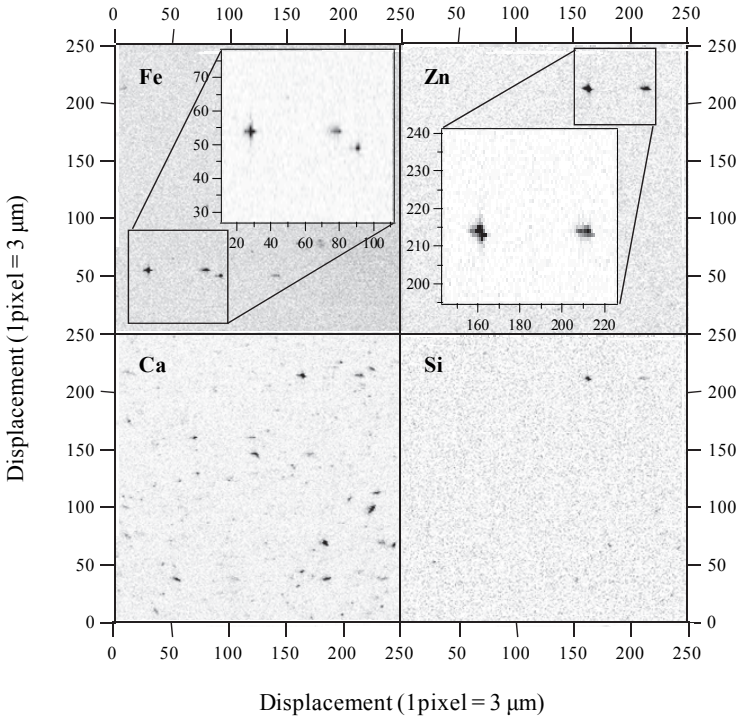

Fig. 9. XRF elemental maps of residuals in individual cloud droplets

4.2 Washout of ADS particles by raindrops

4.2.1 Sampling, handling, and analysis of individual raindrops

Sampling of size-resolved raindrops was conducted on a five-story building of Kyoto University (34.53° N; 135.48° E) during the yellow rain event in the early of April 2001. Rains started to fall in the afternoon of April 7, 2001 across southwest Japan Island as a cold front approached from the west. The front moved into east Japan late on April 7th. Total rain amount and rainfall intensity in this rainfall event were 5.0 mm and 0.8 mm/h, respectively. During sampling period the range of wind speed was 1.0~3.9 m s^{-1} generally blowing from the west. The temperature was around 19.1~19.9°C and average relative humidity was around 100%.

For the purpose of size-classified raindrop sampling, a raindrop-sampling device was employed. This raindrop-sampling device was modified from the "Guttalgor method" introduced by Tenberken and Bächmann (1996). This raindrop collector consists of a Dewar vacuum flask (Jencons Co.) filled with liquid nitrogen, five-stage stainless steel sieves with different mesh size (2.36 mm, 1.7 mm, 1.0 mm, 0.71 mm, 0.5 mm), and back-up stage. Fallen raindrops into the liquid nitrogen were frozen and they sink to lower sieves owing to their higher density. For the successful size-classification of raindrops, sampling duration time should be adjusted considering the rainfall intensity. In this study, raindrop sampling was performed for 5 minutes from the beginning rainfall. The rainfall amount for 5 minutes was 0.4 mm.

For the handling of individual raindrops without evaporation and contamination, we designed a clean air chamber system filled with cooled dry N_2 gas. After sampling, the sieves and back-up stage were pulled out from the Dewar vacuum flask and then frozen raindrops on each sieve were placed into the polyethylene vial by using a vacuum pipette. Fig. 10 shows the individual frozen raindrops collected on a mesh stage (1.7 mm mesh size) and the handling of a frozen raindrop by using a vacuum pipette. As shown in Fig. 10, the raindrops kept their spherical shape during the freezing process.

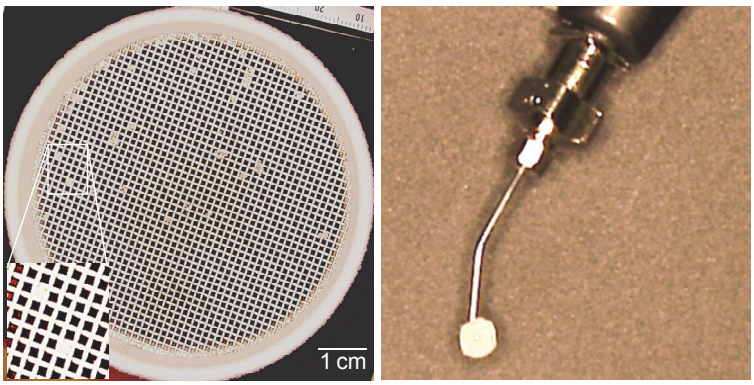

Fig. 10. Individual frozen raindrops collected on a mesh stage (1.7 mm mesh size) (left) and the handling of a frozen raindrop using a vacuum pipette (right)

To separate size-segregated raindrops into soluble and insoluble fractions, frozen raindrops were melted and then 50 μl of rainwater from each raindrop size was centrifuged under the condition of 4000 rpm for 10 min. Centrifuging method can be used to separate the solids from liquid 12). Centrifuging can be effectively used especially for the relatively small amount of liquid sample. When the insoluble particle is placed in a centrifugal field (maximum centrifugal force: 2,670 g), a force higher than gravity pulls the particle down. By centrifuging treatment, the solid insoluble particles could be deposited on a non-hole Nuclepore® film. Also 20 μl of upper soluble fraction was dropped on a non-hole Nuclepore film and then water fraction was evaporated under an infrared lamp. The solid insoluble particles and the residual material of upper solution were subsequently analyzed as the insoluble and soluble fractions, respectively. Elemental concentrations of the soluble and insoluble fractions were determined by PIXE analytical method. For the elemental quantification analysis of the individual solid particles retained in raindrops, the XRF microbeam system equipped at SPring-8 BL-37XU was applied. The analytical procedures and experimental set-up used for both analysers were mentioned earlier.

4.2.2 Replication of individual cloud droplets

Fig. 11 exhibits the variation of major elemental mass concentrations as the function of solubility and raindrop size. Since the giant raindrop, which is larger than 3.5 mm diameter, will be easily split into smaller one, the whole size range of raindrop was considered from 0.2 mm to 3.5 mm diameter. As shown in Fig. 11, every elemental concentration in both soluble and insoluble fractions is found to be strong raindrop size dependence. Though

there is the slight increase of K concentration between 1.7 mm and 2.3 mm raindrop diameter, it shows a strong decrease of every elemental concentration with increasing droplet diameter regardless of solubility. Especially S and Cl show the predominantly higher mass loading in soluble fraction. It is expected that the following several mechanisms are responsible for this raindrop size dependence of elemental concentration (Bächmann et al., 1993):

- Inside the cloud
- The scavenging of particles by CCN mechanism
- The uptake of gases
- The collision and coalescence
- Below the cloud
- The scavenging of particles by impaction, collision, and coalescence
- The uptake of gases
- Raindrop evaporation

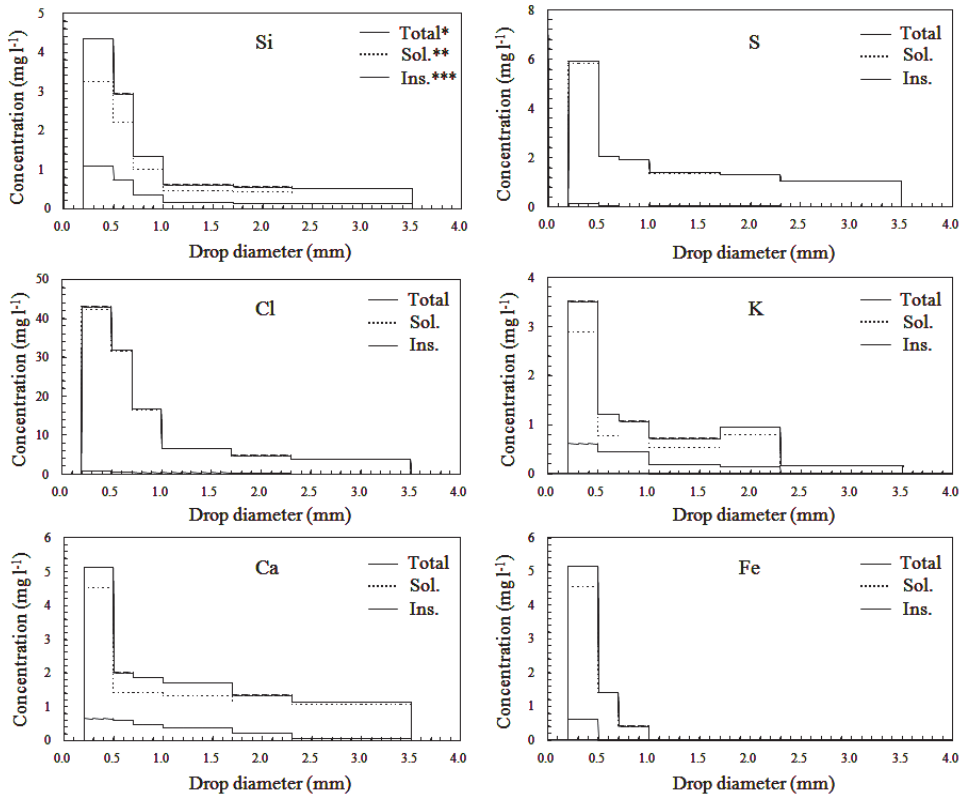

Fig. 11. The variation of major elemental masses as the function of solubility and raindrop size.
*Sum of soluble and insoluble (outer bold)
**Soluble
***Insoluble (inner bold)

Flossman (1994) stated that raindrops within the cloud or near the cloud base have nearly identical concentrations regardless of raindrop size. Moreover, according to Munger's measurement in the coastal stratus clouds (Munger et al., 1983), the continuous decreasing of component concentrations in cloud was not found. On the other hand, at the ground-based measurement in the present study, the dependence of elemental concentration on raindrop diameter was found. Therefore it is suggested that dependence of elemental concentration on drop size measured near and at the ground is only due to below cloud influences (Tenberken & Bächmann, 1996). When raindrops fall from cloud base to ground, due to below cloud scavenging of pollutants the solute concentration in raindrop will be increased. Hans and James (1998) also reported that the scavenging efficiency of pollutants by falling raindrops decreases with increasing raindrop size with the range of 0.2 mm to 4 mm diameter.
In the case of insoluble fraction, the concentration ratios of Si, K, Ca, and Fe in yellow rain (average value of size-classified raindrop samples) to those in non-yellow rain (Park, 1997) are 12.4, 11.4, 13.7, and 10.1, respectively. They also show the overwhelmingly higher ratios at soluble fraction. It is clear that the episodically yellowish rainfall shows a high load for crustal materials in both soluble and insoluble fractions.

4.2.3 Model calculation of elemental mass in size-resolved raindrops

For the purpose of comparing the measured mass concentration of each element to calculated mass concentration in size-resolved raindrop, we made an attempt to determine the each elemental mass concentration as a function of raindrop size by model calculation. The schematic of model concept is illustrated in Fig. 12. This model is a Lagrange type model that set the special coordinates as the one-dimensional vertical direction from below cloud base to ground. For model calculation, we assumed several parameters as following: the uniform distribution of aerosol particles existing in a volume swept by falling raindrops, the stable atmosphere, no diffusion by a rising air current, no evaporation and coalescence of raindrops. When the raindrop with diameter d_r falls for one second, the volume V swept by falling raindrop is described as following equation.

$$V = \frac{\pi {d_r}^2}{4} \upsilon_t \tag{1}$$

where υ_t is the terminal velocity.
When the mass concentration of particles with diameter d_p at ground is defined as $C_{p,0}$ (d_p), and the collection efficiency of raindrop with d_r for particle with diameter d_p is defined as E_0 (d_r, d_p), the mass (m) of particle (d_p) in raindrop (d_r), which falls through V for one second, can be written as following.

$$m = \frac{\pi {d_r}^2}{4} \upsilon_t \cdot C_{p,0}(d_p) \cdot E_0(d_r, d_p) \tag{2}$$

Therefore the total mass (M) of particle (d_p) in raindrop (d_r), which falls through from below cloud base to ground, can be rearranged as following equation.

$$M = \int_0^t \frac{\pi {d_r}^2}{4} \upsilon_t(h, d_r) \cdot C_p(h, d_p) \cdot E(h, d_r, d_p) dt \tag{3}$$

where $\upsilon_t(h, d_r)$ is the terminal velocity of raindrop (d_r) at height (h), $C_p(h, d_p)$ is the mass concentration of particles existing at height (h), $E(h, d_r, d_p)$ is the collection efficiency of raindrop (d_r) for particle (d_p) at height (h).

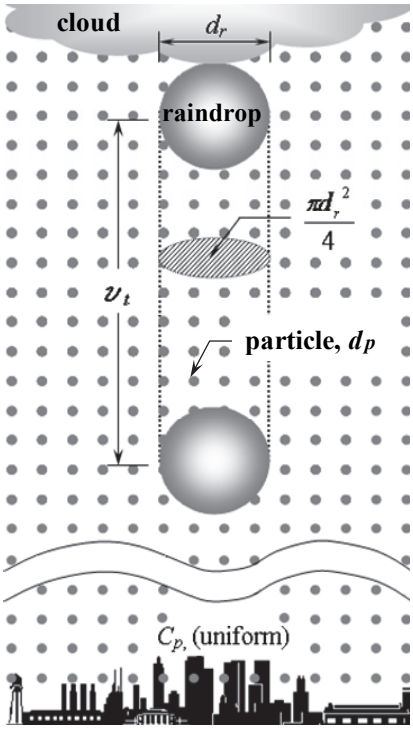

Fig. 12. Schematic of the model used for the calculating each elemental mass concentration as a function of raindrop size at ground

About the terminal velocity of raindrops (U_t, cm s^{-1}), we applied the Beard's (1976) three physically distinct flow regimes: 1) small cloud droplets, 1 μm≤d_0≤20 μm (steady wake, vanishingly small Reynolds number, 10^{-6}≤N_{Re}≤0.01), 2) large cloud droplets to small raindrops, 20 μm≤d_0≤1 mm (steady wake, low to intermediate Reynolds number, 0.01≤N_{Re}≤300), 3) small to large raindrops, 1 mm≤d_0≤7mm (unsteady wake, moderate to large Reynolds number, 300≤N_{Re}≤4000).

Though other mechanisms like diffusiophoresis, electrostatic force, and thermophoresis are comprised in particle scavenging by raindrop in the atmosphere, aerosol particles can be mainly removed through the processes of Brownian diffusion, interception, and impaction. Therefore, in the present study the particle collection efficiency (E) of raindrops including Brownian diffusion (E_{dif}), interception (E_{int}), inertial impaction processes (E_{imp}), and the combined with these three particle scavenging coefficients (E_{com}) as a function of raindrop size were calculated. In order to formulate a correlation for E based on dimensional analysis, the parameters that influence E must be identify (Seinfeld & Pandis, 1998). The parameters are several variables such as volume of raindrop (f, cm^3), scale height (h, m), rain intensity

(I, mm h^{-1}), total number concentration of raindrop (N, m^{-3}), raindrop radius (r_r, μm), Reynolds number (Re), critical Stokes number (S^*), raindrop terminal settling velocity (υ_t, cm s^{-1}), rainwater concentration in the atmosphere (W, mg m^{-3}), vertical distance from the cloud base (z, m), dynamic viscosity of air (μ_a, Pa·s), particle diffusivity (D_p, cm s^{-2}), and dynamic viscosity of water (μ_r, Pa·s). Based on E_{dif}, E_{int}, and E_{imp}, Strauss (1975) proposed the following E_{com} equation that fits experimental data:

$$E_{com}=1-(1-E_{dif})\cdot(1-E_{int})\cdot(1-E_{imp}) \tag{4}$$

In this work, the following E_{dif}, E_{int}, and E_{imp} proposed by Slinn and Hales (1971) were applied.

$$E_{dif}=\frac{4}{Re\cdot Sc}\left(1+0.4Re^{1/2}Sc^{1/3}\right) \tag{5}$$

$$E_{int}=4\frac{r_p}{r_r}\left(\frac{\mu_a}{\mu_r}+(1+2Re^{1/2})\frac{r_p}{r_r}\right) \tag{6}$$

$$E_{imp}=\left(\frac{St-S^*}{St-S^*+2/3}\right)^{3/2} \tag{7}$$

where Re is the Reynolds number of raindrop based on its radius ($(r_r \upsilon_t \rho_a)/\mu_a$). Sc is the Schmidt number of collected particle ($\mu_a/\rho_a D_p$). St is the Stokes number of collected particle ($(2C\rho_p r_p \upsilon_t)/(9\mu_a r_r)$), C is the Cunningham slip factor, ρ_p is the particle density kg m^{-3}. S^* is the critical Stokes number ($(1.2+(1/12)\ln(1+Re))/(1+\ln(1+Re))$).

In the present study, six major components (Si, S, Cl, K, Ca, Fe) were the target of model calculation. To get the elemental mass information at atmosphere, concurrently with the raindrop sampling, the collection of size-classified particles by LPAI (Dylec, LP-20) was conducted at the same sampling site. The detailed specifications of LPAI were described previous study (Ma et al., 2004a).

The PIXE analysis results of soluble and insoluble fractions for the size-segregated ambient particles were applied to the calculation of mass concentrations of **six** elements as a function of raindrop size. The elemental mass concentration at height (h) can be given by

$$C(h)=C_g(0)\exp\left(-\frac{h}{H}\right) \tag{8}$$

where C(h) is the atmospheric concentration of target component at height (h). $C_g(0)$ is the atmospheric concentration of target component at ground. H is the scale height, 900 m.

The height of Mt. Hiei (848 m) which is located close to our raindrop sampling site was a barometer of the height of cloud above ground level because the widely distributed cloud was suspended right above the summit of Mt. Hiei.

The calculated mass concentrations of six elements as a function of raindrop size are plotted with measured results in Fig. 13. Raindrops were fractionated into size class 0.2-0.5, 0.5-0.7, 0.7-1.0, 1.0-1.7, 1.7-2.3, and 2.3-3.5 mm diameter. The phenomenon of the continuous decreasing of elemental mass concentration with increasing raindrop size was shown in both calculated and measured results.

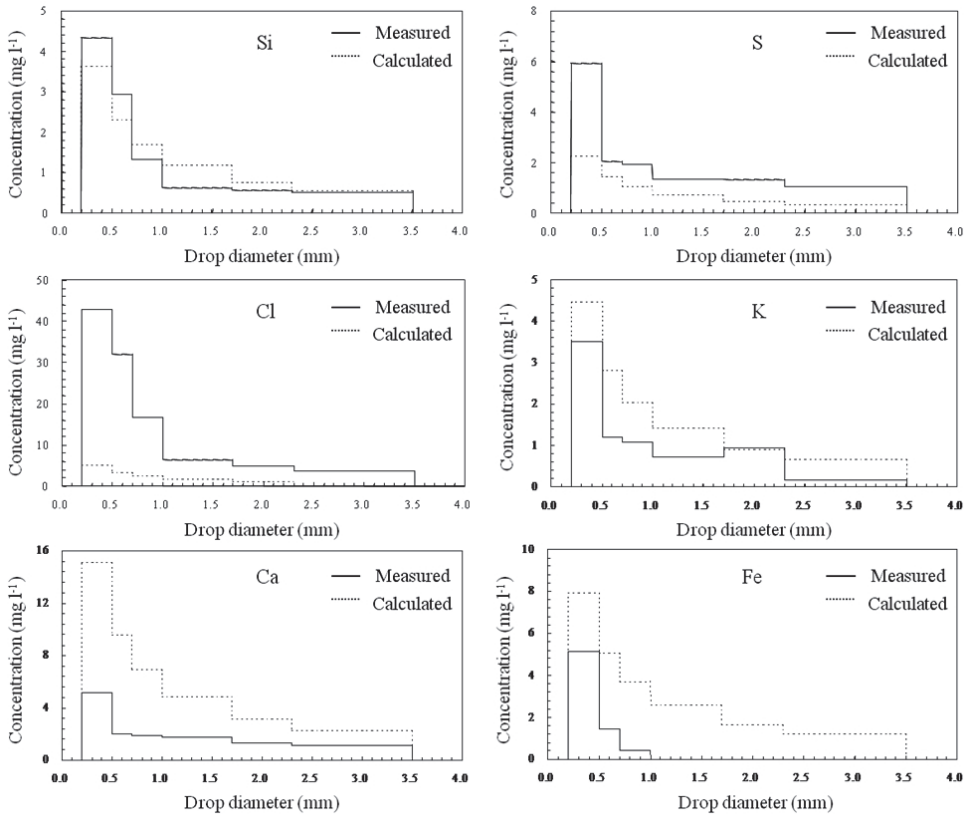

Fig. 13. The plotting of calculated vs. measured mass concentrations for six major elements as a function of raindrop size

A comparatively good agreement was obtained between measured and calculated results for Si, S, and K. However, the calculated Cl mass concentration was considerably under estimated compared with measured results. Whereas, in the case of Ca and Fe, the calculated mass concentrations over estimated. One of the reasons for these discrepancies between measured and calculated levels might be the inhomogeneous particle distribution from below cloud base to ground. Because the physicochemical properties of Asian dust particles will be exceedingly variable according the transport situation, local emission sources, and atmosphere conditions. Furthermore, the long sampling duration time (24 hours) for ambient particle collection can obscure the particle-to-particle composition variations because the particle composition may be altered due to condensation or evaporation of volatile compounds, or chemical reactions. Therefore spatial and temporal inhomogeneities in air mass might lead to disagreement between calculated and measured results. From this point of view, the sampling of atmospheric particles must be done with good time-resolved sampling duration. The continuous sampling of size-resolved raindrop as a function of rainfall amount with the detailed size-classification of fine fraction raindrop with diameter smaller than 0.5 mm is also desirable.

4.2.4 Chemical components of individual particles retained raindrops

By irradiation of the XRF microbeam, it was possible to reconstruct individual particles retained raindrops as elemental maps. Fig. 14 draws the example XRF elemental maps for Fe, Cl, Si, and Ca in individual particles retained in raindrops (1.7 mm<Rd<2.36 mm). These visualized elemental maps for four kinds elements enable us not only to estimate the chemical mixing state of raindrop residual particles, but also to presume the particle scavenging of raindrops. For example, some particles indicate the chemical mixing state with soil derived components and Cl, while others consist of only crustal components. Consequently, from these four kinds of XRF images replayed corresponding to individual residual particles in raindrops, we can simply fractionate the visualized particle images into several groups.

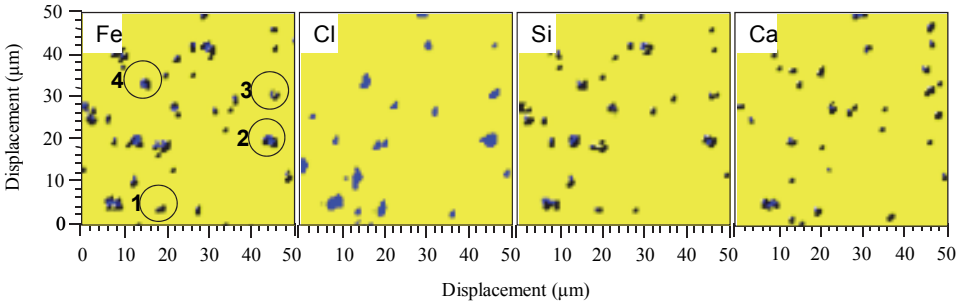

Fig. 14. XRF images of Fe, Cl, Si, and Ca in individual particles retained in raindrops (1.7< Rd <2.36 mm)

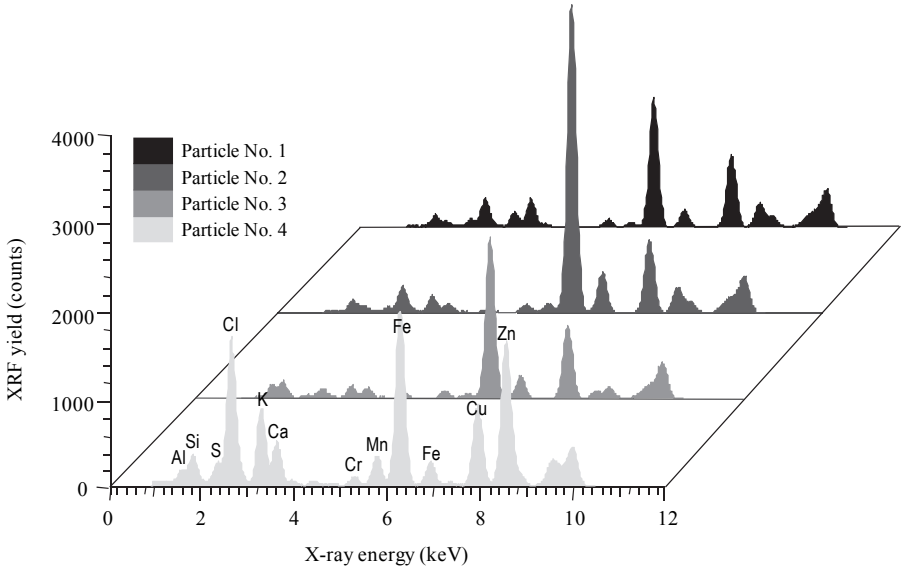

Fig. 15. XRF spectra for four particles indicated in Fig. 14. XRF counts were counted for 100 seconds

The XRF spectra for four particles indicated in Fig. 14 are plotted in Fig. 15. It was possible to resolve the multiple elemental peaks corresponding to X-ray energy of XRF spectra. The XRF count for every element shows the particle-to-particle variation. Among the soil-originated components, especially Fe shows high XRF counts. Several minor trace elements like Cr, Mn, and Cu are also coexisted with crustal elements. However, the XRF peak for Cu was overestimated because the sample holder of our XRF analytical system contains Cu. The elemental mass concentration (mg l^{-1}) for multielement can be quantitatively calculated by X-ray energy and count of each element.

5. Conclusion

As the source of ADS particles, the sands at four different desert areas were to be the target of bulk and single analyses by means of PIXE and SR-XRF analyses, respectively. The physical properties of desert sands like morphology, color, and size were basically determined. Also the chemical characteristics of bulk sands of each desert were specified as the relative elemental ratio. The XRF elemental maps and spectra for a point on individual sands allow us to understand the nature of individual sands. Consequently, the physicochemical properties of desert sands obtained from this study can be helpful to understand what kinds of man-made pollutants and sea-salts are incorporated into natural ADS particles.

By a combination of two different detector systems of micro-PIXE, a broad detection range of elements including Na, Mg, and Al was successively realized. The well drawn elemental spectra and maps from this novel attempt enabled us to visually classify individual ADS particles. It was also possible to sufficiently interpret the mixing state of individual ADS particles with sea-salts, especially portion-to-portion dissimilarity of chemical state in individual ADS particles. In addition to this, the detailed information of elemental micro distribution obtained from the scanning of microbeam with a 1-2 μm beam diameter in and/or on an ADS particle helped us presume the aging processes of ADS particles both in ambient and in-cloud. The relative number fraction of chemically transformed particle type in the size-classified particles collected during ADS event indicates that the chemical mixing states of individual ADS particles are strongly dependent on particle size.

The significant distribution of crustal components on the elemental maps reconstructed by XRF microprobe analysis indicates that a large number of crustal particles were incorporated into cloud droplets during their long-range transport. In other words, ADS particles were effectively scavenged by rain out mechanisms. Elemental concentrations in both soluble and insoluble fractions were found to be strong raindrop size dependence showing a sharp decrease of concentration with increasing raindrop size. Even though the tendency of the continuous decreasing of elemental mass concentration across the raindrop size spectrum was also shown in the model calculation, to improve the results of modeling calculation, the sampling of atmospheric particles with good time-resolved sampling duration is desirable. By a combination of XRF microbeam method, the individual particles retained in size-resolved raindrops were successfully characterized. Though the in-cloud scavenging of ADS particles is also expected, the results of our study make certain of the truth that the wet removal processes is one of final dissipation mechanisms of ADS particles.

6. Acknowledgments

The synchrotron radiation experiments were performed at the SPring-8 with approval of the Japan Synchrotron Radiation Research Institute (JASRI) (Proposal No. 2002B0395-NOS-np, 2002A4029-LM-np). The authors gratefully acknowledge Professor S. Tohno at Graduate School of Energy Science, Kyoto University and Professor S. Hayakawa at Graduate School of Engineering, Hiroshima University for their analytical support. The author wishes to express thanks to all the members, especially Mr. T. Sakai, in the Advanced radiation technology center, Japan Atomic Energy Research Institute for their help of micro-PIXE analysis. The author also gratefully acknowledges Professor M. Kasahara at Institute of Science and Technology Research, Chubu University for his planning and arrangement of micro-PIXE experiment for a long period.

7. References

Avila, A. & Rodà, F.: Red rains as major contributors of nutrients and alkalinity to terrestrial ecosystems at Montseny (NE Spain). *Orsis*, 6, 215-218 (1991)

Bächmann, K.; Haag, I. & Roder, A. (1993). A field study to determine the chemical content of individual raindrops as a function of their size. *Atmospheric Environment*, 27A, 1951-1958

Baez, A.P.; Belmont, R. & Padilla, H. (1995). Measurements of formaldehyde and acetaldehyde in the atmosphere of Mexico City. *Environmental Pollution*, 89, 163-171

Beard, K.V. (1976). Terminal velocity and shape of cloud and precipitation drops. *Journal of Atmospheric Science*, 33, 851-864

Berganetti, G.; Gomes, L.; Coude-Gaussen, G., Rognon, P. & Le Costumer, M. (1989). Present transport and deposition patterns of African dusts to the North-Western Mediterranean. *Journal of Geophysical Research*, 94 D12, 14855-14864

Braaten, D.A. & Cahill, T.A. (1986) Size and composition Asian dust transported to Hawaii. *Atmospheric Environment*, 20, 1105-1109.

Chate, D.M. & Kamra, A.K. (1997). Collection efficiencies of large water drops collecting aerosol particles of various densities. *Atmospheric Environment*, 31, 1631-1635

Darzi, M.D. & Winchester, W. (1982) Aerosol characteristics at Mauna Loa observatory, Hawaii, after east Asia dust storm episodes. *Journal of Geophysical Research*, 87, 1251-1258.

Desboeufs K.V.; Losno, R. & Colin, J.L. (2001) Factors influencing aerosol solubility during cloud processes. *Atmospheric Environment*, 35, 3529-3537.

Duce R.A.; Unni, C.K.; Ray, B.J.; Prospere, J.M. & Merrill, J.T. (1980) Long-range atmospheric transport of soil dust from Asia to the tropical north Pacific: Temporal variability. *Science*, 209, 1522-1524.

Flossman, A.I. (1994). A 2-D spectral model simulation of the scavenging of gaseous and particulate sulfate by a warm marine cloud. *Atmospheric Research*, 32, 233-248

Hallberg, A.; Wobrock, W.; Flossmann, A.I.; Bower, K.N.; Noone, K.J.; Wiedensohler, A.; Hansson, H. C.; Wendisch, M.; Berner, A.; Kruisz, C.; LAJ, P.; Facchini, M. C.; Fuzzi, S. & Arends, B.B. (1997). Microphysics of clouds: Model vs measurements. *Atmospheric Environment*, 31, 2453-2462

Hans, R.P. & James, D.K. (1998). Microphysics of clouds and precipitation. *Atmospheric and Oceanic Sciences Library*, 18, 24-30

Hayakawa, S. (2000) X-ray fluorescence method for trace analysis and imaging. Journal of *Japanese Synchrotron Radiation Research*, 13, 313-318. (in Japanese)

Hayakawa, S.; Ikuta, N.; Suzuki, M.; Wakatsuki, M. & Hirokawa, T. (2001) Generation of an X-ray microbeam for spectromicroscopy at SPring-8 BL39XU. *Journal of Synchrotron Radiation*, 8, 328-330.

Husar, R.B.; Tratt, D.M.; Schichtel, B.A.; Falke, S.R.; Li, F.; Jaffe, D.; Gassó, S.; Gill, T.; Laulainen, N.S.; Lu, F.; Reheis, M.C.; Chun, Y.; Westphal, D.; Holben, B.N.; Gueymard, C.; McKendry, I.; Kuring, N.; Feldman, G.C.; McClain, C.; Frouin, R.J.; Merrill, J.; DuBois, D.; Vignola, F.; Murayama, T.; Nickovic, S.; Wilson, W.E.; Sassen, K.; Sugimoto, N. & Malm, W.C. (2001) The Asian Dust Events of April 1998. *Journal of geophysical research atmospheres*, 106 (D16), 18317-18330.

Hwang, H.J.; Kim, H.K. & Ro, C.U. (2008) Single-particle characterization of aerosol samples collected before and during an Asian dust storm in Chuncheon, Korea. *Atmospheric Environment*, 42, 8738–8746.

Iwasaka, Y.; Yamamoto, M.; Imasu, R. & Ono, A. (1988) Transport of Asian dust (KOSA) particles: importance of weak KOSA events on the geochemical cycle of soil particles. *Tellus*, 40B, 494-503.

Johansson, S.A.E. & Campbell, J.L. (1988) *PIXE*: A novel technique for elemental analysis. New York: John Wiley and Sons, pp.134-140.

Lafon, S.; Rajot, J.-J.; Alfaro, S.C. & Gaudichet, A. (2004) Quantification of iron oxides in desert aerosol. *Atmospheric Environment*, 38, 1211-1218.

Li, R.; Liu, Y. & Zhang, K. (2007) Plant species diversity of wetland ecosystem in an arid and semi-arid region in northwest China. *Frontiers of Forestry in China*, 2(3), 284-290.

Ma, C.-J. (2001). New approaches for characterization of atmospheric particles and acid precipitation, Ph. D. dissertation, Kyoto University

Ma, C.-J.; Kasahara, M.; Hwang, K.C.; Choi, K.C.; Choi, S.B. & Lee, J.J. (2000) Physicochemical characteristics of single Asian dust storm particles. *Journal of Korean Society for Atmospheric Environment*, 16 E, 29-38.

Ma, C.J.; Kasahara, M. & Tohno, S., 2001. A new approach for characterization of single raindrops. *Water, Air and Soil Pollution*, 130, 1601-1606.

Ma, C.-J.; Kasahara, M. & Tohno, S. (2002). Application of PIXE to characterization of size-segregated single raindrops. *International Journal of PIXE*, 12, 7-18

Ma, C.-J.; Kasahara, M.; Tohno, S. & Kamiya, T. (2001). A new approach for characterization of single raindrops, *Water, Air, and Soil Pollution*, 130, 1601-1606

Ma, C.-J.; Kasahara, M.; Tohno, S. & Kim, K.-H. (2008) Physicochemical properties of Asian dust sources. *Asian Journal of Atmospheric Environment*, 2-1, 26-33.

Ma, C.-J. & Kim, K.-H. (2008) A combination of size-resolved particle samplers and XRF microprobe technique for single particle study. *Atmospheric Environment*, 42, 7022-7026.

Ma, C.-J.; Oki, Y.; Tohno, S. & Kasahara, M. (2004a) Assessment of wintertime atmospheric pollutants in an urban area of Kansai, Japan. *Atmospheric Environment*, 38, 2939-2949.

Ma, C.-J.; Tohno, S.; Kasahara, M. & Hayakawa, S. (2004b) Properties of the size-resolved and individual cloud droplets collected in the western Japan during Asian dust storm event. *Atmospheric Environment*, 38, 4519-4529.

Ma, C.-J.; Tohno, S.; Kasahara, M. & Hayakawa, S. (2004c) Properties of individual Asian dust storm particles collected at Kosan, Korea during ACE-Asia. *Atmospheric Environment*, 38, 1133-1143.

Mason, B. (1966) *Principles of Geochemistry*, 3rd edn. Wiley, New York.

Munger, J.W.; Jacob D.J.; Waldman J.M. & Hoffmann M.R. (1983). Fogwater chemistry in an urban atmosphere. *Journal of Geophysical Research*, 88, 5109-5123

Nishikawa, M.; Hao, Q. & Morita, M. (2000) Preparation and Evaluation of Certified Reference Materials for Asian Mineral Dust. *Global Journal of Environmental Research*, 4, 103-113.

Nishikawa, M. & Kanamori, S. (1991) Chemical composition of Kosa aerosol (yellow sand dust) collected in Japan. *Analytical Science*, 7, 1127-1130.

Park, J.H. (1997). Study of physicochemical properties of atmospheric particles and their scavenging. Ph. D. dissertation, Kyoto University (In Japanese).

Rodà, F.; Bellot, J.; Avila, A.; Escarré, A.; Piñol, J. & Terradas, J. (1993). Sahara dust and the atmospheric inputs of elements and alkalinity to Mediterranean ecosystems. *Water, Air, and Soil Pollution*, 66, 277-288

Sakai, T.; Oikawa, M. & Sato, T. (2005) External Scanning Proton Microprobe –A New Method for In-Air Elemental Analysis. *Journal of Nuclear and Radiochemical Sciences*, 6(1), 69-71.

Seinfeld, J.H. & Pandis, S.N. (1998). *Atmospheric Chemistry and Physics*, pp.1003-1013, John Wiley & Sons Press, New York

Slinn, W. G.N. & Hales, J.M. (1971). A revaluation of the role of thermophoresis as a mechanism in and below cloud scavenging. *Journal of Atmospheric Science*, 28, 1465-1471

Song, C.H. & Carmichael, G.R. (1999) The aging process of naturally emitted aerosol (sea-salt and mineral aerosol) during long range transport. *Atmospheric Environment*, 33, 2203-2218.

Song, M.; Lee, M.; Moon, K.J.; Han, J.S.; Kim, K.R. & Lee, G. (2006) Chemical characteristics of fine aerosols during ABC-EAREX2005. *Journal of Korean Society for Atmospheric Environment,* 22, 604-613.

Strauss, W. (1975). *Industrial gas cleaning*. pp. 293-3005, Pergamon Press, New York

Tenberken, B. & Bächmann, K. (1996). Analysis of individual raindrops by capillary zone electrophoresis. *Journal of Chromatograph A*, 755, 121-126

The standards of China loess and Simulated Asian mineral dust (1998). Sino-Japan Friendship Centre for Environmental Protection (SJC), Available from http://www.china-epc.cn/ japan/index_e.htm

Zhang, D. & Iwasaka, Y. (1998) Morphology and chemical composition of individual dust particles collected over Wakasa bay, Japan. *Journal of Aerosol Sciene*, 29, S217-S218.

Zhang, D. & Iwasaka, Y. (2004) Size change of Asian dust particles caused by sea salt interaction: Measurements in southwestern Japan. *Journal of Geophysical Research*, 31, L15102, doi:10.1029/2004GL020087.

Zhang, D.; Iwasaka, Y.; Shi, G.; Zang, J.; Matsuki, A. & Trochkine, D. (2003) Mixture state and size of Asian dust particles collected at southwestern Japan in spring 2000. *Journal of Geophysical Research*, 108, 4760, doi:10.1029/2003JD003869.

13

Genetic Biomarkers Applied to Environmental Air Quality: Ecological and Human Health Aspects

Vera Maria Ferrão Vargas,
Kelly Cristina Tagliari de Brito and Mariana Vieira Coronas
Programa de Pesquisas Ambientais,
Fundação Estadual de Proteção Ambiental Henrique Luís Roessler (FEPAM)
Programa de Pós-graduação em Ecologia,
Universidade Federal do Rio Grande do Sul
Brazil

1. Introduction

Exposure to air pollutants may cause health risks leading to acute respiratory infections, cancer, chronic respiratory and cardiovascular diseases. In 2008, IARC/WHO (International Agency for Research on Cancer/World Health Organization) estimated 12.4 million new cases and 7.6 million deaths from cancer worldwide (WHO, 2009). The highest rate of occurrence was of lung cancer (1.52 million new cases), which was the main cause of death of 1.31 million people. For South and Central America and the Caribbean, in 2008, about one million new cases of cancer and 589 thousand deaths were estimated.

In Brazil, estimates for 2010, also valid for 2011, indicate 489,270 new cases of cancer, and lung cancer was the third most frequent in males (18/100,000) and the fifth in females (10/100,000). However, the rates of occurrence per region for malignant neoplasms of the trachea, bronchi and lungs indicate major variations in the different Brazilian states. For 2010, the highest rates were estimated for Rio Grande do Sul both for males (48.33/100,000) and for females (21.43/100,000) These estimates increased compared to 2003 (46.90/100,000, in males and 16.80/100,000 in females), in this state (Brasil, 2003, 2009).

Although the major causes for the increases of cancer incidence include lifestyle, personal habits and diet, the role of environmental changes caused by the industrial activities favoring the release of chemicals into the environment, polluting air, water, soil and potentially contaminating the food should be considered (Brasil, 2009; WHO, 2009; Yu, 2001). The habit of smoking is the most important risk factor for the development of lung cancer. Compared to non-smokers, smokers are about 20 to 30 times more at risk of developing lung cancer. Generally the rates of occurrence in a given country reflect its cigarette use.

Epidemiological studies indicate that other major risk factors for lung cancer are repeat lung infections, a history of tuberculosis and exposure to certain chemicals mainly found in the occupational environment, such as asbestos, arsenic, beryllium, radon, a radioactive gas, nickel, cadmium and vinyl chloride. In addition there is air pollution, especially exposure to

polycyclic aromatic hydrocarbons (PAHs) and diesel oil smoke, from motor vehicles and industry, and to fine and ultrafine airborne particles. The size and composition of these particles determine their behavior in the respiratory system and the time of residence in the environment (Brasil, 2009; Pagano et al., 1996; Pope III et al., 1995, 2002).

The effects of hazardous substances on the population are expressed after a long period of exposure, making it difficult to take preventive action which will allow reverting or reducing risks. In this context, sensitive methodologies, such as biomarkers, allow defining early biological effects after exposure to environmental toxins (Van der Oost et al., 2003).

Genotoxicity biomarkers have been considered sensitive to the early diagnosis of hazardous compounds, their dispersion routes and potential risks to organisms from different ecosystems including damage to human health. In addition, these assays allow evaluating the effect of interactions between the substances present in the atmospheric compartment. This gives particular characteristics to the mixtures formed (Claxton et al., 2004). The distribution of these mixtures in the environment depends on their physical and chemical properties. Their dispersion and deposition may contaminate soils, rivers, dust and plants and affect different organisms, populations and communities, even far from the original sources. Grantz et al. (2003) highlight its effects on vigor, competitive viability and reproductive fitness at the individual level, with subsequent impacts on the ecosystem structure, function and biodiversity.

The presence of mutagenic compounds in organic extracts of airborne particles was reported for the first time in 1975, and since then research worldwide has sought to quantify, characterize and indicate sources of emission, besides the risk of exposure to air pollutants. Most of these studies investigating mutagenic and carcinogenic properties in urban air reported positive responses (Claxton et al., 2004; Claxton & Woodwall Jr., 2007). Claxton et al. (2004) reviewed the literature for studies that used the *Salmonella*/microsome assay and its variations in urban air samples. This assay represents majority of ambient air mutagenesis literature (Claxton & Woodwall Jr., 2007), it is an useful assay to compare genotoxicity among different locations and conditions (Claxton et al., 2004). The *Salmonella* assay is useful to evaluate complex mixtures influenced by different and diffuse sources, such as the atmospheric compartment. Besides, the associated responses of different strains and the presence of the mammal metabolization fraction *in vitro* (S9 fraction) obtained in this assay, indicate the classes of compound found in the samples.

FEPAM (Fundação Estadual de Proteção Ambiental, state of Rio Grande do Sul, RS, Brasil) has been developing a research program on mutagenic activity in air samples in urban and industrial areas of Rio Grande do Sul, Brazil using the *Salmonella*/microsome assay as a specific marker of the presence of these compounds adsorbed to the particulate matter in the air and its carcinogenic potential. This assay evaluates molecular mutagenic damage, and these changes result in specific genetic markers that allow measuring the presence of agents aggressive to DNA by means of the effect. The international validation and constant improvement include this biomarker in the set of tests that define the potential of genotoxic carcinogenic organic compounds (Brambilla & Martelli, 2009; Claxton et al., 2004; Kado et al., 1986; Maron & Ames 1983).

Because of the complex system that forms the airborne particulate matter and inter-individual variability in exposure, no safe threshold or no main component of these air pollutants can be established below which adverse effects do not occur (WHO, 2006). Studies associating emissions sources, mutagenic activity and chemical characterization of airborne particulate matter help to understand the effects of pollutants. Also, they can

provide better assessment for regulatory agencies to establish more restrictive, safer concentrations of the main biologically active components.
This chapter will emphasize the use of genetic damage biomarkers as early indicators for mainly organic atmospheric pollution and highlight their sensitivity and applicability for areas under different anthropic influences; to compare the mutagenic responses with the particulate matter concentration, a parameter used in different air quality standards; and finally discuss the biological effects observed in assays using samples of different particulate matter size (total suspended particles, TSP, and particles less than 10μm, PM10 and less than 2.5 μm).

2. Airborne particulate matter

Particulate matter (PM) is a complex heterogeneous mixture of extremely small particles and liquid droplets having diverse chemical and physical characteristics. PM is made up of a number of components of solid and liquid particles of organic and inorganic substances suspended in the air, including acids (such as nitrates and sulfates), organic chemicals, metals, and soil or dust particles. The potential of particles to cause health problems varies with size and other physical characteristics, chemical composition and sources.
The particles are identified generally according to their aerodynamic diameter because these determine transport and removal processes in the air and deposition sites and clearance pathways within the respiratory tract. PM has been classified as either TSP (total suspended particulate matter smaller than 100 micrometers in diameter) or PM10 (particles with an aerodynamic larger than 2.5 micrometers and smaller than 10 micrometers in diameter) or PM2.5 (aerodynamic diameter smaller than 2.5 μm) and ultrafine particles, those smaller than 0.1 μm (100 nm).
The inhalable coarse particles (PM10), such as those found near roadways and dusty industries, are the particles that generally pass through the throat and nose and enter the lungs. Once inhaled, these particles can affect the heart and lungs and cause serious health effects. Fine particles (PM2.5), such as those found in smoke and haze, can be directly emitted from sources such as forest fires, or formed from gases from power plants, industries and automobiles. PM2.5 particles are dangerous since, when inhaled, they may reach the peripheral regions of the bronchioles, and interfere with gas exchange inside the lungs.
International and regulating agencies establish limits or recommendations for the different particles. The World Health Organization Air Quality Guidelines (WHO, 2006) recommend more restrictive values for PM10 (50 $\mu g/m^3$, 24 hour mean and 20 $\mu g/m^3$ annual mean) and PM2.5 (25 $\mu g/m^3$, 24 hour mean and 10 $\mu g/m^3$ annual mean). Other publications present staggered targets for particle reduction (Official Journal the European Union, 2008), or defined threshhold values (USEPA, 2008). In Brazil, total suspended particulate (TSP) (240-150 $\mu g/m^3$ 24h mean and 80-60 $\mu g/m^3$ annual mean) and particulate matter less than 10 μm in diameter (PM10) (150 $\mu g/m^3$ 24 h mean and 50 $\mu g/m^3$ annual mean) are regulated by the National Council of the Environment (Brasil, 1990).

3. *Salmonella*/microsome assay

The basic mechanism of the test is to determine changes in the DNA molecule, caused by reverse mutations for prototrophy, using *S. typhimurium* mutants to assess the mutagenic

activity and the carcinogenic potential of chemicals. The indicator strains present different mutations in the histidine *operon*, selected to detect substances that are able to generate base pair substitution or frameshift mutation.

Strains derived from the classical TA98 and TA100 were developed bearing a deficiency in a classical nitroreductase (NR strains) or in an *O*-acetyltransferase (1.8-DNP6 strains) (Rosenkranz et al., 1980; Rosenkranz, 1996), enabling the diagnosis of the presence of mononitro and dinitroarenes, respectively. Watanabe et al. (1989, 1990) developed a series of YGs strains with similar properties – YG1021 (pYG216), YG1024 (pYG219), YG1026 (pYG216), YG1029 (pYG219) – but presenting high enzymatic production. The genes of classical nitroreductase (pYG216) and of *O*-acetyltransferase (pYG219) are inserted in the plasmids, conferring high enzymatic activity and greater sensitivity for nitrocompounds, such as nitroarenes or dinitroarenes, hydroxyamine-compounds and aromatic amines, respectively (Watanabe et al., 1989, 1990).

The assay may be performed by various procedures, the most widely used being plate-incorporation, pre-incubation and microsuspension, which presents a 5 to 10 times higher sensitivity than the traditional Ames test (Kado et al., 1983; Maron & Ames, 1983; Mortelmans & Zeiger, 2000). The test is performed in the presence and absence of an *in vitro* system of metabolic activation, the most commonly used being the microsomal fraction – S9. The S9 was composed of a homogenate from cells of the livers of *Sprague-Dawley* rats pre-treated with a polychlorinated biphenyl mixture (Aroclor 1254) to induce an increase in the P-450 enzymes.

4. Study cases in urban and industrial areas

Our research group in Rio Grande do Sul (RS), Brazil, performed studies to assess the mutagenic activity of air samples in regions under different anthropic influences. Several sites were investigated, ranging from regions with urban predominance such as Porto Alegre, the capital of RS, an area in Triunfo, RS, under the influence of a petrochemical industry, and another where oil industry contaminants predominate, located in an urban residential area in Esteio, RS (Figure 1).

Total airborne particulate matter (TSP, particles <100 μm) samples were collected on Fiberglass filters (AP40-810, 20 cm × 25 cm Millipore) using high-volume sampler (General Metal Works Inc.). Airborne particulate matter less than 10 μm (PM10) and less than 2.5 μm (PM2.5) samples were collected on Teflon® filters (TX40HI20WW, 254 mm × 203 mm) using a high-volume collector (AVG MP10, 1200/CCV) for 24 hours. The filters were weighed and stabilized before and after sampling (45% humidity) to calculate the TSP, PM10 or PM2.5 values expressed in units of $\mu g/m^3$ of sampled air.

Half of each filter was used for the extraction of the organic compounds, pooled or extracted separately according to the study objectives. Each pooled or simple sample was submitted to extraction by sonication with dichloromethane (DCM, CASRN. 75-09-2) (Vargas et al., 1998). Dichloromethane extracts the moderately polar compounds and is the most representative fraction of mutagenic activity (De Martinis et al., 1999) extracting a wide range of compounds from airborne particulate matter. DCM is preferred when the investigator did not want to extract non-organic components that would be toxic to the bacteria used in the assay (Claxton et al., 2004; Marvin & Hewitt, 2007). The percentage of extractable organic matter (EOM%) was calculated, and the mass obtained was compared to half the volume of air sampled (EOM in $\mu g/m^3$), since half the filters were used. Prior to

bioassay performance, the organic extract was dried with gaseous nitrogen and resuspended in dimethyl sulfoxide (DMSO, CASRN. 67-68-5).

Fig. 1. Location of studied sites in the Porto Alegre metropolitan area, Rio Grande do Sul, Brazil.

The different fractions were tested for mutagenicity using the microsuspension method with *Salmonella typhimurium* strains TA98–S9 and TA98+S9 to detect frameshift mutagens; TA98NR and TA98/1,8-DNP6 (TSP samples) or the YG1021 or YG1024 (PM10 and PM2.5 samples) to detect the presence of mononitro, hydroxyamine-compounds and aromatic amines (Kado et al., 1986; Maron & Ames, 1983; Rosenkranz, 1996; Rosenkranz et al., 1980; Watanabe et al., 1989, 1990). The assay response was considered a significant effect when the number of *his*$^+$ revertants per plate observed was double that of the spontaneous yields observed in the negative control, a significant ANOVA ($p \leq 0.05$) accompanied by a significant dose-response curve ($p \leq 0.05$). The significance of linear regressions from the dose–response curves was evaluated by SALANAL software (Salmonella Assay Analysis, version 1.0, Integrated Laboratory Systems of Research Triangle Institute, RTP, North

Caroline, USA) choosing the linear or Bernstein model (Bernstein et al., 1982). The positive responses were expressed as the number of revertants based on volume of air sampled (rev/m^3).

4.1 Mutagenic activity of particulate matter in the urban area of Porto Alegre

Airborne particulate matter was investigated in the city of Porto Alegre (1.420,000 million inhabitants), capital of the RS state, in southern Brazil, 110 km from the coast, at an altitude of approximately 10m (Figure 1). Studies in different areas of the city, airborne size fractions and periods were performed by our research group (Ducatti & Vargas, 2003; Vargas et al., 1998; Vargas, 2003). The area located in the Botanical Gardens District (30°03'12"S, 51°10'29"W) about 1 km from an avenue with traffic ranging from 72,000 to 120,000 vehicles/day during the studied periods, far from large industrial areas was selected to evaluate the mutagenicity of an urban area. This area has unpublished studies performed during 2006 and 2010.

The studies reported were performed during three different periods using different particulate matter sizes: TSP (first period), Summer (December) of 1994 (Vargas et al., 1998), Spring (October) and Summer (December) of 1997 (Ducatti & Vargas, 2003; Vargas, 2003); PM10 (second period), Spring (October/November) and Summer (December) of 2006; PM2.5 (third period), Winter (August) and Spring (September/October) of 2010 (Table 1).

The first studies evaluated TSP (Ducatti & Vargas, 2003; Vargas et al., 1998; Vargas, 2003), and negative results were observed in most of the samples (Figure 2). The concentration of TSP particles agreed with what was expected for the area according to the institutional monitoring of air quality standards and below the legally established limit for Brazil (ranging from 17 to 60 μg/m^3 for October and December, respectively). Mutagenic frameshift responses were observed in December/1997 (4.23 rev/m^3), the highest TSP value, previously characterized as negative for mutagenicity.

Particle fraction (Study year)	Period of sampling	Particle concentration (μg/m^3)	Mean Particle concentration (μg/m^3)
TSP (1994)	December	41	Single filter sample
TSP (1997)	October	17	Single filter sample
	December	60	Single filter sample
PM10 (2006)	October	15	15
	November	24; 37	30.5
	December	76; 14	45
PM2.5 (2010)	August	11; 61; 34	35.3
	September	5; 14; 12; 16	11.7
	October	41; 6; 22	23

Table 1. Urban area: particle fraction, period of sampling and particle concentration.

In second period for PM10, all samples showed positive mutagenic responses and a gradient was observed between the lower and higher values of PM10 concentration (15 to 76 μg/m³) and mutagenic activity. The concentration value of PM10 in December surpassed the limit recommended by WHO (WHO, 2006). The lowest and the highest values were observed in October (TA98-S9, 1.33 ± 0.30 rev/m³; TA98+S9, 0.91 ± 0.14 rev/m³) and December samples (TA98-S9, 17.95 ± 1.37 rev/m³; TA98+S9, 10.36 ± 0.52 rev/m³), respectively (Figure 2). Mutagenic activity decreased in the presence of S9 mix, and this response indicated that the predominant compounds present in the organic particulate matter were direct-acting mutagens. All samples showed increased responses for YGs strains, especially YG1021, indicating that nitroarenes predominated in these samples (Coronas, 2008).

In third period for PM2.5, all the samples showed positive responses for TA98, the highest being obtained without S9. The highest frameshift mutagenicity values expressed in revertants/m³ were found in August pool samples (Figure 2). In one of the filters of this and October pool, the concentration value of PM2.5 surpassed the limit recommended by WHO (WHO, 2006), reaching the value of 61 and 41 μg/m³, respectively (Table 1). On the other hand, the lowest value observed in the study was 5 μg/m³, in one of the September pool filters. The elevation of the mutagenic responses shown by the YG strains indicated the participation of nitro-PAHs in direct mutagenic responses, as well as the presence of hydroxylamine compounds detected by the YG1024 strain (unpublished data).

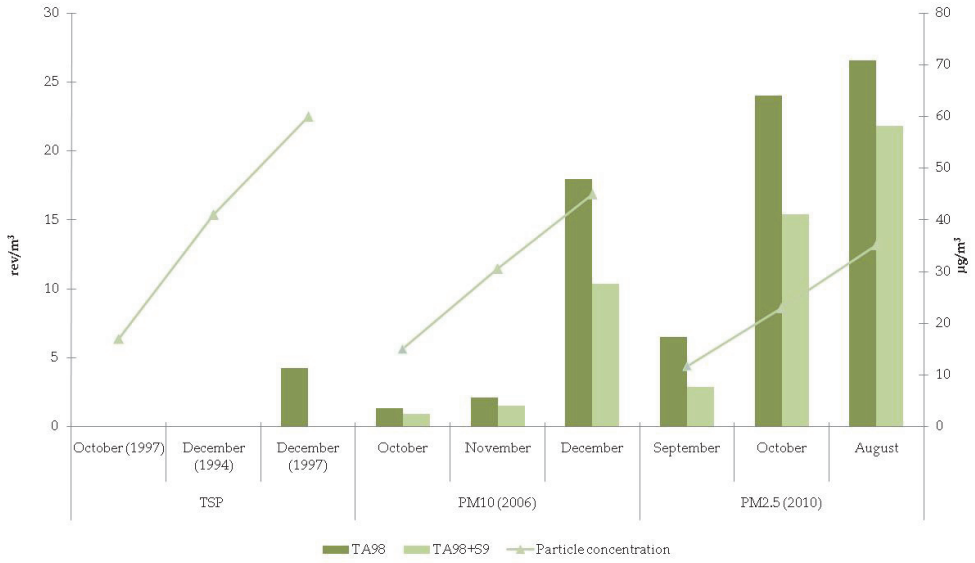

Fig. 2. Mutagenic activity of organic airborne particulate matter extracts evaluated by the *Salmonella*/microsome assay for TA98 strain (revertants/m³) in Porto Alegre urban area ordered by TSP, PM10 or PM2.5 mean concentrations (μg/m³). −S9, +S9, absence, presence of S9 mix fraction. TSP samples were not evaluated in the presence of S9.

4.2 Mutagenic activity of particulate matter in industrial areas

4.2.1 Petrochemical area

An area under the influence of a petrochemical complex situated in the town of Triunfo, RS, in southern Brazil (Figure 1), was studied at different times for mutagenicity of organic compounds adsorbed in TSP and PM10 (Coronas et al., 2008; Vargas, 2003). This station is 6.1 km away from the main smokestack of the central raw material production area of this petrochemical district (benzene, toluene, xylene, ethene, propane and butadiene), located in the main atmospheric dispersion quadrant of this complex and 1.4 km from a federal highway (29°49'35"S, 51°24'56"W). This area (14,600 ha) is 30 km upstream from Porto Alegre, in a mixed rural, urban and industrial area.

The study was performed in two periods (TSP and PM10) subdivided into eleven samplings. The first period for TSP during the winter (July and August) and spring (November) months of 1995 and three pools during different stations (January to April; May to August; September to December) of 2000; and the second for particles less than 10 μm (PM10) during summer (February), fall (April), winter (June, July, August) and spring (November) months of 2005. The particles concentration for both TSP and PM10 were within Brazilian air quality standards, although the sampling of the November/2005 pool presented values above those recommended by WHO (WHO, 2006) in almost all filters samples (Table 2).

Particle fraction (Study year)	Period of sampling	Particle concentration (μg/m³)	Mean Particle concentration (μg/m³)
TSP (1995)	July - August	52; 41; 86	59.7
	November	56; 92	74
TSP (2000)	January - April	31; 27; 38; 51	36.8
	May - August	13; 14; 57; 17	25.3
	September - December	8; 38; 31; 38	28.8
PM10 (2005)	February	11; 34; 25; 24	23.5
	April	28; 19; 31	26
	June	46; 44; 10; 9; 37	29.2
	July	27; 26	26.5
	August	28; 20; 41; 10; 23	24.4
	November	35; 111; 88; 71; 58	72.6

Table 2. Petrochemical area: particle fraction, period of sampling and particle concentration.

All samples evaluated were positives for frameshift mutagens, and the results were generally higher in PM10 than TSP. The highest mutagenic activity was detected for TSP in the 1995 samplings and for PM10 in the July/2005 monthly pool (Figure 3). Mutagenicity for organic extracts of TSP and PM10 samples in rev/m³, showed no relationship with the largest TSP and PM10 magnitudes (μg/m³), thus mutagenic activity

was not directly related to particle concentration. Hence, the increase of this mutagenic induction is a consequence of the specific danger classes of compounds adsorbed in the airborne particulate matter. Figure 3 shows the data in growing order of concentration values of TSP and PM10 in μg/m³.

Most of the samples presented higher responses in assays in the absence of S9 mix metabolization. Studies with nitrosensitive strains performed by Coronas et al. (2008), indicate a significant contribution of nitro and amino derivatives of PAHs to the total mutagenicity of suspended particulates (Apel et al., 2010). In fifty percent of the cases, the nitrosensitive strains were more sensitive for mononitrocompounds or for dinitrocompounds.

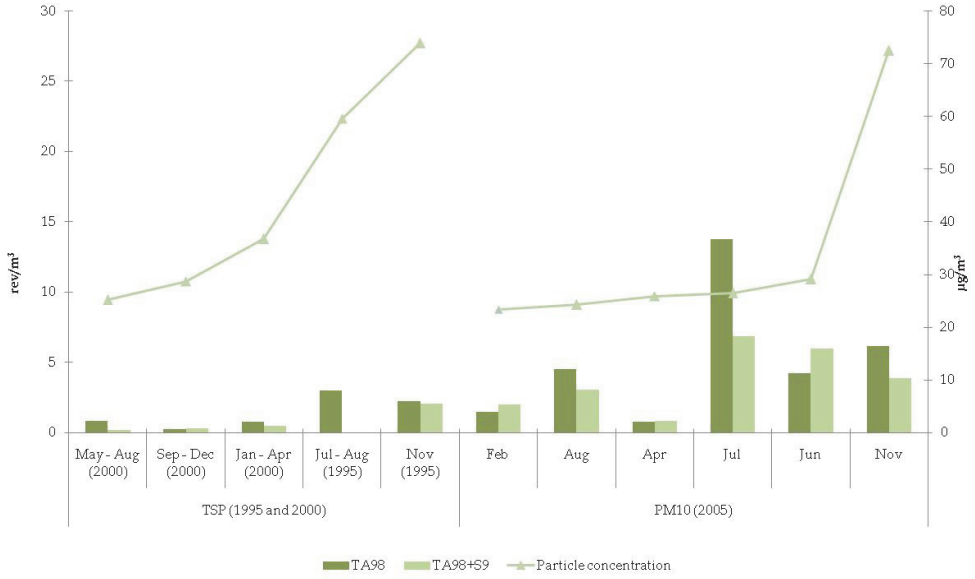

Fig. 3. Mutagenic activity of airborne samples evaluated by the *Salmonella*/microsome assay for TA98 strain (revertants/m³) in Triunfo in an area under the influence of a petrochemical complex ordered by TSP, or PM10 mean concentrations (μg/m³). −S9, +S9, absence, presence of S9 mix fraction.

4.2.2 Oil refinery area

An urban/residential area (29°51'29"S; 51°09'25"W) under the influence of an oil refinery plant was assessed for mutagenicity in airborne particulate matter (Coronas et al., 2009). The refinery is located in the city of Canoas (324,000 inhabitants), close to the region that borders on the neighbour municipality, Esteio (Figure 1). In this area PM10 samples were collected weekly from October to December 2006. The collector was placed in the town of Esteio (80,700 inhabitants), Rio Grande do Sul state, in southern Brazil. The dominant winds there are from the Southeast, and therefore Esteio is most influenced by the plant, and the PM10 collector was installed at a site predisposed to particle deposition. Two automatic stations from the Rio Grande do Sul Environmental Protection State Foundation (FEPAM) measure

PM10, SO_2, NO_X, O_3, CO and meteorological parameters continuously. PM10 organic extracts were also quantified for 16 United States Environmental Protection Agency (EPA) priority polycyclic aromatic hydrocarbons: naphthalene, acenaphthylene, acenaphthene, fluorene, phenanthrene, anthracene, fluoranthene, pyrene, benzo[a]anthracene, chrysene, benzo[b]fluoranthene, benzo[k]flouranthene, benzo[a]pyrene, dibenzo(ah)anthracene, benzo[ghi]perylene, and indeno(1,2,3-cd)pyrene.

During the period studied the concentration of PM10 particles ranged from 9 to 62 μg/m³ (Table 3), and the latter concentration was the only one that surpassed the values recommended by WHO (WHO, 2006). All samples showed positive responses for mutagenesis for TA98 strain (Figure 4).

Particle fraction (Study year)	Period of sampling	Particle concentration (μg/m³)	Mean Particle concentration (μg/m³)
PM10 (2006)	October 1	9; 23	16.0
	October 2	62; 27	44.5
	November 1	19; 46	42.0
	November 2	14; 20	17.0
	November - December	15; 37	26.0
	December	47; 40	43.5

Table 3. Oil Refinary area: particle fraction, period of sampling and particle concentration.

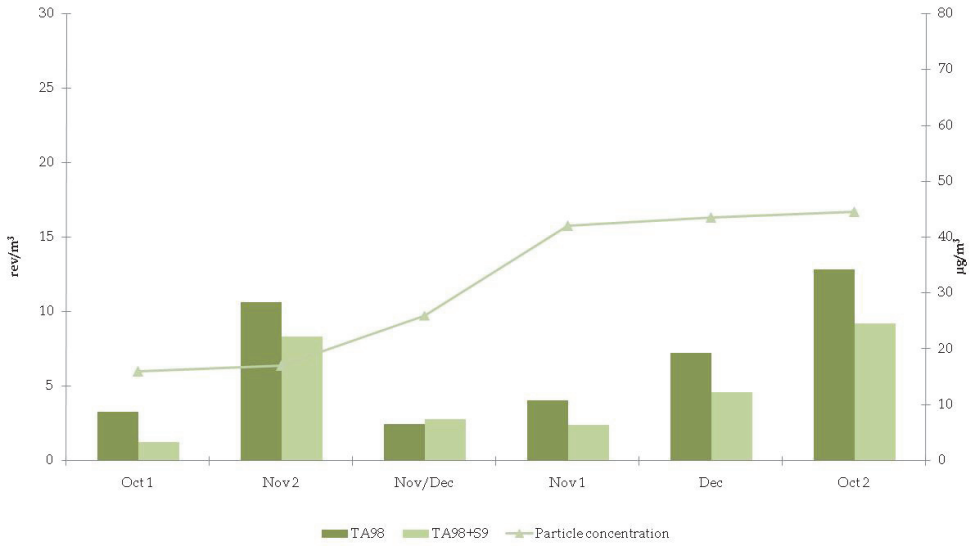

Fig. 4. Mutagenic activity of airborne samples evaluated by the *Salmonella*/microsome assay for TA98 strain in an urban area under the influence of oil refinery plant ordered by PM10 mean concentrations (μg/m³). −S9, +S9, absence, presence of S9 mix fraction.

For most of the samples, the mutagenic activity decreased in the presence of S9 mix, except for Nov/Dec which increased slightly. This response indicated that the predominant compounds present in the organic particulate matter were direct-acting mutagens. All samples showed increased response for mutagenic activity for the YGs nitrosensitive strains (Coronas et al., 2009), indicating the presence of nitrocompounds in the evaluated sites, with preponderance of results involving the YG1024 strain. The PAHs content is shown in figure 5. Sample Oct 2 showed the highest PAHs concentrations and also the highest mutagenicity response. Indeno(1,2,3-cd)pyrene and Benzo(g,h,i)perylene showed higher concentrations than the other PAHs in all samples. Eight of the 16 PAHs analyzed are classified by The International Agency for Research on Cancer (IARC, 2010) as group 1 (carcinogenic to humans: benzo[a]pyrene), group 2A (probably carcinogenic to humans: dibenzo(ah)anthracene) or group 2B (possibly carcinogenic to humans: naphthalene, benzo[a]anthracene, chrysene, benzo[b]fluoranthene, benzo[k]flouranthene, indeno(1,2,3-cd)pyrene). In these samples the carcinogenic PAHs represented more than 66% of the total PAHs concentration (Figure 6).

All samples showed an increased response for mutagenic activity for the YGs strains, indicating the presence of nitrocompounds in the evaluated site (Coronas et al., 2009). Strain YG1024 produced higher values of revertants/µg of EOM in five of the six samples, while at site 2, in an urban area, strain YG1021 showed higher values in most of the samples.

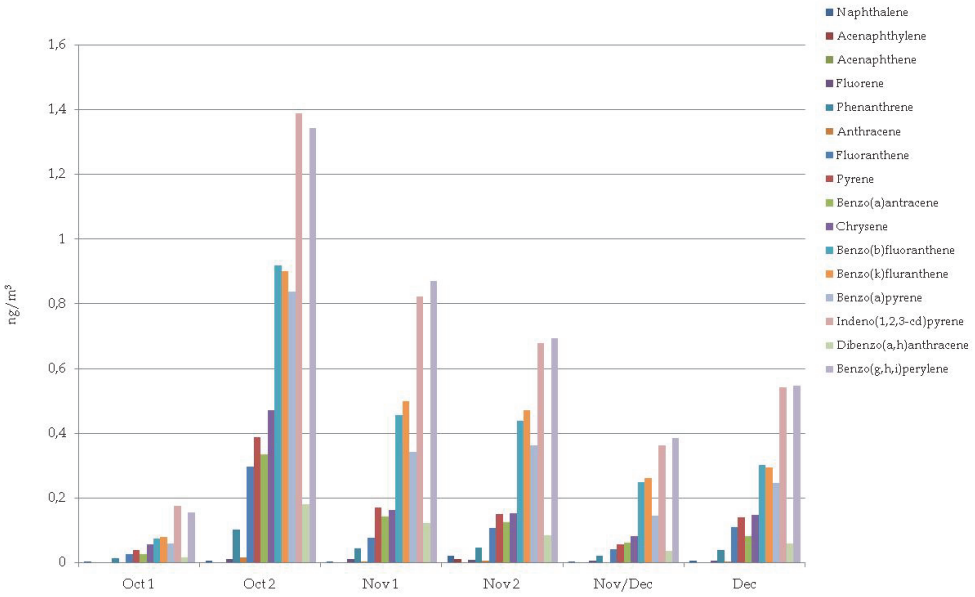

Fig. 5. PAH concentrations (ng/m^3) in PM10 samples from an urban area under the influence of oil refinery plant.

DNA damage in people residing and/or working downwind from this oil refinery was investigated (Coronas et al., 2009). Samples of peripheral blood, buccal mucosa and PM10 were simultaneously collected and evaluated using the comet, micronucleus and

Salmonella/microsome assays, respectively. The subjects showed significantly increased DNA damage in lymphocytes detected by the comet assay and no difference in the frequencies of micronucleated buccal mucosa cells. These genetic lesions were not associated with the tobacco smoking habit, age and recent exposure to X-ray for diagnosis.

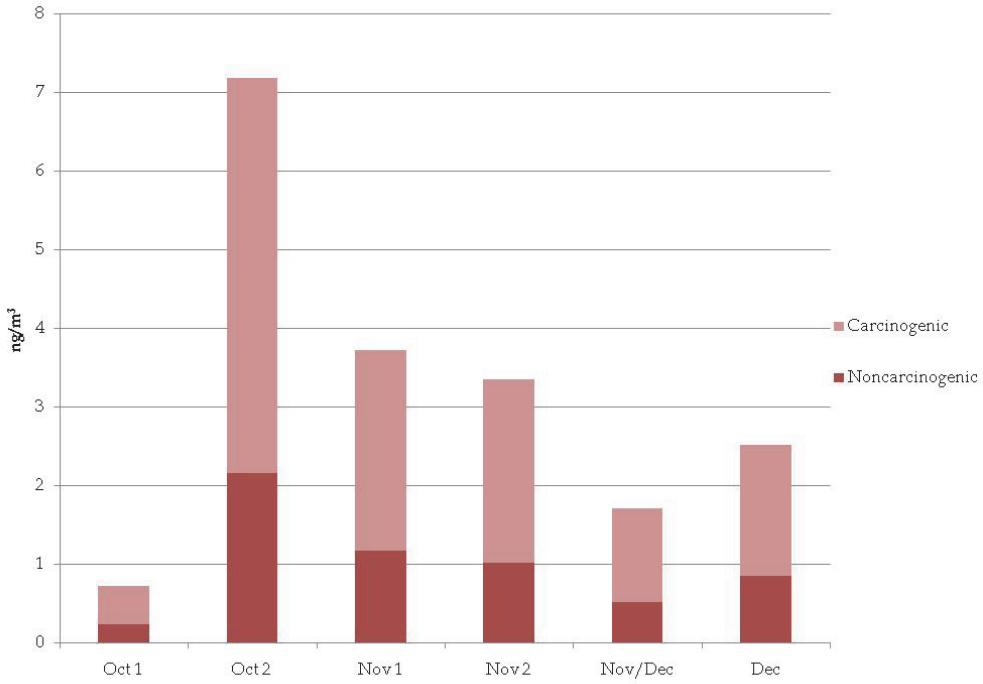

Fig. 6. Concentrations of potentially carcinogenic PAHs (ng/m^3) according to IARC (2010) in PM10 samples from an urban area under the influence of oil refinery plant.

4.3 Discussion

The case studies showed the mutagenicity of TSP, PM10 or PM2.5 DCM-fraction in the urban area of Porto Alegre city and in two industrial regions. One of these areas was under the specific influence of a petrochemical industry and another was influenced by contaminants from an oil refinery, but inserted in an urban area.

The site studied in Porto Alegre city had been used as a reference for the urban area (RS, Brazil) presenting absence or low mutagenic activity in previous studies (Ducatti & Vargas, 2003; Vargas et al., 1998). These studies evaluated TSP organic extracts, which might account for the low mutagenic response, since the lowest particle fractions concentrate organic and mutagenic compounds (Hayakawa et al., 1995; Pagano et al., 1996). An increase in mutagenic induction was observed, generally, for the PM10 and PM2.5 DCM-extracts as the particle diameter diminishes. However, is necessary to

consider that traffic of motor vehicles increased during this new period of diagnosis. Other studies detected the 16 most important PAHs in PM10 at this site (Dallarosa et al., 2005). Just as the capacity to penetrate more deeply into the respiratory tract rises with the decreased diameter of the particle, increased mutagenic activity is also reported in the literature (Claxton et al., 2004).

The studies in urban area appear to indicate a trend between the concentration of TSP, PM10 and PM2.5 and intensity of the mutagenic effect observed. However, this evidence was not clearer in industrial areas. The increase of the mutagenic induction in these areas can be a consequence of the specific hazard classes of compounds adsorbed in the airborne particulate matter.

Although, most concentrations of particulate matter are in accordance with the primary and secondary standards for atmospheric particulate matter TSP and PM10 in Brazil (Brasil, 1990), the different studies showed that the *Salmonella*/microsome assay was sensitive to define areas contaminated by mutagenic compounds (Coronas et al., 2008; Coronas et al., 2009; Ducatti & Vargas, 2003; Pereira et al., 2010; Vargas, 2003).

However, a concentration of 150 $\mu g/m^3$ (Brazilian legal standards for 24 hour-mean) is related to an approximately 5% increase in daily mortality according to the World Health Organization (WHO, 2006). A more restrictive value (50 $\mu g/m^3$ 24 hour-mean) for PM10 concentration is suggested by WHO air quality guidelines to decrease adverse health effects. In the present study, three pools presented filters with values higher than this standard (WHO, 2006): one in an urban area and two pools in areas under industrial influence. For PM2.5 our results showed that one sampling suppressed WHO air quality guidelines (2.5 $\mu g/m^3$ 24 hour-mean) (WHO, 2006).

Approximately half the ambient mutagenicity can be ascribed to atmospheric reaction products of two-to-four-ring PAH. However, PAHs are commonly present in airborne particles and increase mutagenic activity when S9 mix is used (Lewtas, 2007; Claxton et al., 2004), and can explain part of the mutagenic induction observed in these studies. In the area under the influence of the refinery, the presence of PAHs can account for part of the mutagenic activity with S9 mix. In these samplings, 66% of the total concentration of PAHs detected was classified by IARC (IARC, 2010) as potentially carcinogenic. A recently published study of our research group (Pereira et al., 2010) highlighted the presence of carcinogenic PAHs compounds and mutagenic activity in a city located in the main atmospheric dispersion quadrant of a petrochemical industrial complex region (22 km distant), with a long history of mutagenic activity in its atmospheric particulates and water resources (Vargas et al., 2003; Vargas et al., 2008).

Nevertheless, other compounds extracted in the base/neutral fraction (DCM) are responsible for direct mutagenicity in organic samples analyzed by *Salmonella*/microsome assay, for example nitroarenes and aromatic amines (Coronas et al., 2008; Coronas et al., 2009; DeMarini et al., 1994; Pereira et al., 2010; Vargas, 2003; Watanabe et al., 1989; Watanabe et al., 1990). Not all of the mutagenicity can be ascribed to particular compounds, but much of it is due to nitro-PAH lactones and to simpler nitro-PAH (Lewtas, 2007). This supports the importance of co-pollutants in the mutagenic activity of airborne particles. Reactive gases (NO_X, O_3) under photoactive conditions can produce mutagenic compounds from non-mutagenic organic compounds commonly present in ambient air (Claxton et al., 2004). The present comparative study appears to indicate a more significant presence of mononitro compounds in urban areas and dinitro compounds in industrial areas influenced by petrochemical compounds.

5. Conclusions

Salmonella/microsome is the most widely used assay for monitoring mutagenic compounds in airborne particulate matter. Although several mechanisms are associated with cancer due to environmental exposure, the primary event of carcinogenesis by genotoxicity is the mutagenic event. The assay allows modeling carcinogenic potency without identifying all the specific carcinogens present in the mixture, by using strains sensitive to different classes of compounds.

All these results highlight the evidence that the mutagenic activity of airborne particulate matter organic DCM-extracts detects hazardous atmospheric compounds, more closely related to the types and reactivity of compounds adsorbed in airborne particulate matter than to the particle mass. It also indicates that particulate matter concentrations alone do not present sufficiently good air quality standards to avoid damage to the environment and human health. Besides the particulate concentration, the characterization of the present hazardous compounds and the reactivity of the mixture formed by it are essential to support exposure estimates.

Reviews of literature (Claxton et al., 2004; Claxton & Woodwall Jr., 2007) discuss the importance of the results that have already been identified in the *Salmonella*/microsome assay, pointing out that their international standardization and applicability to the definition of the presence of compounds potentially carcinogenic to humans and to define the health risk assessment. Claxton & Woodwall Jr. (2007), present tests in different levels of organisms used to evaluate mutagenic compounds in the air, and emphasize the limitations of some assays regarding mammal responses, such as the metabolic pathways, exposure cycles and extrapolation from observed potency to carcinogenic potency.

Studies in this field of knowledge need to advance with additional work on the mutagenic effects of volatile and semi-volatile organic fractions, metals associated with mutagenic potency and the role of atmospheric transformation in raising the complexity of the samples adsorbed in airborne particulate matter. The chemical identification of compounds in these mixtures is complex. This emphasizes the value of associating biomarkers and chemical analysis, defining the main classes of compounds found in the sample and their dispersion, and predicting effects on ecosystem stability and human health. The integration of *in vitro* and *in vivo* responses complements the understanding of the pathways and action mechanisms of compounds and mixtures. Finally, it is necessary to intensify the efforts in the monitoring of fine particles, such as PM2.5, which concentrate a significant amount of mutagenic substances besides presenting a greater probability of deposition in the smaller conducting airways and alveoli. These studies can favor early measure to protect the environment and human health.

Biological tests like *Salmonella*/microsome assay are a sensitive tool to screen the presence of specific chemical compound classes in environmental monitoring programs to characterize areas under the influence of anthropogenic activities. It should be mentioned that there has been an advance in Brazilian environmental law, in which the state of Rio Grande do Sul included the genotoxic assays, especially *Salmonella*/microsome, to control industrial effluents (CONSEMA, 2006).

6. Acknowledgment

We are grateful to FEPAM's air sampling and quality team for their work. This research was supported by Conselho Nacional de Desenvolvimento Cientifico e Tecnológico (CNPq);

Financiadora de Estudos e Projetos (FINEP) and Aperfeiçoamento de Pessoal de Nível Superior (CAPES).

7. References

Apel, M.A., Coronas, M.V., Rocha, J.A.V. & Vargas, V.M.F. (2010). Análise Exploratória da Incidência de nitronaftalenos no Material particulado Atmosférico em Área de Influência Petroquímica. *J. Braz. Soc. Ecotoxicol*., Vol. 5, No. 1, pp. 55-62.

Bernstein, L., Kaldor, J., McCann, J. & Pike, M.C. (1982). An empirical approach to the statistical analysis of mutagenesis data from the Salmonella test. *Mutation Research*, Vol. 97, pp. 267–281.

Brambilla, G. & Martelli, A. (2009). Update on genotoxicity and carcinogenicity testing of 472 marketed pharmaceuticals. *Mutation Research*, Vol. 681, pp. 209–229.

Brasil, Conselho Nacional do Meio Ambiente. Resolução CONAMA n◦ 003. (28 June 1990). *Padrões Nacionais de Qualidade do Ar,* Diário Oficial da República Federativa do Brasil, pp. 15937–15939, Brasília.

Brasil, Ministério da Saúde, Secretaria Nacional de Assistência à Saúde, Instituto Nacional do Câncer. (2003). *Estimativas da incidência e mortalidade por câncer no Brasil*, Rio de Janeiro, Retrieved from <http://www.inca.gov.br>.

Brasil, Ministério da Saúde, Secretaria Nacional de Assistência à Saúde, Instituto Nacional do Câncer. (2009). *Estimativa 2010: incidência de câncer no Brasil,* Rio de Janeiro, Retrieved from <http://www.inca.gov.br>.

Claxton, L.D., Matthews, P. & Warren, S. (2004). The genotoxicity of ambient outdoor air, a review: Salmonella mutagenicity. *Mutation Research*, Vol. 567, pp. 347–399.

Claxton, L.D. & Woodall Jr, G.M. (2007). A review of the mutagenicity and rodent carcinogenicity of ambient air. *Mutation Research*, Vol. 636, pp. 36-94.

Coronas, MV. (2008). *Biomonitoramento de populações humanas em áreas de exposição a poluentes atmosféricos mutagênicos.* Universidade Federal do Rio Grande do Sul. Instituto de Biociências. Programa de Pós-Graduação em Ecologia, Porto Alegre, Retrieved from <http://hdl.handle.net/10183/13649>.

Coronas, M.V., Horn, R.C., Ducatti, A., Rocha, J.A.V. & Vargas, V.M.F. (2008). Mutagenic activity of airborne particulate matter in petrochemical industrial area. *Mutation Research*, Vol. 650, pp. 196-201.

Coronas, M.V., Pereira, T.S., Rocha, J.A.V., Lemos, A.T., Fachel, J.M.G, Salvadori, D.M.F. & Vargas, V.M.F. (2009). Genetic biomonitoring of an urban population exposed to mutagenic airborne pollutants, *Environment International*, in press, doi:10.1016/j.envint.2009.05.001.

Dallarosa, J.B., Monego, J.G., Teixeira, E.C., Stefens, J.L. & Wiegand, F. (2005). Polycyclic aromatic hydrocarbons in atmospheric particles in the metropolitan area of Porto Alegre, Brazil. *Atmospheric Environment*, Vol. 39, pp. 1609-1625.

DeMarini, D.M., Shelton, M.L. & Bell, D.A. (1994). Mutation spectra in Salmonella of complex mixtures: comparison of urban air to benzo[a]pyrene. *Environmental and Molecular Mutagenesis*, Vol. 24, pp. 262–275.

De Martinis, B.S., Kado, N.Y., Carvalho, L.R.F., Okamoto, R.A. & Gundel, L.A. (1999). Genotoxicity of fractionated organic material in airborne particles from São Paulo, Brazil. *Mutation Research*, Vol. 446, pp. 83-94.

Ducatti, A. & Vargas, V.M.F. (2003). Mutagenic activity of airborne particulate matter as an indicative measure of atmospheric pollution. *Mutation Research,* Vol. 540, pp. 67-77.

Grantz, D.A., Garner, J.H.B. & Johnson, D.W. (2003). Ecological effects of particulate matter. *Environ. Int.*, Vol. 29, pp. 213-239.

Hayakawa, K., Kawaguchi, Y., Murahashi, T. & Miyazaki, M. (1995). Distribution of nitropyrenes and mutagenicity in airborne particulates collected with an Andersen sampler. *Mutation Research,* Vol. 348, pp. 57-61.

IARC, International Agency For Research On Cancer. (2010). *Monographs, Supplement.* Retrieved from <http://monographs.iarc.fr/ENG/Classification/index.php>.

Kado, N.Y., Langley, D. & Eisenstadt, E. (1983). A simple modification of the Samolnella liquid-incubation assay. Icreased sensitivity for detecting mutagens in human urine. *Mutation Research*, Vol. 121, pp. 25-32.

Kado, N.Y., Guirguis, G., Flessel, C., Chan, R., Chang, K. & Wesolowski, J. (1986). Mutagenicity of fine (less than 2.5 microns) airborne particles: diurnal variation in community air determined by a Salmonella micro preincubation (microsuspension) procedure. *Environmental Mutagenesis*, Vol. 8, pp. 53-66.

Lewtas, J. (2007). Air pollution combustion emissions: characterization of causative agents and mechanisms associated with cancer, reproductive, and cardiovascular effects. *Mutation Research*, Vol. 636, pp. 95-133.

Maron, D.M. & Ames, B.N. (1983). Revised methods for the Salmonella mutagenicity test. *Mutation Research*, Vol. 113, pp. 173-215.

Marvin, C.H. & Hewitt, L.M. (2007). Analytical methods in bioassay-directed investigations of mutagenicity of air particulate material. *Mutation Research*, Vol. 636, pp. 4-35.

Mortelmans, K. & Zeiger, E. (2000). The Ames Salmonella/microsome mutagenicity assay. *Mutation Research*, Vol. 455, pp. 29-60.

Official Journal of the European Union. (21 May 2008). Directive 2008/50 CE of the European Parliament and Council of on ambient air quality and cleaner air for Europe. L152/1–L152/44. pp. 1-44.

Pagano, P., Zaiacomo, T., Scaecella, E., Bruni, S., Calamosca, M. (1996). Mutagenic activity of total and particle-sized fractions of urban particulate matter. *Environ. Sci. Techn.*, Vol. 30, No. 12, pp. 3512-3516.

Pereira, T.S., Gotorb, G.N., Beltramia, L.S., Nollab, C.G., Rocha, J.A.V., Brotob, F.P., Comellasb, L.R. & Vargas, V.M.F. (2010). Salmonella mutagenicity assessment of airborne particulate matter collected from urban areas of Rio Grande do Sul State, Brazil, differing in anthropogenic influences and polycyclic aromatic hydrocarbon levels. *Mutation Research*, Vol. 702, pp. 78-85.

Pope III, C.A., Dockery, D.W. & Schwartz, J. (1995). Review of epidemiological evidence of health effects of particulate air pollution. *Inhal. Toxicol,* Vol. 7, pp. 1-18.

Pope III, C.A., Burnett, R.T., Thun, M.J., Calle, E.E., Krewsi, D., Ito, K. & Thurston, G.D. (2002). Lung cancer, cardiopulmonary mortality and long-term exposure to fine particulate air pollution. *Jour. Amer. Med.*, Vol. 287, No. 9, pp. 1132 – 1141.

Rio Grande do Sul, Conselho Estadual do Meio Ambiente. Resolução CONSEMA N º 129/2006. (6 February 2007). *Dispõe sobre a definição de critérios e padrões de emissão para toxicidade de efluentes líquidos lançados em águas superficiais do Estado do Rio Grande do Sul*. Retrieved from <http: www.sema.rs.gov.br>.

Rosenkrantz, H.S., McCoy, E.C., Sanders, D.R., Butler, M., Kiriazides, D.K. & Mermelstein, R. (1980). Nitropyrenes: isolation, identification, and reduction of mutagenic impurities in carbon black and toners. *Science*, Vol. 209, pp. 1039–1043.

Rosenkranz, HS. (1996). Mutagenic nitroarenes, diesel emissions, particulate-induced mutations and cancer: an essay on cancer-causation by a moving target. *Mutation Research*, Vol. 367, pp. 65-72.

USEPA, U.S. Environmental Protection Agency. (2008). *Integrated Review Plan for the National Ambient Air Quality Standards for Particulate Matter.* Research Triangle Park, North Carolina, EPA 452/R-08-004. Retrieved from <http://www.epa.gov/ttnnaaqs/standards/pm/data/2008_03_final_integrated_review_plan.pdf>.

Van der Oost, R., Beyer, J., Vermeulen, N.P.E. (2003). Fish bioaccumulation and biomarkers in environmental risk assessment: a review. *Environmental Toxicology and Pharmacology*, Vol. 13, pp.57–149.

Vargas, V.M.F, Horn, R.C., Guidobono, R.R., Mittelstaedt, A.B. & Azevedo, I.G. (1998). Mutagenic activity of airborne particulate matter from the urban area of Porto Alegre. Brazil. *Genet. Mol. Biol.*, Vol. 21, pp. 247-253.

Vargas, V.M.F. (2003). Mutagenic activity as a parameter to assess ambient air quality for protection of the environmental and human health. *Mutation Research*, Vol. 544, pp. 313-319.

Vargas, V.M.F., Migliavaca, S.M.B, Horn, R.C. & Terra, N.R. (2008). Comparative temporal ecotoxicological study in a river basin influenced by petrochemical industries. *Science of the Total Environment*, Vol. 392, pp. 79-92.

Watanabe, M., Ishidate Jr., M. & Nohmi, T. (1989). A sensitive method for the detection of mutagenic nitroarenes: construction of nitroreductase-overproducing derivatives of Salmonella typhimurium strains TA98 and TA100. *Mutation Research*, Vol. 216, pp. 211-220.

Watanabe, M., Ishidate Jr., M. & Nohmi, T. (1990). Sensitive method for detection of mutagenic nitroarenes and aromatic amines: new derivatives of Salmonella typhimurium tester strains possessing elevated O-acetyl-transferase levels. *Mutation Research*, Vol. 234, pp. 337-348.

WHO, World Health Organization. (2006). Air quality guidelines for particulate matter, ozone, nitrogen dioxide and sulfur dioxide; Global update 2005. Geneva: WHO.

WHO, World Health Organization. (2009). *World Cancer Report, 2008.* International Agency for Research on Cancer, Lyon.

Yu, Mig-Ho. (2001). *Environmental Toxicology: impacts of environmental toxicants on living systems,* Lewis Publishers, New York.

14

An Evaluation of Atmospheric Aerosols in Kanana, Klerksdorp Gold Mining Town, North-West Province of South Africa

Brighton Kaonga and Eno E. Ebenso
North-West University (Mafikeng Campus), South Africa

1. Introduction

Atmospheric aerosols have posed a health challenge by their presence in the atmosphere. In order to control them, they have to be understood in terms of their interactions in the air, their length of suspension and their transportation. It is true to say aerosols have been in the atmosphere since the beginning of time itself. As long as there has been wind, particulate matter has found itself in the air, attributed to nature aerosol emissions. Atmospheric aerosols technically are considered to be suspension of fine solid or liquid particles in a gas (Hinds, 1999). Particles in the air can change their size and composition by condensation of vapour species or evaporation, coagulating with other particles by chemical reaction, or by activation in the presence of water.

The production of atmospheric aerosols or atmospheric particulate matter is of great concern. The effects of inhaling particulate matter which have been widely studied in humans and animals include asthma, lung cancer, cardiovascular issues, and premature death (Pope & Burnett, 2002). The size of the particle is a main determinant of where in the respiratory tract the particle will come to rest when inhaled. Larger particles are generally filtered in the nose and throat and do not necessarily cause problems, but particulate matter smaller than about 10 micrometers (μm), referred to as *PM10*, can settle in the bronchi and lungs and cause health problems. The 10 micrometer (μm) particle size does not represent a strict boundary between respirable and non-respirable particles, but has been agreed upon for monitoring of airborne particulate matter by most regulatory agencies (Seinfeld & Pandis, 2006). Similarly, particles smaller than 2.5 micrometers, *PM2.5*, tend to penetrate into the gas-exchange regions of the lung, and very small particles (< 100 nanometers) may pass through the lungs to affect other organs. PM2.5 leads to high plaque deposits in arteries, causing vascular inflammation and atherosclerosis — a hardening of the arteries that reduces elasticity, which can lead to heart attacks and other cardiovascular problems (Pope & Burnett, 2002).

Airborne particles undergo various physical and chemical interactions and transformation (i.e. atmospheric aging), changes of particle size, structure, and composition (coagulation, restructuring, gas uptake, chemical reaction). Particularly efficient particle aging occurs in clouds, which are formed by condensation of water vapour on pre-existing aerosol particles (cloud condensation and ice nuclei). Most clouds re-evaporate, and modified aerosol

particles are again released from the evaporating cloud droplets or ice crystals (cloud processing). If, however, the cloud particles form precipitation which reaches the Earth's surface, not only the condensation nuclei but also other aerosol particles are scavenged on the way to the surface and removed from the atmosphere. This process, termed "wet deposition", is actually the main sink of atmospheric aerosol particles. Particle deposition without precipitation of hydrometeors (airborne water particles)—that is, "dry deposition" by convective transport, diffusion, and adhesion to the Earth's surface—is less important on a global scale, but is highly relevant with respect to local air quality, health effects (inhalation and deposition in the human respiratory tract), and the soiling of buildings and cultural monuments (Pöschl, 2005). Depending on aerosol properties and meteorological conditions, the characteristic residence times (life-times) of aerosol particles in the atmosphere range from hours to weeks.

Emission of particulate matter by natural means did not present as much health hazards as compared to man-made activities. Natural emissions sources were wind dust, sea sprays and natural fires or biomass burning. But this changed when man began to develop himself; trying to make himself comfortable. The more he became comfortable the more population increased, prompting new developments that consequently led to activities that are now responsible for health threatening atmospheric aerosols. These activities included the improved transportation system, industrial transformation, and consumption of fuel etc. This pattern can be seen in the study area of interest, Kanana in South Africa.

2. Purpose of the research study area

Literature shows that air pollution continues to threaten public health despite tighter emission standards, closer monitoring of air pollution, and reduction of levels of certain types of air pollutants. Averaged over the globe, *anthropogenic* aerosols (those made by human activities) currently account for about 10 percent of the total amount of aerosols in our atmosphere, (Pope and Burnett, 2002). The increased levels of fine chemical particle concentration and composition in the air are linked to health hazards such as heart disease, altered lung function and lung cancer. It is for this reason that an evaluation of the air quality with regard to particulate matter was undertaken in Kanana area in the Klerksdorp gold mining town of the North-West province of South Africa.

2.1 The case of Kanana, Klerksdorp (South Africa)

The North West Province, with its favourable geographical location close to the provincial capital of South Africa, as well as its eco-tourism potential and the mining industry, is one of South Africa's most visited provinces. Touristic attractions include:

- The Sun City/Pilanesberg complex, Magaliesberg, and Hartbeespoort. Recommended new nodes include: Borakalalo Game Reserve, Vredefort Dome, Vaalkop Dam, and Ganyesa /Kalahari.
- Both foreign and local tourists visit the North-West Province. As such international tourist bring in foreign exchange and so contribute greatly to the economy of the country. Map of Kanana and description is shown below. Kanana lies in what is called Orkney gold mining area, within Klerksdorp as can be seen in the map above (26° 58' 0" South, 26° 38' 0" East).

2.2 Environmental strains of the North-West Province

According to the State of the Environment Report overview (2002), North West Province, South Africa is under pressure especially from:

- The Ga-Rankuwa, Brits, Hartebeespoort and Rustenburg area due to industrial mining and other developments. This area is also one of the tourism nodes in the Province that needs to be sustained.
- The main corridors for tourism are: Hartebeespoort-Rustenburg-Sun City-Madikwe Game Reserve; Hartebeespoort-Rustenburg-Zeerust-Mafikeng-Lehurutshe, and Gauteng-Potchefstroom-Klerksdorp-Wolmaransstad-Bloemhof.

The State of the Air Report in South Africa (2005), list polluting sources as industrial and commercial activities; electricity generation especially coal-fired and fuel-turbine power stations; waste treatment and disposal that includes incineration; residential activities that includes burning of coal, paraffin, liquid petroleum (LP) gas, dung and wood; transport (petrol-diesel driven exhaust emissions, road dust raised by vehicles, etc); and agriculture. On the other hand, there are admissions of health-risking particulate matter emissions into the environment by industrial giants like the mines such that the public raised complaints because of poor visibility and too much dust from the smelters and refineries, as well as dust fallout from various tailings dams (Bullock, 2006).

3. Information on sources of particulate matter emissions

Like any other settled areas of the world, Rustenburg, another mining city in the North West Province, has had its effects of human development on the quality of air. Before the onset of industrialization, the air in the town was influenced by the natural phenomenon occurrences; particulate matter in the atmosphere as a result of wind dust, fire-raised atmospheric aerosols and particulate matter emissions as a result of human activities. But the advent of increased population, pressures on the atmosphere also increased as a result of increased human needs. The functioning and quality of the environment got affected as the result of increased human needs. Increased population meant increase in land use such as settlements, agriculture, and industry, to mention but a few.

Industrial development in the form of mining appears to have had more influence in the settlement in Rustenburg and the surrounding towns like Klerksdorp.

3.1 Mining

According to the North-West Freight Transport Databank, Rustenburg town alone contributes about 70% platinum mining of the world. Chrome is also mined extensively. Klerksdorp is mostly a gold mining town. South Africa as a whole is the largest producer of gold in the world. The gold mining sector provides about 56% of miner's employment in the country.
Mining activities produce toxic metals like mercury (Roulet et al., 1999) and so it is important to establish the contribution of particulate matter in the atmosphere.

A

B

Fig. 1. (A & B): Mining processes as a source of particulate matter
Source: State of Air Report in South Africa (2005)

3.2 Transport sector

As a result of large scale mining of platinum and gold, the transport sector has grown tremendously. This includes public as well as commercial vehicles.

Fig. 2. Haulage track with particulate matter emissions
Source: State of Air Report in South Africa (2005)

3.3 Human sector

Mining sector offered great employment opportunities. This attracted people from even surrounding areas thereby putting pressure on municipalities in terms of housing. As a result all forms of settlements mushroomed – both planned and unplanned. Settlements used fuel for cooking and warmth and so produced aerosols that reduced quality of the air in the environment (figure 3).

Fig. 3. Domestic cooking as a source of particulate matter emissions
Source: State of Air Report in South Africa (2005)

3.4 Agricultural sector

Agricultural activities also produced atmospheric aerosols resulting into degradation of air quality in the environment. The burning of agricultural refuse especially is a major source of particulate (Figure 4).

Fig. 4. Agricultural burn offs
Source: State of Air Report in South Africa (2005)

3.5 Environmental refuse treatment

When waste is collected, some of it is burnt as a form of reducing its volume as can be seen in Figure 5 below. Such activities emit particulate matter into the atmosphere thus contributing to the degradation of the air quality.

Fig. 5. An industrial burning activity producing particulate matter (burning tyres).
Source: State of Air Report in South Africa (2005)

3.6 Air quality

The air quality in Kanana is dependent on emissions of pollutants from a variety of activities. The fact that the area is located in a mining town, development as a result of the mines affect it markedly. An example is the change in population levels of the area and how the population becomes distributed. Unplanned or informal settlements arise. These in most cases are of low income group. Generally, the low income group tends to use biofuels and burning of wood for cooking purposes as well as for keeping themselves warm especially during winter. Low income group engage in small time-farming. Since they do not have

adequate resources, their methods of preparing land contribute to production of and emission of particulate matter – especially during burning vegetation for clearing land.
There is some contribution of particulate emissions from such activities as incineration of waste from health institutions, boiler operations by industry and so on. The household use of coal, paraffin, Liquefied Petroleum Gas (LPG) as a source of fuel result into particulate matter being emitted into the air.
The expanded economic activities promote an improvement of road network. Some roads are tarred and others are gravel roads. It is the untarred roads that are a major concern. They become a source of particulate matter emission as a result of the dust that is disturbed by both commercial and private vehicles – trucks hauling material from one place to another cause entailment of dust. Mechanical forces (between the tire and the road surface) for example re-suspend particulate matter that had been deposited thereby increasing aerosol particulates. Re-entrainment of deposited particulate matter can also occur as a result of air blow from vehicle exhausts pipes during operations.
Development translates into more vehicles on the road; the consequence is that both diesel and petrol vehicles produce particulate matter that eventually end up in the atmosphere thereby degrading its air quality. Inter-dependent industry spring up (one manufacturer produces one thing that the other needs in order to proceed with their production), each producing waste in one way or another. Miscellaneous sources of emissions of particulate matter that could be considered are the burning of tires, and dust generated at construction sites.
The mines themselves have a number of activities that produce particulate matter, pollution that is dangerous to communities especially those that live in within areas where mining takes place. Some examples of such activities include operations in the open cast mines, blasting activities, crushing activities, waste discarded as rock dumps, slimes and tailings dams.

3.7 Deposition of particulate matter

The degraded air quality varies throughout each day as more aerosols are emitted and also as they get deposited to the surface of the ground as a result of a number of mechanisms. Some known particulate matter deposition methods include gravity settling, and wet deposition. Particulate matter can also be transported far from their point of emission. Particulate matter gets easily deposited as a result of their particle size diameter. The larger the diameter the better they get deposited by the force of gravity. This phenomenon is further enhanced when aerosol particulates adhere to one another as they get into contact with each other in the atmosphere. This results into formation of agglomerates or large particles having large size diameter. The main forces that cause particulate matter to agglomerate include the London forces – or the van der Waals forces, the electrostatic force and the surface tension of liquids in the atmosphere (Hinds, 1999). The formation of particulate matter of large size diameter is promoted when the atmospheric relative humidity increases to a certain level. As a result, the aerosol particles get scavenged. Aerosol particles experience deposition in still air. This is different from scavenging in conditions of high wind speeds. In this case particulate matter gets blown or transported and get deposited far from the point of emission. High temperatures on the other hand create some air turbulence. This can cause aerosol particle dilution due to air movement.

3.8 Particulate matter and health

The state of the air is of the utmost importance to the health of human beings and living things at large. It is a known fact that particulate matter plays a big role in our physiology;

e.g. breathing particulate matter of size ten micrometres (PM10) or less can affect the respiratory system amongst other health problems. It has been reported from previous studies for instance, that esophageal cancer is high among men and women in northern Iran (Azin et al., 1996). Clearly, the air we breathe does not just contain oxygen, carbon dioxide, nitrogen, water vapor anymore but more other complicated substances. The composition of the air has changed tremendously over the years, more especially with the onset of industrialization on a large scale. Metal mining for example is the leading contributor of toxic emissions to the environment (Earthworks and Oxfam, 2007). Other information that come to mind regarding toxic emissions from the mines are that mining and dust are inseparable. As a consequence, air pollution also comes mainly from silicate dust from ore mining and crushing. The inhalation of aerosol particulates causes a serious health hazard such as development of fibrotic lung disease (Ogola et al., 2001). Some alarming pictures about presence of metals in the atmospheric aerosols have been presented by various researchers. United Nations expressed their concerns regarding toxicity effects of lead even in the lowest doses can impairing the nervous system (UN, 1998). Lead is known to also affect an unborn child (the feotus), infants, as well as young children.

Mercury is known to also attack the central nervous system. It could lead to a disease called Minamata (United Nations University, 1993). Arsenic on the other hand has the ability to attack different sites in the body. It is reported to attack the stomach, the respiratory system, the lungs and others (Harada, 1996).

Both natural and anthropogenic sources of particulates have been discussed above. It is clearly apparent from the data presented below that the concern about the presence of aerosol particulates is very much evident; and that the air quality has been compromised in this chosen area of study.

4. Methodology of data collection

4.1 Sampling of atmospheric aerosols

Sampling of atmospheric aerosols was done using a German Ambient Dust Monitoring instrument Grimm # 180 over a period of 3 months in 2009. The Ambient Dust Monitor is a stationary monitor installed in a measuring shelter (Figure 6), at a clinic for security reasons. This site is about 5 kilometers from the nearest mine. It was chosen for the fact that many people live around the site. It measures continuously concentrations of PM10, PM2.5, and PM1. In this research work, only PM 10 measurements were done. This was decided upon because South Africa Air Quality Guidelines talks only about PM10. The dust monitor presents the airborne dust particulates in micrograms per cubic meter ($\mu g/m^3$). The resolution of the mass calculation set by the manufacturer is 0.1 $\mu g/m^3$ with a flow rate of 72 l/h. The Grimm #180 dust monitor takes continuous air samples by means of a flow controlled pump. In the monitor, the particles are measured by the physical principle of orthogonal light scattering. Particles are illuminated by a laser light and the scattered signal from the particle passing through the laser beam is collected at approximately 90^o by a mirror and transferred to a recipient diode. Each signal of the diode is fed, after a corresponding reinforcement, to a pulse height analyzer then classified to size and transmitted in each size channel. These counts are converted each 6 seconds to a mass distribution from which the different PM values are derived. Results of the measurement are shown on the display as mass distribution in $\mu g/m^3$: PM10, PM2.5, and PM1. The collected data is stored on an AQWeblogger data logger. The data is then retrieved on site or by remote access.

The equipment is shown in Figure 7.

Fig. 6. Measuring station for taking particulate matter measurements
Source: State of Air Report (2005)

Fig. 7. Measuring equipment for taking particulate matter measurements
Source: Grimm # 180 dust monitor manual

5. Results

Results obtained from air samples in the months of April, May, and June 2009 for Kanana, Klerksdorp Gold Mining Town are as presented in the various figures below. In South Africa, April and May are autumn months. June is one of the months in winter season. In the month of April high values (above 70 $\mu g/m^3$) of particulate matter appear 18 times as

can be seen from Fig. 8. The highest value of particulate matter recorded was about 130 μg/m^3 on 20 April, 2009. On the days 18 – 20 April winds blowing were mostly South easterlies as can be seen in Fig. 9. The probability that these winds are responsible for the high particulate matter values are high. Low wind speeds were recorded during these three days – Fig. 10. Low wind speeds favour high particulate matter values. In the month of May, high values (above 70 μg/m^3) of particulate matter appear 11 times as can be seen from Fig. 11. The highest value of particulate matter recorded was about 200 μg/m^3 on 29 May, 2009. Northwest winds prevailed during the time of high recorded values of particulate matter – Fig. 12. Wind speed for this period were below 2ms^{-1}, favouring high particulate matter values – Fig. 13. Wind direction appear not to be the conclusive contributor of high recorded values of particulate matter as can be seen in Fig. 8, 11 and 14. The winter month of June shows the highest value of particulate matter recorded was about 206 μg/m^3 on the 4th day of the month. However high values (above 70 μg/m^3) of particulate matter appear 9 times as can be seen from Fig. 14. In April, on the average winds were mostly southeast for most of the month. These winds appear to have caused the high values of the particulate matter recorded. From Fig. 10, it can be noted that these winds were mostly having speeds of about 2 m/s. The month of May experienced winds blowing from southeast as well. In this month the high values for the particulate matter appear to be blown in from all directions. Wind speeds for these high values were relatively low, less than 2 m/s (Fig. 15).

June, just like April and May, on average winds were mostly southeast for most of the month. Again, these winds appear to have caused the high values of the particulate matter recorded. From Fig. 16, it can be noted that these winds were mostly having speeds of less than 2 m/s as in May. It can be noted from the PM10 graphs and wind speed graphs that wind speeds above 2 m/s had a scouring effect – that is they tended to lower the values of the particulate matter recorded in all the three months.

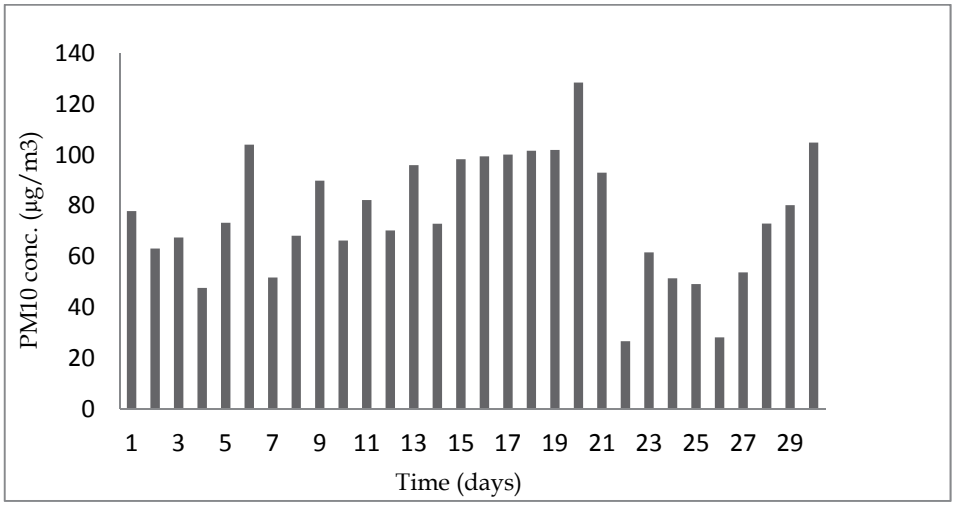

Fig. 8. Daily averages of PM10 concentrations for each day in the month of April 2009 in Kanana

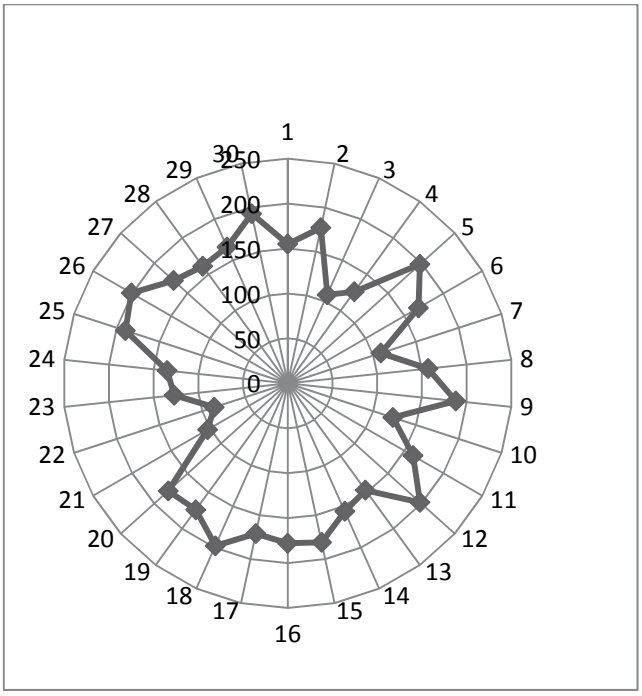

Fig. 9. Wind direction conditions for each day in the month of April 2009 in Kanana

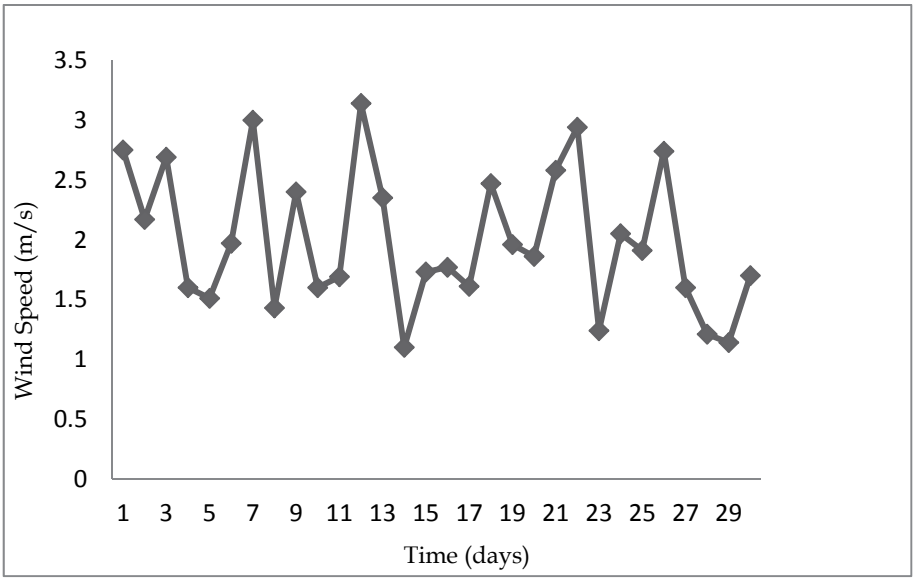

Fig. 10. Wind speed conditions for each day in the month of April 2009 in Kanana

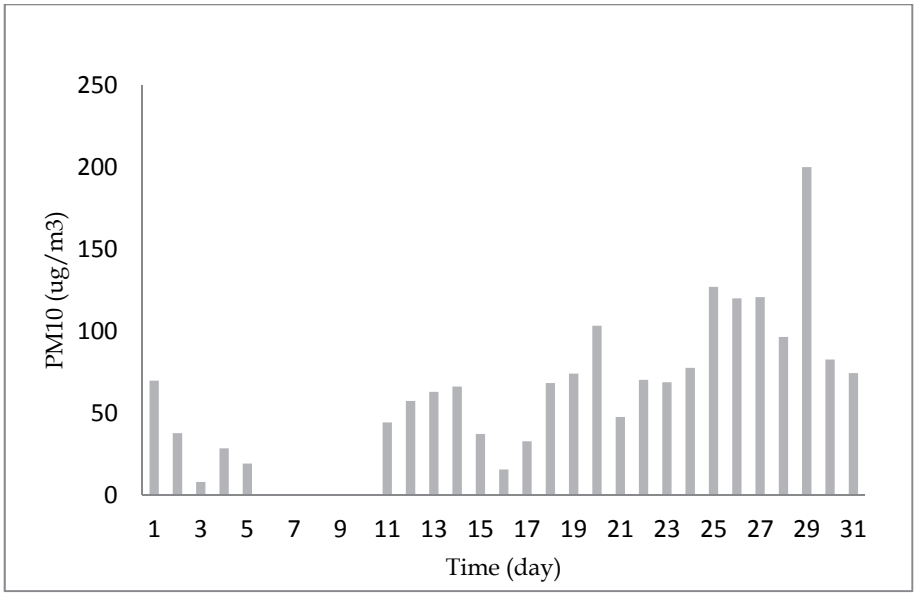

Fig. 11. Daily averages of PM10 concentrations for each day in the month of May 2009 in Kanana

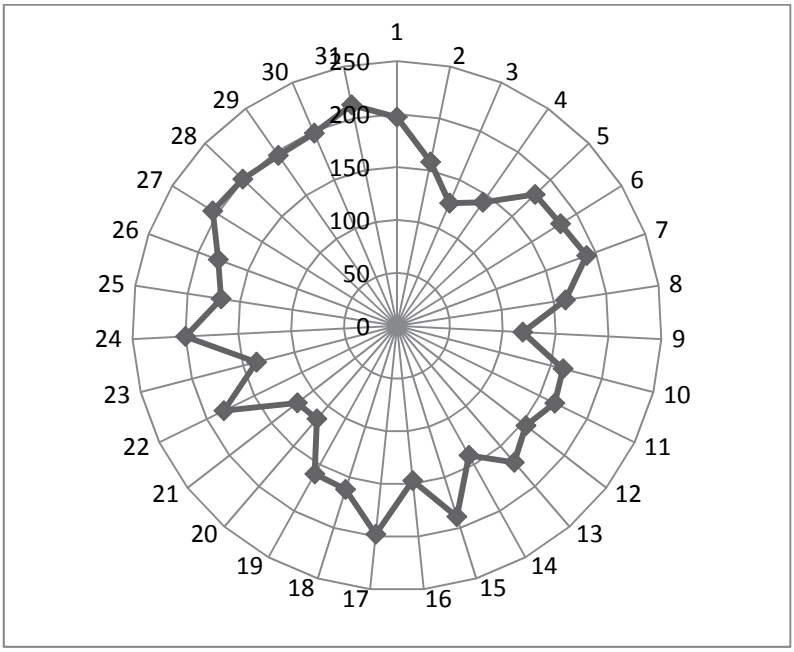

Fig. 12. Wind direction conditions for each day in the month of May 2009 in Kanana

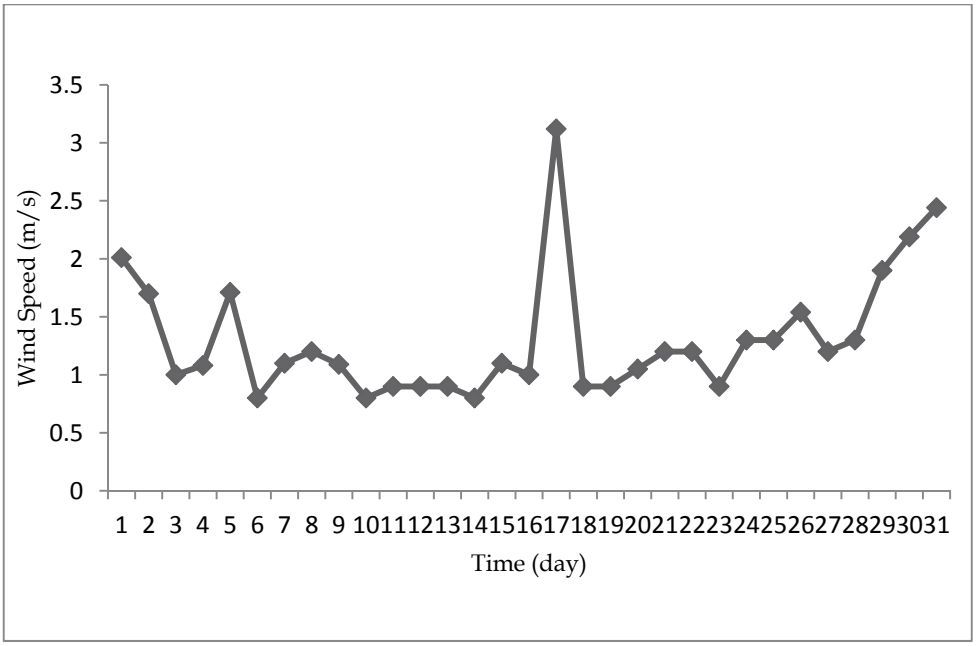

Fig. 13. Wind speed conditions for each day in the month of May 2009 in Kanana

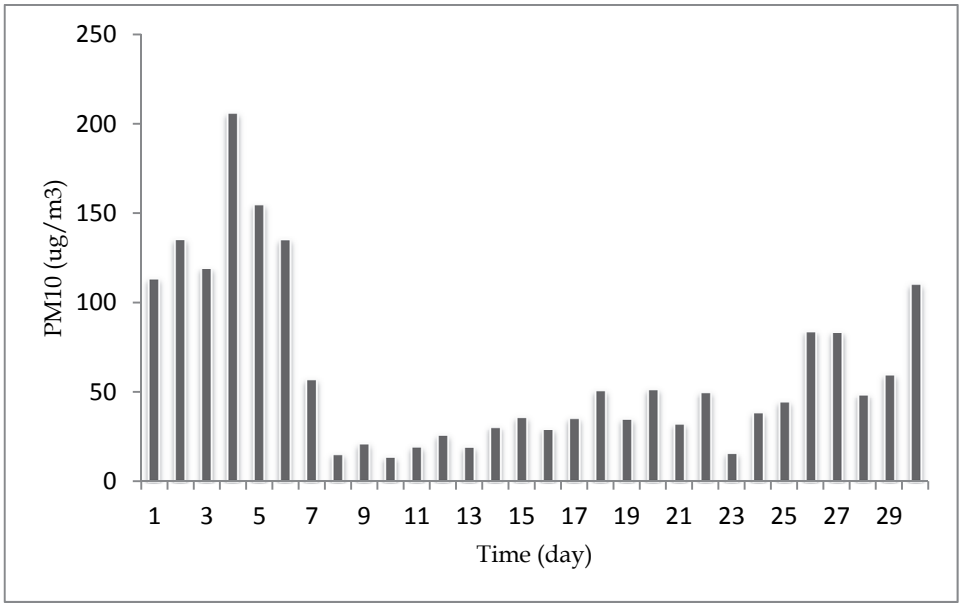

Fig. 14. Daily averages of PM10 concentrations for each day in the month of June 2009 in Kanana

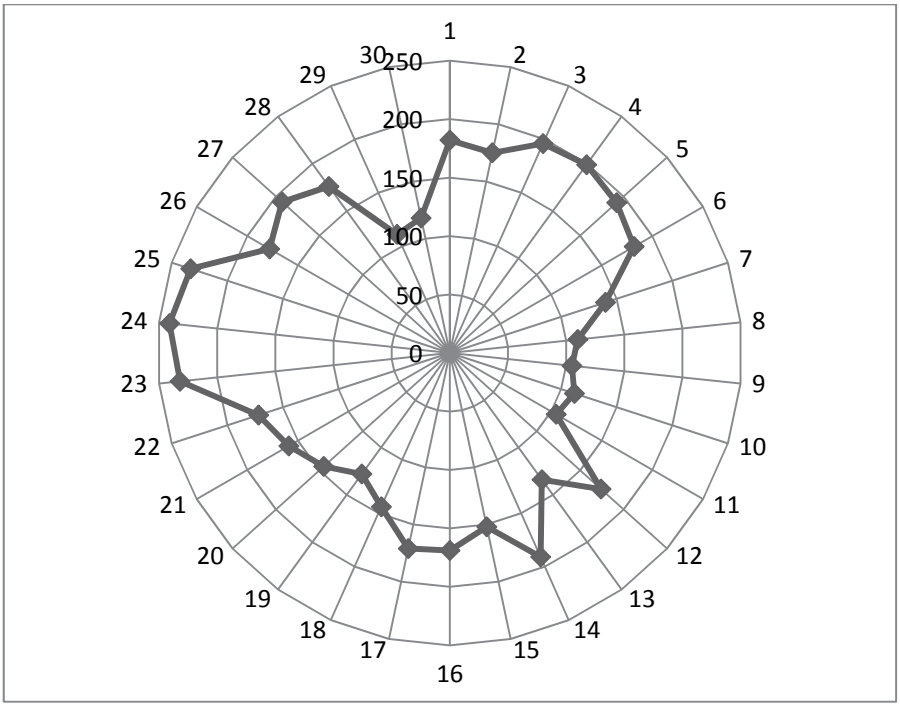

Fig. 15. Wind direction conditions for each day in the month of May 2009 in Kanana

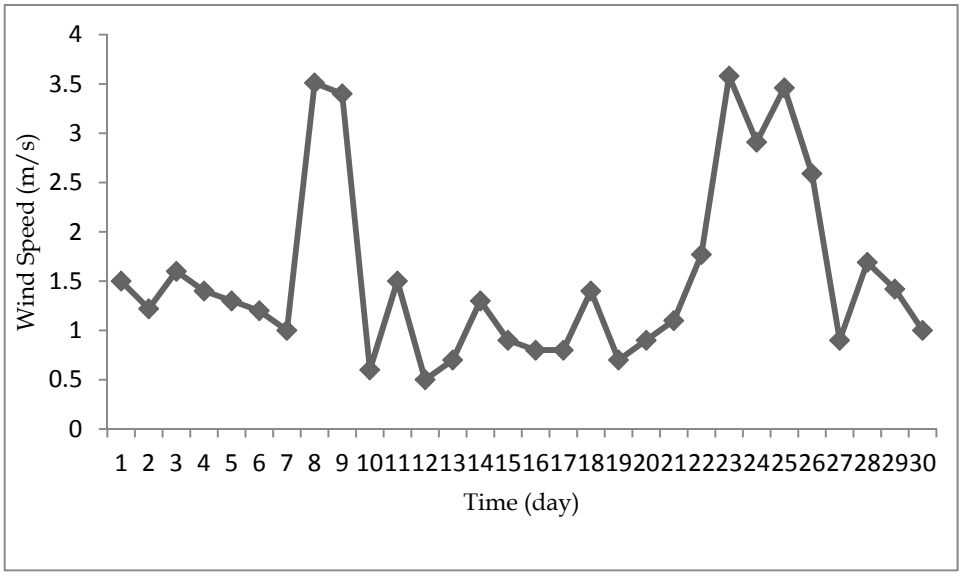

Fig. 16. Wind speed conditions for each day in the month of June 2009 in Kanana

5.1 A comparison – Gold mining and platinum mining PM10 emissions

A comparison of particulate matter emissions between a gold mining area and a platinum mining area for July 2010 was made. As it could be seen from Fig. 17 below, more particulate matter emissions were recorded for Kanana (a gold mining area in Klerksdorp) than for Phokeng (a platinum mining area in Rustenburg). This is not known why it should be so. Perhaps a logical explanation might be as forwarded by report by Earthworks and Oxfam America (2007) that 'gold mining is one of the dirtiest industries in the world'. From the figures below, Kanana showed the highest recording for particulate matter emissions of 180 µg/m^3 on the 20 of July 2010. The highest value for particulate matter emission for Phokeng was 78 µg/m^3 on the 21 of July 2010. Daily average wind speeds for this particular day for Kanana are as shown in Fig. 18.

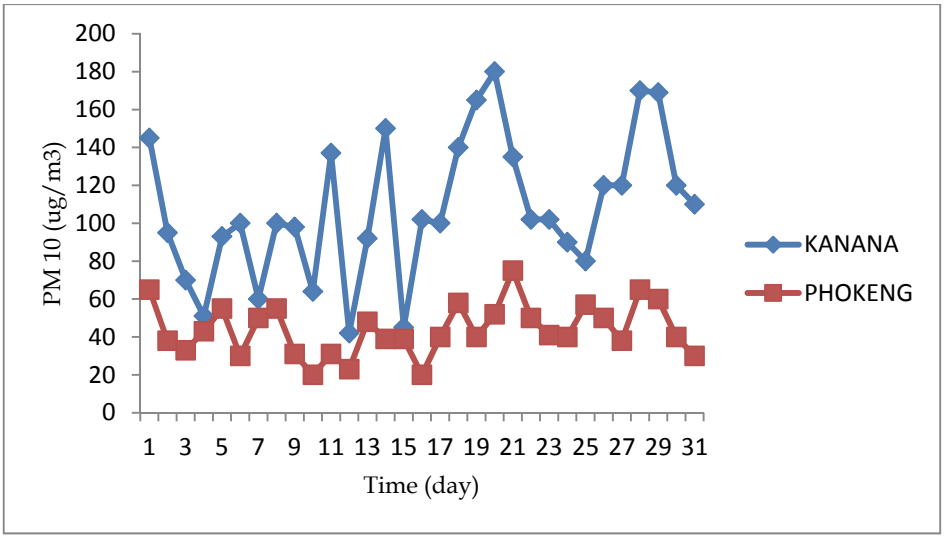

Fig. 17. Comparison of daily averages of PM10 concentrations for each day in the month of July 2010 for Kanana and Phokeng.

Daily average wind speeds for Phokeng are also shown in Fig. 22. Daily average wind speeds for Kanana were generally lower than those of Phokeng. Daily average temperatures for July 2010 for both areas (Kanana and Phokeng) are indicated in Fig. 21 for Kanana and Fig. 23 for Phokeng. There was no precipitation recorded in both places, but relative humidity values are shown in Fig. 20 for Kanana in Klerksdorp, and Fig. 22 for Phokeng in Rustenburg. Relative humidity for Phokeng (the platinum mining area) on a number of days was above 60% where as relative humidity values for Kanana (in the gold mining area) were mostly below 60%. It is possible that this could explain the lower values in the particulate matter recorded in Phokeng the platinum mining area than in Kanana the gold mining area. This is not the case though between the second and the fourth day. But between the ninth and tenth day, the explanation appears to be valid – that high relative humidity could have been responsible for low particulate matter. Low values of relative humidity have corresponded to high values of recorded particulate matter during period 17th to 20th in Kanana gold mining area. These conditions are similar for those prevailing in

Phokeng platinum area and yet particulate matter values for this period 17th to 20th day do not rise as compared to Kanana gold mining area. The explanation that washdown has resulted into lower values of particulate matter recorded because of high relative humidity does not hold.

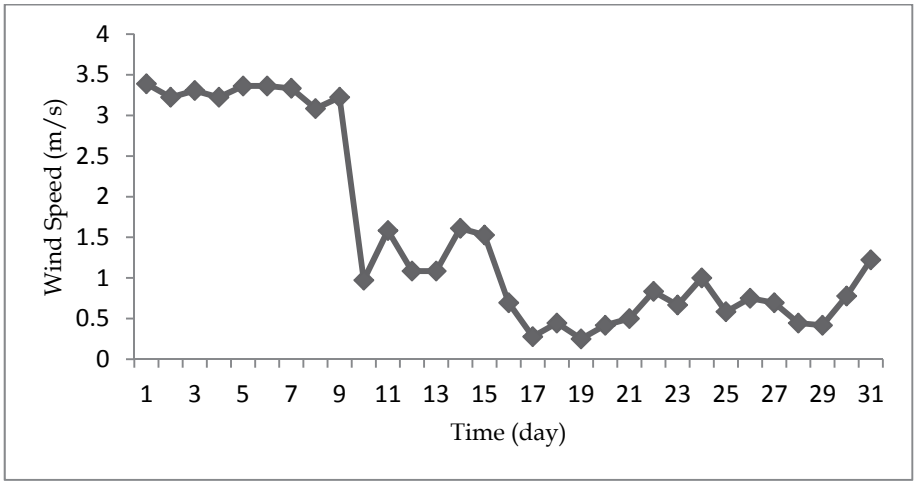

Fig. 18. Wind speed conditions for each day in the month of July 2010 Kanana, in Klerksdorp

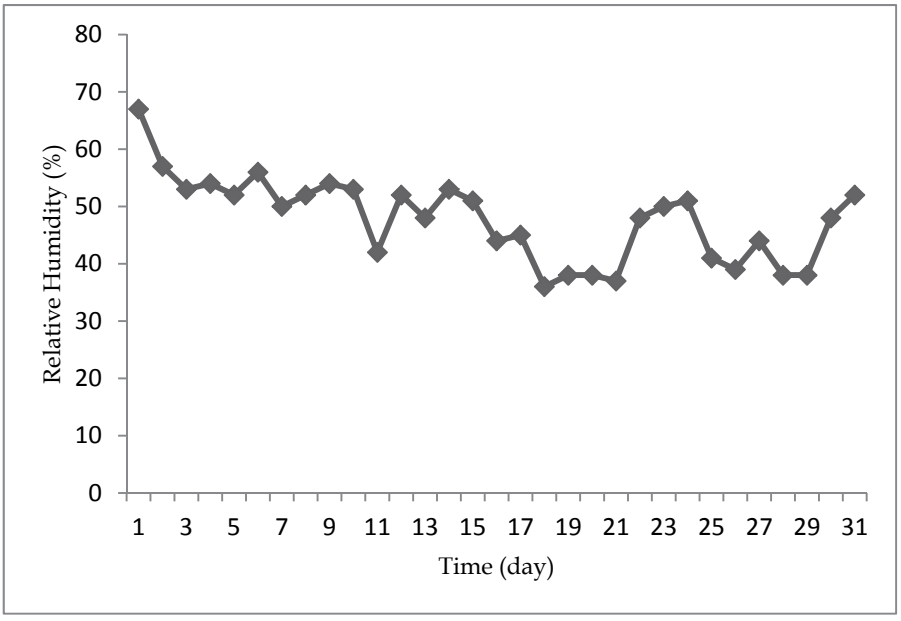

Fig. 19. Relative Humidity conditions for each day in the month of July 2010 Kanana, in Klerksdorp

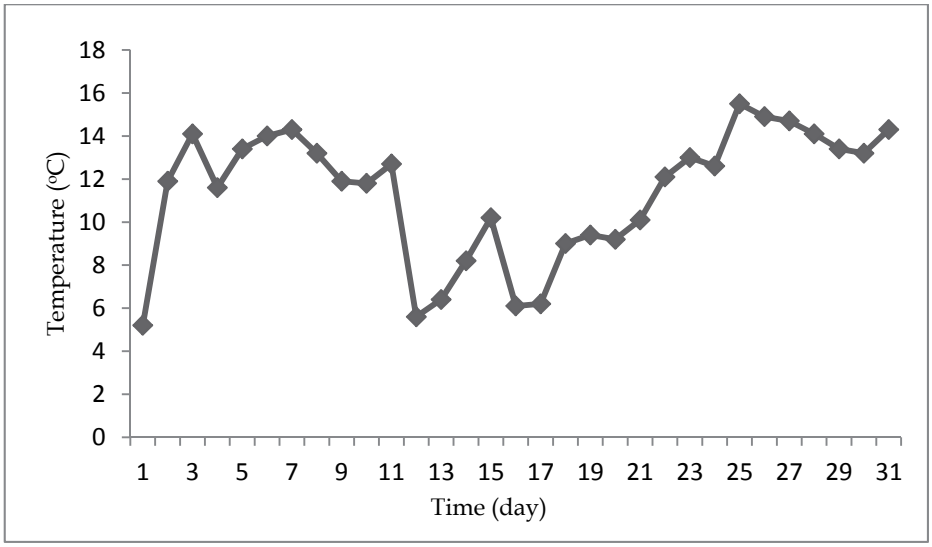

Fig. 20. Temperature conditions for each day in the month of July 2010 Kanana, in Klerksdorp

Fig. 21 and Fig. 23 show temperature variation for each day in July 2010 in each of these two areas. The temperature ranges are similar and so the difference in particulate matter recorded cannot be deduced from temperature comparison either.

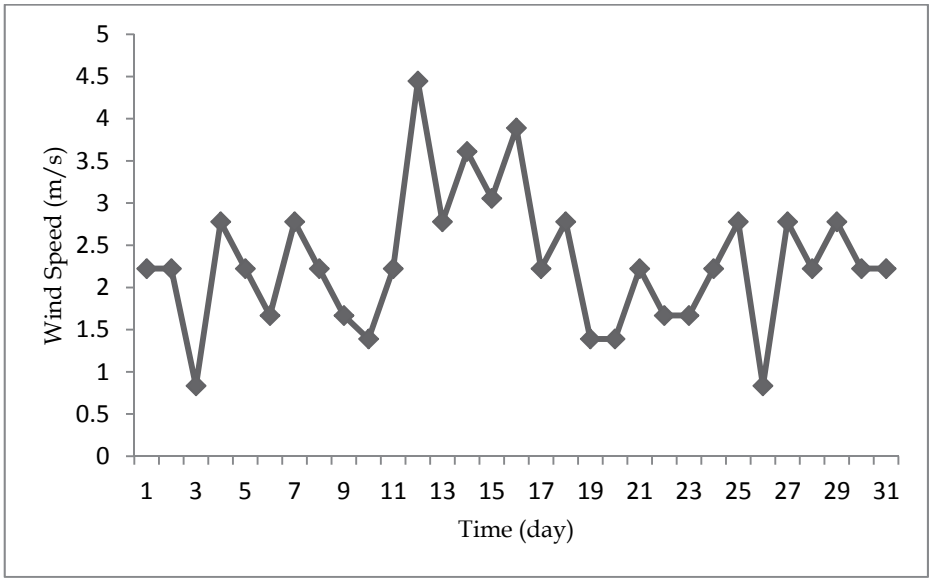

Fig. 21. Wind speed conditions for each day in the month of July 2010 Phokeng, in Rustenburg

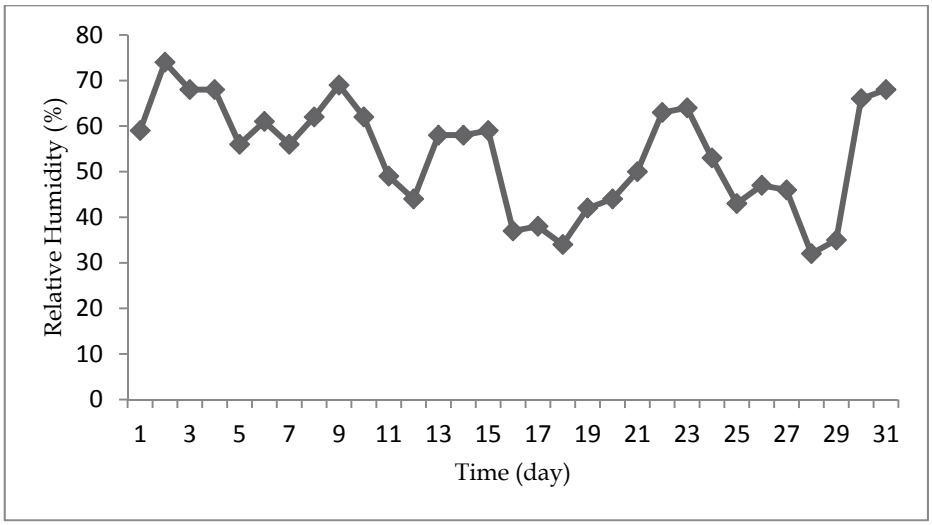

Fig. 22. Relative Humidity conditions for each day in the month of July 2010 Phokeng, in Rustenburg

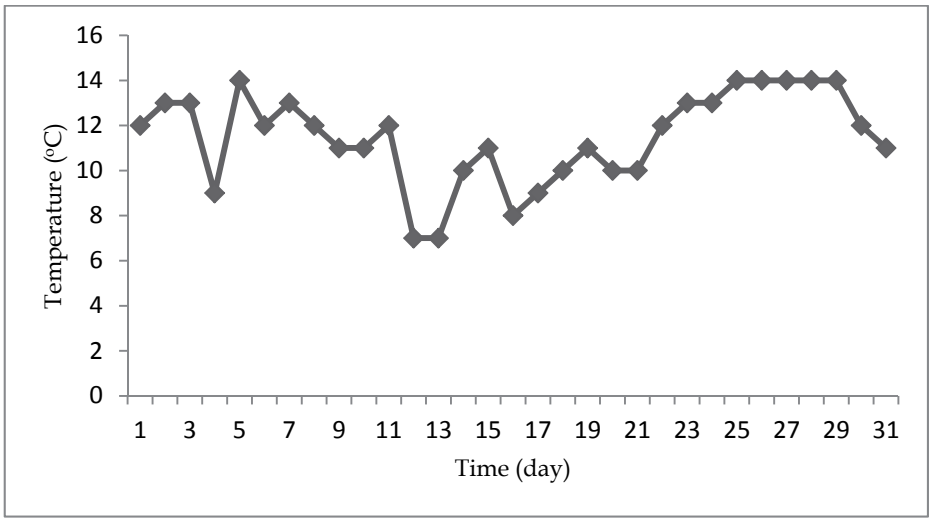

Fig. 23. Temperature conditions for each day in the month of July 2010 Phokeng, in Rustenburg

6. Conclusion

From the results obtained from this study, the following conclusions can be drawn. The results obtained were compared to the South African Air Quality Guidelines (2005) and the World Health Organization, WHO (2005). It was observed that the PM10 values for 24

hourly periods exceeded the 75 μg/m^3 maximum permissible limit for the South African Guidelines, for almost half the month (14 days) in April, 8 days in May, and 9 days in June. According to the World Health Organization Guidelines, WHO (2005) the results obtained in the month of April (26 days), May (17 days), and June (14 days) exceeded the maximum permissible limits of 50μg/m^3. The emissions of particulate matter in the study area are not acceptable, thereby degrading the air quality in the area. This evaluation therefore points towards the possible health risks from presence of particulate matter as can be seen from the experimental data obtained in the study area.

The comparison made between aerosol particulates in Kanana area and aerosol particulates in Phokeng area made interesting revelations. The gold mining area appears to be emitting more particulate matter into the atmosphere than the platinum mining area. It cannot be concluded from this once comparison that gold mining generates more atmospheric aerosols than platinum mining. There could probably be many more activities in Kanana that generate more atmospheric aerosols than in Phokeng. Certainly detailed source point measurements could help determine the causes of the difference in atmospheric aerosols in these two areas. Further studies are ongoing.

7. Acknowledgements

We would like to unreservedly thank Mrs. Thokozile Ramoroa and the organization she works for, the Department of Agriculture, Conservation and Environment Mafikeng, Northwest Province, South Africa, for allowing us to use their air quality monitoring equipment in the areas of this study.

8. References

Azin, F.; Raie, R.M. & Mahmoudi, M.M. (1996). Correlation between the Levels of Certain Carcinogenic and Anticarcinogenic Trace Elements and Esophageal Cancer in Northern Iran. *Ecotoxicology and Environmental Safety* vol.39, 179 – 184

Bullock, S. (2006). Sustainable Development Report. *Anglo Platinum Limited,* Johannesburg, South Africa.

State of the Air Report in South Africa (2005). A report on the state of air in South Africa. *Department of Environmental Affairs*, ISBN 978-0-621-38724-7 Pretoria, South Africa

Eearthworks & Oxfam (2007). *Golden Rules: Making the Case for Responsible Mining*. America.

Harada, M. (1996). Characteristics of industrial poisoning and environmental contamination in developing countries. *Environmental Sciences,* vol. 4 (Suppl), pp. 157–169.

Hinds, W.C. (1999). *Aerosol Technology; Properties, Behavior, and Measurement of Airborne Particles*, (second edition) John Wiley and Sons, ISBN 0-471-19410-7, United States of America.

State of The Environment Report Overview Northwest Province (2002). *Department of Environmental Affairs and Tourism,* Republic of South Africa.

Ogola, JS., Mitullah, WV., and Omulo, MA., (2001). Impact of Gold Mining on the Environment and Human Health: A Case Study in the Migori Gold Belt, Kenya. *Environmental Geochemistry and Health* vol. 24, 141-158.

Pope, C.A., & Burnett, R.T. (2002). Lung Cancer, Cardiopulmonary Mortality, and Long-term Exposure to Fine Particulate Air Pollution. *Journal of the American Medical Association* vol. 287, 1132 – 1141.

Pöschl, U. (2005). Atmospheric Aerosols Composition, Transformation, Climate and Health Effects. *Chemical International* Edition 44, 7520 – 7540.

Roulet, M., Lucotte, M., Farella, N., Serique, G., Coetho, H., Sousa, P., Scarone, A.P., Mergler, D., Guimaråes, J.R.D., and Amorim, M. (1999). Effects of Recent Human Colonisation on the Presence of Mercury in Amazon Ecosystems. *Journal of Water, Air, and Soil Pollution* 112, 3 – 4.

Seinfeld, J.H., & Pandis, S.N.(2006). *Atmospheric Chemistry and Physics; From Air Pollution to Climate Change* (second edition). John Wiley and Sons, United States of America.

South African Air Quality Guidelines (2005). *Department of Environmental Affairs*, Pretoria, South Africa

United Nations University. (1993). Environmental Pollution Control: The Japanese Experience, Papers presented at the United Nation University International Symposium on Eco-Restructuring, 123 pp.

United Nations, (1998). Global Opportunities for Reducing use of Leaded Gasoline, IOMC/UNEP/CHEMICALS/98/9, Switzerland, 59 pp.

World Health Organisation, WHO, (2005). Air quality guidelines for particulate matter, ozone, nitrogen dioxide and sulphur dioxide. WHO Press, Geneva 22pp

15

Some Guidelines to Improve Air Quality Management in Santiago, Chile: From Commune to Basin Level

Margarita Préndez[1], Gerardo Alvarado[2] and Italo Serey[2]
[1]*Universidad de Chile, Facultad de Ciencias Químicas y Farmacéuticas, Santiago,*
[2]*Centro Nacional del Medio Ambiente, Santiago,*
Chile

1. Introduction

1.1 General considerations

Particulate matter is natural or manmade and comes from different sources that determine the variety of its chemical, physical and thermodynamic characteristics.

Particulate matter may be formed by rupture of material and/or by agglomeration of small fragments, including molecules (Prospero and Charlson, 1983; Ondov and Wexler, 1998) and is classified according to its primary or secondary source. Primary particulate matter is emitted directly by sources and secondary particulate matter is formed in the atmosphere by chemical reactions. Primary particulate matter has different sizes, whereas secondary is usually very small (U.S. EPA, 2004). The most important primary natural sources are the dust raised by wind, sea spray, volcanic emissions, forest fires and brush fires. Natural sources include secondary sulphates, nitrates and organic compounds (U.S. EPA, 2004).

Since the mid 60's the city of Santiago de Chile has experienced high levels of air pollution by particulate matter, especially during the autumn-winter period; during the so-called "episodes", which may last even for a few days, the Chilean standards for PM10 air quality (particulate matter <10μm), are overcome, reaching levels considered dangerous to human health, especially to children and the elderly (WHO, 2005).

High levels of air pollution in Santiago are due to a combination of factors: a) geographical and meteorological conditions in the Metropolitan Region, particularly unfavourable for proper dispersion of pollutants, b) the growing economy of the city, c) the large size and functional segregation of the city; d) a progressive increase in transport distances, all the above in spite of technological progress (CONAMA, 1997; CONAMA, 2008).

Particulate matter has a very heterogeneous and changing chemical composition with organic and inorganic components. The studies on the subject were initiated in the mid 70's (Préndez et al, 1984; Trier, 1984, Trier and Silva, 1987; De la Vega et al., 1987, Rojas et al., 1990; Préndez et al. 1991). In 1985, a study conducted by the University of Chile found that diesel vehicles contributed 71% of ambient concentrations of particulate matter, although they represented only 19% of total PM10 emissions. On the contrary, natural dust, the main source of PM10 with 49% of the tons emitted, provided only 15%, and gas industries and vehicles, 6% each.

More recently other studies have confirmed the early ones, giving a different distribution of source contributions (Ortiz et al. 1993; Artaxo et al., 1999; Sienra et al., 2005; Gramsch et al., 2006). The lack of databases of chemical composition of emissions makes the contribution of sources and changes in time difficult to learn. Only some sources have been studied by Préndez et al., (2007). In order to overcome the problem, the Chilean studies use the USEPA database. The last emissions inventory identifies industrial processes, boilers, motor vehicles, recycled dust from the floor, home fireplaces using wood and agricultural burning as the main sources of particulate matter (DICTUC, 2007). There is also a significant fraction of secondary particulate matter (Morata et al., 2007).

The PM10 particle size is harmful to human health when entering the airways. The fine fraction of PM10 (diameter <2.5 μm, PM2.5) is most dangerous because it is 100% breathable, entering and staying longer in the lungs; in addition, its chemical composition is generally more toxic (Préndez, 1993; U.S. EPA, 2004).

Several authors have reported the main effects of particulate matter from Santiago on the population health (Oyanguren, 1972; Ostro et al., 1996; Ostro et al., 1999; Ilabaca et al., 1999; Cifuentes et al., 2000). Pino et al. (2004) established a 5% increases for each increment of 10 $\mu g/m^3$ of PM2.5; Cakmak et al. (2007) established a 4.53% probability of death for 85 $\mu g/m^3$ of PM10 in adults under age 65 and 9.47% over 65 years.

Other proven effects of particulate matter pollution include reduction of visibility, soiling of building facades and clothes, potential problems of dust deposition and acid rain (Préndez et al., 1991; Préndez, 1993; USEPA, 2004).

Since 1997, a Plan of Prevention and Decontamination of Atmospheric Pollution (PPDA) has been implemented in the Metropolitan Region, which includes a series of measures to reduce concentrations of particulate and gaseous pollutants (CONAMA, 1997; CONAMA, 2001; CONAMA 2008). However, in the period 1997-2008, there were 370 days in which concentrations were above the maximum daily alert level (≥ 195 $\mu g/m^3N$ daily concentrations) or pre-emergency level (240 $\mu g/m^3N$ daily concentrations). In most of those days (68%) the monitoring station located in Pudahuel (NW of the city) reached the highest concentration, defining the condition for the adoption of emission control measures and restrictions on the operation of stationary and mobile sources.

The main objective of this study was to identify the causes of high levels of PM10 pollution in Pudahuel in order to contribute to improve the management of air quality in the city of Santiago.

1.2 Environmental management of the Metropolitan Region

The Metropolitan Region (33.5 º S, 70.8 ° W) is a closed basin between the Andes to the east and the Coast Range to the west, the Chacabuco mountain range to the north, and the Cantillana mountain range to the south. Thus, the central valley is surrounded by mountains (altitudes between 1000 and 5000 m) and this fact makes the wind flow and air exchange difficult within the basin, where the city of Santiago is located (Fig. 1).

The first systematic measurements of the levels of air pollution in Santiago were performed in 1964 as recommended by the Pan American Health Organization; in 1976, a network consisting of 5 monitoring stations located in concentric rings around the center of the city was set up (Ulriksen, 1993). Later, (in 1987) the Automatic Monitoring Network of Air Pollutants (MACAM network) was set up, with 4 stations located in the downtown area of the city: Independencia (IS), Plaza Gotuzzo (PGS), Providencia (PS) and Parque O'Higgins

(POS)) and a mobile station, finally located in Las Condes (LCS). In 1997, four stations were added in the external area of the city: Pudahuel (PudS), El Bosque (EBS), La Florida (LFS) and Cerrillos (CES) and two stations PGS and PS were removed. Thus, the present network, called MACAM2 (ASRM, 2008) is formed by seven stations equipped with PM10-TEOM continuous monitors that can provide hourly concentrations of PM10 and continuous monitoring of gases CO, SO_2, NO_2, O_3 and total hydrocarbons (Fig. 1).

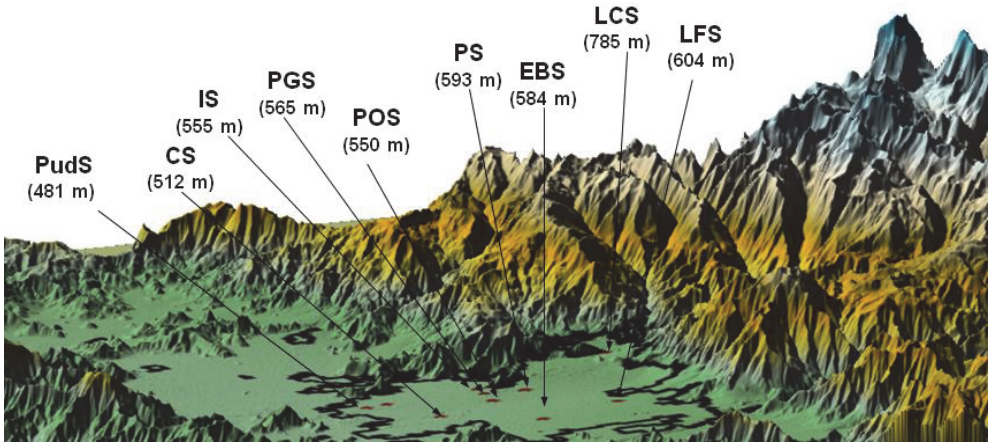

Fig. 1. Air quality stations of MACAM and MACAM2 networks of the Metropolitan Region

In 1988, the Particle Air Quality Index (ICAP) was established in terms of PM10 concentrations for 24h. ICAP was set at 0-149 µg/m^{3}N = ICAP 100 (good); 150-194 µg/m^{3}N = ICAP 200 (regular) and 285-330 µg/m^{3}N = ICAP 500 (dangerous), varying linearly between ranges (ASRM, 2008).
In 1990 the register of sources and the isokinetic testing mandatory for estimating emissions from smokestacks were established and in 1992 emission standards for particulate matter from point sources were set to a gradual reduction of emissions from 112 mg/m^{3}N to 32 mg/m^{3}N as of January 1st, 2005.
In 1996 the Metropolitan Region was declared a saturated area by PM10, TSP, CO and O_3 and latently saturated by NO_2 and ICAP calculation was corresponded to the highest 24-hour mobile concentration of PM10 recorded during the day at one of the network stations MACAM2.
In 1998, PPDA was established, which sets targets for emissions of pollutants in the short, medium and long terms to comply with all air quality standards as of 2012, with regular revisions and updates; in the primary standard it was also established that the 98 percentile of daily concentrations of PM10 during a calendar year must not exceed 150 µg/m^{3}N; in 2001, the maximum allowable annual averages of three consecutive years was set at 50 µg/m^{3}N. Furthermore, in 2000, the use of the methodology of air quality forecast for PM10 in the Metropolitan Region was approved.

1.3 Meteorological characteristics of the Metropolitan Region

During the autumn-winter period, topoclimatic characteristics of the Santiago basin are unfavourable to the dispersion of pollutants (Rutland 1973; Ulriksen 1980; Rutland and

Salinas 1983). Due to the predominance of anticyclonic conditions in the region, forcing the airflow through the large-scale weather systems a weak ventilation of the basin is produced mainly by a system of winds generated locally by the radiative heating of the surface. Therefore, from April to August (austral autumn-winter), the flow of air into the basin is much weaker than in summer (Ulriksen, 1993).

Two configurations of weather conditions have been established associated with days of high concentrations of PM10, called A and BPF types episodes. The A type corresponds to the development of a low pressure area from the Andes to the ocean, accompanied by wind from the east in the lower troposphere and a decrease in the height of the inversion layer of subsidence. The BPF type episode corresponds to a prefrontal condition, with overcast skies and weak ventilation from the NW in the Santiago basin (Rutland and Garreaud, 1995, Rutland and Garreaud, 2004).

During the A type episodes the PudS station usually shows higher concentrations of PM10 than other monitoring stations in the city. During the BPF type episodes however, the maximum concentrations are usually seen in the SW sector of the city. The number of episodes associated to A and BPF configurations that occurred in the Metropolitan Area between 1997 and 2008 are shown in fig. 2. Muñoz et al. (2003), classified the episodes occurring between 2001 and 2003 as "early episodes", with high concentrations of PM10 between 21 and 22h and "late episodes" occurring during the early hours of the next day with a lower peak.

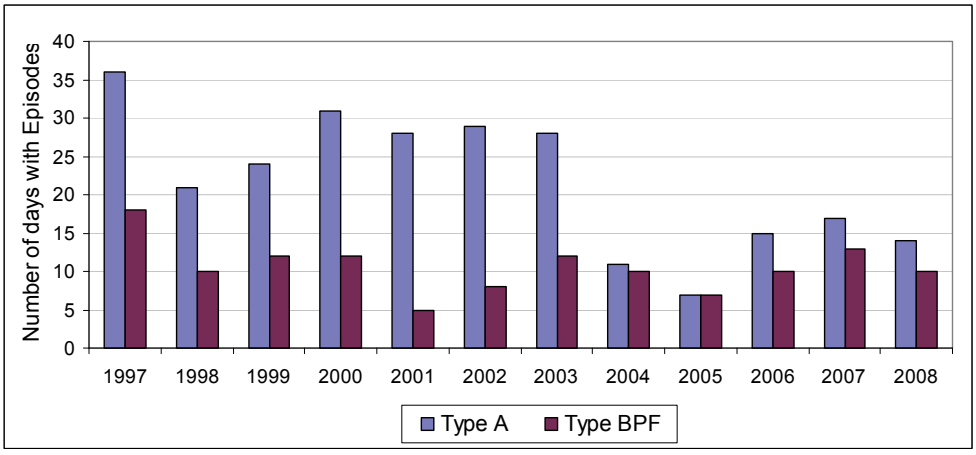

Fig. 2. Number of episodes associated to A and BPF configurations in the Metropolitan Area between 1997 and 2008

2. Materials and method

The study was divided into two stages, the first one corresponding to the identification and study of the causes of high concentrations of PM10 in the area of Pudahuel on days of pollution episodes in Santiago; the second one corresponding to the proposed management actions to reduce the occurrence of high concentrations of PM10, thus improving air quality in Pudahuel and in the city of Santiago.

2.1 Collection and critical study of the information

a. Collection of information of PM10 and meteorology to develop a diagnosis of Pudahuel air quality, considering the official historical information of PM10 (Network of Metropolitan Health Authority, ASRM, and the National Environment Commission, Metropolitan Region, CONAMA RM) and from the National Centre for the Environment (CENMA), with emphasis on the period from 2000 to 2008, including environmental emergencies, Santiago basin weather (average hourly temperature, relative humidity, speed and direction wind, rainy days) and reports of episode forecasting system.
   The information of PM10 and meteorological data used correspond to percentages above 75% of valid data for analysis periods (daily, monthly, yearly). A principal component analysis (PCA) was performed (SPSS version 8.0) and Airviro and Excel software was applied to relate information between PM10 and meteorological data in Pudahuel.
b. Analysis of primary data from two campaigns of measurements of particulate matter by CENMA in 1999 and 2003 (unpublished data) to determine the geographic extent of the area of high concentrations in the area of Pudahuel. The first season held hourly concentrations of PM10 with a continuous monitor (TEOM) between August and September 1999, a period corresponding to the final stage of the management of episodes of PM10 pollution in 1999. Measurements were made at two distant sites: one located within the area of population representativeness (radius of 2 km), 1 km SE (MunPS) and in a suburban area about 6 km SW (LAFS).
   The second campaign was conducted in the winter of 2003 in the area near PudS at the hours of maximum daily PM10 concentrations, 20h to 02h. The study area covers about 6 x 6 km approximately, including the PudS. Days of episodes were privileged. No measurements were made at nights with rain or with fog coming from the coast. A continuous monitor PM10 type nephelometer (TOPAS) was used programmed to record minute PM10 concentrations, installed on the roof of a vehicle. Measurements were carried out at 17 nights between July 10th and September 1st, 2003.
   To calculate hourly averages, early episodes were separated from the later episodes (Muñoz et al., 2003). PM concentrations under study were integrated in geographic maps in a GIS environment processed with SURFER 8.0 software to generate maps of isolines of concentrations for A and BPF type episodes.
c. The chemical and physical characterization of particulate emissions was made using industrial and natural sources taken from the 2005 emissions inventory (DICTUC, 2007) and the emissions data for the year 2008 (CENMA, 2008b); the annual emissions were calculated by multiplying the daily broadcast on operating the emission sources and dividing the daily broadcasting time by the number of hours of operation of the sources. Information is grouped by categories of sources and interpreted by comparison with the behaviour of the PM10.
d. The following factors were analyzed: 1) PM measurements of the two CENMA's campaigns; 2) behaviour of wind during episodes in Pudahuel; 3) behaviour of the system winds in the area of Pudahuel; 4) emissions inventory for Pudahuel area; 5) results of speciation analysis of physical and chemical PM10 emission sources and environmental samples from literature.
   A comparison was made between the average hourly wind speed in Pudahuel and the speeds measured at the other stations using different statistical tests to a confidence

level of at least 95%, including Wilconxon/Mann, Whitney, Kruskal-Wallis and Chi-square using eViews software. The tests were performed separately for A and BPF type episodes registered between 2004 and 2007 using both the original data series and the data series smoothed using moving averages of order 24. Days of episodes were selected with daily concentrations greater than or equal to the value of the standard between 2004 and 2007 and compared with the behaviour of PM10, wind speed and direction using scatter plots, and daily cycles of wind roses.

To identify differences of the contribution of pollutant sources during episodes and no-episodes days the re-analysis of samples published by Artaxo (1999) for the fine and coarse fractions of PM10 in PudS was performed using absolute principal component analysis (SPSS V.8.0). These results were compared with information for the winter of 2005 published by Gramsch (2006).

2.2 Analysis of management actions to reduce PM10 concentrations in Pudahuel

Based on the data of weather, topographic conditions and emission sources the authors built a scenario in the Pudahuel area to promote actions to reduce particulate matter pollution at local level. This approach is supported by the policy of authorities, the pollution of Pudahuel station values taken as key to daily actions for the whole Metropolitan Region.

3. Results and discussion

3.1 Environmental concentrations of particulate matter in Santiago

Fig. 3 shows annual mean concentrations of PM10 for the period 1997-2008 at MACAM2 network stations. In general PudS presents the highest values, except for 2008. There is a general decline of PM10 concentrations towards 2005 and a further increase, except for LCS.

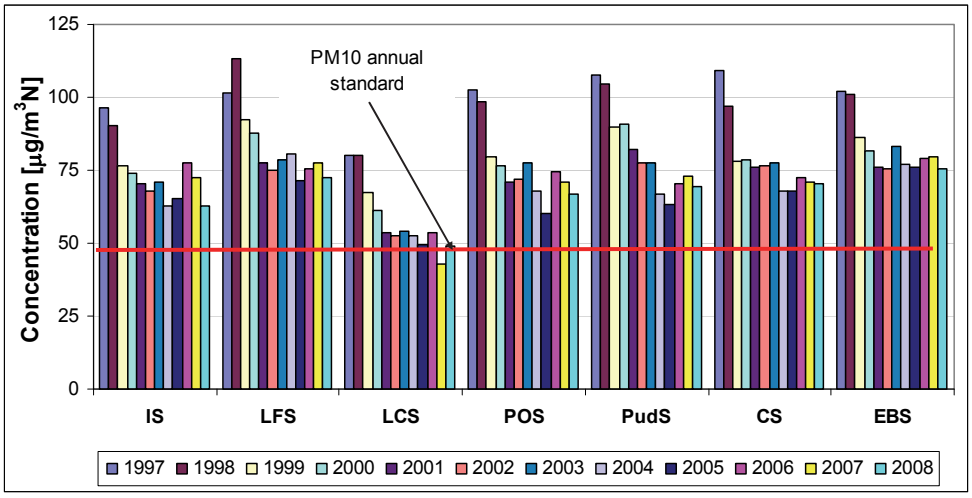

Fig. 3. Annual mean concentrations of PM10 collected with TEOM monitors of MACAM2 network (1997-2008).

This increase is primarily associated with the energy crisis that forced the industries using natural gas to return to diesel oil; however, in 2008 the number of episodes decreases in relation to 2007.

At PudS an exceedance of 26% of the daily standard and 42% of the annual standard has been observed. LCS is the only one always under the current standard. Moreover, in monitoring stations with high levels of PM10 concentration such as Puds, CS, EBS and LFlS, there was a decrease of days under environmental contingency during the period 1997 to 2005 (from 38 to 9 alert; 37 to 2 pre-emergencies, and disappearance of emergencies) as a result of the implementation of measures of PPDA.

Fig. 4 shows that in general, the highest value for daily maximum of 24h rolling averages concentrations, especially on days of high concentrations, corresponds to PudS. The peaks in 1997 were around 380 μg/m³ and in 2008 close to 260 μg/m³.

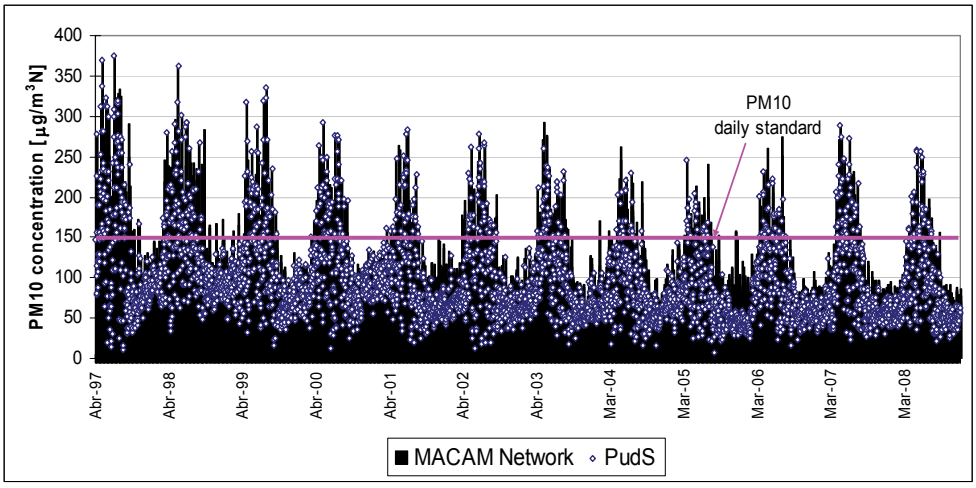

Fig. 4. Highest values for daily maximum of 24h rolling averages concentrations of PM10 in MACAM2 and PudS, 1997 to 2008.

During the period there were 371 days with PM10 alert level, 130 of them exceeding the pre-emergence level, 68% of the highest concentrations corresponding to PudS, most coinciding with A type episodes; in other cases, usually BPF type episodes, the highest concentrations were found at EBS, CS and LFlS stations (CENMA, 2005).

Figs. 5 a) and b) (autumn-winter) and c) and d) (spring-summer) show for most stations two peaks, one at the beginning of the activity of the city (07-09h) and the other associated with the increase in vehicular traffic and atmospheric stability (19-21h); the valleys (12-17h) are associated with an increase in the ventilation of the city. The exact shape of the curves and maximum values depend on each station, but in general, concentrations have declined in the decade under review. For PudS, mean concentrations during autumn and winter had decreased about 22% in the morning peak and about 25% in the afternoon peak. In spring and summer, the concentrations showed a decrease of about 25% in the morning peak and approximately 40% in late afternoon with a not sharply defined maximum.

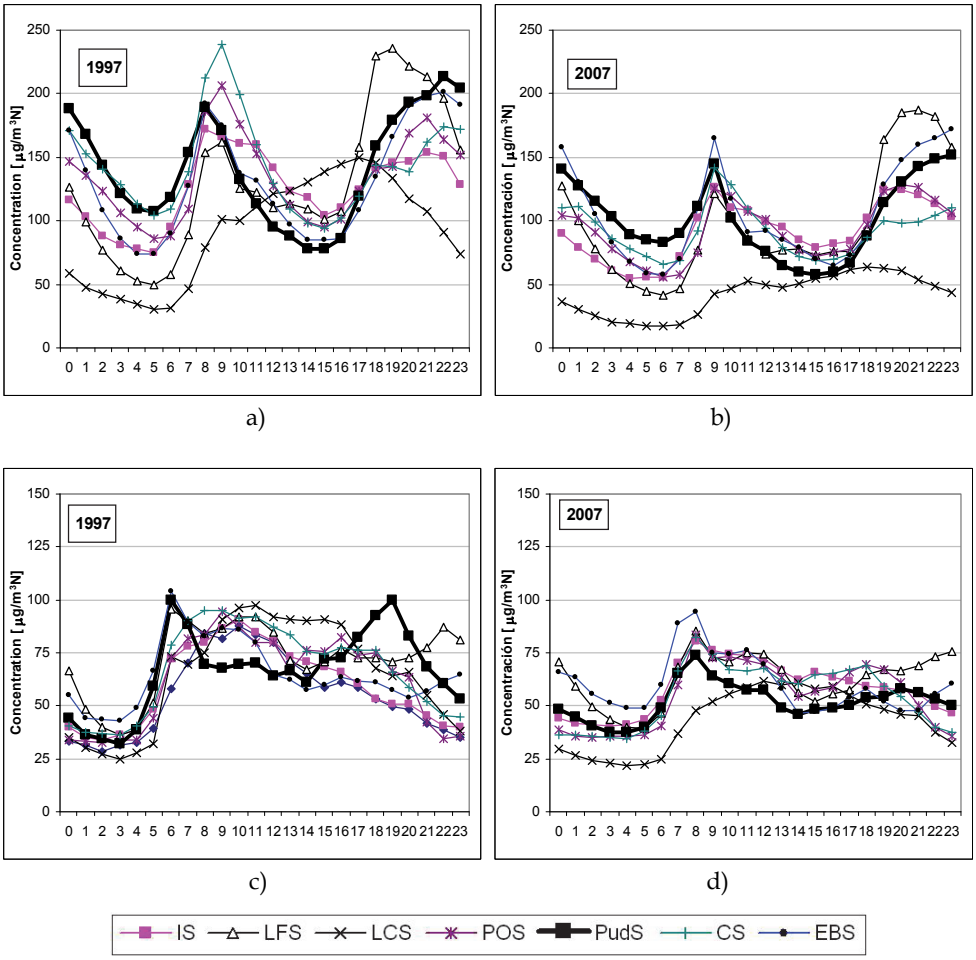

Fig. 5. Mean daily cycles of PM10 for MACAM2 network stations, fall-winter period: a) 1997; b) 2007; spring-summer period: c) 1997, d) 2007.

3.2 PM concentrations in Pudahuel

Fig. 6 shows that the mean concentrations of PM10 for the autumn-winter period are almost twice the mean concentrations during spring-summer. Between 2006 and 2008, the average from April to August of PM10 has been close to 95 µg/m³N, slightly higher than for the years 2004 and 2005 (~ 82 µg/m³N) and clearly lower than those for the years 1997 and 1998 (> 125 µg/m³N).

Analysis of the concentrations of fine (<2.5 µm) and coarse (> 2.6 - <10 µm) fractions of PM10, showed similar values except for the years 2004 and 2008 when the fine fraction exceeded the coarse fraction for more than 10 µg/m³N. Averages of the spring-summer period have remained above 50 µg/m³N, the value established as a limit on the annual standard for PM10.

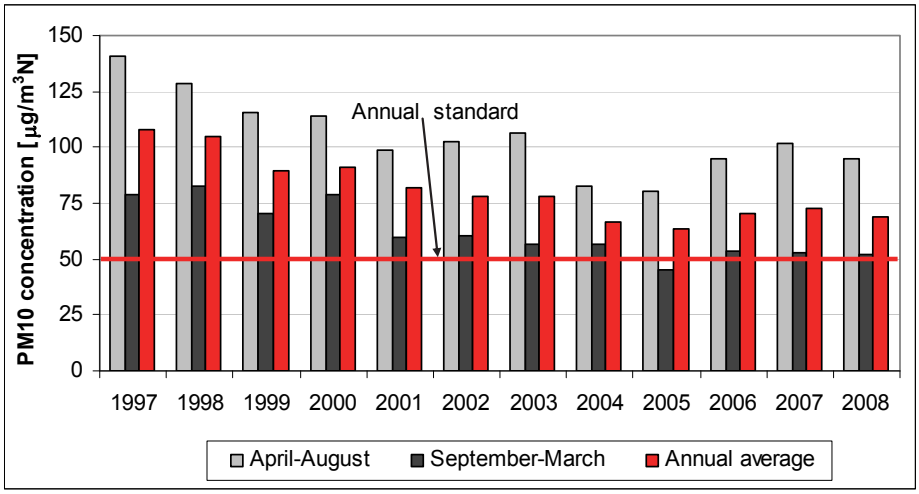

Fig. 6. Mean concentrations of PM10 for April-August and September-March periods and for the mean annual concentrations for the years 1997 to 2008.

Analysis of the annual cycles for monthly mean concentrations of PM10 and PM2.5 at PudS between 1997 and 2008 identifies the mean maximum between May and July for the autumn-winter concentrations and the mean minimum between October and November for spring-summer. For the 1997 to 2003 period the maximum monthly mean concentrations of PM10 and PM2.5 are close to 150 µg/m^{3}N and 75 µg/m^{3}N, respectively. In 2004, the lowest mean monthly maximum of PM10 was 100 µg/m^{3}N, the historically lowest value for Pudahuel; the lowest mean monthly maximum for PM2.5 occurred in 2005, with 50 µg/m^{3}N. Since 2006 concentrations have increased again, with recorded monthly mean maxima of PM10 and PM2.5 of 132 µg/m^{3}N and 60 µg/m^{3}N, respectively.
Between 2004 and 2007, 50 A type and 38 BPF type episodes occurred in Santiago, (CENMA, 2008). PudS showed, 56% of the time, the highest concentrations during A type episodes and only 11% during BPF type. Table 1 shows the concentrations for the 11 largest PM10 episodes at PudS, for that period.

Date	13-06-04	11-07-04	16-04-05	30-04-06	14-06-06	09-05-07	12-05-07	24-05-07	28-05-07	03-06-07	29-06-07	11-07-04
PM10 conc. (µg/m^{3}N)	221	231	246	232	223	226	289	274	223	246	273	221
Episode Type	A	A	A	A	B	A	B	A	B	A	A	A

Table 1. Characteristics of the 11 major episodes of PM10 concentrations at Pudahuel station for the years 2004 to 2007.

Fig. 7 a) and b) show a clear difference between the concentrations of the daily cycles of PM10 and PM2.5 during the 11 days of the major episodes and the mean concentrations for the autumn-winter period for the years 2004 to 2007. The morning peak during the episodes

days show an increase of almost 85% for PM10 and 67% for PM2.5 in relation to the mean for the autumn-winter period; during the afternoon of the episode days PM concentrations fall and then about 17h they begin to increase again, reaching, from 21 to 23h, 2.9 and 3.8 higher levels for PM10 and PM2.5 respectively, compared with the mean for the autumn-winter period.

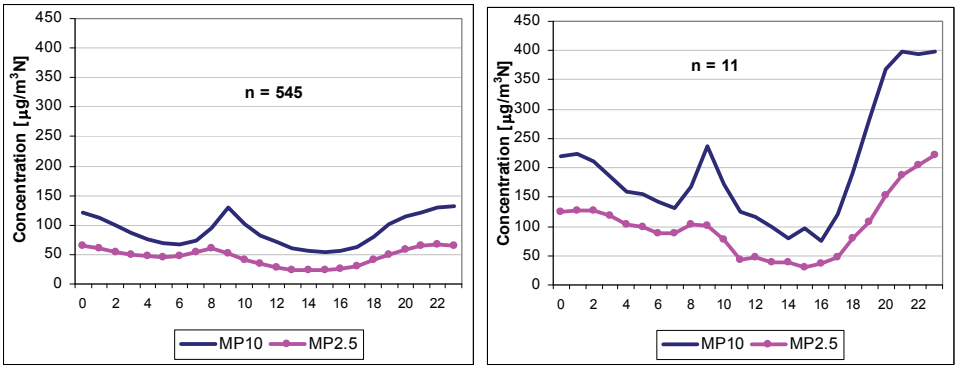

a) b)

Fig. 7. Mean daily cycles of PM10 and PM2.5 at Puds for the years 2004 to 2007: a) April-August period; b) the 11 episodes. Numbers of data included.

Considering the concentrations of fine and coarse fractions for 48 h for the 11 days of the major episodes, it can be seen that the maxima do not coincide exactly at the same times, as shown in Fig. 8. The maxima are separated by 2-3 hours. In the morning both fractions decrease their concentrations, but the fine fraction maintains higher values, reaching 127 µg/m^{3}N at 07h while the coarse fraction goes to 68 µg/m^{3}N at 06h. The increase in city activities and vehicle emissions also increases the concentrations of the fine (140 µg/m^{3}N at 07h) and coarse (170 µg/m^{3}N at 08h) fractions. After the morning peak, concentrations decrease to minimum values in the afternoon, around 30 µg/m^{3}N for the fine fraction and around 50 µg/m^{3}N for the coarse fraction.

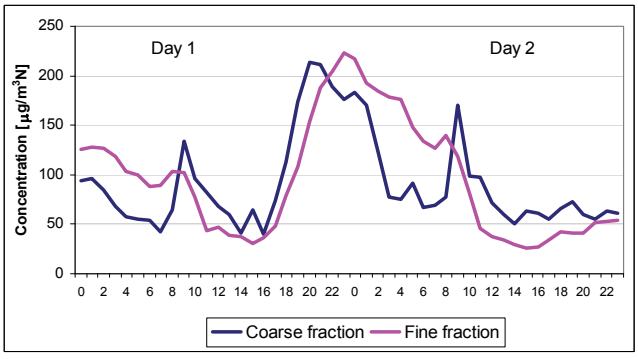

Fig. 8. 24 h PM10 mean concentrations profile for fine and coarse fractions for the 11 major events between 2004 and 2007.

The decrease in concentrations and the end of episodes occurs with increase in ventilation, height of the atmospheric boundary layer and moist coastal air intake
The profile of PM10 mean daily cycle for working days (Monday to Friday) and weekends (Saturday and Sunday) do not show significant differences, except for maximum concentration values in the morning and evening. Every Sunday morning shows concentrations 30% lower than the rest of the week. Conversely, the maximum night is 10 to 30% higher on Sunday and Saturday than on weekdays. However, results show that this increase is not related to the episodes. The mean daily cycle of temperature and wind speed, do not show significant variation during the different days of the week.

3.3 Extent of the geographical area of elevated concentrations during episodes of air pollution in Pudahuel

3.3.1 Pudahuel 1999 campaign

Fig. 9 shows similarities of the daily PM10 concentrations between MunPS (1km SE of PudS) and PudS stations and their great differences compared with LaFS (6km SW of PudS) for most days, except on August 8, 14, 25 and 28 when PudS concentrations were higher than at MunPS; LaFS concentrations were approximately 50% less than the PudS value.

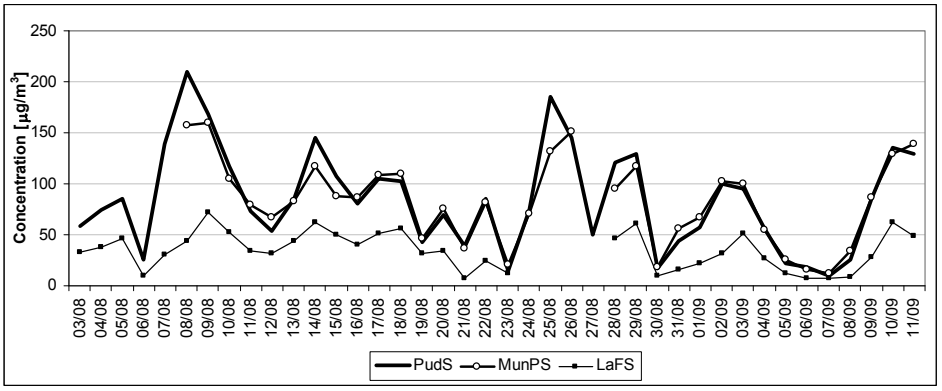

Fig. 9. PM10 daily concentrations at different stations in Pudahuel during August-September 1999

The daily cycle analysis confirmed the similarity of behaviour between PudS, and MunPS and their differences with LaFS, noting that the maxima at PudS are about 21% higher than at LaFS. During the afternoon, the concentrations at MunPS are higher than at PudS, probably due to the increased activity within the Municipality premise, where the MunPS is located.
The above results show that spatial variability of concentrations in the Pudahuel area, during episode days, even within the area of population representativeness (radius of 2 km), does not depend on the weather, but on local conditions of the sites under study. During the days exceeding the PM10 daily standard at PudS, PM10 concentrations at MunPS as well as at LAFS are within the standard.

3.3.2 Pudahuel 2003 campaign

Results of the measured concentrations, including 7 days of episodes (5 of A type and two BFP type) show higher values between 20h and 23 h (early episodes) than between 23h and

02 h the next day (later episodes). The highest concentrations of PM10 may be associated with local illegal burning, home heating and dust rising from bad roads by vehicle traffic. These measurements confirmed the results of the 1999 campaign showing lower concentrations at MunS than at PudS during the night.

The analysis of georeferencing mean PM10 concentrations showed that between 20 and 23h on the days of early A type episodes values increase towards the north of PudS, reaching mean concentrations of 700 µg/m³N (Fig. 10); in this area, illegal burning and dust rising from the streets by vehicular traffic were visually identified. In other sectors, mean concentrations were much smaller and in general PM10 concentrations tended to decrease towards the south of the Commune. On the other hand, the mean PM10 concentrations between 23h and 02h during late A type episode days show a decrease in concentrations throughout the area under study compared with the period 20h to 23h, with maxima in the north of 450 µg/m³N; in other sectors concentrations are only slightly lower.

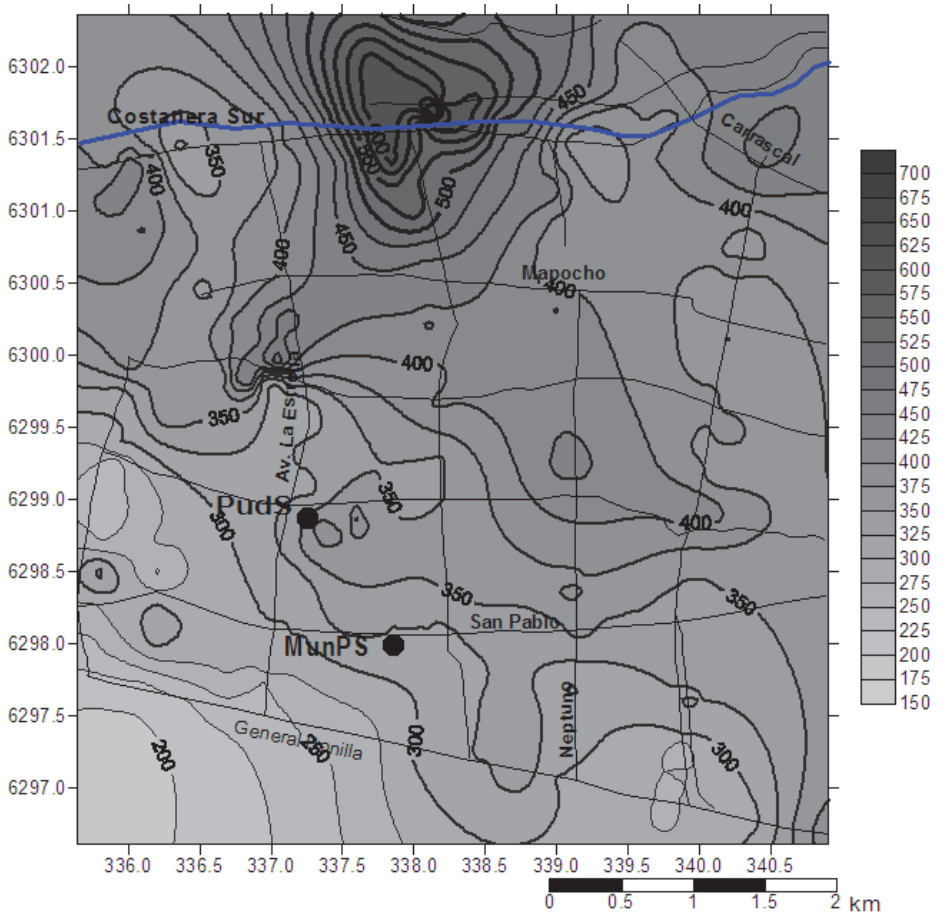

Fig. 10. Spatial distributions of mean PM10 concentrations between 20 and 23 hours, on the days of early A type episodes. July 25th to September 1st, 2003.

The mean hourly PM10 concentrations during early episode days (20 to 23 h) for BPF type episodes are lower than those during A type episodes.
On the days of BPF type episodes, PM10 peaks between 20 and 23h are located in the NW area of Pudahuel, reaching maximum concentrations about 550 µg/m^{3}N; about 2 km from PudS, the hourly mean concentrations are approximately 300 µg/m^{3}N decreasing towards areas located southwest of the station, reaching approximately 225 µg/m3N in the area of MunPS. In addition, lower concentration islands appear in areas of high concentrations, which could be attributed in part to differences in the ground level and to local conditions. The mean hourly concentrations between 23 and 02h during late BPF type episodes are lower than those recorded between 20 and 23h, and similar to levels in A type episodes.

3.4 Meteorological variables in the urban area of Santiago during episode days

Temperature and relative humidity measured in days of A type episodes show similarities between the values recorded at PudS and the other stations, except for LCS, for relative humidity, whereas there are differences for wind speed and direction recorded at PudS as shown in Fig. 11 for daily cycles and prevailing directions at hours of highest concentration (18 to 23h).
The correlation coefficients for wind speed with a confidence level of 95% for 1200 observations at each of the stations show a value of -0.25 between PudS and LCS and values between 0.43 and 0.69 between PudS and the rest of the network stations, for wind direction; the correlation coefficients between PudS and the rest of the stations are below 0.4.

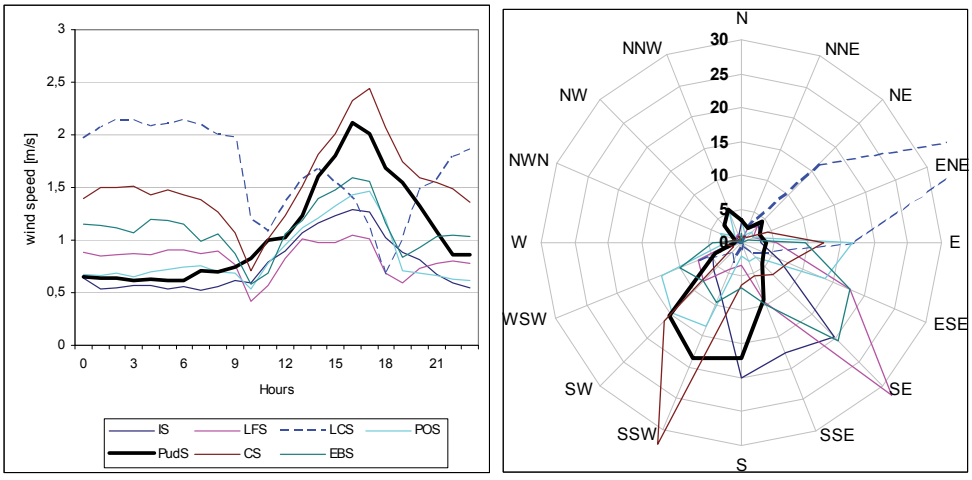

a) b)

Fig. 11. a) Daily cycles of wind speed; b) directions prevailing during hours of high concentrations (18 to 23h) for 50 days of A type episodes between 2004 and 2007 at MACAM2 network stations

Fig. 12 shows an inverse correlation between daily PM10 concentrations and wind speed recorded at PudS. Nevertheless, the site showed the highest and also the lowest daily PM10

concentration at the lowest wind velocity. For temperature, relative humidity and wind direction, no definite relationship was found.

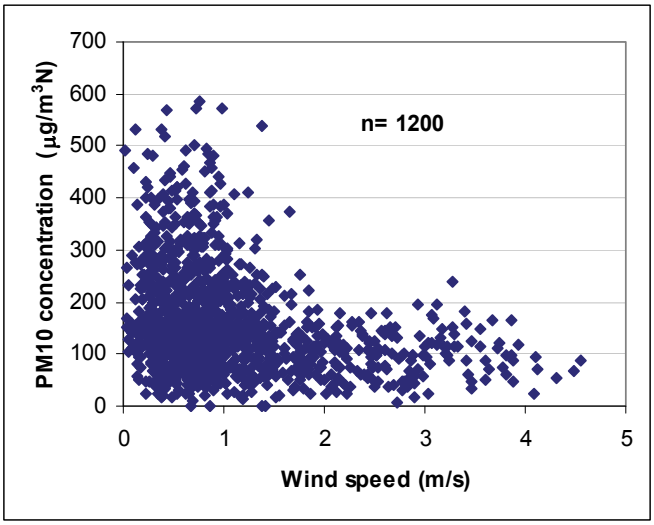

Fig. 12. Daily concentrations of PM10 as a function of wind speed at Pudahuel station, years 2004 to 2007.

The results of different statistical tests show, with a confidence level of 95% or 99%, that the wind speed measured at PudS is different from the rest of the stations, including days of A and BPF type episodes for the years 2004 to 2007. This result is consistent with that obtained by Gramsch et al. (2006) who classified the MACAM2 network stations for PM10 in 5 groups, leaving PudS alone in one of them.

Fig. 13 shows that wind direction from different areas of the city goes to the PudS area at the hours of highest PM10 concentration (18 to 23h) for days of A type episodes. At PudS, the predominant component is SW with wind speeds close to 0.8 m/s. During days of BPF type episodes, wind direction at LFlS and LCS is also towards the Pudahuel area, but with less intensity. At other stations there is great variability in wind direction from the SE, S and SW sectors with no component from the North.

Differences between the daily cycle of wind speed at stations in the eastern (LFS and LCS), central-south (EBS), and western (PudS) sectors of the city for days of A and BPF type episodes during which the daily concentrations of PM10 at PudS are higher than the standard limit value are shown in Fig.14. At LFlS and LCS the daily cycle is affected by a mountain-valley breeze effect that produces changes in wind direction and intensity about 10 AM and 18PM, being more pronounced at LCS where higher speeds are reached during the morning and night. On the contrary, the minimum speed is recorded during the night and early morning at PudS and EBS, and the maximum speed is reached in the afternoon, an hour before the minimum intensity at LCS.

At PudS, in the afternoons the wind speeds are higher during the A type episodes than during BPF type episodes. A similar situation occurs at LCS and EBS.

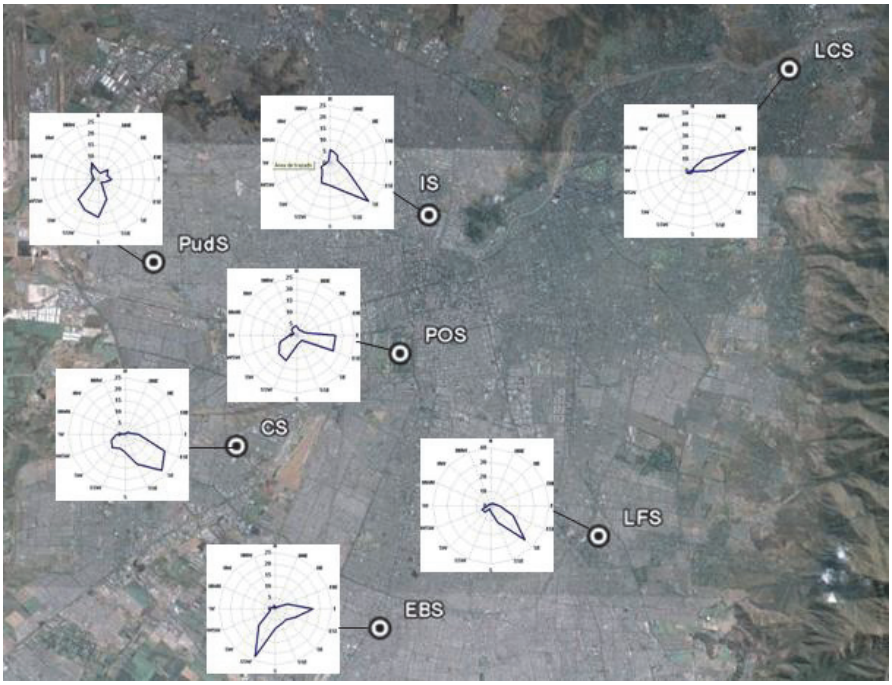

Fig. 13. Prevailing wind directions for days of A type episodes, at the hours of highest concentration of PM10 (18 to 23h) at MACAM2 network stations, years 2004 to 2007

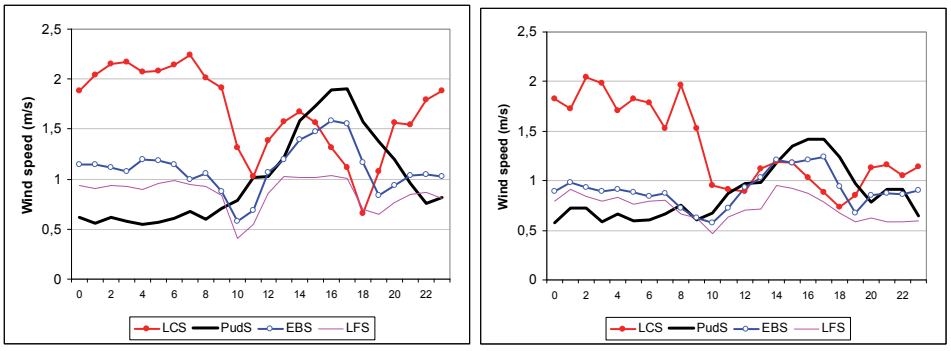

a) b)

Fig. 14. Mean daily wind speed at LCS, LFS, EBS and PudS for A type (a) and BPF type (b) episodes during years 2004 to 2007.

3.4.1 Behaviour of hourly PM10 concentrations of local wind at Pudahuel station

Figs. 15 a) and b) show a negative correlation between hourly and daily PM10 concentrations and wind speed, respectively, recorded at PudS. The highest hourly concentrations (> 400 μg/m^{3}N) occurred with wind speeds between 0.5 and 1.5 m/s. Some high concentrations, with

speeds higher than 3 m/s, occurred in the afternoon during April, 2005. With wind speeds of 5 m/s the PM10 concentrations are lower than 100 µg/m³N. Most days that exceed the value of the daily standard for PM10 have wind speeds averaging less than 1.5 m/s. In addition, there is no correlation between concentrations of PM10 and a predominant wind direction, particularly for very low wind speeds, unlike high speeds, for which a predominant direction remains for several hours. These results are broadly consistent with those reported by Muñoz et al. (2003).

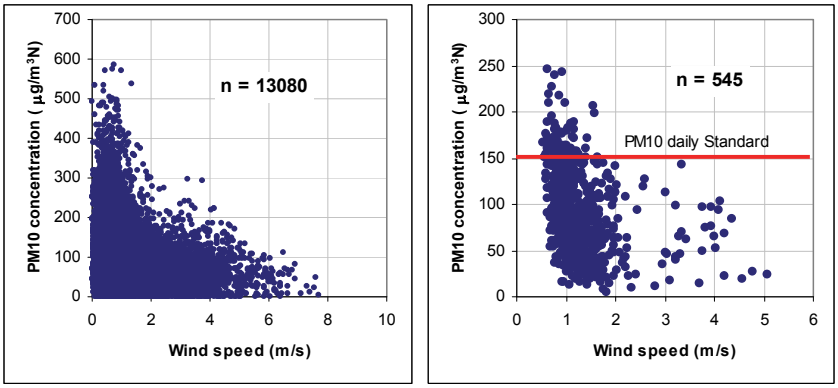

a) b)

Fig. 15. Correlation between PM10 concentrations and wind speed at Pudahuel station. Period April to August, years 2004 to 2007; a) hourly values, b) daily values.

Fig. 16 shows the mentioned inverse correlation between mean concentrations of PM10 and wind speed. From 19h wind speed is less than 1.5 m/s and PM10 concentrations reach values close to 260 µg/m³N around 23h, coinciding with declining wind speed values to under 1 m/s, which suggests an impact of local emission sources more than the impact of distant sources that require wind to be transported.

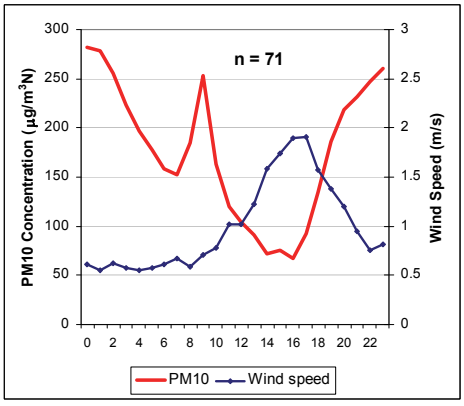

Fig. 16. Daily cycle of mean hourly concentrations of PM10 and wind speed, on days with PM10 concentrations above the standard. April-August period of 2004 to 2007 at Pudahuel station.

Fig. 17 shows the effect of the wind on episode days (35 days of A type, 19 days of BPF type) and 491 days under daily PM10 standard. It is again clear an inverse relationship between PM10 concentrations and wind speed including producing concentrations below the standard. This condition is more intense, from 18h, during days of A type episode than during days of BPF type episodes. At early morning the wind strength for the days of A and BPF type episodes remains close to 0.6 m/s. During days of episodes PM10 concentrations have at PudS a sharp increase around 08h associated with the begin of the city activity and vehicular traffic; during the afternoon, hours of more ventilation, occurs minimum concentrations.

Days of A type episodes show a different cycle of wind speed at LCS compared with Pudahuel, which means that during the night and early morning wind speed is greater (2 - 2.5 m/s). Along the day the wind intensity decreases and there is a change of direction from WSW to ENE at 10h, with a minimum of 1 m/s and from ENE to WSW at 18h, with a minimum of about 0.7 m/s. Days of BPF type episodes, show similar behaviour with lower intensity of the wind, especially at peak concentration hours at PudS (between 18 and 23h).

Consequently, the daily cycle of PM10 concentrations at LCS during episode days, is smaller than that at Pudahuel, even on occasions where PM10 concentrations at PudS have levels of alert or pre-emergency. The situation is similar during days of A and BPF type episodes, but the latter reach lower concentrations and higher wind speeds.

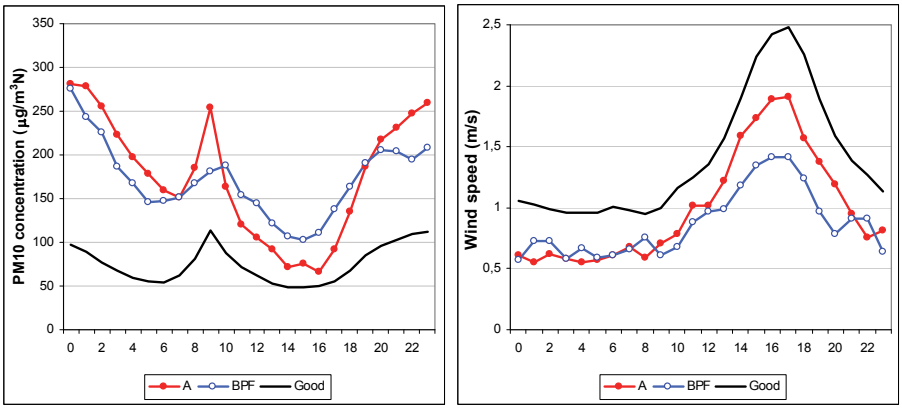

a) b)

Fig. 17. Daily cycle a) mean hourly concentrations of PM10 and b) wind speed for days of A and BPF type episodes and days below the standard. April-August period of 2004 to 2007 at Pudahuel station.

3.5 Contribution of PM10 emission sources to PM10 environmental concentrations in Pudahuel

In the Pudahuel Commune, DICTUC (2007) has identified 147 stationary sources, mainly backup generators, bakery ovens and industrial boilers (CENMA, 2008b). Major stationary sources close to PudS are bakeries, bus terminals, and industrial boilers. The emissions of PM10 of Pudahuel Commune correspond to 1.5% of total emissions of industrial and mobile sources of the Metropolitan Region, as shown in Table 2.

	Light vehicles	Heavy trucks	Clean buses	Other buses	Industry	Total
Pudahuel	2,0	26,8	2,2	3,1	6,6	45,1
MR	514,0	763,0	221,0	94,0	1266,9	3017,2
% Pudahuel	0,4	3,5	1,0	3,3	0,5	1,5

Source: CENMA, 2008b and CONAMA, 2009

Table 2. PM10 emissions from mobile sources and industry to Pudahuel and Metropolitan Region, expressed as tons per year.

Table 3 shows the importance of estimating not only annual but also hourly emissions for major categories of industrial Pudahuel sources especially from 18h until the early hours of the next day, hours during which the PM10 environmental concentrations increase. For instance, backup power generator industries work just a few hours (79% of the hourly emissions), usually at night, during winter days in order to not exceed the limits of electricity consumption and pay fines to the electricity distribution companies.

Source category	Number of sources	Emission	
		Annual t/year	Hourly kg/h
Power Generators	36	1,0	6,2
Industrial Boilers	22	2,9	0,5
Heating Boilers	30	1,1	0,3
Bakery Ovens	39	0,4	0,4
Other Ovens	6	0,5	0,2
Others	14	0,7	0,3
TOTAL	147	6.6	7.9

Source: CENMA, 2008b and CONAMA, 2009

Table 3. PM10 emissions from categories of industrial sources of Pudahuel

Figs. 18 a) and b) show that heavy trucks and buses are the major emission mobile sources in the area that includes the Pudahuel and other nearby Communes (DIMEC, 2007; DIMEC, 2007a). The flow is normalized to peak flow (09h) for working days (Monday to Friday) and weekends (Saturday and Sunday). The flow of heavy trucks has a similar behaviour every day, with a maximum between 10h and 13h. During the evening the flow decreases by 30% compared with the morning. On Sunday, the morning flow decreases by 30% in relation to the week maxima, but it has the highest values at night, between 21h and 22h. Buses (diesel) show differences in the flow of working days and weekends. During the week, there is an increase before the peak, which may be associated with the departure of buses from the large number of bus terminal stations in the area. Between 10h and 22h the flow remains between 90%-100%, of the rush hour, but between 23h and 06h the movement is virtually null. On Saturday morning circulation is equivalent to about 80% and during Sunday afternoon, about 50% of working days.

Mobile and industrial sources show lower emissions on weekends, which do not explain the increased concentrations of PM10 during weekend nights, so that increased concentrations

should be associated with untested local sources, including all kinds of home heating fuels and the dust recycled from streets and roads, by a greater flow of private vehicles.

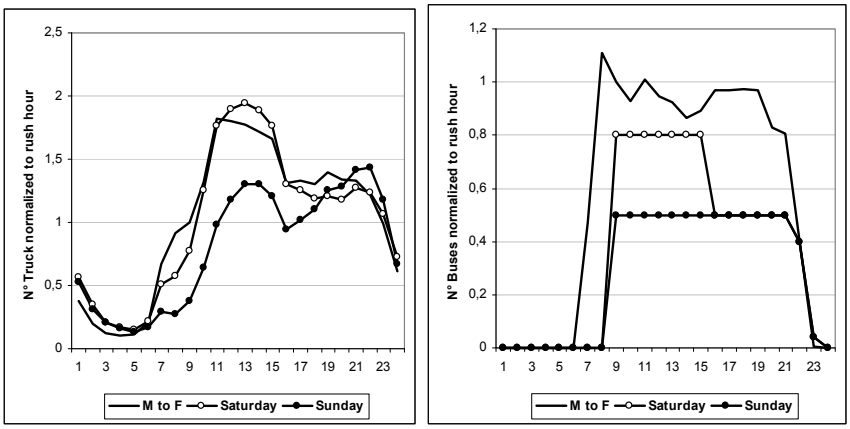

a) b)

Source: DIMEC, 2007 and DIMEC, 2007a

Fig. 18. Daily cycle flow normalized to peak in sector 5 for: a) heavy trucks, b) buses

According to Artaxo (1999) the chemical analysis of the fine and coarse fractions of PM10 in PudS during the winter of 1998 shows 3 major sources: soil dust, transport and copper smelting (S + As + Cu). In the coarse fraction, 88% (73 μg/m³) was attributed to soil dust, 9% to sources emitting S + As + Cu, and 3% to transport. For the fine fraction, the main source was associated to copper smelting with 48% (15 μg/m³), 32% to transport and 20% to soil dust. Reanalysis of that information done for this study, separating the episode days (alerts and pre-emergency) from the good days (concentrations <100 μg/m³) maintains the 3 sources but shows an increase in the concentrations in both fractions on the episode days. In addition, there is a change in the relative contribution of the sources of fine and coarse fractions. The largest increase is for element concentrations associated with the smelting of Cu (6 to 22 μg/m³) followed by soil dust (5 to 11 μg/ m³); for the coarse fraction, the major increase corresponds to soil dust (60 to 135 μg/m³), smelting of Cu (44 μg/m³) and transport (20 μg/m³). These results indicate that despite the measures taken by the government (CONAMA, 1997) to reduce emissions from factories and transportation for episode days, an increase in PM10 concentrations is occurring, associated with the 3 sources, especially the coarse fraction. Similar results, but for smaller PM10 concentrations, were obtained by Gramsch (2006), in a campaign conducted in 2005. It is interesting to note that this study assigns 50% of PM2.5 to carbon (39% to organic C and 11% to inorganic C).

3.6 Guidelines to improve the management of air quality of Pudahuel and Santiago basin

The first version of PPDA for the Metropolitan Region (CONAMA, 1997) considered 139 measures to improve air quality throughout the city of Santiago, including 104 actions to direct and permanently reduce emissions of major pollution sources; 26 management actions for pollution episodes (PGEC), including events of alert, pre-emergency, and

emergency: 9 actions for indirect reduction of emissions, i.e., public participation and education.

The PPDA considered a revision and update twice to meet in force the primary standard for the year 2012. Initially, structural measures were considered with a strong impact on reducing industrial emissions of particulate matter and gases, namely modernization of public transport, use of cleaner fuels and accomplishment of goals for reducing industrial emissions. Later, the revision and update of the plan (CONAMA, 2009), strengthened and deepened structural measures to reduce the fine fraction of PM10 by controlling and reducing NO_x emissions, some VOCs, SO_x and NH_3.

In the case of Pudahuel, those measures are of weak impact considering that the industrial sources of the commune represent only 1.5% (147 sources) of the total annual emissions in the Metropolitan Region. However, the backup power generator groups correspond to 79% of hourly night emissions.

The PGEC of the PPDA has three components: 1) Forecast of air quality for PM10, 2) permanent control of emission sources during critical events and 3) public communication of air quality, recommendations and actions. For the period April 1st to August 31th it also establishes permanent actions including restriction of circulation for vehicles without catalytic converters, prohibition of agricultural burning in the entire Metropolitan Area and sweeping of streets according to budget availability. During episodes some of these restrictions are increased depending on the quality of the episode (alert, pre-emergency or emergency).

The forecasting system for PM10 episodes established in 2000 has a preventive nature, recommending actions depending on the probable 24h rolling averages maximum for the next day. The announcement is made about 21h on television and on the CONAMA website. Results show that for short episodes (1 day) actions are taken when the problem has already occurred. Fig.19 illustrates the case on May 21, 2006.

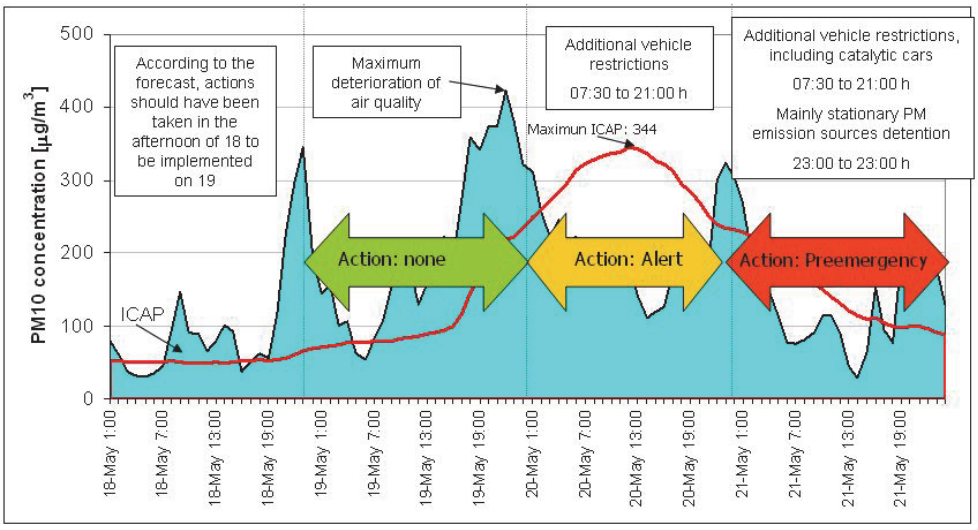

Source: CENMA, 2007

Fig. 19. Episode of May 21, 2006

To improve the management of air quality we suggest that the recommendation proposed by CENMA (2008) be taken into account by changing the present forecasting procedure to considering the use of the mean value from 06h to 05h of the previous day and move the announcement of the action to 18h, warning when high concentrations are detected at night time, especially at PudS. In addition, it was recommended that forecasting point models for the periods of high concentrations be developed, usually between 18h and 23h.
PPDA measurements are applied to the entire Metropolitan Area, with no specific proposals for individual Communes. For Pudahuel the results show an increase in both fractions of PM10 (fine and coarse) in recent years. Regarding the coarse fraction, there are many diffuse sources of recycled dust, which involves implementing specific actions to reduce these emissions, including an important increase in green area surfaces. For the fine fraction there should be greater control and an educational campaign to prevent the wrong environmental practices detected. Other specific actions for the Pudahuel area might include:
i) development of programs to improve the conditions of streets and roads, access to terminals bus stations and street sweeping program to meet for example, the standard of the State of California (USA); ii) improvement in the control of industries, households, small size sources using firewood, particularly on episode days; iii) development of incentive programs for the setting up of mitigation and control systems to decrease emission sources; iv) development of programs to improve thermal insulation and housing subsidies for the purchase of clean-fuel heating equipment operating on clean fuels; v) creation of media mechanisms (Internet, radio or community television, neighbourhood associations and others) to prevent exposure and physical activity of the population during periods of high concentrations of PM10.

4. Conclusions

The results of this study support the existence of spatial heterogeneity of air quality for the population of the city of Santiago. Pudahuel commune has its own characteristics, due to both meteorological conditions and to emissions sources of particulate matter that determine the concentrations of this pollutant observed in some days of the autumn-winter period. Consequently, the concentrations observed are not necessarily representative of the Metropolitan Area. As a result, management of episodes can not be based only on PM10 concentrations observed at Pudahuel station.
It is clear that a very specific campaign must be implemented to decontaminate Pudahuel. But it is also clear that there is a necessity to implement an environmental policy to manage air quality as a support to health and quality of life of people living or working in specific communes. These actions should be subsidized by the State or should be included in measures funded by private companies for instance as part of corporate social responsibility activities.
Since the environmental policy began to be implemented in Chile, the authority has used the "prevention principle" to determine PPDA actions, which may have certain advantages when the State has some level of basic information on air quality. This idea has led the authorities to consider PudS as key to determining environmental alerts. This study shows that, given the spatial heterogeneity of air pollution, a more detailed knowledge of pollution in Santiago would focus on more effective measures at local level which could be managed from the same municipalities in coordination with the metropolitan government.

5. Acknowledgment

Authors acknowledge to Laura Ortiz and Victor Sanhueza for technical support and statistical analysis.

6. References

Artaxo, P. 1999. Final Report Aerosol Characterization Study in Santiago de Chile -1999. Santiago, CONAMA RM. 69p

Artaxo, P., Oyola, O. and Martinez, R. 1999. Aerosol composition, Size Distribution, and Source Apportionment in Santiago de Chile. Nuclear Instruments and Methods B, 150:409-416.

ASRM, 2008. Historia de la red MACAM. Santiago, SEREMI Salud. Available from <http://www.seremisaludrm.cl/sitio/pag/aire/Indexjs3airesist_monit.asp>

Cakmak, S., Dales RS. and Blanco C. 2007. Air pollution and Mortality in Chile: Susceptibility among the Elderly. Environmental Health Perspectives. 115(4): 524 – 527p

CENMA, 2005. Análisis comparativo de condiciones meteorológicas asociadas a episodios de Contaminación Atmosférica en Santiago, durante los períodos de otoño-invierno 1997 a 2005. Report for CONAMA RM. September, 2005.

CENMA, 2008. Análisis comparativo de condiciones meteorológicas asociadas a episodios de Contaminación Atmosférica en Santiago, durante los períodos de otoño-invierno 1997 a 2008. Report for CONAMA RM. September, 2008.

CENMA, 2008b. Actualización del inventario de emisiones de contaminantes atmosféricos de la Región Metropolitana, Año Base 2007. Report for CONAMA. December, 2008.

Cifuentes, L., L. Lave, Vega, J. and Kopfer, K. 2000. Effect of the fine fraction of particulate matter vs the coarse mass and other pollutants on daily mortality in Santiago, Chile. Journal of the Air & Waste Management Association, 50:1287-1298

CONAMA, 1997. Plan de Prevención y Descontaminación Atmosférica para la Región Metropolitana. Santiago, CONAMA RM.

CONAMA, 2001. Anteproyecto de Revisión, Reformulación y Actualización del Plan de Prevención y Descontaminación Atmosférica para la Región Metropolitana. Santiago, CONAMA RM.

CONAMA, 2008. Anteproyecto de Revisión, Reformulación y Actualización del Plan de Prevención y Descontaminación Atmosférica para la Región Metropolitana. Santiago, CONAMA RM.

CONAMA, 2009. Segunda Actualización del Plan de Prevención y Descontaminación Atmosférica de Santiago. Santiago, CONAMA RM.

De La Vega, V., Fuentes, H., Ortiz, J. and Préndez, M. 1987. Balance de masa en aerosoles atmosféricos de Santiago de Chile. Bol. Soc. Chil. Quím., 32, 187-197.

DICTUC, 2007. "Actualización del Inventario de Emisiones de Contaminantes Atmosféricos en la Región Metropolitana 2005". Santiago, CONAMA RM.

DIMEC, 2007. Actualización de Factores de Emisión para Vehículos Livianos y Medianos. Final Report. Departamento de Ingeniería Mecánica, Universidad de Chile.

DIMEC, 2007a. Investigación de Factores de emisión Para Vehículos de Carga. Final Report. Departamento de Ingeniería Mecánica, Universidad de Chile.

Gramsch, E. 2006. Análisis Retrospectivo de Filtros de Material Particulado MP10 en sus fracciones fina y gruesa para estaciones de la Red MACAM2 II en el período 2003-2006. Final Report, Diciembre 2008. Universidad de Santiago de Chile.

Gramsch, E., Cereceda-Balic, F., Oyola, P. and Von Baer, d. 2006. Examination of pollution trends in Santiago de Chile with cluster analysis of PM10 and Ozone data. Atmospheric Environment 40: 5464–5475

Ilabaca, M., Olaeta, I., Campos, E., Villaire, J. and Tellez-Rojo, M. 1999. Association between levels of fine particulate and emergency visits for pneumonia and other respiratory illnesses among children in Santiago, Chile. J Air Waste Manag Assoc 49:154–163.

Morata, D. Polve, M, Vales, A. Belmar, M. 2007. Characterisation of aerosol from Santiago, Chile: an integrated PIXE–SEM–EDX study. Environ Geol DOI 10.1007/s00254-007-1141-8

Muñoz, R., Garreau, R., Fuenzalida, H. and Schmitz, R. 2003. Meteorología y Modelación de la Calidad del Aire en la Región Metropolitana. Final Report. Departamento de Geofísica, Universidad de Chile.

Ortiz, J., Apablaza, N., Campos, C., Zolezzi, S. and Préndez, M. 1993. Tropospheric Aerosols Above the Thermal Inversion Layer of Santiago, Chile: Size distribution of Elemental Concentration. Atmospheric Environment 27A(3).

Ondov, J. M. and Wexler, A. S. 1998. Where Do Particulate Toxins Reside? An Improved Paradigm for the Structure and Dynamics of the Urban Mid-Atlantic Aerosol. Environ. Sci. Technol. 32:2547-2555.

Ostro, B., Sanchez, JM., Aranda, C. and Eskeland, G. 1996. Air Pollution and Mortality: Result form a Study of Santiago, Chile. Journal of Exposure Analysis and Environmental Epidemiology 6:97-114.

Ostro, B., Eskeland, G., Sanchez, J. and Feyzioglu T., 1999. Air pollution and health effects: A study of medical visits Among Children in Santiago, Chile. Environmental Health Perspectives. 107(1): 69-73p.

Oyanguren, H. 1972. Bronquitis crónica en un área urbana y una rural de Santiago y su relación con el grado de contaminación atmosférica". Rev. Med. de Chile.100-101, 1972

Pino, P., Walter, T., Oyarzun, M., Villegas, R. and Romieu, I., 2004. Fine particulate matter and wheezing illnesses in the first year of life. Epidemiology 15, 702–708.

Préndez, M., Ortiz, J., Cortes, E. and Cassorla, V. 1984. Elemental composition of the airborne particulate matter from Santiago City, Chile, 1976. J. Air Pollut. Control Ass. 34, 54-56.

Préndez, M. 1993. Características de los Contaminantes Atmosféricos. En: Sandoval, H. Préndez, M. and Ulriksen, P. (Eds). Contaminación Atmosférica de Santiago: Estado Actual y Soluciones. pp. 109-186.

Préndez, M., Ortiz, J., Zolezzi, S., Campos, C. and Apablaza, N. 1991. Aerosoles atmosféricos de naturaleza inorgánica. Contaminación en Santiago de Chile. Revista Chilena de Enfermedades Respiratorias, 7(4), 224-237.

Préndez, M., Corvalan, R. and Cisternas, M. 2007. Caracterización física y química del material particulado de fuentes estacionarias: incidencia sobre la aplicación de un sistema de compensación de emisiones en la Región Metropolitana de Santiago. Revista Internacional Tecnológica, CIT, Vol 18 (2), 39-103.

Prospero, J. M. y Charlson, R. 1983. The atmospheric Aerosol System: A Review. Review of Geophysics and Space Physics. 21 (7): 1607 – 1629.

Rojas, C., Artaxo, P. and Van Grieken, R. 1990. Aerosols in Santiago de Chile: A study using receptor modelling with X-ray fluorescence and single particle analysis. Atmospheric Environment 24B (2): 227-241.

Rutllant, J. 1973. Factores meteorológicos en la contaminación atmosférica de Santiago. Resultados de mediciones 1971-1972. Publicación No. 164, Departamento de Geofísica, Universidad de Chile

Rutllant, J. and Salinas, H. 1983. Caracterización meteorológica de situaciones de alto potencial de contaminación atmosférica en Santiago. Tralka, 2(1):57-16

Rutllant, J. and Garreaud, R. 1995. Meteorological Air Pollution Potential for Santiago, Chile: Towards an Objetive Episode Forecasting. Environmental Monitoring and Assesment 34: 223-244.

Rutllant, J. and Garreaud, R., 2004. Episodes of strong flow down the western slope of the subtropical Andes. Monthly Weather Review 132, 611–622.

Sienra, M., Rosazza, N. and Préndez, M. 2005. Polycyclic aromatic hydrocarbons and their molecular diagnostic ratios in urban atmospheric respirable particulate matter. Atmospheric Research 75: 267–281

Trier, A. 1984. Observations on inhalable atmospheric particulate in Santiago, Chile, J. Aerosol Science, 15: 419-421.

Trier, A., and Silva, C. 1987. Inhalable urban atmospheric particulate matter in a semi-arid climate: the case of Santiago de Chile. Atmospheric Environment, 21: 419-983.

Ulriksen, P. 1980 Variaciones diarias de la altura de la capa superficial de mezcla sobre Santiago. Tralka 1 (2):143-151.

Ulriksen, P. 1993. Factores Meteorológicos de la Contaminación Atmosférica de Santiago. En: Sandoval, H. Préndez, M. y Ulriksen, P. (Eds). Contaminación Atmosférica de Santiago: Estado Actual y Soluciones. pp. 37-60.

US EPA, 2004. Air Quality Criteria for Particulate Matter, EPA/600/P-99/002aF. Research Triangle Park, NC, October 2004.

WHO, 2005. Air quality guidelines global update 2005. Report on a working group meeting. Bonn, Germany, October 18-20th, 2005.
[www.euro.who.int/Document/E87950.pdf].

16

Multi-Year Assessment of Airborne Metals in Fallon, Nevada, using Leaf-Surface Chemistry

Paul R. Sheppard[1], Gary Ridenour[2] and Mark L. Witten[3]
[1]*Laboratory of Tree-Ring Research, University of Arizona, Tucson, Arizona 85721*
[2]*625 W. Williams Ave., Suite B, Fallon, Nevada 89406*
[3]*Odyssey Research Institute, Tucson, Arizona, 85710*
USA

1. Introduction

1.1 Fallon, Nevada

Spatial patterns of airborne metals are described from leaf-surface chemistry of trees in Fallon, Nevada (Fig. 1a), where a cluster of childhood leukemia began in 1997. Officially, 16 cases of childhood leukemia were diagnosed from 1997 to 2002 inclusive (Expert Panel, 2004), and one additional case was reported in December 2004 (Nevada State Health Division, 2004). Although the cluster is thought to have abated (Reno Gazette-Journal, 11 October 2008), at least one additional case of childhood leukemia has occurred in Fallon since 2004 (Lahontan Valley News, 15 October 2010). Given Fallon's pediatric population of about 2500 children up to 19 years in age (U.S. Census, 2000) and a national expected rate of childhood leukemia of 4.1 cases per 100,000 children up to 19 years in age per year (U.S. NCI, 2003), the expected rate of childhood leukemia for Fallon should be only one case every ten years.

This cluster, deemed "one of the most unique ever reported" (Steinmaus et al., 2004; Steinmaus et al., 2005), prompted multiple investigations to determine if an environmental cause might have been responsible. Research focused on drinking water (Moore et al. 2002; Shaw et al., 2005; Walker & Fosbury 2009; Walker et al., 2006), jet fuel (U.S. ATSDR, 2002), pesticides (Rubin et al., 2007; U.S. CDC, 2003), surface water (U.S. ATSDR, 2003a), outdoor air (U.S. ATSDR, 2003b), surface soil and indoor dust (U.S. ATSDR, 2003c), potential lingering effects of underground nuclear bomb testing in the area (Seiler, 2004), and groundwater (Seiler et al., 2005). A non-environmental hypothesis–population mixing–was also considered (Kinlen & Doll, 2004; Wakeford, 2004]. Few definitive conclusions emerged from these studies, prompting an interpretation that Fallon had been given a "clean bill of health" by the US Agency for Toxic Substances and Disease Registry and the US Centers for Disease Control (Lahontan Valley News, 8 August 2007). However, this interpretation is questionable (Pleil et al., in press), and the need to monitor the environment of Fallon continues to exist.

To monitor the environment of Fallon, we have employed multiple techniques, all of which have shown notable patterns of airborne tungsten and cobalt. Elevated tungsten and cobalt was identified in airborne particulates of Fallon relative to comparison towns (Sheppard et al., 2006a) and in lichens within Fallon compared to outlying desert areas (Sheppard et al.,

2007b). Tungsten and cobalt maxima were found in surface dust (fallout from air) near the center of Fallon, just north and west of the crossroads of the main highways (Sheppard et al., 2007a). Dendrochemistry showed that tungsten began increasing in Fallon tree rings by the mid-1990s, coinciding roughly with the onset of the cluster of childhood leukemia (Sheppard et al., 2007c). From direct microscopy analysis of airborne tungsten particles in Fallon, they are anthropogenic in origin, not natural (Sheppard et al., 2007d).

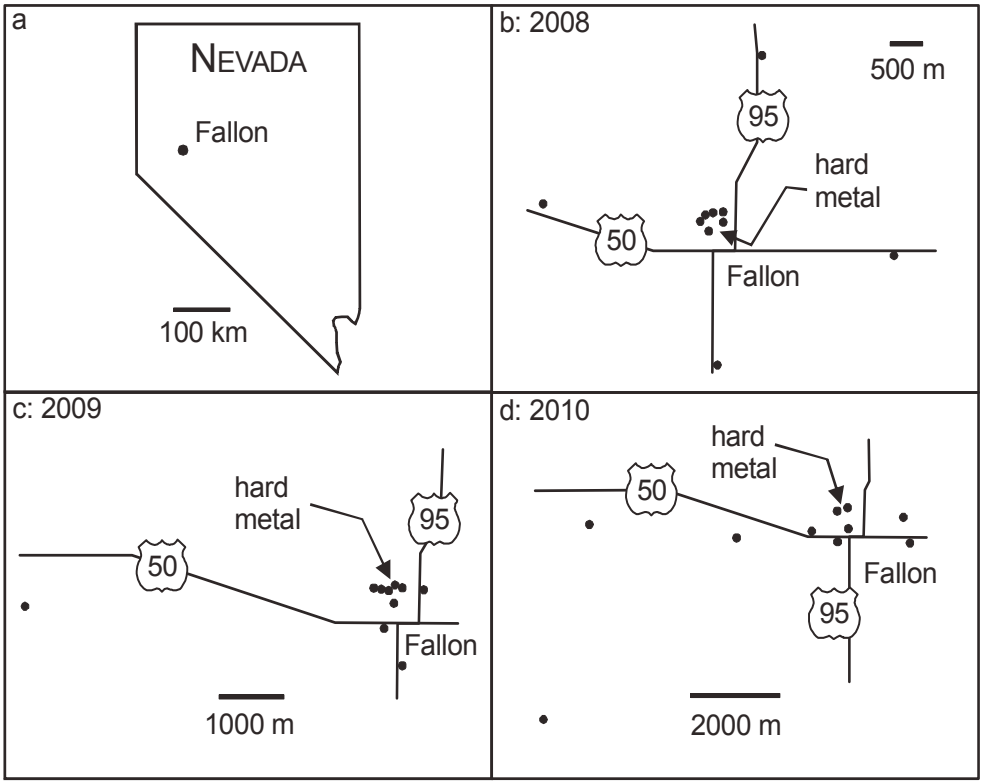

Fig. 1. Maps of Nevada, showing Fallon (a) and of Fallon, showing trees from which leaves were collected each year from 2008 through 2010 (b-d). An industrial facility performing hard-metal metalurgy is located just northwest of the main intersection of Highways 95 and 50.

1.2 Leaf-surface chemistry to assess air quality

An environmental monitoring technique that is applicable for assessing air quality is leaf-surface chemistry, the measurement and interpretation of element concentrations in particulates that accumulate on surfaces of leaves of trees and other plants. Leaf-surface chemistry indicates atmospheric chemistry (Wittig, 1993), including airborne metals (Rautio et al., 1998). Leaves are easy to collect (Aksoy et al., 1999), so spatial and temporal arrays of samples can be obtained quickly (Loppi et al., 1997). Leaf-surface particulates reflect the chemical composition of recent accumulations, on the order of weeks to months or perhaps an entire growing season depending on the occurrence of precipitation (Alfani et al., 1996b).

By collecting leaves across a region, differing accumulations of airborne metals can be mapped, thereby pinpointing source areas (Aboal et al., 2004). Paired studies of leaf-surface accumulations with ground-surface dust and/or airborne particulates can be particularly fruitful for confirming airborne chemistry and identifying spatial patterns of metals (Bargagli 1993; Čeburnis and Steinnes 2000). Because of these advantages, many case studies exist worldwide using leaf-surface chemistry to quantify atmospheric loading of heavy metals and/or identify their spatial patterns (e.g., Aksoy and Öztürk, 1997; Aksoy et al., 1999; Alfani et al., 1996a; Dasch, 1987; Gupta et al., 2004; Rossini Oliva and Mingorance, 2006; Salve et al., 2006; Ward, 1977;). More specifically, leaf-surface chemistry was done in Fallon in 2007, and it showed elevated peaks of airborne tungsten and cobalt just northwest of the center of town (Sheppard et al., 2009a).

1.3 Objective

For years now, we have been collecting various biological samples in and around Fallon for the purpose of assessing air quality there. Total suspended (airborne) particulate samples were collected in March and November 2004. Lichens and surface dust were collected in March 2005. Tree leaves were first collected in October 2007. Tree-ring samples have been collected multiple times since 2002. As time progresses, this time series of observations of air quality of Fallon becomes more and more precious by virtue of the ability to discern change in air quality through time. Therefore, it is important that regular monitoring of air quality of Fallon be maintained. A relevant Nevada state agency charged with environmental monitoring and protection has stated no plans for doing investigations in Fallon (Lahontan Valley News, 3 December 2005), but we are carrying on with environmental monitoring in Fallon.

Weighing advantages and disadvantages of various environmental monitoring techniques (Sheppard et al., 2009b), we have chosen leaf surface chemistry as the technique with which to continue monitoring Fallon air quality. Accordingly, leaves from trees of Fallon were collected in October of 2008, 2009, and 2010. The objective of this chapter is to describe the surface chemistry of these leaves to update spatial patterns of airborne tungsten and cobalt in Fallon.

2. Methods

2.1 Site description

Fallon is a small, rural, farming community (Greater Fallon Area Chamber of Commerce, 2008) located in west-central Nevada (Fig. 1a). Its climate is cool to mild and dry, with a mean annual temperature and precipitation of 10.7° C and 127 mm, respectively, as typified from meteorological data from Fallon (monthly data from 1931 to 2010 obtained on-line from the National Climatic Data Center, NOAA 2010). Along with service industries and small businesses, Fallon has a facility that does hard-metal metallurgy, which includes tungsten carbide and cobalt (Harris and Humphreys, 1983). The hard-metal facility has been considered a candidate source of tungsten within Fallon generally (Reno Gazette-Journal, 5 February 2003) and more specifically of elevated tungsten and cobalt in total suspended particulates and in surface dust of Fallon (Sheppard et al., 2006a, 2007a).

2.2 Leaf collection

Tree leaves were collected in mid- to late-October of the years 2008, 2009, and 2010. All trees sampled were deciduous species, so results of this study reflect accumulations of airborne particulates onto leaf surfaces during just the growing season of each year. During the leaf

season (May–October) of all four years 2007–2010, measurable rainfall was recorded in varying amounts at the nearby Fallon Naval Air Station (Fig. 2; daily data obtained on-line from the National Climatic Data Center, NOAA 2010).

All trees sampled were broadleaf species, in part because conifer species are not common in Fallon but also because broad leaves provide ample surface for accumulating airborne particulates. Tree species was not held constant during collecting because no single species predominates throughout all parts of Fallon. The urban forest of Fallon contains many kinds of trees, and elm (*Ulmus*), mulberry (*Morus*), cottonwood (*Populus*), and ash (*Fraxinus*) were the most common tree types sampled. Accumulation of aerosols onto leaves can be affected by leaf characteristics such as roughness, pubescence, moisture, and stickiness (Wedding et al., 1977), but these characteristics of leaves do not vary appreciably across the tree species sampled in this study.

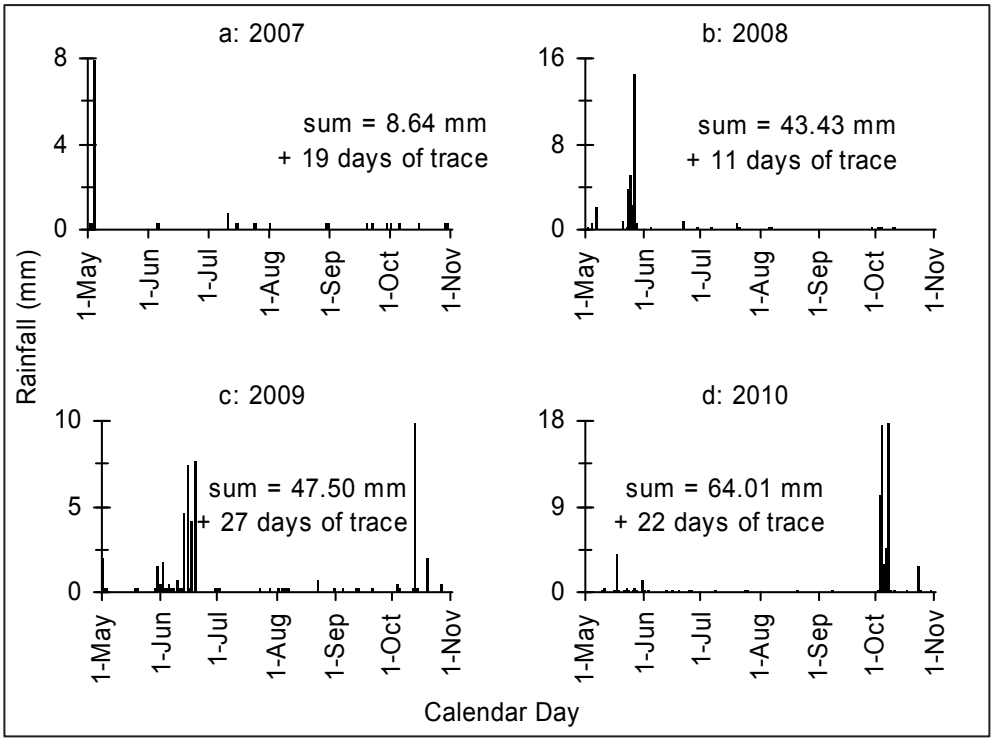

Fig. 2. Daily rainfall in Fallon during May through October for each year of leaf collection, 2007 through 2010. Short marks indicate days with only a trace of rainfall (<0.25 mm). Data from NCDC, NOAA. Graph for 2007 is modfied from Sheppard et al. (2009a).

Trees were selected for sampling at differing spatial densities from one year to the next. In 2008 and 2009, some trees were sampled within 0.25 km of the hard-metal facility, i.e., very near to it, while others were sampled farther away (Fig. 1b,c). In 2010, trees were sampled along a more even continuum of distance from the hard-metal facility (Fig. 1d). Sampling near the hard-metal facility does not represent biased sampling on our part, as has been suggested by others (Sueker, 2006). Rather, this is an example of targeted sampling (e.g.,

Seinfeld, 1972) to take advantage of prior knowledge that the area of the hard-metal facility is known to be where peak loadings of airborne tungsten and cobalt have occurred and where spatial variability in airborne tungsten and cobalt has been high (Sheppard et al., 2006b). In each year 2008–2010, leaves from just 10 trees were sampled, as opposed to the 95 trees sampled in 2007 (Sheppard et al., 2009a). It is no longer necessary to sample extremely intensively to discern patterns of airborne tungsten and cobalt in Fallon. Geographic coordinates were recorded for each sampled tree to facilitate mapping.

From each tree sampled, an outer branchlet of several leaves was clipped off with pruning cutters from a height of about 2 m above ground. The aspect of each tree sampled was not held constant or patterned, so sampling was effectively random across trees. None of the trees sampled was next to other trees, so there is no forest canopy effect in this study (Dasch, 1987). Branchlets were stored in clean paper bags during fieldwork. Later, leaves were trimmed from their petioles using clean, ceramic (non-metal) scissors.

2.3 Chemical measurement

Leaf tissues themselves were not measured for metals content, but rather rinse water solutions of particulates from the leaf surfaces were measured. Consequently, this study reflects airborne metals that accumulate on leaf surfaces, not soil-derived metals that move through the trees to leaf tissues (Wolterbeek and Bode, 1995). Trimmed leaves were placed in clean, 50-ml polypropylene vials, and tepid, de-ionized water was added to completely submerge the leaves. The vials were capped tightly and shaken lightly for two hours (Little, 1973). Rinse solutions were poured into new, clean polyurethane vials. Rinsed leaves were then oven dried at 50° C for several days and weighed to ±0.0001 g.

Rinse solutions were filtered with acid-washed GHP Acrodisc syringe filters (less than 0.2 μm) and acidified to pH less than 2 with certified pure nitric acid. Measurement was performed using inductively coupled plasma, mass spectroscopy ICP-MS (Elan DRC-II, Perkin Elmer, Shelton, CT). Most analytes were measured in standard mode (e.g., vanadium, nickel, copper, zinc, arsenic, cadmium, cesium, tungsten, lead, and uranium), while chromium and cobalt were measured using the dynamic reaction cell (DRC) flushed with ammonia gas. For all elements measured, detection limits were sub-ppb based on three standard deviations from the mean of 11 replicate measurements.

2.4 Quantitative analysis

Measured contents of metals in rinse solutions were standardized to oven dry mass of leaves measured. Oven dry leaf masses were first transformed to the ¾ power before this standardization step. This transformation incorporates a concept of diminishing returns whereby leaf area increases ever more slowly as leaf mass increases, i.e., at a power of ¾ of leaf mass (Niklas & Cobb, 2008). This transformation was not done originally with the 2007 leaf collection (Sheppard et al., 2009a), but it has since been done on that data set in addition to the data from 2008–2010.

The 2008 and 2009 collections were analyzed by testing medians of element concentrations from trees near the hard-metal facility versus trees away from it. The Mann-Whitney test of medians (Sokal & Rohlf, 1981) was used to assess significance between near trees versus far trees, with the alternative hypothesis being one-tailed, i.e., that element concentrations of trees near the hard-metal facility were higher than those of trees farther away. The 2010 collection was analyzed by plotting concentration values by distance from the hard-metal facility and assessing the strength of a power function model for each element.

3. Results

3.1 Year 2008

From leaves of 2008, tungsten and cobalt show the largest differences between trees near the hard-metal facility versus trees away from it. Tungsten and cobalt medians were 38 times and 16 times more concentrated on surfaces of leaves of trees near the facility than trees far away (Table 1). These differences are highly significant.

element	Concentration ($\mu g \cdot g^{-(3/4)}$)		Near: Far	p value
	Near (n=6)	Far (n=4)		
tungsten	0.793	0.021	37.76	0.007
cobalt	2.052	0.131	15.66	0.007
nickle	0.526	0.040	13.15	0.021
cesium	0.045	0.004	11.25	0.021
sodium	3934	406	9.69	0.035
tantalum	0.0045	0.0005	9.00	0.007
rubidium	7.53	0.94	8.01	0.021
magnesium	2603	329	7.91	0.055
zirconium	0.051	0.011	4.64	0.007
lead	0.037	0.008	4.63	0.013
silicon	331	87	3.80	0.035
beryllium	0.0018	0.0005	3.60	0.143
copper	0.596	0.187	3.19	0.055
phosphorus	631	218	2.89	0.120
titanium	2.18	0.78	2.79	0.083
molybdenum	0.086	0.032	2.69	0.035
vanadium	0.067	0.028	2.39	0.007
strontium	18.0	7.7	2.34	0.169
zinc	3.00	1.32	2.27	0.013
potassium	17229	7715	2.23	0.083
chromium	0.021	0.010	2.10	0.035
gallium	0.036	0.018	2.00	0.228
barium	1.26	0.76	1.66	0.228
lithium	14.9	10.3	1.45	0.457
calcium	5063	3554	1.42	0.169
arsenic	0.188	0.157	1.20	0.375
aluminum	8.7	10.6	0.82	Ø
barium	264	410	0.64	Ø
manganese	37	207	0.18	Ø
selenium	0.001	0.027	0.04	Ø
iron	18	563	0.03	Ø

Table 1. Results for the 2008 collection, sorted by the ratio Near:Far, i.e., the ratio of the median value of trees near the hard-metal facility versus trees farther away from it. Concentration values are medians. P value is for Mann-Whitney testing of no difference between median values versus the one-tailed alternative that the near median is greater than the far median (Sokal & Rohlf, 1981).

Other elements measured show smaller differences between trees near the hard-metal facility versus trees away from it. Most elements show near:far ratios of less than 10, and most of these differences are less significant statistically than the differences for tungsten and cobalt (Table 1). Of these other elements, nickel and cesium show the highest near:far ratios, both above 10. Cesium showed notable spatial variability in the 2007 collection (Sheppard et al., 2009a), and this replication of spatial variability in cesium makes that element potentially interesting environmentally in Fallon.

3.2 Year 2009

From leaves of 2009, tungsten and cobalt show the largest differences between trees near the hard-metal facility versus trees away from it. Tungsten and cobalt medians were 12 times and 7 times more concentrated on surfaces of leaves of trees near the facility than trees far away (Table 2). These differences are highly significant.

Other elements measured show smaller differences between trees near the hard-metal facility versus trees away from it. Other elements show near:far ratios of 3.0 or less, and most of these differences are less significant statistically than the differences for tungsten and cobalt (Table 2). No other element measured shows spatial variability that is especially notable or potentially interesting environmentally in Fallon.

3.3 Year 2010

From leaves of 2010, the negative power model of tungsten concentration as a function of distance from the hard-metal facility is very strong. The R^2 value of the tungsten model is 62% (Fig. 3a), much higher than other elements (Fig. 3b-i). The negative power model of cobalt concentration as a function of distance from the hard-metal facility is weaker but still notable. The R^2 value of the cobalt model is 12%, though that is without an obvious high outlying value from the tree that was nine km away from the facility (Fig. 3b).

element	Concentration ($\mu g \cdot g^{(-3/4)}$)		Near: Far	p value
	Near (n=4)	Far (n=6)		
tungsten	0.176	0.015	11.73	0.007
cobalt	0.757	0.113	6.70	0.007
selenium	0.015	0.005	3.00	0.055
calcium	1329	507	2.62	0.120
iron	1.760	0.924	1.90	0.120
chromium	0.009	0.005	1.80	0.083
potassium	2814	1945	1.45	0.297

Table 2. Results for the 2009 collection, sorted by the ratio Near:Far, i.e., the ratio of the median value of trees near the hard-metal facility versus trees farther away from it. Concentration values are medians. P value is for Mann-Whitney testing of no difference between median values versus the one-tailed alternative that the near median is greater than the far median (Sokal & Rohlf, 1981).

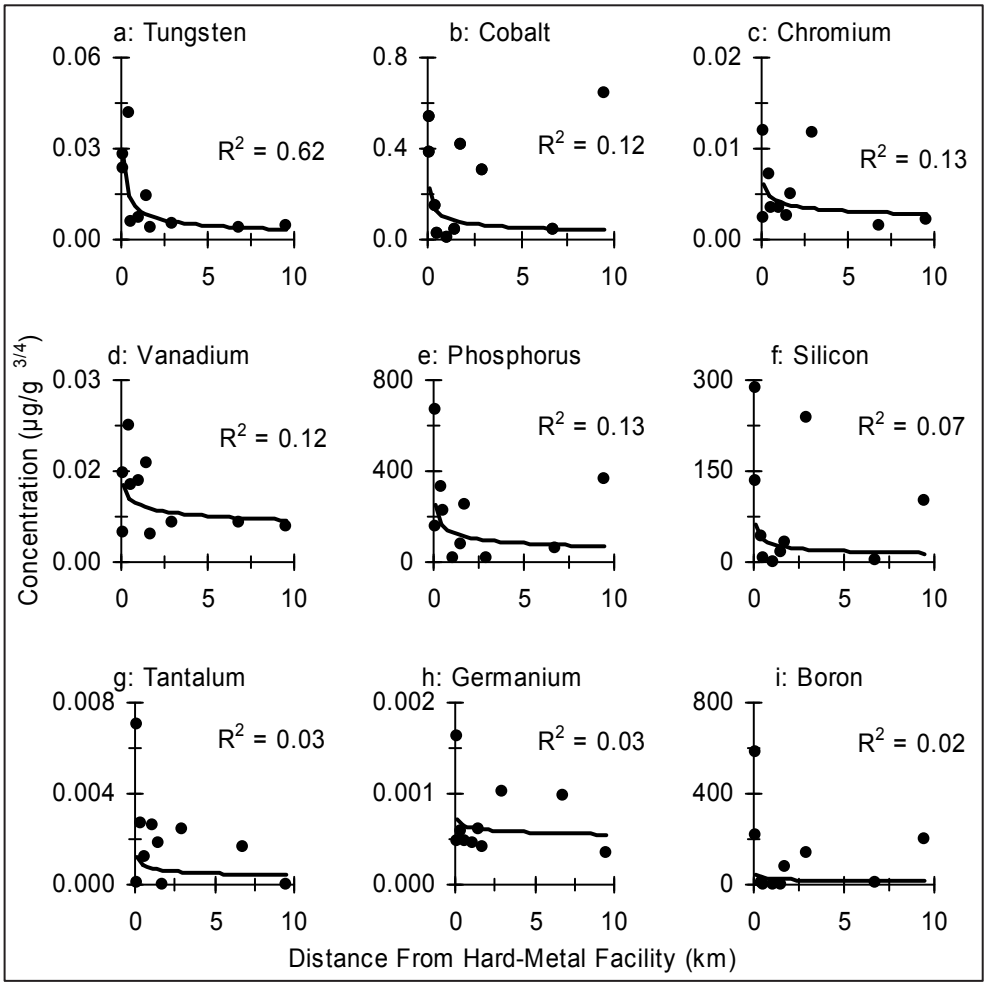

Fig. 3. Leaf surface concentration (mass of element per oven dry mass of leaf raised to the ¾ power) of elements as a function of distance from the hard-metal facility (km) for the 2010 collection. The R^2 value for cobalt is without the outlying value included.

The negative power models of other elements measured are weaker than that of tungsten. Chromium, vanadium, and phosphorus have R^2 values about as strong as that of cobalt (Fig. 3c-e), while other elements have very weak R^2 values (Fig. 3f-i).

3.4 Years 2007–2010

A temporal pattern in absolute maximum values emerged for elements that have been measured all four years. Maximum concentrations of tungsten, cobalt, and chromium have declined fairly steadily from 2007 through 2010 (Table 3). A possible explanation of this trend is that total summer rainfall for Fallon has steadily increased from 2007 through 2010 (Table 3). Maximum concentrations of these three elements show clear negative

relationships with total summer rainfall, each with strong R^2 values (Fig. 4). Rainfall has the obvious potential effect of cleaning leaf surfaces of dust that leaves catch throughout the growing season.

4. Discussion

This work confirms various advantages of leaf-surface chemistry as a technique for assessing air quality. As a relatively easy and inexpensive method, many leaf samples can be collected and analyzed, either for fine-turning spatial variability of air quality at one point in time (Sheppard et al., 2009a) or for assessing temporal variability of air-quality for one area (this study).

Year	Maximum Concentration ($\mu g \cdot g^{-(3/4)}$)			Summer Rainfall (mm)
	Tungsten	Cobalt	Chromium	
2007	16.40	6.70	0.089	8.64
2008	4.78	8.47	0.052	43.43
2009	0.39	1.29	0.021	47.50
2010	0.04	0.64	0.012	64.01

Table 3. Maximum concentration of tungsten, colbalt, and chromium for each year of collecting leaves in Fallon, and total summer (May through October) rainfall recorded at the Fallon Naval Air Station.

Notable findings emerged from this work. One, maximum values of airborne tungsten and cobalt in Fallon have been varying through time at the annual scale. Absolute values from leaf-surface chemistry are standardized for multiple procedural sources of variation (e.g., differing solution volumes and leaf sizes), so the interannual variability in airborne tungsten and cobalt shown here is probably environmental in nature. A logical explanation for this variability is differing summer rainfall totals from year to year.

Two, even during a summer leaf season with high rainfall (i.e., 64 mm in 2010), which logically should reduce absolute values of airborne metals on leaf surfaces, spatial patterns of airborne elements are still discernible with leaf-surface chemistry. This illustrates the robustness of this technique for assessing air quality, at least in environments that are relatively arid to begin with.

In general, long-term environmental monitoring is extremely valuable. Multi-year assessment research allows for discovering slow changes in environmental quality (Johnston, 1991), some of which could have implications for public health. Given the temporal variability of air quality in Fallon, it seems imperative that environmental monitoring and assessment of Fallon, especially for air quality, be continued. Even without considering linkage between exposure to airborne tungsten and cobalt and human illness, merely knowing that airborne tungsten and cobalt are elevated in Fallon and that their airborne loadings are changing through time logically suggests that continuing monitoring and assessment is prudent. Leaf-surface chemistry is a suitable technique for such long-term assessment.

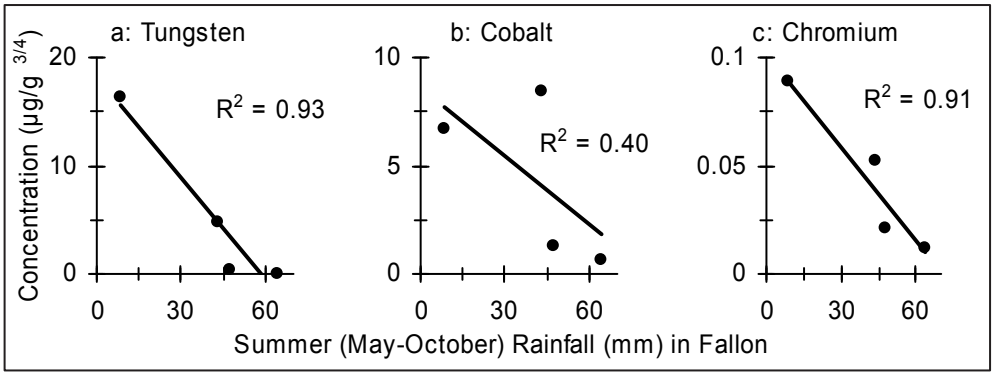

Fig. 4. Maximum concentration (mass of element per oven dry mass of leaf raised to the ¾ power) of tungsten (a), cobalt (b), and chromium (c) as a funtion of total summer (May–October) rainfall (mm) recorded in Fallon for each year (2007–2010).

5. Conclusion

Leaf-surface chemistry is an effective technique for assessing air quality, including for loadings of airborne metals and especially in urban settings. From leaf-surface chemistry, the center area of Fallon is shown to continue having elevated airborne tungsten and cobalt relative to outlying areas around Fallon. Interannual variability in absolute maximum values is notable.

It cannot be concluded from only environmental data that elevated airborne tungsten and/or cobalt cause childhood leukemia. Such a connection requires direct biomedical testing. Nonetheless, given that childhood leukemia in Fallon is the "most unique cluster ever reported" (Steinmaus et al. 2004) and that Fallon is distinctive environmentally by its elevated airborne tungsten and cobalt particulates, it stands to reason that additional biomedical research is warranted to assess the leukogenicity of airborne tungsten and cobalt (e.g., Fastje et al., 2009; Kalinich et al. 2005; Miller et al., 2001; Radcliffe et al., 2010; Steinberg et al. 2007; Sun et al. 2003).

6. Acknowledgments

Mary Kay Amistadi assisted in this project. ICP-MS measurements were conducted at the Arizona Laboratory for Emerging Contaminants of the University of Arizona. Coauthors on original publications of the University of Arizona research in Fallon are acknowledged. Original ecologic research by the University of Arizona was funded in part by the Cancer Research and Prevention Foundation and the Gerber Foundation, neither of which is otherwise responsible for content of this paper. This leaf-surface chemistry research was funded in part by the US Environmental Protection Agency. This article does not necessarily reflect the views of the U.S. Environmental Protection Agency and no official endorsement should be inferred. Sheppard and Witten have provided documents, data, and a declaration in Case CV03-03482, Richard Jernee et al. vs Kinder Morgan Energy et al., and CV03-05326, Floyd Sands et al. vs Kinder Morgan Energy et al., Second Judicial District

Court of Nevada, Washoe County, which are related to the childhood leukemia cluster of Fallon. In those cases, the law firm of Dunlap and Laxalt, representing the plaintiffs, with full disclosure to all defendants and their counsel, made an unsolicited donation of $15,000 to assist Witten and Sheppard in furthering their research, with a request that defendants provide similar donations.

7. References

Aboal, J.R.; Fernández, J.A. & Carballeira, A. (2004). Oak Leaves and Pine Needles as Biomonitors of Airborne Trace Elements Pollution. *Environmental and Experimental Botany*, Vol. 51, No. 3, (June 2004), pp. 215-225, ISSN 0098-8472

Aksoy, A.; Hale, W.H.G. & Dixon, J.M. (1999). *Capsella bursa-pastoris* (L.) Medic. as a Biomonitor of Heavy Metals. *Science of the Total Environment*, Vol. 226, No. 2-3, (February 1999), pp. 177-186, ISSN 0048-9697

Aksoy, A. & Öztürk, M.A. (1997). *Nerium oleander* L. as a Biomonitor of Lead and Other Heavy Metal Pollution in Mediterranean Environments. *Science of the Total Environment*, Vol. 205, No. 2-3, (October 1997), pp. 145-150, ISSN 0048-9697

Alfani, A.; Bartoli, G.; Rutigliano, F.A.; Maisto, G. & deSanto, A.V. (1996a). Trace Metal Biomonitoring in the Soil and the Leaves of *Quercus Ilex* in the Urban Area of Naples. *Biological Trace Element Research*, Vol. 51, No. 1, (January 1996), pp. 117-131, ISSN 0163-4984

Alfani, A.; Maisto, G.; Iovieno, P.; Rutigliano, F.A. & Bartoli, G. (1996b). Leaf Contamination by Atmospheric Pollutants as Assessed by Elemental Analysis of Leaf Tissue, Leaf Surface Deposit and Soil. *Journal of Plant Physiology*, Vol. 148, No. 1-2, (April, 1996), pp. 243-248, ISSN 0176-1617

Bargagli, R. (1993). Plant Leaves and Lichens as Biomonitors of Natural or Anthropogenic Emissions of Mercury. In: *Plants as Biomonitors*, B. Markert, (ed.), 461-484, VCH, ISBN 3527300015, Weinheim, Germany

Čeburnis D. & Steinnes E. (2000). Conifer Needles as Biomonitors of Atmospheric Heavy Metal Deposition: Comparison with Mosses and Precipitation, Role of the Canopy. *Atmospheric Environment*, Vol. 34, No. 25, (July 2000), pp. 4265-4271, ISSN 1352-2310

Dasch, J.M. (1987). Measurement of Dry Deposition to Surfaces in Deciduous and Pine Canopies. *Environmental Pollution*, Vol. 44, No. 4, (1987), pp. 261-277, ISSN 0269-7491

Expert Panel. (2004). *Final Report and Recommendations to the Nevada State Health Division*. Expert Panel on Childhood Leukemia in Churchill County, Nevada

Fastje, C.D.; Le, K.; Sun, N.N.; Wong, S.S.; Sheppard, P.R.; Witten, M.L. (2009). Pre-natal exposure to tungstate is associated with decreased transcriptome-expression of the putative tumor suppressor gene, DMBT1: implications for childhood leukemia. *Land Contamination and Reclamation*, Vol. 17, No. 1, (March 2009), pp. 169-178, ISSN 0967-0513

Greater Fallon Area Chamber of Commerce. (2008). *History of Fallon*. Accessed 1 March 2010, Available from: http://www.fallonchamber.com

Gupta, A.; Kumar, R.; Kumari, K.M. & Srivastava, S.S. (2004). Atmospheric Dry Deposition to Leaf Surfaces at a Rural Site of India. *Chemosphere*, Vol. 55, No. 8, (May 2004), pp. 1097-1107, ISSN 0045-6535

Harris, P.M. & Humphreys, D.S.C. (1983). *Tungsten: A Review*. Occasional Papers of the Institution of Mining and Metallurgy, Paper 2, Institution of Mining and Metallurgy, ISBN 0900488654, London, England

Johnston, A.E. (1991). Benefits from Long-Term Ecosystem Research. In: *Long-Term Ecological Research: An International Perspective*, P.G. Risser (ed.), 89–114, Wiley, ISBN 0471930059, Chichester, England

Kalinich, J.F.; Emond, C.A.; Dalton, T.K.; Mog, S.R.; Coleman, G.D.; Kordell, J.E.; Miller, A.C. & McClain, D.E. (2005). Embedded Weapons-Grade Tungsten Alloy Shrapnel Rapidly Induces Metastatic High-Grade Rhabdomyosarcomas in F344 Rats. *Environmental Health Perspectives*, Vol. 113, No. 6, (June 2005), pp. 729-734, ISSN 0091-6765

Kinlen, L. & Doll, R. (2004). Population Mixing and Childhood Leukaemia: Fallon and Other US Clusters. *British Journal of Cancer*, Vol. 91, No. 1, (July 2004), pp. 1-3, ISSN 0007-0920

Lahontan Valley News. (3 December 2005). *Study Finds Higher Levels of Tungsten, Cobalt in Fallon Air*

Lahontan Valley News. (8 August 2007). *Study: Fallon Tungsten Particles Not Natural*

Lahontan Valley News. (15 October 2010). *Obituary: Halycon Marie Bice*

Little, P. (1973). A Study of Heavy Metal Contamination on Leaf Surfaces. *Environmental Pollution*, Vol. 5, No. 3, pp. 159-172, ISSN 0269-7491

Loppi, S.; Nelli, L.; Ancora, S. & Bargagli, R. (1997). Passive Monitoring of Trace Elements by Means of Tree Leaves, Epiphytic Lichens and Bark Substrate. *Environmental Monitoring and Assessment*, Vol. 45, No. 1, (March 1997), pp. 81-88, ISSN 0167-6369

Miller, A.C.; Mog, S.; McKinney, L.; Luo, L.; Allen, J.; Xu, J.Q. & Page, N. (2001). Neoplastic Transformation of Human Osteoblast Cells to the Tumorigenic Phenotype by Heavy Metal-Tungsten Alloy Particles: Induction of Toxic Effects. *Carcinogenesis*, Vol. 22, No. 1, (January 2001), pp. 115-125, ISSN 0143-3334

Moore, L.E.; Lu, M. & Smith, A.H. (2002). Childhood Cancer Incidence and Arsenic Exposure in Drinking Water in Nevada. *Archives of Environmental Health*, vol. 57, No. 3, (May-June 2002), pp. 201-206, ISSN 0003-9896

Nevada State Health Division. (2004). *New Childhood Leukemia Case Confirmed*. News Release, 20 December 2004

Niklas, K.J. & Cobb, E.D. (2008). Evidence for "Diminishing Returns" From the Scaling of Stem Diameter and Specific Leaf Area. *American Journal of Botany*, Vol. 95. No. 5, (May 2008), pp. 549-557, ISSN 0002-9122

NOAA. (2008). *National Climatic Data Center*. National Oceanic and Atmospheric Administration. Accessed 1 March 2010, Available from: http://www.ncdc.noaa.gov/oa/ncdc.html

Pleil, J.D.; Sobus, J.; Sheppard, P.R.; Ridenour, G. & Witten, M.L. (In press). Strategies for Evaluating the Environment-Public Health Interaction of Long-Term Latency

Disease: The Quandary of the Inconclusive Case-Control Study. *Chemico-Biological Interactions*, ISSN 0009-2797

Radcliffe, P.M.; Leavens, T.L.; Wagner, D.J.; Olabisi, A.O.; Struve, M.F.; Wong, B.A.; Tewksbury, E.; Chapman, G.D. & Dorman, D.C. (2010). Pharmacokinetics of Radiolabeled Tungsten (^{188}W) in Male Sprague-Dawley Rats Following Acute Sodium Tungstate Inhalation. *Inhalation Toxicology*, Vol. 22, No. 1, (January 2010), pp. 69-76 ISSN 0895-8378

Rautio, P.; Huttunen, S. & Lamppu, J. (1998). Element Concentrations in Scots Pine Needles on Radial Transects Across a Subarctic Area. *Water Air and Soil Pollution*, Vol. 102, No. 3-4, (March 1998), pp. 389-405, ISSN 0049-6979

Reno Gazette-Journal (Frank X. Mullen). (5 February 2003). *No Pollution Controls in Tungsten Plant*

Reno Gazette-Journal (Frank X. Mullen). (11 October 2008). *Metal Remains at Heart of Fallon Leukemia Inquiry*

Rossini Oliva, S. & Mingorance, M.D. (2006). Assessment of Airborne Heavy Metal Pollution by Aboveground Plant Parts. *Chemosphere*, Vol. 65, No. 2, (October 2006), pp. 177-182, ISSN 0045-6535

Rubin, C.S.; Holmes, A.K.; Belson, M.G.; Jones, R.L.; Flanders, W.D.; Kieszak, S.M.; Osterloh, J.; Luber, G.E.; Blount, B.C.; Barr, D.B.; Steinberg, K.K.; Satten, G.A.; McGeehin, M.A. & Todd, R.L. (2007). Investigating Childhood Leukemia in Churchill County, Nevada. *Environmental Health Perspectives*, Vol. 115, No. 1, (January 2007), pp. 151-157, ISSN 0091-6765

Salve, P.R.; Maurya, A. & Wate, S.R. (2006). Atmospheric Dry Deposition on Leaves at an Urban Location. *Bulletin of Environmental Contamination and Toxicology*, Vol. 77, No. 6, (December 2006), pp. 834-837, ISSN 0007-4861

Seiler, R.L. (2004). Temporal Changes in Water Quality at a Childhood Leukemia Cluster. *Ground Water*, Vol. 42, No. 3, (May-June 2004), pp. 446-455, ISSN 0017-467X

Seiler, R.L.; Stollenwerk, K.G. & Garbarino, J.R. (2005). Factors Controlling Tungsten Concentrations in Ground Water, Carson Desert, Nevada. *Applied Geochemistry*, Vol. 20, No. 2, (February 2005), pp. 423-441, ISSN 0883-2927

Seinfeld, J.H. (1972). Optimal Location of Pollutant Monitoring Stations in an Airshed. *Atmospheric Environment*, Vol. 6, No. 11, (1972), pp. 847-858, ISSN 1352-2310

Shaw, W.D.; Walker, M.; & Benson, M. (2005). Treating and Drinking Well Water in the Presence of Health Risks from Arsenic Contamination: Results from a US Hot Spot. *Risk Analysis*, Vol. 25, No. 6, (December 2005), pp. 1531-1543, ISSN 0272-4332

Sheppard, P.R.; Hallman, C.L.; Ridenour, G. & Witten, M.L. (2009a). Spatial Patterns of Tungsten and Cobalt on Leaf Surfaces of Trees in Fallon, Nevada. *Land Contamination and Reclamation*, vol. 17, No. 1, (March 2009), pp. 31-41, ISSN 0967-0513

Sheppard, P.R.; Ridenour, G.; Speakman, R.J. & Witten, M.L. (2006a). Elevated Tungsten and Cobalt in Airborne Particulates in Fallon, Nevada: Possible Implications for the Childhood Leukemia Cluster. *Applied Geochemistry*, Vol. 21, No. 1, (January 2006), pp. 152-165, ISSN 0883-2927

Sheppard, P.R.; Ridenour, G.; Witten, M.L. (2009b). Multiple Techniques for Researching Airborne Particulates: A Comprehensive Case Study of Fallon, Nevada. In: *Airborne Particulates*, M. Cheng & W. Liu (eds.), 141-156, Nova Science Publishers, ISBN 9781606929070, New York

Sheppard, P.R.; Speakman, R.J.; Ridenour, G.; Glascock, M.D.; Farris, C. & Witten, M.L. (2007a). Spatial Patterns of Tungsten and Cobalt in Surface Dust of Fallon, Nevada. *Environmental Geochemistry and Health*, Vol. 29, No. 5, (October 2007), pp. 405-412, ISSN 0269-4042

Sheppard, P.R.; Speakman, R.J.; Ridenour, G. & Witten, M.L. (2006b). Reply to Comment on "Elevated Tungsten and Cobalt in Airborne Particulates in Fallon, Nevada: Possible Implications for the Childhood Leukemia Cluster", by Blasland, Bouck and Lee, Inc. *Applied Geochemistry*, Vol. 21, No. 6, (June 2006), pp. 1083-1088, ISSN 0883-2927

Sheppard, P.R.; Speakman, R.J.; Ridenour, G. & Witten, M.L. (2007b). Using Lichen Chemistry to Assess Airborne Tungsten and Cobalt in Fallon, Nevada. *Environmental Monitoring and Assessment*, Vol. 130, No. 1-3, (July 2007), pp. 511-518, ISSN 0167-6369

Sheppard, P.R.; Speakman, R.J.; Ridenour, G. & Witten, M.L. (2007c). Temporal Variability of Tungsten and Cobalt in Fallon, Nevada. *Environmental Health Perspectives*, Vol. 115, No. 5, (May 2007), pp. 715-719, ISSN 0091-6765

Sheppard, P.R.; Toepfer, P.; Schumacher, E.; Rhodes, K.; Ridenour, G. & Witten, M.L. (2007d). Morphological and Chemical Characteristics of Airborne Tungsten Particles of Fallon, Nevada. *Microscopy and Microanalysis*, Vol. 13, No. 4, (August 2007), pp. 296-303, ISSN 1431-9276

Sokal, R.R. & Rohlf, F.J. (1981). *Biometry*. WH Freeman and Co., ISBN 0716712547, San Francisco, California

Steinberg, K.K.; Relling, M.V.; Gallagher, M.L.; Greene, C.N.; Rubin, C.S.; French, D.; Holmes, A.K.; Carroll, W.L.; Koontz, D.A.; Sampson, E.J. & Satten, G.A. (2007). Genetic Studies of a Cluster of Acute Lymphoblastic Leukemia Cases in Churchill County, Nevada. *Environmental Health Perspectives*, Vol. 115, No. 1, (January 2007), pp. 158-164, ISSN 0091-6765

Steinmaus, C.; Lu, M.; Todd, R.L. & Smith, A.H. (2004). Probability Estimates for the Unique Childhood Leukemia Cluster in Fallon, Nevada, and Risks Near Other U.S. Military Aviation Facilities. *Environmental Health Perspectives*, Vol. 112, No. 6, (May 2004), pp. 766-771, ISSN 0091-6765

Steinmaus, C. & Smith, A.H. (2005). The Highly Unusual Cluster of Childhood Leukaemia in Churchill County, Nevada. *Epidemiology*, Vol. 16, No. 5, (September 2005), pp. S51-S51, 1044-3983

Sueker, J.K. (2006). Comment on "Elevated Tungsten and Cobalt in Airborne Particulates in Fallon, Nevada: Possible Implications for the Childhood Leukemia Cluster" by P.R. Sheppard, G. Ridenour, R.J. Speakman and M.L. Witten. *Applied Geochemistry*, Vol. 21, No. 6, (June 2006), pp. 1083-1085, ISSN 0883-2927

Sun, N.N.; Fastje, C.D.; Wong, S.S.; Sheppard, P.R.; Ridenour, G.; Hyde, J.D.; Macdonald, S. & Witten, M.L. (2003). Dose-Dependent Transcriptome Changes by Metal Ores on a

Human Acute Lymphoblastic Leukemia Cell Line. *Toxicology and Industrial Health*, Vol. 19, No. 7-10, (2003), pp. 157-163, ISSN 0748-2337

U.S. ATSDR. (2002). *Evaluation of Potential Exposures from the Fallon JP-8 Fuel Pipeline*. Agency for Toxic Substances and Disease Registry, Accessed 1 March 2010, Available from http://www.atsdr.cdc.gov/HAC/pha/PHA.asp?docid=952&pg=0

U.S. ATSDR. (2003a). *Surface Water, Sediment, and Biota Human Exposure Pathway Analysis for Churchill County: Fallon Leukemia Project, Fallon, Churchill County, Nevada*. Agency for Toxic Substances and Disease Registry, Accessed 1 March 2010, Available from http://www.atsdr.cdc.gov/HAC/pha/fallonwater/finalwater.pdf

U.S. ATSDR. (2003b). *Air Exposure Pathway and Assessment: Fallon Leukemia Cluster Investigation*. Agency for Toxic Substances and Disease Registry, Accessed 1 March 2010, Available from http://www.atsdr.cdc.gov/HAC/PHA/fallonair/finalair.pdf

U.S. ATSDR. (2003c). *Pathway Assessment for Churchill County Surface Soils and Residential Indoor Dust: Fallon Leukemia Project, Fallon, Churchill County, Nevada*. Agency for Toxic Substances and Disease Registry, Accessed 1 March 2010, Available from http://www.atsdr.cdc.gov/HAC/pha/fallonsoil/finalsoil.pdf

U.S. CDC. (2003). *A Cross-Sectional Exposure Assessment of Environmental Exposures in Churchill County, Nevada*. Centers for Disease Control and Prevention, Accessed 1 March 2010, Available from http://www.cdc.gov/nceh/clusters/fallon

U.S. Census. (2000). *United States Census 2000*. Accessed 1 March 2010, Available from http://www.census.gov/main/www/cen2000.html

U.S. NCI. (2003). *Age-Adjusted SEER Incidence and the U.S. Death Rates and 5-Year Relative Survival Rates by Primary Cancer Sites, Sex, and Time Period*. SEER Cancer Statistics Review, 1975-2000, Table XXVII-3: Childhood Cancers, U.S. National Cancer Institute. Accessed 1 March 2010, Available from http:// www.seer.cancer.gov

Wakeford, R. (2004). Extreme Childhood Leukaemia Cluster at Fallon, Nevada. Journal of Radiological Protection, Vol. 24, No. 2, (June 2004), pp. 183-184, ISSN 0952-4746

Walker, M. & Fosbury, D. (2009). Arsenic, $As^{(III)}$, and Tungsten in Nevada County's Private Water Supplies. *Journal of Water and Health*, Vol. 7, No. 2, (June 2009), pp. 293-301, ISSN 1477-8920

Walker, M.; Shaw, W.D. & Benson, M. (2006). Arsenic Consumption and Health Risk Perceptions in a Rural Western US Area. *Journal of the American Water Resources Association*, Vol. 42, No. 5, (October 2005), pp. 1363-1370, ISSN 1093-474X

Ward, N.I.; Brooks, R.R. & Roberts, E. (1977). Silver in Soils, Stream Sediments, Waters and Vegetation Near a Silver Mine and Treatment Plant at Maratoto, New Zealand. *Environmental Pollution*, 13, No. 4, (August 1977), pp. 269-280, ISSN 0269-7491

Wedding, J.B.; Carlson, R.W.; Stukel, J.J. & Bazzaz, F.A. (1977). Aerosol Deposition on Plant Leaves. *Water Air and Soil Pollution*, Vol. 7, No. 4, (1977), pp. 545-550, ISSN 0049-6979

Wittig, R. (1993). General aspects of biomonitoring heavy metals by plants. In: *Plants as Biomonitors*, B. Markert, (ed.), 3-27, VCH, ISBN 3527300015, Weinheim, Germany

Wolterbeek, H.T. & Bode, P. (1995). Strategies in Sampling and Sample Handling in the Context of Large-Scale Plant Biomonitoring Surveys of Trace Element Air Pollution. *Science of the Total Environment*, Vol. 176, No. 1-3, (December 1995), pp. 33-43, ISSN 0048-9697

17

Organic Compounds in Airborne Particles and their Genotoxic Effects in Mexico City

Villalobos-Pietrini R.[1], Amador-Muñoz O.[1], Valle-Hernández B.L.[1], Gómez-Arroyo S.[1], Waliszewski S.[2] and Jazcilevich A.D.[1]
[1]*Centro de Ciencias de la Atmósfera, Universidad Nacional Autónoma de México*
[2]*Instituto de Medicina Forense, Universidad Veracruzana*
México

1. Introduction

Air pollution is a local, regional and global problem concerning natural and human activities. The atmospheric pollution in urban areas is of great importance since those centers are densely populated and the degree of exposure to toxics in the air has a major impact on the inhabitants, compared to the exposure of people not living in them. Many urban areas experience uncontrolled growth which is especially acute in developing countries and leads to increasing demands for energy, transportation, and commercial and industrial activities (Lawrence et al., 2007). Although people in some microenvironments can be exposed to concentrations of specific pollutants higher than those for individuals exposed outside, our interest is in environmental atmospheric pollutants and specifically in atmospheric organic aerosols. This chapter will give a brief overview of the organic compounds in airborne particles and their impact on climate and air quality, chemical composition and source apportionment, as well as on instrumental determination and atmospheric transformation, besides their toxic effects and to risk human health. We will present those studies related with the organic chemical speciation of the compounds, particularly emphasizing polycyclic aromatic hydrocarbons, which are known to be ubiquitous environmental mutagens and carcinogens, and we will discuss the genotoxic effects of those compounds in Mexico City (MC); finally, we will describe the recent work and future studies of our research group.

2. Airborne particles

Aerosol is constituted by a mixture of gases and suspended particles (liquid and solid). However, the particulate phase is commonly referred to as aerosol. Aerosols have been considered to play a significant role in atmospheric chemistry physical processes, meteorology and climate change, justifying in all cases the impact on humans. Their study will add to the knowledge regarding their transport and atmospheric processes, their spatial and temporal behavior and their impact on materials, visibility, climate and human health. In this sense, the particle phase of an aerosol, called airborne particles, is of relevance to

public health due to their proven morbidity and mortality effects on humans (Pope & Dockery, 2006). The magnitude of these effects generally depends upon their seasonal behavior, sources, chemical composition, number, mass, surface area and size, which increases the human health risk when the particles are inhaled because particle size is inversely proportional to the deep deposition area in the respiratory system (Sugita et al., 2004). An essential step is to measure these variables which may all be important physical-chemical properties that influence particle toxicology (Sen et al., 2007). The risk to human health is related with a long period of exposure to environmental pollutants, which increases in children and elderly persons. Human exposure to particles for both a short- and a long-term has been associated with measures of genetic damage (Lewtas, 2007). Airborne particles can be generated through grinding activities, soil resuspension due to wind or other natural processes as soil erosion, or they can be a product of the incomplete combustion of fossil and non-fossil materials as well as a result of chemical reactions and condensation onto preexistent particles (Solomon et al., 2001). Their chemical composition is a complex mixture that depends upon several factors as emission sources, geographic and climatic conditions, atmospheric reactivity, and the like.

The main process of aerosol production in nature and the most important mass-transfer via gas-phase and particle-phase is by condensation, through a supersaturated vapor initiated by the presence of small particles (heterogeneous or homogeneous nucleation) or ions that serve as sites for particle formation (Hinds, 1999). Micrometer-sized particles are strongly attached to any surface they contact through the London -van der Waals forces-, which is one of the most important adhesive forces to form aggregates (Hinds, 1999). Particle size, density and shape are some of the physical properties that influence pulmonary deposition, ground deposition rate, aging during atmospheric transport and residence time in the air. These properties help identify emission sources and /or the atmospheric formation process. Size, which ranges from 10 nm to 100 μm and is commonly analyzed by lognormal distributions, is one of the most important physical properties of the particles. It is measured in terms of the aerodynamic diameter defined as the equivalent spherical particle diameter that has a density of 1 g cm^{-3} with the same settling velocity as the target particle, and it is used for characterizing filtration, respiratory deposition and the performance of many types of air cleaners and air particle samplers.

3. Organic aerosol

3.1 Impact on climate and air quality

Aerosol particles influence the Earth's radiative and hydrological balance (Ramanathan et al., 2001). Knowledge of their contribution to radiative forcing is still uncertain (IPCC, 2007). Soot particles, which are aggregated carbonaceous spherules of tens of nanometers in size, and which have graphitic structures, are emitted from incomplete combustion of fossil fuel, biofuel, and biomass carbon together with organic matter. Soot particles contribute to the warming effect in the atmosphere through absorption of sunlight (Bong & Bergstrom, 2006). Black carbon is found throughout the atmosphere, and it is thought to be the most important component to aerosol absorption of solar radiation although attention has recently turned to "brown" organic carbon (Sun et al., 2007) as a source of significant absorption, particularly in the near-UV. The scattering and absorption of incoming solar radiation is also affected by the organic aerosol component (Jacobson et al., 2000). Organics can alter the hygroscopicity

of the particles (Thomas et al., 1999), and this changes the radiative forcing that involves cloud condensation and nuclei formation; such forcing may have opposite signs depending on the type of particulate carbon (NRC, 1996). Emissions of organic species have the potential to influence aerosol-cold cloud interactions and climate (Cziczo et al., 2004). The hygroscopicity of atmospheric aerosols has a considerable effect on particle size and therefore on visibility (Vasconcelos et al., 1994). Dissolved and surface-active organic compounds in droplets and aerosols affect the albedo of clouds and rain development (Facchini et al., 1999). Size distributions as well as the optical and hydrophilic properties of organic particles are also uncertain due to the lack of data (Liousse et al., 2005), in part owing to the complexity of the organic content which may involve several hundreds of compounds of a different chemical class and which have different biological effects. Although biological particles such as spores, bacteria, algae, pollen, vegetation and insect debris, animal cell fragments, and the like (Winiwater et al., 2009) can be considered as part of the particle organic fraction, their discussion goes beyond this chapter.

3.2 Chemical composition and source apportionment

Organic aerosol (OA) represents the second most abundant component after sulfates and nitrates in particles < 1 μm (Jacobson et al., 2000) and contributes to 10-80 % of their total mass (Hildemann et al., 1996; Rogge et al., 1993a). The specific organic chemical composition of aerosol includes n-alkanes, sugar derivatives, aldehydes, mono- and di-carboxylic acids, substituted phenols, polycyclic aromatic hydrocarbons (PAH) and their derivatives, ketones, quinones, diterpenoids acids and some nitrogen-compounds (Rogge et al., 1993a, 1993b, 1993c, 1993d), all of which are emitted from a variety of natural and anthropic sources. The range of their molecular weight, vapor pressure, polarity, reactivity and the like, have limited the chemical speciation ~10 % of the total mass (Rogge et al., 1993a), and recent efforts have focused on methods that classify the OA (Zhang et al., 2005). Polycyclic organic matter (POM) is considered by the Air Clean Act of the USA as one of the 189 air pollutants most risky for humans (Kelly et al., 1994). Among these, PAH and their nitro-derivatives (nitro-PAH) are very important, given their mutagenic and carcinogenic properties (IARC, 1983, 1989; Rosenkranz & Mermelstein, 1983). PAH are primary pollutants emitted from combustion sources, while the nitro-PAH are also primary pollutants, but they are generated by combustion mainly from diesel engines and they are also formed in the gas phase by the interaction between PAH and NOx with OH radical during the day and with NO_3 radical during the night (Atkinson et al., 1990; Nielsen, 1984). Opposite to adverse effects of POM, fatty acids have showed antimutagenic properties (Hayatsu et al., 1988). In MC, the palmitic and stearic acids were the most abundant fatty acids (Villalobos-Pietrini et al., 2008). Fatty acids and n-alkanes are two of the most abundant organics which make up organic aerosol (Feng et al., 2007), and although no adverse effects on human health for n-alkanes have been reported, they are used as anthropic and biogenic emission markers (Amador-Muñoz et al., 2011; Kavouras et al., 1999).

Depending on the emitted amount, some organic compounds can be used as tracers of emitting sources or atmospheric transformations (Rogge et al., 1993a; Schauer et al., 1996). The development of effective control strategies for airborne organic pollution is necessary for good air quality. The knowledge of emission sources in each site is extremely important to satisfy this demand. Two methods have been widely employed to evaluate source contribution: source-oriented models and receptor-oriented-models (Schauer et al., 1996).

Source modeling uses emissions data and fluids mechanics to predict pollutant concentrations at a specific receptor site. Receptor modeling infers source contributions based on the best-fit linear combination of the chemical compositions of the effluents from specific emission sources needed to reconstruct the chemical composition of specific atmospheric samples (Watson, 1984). Schauer et al. (1996) constructed a chemical mass balance (CMB) receptor modeling based on the use of organic tracers that has been widely accepted. Dual diagnostic ratios to determine the origin of the atmospheric pollutants have also been employed (Ravindra et al., 2008); however, the huge uncertainty due to different methodologies and reactivity of the pollutants (Robinson et al., 2006a, 2006b) suggests that this method must be used with caution because it is difficult to discriminate between sources (Ravindra et al., 2006). The other limitation is that interpretation is ambiguous, because it depends on the ratio considered and on the source profile chosen (Goriaux et al., 2006). However, the diagnostic ratio with similar physicochemical properties for example among PAH can be used to minimize bias due to chemical reactivity, volatility, and solubility of PAH species. Diagnostic atomic ratios have been recently employed as a metric degree of oxidation of organic species in the atmosphere to describe organic mixtures in the organic aerosol (Kroll et al., 2011). Aiken et al. (2008) used oxygen-to-carbon (O/C) ratios to characterize the oxidation state of OA. The O/C from ambient urban OA for primary emissions was 0.2, and it increased to 0.8 because of photochemical processing and secondary OA formation. They also analyzed the high resolution OA spectra generated from High-Resolution Time-of-Flight Aerosol Mass Spectrometer (HR-ToF-AMS) by Positive Matrix Factorization (PMF) analysis, and they were able to identify emissions from chemically-reduced urban primary, oxygenated OA, and biomass burning OA that correlated with levoglucosan and acetonitrile. PMF has several advantages over common versions of factor analytical approaches based on the correlation matrix (Lanz et al., 2007). Principal components analysis (PCA) is the most widely multivariate statistical technique used in atmospheric science to simplify the interpretation of complex systems; it is also used to reduce the dimensionality of the variables into a smaller set of linear combinations that explain the greatest variance of the original set, called factors, which can be interpreted as an emission source or a chemical interaction. In general, each factor from PCA is associated with a source characterized by its chemical marker. Amador-Muñoz et al. (2011) applied PCA to show that in the Northeast (NE) of the Mexico City Metropolitan Area (MCMA) the main sources were diesel combustion, in Central (C) Mexico City they were gasoline combustion and in the Southwest (SW) they were of biogenic origin. Furthermore, the authors were able to describe the origin of the particles less than 2.5 μm ($PM_{2.5}$) in the Northwest (NW) and Southeast (SE) associated to primary sources, while in the NE, in Central MC and the SW the $PM_{2.5}$ had a secondary origin.

3.3 Instrumental determination

The OA consists of hundreds of compounds with a wide range in polarity and aqueous solubility. Knowledge of these compounds implies a better understanding of aerosol organics in atmospheric processing (Pang et al., 2006). Bulk aerosol characteristics have been measured using infrared spectroscopy, nuclear magnetic resonance, ion chromatography and aerosol mass spectrometry (Allan et al., 2003; Schmeling et al., 2000; Suzuki et al., 2001). In real-time particle mass spectrometric analysis, techniques have been developed for atmospheric measurements (Canagaratna et al., 2007). The application of the HR-ToF-AMS

is an example of on real-time measurement elemental analysis and organic aerosol (Aiken et al., 2007); however, incomplete speciation of chemical composition remains a challenge. A number of different ambient ionization techniques (Venter et al., 2008) are promising for identifying the organic component of SOA. For example, desorption electrospray ionization has been applied to particles collected on filters either with or without extraction (Laskin et al., 2010). One of these new ambient ionization techniques is the atmospheric solids analysis probe mass spectrometry, which was applied to identify organics in particles from laboratory systems as well as from ambient air, with a minimal sample preparation (Bruns et al., 2010).

Off-line organic composition of atmospheric aerosols has been characterized by a number of studies by their collection on filters or impactors, followed by solvent extraction, evaporation, derivatization and analysis using several analytical techniques (Laskin et al., 2009; Zheng et al., 2006). One approach is detailed chemical characterization through identification and quantification of individual constituents by gas or liquid chromatography coupled with mass spectrometry (GC-MS and LC-MS, respectively). Currently, off–line measurements are the procedures most employed to elucidate the organic aerosol composition, although the identified components depend on the details of the analytical techniques used, and both positive and negative artifacts can occur during sampling (Turpin et al., 2000). Determination of the carbon content associated to the atmospheric aerosol is carried out by various extraction techniques. The two most commonly used methods are thermal extraction and solvent extraction. Thermal extraction is used to differentiate between organic carbon and elemental carbon (Johnson et al., 1981) or to characterize the organic chemical composition (Vogt et al., 2007). Solvent extraction (Alves et al., 2000; Tran et al., 2007) is a method by which the organic matter extracted with organic solvents is used to determine the organic mass concentration (Alves et al., 2000; Villalobos-Pietrini et al., 2006), to speciate organic compounds (Amador-Muñoz et al., 2010, 2011; Valle-Hernández et al., 2010) and to perform genotoxic studies (Villalobos-Pietrini et al., 2006, 2007). Gas chromatography-mass spectrometry is the analytical technique most used to characterize their composition. Recently, two-dimensional comprehensive gas chromatography (GCxGC) coupled to time of fly mass spectrometry (TOF/MS) has focused attention on some studies because of the increased resolution and sensitivity of organic compounds in aerosol samples (Welthagen et al., 2003). Thermal desorption aerosol (TAG) was developed for in-situ identification of organic aerosols (William et al., 2006), and a newer version of this system coupled to GCxGC (2D-TAG) was applied for the time-resolved measurement of organic compounds in ambient aerosols (Goldstein et al., 2008), showing extraordinary improved separation capabilities for the OA. Although GCxGC offers a great deal of information at the molecular level, quantitative analysis has been less developed (Amador-Muñoz & Marriott, 2008). In a recent paper, we proposed a simple method based on isotope-dilution mass spectrometry to quantify PAH on aerosol samples employing a reference material of urban dust (NIST SRM1649a). Results agreed well with certified PAH (Amador-Muñoz et al., 2008), without a pre-treatment of the samples after their organic extraction.

3.4 Atmospheric transformation

Primary Organic Aerosol (POA) is emitted directly as particles by anthropic or natural sources, whereas Secondary Organic Aerosol (SOA) is formed in the atmosphere through

chemical reactions that result from the more volatile species conversion into lower volatility oxidized condensation products and the subsequent partition to the particulate phase (Kanakidou et al., 2005; Pöschl, 2005). The formation of SOA is impacted by the amount and reactivity of gas-phase precursors, the presence of oxidants in the atmosphere, incoming solar radiation, the chemical composition of existing particles, and meteorological parameters as relative humidity and temperature (Pöschl, 2005). On a global scale, biogenic volatile organic compounds (VOCs) account for ~ 90% of VOC emissions and of SOA formation (Hallquist et al., 2009). SOA particles scatter radiation, act as cloud condensation or ice nuclei, and have influence on the Earth's radiation balance and climate (Hallquist et al., 2009; IPCC, 2007). However, emission sources, atmospheric transformation, and properties of OA remain poorly understood, and consequently offer uncertain information for chemical-transport models (Hallquist et al., 2009; Kanakidou et al., 2005). Current modeling assumptions and the oxidation of VOC gaseous precursors can not explain the SOA levels in polluted regions (Volkamer et al., 2006) as in the case of biogenic SOA levels formed in clean regions (Slowik et al., 2010). Evidence for new precursors and pathways of SOA formation has recently been described, in particular, the semi-volatile character of POA (Robinson et al., 2007), which has been modeled as a group of hydrophobic non-volatile compounds in particulate phase. POA coexist with semi-volatile organic compounds (SVOC) of low volatility that are in the particle-phase; besides, POA also coexist with intermediate-volatile organic compounds (IVOC) which are highly volatile and are in the gas-phase. Both groups are ignored in SOA modeling and commonly not included in VOC emission inventories (Robinson et al., 2007). They are composed of species such as long-chain alkanes, which can be oxidized to produce a large amount of lower volatility precursors that are likely to partition to the aerosol phase. Unfortunately many IVOCs and SVOCs are not separable by GC-MS and they are part of the "unresolved complex mixture", which lead to the need to parameterize their amounts and SOA formation (Robinson et al., 2007). The treatment of the POA emissions is a huge uncertainty (Murphy & Pandis, 2009). In addition to anthropic emissions, the POA emitted from biomass burning (BB) should also be considered semi-volatile (Huffman et al., 2009). These SVOC are oxidized quickly in the gas-phase (Yokelson et al., 2009). Gas-particle partitioning is another important parameter to be considered in the modeling of the dynamics of biogenic SOA formation. The gas/aerosol partitioning is assumed to be governed by equilibrium partitioning into an absorptive, well-mixed liquid or amorphous organic matter phase (Pankow, 1994), yet Virtanen et al. (2010) recently presented experimental evidence that biogenic SOA particles are amorphous solid state (glassy state) under ambient conditions. This result may influence the kinetics and thermodynamics of SOA formation and transformation, impacting several processes: the partitioning of semi-volatile compounds, the rate of heterogeneous chemical reactions, the particles' ability to accommodate water, cloud condensation or ice nuclei, and the atmospheric lifetime of the particles (Mikhailov et al., 2009). All of these important physical-chemical parameters will have implications for air quality and climate. The improved agreement between observed and predicted SOA when including SI-SOA in both studies also suggested that the POA emissions inventory in MC does not include SVOC that evaporate after POA emission.

Stone et al. (2010) calculated anthropic secondary organic carbon (SOC) as 20-25% of ambient OC at peripheral and urban sites of MC, while biogenic SOC was less abundant but relatively twice as important at the peripheral site. The OC that was not attributed to

secondary sources or to primary sources in a previous study (Stone et al., 2008) showed temporal consistency with BB events, as demonstrated by the correlation with levoglocusan. Based on a factor analysis, Amador-Muñoz et al. (2011) observed that organic matter in $PM_{2.5}$ did not originate in primary emission sources (petrogenic combustion, pyrolysis or biogenic emissions) in the MCMA, and that the weak correlations between organic matter vs. $PM_{2.5}$ (except in the SW), heavy PAH, n-alkanes and nitro-PAH (except in the SW), indicated that organic matter was formed by processes different from the other variables, where BB would play an important emission source. In this sense, organic matter was probably explained by the emissions and the aging of Mexico Basin outflow and not from inside the Mexico Basin. The oxidation level of the organic matter around MCMA was classified based on the ratios between organic matter vs. some n-alkanes sum and organic matter vs. some heavy PAH (Fig. 1). These compounds were selected due to their chemical stability and no evaporative losses in the atmosphere (Schauer et al., 1996).

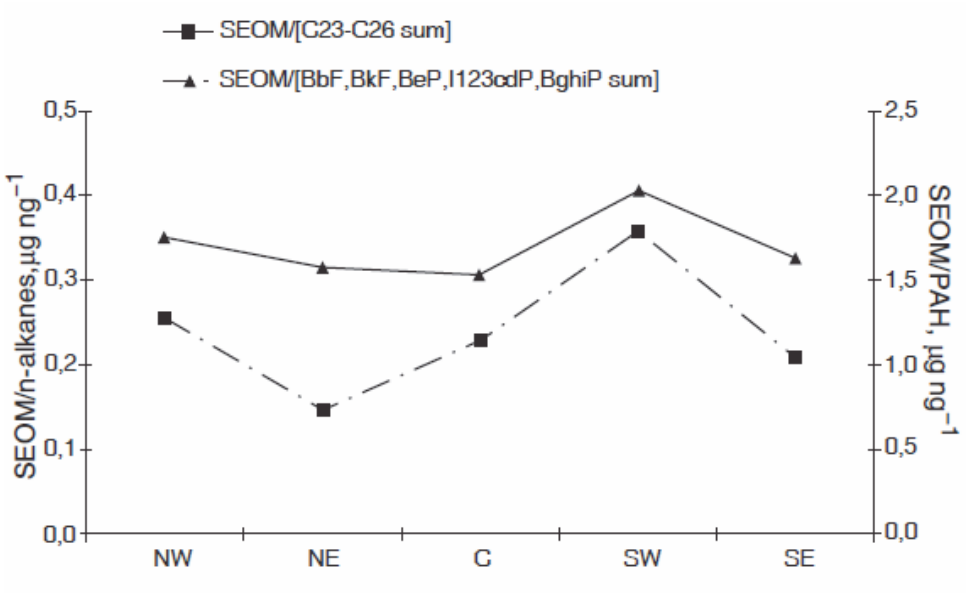

Fig. 1. Annual median ratios of SEOM/[C_{23}–C_{26} sum] (dashed line) and SEOM/[BbF,BkjF, BeP,I123cdP and BghiP sum] (continuous line) of five sites around the MCMA during 2006. Taken from Amador-Muñoz et al. (2011).

Results showed that organic chemical composition in the SW was dominated by secondary organic species with a higher oxidation level with respect to organic compounds in the NE. The non-significant difference of ratios among the Central area, the NW and the SE suggests an organic composition with mixed secondary and primary organic compounds. This matches up with a decrease in the ratios between PAH and humidity, probably due to a major coverage of oxidized organic compounds during the transport of pollutants from NE to SW, as it has been established elsewhere in MC (Baumgardner et al., 2007; Thornhill et al., 2008; Volkamer et al., 2006).

At present, the sources and composition of OA are uncertain, with current models under predicting SOA by large factors (Volkamer et al., 2006), and the models have difficulty in predicting the loadings, spatial and temporal variability, and degree of oxidation of ambient OA (Kroll et al., 2011). Some studies related with aerosol modeling have been performed at the Centro de Ciencias de la Atmósfera, UNAM. In a recent investigation, Díaz-Nigenda et al. (2010) studied the effect of particle less than 10 μm (PM_{10}) from aeolian erosion episodes in MC using the wind erosion and air quality model Multiscale Climate and Chemistry Model during specific episodes in 2006 and 2008. In all extreme PM_{10} episodes, wind erosion was a major cause of high PM_{10} concentrations in MC, mainly originated in agricultural lands and the Texcoco areas from the NE, East and SE. 3D analysis of the modeling results showed that transport of PM_{10} is accelerated horizontally when nearby confluences are formed generating low pressure systems and vertical transport of the particles is enhanced. Confluence lines are a main factor for vertical mechanical convection of dust particles. In the case of the November 2008 episode, the particles were transported to the mixing layer height and then transported out of the Basin of Mexico. Jazcilevich et al. (2003) used a prognostic air quality model to show vertical fumigation episodes due to the complex orography of the MCMA where reactive and non-reactive atmospheric pollutants can travel near the surface, be transported vertically and land in an area opposite to its initial route due to convective downward currents, changing the surface pollutant concentrations on the landing area. Another meteorological mechanism shown by Jazcilevich et al. (2005) gives rise to high atmospheric pollution episodes over the MCMA: a local confluence line created when two airflows meet over the city almost canceling their horizontal speed, accumulating pollutants and favoring photochemical reactions. It was concluded that the occurrences of the confluence lines over MCMA are relatively common during the autumn–winter period. The confluence phenomenon explains why the measured pollutant assumes its distribution. It also explains how biogenic and anthropic photochemical smog precursors can meet within the Basin of Mexico aiding to the formation of ozone.

4. Studies of organic aerosol in Mexico City Metropolitan Area

The MCMA is located in a basin on the central Mexican plateau with a population of around 20 million, in addition to 4 million vehicles and 35,000 industries. It has tropical latitude, an urban area of about 3,500 km^2 at 2,240 m altitude, and is surrounded by high mountains on three sides, degrading the air quality (Fast et al., 2007). One of the first campaigns to provided comprehensive information into meteorological measurements and particulate composition in the MCMA was the IMADA-AVER study (Investigación sobre Materia Particulada y Deterioro Atmosférico-Aerosol and Visibility Evaluation Research) carried out in February–March 1997 (Doran et al., 1998). A subsequent campaign developed during April 2003 (MCMA-2003) generated observations of oxidant precursors, photochemical products, radicals species, speciated VOCs, particulate matter, as well as meteorology and emissions information (Molina et al., 2007). The most recent and intensive campaign named MILAGRO (Megacity Initiative: Local and Global Research Objectives), characterized the pollutant emissions in MC and their transformation and impact on the atmosphere from local to global scales. The study involved multiple ground sites inside and downwind from MC, as well as multiple research aircraft (http://mce2.org/, Molina et al., 2010).

4.1 Chemical speciation

Carbon is one of the major contributors to fine particle mass. It can be found as elemental (EC) and organic carbon (OC). Chow et al. (2002) reported crustal material (~50%), carbon (~32%) and sulfate, ammonium and nitrate (~17%) as the main components of PM_{10}, while those $PM_{2.5}$ were carbon (~50%), crustal material (~30%), and sulfate, ammonium and nitrate (~15%), around and in MC during February and March 1997. $PM_{2.5}$ contributed to ~50% of PM_{10} mass. Chemical composition mass was heterogeneous among sites. In November of the same year, the chemical analysis of aerosols measured in the SW indicated again that soot, organic compounds, and sulfate dominate their composition (Baumgardner et al., 2000), and that the relative fractions of sulfate that make up their composition are controlled by water vapor and cloud droplets. Baumgardner et al. (2002) suggested that black carbon in urban areas can be estimated by carbon monoxide measurements. Salcedo et al. (2006) determined that organic and elemental carbon constituted ~66% of fine particle concentration, while inorganic and crustal species accounted for the remaining ~33% during MCMA-2003. The concentrations and compositions were consistent at various locations within MC, suggesting widespread sources of precursors and secondary aerosol formation. The OA total mass can be estimated from the organic carbon content commonly multiplying by a conversion factor of 1.4 (Turpin & Lim, 2001), although it can vary from 1.0 to 2.5 depending on location (Pang et al., 2006).

Although total carbon (EC+OC) determination is an important parameter to explain several atmospheric conditions due to particles found there, the chemical speciation is a key to comprehensively understand, for example, source apportionment, concentration levels, chemical transformation, air quality models and human health risk. One of the most important groups in airborne particles in terms of health risk are polycyclic aromatic compounds (PAC), which include PAH, oxygenated-PAH, nitro-PAH, amino-PAH, and heterocyclic aromatic compounds (Finlayson-Pitts & Pitts, 1997). PAC is a fraction of several classes of organic compounds found in atmospheric aerosol. Among them, PAH have been the most studied PAC in gas and particle phases, in part owing to carcinogenic effects (Denissenko et al., 1996; IARC, 1983, 1989) and genotoxic properties (Villalobos-Pietrini et al., 2007), although their derivatives as nitro- and oxy-compounds can represent a higher risk than their parent PAH (Durant et al., 1996). PAH are present in a larger proportion in fine particles (Allen et al., 1996; Amador-Muñoz et al., 2010). The main intake route by humans is the respiratory system; the particles generally occur as complex mixtures emitted as a result of incomplete combustion processes and are generated from both natural and anthropic sources (ATSDR, 1995). Several studies have been developed to determine PAH in MC, including on-real and off-real time analysis.

4.1.1 On-real time PAH measurements

Velasco et al. (2004) measured personal exposure to PAH in different outdoor and indoor environments, as well as along roadways in MC developed in December 2001. PAH were analyzed based on the aerosol surface properties using a photoelectric aerosol sensor (PAS) which quantifies bulk particle-bound PAH (PPAH) (Burtscher & Siegmann, 1993). For outdoor environments (bus stations) PPAH concentrations varied from 17 to 582 ng m^{-3}. For indoor environments the major contributors were hand smokers, poorly adjusted pilot stoves, inefficient ventilation and faulty air-conditioning systems. Marr et al. (2004) measured PPAH with a PAS during October 2002 at three points in MC with a high influence of diesel combustion. Median PPAH concentrations in roadways along MC ranged

from 60 to 910 ng m^{-3}. Particles freshly emitted by vehicles, PPAH and elemental carbon concentrations were well correlated, suggesting that surface PPAH concentrations may diminish with particle aging. In a subsequent study, Marr et al. (2006) compared different methods for characterization of PAH concentrations in the SE of MC during April 2003 (MCMA-2003). The diurnal concentration patterns captured by aerosol photoionization and aerosol mass spectrometry were generally consistent. Ambient PPAH typically show a peak at ~ 110 ng m^{-3} during morning rush hour, with a quick decrease due to sources in activity pattern, air dilution and surface coated by secondary organic aerosol. Speciated measurements suggest that motor vehicles are the predominant daytime source of PPAH, while wood and garbage burnings are important nighttime sources. Jiang et al. (2005) estimated PAH from motor vehicles in MC during April 2003 (MCMA-2003). On the basis of ~ 30,000 exhaust measurement points that represent a variety of vehicle types and driving conditions, and supported by a method of automatically identifying exhaust plumes, an estimate was made of an emission inventory and a fleet-average emission factor of 57±6 tons PPAH per year, not including cold start emissions. However, this estimate may be low by ~10% due to the lower response type of the PAS. Dzepina et al. (2007) reported the technical aspect of particle-bound PAH analysis using real-time quadrupole aerosol mass spectrometer (Q-AMS) and the comparison with PAS and GC-MS analysis. A subtraction method to remove the contribution of non-PAH organics to the ion signals of the PAH in ambient data was developed. The mass concentration of ambient PAH from 202 to 328 g mol^{-1}, as well as their sum was reported with an uncertainty of +35% and -38%. Comparisons with PAH-PAS measurements were well correlated, while those of PAH concentrations in filter determined by GC-MS analysis were in agreement for some PAH and higher for others. The signals of ambient cyclopenta[*cd*]pyrene and dicyclopentapyrenes were higher by Q-AMS than by GC-MS analysis of filter samples, suggesting artifacts during filter sampling. Thornhill et al. (2008) measured PAH with PAS at several sites throughout MC during the MILAGRO campaign. PPAH concentrations in the north of Central exhibited a consistent diurnal pattern and frequently exceeded 200 ng m^{-3} during the morning rush hour. PPAH concentrations were poorly correlated in space, and therefore for risk assessment studies, a single monitoring site was not adequate to represent an individual's exposure. PPAH were strongly correlated with NOx, reflecting the importance of diesel combustion engines. Results suggested that primary particles emitted from combustion are rapidly coated by secondary aerosol in MC, protecting PPAH against photodegradation or heterogeneous reactions, increasing the PPAH lifetime in the atmosphere. Since some other organic compounds can be ionized by the PAS and contribute to their signal (Matter et al., 1999), PPAH should be considered a relative, rather than absolute, indicator of the concentration of PPAH, elemental carbon and some trace amounts of other organics (Baumgardner et al., 2007). Given this uncertainty, a mass concentration of PPAH in the SW of MC during April 2005 was reported by Baumgardner et al. (2007). A reproducible diurnal pattern with the daily maxima (~120 ng m^{-3}) occurring from 6 to 8 a.m. was observed, and the maximum occurred at the same time as the condensation nuclei (CN), indicating that the majority of the particles containing PAH are quite small, which are those that dominate the CN concentration. A rapid decrease of PPAH, similar to findings by Marr et al. (2004, 2006) and Thornhill et al. (2008), was observed, suggesting a removal process by photochemical reactions which suppresses the response of the PAS; however, caution is recommended in using this type of analyzer for studying urban PPAH.

4.1.2 Off-real time PAH measurements

Several Mexican research groups have contributed to determine specific PAH in aerosol based on off-real time measurements. Our Environmental Mutagenesis Group (EMG) is one of them. It is dedicated to evaluating not only PAH, but also several organic compounds in aerosols, their temporal and spatial behavior, sources and genotoxic effects. The follow studies were done using high volume samplers for PM_{10} in the SW of MC on the campus of Universidad Nacional Autónoma de México, considered as a pollutants receptor site (Amador-Muñoz et al., 2011; Guzmán-Torres et al., 2009). In all campaigns, the analyses were done by GC-MS operated in electron impact mode. Calderón-Segura et al. (2004) measured PAH present in PM_{10} in April, August and November 1997. The highest concentrations were obtained in dry-season (November), while the lower ones were obtained in rainy season (August). Furthermore, the effects of seasonal weather on genotoxicity, mitotic changes and cytotoxicity in human cells exposed to extracts of airborne particles were evaluated as will be shown in the section on toxic effect and human health risk. Bravo et al. (2006) proposed a multivariate linear model made up with data from August 1998 to September 2000 to estimate PM_{10} as a function of meteorological parameters behavior. The model was evaluated to estimate non-seasonal PM_{10} concentrations from November 2000 to June 2001 ($r=0.57$, $p<0.05$). PM_{10} concentration values from February to May 1998 were higher than the rest of the data, due to the abundant emissions of smoke from the forest fires in the surroundings of the sampling site and confirmed by the presence of high amounts of retene (Fig. 2), which is a branched PAH considered a molecular marker of wood burning (Ramdahl, 1983).

In addition to retene, specific PAH were quantified by Villalobos-Pietrini et al. (2006). The presence of benzo[*ghi*]perylene, coronene and indeno[*1,2,3-cd*]pyrene as the most abundant PAHs (Fig. 3) indicate vehicles with gasoline combustion as the main source (Miguel et al., 1998), in spite of the wood burning presence. Statistical analysis suggested that fluoranthene and benz[*a*]anthracene could also mainly originate in wood combustion, which was the opposite for perylene and coronene, where the fires were not their principal origin.

In a subsequent study, Amador-Muñoz et al. (2010) evaluated the seasonal behavior of particle mass, solvent extracted organic matter (SEOM) and PAH in dry (October 1998-February 1999) and rainy (June-October 1999) season, using a cascade impactor with six stages (<0.49-10 μm). Higher mass concentrations were distributed in particles with diameters < 3.0 μm in both seasons (Fig. 4). The most abundant PAH detected in this study were coronene, benzo[*ghi*]perylene, and indeno[*1,2,3-cd*]pyrene, indicating vehicular gasoline combustion. Heavy PAH were distributed in fine particles, while light PAH were more abundant in coarse particles. SEOM in particles <0.95 μm indicated an organic composition with a higher water-affinity than in greater particle sizes. SEOM mass/particle mass ratios were higher in the rainy season compared to the dry season for five stages (except for $0.95>d\geq0.49$ μm range), suggesting higher amounts of organic compounds per mass unit of inhaled particles in the rainy season than in the dry season. Greater human risk in the dry season was determined when the potential doses of carcinogenic PAH by inhalation were evaluated. In a campaign carried out from February to April in 2004 at the same sampling zone (Saldarriaga et al., 2008), we found higher concentrations of coronene, benzo[*ghi*]perylene, benzo[*b+j+k*]fluoranthenes and indeno[*1,2,3-cd*]pyrene in PM_{10}, indicating again a strong contribution from incomplete combustion of gasoline.

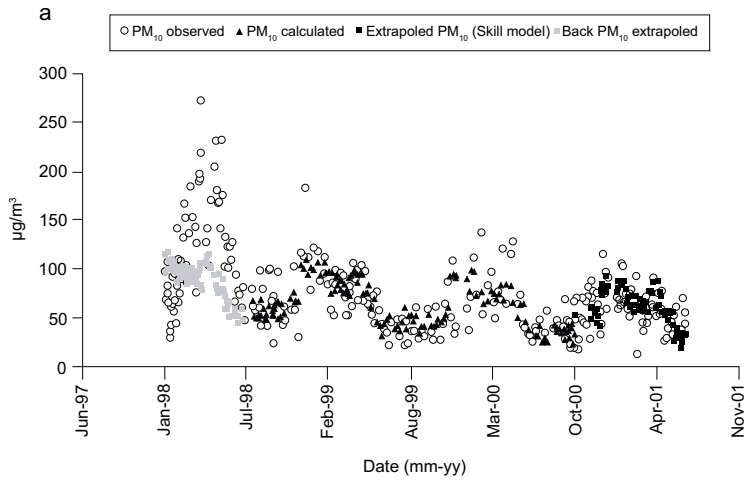

Fig. 2. Observed and estimated PM_{10} vs. date from January (1998) to June (2001). SWof MC. Higher values (> 200 µg m^{-3}) due to forest fires. Taken from Bravo et al. (2006).

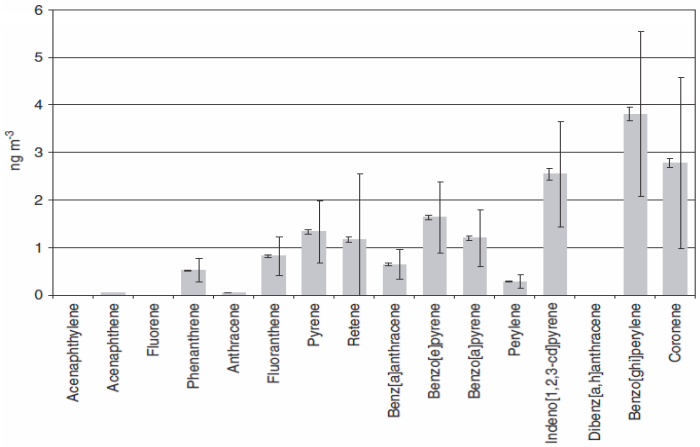

Fig. 3. PAH annual mean concentrations in SW of MC during 1998; the smaller deviation lines indicate the uncertainty associated to measurements, and the largest lines represent the standard deviations. Taken from Villalobos-Pietrini et al. (2006).

Other Mexican research groups have also contributed to studies on PAH concentrations in airborne particles in the MCMA. In a study carried out in 2003 (November and December) in the NW (UAM-A) of MC, Mugica et al. (2010a) reported PAH in PM_{10}, employing high-volume samplers and GC-MS analysis developed in different seasons and sites. Benzo[*ghi*]perylene was the most abundant PAH, associated to vehicle emissions. Guzmán-Torres et al. (2009) carried out a study during March 2003 at two sites in MC: Center (source site) and SW (receptor site). Higher PAH concentrations were found during the morning period, while the ratios between organic and elemental carbon also measured indicated that

the SW is impacted by secondary aerosols during the afternoon hours. Similar to the last mentioned studies, benzo[*ghi*]perylene was the most abundant PAH, suggesting exhaust emission by light-duty vehicles as an important contributor to the atmospheric PAH burden. In a subsequent campaign by Mugica et al. (2010a) from February 2005-2006, spatial and seasonal PM_{10}-PAH differences were found among four sites in MCMA. The highest amount of PAH was found in the NE (Xalostoc) (considered as the most important industrial area in the MCMA), while the lowest was found in the NW (UAM-A). Dry-cold season (October to February) showed PAH levels up to three times greater than rainy (June-September) and dry-warm (February-May) seasons. A high number of thermal inversions and calm wind events during dry-cold season, and photochemical reactivity and evaporation on PAH during dry-warm season, explained the temporal PAH variations. In a similar period (February 2005 to January 2006), Mugica et al. (2010b) characterized and evaluated the seasonal behavior of PAH in the gas phase and in PM_{10} in the NW (UAM-A) of MC. Vapor-phase PAH comprised 86–97% of the total PAH mass. Major PAH concentrations in dry-cold season were found. Vehicular emissions and diesel and gas combustion were the most important PAH sources. Similar to other studies, benzo[*ghi*]perylene was the most abundant PAH. A more recent campaign developed by the same group from April 2006 to March 2007 in the North of MC (CINVESTAV), benzo[*ghi*]perylene was the PAH most abundant followed by indeno[*1,2,3-cd*]pyrene. Dry-cold season showed the highest PAH concentrations with respect to warm and rainy season. Table 1 shows a comparison of PAH concentrations in PM_{10} developed in the MCMA.

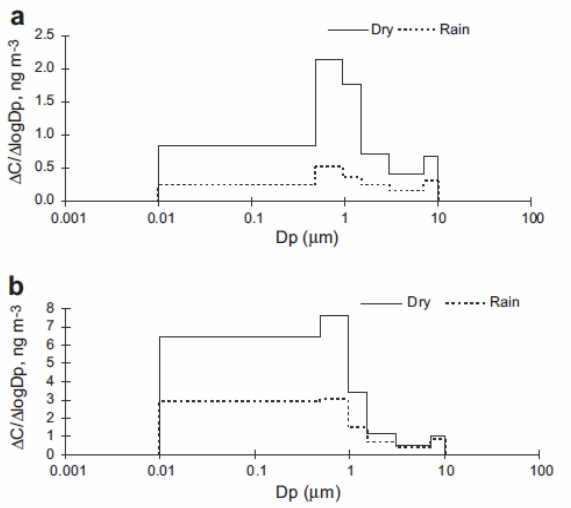

Fig. 4. Median seasonal PAH mass concentrations (ΔC/ΔlogDp) in six diameter ranges of a. Light PAH sum (phenanthrene, anthracene, retene, fluoranthene and pyrene) and b. Heavy PAH sum (benzo[*a*]anthracene, chrysene, triphenylene, benzo[*b*]fluoranthene, benzo[*j*]fluoranthene, benzo[*k*]fluoranthene, benzo[*e*]pyrene, benzo[*a*]pyrene, perylene, indeno[*1,2,3-cd*]pyrene, dibenzo[*a,h*]anthracene, benzo[*ghi*]perylene and coronene), during dry (October 1998–February 1999) and rainy (June–October 1999) seasons at SW of MC, Dp – aerodynamic particle diameter. Taken from Amador-Muñoz et al. (2010).

PAH	SW[1] (98)	SW[2a] (98-99)	SW[2b] (98-99)	Central[3a] (03)	SW[3b] (03)	SW[4] (04)	SW[5a] (05-06)*	SW[5b] (05-06)*	SW[5c] (05-06)*	Central[5a] (05-06)*	Central[5b] (05-06)*	Central[5c] (05-06)*
Acenaphthylene	n.f.	n.r.	n.r.	201	85	n.r.	n.r.	n.r.	n.r.	n.r.	n.r.	n.r.
Acenaphthene	46	n.r.	n.r.	35	29	n.r.	n.r.	n.r.	n.r.	n.r.	n.r.	n.r.
Fluorene	n.f.	n.r.	n.r.	85	23	n.r.	< 200	< 200	< 500	100-300	100-300	< 500
Phenanthrene	516	337	153	561	249	n.r.	200-500	200-500	500-1 000	500-1 000	500-1000	1 000-1 500
Anthracene	49	87	85	133	76	n.r.	n.r.	n.r.	n.r.	n.r.	n.r.	n.r.
Fluoranthene	815	659	203	1 438	681	200	500-800	400-600	500-1 000	1 000-1 500	1 000-1 500	2 000-3 000
Pyrene	1 330	848	242	1 702	791	n.r.	600-1 000	600-1 000	1 000-1 500	1 200-1 600	1 500-2 000	2 000-3 000
Retene	1 162	512	181	n.r.	n.r.	30	n.r.	n.r.	n.r.	n.r.	n.r.	n.r.
Benzo[*a*]anthracene	639	525	138	2 174	887	180	1 000-1 200	1 100-1 400	1 000-1 500	1 500-2 000	1 500-2 000	2 000-3 000
Chrysene	1 204[I]	728[I]	214[I]	3 132	1 441	240[I]	1 200-1 500	1 000-1 300	1 000-1 500	3 000-3 500	1 500-1 800	5 000-7 000
Benzo[*b*]fluoranthene	3 388[II]	1603	703	3 412	1 560	740[IV]	1 500-1 800	1 500-1 800	1 500-2 500	2 000-2 500	3 000-3 200	5 000-7 000
Benzo[*k*]fluoranthene	n.r.	1 021[III]	425[III]	2 858	1 474	n.r.[IV]	1 200-1 500	1 000-1 300	1 000-1 500	2 000	1 000-1 300	3 500-5 000
Benzo[*e*]pyrene	1 630	1 304	556	n.r.	n.r.	370	n.r.	n.r.	n.r.	n.r.	n.r.	n.r.
Benzo[*a*]pyrene	1 195	786	322	4 004	1 522	320	1 200-1 500	1 000	1 000-1 500	3 500-4 000	4 000	5 000-6 000
Perylene	282	225	126	n.r.	n.r.	n.r.	n.r.	n.r.	n.r.	n.r.	n.r.	n.r.
Indeno[*1,2,3-cd*]pyrene	2 541	1 821	887	5 660	2 516	670	1 400-1 600	1 500-1 800	1 000-1 500	4 000-4 500	5 000-5 500	12 000-14 000
Dibenzo[*a,h*]anthracene	n.f.	186	115	887	734	70	1 000	1 000	1 000-1 500	500-1 000	500-1 000	1 000-1 500
Benzo[*ghi*]perylene	3 802	3 065	1 520	7 174	2 777	870	1 600-2 000	2 000	2 500-3 000	5 000	6 000-7 000	16 000-18 000
Coronene	2 776	3 167	1 544	n.r.	n.r.	1 250	n.r.	n.r.	n.r.	n.r.	n.r.	n.r.
∑PAH	21 634	17 371	7 359	34 300	15 600	4 900	n.r.	n.r.	n.r.	n.r.	n.r.	n.r.

Table 1. Comparison of PAH concentration (pg m^{-3}) in PM10 among different sites and seasons carried out in the MCMA. The year of the campaign is indicated in parenthesis.

PAH	NW[6a] (05-06)	NW[6b] (05-06)	NW[6c] (05-06)	N[5d] (06-07)*	N[5e] (06-07)*	N[5f] (06-07)*
Acenaphthylene	n.r.	n.r.	n.r.	n.r.	n.r.	n.r.
Acenaphthene	n.r.	n.r.	n.r.	n.r.	n.r.	n.r.
Fluorene	100	100	300	500-800	100-300	400-600
Phenanthrene	80	50	260	500-800	500-800	700-900
Anthracene	n.r.	n.r.	n.r.	n.r.	n.r.	n.r.
Fluoranthene	120	110	250	700-900	600-800	1 200-1 400
Pyrene	350	250	580	1 000-1 100	700-900	1 400-1 600
Retene	n.r.	n.r.	n.r.	n.r.	n.r.	n.r.
Benzo[*a*]anthracene	220	440	1 580	1 000-1 300	1 000	1 400-1 600
Chrysene	240	270	1 360	1 100-1 400	800-1 000	1 000
Benzo[*b*]fluoranthene	150	280	1 740	1 000-1 300	1 400-1 600	2 800-3 000
Benzo[*k*]fluoranthene	120	210	1 150	1 100-1 400	1 000-1 200	1 800-2 000
Benzo[*e*]pyrene	n.r.	n.r.	n.r.	n.r.	n.r.	n.r.
Benzo[*a*]pyrene	250	290	810	1 400-1 600	1 300-1 500	2 300-2 500
Perylene	n.r.	n.r.	n.r.	n.r.	n.r.	n.r.
Indeno[*1,2,3-cd*]pyrene	70	90	390	1 800-2 000	1 700-1 900	3 200-3 400
Dibenzo[*a,h*]anthracene	110	270	900	1 100-1 400	1 100-1 300	1 300-1 500
Benzo[*ghi*]perylene	340	380	1 360	1 800-2 000	1 700-1 900	3 400-3 600
Coronene	n.r.	n.r.	n.r.	n.r.	n.r.	n.r.
∑PAH	1 990	2 760	10 480	n.r.	n.r.	n.r.

Continuation of Table 1.

SW (Pedregal), NW (UAM-A), N (CINVESTAV), * Range of approximated values since they were obtained directly from figures described by Mugica et al. (2010a), n.f. – not found, n.a. – not analyzed, n.r. – not reported, [I] Chrysene+Triphenylene, [II] Benzo[*b*+*k*]fluoranthenes, [III] Benzo[*j*+*k*]fluoranthenes, [IV] Benzo[*b*+*j*+*k*]fluoranthenes

[1] Villalobos-Pietrini et al. (2006). PAH annual mean concentrations (adjusted to standard conditions in 25°C and 1 atm) from January to December 1998. Forest fires were present from February to May 1998 (Bravo et al., 2006). SW is a residential and commercial zone, with green areas. 24 h collection, high volume samplers (1.13 m^3 min^{-1}).

[2] Amador-Muñoz et al. (2010). PAH seasonal median concentrations (adjusted to standard conditions in 25°C and 1 atm):

[a] Dry-cold season (October 1998-February 1999) and [b] Rainy season (June-October 1999). SW is a residential and commercial zone, with green areas. 24 h collection, in a cascade impactor on high volume samplers (1.13 m^3 min^{-1}), PAH in PM_{10} was calculated as the sum of all stages.

[3] Guzmán-Torres et al. (2009). PAH monthly mean concentration in March 2003 (Dry-warm season). [a] The zone is highly impacted by vehicular emissions, and it was considered as a source site, [b] The zone is a low density residential area with low vehicular flow, and it was considered as a receptor site during the prevalent diurnal wind directions. 8 h collection, high volume samplers (1.13 m^3 min^{-1}).

[4] Saldarriaga et al. (2008). PAH seasonal mean concentration (adjusted to standard conditions in 25°C and 1 atm) from February to April 2004 (Dry-warm season). SW is a residential and commercial zone, with green areas, 24 h collection, high volume samplers (1.13 m^3 min^{-1}).

[5] Mugica et al. (2010a). PAH seasonal mean concentration: [a] February-May 2005 (Dry-warm season), [b] June-September 2005 (Rainy season), [c] October 2005-February 2006 (Dry-cold season), [d] Dry-warm season, [e] Rainy season, [f] Dry-cold season. Months were not specified for [d,e,f]. Center zone is close to downtown MC with heavy and light traffic on many avenues, and N (CINVESTAV) site has intense industrial activities, surrounded by main roads with large transit volumes, connecting northern and central regions of the MCMA, 24 h collection, high volume samplers (1.13 m^3 min^{-1}).

[6] Mugica et al. (2010b). PAH seasonal mean concentration: [a] February-May 2005 (Dry-warm season), [b] June-September 2005 (Rainy season), [c] November 2005-January 2006 (Dry-cold season). NW (UAM-A) is an urbanized zone with mixed land occupation of housing and industrial areas, 24 h collection, high volume samplers (1.13 m^3 min^{-1}).

PAH sum concentrations in the SW during 2003 found by Guzmán-Torres et al. (2009) were similar to those found by Amador-Muñoz et al. (2010) compared with the dry season during 1998-1999, but higher compared with the rainy season in 1999. PAH sum in the Center and the SW reported by Guzmán-Torres et al. (2009) were similar to those described by Mugica et al. (2010a) during 2005-2006, but three times higher than those reported by Saldarriaga et al. (2008) for the SW during 2004. The NW of the city showed lower PAH concentrations during 2005-2006 (Mugica et al. 2010b) compared to PAH in the North during 2006-2007. PAH differences in space were also observed by Thornhill et al. (2008), where different primary emission sources resulted in different PAH emitted concentrations in $PM_{10.}$ This spatial heterogeneity implies the importance of the primary emission combustion sources in each site and implies that PAH concentrations in PM_{10} in a specific site can not be extrapolated to other sites. This is important since the development of effective control strategies for fine particulate air pollution abatement requires knowing the importance of the diverse sources that contribute to the particulate matter concentrations at ambient air monitoring sites (Atkinson & Lewis, 1974).

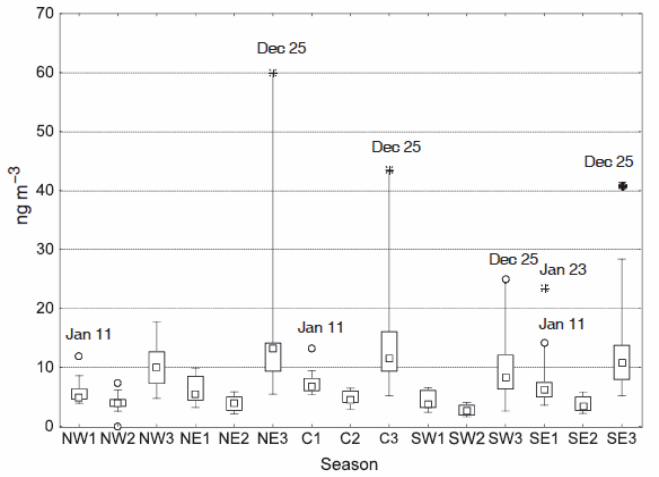

Fig. 5. Median (middle squares) seasonal heavy PAH sum (benzo[*a*]anthracene, chrysene, triphenylene, benzo[*b*]fluoranthene, benzo[*j*]fluoranthene, benzo[*k*]fluoranthene, benzo[*e*]pyrene, benzo[*a*]pyrene, perylene, indeno[*1,2,3-cd*]pyrene, dibenzo[*a,h*]anthracene, dibenzo[*a,c*]anthracene and benzo[*ghi*]perylene) mass concentrations of five sites around MCMA during 2006. Boxes — 25–75% and whiskers — 10th–90th percentiles, circles — outliers, asterisks — extremes values. 1—Dry season 1 (January–April), 2—Rainy season (May–October), 3—Dry season 2 (November–December). Taken from Amador-Muñoz et al. (2011).

Stone et al. (2008) determined PAH, alkanes, hopanes, steranes, carboxylic acids and levoglucosane in $PM_{2.5}$ in the North of MC during the MILAGRO campaign. Motor vehicles accounted for 49% of OC in the urban area and 32% on the periphery. The OC generated by biomass burning ranged from 5–26% at the urban site and 7–39% at the peripheral site. The remaining OC not related to primary sources showed a strong correlation with real-time water soluble organic carbon which was considered to be secondary in nature. Amador-Muñoz et al. (2011) determined PAH, nitro-PAH, n-alkanes and solvent extracted organic matter (SEOM) in

$PM_{2.5}$ in five simultaneously sites in MC. Instead, a uniform distribution of $PM_{2.5}$, SEOM, biogenic n-alkanes (C_{24}-C_{33}) and nitro-PAH was observed in the MCMA regarding gravimetric mass concentration, while petrogenic n-alkanes ($<C_{23}$), fossil fuel combustion n-alkanes ($23 \leq Cmax \leq 26$) and PAH (Fig. 5) showed mass heterogeneity in the MCMA. Spatial PAH heterogeneity across MCMA was observed as in the case of PAH in PM_{10}, suggesting again a significant impact of combustion primary sources in each site. These last authors also described that the highest mass concentrations of PAH occurred in the dry season with respect to the rainy season (Fig. 5). Bonfires and fireworks were probably responsible for extreme values of PAH. Benzo[*ghi*]perylene was again the most abundant PAH.

Table 2 shows a comparison of PAH concentrations in $PM_{2.5}$ developed in MCMA. The most abundant light PAH were found in the NE zone, because it is known (Miguel et al., 1998) that this type of PAH are mainly emitted by diesel combustion, which suggests this source is a main generator in the area (Amador-Muñoz et al., 2011). The majority of the heavy PAH were more abundant in the Central zone, suggesting gasoline combustion as main source (Miguel et al., 1998). Regarding seasonal variation, there was greater concentration of PAH in $PM_{2.5}$ in the dry-cold season. Concentrations quite similar to those PAH found by Stone et al. (2008) in the Northern zone (urban site) were observed with those in the NW and the NE reported by Amador-Muñoz et al. (2011).

PAH	N[1a, *]	NE[1b, *]	NW[2]	NE[2]	C[2]	SW[2]	SE[2]
Naphthalene	n.a.	n.a.	107	588	151	96	89
Acenaphthylene	n.a.	n.a.	50	76	49	25	39
Acenaphthene	n.a.	n.a.	0	0	0	0	0
Fluorene	n.a.	n.a.	16	60	0	0	0
Phenanthrene	n.a.	n.a.	173	386	199	115	134
Anthracene	n.a.	n.a.	40	66	40	23	26
Fluoranthene	n.a.	n.a.	223	554	222	139	187
Pyrene	n.a.	n.a.	285	711	292	178	241
Benzo[*a*]anthracene	n.a.	n.a.	219	313	254	140	207
Chrysene+Triphenylene	n.a.	n.a.	598	883	662	391	477
Benzo[*b*]fluoranthene	572	475	576	548	764	402	601
Benzo[*k*]fluoranthene	487	317	n.r.	n.r.	n.r.	n.r.	n.r.
Benzo[*j*+*k*]fluoranthenes	n.a.	n.a.	486	506	534	347	517
Benzo[*e*]pyrene	597	438	313	383	474	275	408
Benzo[*a*]pyrene	n.a.	n.a.	380	404	455	265	452
Perylene	n.a.	n.a.	105	110	118	69	94
Indeno[*1,2,3-cd*]pyrene	475	353	500	477	690	408	608
Dibenzo[*a,c*]anthracene	n.a.	n.a.	38	53	38	23	50
Dibenzo[*a,h*]anthracene	110	97	63	60	73	46	94
Benzo[*ghi*]perylene	1108	548	1333	1229	1840	1119	1619

Table 2. Comparison of PAH mass concentrations (pg m^{-3}) in $PM_{2.5}$ at different sites in the MCMA.

n.a. – not analyzed, n.r. – not reported. * Values were updated to standard conditions (298 K, 1 atm), which represent ~ 21.5 % more than real values.

[1] Stone et al. (2008). [a] Urban zone, [b] Suburban zone. Average of the sampling days (17-30, March 2006). $PM_{2.5}$ was collected with medium volume samplers on quartz fiber filters, during 12 h.

[2] Amador-Muñoz et al. (2011). Annual medians (January to December 2006). $PM_{2.5}$ were collected with high volume samplers on glass fiber filters covered with Teflon during 24 h.

4.1.3 Nitro-PAH in PM_{10} and in $PM_{2.5}$

In addition to PAH determination, another important class in terms of human health risk is their nitro derivatives by their mutagenic and carcinogenic properties mentioned earlier. In a PM_{10} sampling carried out from February to April in 2004 in the SW of MC, Saldarriaga et al. (2008) found 9-nitroanthracene, indicating direct emission from diesel combustion, and heterogeneous nitrating reactions on sorbed particles, while 2-nitrofluoranthene, indicated atmospheric transformation. The total average concentration of PAH was 14 times greater than that of nitro-PAH, whereas the n-alkanes concentration was 17 times greater than that of PAH.

In an effort with researchers of Universidad Autónoma Metropolitana Unidad Aztcapotzalco, we carried out a campaign to determine nitro-PAH in $PM_{2.5}$ and in PM_{10} sampled simultaneously (Valle-Hernández et al., 2010). The study was developed in three seasons from April 2006 to February 2007 in the North of MC. The analytical extraction and purification method for nitro-PAH was evaluated employing a standard reference with and without matrix, the former giving the best results. Eight PAH in PM_{10} were quantified by GC-MS operating in the negative chemical ionization mode. Nitro-PAH sum ranged from 111 to 819 pg m^{-3}, depending on the season. The greatest concentration was for 9-nitroanthracene, detected during the dry-cold season. This nitro-PAH showed greater concentrations than those found in the SW by Saldarriga et al. (2008), while the 2-nitrofluoranthene was lower. This suggests more sources of diesel combustion in the North, whereas more secondary organic aerosol is present in the SW.

Table 3 shows the medians of nitro-PAH mass concentrations in $PM_{2.5}$ during 2006 and early 2007 in different zones in MC. 2-Nitrofluoranthene (2-NFlt) and 9-Nitroanthracene (9-NAnt) appear to be among the most abundant nitro-PAH in $PM_{2.5}$. The North showed a higher mass of 9-NAnt with respect to the other sites, probably emitted from diesel combustion of heavy trucks (Feilberg et al., 2001) circulating in a major proportion in this area. 2-NFlt was the nitro-PAH with the highest concentration found in the Central zone, where the presence of this compound is exclusively attributed to atmospheric formation (Nielsen, 1984). At present, nitro-PAH have only been determined by our research group in the MCMA. Valle-Hernández et al. (2010) and Amador-Muñoz et al. (2011) have described their seasonal

nitro-PAH	N[1]	NW[2]	NE[2]	C[2]	SW[2]	SE[2]
9-Nitroanthracene	45.7	36.8	36.0	35.7	27.7	35.8
9-Nitrophenanthrene	13.7	n.f.	n.f.	n.f.	n.f.	n.f.
3-Nitrophenanthrene	14.7	n.f.	n.f.	n.f.	n.f.	n.f.
2-Nitrofluoranthene	41.7	52.8	59.4	67.4	47.8	52.9
3-Nitrofluoranthene	3.1	n.f.	n.f.	n.f.	n.f.	n.f.
1-Nitropyrene	10.9	n.a.	n.a.	n.a.	n.a.	n.a.
7-Nitrobenzo[*a*]anthracene	16.3	9.3	11.3	15.7	8.7	14.4
6-Nitrochrysene	1.7	n.f.	n.f.	n.f.	n.f.	n.f.

Table 3. Comparison of nitro-PAH mass concentrations (pg m^{-3}) in $PM_{2.5}$ at different sites (urban zones) in MC. The values are adjusted to standard conditions (298 K, 1 atm), n.f. – not found, n.a. – not analyzed.

[1] Valle-Hernández et al. (2010). Medians of the sampling days (April 2006 to February 2007, twice per month). $PM_{2.5}$ was collected with high volume samplers on quartz fiber filters during 24 h.
[2] Amador-Muñoz et al. (2011). Annual medians (January to December 2006). $PM_{2.5}$ were collected with high volume samplers on glass fiber filters covered with Teflon during 24 h.

behavior classified in three periods: dry-warm, rainy and dry-cold. The highest concentrations of nitro-PAH in $PM_{2.5}$ were found during the dry-cold season and the lowest values corresponded to the rainy season in both studies. In general, quite similar concentrations in both studies of those similar nitro-PAH were found.

Annual median of nitro-PAH in PM_{10} and in $PM_{2.5}$ in the N of MC is depicted in Fig. 6 (Valle-Hernández et al., 2010). All nitro-PAH exhibited similar behaviors and concentrations between PM_{10} with respect to $PM_{2.5}$, suggesting that these compounds are mainly located in $PM_{2.5}$. One exception was for 9-NAnt with greater concentration and variability in PM_{10}, probably given by a mixing of primary and secondary origins (Bamford & Baker, 2003; Pitts et al., 1978).

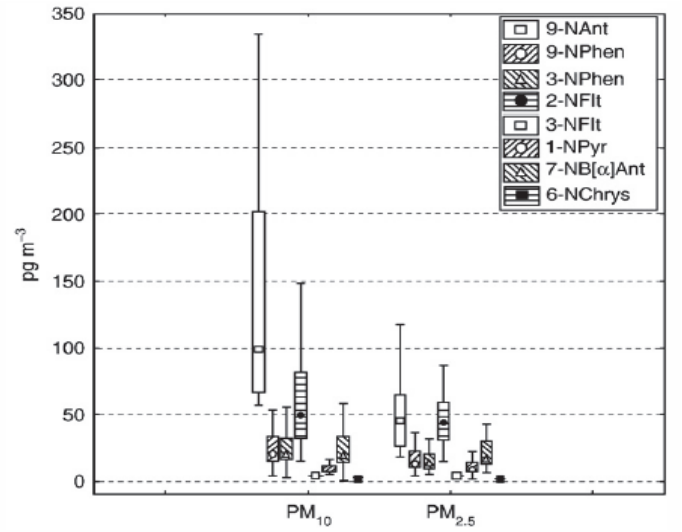

Fig. 6. Annual median concentrations (middle square), boxes 25–75% and whiskers 10th–90th percentiles of the nitro-PAH in PM_{10} and $PM_{2.5}$ during 2006-2007 at North of MC. Taken from Valle-Hernández et al. (2010).

Analytical methodology optimization is another important activity developed by the EMG focused to reduce the uncertainty and increase the efficiency in the measurements. A recent purification procedure based on solid phase extraction was proposed for determining oxy-PAH from PAH and n-alkanes in $PM_{2.5}$ (Murillo-Tovar et al., 2010). Multivariate parameters were adjusted on a standard mixture, and on a different amount of solvent extracted organic matter (SEOM) spiked with pure standard mixture solutions. Cyanopropylsilyl-bonded phase material was the selected stationary phase. Oxy-PAH was totally separated from n-alkanes and PAH by applying different SEOM pooled masses. Fig. 7 shows an example of the separation obtained. Mean recoveries ± confidence intervals (95%) for n-alkanes ranged from 53±17% (n-tetracontane) to 101±11% (n-hexacosane); for PAH from 58±5% (phenanthrene) to 85±9% (benzo[k]fluoranthene); and for oxy-PAH from 68±12% (9,10-dihydrobenzo[a]pyren-7(8H)one) to 108±9%(1,2-benzopyrone). This method is an efficient fractionation procedure to apply to oxy-PAH, PAH and n-alkanes in complex organic mixtures extracted from $PM_{2.5}$.

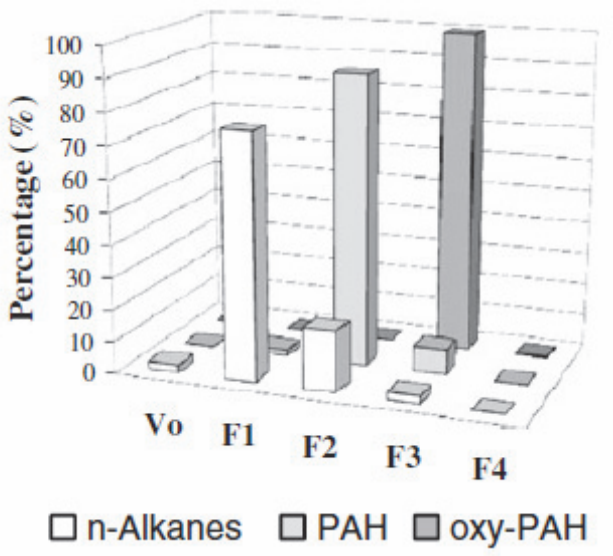

Fig. 7. Percentage distributions (mass per fraction) of organic classes in a real sample by applying 8.5 mg of SEOM pooled mass. Vo – Death volume, F1 to F4 – Organic fractions. Taken from Murillo-Tovar et al. (2010).

4.2 Toxic effects and human health risk

New methods have been developed to identify mutagens related to potential carcinogens more efficiently (Lewtas, 1988) in airborne complex mixtures combining bioassay directed fractionation and chemical characterization (Schuetzle & Lewtas, 1986). Several Environmental Agencies around the world have tried to regulate the air particle concentrations in a defined period of time; however, there are no threshold values under which humans are protected. The permissible limits are restricted to mass concentrations and should be important to relate those compounds with mutagenic and carcinogenic effects.

Airborne particles are formed by complex mixtures of hundreds of compounds, some of which are extracted organic matter (EOM) potentially mutagenic, cytotoxic and carcinogenic (Lewtas, 1993; Villalobos-Pietrini et al., 2006, 2007). For this reason special attention has been applied in assays to evaluate the genotoxicity produced by these pollutants. The *Salmonella* assay (Ames test) has been a convenient and usable test to compare genotoxic activity. Pitts et al. (1975) were the first authors who treated *Salmonella typhimurium* with EOM adsorbed airborne particles, now recognized as a bioassay of the reference Ames test to detect a wide range of chemicals that can produce genetic damage leading to gene mutation (Mortelmans & Zieger, 2000) in the histidine operon of the mentioned bacteria that revert to wild type condition (Ames et al., 1973). When an agent induces a reversion in the mentioned operon, then the bacteria can synthesize the amino acid and can reproduce itself, when it is more mutagenic, the revertant cells increase. As the bacteria cannot metabolize some chemicals, it is useful to include in the test the metabolic activation of mammals known as enzymatic fraction S9 (Ames et al., 1975).

The use of some strains allows recognizing whether the effect is in a direct acting mutation (without S9) or if it includes the mammal metabolism (with S9) by indirect acting mutagens. Therefore, it is important to choose the strains based on the purpose of the study. When rural and urban monitoring sites are studied during different seasons in the year, the plate incorporation assay with TA98 and TA100 furnishes more reproducible and comparative results (Claxton et al., 2004); when the effect of series of strains are compared, the strains YG are more sensitive to mutagenic nitroaromatic than the TA (Claxton et al., 2001). When the sample amount is very small, another important change in the technique is the microsuspension assay that is more sensitive than the plate incorporation assay, this last one differing in the increment of the number of bacteria and in the time of contact to them (Kado et al., 1983, 1986).

Biological effects of organic matter in vivo and in vitro have been scarcely developed in Mexico. Recent studies have shown different responses as a function of their own biological mechanisms. In a study carried out in SW of MC, Villalobos-Pietrini et al. (2006) observed that the mutagenicity of strain TA98+S9 did not correlate with the monthly concentration of PM_{10} and of EOM, while strains TA98-S9 and YG1021 correlated well, which suggests that there exist different emission sources of direct and indirect pollutants. The same organic compounds selectively separated in less complex groups (Fig. 8a, b), means fractioning the PM_{10} in fractions of increasing polarity: 1) hexane; 2) hexane-methylene chloride (6:4); 3) methylene chloride; and 4) methanol. In 77 % of the cases, mutagenic activity was higher in the sum of fractions than in their EOM (Villalobos-Pietrini et al., 2007). The same study revealed that the moderately polar and the polar fractions induced higher mutagenicity in relation to less polar fractions, and perhaps this effect depends upon mass concentration of organic matter; these polar fractions are correlated with thermal inversions in the dry-cold season (Villalobos-Pietrini et al., 2007).

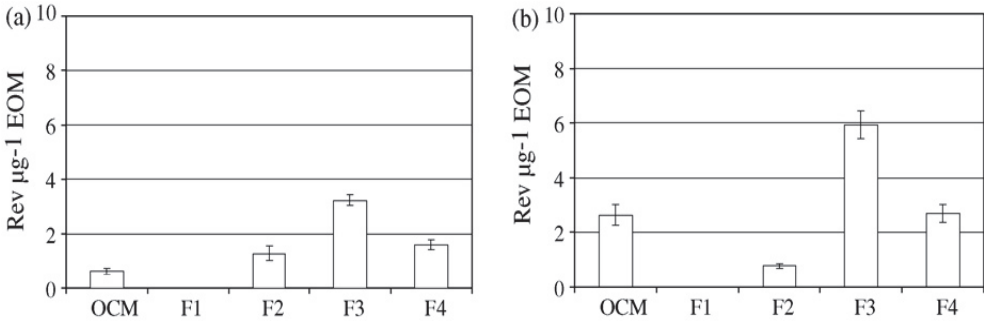

Fig. 8. Mutagenic potency of extracted organic matter (EOM) of January 1998 in the organic complex mixture (OCM) and in its fractions; (a) with TA98 + S9 and (b) with YG1021. Taken from Villalobos-Pietrini et al. (2007).

Several studies have been made using the sister chromatid exchange (SCE) which is a sensitive biomarker to detect genotoxicity. It represents symmetric change between homologous loci of replication products. SCE occur without loss of DNA and do not change the morphology of chromosome. This assay is based on the incorporation of the 5-bromodeoxyuridine (BrdU), an analog of the DNA base thymidine inside the DNA cell that replicates twice (Latt et al., 1981). In addition to SCE analysis, the BrdU differential staining

method can be used to asses the effect of the compounds in cell replication proliferation kinetics and in the replication index in human blood culture as a useful tool in genotoxicity testing. In this way, Calderón-Segura et al. (2004) assayed the EOM from PM_{10} collected in three seasons in MC to evaluate SCE (genotoxicity), mitotic index (cytotoxicity) and replication index (cytokinetic) in human lymphocyte cultures. The SCE obtained was dose-dependent with the greatest effect in response to indirect acting mutagens. The direct acting mutagens produced significant effects as well, but in lower frequency. The results show that the EOM effect also depended on the weather because in April (dry-warm), August (rainy-warm) and November (dry-cold) different responses were obtained. The lowest was observed in August and the highest in November, both of the direct (without S9) and indirect-acting mutagens (with S9) due to the fact that the content of PAH was different, possibly because the heavy rains in August reduce the amount of EOM and in November frequent thermal inversions tend to prevent the dispersion of contaminants, because of the atmospheric stability favoring photochemical reactions, among other reasons. Cytokinetics showed a decrease as the concentration of EOM increased independently of bioactivation and weather. Cytotoxicity occurred when higher concentrations of EOM were used.

Another useful assay to evaluate the effect of the compounds on the DNA is alkaline single cell gel electrophoresis, also called comet assay. This is a rapid and sensitive technique to analyze the damage to the DNA in individual cells on alkaline conditions (pH > 13) that detects the effects of different compounds on DNA at the individual cell level. It is based on the migration of DNA in an electric field, and its displacement from the nucleus could be used as an indicator of DNA damage (Östling & Johanson, 1984); the alkaline version is capable of detecting DNA single-strand breaks and alkali-labile sites. The name refers to the fact that the head has no DNA damage while the tail is the fragmented DNA. Rojas et al. (2000) used the comet assay in exfoliated tear duct epithelial cells of young adults, residents of the Northern and the Southern areas of MCMA; individuals in the last area showed the highest frequencies of DNA damage by the environmental pollution exposure. Gutiérrez-Castillo et al. (2006) made two fractions with the particle matter (PM), one a water soluble and the other an organic soluble. They treated the human cell line lung epithelial with both extracts and applied to them the alkaline single cell gel electrophoresis, concluding that more DNA damage was induced by the extracts obtained of the water soluble fraction, and that PM composition was more important than PM mass for producing genotoxicity.

Another genotoxic damage biomarker is the micronucleus assay that is based on chromosomal effects produced by the EOM that impact the chromosomes and produce fragments (clastogenic effect) or alter complete chromosomes (aneugenic effect) that are not included in the main nuclei of the daughter cells during mitosis; they remain in the cytoplasm and are present in the interphase cell as small nuclei. Roubisek et al. (2007) exposed human alveolar epithelial cells and found significant correlation between the induction of micronuclei and the presence of PAH, obtaining higher frequencies of micronuclei in the water–soluble industrial extracts than in residential extracts.

An increase in morbidity and mortality was associated with the exposure to urban PM_{10} obtained in three zones of the MCMA (North, Center and South), which were cytotoxic, genotoxic and proinflammatory (Alfaro-Moreno et al., 2002, 2007; García-Cuellar et al., 2002; Osornio-Vargas et al., 2003;). Montiel-Dávalos et al. (2010) showed that oxidative stress and apoptosis (programmed cellular death) are induced in human endothelial cells exposed to MC particulate matter. PM_{10} induced impairment of the antioxidant defense systems, without changes in cell viability (Chirino et al., 2010).

Furthermore, this has been described in children chronically exposed to complex mixtures of air pollutants in the SW of urban areas of MC, producing respiratory damage, as well as systemic and endothelial inflammation (Calderón-Garcidueñas et al., 2006), also residents of MC who are exposed to strong pollution present neuroinflammation and neurodegeneration, suggesting that the brain is affected by pollutants (Calderón–Garcidueñas et al., 2010). Barraza-Villarreal et al. (2008) show that the exposure to $PM_{2.5}$ provokes airway inflammation and decrement of lung function, and Holguin et al. (2003) observed that the concentrations of $PM_{2.5}$ are related with cardiac dysfunction especially in elderly persons in MCMA.

Another research related to organic matter of airborne particles refers to the content of PAH, which recognizes how the carcinogenic and mutagenic potential compounds are emitted by incomplete combustion and vegetation burning. In the MCMA, the most abundant PAH in the fine particulate matter are usually benzo[*ghi*]perylene, coronene and indeno[*1,2,3-cd*]pyrene with indirect acting mutagenic activity, and the most abundant nitro PAH are 2-nitrofluoranthene and 9-nitroanthracene (Amador-Muñoz et al., 2011), with direct acting mutagenic effects (Villalobos-Pietrini et al., 2007). Due to their lipophilic characteristics, the PAH may penetrate the cell membrane and change its properties inducing their effects through activation of aryl hydrocarbon receptors (AhR) and of cytochromes CYP that metabolize PAH, which leads to ROS formation and reactive metabolites that can covalently bind to nucleophilic sites on macromolecules and alter signaling pathways that are involved in cell survival proliferation, inflammatory response and cell death (Schwarze et al., 2010). This seems to cause changes in ion transport, in intracellular pH as well as lysosomal breakage. Along with PAH, other compounds (as transition metals and some quinones) have the potential to interact with airway epithelial cells and macrophages to generate ROS which have been linked to respiratory inflammation and other adverse effects (Cho et al., 2005; Xia et al., 2004).

In order to reduce the human health risk caused by airborne pollutants, researchers must continue studies on their chemical characterization, distribution, formation and sources emission, as well as on their effects such as complex mixture and their fraction, so as to detect compounds that cause damage and discover their mechanism of action.

5. Conclusions

Organic aerosol in the atmosphere is composed by hundreds of organics from primary or secondary origin. The knowledge of their composition is of relevant importance due to their impact on climate, chemical and physical processes, modeling and human health. New analytical techniques have been recently developed to identify and quantify the organics in the complex mixtures, where mass spectrometry has been the most employed. Multivariate statistical techniques are the most useful methods to classify pollutant sources. Given their mutagenic and carcinogenic effects, PAH have been the organic compounds most studied in the MCMA. They have been determined mostly in particle phase showing spatial heterogeneity around MCMA in both on-real and off-real time measurements. Benzo[*ghi*]perylene has been the most abundant PAH determined in all studies and it must be considered for health studies due to the indirect correlation with in vitro ROS formation. The cold dry-season (November-February) contained the highest organic pollutant concentrations, while the rainy season (May-October) showed the lowest. Indirect mutagenic activities in the Ames test have showed significant correlation with PAH when

they are not mixed with other compounds, suggesting a greater risk for those people exposed to direct emissions rich in these compounds. Results of the Environmental Mutagenesis Group (EMG) suggest heterogeneity in PAH concentrations around MCMA, indicating higher human health risk for those living in Downtown of MC, based on the higher mass per cubic meter of inhaled air containing carcinogenic PAH. Different oxidation degrees of the organic matter were observed in the MCMA, indicating aging of the aerosol from the NE to the SW.

6. Future research

Organic aerosol on climate, atmospheric chemistry and the impact on human health are uncertain and scarcely known. Therefore, more comprehensive data on spatial and seasonal distribution is needed to investigate further the regional nature of airborne particles and their organic composition, so as to support the development of strategies for reducing ambient concentrations. Although off–line measurements techniques are the most employed to elucidate the specific organic aerosol composition, the components are dependent on the details of the analytical techniques used, and both positive and negative artifacts can occur during sampling (Turpin et al., 2000), thus indicating that and more research is needed in this field.

Studies on PAH determination in MCMA should be included in regulations in order to properly establish air quality standards according to their atmospheric conditions. This is why part of our future research will be focused on obtaining emissions due to the introduction of new car technologies (Jazcilevich et al., 2011), and the use of mixtures of ethanol and bio-diesel in vehicles, an international trend that Mexico might follow. At present, secondary organic aerosols are underestimated by the current models due to the extreme chemical complexity which has prevented the precise measurement and prediction of the oxidation process associated with the formation and evolution of atmospheric organic aerosol. Further studies are needed to improve estimations and to understand the relative importance of anthropic versus natural aerosol precursors. Analytical methodology optimization to determine organic aerosols is a continuous challenge to evaluate new analytical methodologies increasing precision and efficiency, and decreasing uncertainty in the measurements of the target compounds in the complex mixture of the organic aerosol. These methods are developed under the criteria of "green chemistry" to reduce the consumption of materials and time and therefore, to reduce waste and energy. New approaches are being developed to bio-direct the effect of specific organic pollutants on specific cultures of epithelial cells, human lymphocytes and bacterial assays, all of them for explaining different action mechanisms to know the risk of people exposed living mainly in urban centers.

7. Acknowledgments

We thank Jose Ramón Hernández, Agustín Eguiarte, Wilfrido Gutiérrez, Manuel García, Josué Vázquez, Alfredo Rodríguez, Delibes Roman, Guadalupe Zitlalpopoca and Geraldine González their technical assistance. Claudio Amescua and Pietro Villalobos by their writing assistance. A-M O acknowledges the Programa de Maestría y Doctorado en Ciencias Químicas-UNAM for the facilities given during doctorate studies. VH-BL acknowledges the CONACyT for the studentship given during her Doctorate studies in the Posgrado de Ciencias de la Tierra-UNAM. We thank to PAPIIT IN116810-UNAM, ICYT-GDF PICS08-31, UC532MEXUS, CONACYT-SEMARNAT CO1-0822/A1 and 23600 their financial support.

8. References

Aiken, A.C.; DeCarlo, P.F. & Jimenez, J.L. (2007). Elemental Analysis of Organic Species with Electron Ionization High-Resolution Mass Spectrometry. *Analytical Chemistry* 79, 8350–8358.

Aiken, A.C.; DeCarlo, P.F.; Kroll, J.H.; et al. (2008). O/C and OM/OC Ratios of Primary, Secondary, and Ambient Organic Aerosols with High-Resolution Time-of-flight Aerosol Mass Spectrometry, *Environmental Science and Technology*, 42, 4478–4485.

Alfaro-Moreno, E.; Martínez, L.; García-Cuellar, C.; et al. (2002). Biologic Effects Induced in Vitro by PM_{10} from Three Different Zones of Mexico City. *Environmental Health Perspectives*, 110, 715-720.

Alfaro-Moreno, E.; López-Marure, R.; Montiel-Dávalos, A.; et al. (2007). E-Selectin Expression in Human Endothelial Cells Exposed to PM_{10}: The Role of Endotoxin and Insoluble Fraction. *Environmental Research*, 103, 221-228.

Allan, J.D.; Alfarra, M.R.; Bower, K.N.; et al. (2003). Quantitative Sampling Using an Aerodyne Aerosol Mass Spectrometer – 2. Measurements of Fine Particulate Chemical Composition in Two U.K. Cities. *Journal of Geophysical Research Atmospheres*, 108, NO. D3, 4091, doi:10.1029/2002JD002359.

Allen, J.O.; Dookeran, N.M.; Smith, A.K.; et al. (1996). Measurement of Polycyclic Aromatic Hydrocarbons Associated with Size-segregated Atmospheric Aerosols in Massachusetts. *Environmental Science and Technolology*, 30, 1023-1031.

Alves, C.A.; Pío, C.A. & Duarte, A.C. (2000). Particulate Size Distributed Organic Compounds in a Forest Atmosphere. *Environmental Science and Technolology*, 34, 4287-4293.

Amador-Muñoz, O. & Marriott, P.J. (2008). Quantification in Comprehensive Two-dimensional Gas Chromatography and a Model of Quantification Based on Selected Summed Modulated Peaks. *Journal of Chromatography A (50th anniversary)*, 1184, 323-340.

Amador-Muñoz, O.; Villalobos-Pietrini, R.; Aragón-Piña, A.; et al. (2008). Quantification of Polycyclic Aromatic Hydrocarbons Based on Comprehensive Two-dimensional Gas Chromatography-Isotope Dilution Mass Spectrometry. *Journal of Chromatography A*, 1201, 161-168.

Amador-Muñoz, O.; Villalobos-Pietrini, R.; Agapito-Nadales, M.C.; et al. (2010). Solvent Extracted Organic Matter and Polycyclic Aromatic Hydrocarbons Distributed in Size-segregated Airborne Particles in a Zone of México City: Seasonal Behavior and Human Exposure. *Atmospheric Environment*, 44, 122–130.

Amador-Muñoz, O.; Villalobos-Pietrini, R.; Miranda, J.; et al. (2011). Organic Compounds of $PM_{2.5}$ in Mexico Valley: Spatial and Temporal Patterns, Behavior and Sources. *Science of the Total Environment*, 409, 1453-1465.

Ames B.N.; Durston, W.E.; Yamasaki, E.; et al. (1973). Carcinogens are Mutagen: A Simple Test System Combining Liver Homogenates for Activation and Bacteria for Detection. *Proceedings of the National Academy of Sciences USA*, 70, 2281-2285.

Ames, B.N.; Mccann, J. & Yamasaki, E. (1975). Methods for Detecting Carcinogens and Mutagens with *Salmonella*/Mammalian-Microsome Mutagenicity Test. *Mutation Research*, 31, 347-364.

Atkinson, S.E. & Lewis, D.H. (1974). A Cost-Effectiveness Analysis of Alternative Air Quality Control Strategies. *Journal of Environmental Economics and Management*, 1, 237-250.

Atkinson. R.; Arey, J., Zielinska, B.; et al. (1990). Kinetics and Nitro-Products of the Gas-Phase OH and NO_3 Radical-initiated Reactions for Naphthalene-d_8, Fluoranthene-d_{10}, and Pyrene. *International Journal of Chemical Kinetics*, 22, 999-1014.

ATSDR (Agency for Toxic Substances and Disease Registry) (1995).Toxicology Profile for Polycyclic Aromatic Hydrocarbons, US Department of Health and Human Services, Atlanta, GA., http://www.atsdr.cdc.gov/toxprofiles/tp69.pdf.

Bamford, H.A. & Baker, J.E. (2003). Nitro-Polycyclic Aromatic Hydrocarbon Concentrations and Sources in Urban and Suburban Atmospheres of the Mid-Atlantic Region. *Atmospheric Environment*, 37, 2077–2091.

Barraza-Villarreal, A.; Sunyer, J.; Hernández-Cadena, L.; et al. (2008). Air Pollution, Airway Inflammation, and Lung Function in a Cohort Study of Mexico City Schoolchildren. *Environmental Health Perspectives*, 116, 832-838.

Baumgardner, D.; Raga, G.B.; Kok, G.; et al. (2000). On the Evolution of Aerosol Properties at a Mountain Site Above Mexico City. *Journal of Geophysical Research Atmospheres*, 105, 22243-22253.

Baumgardner, D.; Raga, G.B.; Peralta, O.; et al. (2002). Diagnosing Black Carbon Trends in Large Urban Areas Using Carbon Monoxide Measurements. *Journal of Geophysical Research*, 107, NO. D21, 8342, doi:10.1029/2001JD000626.

Baumgardner, D.; Kok, G.J. & Raga, G.B. (2007). On the Diurnal Variability of Particle Properties Related to Light Absorbing Carbon in Mexico City. *Atmospheric Chemistry and Physics*, 7, 2517–2526.

Bond, T. C. & Bergstrom, R. W. (2006). Light Absorption by Carbonaceous Particles: An Investigative Review. *Aerosol Science and Technology*, 40, 27–67.

Bravo, J.L.; Amador-Muñoz, O.; Villalobos-Pietrini, R. et al. (2006). Influence of Some Meteorological Parameters and Forest Fires on PM_{10} Concentrations in a Southwest Zone of Mexico Valley. *International Journal of Environment and Pollution*, 26, 142-155.

Bruns, E.A.; Perraud, V.; Greaves, J. & Finlayson-Pitts, B.J. (2010). Atmospheric Solids Analysis Probe Mass Spectrometry: A New Approach for Airborne Particle Analysis, *Analytical Chemistry* 82, 5922-5927.

Burtscher, H. & Siegmann, H. C. (1993). Photoemission for in Situ Analysis of Particulate Combustion Emissions. *Water, Air, & Soil Pollution*, 68, 125-136.

Canagaratna, M.R.; Jayne, J.T.; Jimenez, J.L.; et al. (2007). Chemical and Microphysical Characterization of Ambient Aerosols with the Aerodyne Aerosol Mass Spectrometer. *Mass Spectrometry Reviews*, *26*, 185–222.

Calderón-Segura, M.E.; Gómez-Arroyo, S.; Villalobos-Pietrini, R.; et al. (2004). The Effects of Seasonal Weather on the Genotoxicity, Cytokinetic Properties, Cytotoxicity and Organochemical Content of Extracts of Airborne Particulates in Mexico City. *Mutation Research*, 558, 7-17.

Calderón-Garcidueñas, L.; Mora-Tiscareño, A.; Fordham, L.A.; et al. (2006). Lung Radiology and Pulmonary Function of Children Chronically Exposed to Air Pollution. *Environmental Health Perspectives*, 114, 1432-1437.

Calderón-Garcidueñas, L.; Franco-Lira, M.; Henríquez-Roldán, C.; et al. (2010). Urban Air Pollution: Influences On Olfactory Function and Pathology in Exposed Children and Young Adults. *Experimental and Toxicology Pathology*, 62, 91-102.

Chirino, Y.I.; Sánchez-Pérez, Y.; Osornio-Vargas, A.R.; et al. (2010). PM_{10} Impairs the Antioxidant Defense Systems and Exacerbates Oxidative Stress Driven Cell Death. *Toxicology Letters*, 193, 209-216.

Cho, A. K.; Sioutas, C.; Miguel, A. H.; et al. (2005). Redox Activity of Airborne Particulate Matter at Different Sites in the Los Angeles Basin. *Environmental Research*, 99, 40–47.

Chow, J.C.; Watson, J.G.; Edgerton, S.A.; et al. (2002). Chemical Composition of $PM_{2.5}$ and PM_{10} in Mexico City During Winter 1997. *The Science of the Total Environment*, 287, 177-201.

Claxton, L.D.; Warren, S.; Zweidinger, R.; et al. (2001). A Comparative Assessment of Boise, Idaho, Ambient Air Fine Particle Samples Using the Plate and Microsuspension Salmonella Mutagenicity Assays. *The Science of the Total Environment*, 275, 95-108.

Claxton, L.D.; Matthews, P.P. & Warren, S.H. (2004). The Genotoxicity of Ambient Outdoor Air, a Review: *Salmonella* Mutagenicity. *Mutation Research*, 567, 347-399.

Cziczo, D.J.; DeMott, P. J.; Brooks, S.D.A.; et al. (2004). Observations of Organic Species and Atmospheric Ice Formation, *Geophysical Research Letters*, 31, L12116, doi:10.1029/2004GL019822.

Denissenko, M.F.; Pao, A.; Tang, M.; et al. (1996). Preferential Formation of Benzo[*a*]pyrene Adducts at Lung Cancer Mutational Hotspots in P53. *Science*, 18, 430–432.

Díaz-Nigenda, E.; Tatarko, J.; Jazcilevich, A.D.; et al. (2010). A Modeling Study of Aeolian Erosion Enhanced by Surface Wind Confluences over Mexico City. *Aeolian Research* 2, 143-157.

Doran, J.C.; Abbott, S.; Archuleta, J.; et al. (1998). The IMADA-AVER Boundary-layer Experiment in the Mexico City Area. *Bulletin of the American Meteorological Society*, 79, 2497–2508.

Durant, J.L.; Busby, W.F. Jr.; Lafleur, A.L.; et al. (1996). Human Cell Mutagenicity of Oxygenated, Nitrated and Unsubstituted Polycyclic Aromatic Hydrocarbons Associated with Urban Aerosols. *Mutation Research*, 371, 123–157.

Dzepina, K.; Arey, J.; Marr, L. C.; et al. (2007). Detection of Particle-phase Polycyclic Aromatic Hydrocarbons in Mexico City Using an Aerosol Mass Spectrometer. *International Journal of Mass Spectrometry*, 263, 152–170.

Facchini, M.C.; Fuzzi, S.; Zappoli, S.; et al. (1999). Partitioning of the Organic Aerosol Component between Fog Droplets and Interstitial Air. *Journal of Geophysical Research Atmospheres*, 104, 26821-26832.

Fast, J.D.; de Foy, B.; Rosas, F.A., et al. (2007). A Meteorological Overview of the MILAGRO Field Campaigns. *Atmospheric Chemistry and Physics*, 7, 2233-2257.

Feilberg, A.; Poulsen, M.W.; Nielsen, T.; et al. (2001). Occurrence and Sources of Particulate Nitropolycyclic Aromatic Hydrocarbons in Ambient Air in Denmark. *Atmospheric Environment*, 35, 353–366.

Feng, J.; Guo, Z.; Chan, C.K.; et al. (2007). Properties of Organic Matter in PM2.5 at Changdao Island, China-A Rural Site in the Transport Path of the Asian Continental Outflow. *Atmospheric Environment*, 41, 1924-1935.

Finlayson-Pitts, B.J. & Pitts, J.N. (1997). Tropospheric Air Pollution: Ozone, Airborne Toxics, Polycyclic Aromatic Hydrocarbons, and Particles. *Science*, 276, 1045–1052.

García-Cuellar, C.; Alfaro-Moreno, E.; Martínez-Romero, F.; et al. (2002). DNA Damage Induced by PM_{10} from Different Zones of Mexico City. The *Annals of Occupational Hygiene*, 46, Supplement 1, 425-428.

Goldstein, A.H.; Worton, D.R.; Williams, B.J.; et al. (2008). Thermal Desorption Comprehensive Two-dimensional Gas Chromatography for in-situ Measurements of Organic Aerosols. *Journal of Chromatography* A, 1186, 340-347.

Goriaux, M.; Jourdain, B.; Temime, B.; et al. (2006). Field Comparison of PAH Measurements Using a Low Flow Denuder Device and Conventional Sampling Systems. *Environmental Science and Technology*, 40, 6398–6404.

Gutierrez-Castillo, M.E.; Roubicek, D.A.; Cebrían-García, M.E.; et al. (2006). Effect of Chemical Composition on the Induction of DNA Damage by Urban Airborne Particulate Matter. *Environmental and Molecular Mutagenesis*, 47, 199-211.

Guzmán-Torres, D.; Eiguren-Fernández, A.; Cicero-Fernández, P.; et al. (2009). Effects of Meteorology on Diurnal and Nocturnal Levels of Priority Polycyclic Aromatic Hydrocarbons and Elemental and Organic Carbon in PM_{10} at a Source and a Receptor Area in Mexico City. *Atmospheric Environment*, 43, 2693–2699.

Hallquist, M.; Wenger, J.C.; Baltensperger, U.; et al. (2009). The Formation, Properties and Impact of Secondary Organic Aerosol: Current and Emerging Issues. *Atmospheric Chemistry and Physics*, 9, 5155–5236.

Hayatsu, H.; Arimoto, S. & Negishi, T. (1988). Dietary Inhibitors of Mutagenesis and Carcinogenesis. *Mutation Research*, 202, 429-446.

Hildemann, L.M.; Rogge, W.F.; Cass, G.R.; et al. (1996). Contribution of Primary Aerosol Emissions from Vegetation-derived Sources to Fine Particle Concentrations in Los Angeles. *Journal of Geophysical Research*, 101, 19541-19549.

Hinds, W.C. (1999). *Aerosol Technology, Properties, Behavior, and Measurements of Airborne Particles*. Wiley Interscience, New York.

Holguín, F.; Téllez-Rojo, M.M.; Hernández, M.; et al. (2003). Air Pollution and Hearth Rate Variability Among the Elderly in Mexico City. *Epidemiology*, 14, 521-527.

Huffman, J.A.; Docherty, K.S.; Aiken, A.C.; et al. (2009). Chemically-resolved Aerosol Volatility Measurements from Two Megacity Field Studies. *Atmospheric Chemistry and Physics*, 9, 7161–7182.

IARC (International Agency for Research on Cancer) (1983). Polynuclear Aromatic Compounds, Part 1, Chemical, Environmental and Experimental Data. Summary of Data Reported and Evaluation, In: *IARC Monographs on the Evaluation of Carcinogenic Risks to Humans,* World Health Organization, International Agency for Research on Cancer, 1983 updated 1998, http://monographs.iarc.fr/ENG/Monographs/vol32/volume32.pdf.

IARC (International Agency for Research on Cancer) (1989). Diesel and Gasoline Engine Exhausts and Some Nitroarenes. Summary of Data Reported and Evaluation, In: *IARC Monographs on the Evaluation of Carcinogenic Risks to Humans*, World Health Organization, International Agency for Research on Cancer, Updated 1998. http://monographs.iarc.fr/ENG/Monographs/vol46/volume46.pdf.

IPCC. Climate Change (2007). *The Physical Science Basis, Contribution of Working Group I to the Fourth Assessment Report of the Intergovernmental Panel on Climate Change*. S. Solomon, D. Qin, M. Manning, Z. Chen, M. Marquis, K.B. Averyt, M. Tignor & H.L Miller (Eds)., Cambridge University Press, Cambridge, United Kingdom and New York, USA, 996 p.

Jacobson, M.C. ; Hansson, H.C. ; Noone, K.J.; et al. (2000). Organic Atmospheric Aerosols: Review and State of the Science. *Reviews of Geophysics*, *38*, 267-294.

Jazcilevich, A.D.; García, A.R. & Ruíz-Suárez, L.G. (2003). A Study of Air Flow Patterns Affecting Pollutant Concentrations in the Central Region of Mexico. *Atmospheric Environment*, 37, 183-193.

Jazcilevich, A.D.; García, A.R. & Caetano, E. (2005). Locally Induced Surface Air Confluence by Complex Terrain and its Effects on Air Pollution in the Valley of Mexico. *Atmospheric Environment*, 39, 5481-5489.

Jazcilevich, A.D.; García, A.R.; Grutter, M.; et al. (2011). An Evaluation of the Hybrid Car Technology for the Mexico Mega City. To appear in *Journal of Power Sources*.

Jiang, M.; Marr, L.C.; Dunlea, E.J.; et al. (2005). Vehicle Fleet Emissions of Black Carbon, Polycyclic Aromatic Hydrocarbons, and other Pollutants Measured by a Mobile Laboratory in Mexico City. *Atmospheric Chemistry and Physics*, 5, 3377-3387.

Johnson, R.L., Shah, J.J.; Cary, R.A.; et al. (1981). An Automated Thermal-optical Method for the Analysis of Carbonaceous Aerosol, In: *Atmospheric Aerosol: Source/Air Quality Relationships*, E.S. Macias & P.K. Hopke (Eds.), 223-233. Vol ACS Symposium Series No. 167. American Chemical Society, Washington, DC.

Kado, N.Y.; Langley, D. & Eisenstadt, E. (1983). A Simple Modification of the *Salmonella* Liquid-Incubation Assay. Increased Sensitivity for Detecting Mutagens in Human Urine. *Mutation Research*, 121, 25-32.

Kado, N.Y.; Guirguis,N.G.; Flessel, C.P.; et al. (1986). Mutagenicity of Fine (< 2.5 μm) Airborne Particles: Diurnal Variation in Community Air Determined by a Salmonella Micro Preincubation (Microsuspension) Procedure. *Environmental Mutagenesis*, 8, 53-66.

Kanakidou, M.; Seinfeld, J.H.; Pandis, S.N.; et al. (2005). Organic Aerosol and Global Climate Modelling: A Review. *Atmospheric Chemistry and Physics*, 5, 1053–1123.

Kavouras, I.G.; Lawrence, J.; Koutrakis, P.; et al. (1999). Measurement of Particulate Aliphatic and Polynuclear Aromatic Hydrocarbons in Santiago de Chile: Source Reconciliation and Evaluation of Sampling Artifacts. *Atmospheric Environment*, 33, 4977-4986.

Kelly, T.J.; Mukund, R.; Spicer, C.W.; et al. (1994). Concentrations and Transformations of Hazardous Air Pollutants. *Environmental Science and Technolology*, 28, 378A-387A.

Kroll, J.S. ; Donahue, N.M. ; Jimenez, J.L. ; et al. (2011). Carbon Oxidation State as a Metric for Describing the Chemistry of the Atmospheric Organic Aerosol. *Nature Chemistry*, 3, 133-139.

Lanz, V.A.; Alfarra, M.R., Baltensperger, U.; et al. (2007). Source Apportionment of Submicron Organic Aerosols at an Urban Site by Factor Analytical Modelling of Aerosol Mass Spectra. *Atmospheric Chemistry and Physics*, 7, 1503–1522.

Laskin, A.; Smith, J. S. & Laskin, J. (2009). Molecular Characterization of Nitrogen-Containing Organic Compounds in Biomass Burning Aerosols Using High-Resolution Mass Spectrometry *Environmental Science and Technology*, *43*, 3764–3771.

Laskin, J.; Laskin, A.; Roach, P. J.; et al. (2010). High- Resolution Desorption Electrospray Ionization Mass Spectrometry for Chemical Characterization of Organic Aerosols *Analytical Chemistry*, 82, 2048–2058.

Latt, S.; Allen, J.; Blom, S.; et al. (1981). Sister Chromatid Exchanges in Human Lymphocytes after Exposure to Diagnostic Ultrasound. *Science,* 205, 1273-1275.

Lawrence, M.G.; Butler, T. M.; Steinkamp, J.; et al. (2007). Regional Pollution Potentials of Megacities and Other Major Population Centers. *Atmospheric Chemistry and Physics*, 7, 3969– 3987.

Lewtas, J. (1988). Genotoxicity of Complex Mixtures: Strategies for the Identification and Comparative Assessment of Airborne Mutagens and Carcinogens from Combustion Sources. *Fundamental and Applied Toxicology*, 10, 571-589.

Lewtas, J. (1993). Complex Mixtures of Air Pollutants: Characterizing the Cancer Risk of Polycyclic Organic Matter (POM). *Environmental Health Perspectives*, 100, 211-218.

Lewtas, J. (2007). Air Pollution Combustion Emissions: Characterization of Causative Agents and Mechanisms Associated with Cancer, Reproductive, and Cardiovascular Effects. *Mutation Research*, 636, 95-133.

Liousse, C.; Michel, C.; Bessagnet, B.; et al. (2005). O-D-Modelling of Carbonaceous Aerosols over Greater Paris Focusing on the Organic Particle Formation. *Journal of Atmospheric Chemistry*, 51, 207-221.

Marr, L.C.; Grogan, L.A.; Worhrnschimmel, H.; et al. (2004). Vehicle Traffic as a Source of Particulate Polycyclic Aromatic Hydrocarbon Exposure in Mexico City. *Environmental Science and Technology*, 38, 2584–2592.

Marr, L.C.; Dzepina, K.; Jimenez, J.L.; et al. (2006). Sources and Transformations of Particle-bound Polycyclic Aromatic Hydrocarbons in Mexico City. *Atmospheric Chemistry and Physics*, 6, 1733–1745.

Matter, U.; Siegmann, H. C. & Burtscher, H. (1999). Dynamic Field Measurements of Submicron Particles from Diesel Engines, *Environmental Science and Technology*, 33, 1946–1952.

Miguel, A.H.; Kirchstetter, T.W.; Harley, R.A.; et al. (1998). On-road Emissions of Particulate Polycyclic Aromatic Hydrocarbons and Black Carbon from Gasoline and Diesel Vehicles. *Environmental Science and Technology*, 32, 450–455.

Mikhailov, E.; Vlasenko, S.; Martin, S.T.; et al. (2009). Amorphous and Crystalline Aerosol Particles Interacting with Water Vapor: Conceptual Framework and Experimental Evidence for Restructuring, Phase Transitions and Kinetic Limitations. *Atmospheric Chemistry and Physics*, 9, 9491–9522.

Molina, L.T.; Kolb, C.E.; de Foy, B.; et al. (2007). Air Quality in North America's most Populous City – Overview of the MCMA-2003 Campaign. *Atmospheric Chemistry and Physics*, 7, 2447-2473.

Molina, L. T.; Madronich, S.; Gaffney, J. S.; et al. (2010). An Overview of the MILAGRO 2006 Campaign: Mexico City Emissions and their Transport and Transformation. *Atmospheric Chemistry and Physics*, 10, 8697-8760.

Montiel-Dávalos, A.; Ibarra-Sánchez, M de.J.; Ventura-Gallegos, J.L.; et al. (2010). Oxidative Stressand Apoptosis are Induced in Human Endothelial Cells Exposed to Urban Particulate Matter. *Toxicology in Vitro*, 24, 135-141.

Mortelmans, K. & Zeiger, E. (2000). The Ames *Salmonella*/microsome Mutagenicity Assay. *Mutation Research*, 455, 29-60.

Mugica V., Torres M., Salinas E., et al. (2010a). Polycyclic Aromatic Hydrocarbons in the Urban Atmosphere of Mexico City. In: *Air pollution,* V. Villanyi (Ed.), 75-97, Scyio, ISBN 978-953-307-143-5, Rijeka, Croatia.

Mugica, V.; Hernández, S.; Torres, M.; et al. (2010b). Seasonal Variation of Polycyclic Aromatic Hydrocarbons Exposure Levels in Mexico City. *Journal of the Air & Waste Management Association*, 60, 548-555.

Murillo-Tovar, M.A.; Amador-Muñoz, O.; Villalobos-Pietrini, R.; et al. (2010). Selective Separation of Oxy-PAH from n-alkanes and PAH in Complex Organic Mixtures Extracted from Airborne Particulate Matter ≤ 2.5 μm. *Chromatographia* 72, 913-921.

Murphy, B. N. & Pandis, S. N. (2009). Simulating the Formation of Semivolatile Primary and Secondary Organic Aerosol in a Regional Chemical Transport Model. *Aerosol Science and Technology*, 43, 4722–4728.

Nielsen, T. (1984). Reactivity of Polycyclic Aromatic Hydrocarbons Toward Nitrating Species. *Environmental Science and Technology*, 18, 157–163.

NRC (Nacional Research Council) (1996). A Plan for a Research Program on Aerosol Radiative Forcing and Climate Change. National Academic Press, Washington DC.

Osornio-Vargas, A.R.; Bonner, J.C; Alfaro-Moreno, E.; et al. (2003). Proinflammatory and Cytotoxic Effects of Mexico City Air Pollution Particulate Matter in Vitro are

Dependent on Particle Size and Composition. *Environmental Health Perspectives*, 111, 1289-1293.

Östling, O. & Johanson, K.J. (1984). Microelectrophoretic Study of Radiation-Induced DNA Damages in Individual Mammalian Cells. *Biochemical and Biophysical Research Communications*, 123, 291-298.

Pang, Y.; Turpin, B. J. & Gundel, L. A. (2006). On the Importance of Organic Oxygen for Understanding Organic Aerosol Particles. *Aerosol Science and Technology*, 40, 128–133.

Pankow, J.F. (1994). An Absorption Model of the Gas/aerosol Partitioning Involved in the Formation of Secondary Organic Aerosol. *Atmospheric Environment*, 28, 189-193.

Pankow, J.F. & Chang, E.I. (2008). Variation in the Sensitivity of Predicted Levels of Atmospheric Organic Particulate Matter (OPM). *Environmental Science and Technology*, *42*, 7321–7329.

Pitts, J.N.; Doyle, G.J. ; Lloyd, A.C.; et al. (1975). Chemical Transformations in Photochemical Smog and their Applications to Air Pollution Control Strategies In: *Second Annual Report, National Science Fundation – Research Applied to National Needs*, grant no. AEN73-02904-A02, 1975, Washington, DC (M.D. Waters, S. Nesnow, J.L. Huisingh, S. Sandhu & L.D. Claxton (Eds.)), Application of Short-term Bioassays in the Fractionation and Analysis of Complex Environmental Mixtures, Plenum Press, New York.

Pitts, J.; Cawenberghe, K.; Grossjean, D.; et al. (1978). Atmospheric Reactions of Polycyclic Aromatic Hydrocarbons: Facile Formation of Mutagenic Nitro Derivatives. *Science*, 202, 515–519.

Pope, C.A. & Dockery, D.W. (2006). Health Effects of Fine Particulate Air Pollution: Lines that Connect. *Journal of the Air and Waste Management Association*, 56, 709-742.

Pöschl, U. (2005). Atmospheric Aerosols: Composition, Transformation, Climate and Health Effects. *Angewandte Chemie International Edition*, *44*, 7520–7540.

Ramanathan, V.; Crutzen, P.J.; Kiehl, J.T.; et al. (2001). Atmosphere – Aerosols, Climate, and the Hydrological Cycle. *Science*, 294, 2119–2124.

Ramdahl, T. (1983). Retene—a Molecular Marker of Wood Combustion in Ambient Air. *Nature*, 306, 580–582.

Ravindra, K.; Bencs, L.; Wauters, E.; et al. (2006). Seasonal and Site Specific Variation in Vapor and Aerosol Phase PAHs over Flanders (Belgium) and their Relation with Anthropogenic Activities. *Atmospheric Environment*, 40, 771–785.

Ravindra, K.; Sohki R. & Van Grieken, R. (2008). Atmospheric Polycyclic Aromatic Hydrocarbons: Source Attribution, Emission Factors and Regulation. *Atmospheric Environment*, 42, 2895-2921.

Robinson, A.L.; Donahue, N.M. & Rogge, W.F. (2006a). Photochemical Oxidation and Changes in Molecular Composition of Organic Aerosol in the Regional Context. *Journal of Geophysical Research*, 111, D03302, doi:10.1029/2005JD006265.

Robinson, A.L.; Subramanian, R.; Donahue, N.M.; et al. (2006b). Source Apportionment of Molecular Markers and Organic Aerosols 1. Polycyclic Aromatic Hydrocarbons and Methodology for Data Visualization. *Environmental Science and Technology* 40, 7813–7820.

Robinson, A. L.; Donahue, N.M.; Shrivastava, M.K.; et al. (2007). Rethinking Organic Aerosols: Semivolatile Emissions and Photochemical Aging. *Science*, 315, 1259–1262.

Rogge, W.F.; Mazurek. M.A.; Hildemann, L.M.; et al. (1993a). Quantification of Urban Organic Aerosols at a Molecular Level: Identification, Abundance and Seasonal Variation. *Atmospheric Environment*, 27A, 1309-1330.

Rogge, W.F.; Hildemann, L.M; Mazurek, M.A.; et al. (1993b). Sources of Fine Organic Aerosol. 4. Particulate Abrasion Products from Leaf Surfaces of Urban Plants. *Environmental Science and Technology*, 27, 2700-2711.

Rogge, W.F.; Hildemann, L.M.; Mazurek, M.A.; et al. (1993c). Sources of Fine Organic Aerosol. 2. Non catalyst and Catalyst-equipped Automobiles and Heavy-duty Diesel Trucks. *Environmental Science and Technology*, 27, 636-651.

Rogge, W.F.; Hildemann, L.M.; Mazurek, M.A.; et al. (1993d). Sources of Fine Organic Aerosol. 3. Road Dust, Tire Debris, and Organometallic Brake Lining Dust: Roads as Sources and Sinks. *Environmental Science and Technology*, 27, 1892-1904.

Rojas, E.; Valverde, M.; López, M.C.; et al. (2000). Evaluation of DNA Damage in Exfoliated Tear Duct Epithelial Cells from Individuals Exposed to Air Pollution Assessed by Single Cell Gel Electrophoresis Assay. *Mutation Research*, 468, 11-17.

Rosenkranz, H.S. & Mermelstein, R. (1983). Mutagenicity and Genotoxicity of Nitroarenes, all Nitro-containing Chemicals were not Created Equal. *Mutation Research*, 114, 217-267.

Roubicek, D.A.; Gutiérrez-Castillo, M.E.; Sordo, M.; et al. (2007). Micronuclei Induced by Airborne Particulate Matter from Mexico City. *Mutation Research*, 631, 9-15.

Salcedo, D.; Onasch, T.B.; Dzepina, K.; et al. (2006). Characterization of Ambient Aerosols in Mexico City during the MCMA-2003 Campaign with Aerosol Mass Spectrometry: Results from the CENICA Supersite. *Atmospheric Chemistry and Physics*, 6, 925–946.

Saldarriaga, H.; Villalobos-Pietrini, R.; Solano, G.; et al. (2008). Aliphatic, Polycyclic Aromatic Hydrocarbons and Nitrated-Polycyclic Aromatic Hydrocarbons in PM_{10} in Southwestern Mexico City. *Polycyclic Aromatic Compounds*, 28, 578-597.

Schauer, J.J.; Rogge, W.F.; Hildemann, L.M.; et al. (1996). Source Apportionment of Airborne Particulate Matter Using Organic Compounds as Tracers. *Atmospheric Environment*, 30, 3837-3855.

Schmeling, M.; Russell, L.M.; Erlick, C.; et al. (2000). Aerosol Particle Chemical Characteristics Measured from Aircraft in the Lower Troposphere During ACE-2. *Tellus* B, 52, 185–200.

Schuetzle, D. & Lewtas, J. 1986. Bioassay-Directed Chemical Analysis in Environmental Research. *Analytical Chemistry*, 58, 1060A-1075A.

Schwarze, P.E.; Totlandsdal, A.I.; Herseth J.I.; et al. (2010). Importance of Sources and Components of Particulate Air Pollution for Cardio-Pulmonary Inflammatory Responses, In: *Air pollution,* V. Villanyi (Ed.), 47-73, Scyio, ISBN 978-953-307-143-5, Rijeka, Croatia.

Sen, B.; Mahadevan, B. & DeMarini, DM. (2007). Transcriptional Responses to Complex mixtures—A Review. *Mutation Research*, 636, 144-177.

Slowik, J.G.; Stroud, C.; Bottenheim, J.W.; et al. (2010). Characterization of a Large Biogenic Secondary Organic Aerosol Event from Eastern Canadian Forests. *Atmospheric Chemistry and Physics*, 10, 2825–2845.

Solomon, P.A.; Norris, G.A.; Landis, M.S. ; et al. (2001). Chemical Analysis Methods for Atmospheric Aerosols Components, In: *Aerosol Measurements: Principles, Techniques, and Application*,. K. Willeke & P. Baron (Eds.) 261-293, Wiley, New York.

Stone, E.A.; Snyder, D.C.; Sheesley, R.J.; et al. (2008). Source Apportionment of Fine Organic Aerosol in Mexico City during the MILAGRO Experiment 2006. *Atmospheric Chemistry and Physics*, 8, 1249-1259.

Stone, E.A.; Curtis J. Hedman, J.; et al. (2010). Insights into the Nature of Secondary Organic Aerosol in Mexico City during the MILAGRO Experiment 2006. *Atmospheric Environment*, 44, 312-319.

Sugita, K.; Goto, S.; Endo, O.; et al. (2004). Particle Size Effects on the Deposition Ratios of Airborne Particle in Respiratory Tracts. *Journal of Health Science*, 50, 185–188.

Sun, H.; Biedermann, L. & Bond, T. C. (2007). The Color of Brown Carbon: A Model for Ultraviolet and Visible Light Absorption by Organic Carbon Aerosol. *Geophysics Research Letters*, 34, L17813- doi: 10.1029/2007GL029797.

Suzuki, Y.; Kawakami, M. & Akasaka, K. (2001). H-1 NMR Application for Characterizing Water-soluble Organic Compounds in Urban Atmospheric Particles. *Environmental Science and Technology,* 35, 2656–2664.

Thomas, E.; Rudich, Y.; Trakhtenberg, S.; et al. (1999). Water Adsorption by Hydrophobic Organic Surfaces: Experimental Evidence and Implications to the Atmospheric Properties of Organic Aerosols. *Journal of Geophysical Research*, 104, 16053-16059.

Thornhill, D.A.; de Foy, B.; Herndon, S.C.; et al. (2008). Spatial and Temporal Variability of Particulate Polycyclic Aromatic Hydrocarbons in Mexico City. *Atmospheric Chemistry and Physics*, 8, 3093–3105.

Tran, T.; Amador-Muñoz, O.; Purcaro, G.; et al. (2007). Gas Chromatographic Analysis of Polyaromatic Hydrocarbons, In: *Environmental Impact of Polynuclear Aromatic Hydrocarbons.* C. Anyakora (Ed.) 331-378, Research Signpost, Kerala, India.

Turpin, B.J.; Saxena, P. & Andrews, E. (2000). Measuring and Simulating Particulate Organics in the Atmosphere: Problems and Prospects. *Atmospheric Environment*, 34, 2983-3013.

Turpin, B.J. & Lim, H.J. (2001). Species Contributions to $PM_{2.5}$ Mass Concentrations: Revisiting Common Assumptions for Estimating Organic Mass. *Aerosol Science and Technology*, *35*, 602–610.

Valle-Hernández, B.L.; Mugica-Alvarez, V.; Salinas-Talavera, E.; et al. (2010). Temporal Variation of Nitro-polycyclic Aromatic Hydrocarbons in PM_{10} and $PM_{2.5}$ Collected in Northern Mexico City. *Science of the Total Environment*, 408, 5429-5438.

Vasconcelos, L.A.; Macias, E.S. & White, W.H. (1994). Aerosol Composition as a Function of Haze and Humidity Levels in the Southwestern US. *Atmospheric Environment*, 28, 3679-3691.

Velasco, E.; Siegmann, P. & Siegmann, H. C. (2004). Exploratory Study of Particle-bound Polycyclic Aromatic Hydrocarbons in Different Environments in Mexico City. *Atmospheric Environment*, 38, 4957–4968.

Venter, A.; Nefliu, M. & Cooks, R.G. (2008). Ambient Desorption Ionization Mass Spectrometry. *Trends in Analytical Chemistry*, 27, 284–290.

Villalobos-Pietrini, R.; Amador-Muñoz, O.; Waliszewski, S.; et al. (2006). Mutagenicity and Polycyclic Aromatic Hydrocarbons Associated with Extractable Organic Matter from Airborne Particles $\leq$ 10 μm in Southwest Mexico City. *Atmospheric Environment*, 40, 5845-5857.

Villalobos-Pietrini, R.; Hernández-Mena, L.; Amador-Muñoz, O.; et al. (2007). Biodirected Mutagenic Chemical Assay of PM_{10} Extractable Organic Matter in Southwest Mexico City. *Mutation Research*, 634, 192-204.

Villalobos-Pietrini, R.; Amador-Muñoz, O.; Flores-Márquez, A.R.; et al. (2008). Materia Orgánica Extraída de las Aeropartículas de la Ciudad de México y sus Efectos Genotóxicos. *TIP, Revista Especializada en Ciencias Químico-Biológicas de la Facultad de Estudios Superiores Zaragoza, UNAM*, 11, 105-109.

Virtanen, A.; Joutsensaari, J.; Koop, T.; et al. (2010). An Amorphous Solid State of Biogenic Secondary Organic Aerosol Particles. *Nature*, 467, 824-826.

Vogt, L.; Gröger, T. & Zimmermann, R. (2007). Automated Compound Classification for Ambient Aerosol Sample Separations Using Comprehensive Two-dimensional Gas

Chromatography–time-of-flight Mass Spectrometry. *Journal of Chromatography A*, 1150, 2–12.

Volkamer, R.; Jimenez, J.L.; San Martini, F.; et al. (2006). Secondary Organic Aerosol Formation from Anthropogenic Air Pollution: Rapid and Higher than Expected. *Geophysical Research Letters,* 33, L17811. doi:10.1029/2006GL026899.

Watson, J. G. (1984). Overview of Receptor Model Principles. *Journal of the Air pollution Control Association,* 34, 619-623.

Welthagen, W.; Schnelle-Kreis, J. & Zimmermann, R. (2003). Search Criteria and Rules for Comprehensive Two-dimensional Gas Chromatography–time-of-flight Mass Spectrometry Analysis of Airborne Particulate Matter. *Journal of Chromatography* A, 1019, 233-249.

Williams, B.J.; Goldstein, A.H.; Kreisberg, N.M.; et al. (2006). An In-Situ Instrument for Speciated Organic Composition of Atmospheric Aerosols: Thermal Desorption Aerosol GC/MS-FID (TAG). *Aerosol Science and Technology*, 40, 627-638.

Winiwarter, W.; Bauer, H.; Caseiro, A.; et al. (2009). Quantifying Emissions of Primary Biological Aerosol Particle Mass in Europe. *Atmospheric Environment*, 43, 1403–1409.

Xia, T.; Korge, P.; Weiss, J. N.; et al. (2004). Quinones and Aromatic Chemical Compounds in Particulate Matter Induce Mitochondrial Dysfunction: Implications for Ultrafine Particle Toxicity. *Environmental Health Perspectives* 112, 1347-1358.

Yokelson, R. J.; Crounse, J.D.; DeCarlo, P.F.; et al. (2009). Emissions from Biomass Burning in the Yucatan. *Atmospheric Chemistry and Physics*, 9, 5785–5812.

Zhang, Q.; Alfarra, M.R.; Worsnop, D.R.; et al. (2005) . Deconvolution and Quantification of Hydrocarbon-like and Oxygenated Organic Aerosols Based on Aerosol Mass Spectrometry. *Environmental Science and Technology*, 39, 4938–4952.

Zheng, M.; Ke, L.; Edgerton, E.S.; et al. (2006). Spatial Distribution of Carbonaceous Aerosol in the Southeastern United States Using Molecular Markers and Carbon Isotope Data; *Journal of Geophysical Research Atmosphere*, 111, D10S09, doi:10.1029/2005JD006777.